UNIVERSITY OF CALGARY

Mechanisms of Heavy Oil Recovery by Waterflooding

By

An Mai

A THESIS

SUBMITTED TO THE FACULTY OF GRADUATE STUDIES

IN PARTIAL FULFILMENT OF THE REQUIREMENTS FOR THE

DEGREE OF DOCTOR OF PHILOSOPHY

DEPARTMENT OF CHEMICAL AND PETROLEUM ENGINEERING

CALGARY, ALBERTA

APRIL, 2008

Canada

ABSTRACT

Waterflooding is a common technology applied in heavy oil reservoirs after primary production, but the actual recovery mechanisms are still poorly understood. Due to the adverse mobility ratio between oil and water, injected water will tend to finger through the oil, leaving large portions of the reservoir unswept. Breakthrough of water will occur early in the life of a waterflood, followed by further oil production at high water cuts. Viscous instability theory can be used to describe the oil recovered up to breakthrough, but the mechanisms leading to oil recovery at later times have been largely unexplored. In this work, a suite of experiments was performed to investigate the relative significance of viscous and capillary forces on heavy oil waterfloods after water breakthrough.

Experiments performed in dead oil systems varied the oil viscosity, water injection and sand permeability. At lower injection rates and in higher permeability sands, optimal oil recovery was obtained. Normalized oil production rates could also be sustained at low water injection rates, and rates became relatively insensitive to the pressure gradient across the core. This showed that viscous forces are not responsible for oil production after water breakthrough. Similar trends were observed in systems where waterflooding was performed at the conclusion of primary production, indicating that the same recovery mechanisms were present in dead oil core floods and in cores after primary production.

The response of the cores to low rate waterflooding indicated that capillary forces are an important contributor to heavy oil recovery. This was further investigated through CT imaging of fast versus slow waterfloods, and through an NMR study of fluids redistribution under static and flowing conditions. It was concluded that heavy oil recovery after breakthrough is mainly due to water imbibition and film thickening in water wet sands. This effect can be manifested in reduced apparent relative permeability to water at low injection rates. An empirical correlation was also developed, which can make predictions of oil recovery for a wide range of conditions in linear, water wet systems.

iii

ACKNOWLEDGEMENTS

During the course of this work many people near and far have lent their support, whether in direct help or to provide encouragement. I would like to take this opportunity to thank them for making this phase of my life more enjoyable.

I would like to thank Dr. Kantzas for his guidance and patience over the past few years. His trust in my ability and skills has encouraged me countless times throughout the course of my research. I would also like to thank Mr. John Schnitzler for his help in sealing my cores at times when the situations seem hopeless. The help of Mr. Jun Gao and Ms. Xiaodong Ji were also greatly appreciated, as was computer support from Mr. Michael Erath and Mr. Darrell Hodgson. I would also like to thank Mr. Dave Moon for his help with the micro-CT measurements and Mr. Yubin Li for his help in analyzing the CT images.

Financial support for this project was received from NSERC, COURSE and the Canada Research Chair in Energy and Imaging, with its industrial affiliates (Shell, Nexen, Devon, PetroCanada, Canadian Natural, ET Energy, Suncor, Schlumberger, CMG, Laricina and Paramount). The additional support from Laricina Energy Ltd. is deeply appreciated.

There have been many others who have provided their ears and their shoulders for me through some difficult times and to these people I express my heartfelt thanks. To my friends who have made the long time spent at the university seem shorter (particularly Jon, Paige and Tan), and to the past students of TIPM Laboratory who have shared my many frustrations. To my family (Mom, Dad, Trung, Binh and Vy) for always being there to cheer me on and especially when I felt like quitting. And finally to my extended family in Vietnam, for their love which transpired the long distance between us.

To my parents (Loc Mai and Hong Bui),

my husband (Trung Nguyen),

and my very best friend (Jon Bryan).

For they have stood by me

through my most glorious moments

as well as my darkest years.

TABLE OF CONTENTS

LIST OF FIGURES

LIST OF TABLES

NOMENCLATURE

A   cross-section area open to flow (m^2)

AEUB   Alberta Energy and Utilities Board

AI_w amplitude index of water

°API   density as defined by the American Petroleum Institute

A_w NMR amplitude of water

A_{w_f} NMR amplitude associated with water in films

A_{w_fs} NMR amplitude when the core is fully saturated with water

A_{w_p} NMR amplitude associated with water in pores

BPR   back pressure regulator

CT   Computerized Tomography

CTn   CT number

C*   wettability constant

d   drop diameter (scale divisions)

D   diameter of the sandpack (m)

DI   deionized water

DO   dead oil

E_A total sweep efficiency (fraction)

E_{Abt} the areal sweep efficiency at breakthrough (fraction)

f   calibration factor for the spinning drop tensiometer (mm/scale division)

f_{o2} fraction of oil flowing out of the outlet

f_w fraction of water in the flowing stream (as a fraction of total flow rate)

g   acceleration due to gravity (m/s^2)

GOR   gas oil ratio

h_1, h_2 heights above a certain reference level of water (m)

I_{sr} Instability number

JBN   Johnson-Bossler-Naumann

k   permeability of the porous medium (D)

K   factor of proportionality

k_{ri} relative permeability of component i (fraction)

k_{wor} permeability to water at the irreducible oil saturation S_{or}

k_{oiw} permeability to oil at the connate water saturation S_{wi}

l   thickness of sand (m)

L   length of sandpack (m)

L_a characteristic length of the matrix block (m)

L_w distance penetrated in the Wasburn equation (m)

LM 70   Lane Mountain 70 sand

M   mobility ratio

m   mass (g)

n   fitting exponent used by Abrams (which is equal to 0.4)

N_{ca} capillary number

N_{ca}^{*} Abram's capillary number

N_g ratio of the gravitational forces to the viscous forces

NMR   Nuclear Magnetic Resonance

n_r angular velocity (rpm)

N_w volume of water imbibed (m^3)

OGIP   original gas in place

OOIP   original oil in place

P   pressure (kPa)

P_c capillary pressure (kPa)

P_{visc} viscous pressure drop (kPa)

PSD   particle size distribution

PV   pore volume (m^3)

q   volume of water flowing across a unit area in unit time (m/s)

Q   volumetric flow rate (m^3/s)

q_i injection rate of fluid i (m^3/s)

Q_i pore volumes of water injected

Q_o cumulative oil production (m^3)

Q_∞ ultimate cumulative oil production (m^3)

r   radius of capillary tube (m)

R   recovery after 5 PVs of water injected from empirical relationship (%OOIP)

R_{bt} recovery at breakthrough (%OOIP)

RE   recovery efficiency

RF_Eff recovery efficiency of a waterflood (%OOIP/PV)

R_1, R_2 radii of the pore body and pore throat in the Laplace equation (m)

S_w water saturation (fraction)

$\overline{S}_w$ average water saturation (fraction)

S_{wc} connate water saturation (fraction)

S_{wi} initial water saturation (fraction)

S_{w2} water saturation at production outlet (fraction)

S_{or} residual oil saturation (fraction)

$\overline{S}_{wbt}$ average water saturation in the core at breakthrough (fraction)

S/V   surface to volume ratio (m^{-1})

T_2 NMR transverse relaxation time (ms)

T_{2B} NMR bulk relaxation (ms)

T_{2gm} geometric mean relaxation time (ms)

T_{2s} NMR surface relaxation (ms)

t_D dimensionless time

t_s scaled time ($s^{1.5}/m^2$)

USBM United States Bureau of Mining

V   volume (m^3)

W_i pore volumes of water injected

X_0 location where the frontal perturbation or the viscous fingers start to form (m)

z   height measured from the datum level (m)

α   angle of the formation dip to the horizontal plane

γ   interfacial tension between oil and water (mN/m)

ΔP_i pressure drop of component i (kPa)

Δρ   water-oil density difference (kg/m³)

$\Delta\Phi$ the change in piezometric pressure (kPa)

$\varepsilon_w, \varepsilon_o$ adjustable exponents for relative permeability

θ contact angle (measured through the water phase)

λ dimensionless empirical constant

μ viscosity of the fluid (mPa·s)

μ_m the mixture viscosity (mPa·s)

ν the injected velocity (m/s)

ν_{HP} velocity from Hagen-Poiseuille's equation (m/s)

ν_{pore} interstitial velocity (m/s)

ρ density of fluid (kg/m³)

ρ_s surface relaxivity (μm/s)

σ_e the effective or the pseudo-interfacial tension (mN/m)

σ_{os} interfacial tension between solid and oil (mN/m)

σ_{ow} interfacial tension between oil and water (mN/m)

σ_{ws} interfacial tension between water and solid (mN/m)

υ_t total fluid velocity (m/s)

ϕ the rock porosity (fraction)

ω a rate of convergence constant for Aronofsky's model

CHAPTER 1: INTRODUCTION

The Canadian deposits of heavy oil and bitumen are some of the largest in the world. Recent estimates by the AEUB (2007) suggest that this resource could exceed 270 billion m³ in Alberta alone. With a rising worldwide demand for oil and steadily declining conventional oil reserves, the Canadian oil sands will help Canada to remain an important energy source for the world. Around 82% of the oil in Alberta must be recovered by *in-situ* methods (AEUB, 2007). Of the total oil resource available, recent estimates (Radler, 2006) have put the Canadian oil reserves at approximately 28 billion m³ (179 billion bbls). These reserves are second only to Saudi Arabia (Radler, 2006), and the vast majority of these reserves are located in the Alberta oil sands (Alberta Energy, 2005). Of these reserves, almost 23 billion m³ of oil must be recovered using *in-situ* methods, which includes thermal, solvent and primary recovery of heavy oil and bitumen.

Heavy oil is a special class of this unconventional oil, which has viscosity ranging from 50 – 50,000 mPa·s (cP), and low API gravity. In Alberta alone, heavy oil deposits account for approximately 2% (5.7 billion m³) of the total oil sand resource base (AEUB, 2007). While this seems to be only a small fraction of the Canadian Heavy Oil resource, this is still a significant amount of oil that is available for recovery. Heavy oil reservoirs are often found in high porosity, high permeability, unconsolidated sand deposits. Permeability of the sand averages in the range of 3 D (Albartamani *et al*., 1999), but oil does not flow easily due to its high viscosity. Therefore, most heavy oil recovery methods focus at least partially on either reducing the oil viscosity or somehow improving flow at reservoir conditions.

At the initial reservoir temperature and pressure, the oil may contain dissolved solution gas, thus a fraction of the oil can be recovered using the energy from heavy oil solution gas drive. Primary production from heavy oil operations currently accounts for approximately 63% of *in-situ* Canadian heavy oil production (AEUB, 2007). Other countries, notably Venezuela, also contain significant heavy oil deposits capable of

sustaining some primary production at initial reservoir pressures (Radler, 2006). Primary production can recover around 5% of the oil in place (AEUB, 2007), leaving significant oil volumes in the reservoir for potential secondary recovery. In Alberta alone, this translates to a resource base of 5.4 billion m³ remaining oil for further exploitation, and massive other heavy oil volumes are available in the Venezuela oil sands. At this state, however, the reservoir energy has been depleted so another fluid must be injected into the reservoir in order to displace oil to production wells. The oil no longer contains dissolved solution gas, thus its viscosity is also higher than at initial reservoir conditions. As a result, most secondary or enhanced oil recovery methods focus on the injection of steam, heat or hydrocarbon solvent to reduce the oil viscosity.

Many of the reservoirs in Alberta and Saskatchewan are relatively small or thin, and the sand has been disturbed to an unknown extent during the production of sand in primary production. This sand production leads to the generation of high permeability "wormholes", which may or may not connect injectors and producers (Tremblay *et al.*, 1996, Tremblay *et al.*, 1999). As a result, issues regarding sweep efficiency and good reservoir contact in secondary recovery schemes become paramount to the success of these operations. In many heavy oil reservoirs, the conditions are such that expensive thermal or hydrocarbon solvent processes will likely not be applicable. New solutions for inexpensive secondary recovery techniques are needed to continue production from heavy oil deposits (Selby *et al.*, 1989).

Waterflooding is a common technique for secondary oil recovery in conventional oil reservoirs. When oil and water viscosity are similar, the theory of oil displacement by water is relatively well described (Buckley and Leverett, 1942). In water wet, homogeneous rock, water displaces oil in a stable fashion, and residual oil is trapped due to capillary forces. Recovery from these reservoirs is on the order of around 60 – 70% of the oil in place (Abrams, 1975). In heavy oil systems, the extremely high oil viscosities lead to adverse mobility ratio conditions, thus water will tend to "finger" through the oil,

and recoveries are expected to be extremely low (van Meurs and van der Poel, 1958; Haberman, 1960).

Despite the poor recoveries predicted theoretically, there have been numerous reports of heavy oil waterfloods performed in the literature (Adams, 1982; Smith, 1992; Forth *et al*., 1997; Miller, 2006). All of these studies reported poor sweep efficiencies and overall recovery, however it is significant that in all cases some oil was recovered despite the highly adverse mobility ratios in the waterfloods. Laboratory studies of waterflooding in heavy oil systems also demonstrate that some oil can be recovered by controlled injection of water. Although heavy oil waterflood responses cannot be readily predicted through theory (Adams, 1982), waterfloods have still been carried out in heavy oil reservoirs in Alberta and Saskatchewan for the past 50 years (Kumar *et al*., 2005; Miller, 2007).

Waterflooding is often employed at least initially in many heavy oil reservoirs after primary recovery has been completed. Despite the adverse mobility ratio, water injection is relatively inexpensive, and may be economic despite the low ultimate recoveries predicted (Alikhan *et al*., 1983). Operators also have many years of experience in properly controlling waterfloods. An additional value of waterflooding is that, if more expensive EOR options are being considered for a given field, waterflooding is a low-risk option that can be used to recover some additional oil while more advanced lab and pilot studies are being designed. Moreover, in many marginal heavy oil pools that would not be economic for expensive EOR projects, waterflooding may be the only option for recovering some heavy oil after the conclusion of primary production.

Although heavy oil waterfloods are preformed regularly in western Canada, there is a surprising lack of information regarding the mechanisms by which water can recover viscous oil. This thesis first provides a description of fluids trapping and flow at both a pore scale and macroscopic level, and details the available literature published for heavy oil waterflood systems. Experimental data is then collected (approximately 30 core floods in total) in heavy oil sand packs, both with and without previous primary

production. The data that is produced is used to perform a thorough investigation into the relative significance of viscous and capillary forces in heavy oil systems, and to develop methods for predicting recovery of viscous oil by waterflooding.

CHAPTER 2: RESEARCH PROPOSAL AND OUTLINE

This overall goal of this thesis is to identify and quantify the mechanisms by which heavy oil can be recovered through waterflooding. In order to fulfill this objective, an experimental work plan has been developed that measures the response of heavy oil waterfloods in unconsolidated sand packs at ambient conditions. In each core flood, pressures and produced fluid volumes are monitored in order to obtain information for the development of relative permeability type curves. In addition, *in-situ* saturations may also be measured through the use of Computerized Tomography (CT) scanning and low field nuclear magnetic resonance (NMR) techniques. The waterfloods performed have been designed specifically to vary the contribution of viscous and capillary forces so as to develop an improved understanding of how these systems will respond both at early times (before water breakthrough) and late times (after water breakthrough).

Specifically, this research aims at addressing some of the uncertainties in interpreting heavy oil waterflood responses. The questions to be answered are as follows:

- What is the effect of higher oil viscosities on both breakthrough recovery and total waterflood recovery?
- What is the effect of water injection rate on oil production rates and recovery?
- What is the effect of varying sand permeability on oil production rates and recovery?
- What is the mechanism responsible for continued oil recovery even after water breakthrough occurs and the pressure gradient in the core is low?
- Where is injected water distributed in a heavy oil waterflood, both before and after water breakthrough occurs?
- Do primary heavy oil waterfloods perform similarly to secondary waterfloods (i.e. after primary production)?
- What is the best strategy for waterflooding heavy oil?
- Is it possible to make predictions of recoveries that can be expected for a heavy oil waterflood in a given reservoir?

The following sections describe both the hypothesis behind this research and the outline of the subsequent chapters in the thesis.

2.1 Research Hypothesis

Conventional thought in heavy oil waterflooding states that due to the high oil viscosity, capillary forces are negligible in relation to the magnitude of the viscous forces. This is in direct contrast to light oil waterfloods, where capillary forces govern the fluid trapping and final residual oil saturation. In heavy oil systems, the parameter given the most concern is the mobility ratio, and its effect on viscous fingering and breakthrough recovery (Chouke *et al.*, 1969; Peters and Flock, 1981; Bentsen, 1985). It is a well-known fact that under adverse mobility flow, waterfloods are unstable and the breakthrough recovery will be much lower than in conventional oil.

In heavy oil waterfloods, water breakthrough occurs very early in the life of a waterflood. Subsequent production comes from water cycling, or production of oil/water mixtures at very high water cuts (Miller, 2007). It is surprising that, despite the importance of post-breakthrough oil recovery, this has received very little attention in the literature. Therefore, the major focus of this research is to examine the mechanisms responsible for oil production both before and after breakthrough.

The hypothesis suggested in this work is that at early times, when water is injected into a porous medium containing high viscosity heavy oil, viscous forces dominate as is expected. After water breakthrough, however, further injected water will preferentially pass through low-resistance continuous water channels, and when the pressure gradient in the reservoir is low there will be essentially no viscous driving force for water to displace oil. Therefore, this work proposes that after water breakthrough capillary imbibition of water is the dominant mechanism responsible for oil recovery. The concept is that injected water flows preferentially into the continuous water channels formed during viscous fingering. Once in these channels, however, water also may invade the bypassed regions of the core through imbibition. Due to the presence of poor sweep efficiency and

viscous fingering, this bypassed oil will still be mainly continuous, therefore oil can be slowly displaced out of pores by imbibing water, and the overall recovery from a heavy oil waterflood may be much higher than what is expected based only on the mobility ratio between the water and oil.

The Young-Laplace equation for capillary pressure (Dullien, 1992) does not include any effect of oil viscosity, therefore imbibition will theoretically occur into water wet sands for any fluid viscosity. However, invading water must first displace viscous heavy oil, which is much less mobile than the water. Therefore, imbibition is expected to be a very slow process in heavy oil systems. Under high rate water injection, only a small portion of water will imbibe into the porous medium while most of the water will simply cycle through the continuous water channels. Therefore, the influence of capillary forces will be much less significant in high rate waterflooding. If water is injected at low rates, however, more time is provided for water to imbibe into the bypassed core. While this leads to slow oil production, the overall recovery from waterflooding can theoretically approach similar values as for conventional oil.

2.2 Outline of the Thesis

Chapter 3 of the thesis summarizes the pertinent theory required for properly interpreting a heavy oil waterflood. This chapter begins by describing the forces in single phase and multi-phase flow, and trapping in porous media. The theory describing conventional oil waterflooding and residual oil is then presented. This chapter then outlines the theories of instability number and its influence on breakthrough recovery in heavy oil systems. Finally, concepts of wettability and imbibition are discussed.

Chapters 4 and 5 provide an outline of the experimental work plan followed in this study. Chapter 4 describes the procedure followed for all the core flood and rock/fluid testing, while Chapter 5 summarizes the properties of all core floods performed.

Chapter 6 details the primary production performed in two large sand packs. The depletion data is interpreted to explain the response of both systems to a fixed rate pressure decline. The primary production data obtained are also compared against previous data generated by other authors. The secondary objective of this chapter is to identify the state of the cores at the end of primary production. Specifically, the regions of high gas saturation and the location of the residual oil are identified. This has a direct impact into how subsequent waterfloods will respond in these systems.

Chapter 7 provides the results of the experimental program developed for waterflooding in dead (gas-free) heavy oil systems. The parameters varied in the core floods are the oil viscosity and the water injection rate. By altering these parameters in similar pore systems, the relative magnitude of the viscous forces is varied so that the influence of capillary forces could be inferred. The effect of altering the sand permeability is also examined. This data considers both oil recovery up to breakthrough and the oil recovery after five pore volumes of brine injection.

Chapter 8 summarizes the results similar experiments, but on systems after primary production. Waterfloods are performed on the two cores depleted in Chapter 6, and also on two other cores previously depleted by Goodarzi and Kantzas (2006). While these cores all contain a single heavy oil, the effect of changing the water injection rate is still studied, in order to compare the results against the correlations observed in the dead oil core floods in Chapter 7.

The results of Chapters 7 and 8 provide evidence for the impact of capillary forces and water imbibition on heavy oil waterfloods. Chapter 9 utilizes the results of studies performed in NMR transparent core holders, and the spectra obtained during waterflooding are interpreted to provide quantitative evidence of imbibition at the pore scale. The data presented in this chapter provide empirical evidence of water film thickening and imbibition. Once this evidence has been provided, Chapter 10 quantifies the importance of the water imbibition on flow rates and recovery after breakthrough.

Finally, Chapter 11 provides an analysis of the dead oil waterflooding data, and investigates how to predict the waterflood response in heavy oil systems. Apparent relative permeability curves are calculated, and correlations are presented for predicting oil recovery.

CHAPTER 3: THEORY

Waterflooding of oil reservoirs is a well-recognized technique for oil recovery after primary production. The theory of waterflooding in conventional oil has been developed over many years, thus it is well understood and documented. It is tempting to apply the theoretical and operational knowledge of conventional waterflooding heavy oil reservoirs, with a simple correction for the higher oil viscosity. However, the assumptions made in the conventional waterflood theory are not applicable in heavy oil reservoirs (Miller, 2006). To complicate matters even further, the nature of waterflooding in heavy oil is still relatively unknown due to its complexity. Field results of waterflooding are rare, and only limited laboratories heavy oil waterflooding studies exist that attempt to explain recovery mechanisms. In this chapter, the waterflooding theory of conventional oil and heavy oil is explored to identify the differences in these systems, and to shed light upon possible heavy oil recovery mechanisms.

As proposed in the Chapter 2, imbibition was considered as a possible mechanism aiding in the recovery of heavy oil during waterflood. Thus, it is also important to discuss the wettability of the oil sands and the various characteristics of imbibition that have been reported in the literature. The majority of research concerning imbibition has focused on imbibition of water from fractures to recover oil or gas from rock matrices. Thus, while most of the models developed could not be used directly to describe the imbibition phenomenon that occurs while water is flowing in heavy oil reservoirs, they still provide a starting point for understanding imbibition in these complex systems.

3.1 Flow in Porous Media

Fluid flow in porous media at a microscopic scale is a very important parameter in determining the success of the recovery of oil. Single-phase flow is well described by Darcy's Law. However, the introduction of another fluid into the porous medium adds more complexity to the flow process and its description. When two immiscible fluids are present in a core, under equilibrium there exists a capillary interface between the phases.

This interface must be considered as it plays an important role in recovery and trapping of oil. Under flowing conditions, the immiscible fluids can theoretically represented by relative permeability concepts. However, when heavy oil is flowing with water, the relative permeability measured might not be representative of actual pore level events.

3.1.1 Single Phase Flow

The flow of a fluid through a porous medium can be described by Darcy's Law. In 1856 Darcy published the results from his study of downward flow of water through filter sands. He observed that when water flows vertically downward through a column of sand, the volume of water passing through the sand per unit time is (King Hubbert, 1956):

$$q = -K \frac{(h_2 - h_1)}{l}$$ Eqn (3.1)

Where q = volume of water flowing across a unit area in unit time

h_1, h_2 = heights above a certain reference level of water

l = thickness of sand

K = factor of proportionality.

It must be noted that this equation was derived empirically based solely on Darcy's observations. This is known as Darcy's Law and is widely used in the oil and gas industry as one of the most important fundamental equations. At the point of inception, K was not known as "permeability", but rather a constant that is a property of the sandpack. Its general application in porous media has been modified and expressed as (Dullien, 1992):

$$\frac{Q}{A} = -\frac{k}{\mu} \frac{\Delta \Phi}{L}$$ Eqn (3.2)

With the change in piezometric pressure given by the symbol $\Phi = {}^P\!\!\diagup\!\!_{\rho g} + z$

Where Q = volumetric flow rate

     A = cross-section area open to flow

     k = permeability of the porous medium

     μ = viscosity of the fluid

     L = length of sandpack

     ΔΦ = the change in piezometric pressure

     ρ = density of fluid

     g = acceleration due to gravity

     z = height measured from the datum level.

The parameters used in the measurement of Darcy's Law are illustrated in Figure 3.1.
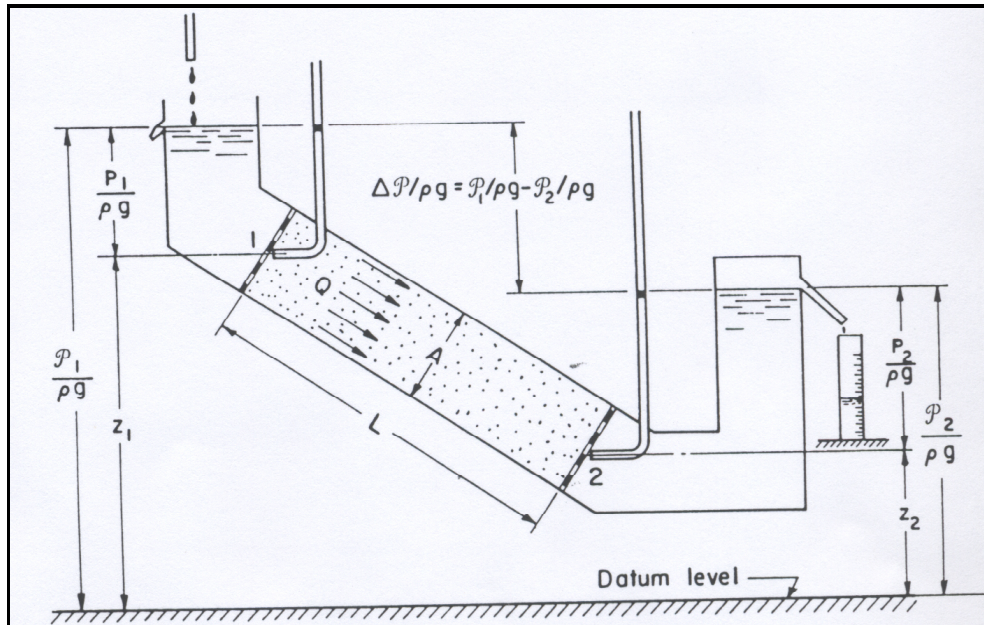
Figure 3.1: Single phase flow through porous media
(from Dullien, 1992)

Darcy's Law was derived for uni-directional, steady flow at relatively slow rates. In fact, Darcy's Law fails when inertial forces become significant (King Hubbert, 1956). This is often incorrectly attributed to the presence of turbulent flow. Turbulence occurs when the inertial forces become predominant over the resistive forces, and its presence corresponds to higher values of Reynolds number, which is defined as:

$$Re = Dv\rho / \mu \qquad\qquad\qquad\qquad \text{Eqn (3.3)}$$

Where D is the average diameter of the grain and v is the injected velocity.

At higher velocity flow ranges the relationship between flow rate and pressure gradient begins becomes non-linear. The transition is gradual, however different values of the critical Re representing the transition point have been cited in the literature. In general, turbulence in a pipe is expected when Re = 2,300 (Boyle, 1986). King Hubbert (1956) states that for Re values greater than one, Darcy's Law is no longer valid. Macdonald *et al*. (1979) state that the deviation from Darcy's Law occurs for the range of Re/(1-ϕ) of 1 – 10, where ϕ is the rock porosity. For an average oil sand porosity of around 36%, this corresponds to deviation from Darcy's law when Re $\approx$ 1.5 – 15. Therefore, it can be concluded that in porous media even when flow is still far below the rates expected for turbulence, inertial forces can still become significant and Darcy's Law will no longer be valid. In the range of flow rates expected in flow in oil reservoirs, however, Darcy's Law is expected to be valid except for situations like high rate flow of gases near well bores.

Throughout the years, many people have attempted to give Darcy's Law, which was derived empirically, a more general physical formulation. From direct derivation of the Navier-Stokes equation, King Hubbert (1956) had found an expression for flow that is similar to Darcy's Law. He also had found that this law is only valid when the flow is slow, such that the inertial forces are negligible compared to the forces arising from velocity. This validation of Darcy's Law was extremely important since it provided a

fundamental basis to this expression, which is easily the most recognized equation in reservoir engineering.

3.1.2 Capillary Pressure

The next level of complexity from single-phase fluid flow is that of two immiscible fluids in static equilibrium. When static immiscible fluids are in contact with each other, they are separated by a thin layer known as the interface. The surface energy related to this fluid interface controls the saturations, distributions, and displacement of the phases in porous media (Green and Willhite, 1998). An example of a liquid in contact with air or its own vapor is shown in Figure 3.2.
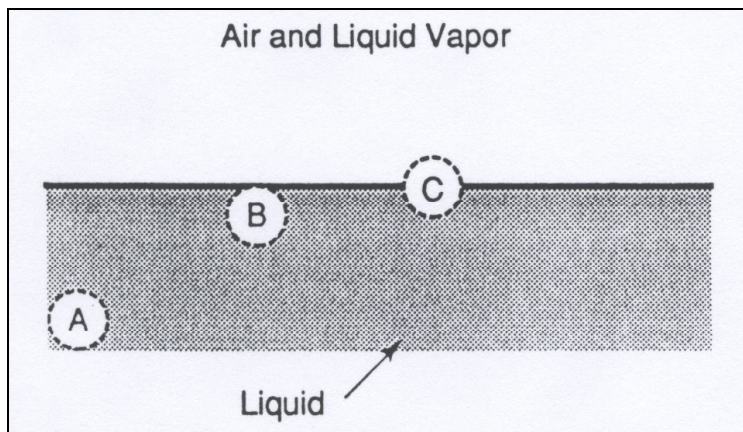
Figure 3.2: Different molecular positions in a liquid-gas interface
(from Green and Willhite, 1998)

A, B and C are molecules of the liquid phase. Molecules that are well below the surface (A) are attracted equally in all directions due to cohesive forces, while molecules B and C close to the interface are attracted unequally with a net downward force that tries to pull these molecules back into the liquid phase. Thus, the surface acts like a stretched membrane, and tends to minimize its area as much as possible (Green and Willhite, 1998). Surface tension is the force acting on the surface for a unit length of the surface.

The term surface tension is used in the situation where a liquid is in contact with its vapor or with air. When there is an interface between two immiscible liquids, or between a liquid and a solid, the term interfacial tension is used. In the situation where waterflooding is employed as a recovery mechanism, the interfacial tension between oil and water is an important parameter. However, in heavy oil systems it is not trivial to determine the interfacial tension between oil and water. This will be further discussed in Chapter 4.

Fluid distributions in porous media are not only controlled by the interfacial tension but also by the wettability of the rock. Wettability is defined as a tendency of a fluid to spread or adhere to a solid surface in the presence of a second immiscible fluid (Anderson, 1986a). A more thorough discussion on wettability will be presented later; in this section only simple definitions will be discussed.

When two immiscible phases are placed in contact with a solid surface, due to the wetting preference of the solid, one phase is generally attracted more strongly to the solid than the other. The phase is called the wetting phase, while the other fluid is termed the non-wetting phase. A schematic of oil wet and water wet systems is shown in Figure 3.3.
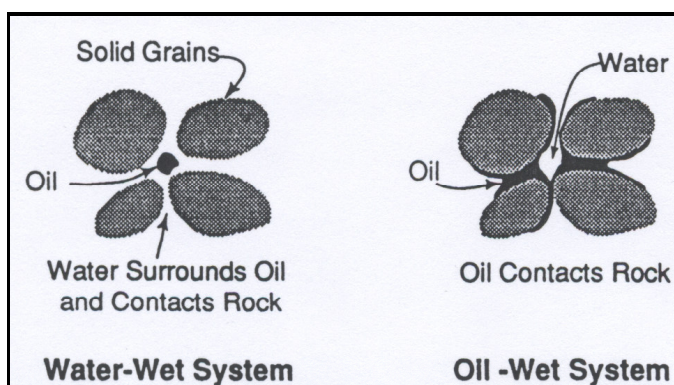
Figure 3.3: Schematic distribution of oil and water in systems of varying wettability (from Green and Willhite, 1998)

This figure shows that in a preferentially water-wet reservoir, water spreads to cover the sand grains, thus oil will occupy the middle of the pores. In contrast, in the oil wet system, the opposite will occur. Therefore in addition to interfacial tension, fluids distribution and flow pathways are also controlled by the rock wettability.

Wettability is a measure of the adhesion forces between the two different fluids and the rock surface. Although these forces cannot be measured directly, wettability can be quantified by examining the interfacial forces. Figure 3.4 shows the forces acting on a water droplet on a solid surface in a continuous oil phase.
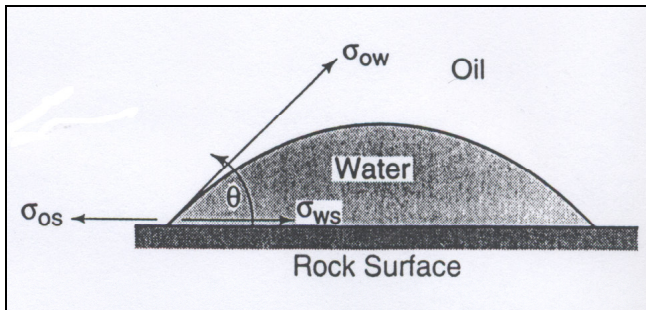
Figure 3.4: Schematic of a droplet on water surrounded by oil on a water-wet rock (from Green and Willhite, 1998)

A force balance on this droplet yields:

$$\sigma_{os} - \sigma_{ws} = \sigma_{ow} \cos \theta \qquad \qquad \text{Eqn (3.4)}$$

Where σ_{os} = interfacial tension between solid and oil

$\quad \sigma_{ws}$ = interfacial tension between water and solid

$\quad \sigma_{ow}$ = interfacial tension between oil and water

$\quad \theta$ = contact angle (measured through the water phase).

Only the interfacial tension between oil and water can be evaluated through laboratory methods, however by also measuring the contact angle the rock wettability can be

directly determined. The solid is water wet for $\theta < 90°$ and is oil wet for $\theta > 90°$. A system is strongly water wet if θ is close to $0°$, while it is strongly oil wet if θ approaches $180°$. Most reservoirs are not strongly wetted by either fluid, and contact angles will also be non-trivial to measure in actual porous media where the rock interface is not flat (Rosen, 1989).   However, it should be understood that regardless of whether wettability can be measured easily, there does exist a wetting preference for the rock that will lead to fluids re-distributing in porous media.

The presence of two immiscible fluids in the same porous medium induces a pressure difference across the fluid interface. This is called capillary pressure. An illustration of the capillary pressure in a tube of constant diameter is shown in Figure 3.5.
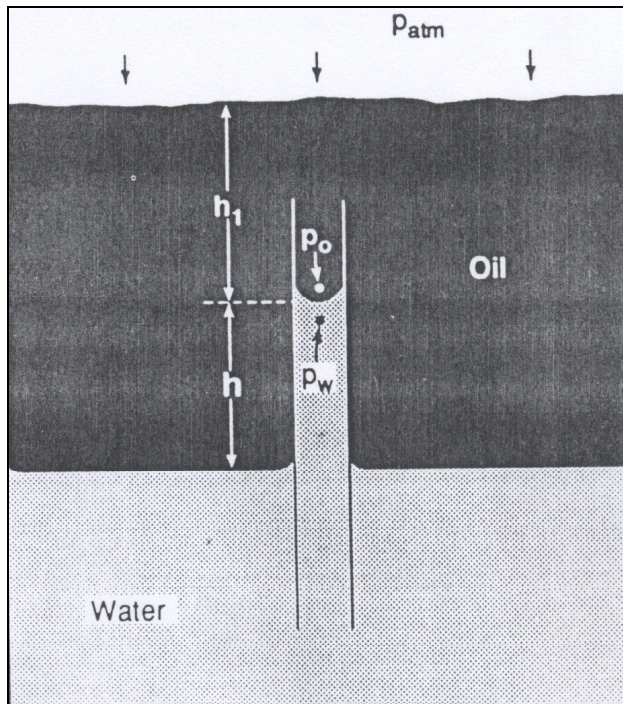
Figure 3.5: Schematic of capillary pressure of oil and water in a water wet capillary tube (from Green and Willhite, 1998)

From the force balance of the fluids in this tube, an expression for capillary pressure (P_c) could be found. This is known as the Young-Laplace equation.

$$P_c = \frac{2\sigma_{ow}\cos\theta}{r}$$
Eqn (3.5)

Where r is the radius of the capillary tube and θ is the angle between the water interface and the wall of the tube.

The description of the capillary action in a tube is an ideal situation, which cannot be used to describe the true phenomenon in a pore. Leverett (1941) developed a more appropriate equation for a wetting fluid occupying a pendular ring structure at the point where two unconsolidated solid spheres join:

$$P_c = \sigma\left(\frac{1}{R_1} + \frac{1}{R_2}\right)$$
Eqn (3.6)

The radii R_1 and R_2 in Eqn (3.6) are defined in the schematic shown in Figure 3.6.
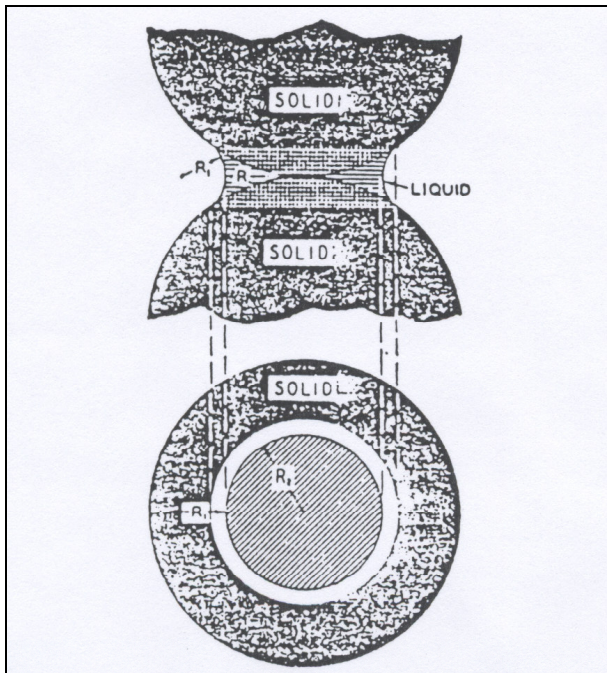
Figure 3.6: Principal radii governing capillary pressure at the joining of two solids (from Leverett, 1941)

This equation was developed to describe the condition where water exists in the crevices between the sand grains.

The discussion on capillary pressure has so far been restricted to the scale of a single pore. In porous media where the pore structure is a complex network of various pore sizes, these simple models cannot adequately describe the full effect of capillary pressure. Capillary pressure depends on many factors such as wettability, interfacial tension, pore geometry, surface roughness and the rock saturation history.

When a non-wetting fluid is displacing a wetting fluid, the process is called drainage. The reverse process, where the wetting fluid is displacing the non-wetting fluid, is called imbibition. In general, an understanding of capillary pressure and how it relates to recovery in a given reservoir is obtained by measuring the capillary pressure over the complete range of saturations. An example of a capillary curve for water is shown in Figure 3.7. In this figure, S_{wi} is the initial water saturation and S_{or} is the residual oil saturation.
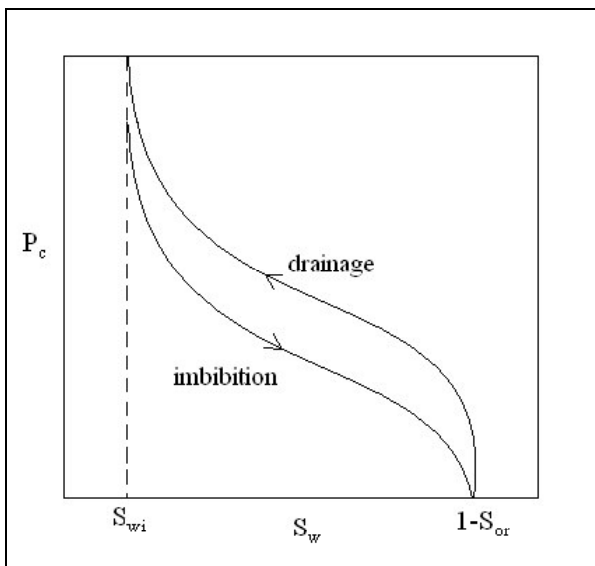
Figure 3.7: Example of a capillary pressure curve showing drainage and imbibition

For reservoir studies and applications, water/oil capillary pressure data are required for waterflooding. However, this data is difficult to measure, thus it is rarely obtained. Air/water and air/oil capillary pressure data are generally more commonly obtained (Takamura and Isaacs, 1989). The data is then often simply extrapolated to oil/water systems by applying a different interfacial tension for the same pore size distribution in the rock. However, this approach neglects differences in rock wettability in oil/water versus air/water systems, and the capillary pressures predicted may not be correct.

There are two common methods of determining the water-oil capillary pressure curves: porous plate and centrifuge. In the porous plate method, a water-saturated sample is placed in oil. The pressure of the oil is increased in steps, thus forcing oil into the core (drainage). When equilibrium is reached at any pressure the produced water volume is collected. This process is very slow, and in some cases, a full curve may require up to 40 days (Anderson, 1986b). In the centrifuge method, the same concept is applied, however, in this case due to the application of high centrifugal forces the capillary pressure curve can be obtained much more quickly. The sample is centrifuged at various speeds, which can be converted into non-wetting phase pressure, and the produced wetting phase at each speed is also collected. One other method for measuring capillary pressure is mercury injection, which is applied in mercury/air systems. Mercury has high surface tension and is perfectly non-wetting (i.e. its contact angle is 180°). This method is capable of measuring a pore size distribution in a short period of time, but mercury poses health risks and is also not a native reservoir fluid so once again extrapolating this information to oil/water systems assumes that a different wettability will not strongly affect the capillary pressure curve.

The various methods of measuring capillary pressure are normally performed at ambient conditions. When it is required to perform them at reservoir temperature and pressure, methods such as the centrifuge or porous plate may no longer be possible. For heavy oil and unconsolidated sand, measurements are even more difficult since the oil does not

flow easily, and the pore size distribution of the sand is a function of the overburden pressure applied. This will be discussed further in Chapter 4.

3.1.3 Multiphase Flow

When there is more than one immiscible fluid flowing through the porous medium, the fluids interfere with one another and their overall flow is described by relative permeability. Relative permeability is a measure of the ability of a porous medium to conduct flow of a given fluid in the presence of other immiscible fluids (Maini *et al*., 1990). Obviously multiphase flow in porous media is a complicated process that depends on many different factors. Relative permeability is a function of fluid distributions, which are affected by both the pore structure and pore size distribution. Relative permeability is also governed by the rock wettability, saturation history, interfacial tension, viscosity ratios, density ratios and fluid flow velocities. Due to the complex nature of the porous medium, it is not possible to simulate the combination of all these effects, thus it is necessary to measure the relative permeability experimentally. Unfortunately, these measurements are not necessarily easy to perform accurately in all systems.

Relative permeability is measured from laboratory core floods in steady state or unsteady state experiments. In order to derive the relative permeabilities from laboratory results, either explicit or implicit methods of fitting the data can be used. It must be emphasized that the development of these methods was based on analysis of conventional oils, thus their applications in heavy oil may not be correct since the required assumptions are not met in heavy oil systems.

3.1.3.1 Steady State and Unsteady State Method

Laboratory data for the purpose of relative permeability extraction can be obtained by either the steady state or unsteady state method. However, since the steady state method requires a long period of time to yield a complete relative permeability

curve, the unsteady state approach is generally more favorable (Sarma *et al.*, 1990). However, even this method is only applicable when the displacement itself is stable.

In the steady state method, two fluids are injected simultaneously at a fixed ratio of known flow rates. Steady state is achieved when the inflows equal the outflows and the pressure drop across the sample is constant. This process is very time consuming; it may require anywhere from 2 – 40 hours or even longer for a given flow rate, depending on the sample permeability and oil viscosity (Dullien, 1992). The ratio of oil and water flow rates is varied over a wide range in order to obtain saturation-dependent pressure information. The data collected in the steady state method is the pressure gradient for the oil and water injection, the fluid flow rates and the assumed saturations obtained from the ratio of the fluid injection rates.

The relative permeability for each fluid (i) would be calculated by using the following equation:

$$q_i = \left(\frac{k_{ri} kA}{\mu_i} \right) \left(\frac{\Delta P_i}{L} \right) \qquad\qquad \text{Eqn (3.7)}$$

Where k_{ri} is the relative permeability of phase "i". The injection pressure (ΔP_i) of each fluid is monitored by using pressure transducers at the inlet to the core. Aside from being time consuming, there is some question of whether data collected using the steady state method is representative of how oil and water will flow during an actual waterflood.

The unsteady state method is also known as the external drive method. In this configuration, one fluid is injected (such as water) to displace the other fluid (such as oil). The displacement is generally assumed to be linear and homogeneous with length. The relative permeability is calculated from the produced fluids and the total pressure drop measured across the core, as opposed to individual oil and water pressures. The relative permeability calculations are more complex compared to those performed in the steady

state method, since now the difference between the oil and water pressure cannot be measured directly. Nevertheless, the unsteady state method is considerably faster to perform experimentally than the steady state. There are various limitations to this method as well. The pressure differential has to be significant to eliminate the outlet end effects, and the experimental conditions need to be carefully selected to yield a range of saturations for the development of the relative permeability curves. Additionally, if the displacement is not linear or homogeneous with length, the validity of the results becomes questionable.

Along with Sarma and Bentsen (1987), many researchers have investigated whether the steady state and unsteady state methods yield the same values for relative permeability. It is generally accepted that unsteady state will often yield essentially the same results as steady state methods (Dullien, 1992). However, there have also been numerous cases where researchers have seen otherwise, especially when heavy oil is used (Maini, 1998).

3.1.3.2 Implicit vs. Explicit Methods in Conventional Oils

Using the recorded core flooding data (flow rates and differential pressure) obtained in an unsteady state experiment, implicit and explicit methods are then used to determine the relative permeability curves. Before this can be done, it first must be ensured that the waterflood was performed under stable displacement conditions. The stability condition has been developed by Rapoport and Leas (1953). For small values of the scaling coefficient ($Lv\mu_w$), which has units of cm²/min·cP, the flooding behavior is influenced by capillary end effects. The flood will therefore be dependent upon injection rate, the length of the core and the fluid viscosities. Rapoport and Leas (1953) showed that when the scaling coefficient is less than 1, breakthrough recovery is a function of the scaling coefficient and the data collected is not representative of true relative permeability. When the scaling coefficient is greater than 1 the breakthrough recovery does not change with changing fluid viscosity or injection rate, thus this is the point of stabilized flow where capillary end effects do not influence the behavior of the

waterflood. At this condition, the core flood data collected can be used to infer the relative permeability of the core as a function of water saturation.

The implicit method of determining relative permeability involves using a reservoir simulator to obtain the relative permeability curves through history matching. The main advantage of the implicit method is that the effects of capillary pressure can be included in the simulator. This method generally used a parametric form of the relative permeability curve (Maini, 1998). The simplest form of the implicit method is in the following exponential form:

$$k_{rw} = k_{wor} \left(S_e\right)^{\varepsilon_w} \qquad\qquad \text{Eqn (3.8)}$$

$$k_{ro} = k_{oiw} \left(1 - S_e\right)^{\varepsilon_o} \qquad\qquad \text{Eqn (3.9)}$$

with,

$$S_e = \frac{S_w - S_{w,min}}{(1 - S_{or}) - S_{wc}} \qquad\qquad \text{Eqn (3.10)}$$

Where k_{wor} = the relative permeability to water at S_{or}

k_{oiw} = the relative permeability to oil at S_{wi}

ε_w and ε_o = exponents that are adjustable

S_{wc} = connate water saturation.

The modeling errors inherent in the implicit method can be reduced by using more sophisticated mathematical models, such as those developed by Sigmund and McCaffery (1979).

The explicit approach is much simpler. The most common explicit methods are those developed by Johnson-Bossler-Naumann (JBN) and Jones-Roszelle. These methods are

discussed in great details by Johnson *et al*. (1959) and Jones and Roszelle (1978). These are analytical methods that can be used to calculate relative permeability for the production points measured.

The Jones-Roszelle method is actually an extension of the JBN method. The distinction is that Jones and Roszelle (1978) observed that the JBN method could cause significant error in the evaluation of the derivatives, so as an improvement they proposed the use of graphical techniques to eliminate the use of numerical derivatives. Essentially, this method uses the same equations and assumptions to obtain the relative permeabilities. The Jones-Roszelle method also ignores gravity effects and capillary pressures while using the same equations proposed by Welge and JBN. Another minor difference is that Jones and Roszelle expressed k_{ro} and k_{rw} as relative to absolute permeability whereas JBN's relative permeabilities are relative to the pre-waterflood condition (oil flowing at S_{wi}).

It must be noted that although the explicit methods are simple to perform, any inaccuracies in the measured data are amplified through the numerical or even graphical differentiation. Therefore, there might be extensive scattering in the relative permeability curves calculated. It was observed by various researchers (Batycky *et al*., 1981; Tao and Watson, 1984a, 1984b; Kerig and Watson, 1986; Sarma *et al*., 1990) that the inaccuracies in the data measurement become amplified by the process of differentiation. Tao and Watson (1984) found that the errors from differentiation of data can be significant. Despite these issues, analytical explicit methods of calculating relative permeability are valuable because they allow for a fast visual comparison of the behaviour of different systems.

3.1.3.3 Relative Permeability Determination for Heavy Oil Systems

The fact that the simultaneous flow of heavy oil and water in porous media is not well understood adds more uncertainty to an already complicated problem. Maini (1998) has pointed out that the multiphase flow model obtained from conventional oil does not

adequately describe heavy oil systems, where issues of viscous fingering and bypassing of oil lead to poor sweep efficiency and water not contacting the complete area of the core. However, numerical simulation and reservoir studies often require relative permeability information, thus it is usually still necessary to obtain this information.

The first difficulty in measuring relative permeability in heavy oil systems lies in the fact that most heavy oil reservoirs are unconsolidated sand, which could not be preserved during the coring process. As a result, the core pore structures and permeability may have been altered before samples can be measured in the laboratory. In addition, some heavy oil reservoirs also show variations in oil composition and viscosity with depth (Maini, 1998; Larter *et al*., 2006; Bryan *et al*., 2007). This means that not only may permeability vary in the reservoir, but that the oil viscosity may also not be constant. There have been reports of slippage in flowing heavy oil systems (Dullien, 1992), which leads to apparent oil relative permeability values that are abnormally high. Finally, due to the adverse mobility ratio, a significant number of pore volumes of fluid injection are required to reach the true value of S_{or}, so most laboratory core floods only cover a limited range of water saturation.

The steady state method of measuring relative permeability is rarely performed with heavy oil due to experimental difficulties (Maini, 1998). Similar to conventional oil the most popular method is external drive (i.e. waterflooding) at high flow rates. However, at high flow rates the effect of viscous forces is high as well, which leads to severe viscous fingering. This has lead many researchers (Maini, 1998; Wang *et al*., 2006) to observe that in heavy oils relative permeability is a function of flow rate. Due to many experimental difficulties associated with getting accurate data, Maini (1998) proposed the use of pseudo-relative permeability curves as opposed to the true relative permeability, which could only be obtained from steady state results.

The criterion of stable flow for unsteady state measurements has also led to other difficulties in heavy oil systems. The Rapoport and Leas (1953) criterion of stability is

not applicable for heavy oil, because in order to have stable flow water must be injected at extremely slow rates to limit viscous fingering. At these rates, Rapoport and Leas (1953) report that capillary end effects may be present and will lead to incorrect breakthrough recoveries. Therefore it is impossible to satisfy the stability criterion for heavy oil systems.

Once core flood data has been generated, the implicit method could be used to extrapolate relative permeability curves. However, there are several problems when using the implicit method in heavy oil systems. Normally the capillary pressure curve for the rock/fluid system used in the relative permeability test was not measured. Also, the true value of residual oil saturation may never be obtained from the experiment since it is unlikely that at low injection rates, sufficient pore volumes of fluid will be injected. The use of the explicit method for heavy oil does not pose any extra difficulties; it is subjected to the same problems as conventional oil. However, it still may not be possible to construct a full relative permeability curve with water saturation ranging from S_{wi} to S_{or} due to the fact that an exceedingly large number of pore volumes of water must be injected before S_{or} is reached.

Despite the difficulties facing the determination of relative permeability information for heavy oil systems, this information should still be collected. Even if the quality of the data is suspect, it can still be used to provide an approximation for describing the flow of heavy oil and water in the porous medium during waterflooding.

3.2 Waterflooding of Conventional Oil Reservoirs

Waterflooding is by far the most common method of fluid injection in conventional oil reservoirs (Craig, 1971). This is due to the fact that water is readily available, and can provide a cost effective method to recover oil after primary depletion. In addition, owing to its low viscosity, water can be injected with relative ease. Water has also proven to be quite efficient in displacing conventional oil (Craig, 1971).

The recovery of oil via water injection is well described and documented. For waterflooding of conventional oil, its performance can be evaluated by various analytical methods. The efficiency of oil displacement by water is well represented by the Frontal Advance Theory, which was developed by Leverett (1941). In the literature, one can find abundant sources that provide correlations to predict breakthrough and post-breakthrough recovery both at microscopic and macroscopic scales. Throughout the years, many researchers have amassed a large data bank that shows a correlation between S_{or} and a dimensionless number known as capillary number (N_{ca}). The capillary number is also generally used to provide a guideline for improving oil recovery after waterflooding. Empirical relationships have also been observed for field waterfloods, where other concerns such as areal sweep efficiency will also affect the overall oil recovered.

3.2.1 Frontal Advance Theory

Leverett (1941) started with Darcy's law for both oil and water to obtain an expression for fractional flow of water:

$$f_w = \frac{1 + \dfrac{kk_{ro}}{\upsilon_t \mu_o}\left(\dfrac{\partial P_c}{\partial L} - g\Delta\rho\sin\alpha_d\right)}{1 + \dfrac{\mu_w}{\mu_o}\dfrac{kk_{ro}}{kk_{rw}}} \qquad\qquad \text{Eqn (3.11)}$$

Where f_w = fraction of water in the flowing stream (as a fraction of total flow rate)

υ_t = total fluid velocity

$\Delta\rho$ = water-oil density difference

α = angle of the formation dip to the horizontal plane.

It must be noted that with all the proper conditions met for waterflooding in conventional oil, the fractional flow of water is a function of water saturation only. This is due to the fact that relative permeability and capillary pressure are both functions of saturation alone. The capillary pressure gradient can be written as:

$$\frac{\partial P_c}{\partial L} = \frac{\partial P_c}{\partial S_w} \frac{\partial S_w}{\partial L}$$ Eqn (3.12)

$\dfrac{\partial S_w}{\partial L}$ is not available, thus $\dfrac{\partial P_c}{\partial L}$ is difficult to obtain directly. However, the assumption that is commonly made is that at steady state, the same pressure gradient exists in both the oil and water channels. Therefore, P_c is constant for any water saturation, and $\dfrac{\partial P_c}{\partial L} = 0$.

By neglecting $\dfrac{\partial P_c}{\partial L}$ Eqn (3.11) becomes:

$$f_w = \frac{1 - \dfrac{kk_{ro}}{\upsilon_t \mu_o}(g\Delta\rho\sin\alpha_d)}{1 + \dfrac{\mu_w}{\mu_o}\dfrac{kk_{ro}}{kk_{rw}}}$$ Eqn (3.13)

When injecting in a horizontal system $\sin\alpha_d = 0$, thus Eqn (3.13) simplifies again:

$$f_w = \frac{1}{1 + \dfrac{\mu_w}{\mu_o}\dfrac{kk_{ro}}{kk_{rw}}}$$ Eqn (3.14)

In 1942, Buckley and Leverett presented the frontal drive equation as a direct function of the fractional flow of water:

$$\left(\frac{\partial L}{\partial t}\right)_{S_w} = \frac{Q_t}{A\phi}\left(\frac{\partial f_w}{\partial S_w}\right)_t$$ Eqn (3.15)

The parameter "L" in Eqn (3.15) is the length of the water-front in the system.

This equation was obtained based on the mass balance of fluids entering, leaving and accumulating in a small element of the porous medium. The assumptions made behind this equation are that there is no mass transfer between the phases and that the phases are incompressible.

By integrating Eqn (3.15), the expression for L becomes:

$$L = \frac{W_i}{A\phi}\left(\frac{df_w}{dS_w}\right)$$ Eqn (3.16)

Where W_i is the pore volumes of water injected.

This equation can be used to calculate the location of the water-front, or the average water saturation distribution during the flood.

Despite the fact that Eqn (3.16) is very useful, many researchers have been hesitant to use it due to the fact that Eqn (3.15) implies that two saturations would have the same velocity (Craig, 1971). Buckley and Leverett (1942) have noted that the relationship between S_w and L actually contains multiple solutions consisting of real and imaginary number components. In Figure 3.8 the "real" component is the solid line, whereas the "imaginary" component is shown as the dashed line. The position of L_1 is chosen such that the shaded areas are equaled.
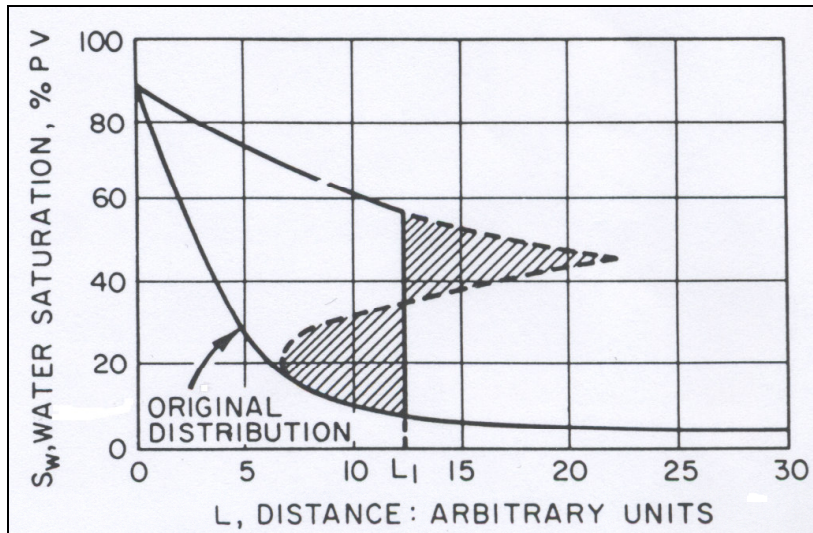
Figure 3.8: Buckley-Leverett solution for water saturation vs. length
(from Craig, 1971)

In 1952, Welge showed that a tangent to the fractional flow curve is equivalent to the balancing of areas, as suggested by Buckley and Leverett (1942) as a solution to the saturation discontinuity. Welge (1952) also showed that:

$$Q_i = \frac{1}{\left(\dfrac{df_w}{dS_w}\right)_{S_{w2}}}$$
Eqn (3.17)

Where Q_i is the pore volumes of water injected. This equation provides a relationship between the cumulative water volume injected and the water cut in the production end after water has broken through. With these equations, graphical or numerical solutions are straightforward to obtain in conventional oil waterfloods.

It must be emphasized that Buckley-Leverett frontal advance theory assumes that water displaces oil as a straight interface (Craig, 1971) as shown in Figure 3.8. This is only true in the cases where the fluid viscosities are similar. However, this method still provides a simple analytical way of predicting the behavior of waterflooding of conventional oil.

3.2.2 Breakthrough Recovery

From the Frontal Advance Theory, the recovery at breakthrough can be predicted. When L is equal to the length of the core:

$$L = \frac{W_i}{A\phi}\left(\frac{df_w}{dS_w}\right)_f \qquad \text{Eqn (3.18)}$$

In this expression, the subscript "f" denotes the condition at the flood front at breakthrough (i.e. when the flood front reaches L), and the total oil recovered is equal to W_i, since until breakthrough the volume of water injected is the same as the oil volume produced.

The average water saturation in the core at breakthrough is then:

$$\overline{S}_{wbt} = S_{wc} + \frac{W_i}{A\phi L} \qquad \text{Eqn (3.19)}$$

Combining Eqn (3.18) and Eqn (3.19) yields:

$$\overline{S}_{wbt} - S_{wc} = \frac{1}{\left(\dfrac{df_w}{dS_w}\right)_f} = \frac{S_{wf} - S_{wc}}{f_{wf}} \qquad \text{Eqn (3.20)}$$

This implies that from the tangent of the fractional curve, the point of intersection gives the water saturation at the front.

The Frontal Advance Theory can only be used if relative permeabilities are known. In cases where relative permeability information is not available, breakthrough recovery can be alternatively predicted using the general trend established with a dimensionless number known as the capillary number. Moore and Slobod (1956) were the first to show

that the oil saturation existing in Berea sandstone outcrops at breakthrough could be related to $\nu\mu/\sigma\cos\theta$, as shown in Figure 3.9.
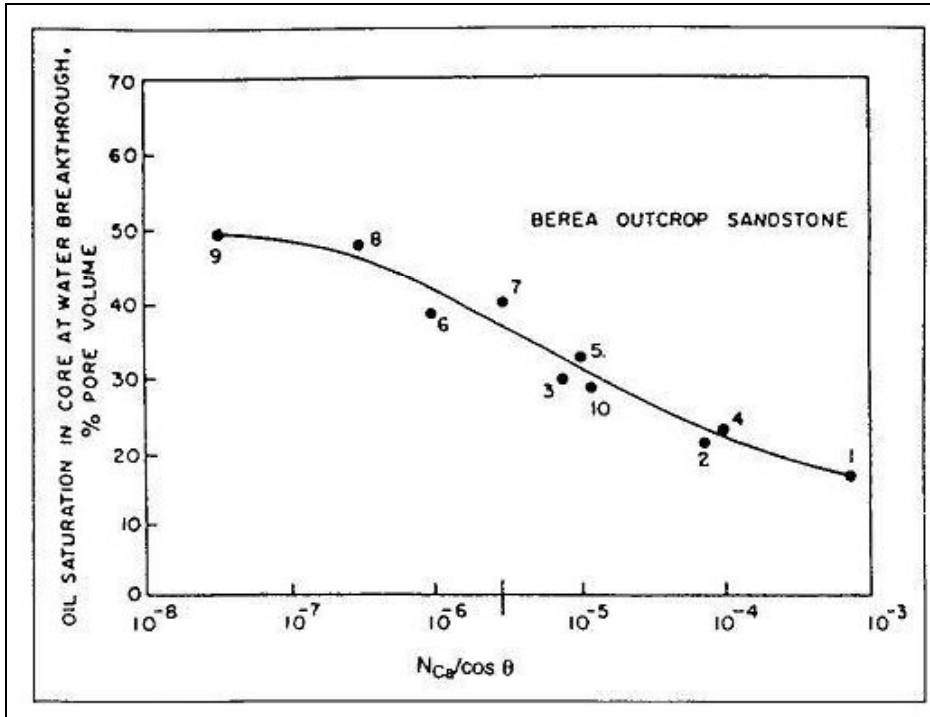
Figure 3.9: S_{or} at breakthrough vs. $\nu\mu/\sigma\cos\theta$

(from Moore and Slobod, 1956)

In a broader generalization, Abrams (1975) provided data for waterflooding recovery for both sandstones and limestone. Abrams (1975) plotted S_{or} at breakthrough against the dimensionless number obtained earlier by Moore and Slobod (1956). In an attempt to eliminate the scattering and to better describe the ratio of viscous to capillary forces, Abrams included oil viscosity, relative permeability effects, and the influence of pore structure on capillary displacement and trapping process. However, he found that with the exception of oil viscosity, the correlation predictions were not improved significantly by the addition of these extra variables to the dimensionless group. Upon close inspection of the results, Abrams (1975) observed that S_{or} obtained for low viscosity ratios of water to oil is lower than those of high viscosity ratios, even though the dimensionless group yielded the same value. To correct for this, he then modified the

dimensionless group to include the viscosity ratio term in this format: $\dfrac{\nu\mu_w}{\sigma}\left(\dfrac{\mu_w}{\mu_o}\right)^n$.

Various values of n were tried, and the best fit of the results for Abram's data was obtained when n = 0.4, as shown in Figure 3.10.
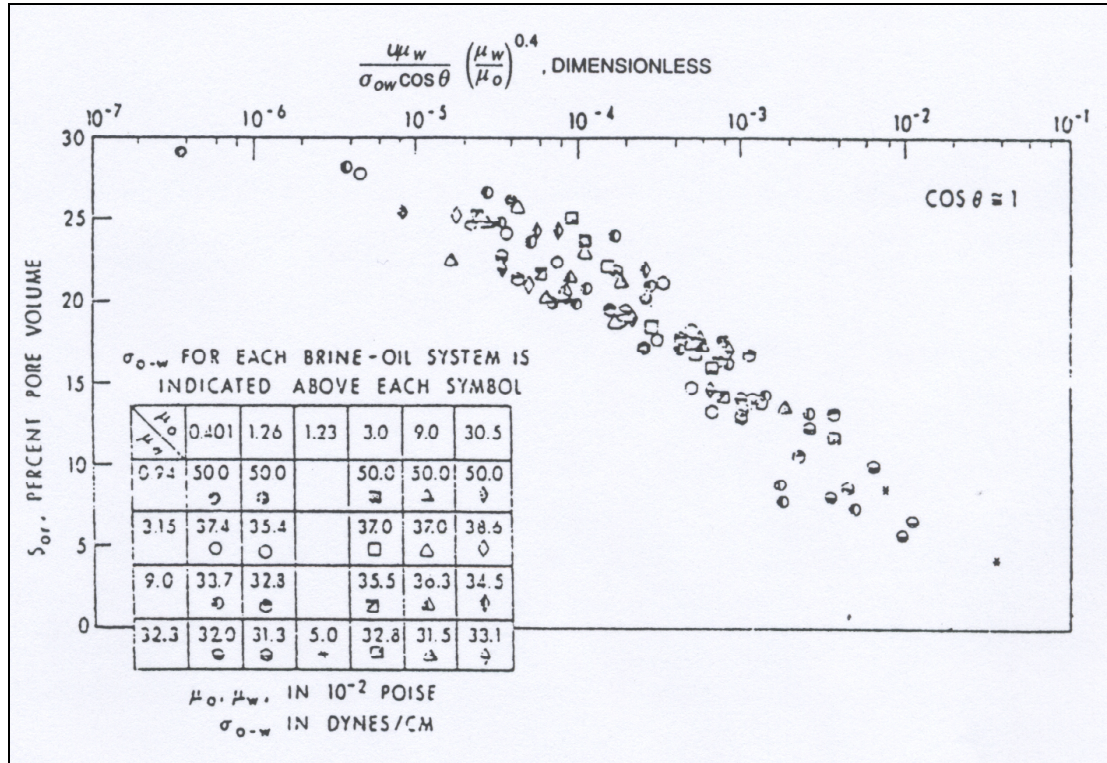
Figure 3.10: Dimensionless number to predict Sor in systems of varying oil viscosity (from Abrams, 1975)

It must be noted that the highest oil viscosity employed by Abrams was only 30.5 mPa·s (cP), thus for actual heavy oil like what is found in the oil sands of Canada or Venezuela, the value of the exponent might be different.

The different models for predicting breakthrough recovery presented up to this point concerns one-dimensional flow, such as what is found in core flooding. However, in field applications flow is often three-dimensional, where injectors and producers are subjected to various patterns. Throughout the literature, various correlations have been

developed to predict the areal sweep efficiency at breakthrough for different well patterns. Areal sweep efficiency is the macroscopic recovery of the flood. E_{Abt}, the areal sweep efficiency at breakthrough, is the ratio of the area contacted by water at breakthrough to the total pattern area. Various pattern areas are shown in Figure 3.11.
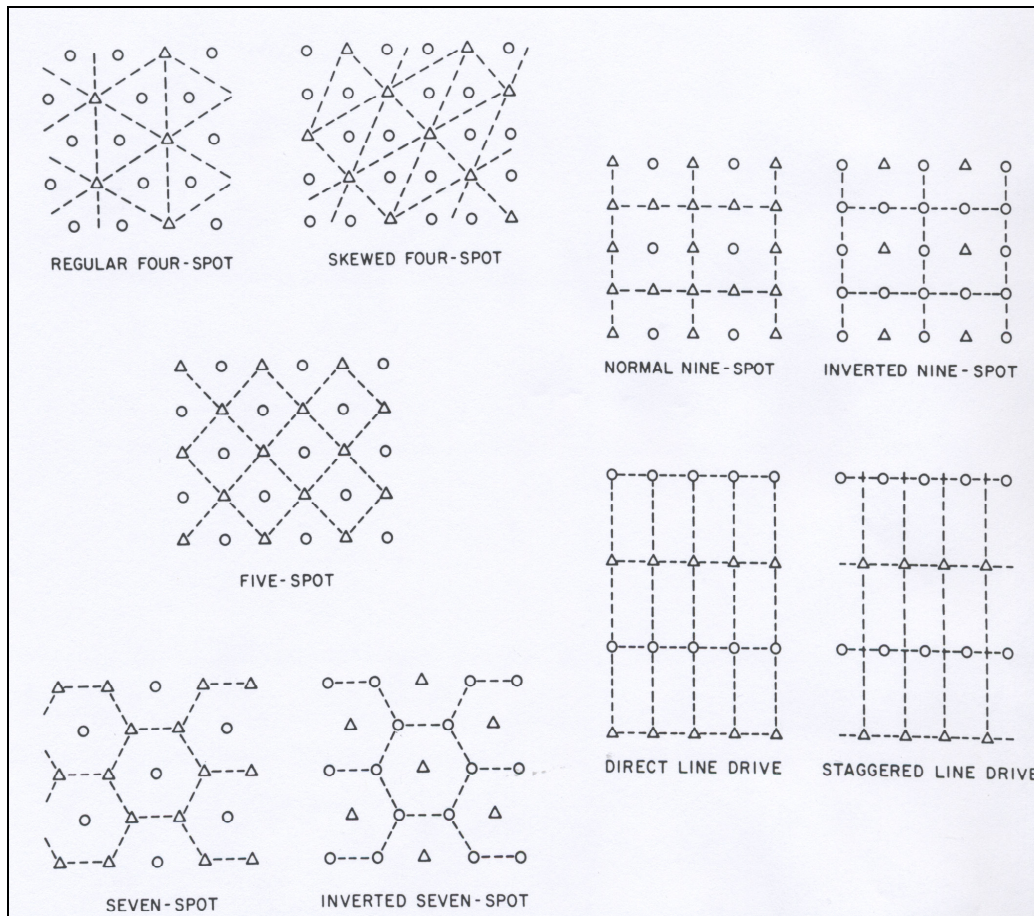
Figure 3.11: Schematics of different waterflood configurations
(from Craig, 1971)

The areal sweep efficiency is a function mainly of mobility ratio (M), which is defined as the mobility of the displacing phase divided by the mobility of the displaced phase. For waterflooding applications, when water is displacing oil, the mobility ratio could be expressed as:

$$M = \frac{\mu_w}{k_{rw}} \frac{k_{ro}}{\mu_o}$$
Eqn (3.21)

For direct line drive patterns (Craig, 1971):

$E_{Abt} = 0.5472 + 0.3959 \log (M^{-1} + 0.3)$
Eqn (3.22)

For staggered line drive patterns (Craig, 1971):

When M < 1: $E_{Abt} = 0.794 + 0.1179 \log (M^{-1} - 0.5)$
Eqn (3.23)

When M > 1: $E_{Abt} = 0.515 + 0.7807 \log (M^{-1} + 0.5)$
Eqn (3.24)

For five-spot patterns (Craig, 1971):

$E_{Abt} = 0.626 + 0.3836 \log (M^{-1} + 0.4)$
Eqn (3.25)

The total recovery is therefore a function of both microscopic and macroscopic sweep efficiency.

3.2.3 Recovery after Breakthrough

Generally, many sources in the literature agree that recovery at breakthrough is fairly similar to the recovery at the termination of the waterflood. The assumption inherent to these observations is that the reservoirs are generally water wet, so waterflooding is an imbibition process. This is true of many conventional oil, sandstone reservoirs. In an imbibition process, waterflooding of conventional oil yields insignificant oil after breakthrough, as can be seen from the recovery profile of conventional oil due to waterflood shown in Figure 3.12.
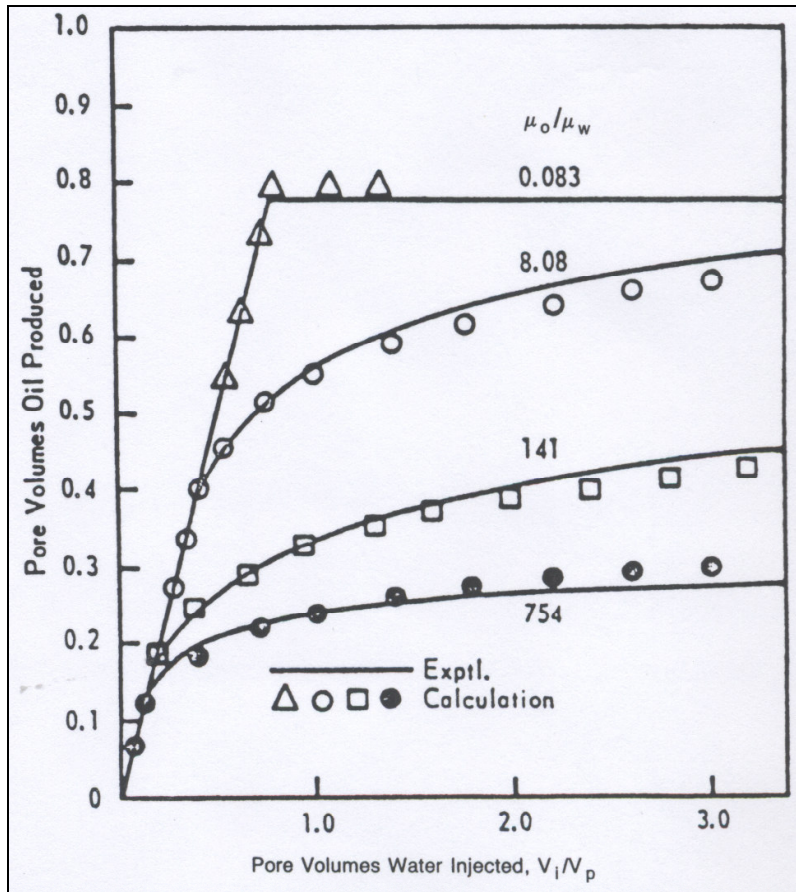
Figure 3.12: Core waterflood recoveries for oils of varying viscosity
(from Craig, 1971)

The low recovery after water breakthrough in Figure 3.12 can be traced back to a capillary number understanding of displacement. In a conventional oil waterflood, water moves in a piston-like fashion through the core, and any oil that is behind the water front exists as discontinuous ganglia trapped by capillary forces. The result of this is that when water breaks through, there is only a small region ahead of the flood front that is still open to additional oil production. In more heterogeneous porous media or situations of higher oil viscosity (as shown in Figure 3.12), more oil can still be recovered after breakthrough since the water front had by-passed some continuous oil at the point of breakthrough. The recovery after breakthrough can be estimated by various methods. When the relative permeability of both water and oil are available, recovery after

breakthrough could be calculated through the means of the extended Welge's method (Craig, 1971):

$$\overline{S}_w - S_{w2} = Q_i f_{o2}$$ Eqn (3.26)

Where $\overline{S}_w$ = average water saturation

S_{w2} = water saturation at production outlet

f_{o2} = fraction of oil flowing out of the outlet.

This method was developed for one-dimensional flow conditions. In field applications the flow is often two-dimensional, thus the recovery is expressed in different terms. Various relationships have been established to predict the recovery of oil after water breakthrough in specific well configurations. In terms of areal sweep efficiency, Dyes (1952) showed that as water was continuously injected after breakthrough, eventually the areal sweep efficiency would reach 100%. Craig (1971) agreed that this was seen in four-spot, five-spot, seven-spot, nine-spot and line drives. There are various correlations to predict the areal sweep efficiency after breakthrough of these various well configurations. Garb (1980) presented a general correlation to predict the overall sweep efficiency (E_A) after breakthrough for all patterns.

$$E_A = 0.2777 \ln\left(\frac{Q}{Q_t}\right) + E_{Abt}$$ Eqn (3.27)

3.2.4 Residual Oil after Waterflooding of Conventional Oil

Trapping of oil in a porous medium is not understood completely and cannot be fully described mathematically (Green and Willhite, 1998). However, it is known that the trapping of oil is dependent on the pore structure of the porous medium, the interfacial tension of the fluids, and flow instabilities. Even though it is not possible to analyze the nature of trapped oil, there are many models to investigate the forces present during trapping.

The simplest model of trapping is in a single capillary, as shown in Figure 3.13.
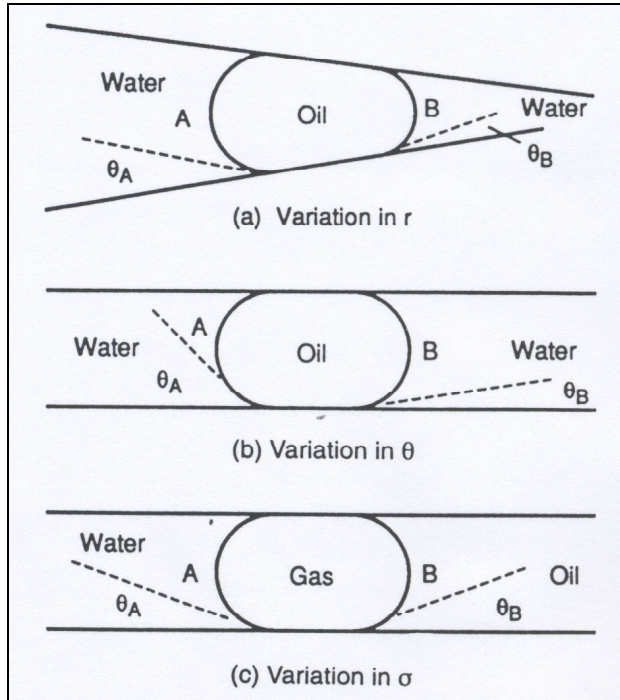
Figure 3.13: Trapping of a non-wetting droplet in a capillary tube

(from Green and Willhite, 1998)

By balancing the pressures in situations (a) and (b), the following relationship is obtained:

$$P_A - P_B = 2\sigma_{ow}\left(\frac{\cos\theta_A}{r_A} - \frac{\cos\theta_B}{r_B}\right)$$
Eqn (3.28)

An equation of this form provides a means to understand how droplets are trapped, and to calculate the pressure drop necessary to mobilize this trapped oil.

Pore channels in reservoir rocks are often irregularly shaped channels, thus the trapping in Figure 3.12 is an idealized version of actual conditions. The single capillary theory

was extended by Moore and Slobod (1956) to consider flow in two parallel capillaries, as shown in Figure 3.14.
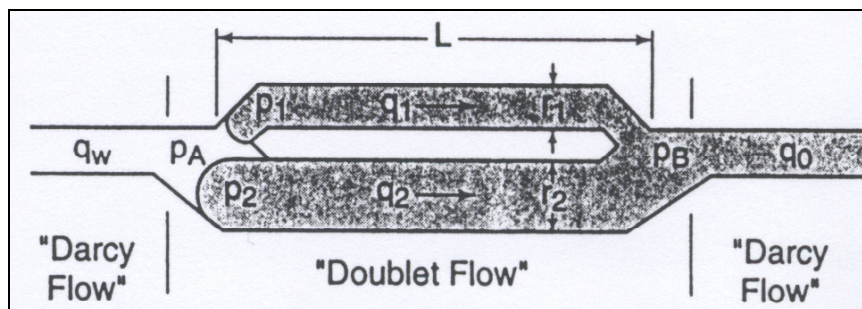
Figure 3.14: Displacement of oil in a pore doublet
(from Green and Willhite, 1998)

Even though this model still does not include all the complexities of actual rock pores, the pore doublet model (Moore and Slobod, 1956) is still very crucial in the understanding of oil trapping. Through this work, they developed the relationship between recovery and a dimensionless group, which was later defined as the capillary number. This work was based on the assumptions that the pores are water wet, and that the viscosities of oil and water are similar.

Moore and Slobod (1956) concluded that unless incredibly high flow rates are employed in water wet reservoirs, the capillary pressure difference in the large versus the small pore is the dominant factor controlling the movement of fluids. An analysis of the ratio of forces in the large and small connected capillary tubes in their theoretical pore doublet shows that unless the wetting phase is injected at unreasonably high rates, flow will occur first into the smaller capillary (Moore and Slobod, 1956). Thus, they concluded that trapping of the oil occurred more frequently in larger pores, as is commonly accepted in imbibition theory.

It was later shown by Chatzis and Dullien (1983) and Dullien (1992) that in for the range of values that are typical of normal waterflooding operations, the theoretical pore doublet model is actually not applicable. In fact, the model predicts countercurrent displacement

of the two interfaces, with flow advancing in the smaller capillary but retreating in the larger capillary. These calculations have been performed for both conventional and heavy oil systems, and are shown in Appendix A. Through visual experiments, it was shown (Chatzis and Dullien, 1983) that under continued flow water will eventually invade the larger pore and there will not actually be trapping of non-wetting fluid in the pore doublet model. Thus while the model can serve to demonstrate that flow of the wetting phase will happen preferentially in smaller pores, the model does not properly explain the presence of residual oil after waterflooding.

The discussion on trapping up to this point pertains to cases where the porous medium is water wet. For a more general case, wettability determines the nature and extent of trapping. The non-wetting phase would be trapped as isolated droplets, whereas the wetting phase would be trapped in small crevices or thin films surrounding the sand grains. When a non-wetting phase is trapped, the ganglia will generally tend to reside in large pores. However, in the case of the wetting phase being displaced, it will be trapped over a larger distance in the porous medium. The effect of wettability on the magnitude of trapping is not clear. It is generally expected that if the reservoir is water wet, the residual oil saturation should be larger than the case where the reservoir is oil wet due to oil being trapped in much larger pores. There are various sources in the literature, which have presented evidence to show that residual oil saturation of water wet media is lower than that of oil wet. For example, Newcombe *et al*. (1955) showed that the residual oil saturation after 8 pore volumes of brine injected decreased as the system became more water wet. However, there are other sources that show that the magnitude of residual oil saturation is not a strong function of wettability (Green and Willhite, 1998). This indicates that wettability might not be the only factor influencing the residual oil saturation. Thus, it is not possible to validate the effect of wettability on the amount of oil being trapped, although the location of the trapped phase is certainly dependent upon the wettability.

There is also a significant amount of experimental data available regarding the trapping of residual oil in the porous medium. The results of numerous core flooding experiments in water wet porous media all show that the residual oil saturation can be directly related to the capillary number. This implies that along with wettability, the condition at the front dictates the amount of oil will be trapped.

3.2.5 Improved Oil Recovery

From the analysis of the pore double model (Moore and Slobod, 1956), a dimensionless group emerged that relates the effect of viscous to capillary forces. This dimensionless group, also known as the capillary number, is defined below:

$$N_{ca} = \frac{\nu \mu_w}{\sigma_{ow}} \qquad\qquad\qquad \text{Eqn (3.29)}$$

It was previously shown in Figure 3.9 that as the capillary number increases, the residual oil saturation in the core decreases. Various expressions of the capillary number can be found in literature. Chatzis and Morrow (1984) have noted that there are more than ten expressions for capillary number, and they are generally equivalent to each other. In some cases, $(\cos\theta)$ is included along with the oil/water interfacial tension in the denominator. Some authors have also used the interstitial velocity while some other use Darcy velocity (Green and Willhite, 1998). Abrams (1975) modified the equation empirically to include the effect of slightly higher oil viscosity, as shown earlier in Figure 3.9. In core flooding experiments, the product of the water velocity and viscosity can be extracted from the produced fluid data. Using Darcy's Law, where $\nu\mu_w = \frac{Q}{A}\mu_w = k\frac{\Delta P}{L}$, an alternative expression of N_{ca} is:

$$N_{ca} = \frac{k\Delta P}{L\sigma_{ow}} \qquad\qquad\qquad \text{Eqn (3.30)}$$

In Eqn (3.30), the residual oil in the core is shown to be related to the product of the rock permeability and the pressure gradient that can be established in the system. This indicates that residual oil should be lower in a higher permeability rock, or in a system that can sustain a high pressure gradient to force fluids through the rock pores. In this manner, residual oil saturation can be related to easily-measured waterflood parameters. Unfortunately, in systems with high rock permeability values, it is difficult to establish high pressure gradients since fluids can flow with relative ease in the porous media. Therefore, although Eqn (3.30) theoretically can be correlated to reductions in residual oil saturation, this is not easy to achieve in practice.

Dullien (1992) derived a capillary number for mobilization of an oil droplet a strongly water wet capillary tube. This version of the capillary number was shown to be:

$$N_{ca} = \frac{4v\mu L}{\sigma r} \qquad\qquad \text{Eqn (3.31)}$$

In this equation, r is the radius of the capillary tube and L is the length of the tube. In order to extend this equation to use in porous media ($r = \sqrt{\dfrac{8k}{\phi}}$) and to predict residual oil saturation in the field, the capillary number can be re-written as:

$$N_{ca} = \frac{\sqrt{2}v\mu L}{\sigma\sqrt{k\phi}} \qquad\qquad \text{Eqn (3.32)}$$

The problem with this expression is that it essentially predicts that in longer systems, the capillary number is larger, indicating that the viscous forces are more important. However, this is only true if the porous medium is a single long capillary tube. In an actual reservoir, there are many sand grains and many paths of displacement, which means that the capillary effect should be much larger. Thus, this equation should not be

applicable when relating the relative importance of viscous to capillary forces for field scale.

The relationship between recovery and capillary number presented earlier was for the condition at which water is injected into a core to displace oil that still exists at relatively high saturations. Green and Willhite (1998) state that the same type of correlation is also expected to mobilize the oil once it has been trapped, but that there is hysteresis between the trapping and mobilization process. Therefore, the capillary numbers required to recover trapped oil ganglia may be significantly higher than those in Figure 3.8. Moore and Slobod (1956) have shown that the magnitude of trapping depends on the condition at the interface between the displacing and displaced phases. This point was illustrated by a set of experiments in which waterfloods were carried out at 0.61 m/D (2 ft/D), 61 m/D (200 ft/D) and a combination of both rates (Moore and Slobod, 1956). The residual oil saturation obtained from 61 m/D was lower than that of 0.61 m/D, which is expected from capillary number analysis (N_{ca} of the 61 m/D waterflood is two orders of magnitude higher than N_{ca} at 0.61 m/D). However, the combination of both slow and fast injection rate yielded a residual oil saturation smaller than 0.61 m/D alone, but still much higher than 61 m/D. This shows that once the oil has been trapped, it is not easy to reverse the process. More importantly, the results also show that recovery is better at a higher injection rate, where the capillary number is also higher. This application is understandable in conventional oil, where a higher waterflooding rate provides a more significant pressure gradient to remove the oil existing in smaller pores before the oil phase becomes trapped.

In general, the capillary number can theoretically be used to provide a guideline to improve oil recovery. The ratio of viscous to capillary force could also be improved by reducing the interfacial tension between oil and water through the use of surfactants (Reisberg and Doscher, 1956), or the interfaces could be eliminated completely through miscible processes (Green and Wilhite, 1998). This is the realm of enhanced oil recovery, and is outside the scope of a discussion on waterflooding.

3.3 Waterflooding of Heavy Oil Reservoirs

The definition of heavy oil can vary significantly. Jayasekera and Goodyear (2000) defined heavy oil as *in-situ* oil with a viscosity greater than 5 mPa·s (cP), indicating an adverse mobility ratio between oil and water. This definition is considerably lower than what is generally accepted as heavy oil. Miller (2006) stated that the definition of heavy oil is based on API gravity (≤ 20 °API) rather than viscosity. According to Miller, the failure to set a limit on viscosity is due to the fact that there are problems in accurately measuring viscosity, especially for viscous oil. However, he used a limit of 1,000 to 2,000 mPa·s, whereas Farouq-Ali and Thomas (2000) believed the upper limit to be 1,200 mPa·s. Other sources have placed a limit for determining an oil to be heavy, which is much lower than these numbers.

Waterfloods in heavy oil reservoirs are very different than those of conventional oil. These differences are due to several factors. First is the high absolute permeability of the oil sands, which are characterized by having large pore throats with low aspect ratio (Smith, 1992). The most important distinction for these reservoirs, however, is the displacement instability, which occurs as a result of the adverse mobility ratio. This poor mobility ratio induces the formation of viscous fingers during waterflooding, which leads to early water breakthrough and poor macroscopic sweep efficiency at breakthrough. Thus, significant oil can be recovered after water breakthrough, and overall the recovery of heavy oil waterfloods tends to be fairly low.

Theoretical development for waterflood recovery predictions in heavy oil reservoirs is sparse. Smith (1992) gave an overview of waterflooding of heavy oils, in which he listed the mechanisms that could potentially aid in the continuous recovery of oil after water breakthrough as: pressure support in the reservoir, multi-phase expansions, gas/oil control (again due to pressure support), water imbibition and gravity drainage of oil. However, he offered few details for these mechanisms.

Most research into heavy oil waterflooding has focused on the recovery before breakthrough, the development of models to predict when viscous fingering will occur and the reduced breakthrough recovery that will be the result of these fingers. There have been significant developments in viscous fingering theory to explain early water breakthrough, but there is very little discussion regarding the recovery of oil after breakthrough in the literature. Smith (1992) is one of the few researchers who have identified the importance of capillary imbibition in heavy oil systems. He proposed that at low displacement rates, capillary imbibition could be a significant process after the early arrival of water, where oil production continues to yield ultimately high recovery. Generally, there is very limited field production results reported in the literature for waterflooding of heavy oil. A more recent summary of this data is provided by Kumar *et al*. (2005). Some of the reported results for laboratory and field waterflood trials in heavy oil systems are discussed later in this chapter.

3.3.1 Viscous Fingering

In waterflooding cases where the viscosity of oil is higher than that of water, the displacement front between oil and water is not even (Demetre *et al*., 1982; Coskuner and Bentsen, 1988; Sigmund *et al*., 1988). Since water is much more mobile than the viscous oil, injected water will tend to finger through the sand, bypassing large portions of continuous oil. Figure 3.15 shows a schematic of these viscous fingers.

Engelberts and Klinkenberg (1951) were the first to name this phenomenon as viscous fingering. Viscous fingering occurs when a high mobility fluid is displacing a fluid of much lower mobility. Such cases occur in heavy oil waterflooding, or in gas flooding where miscibility is not obtained.

(VISCOSITY RATIO 146)
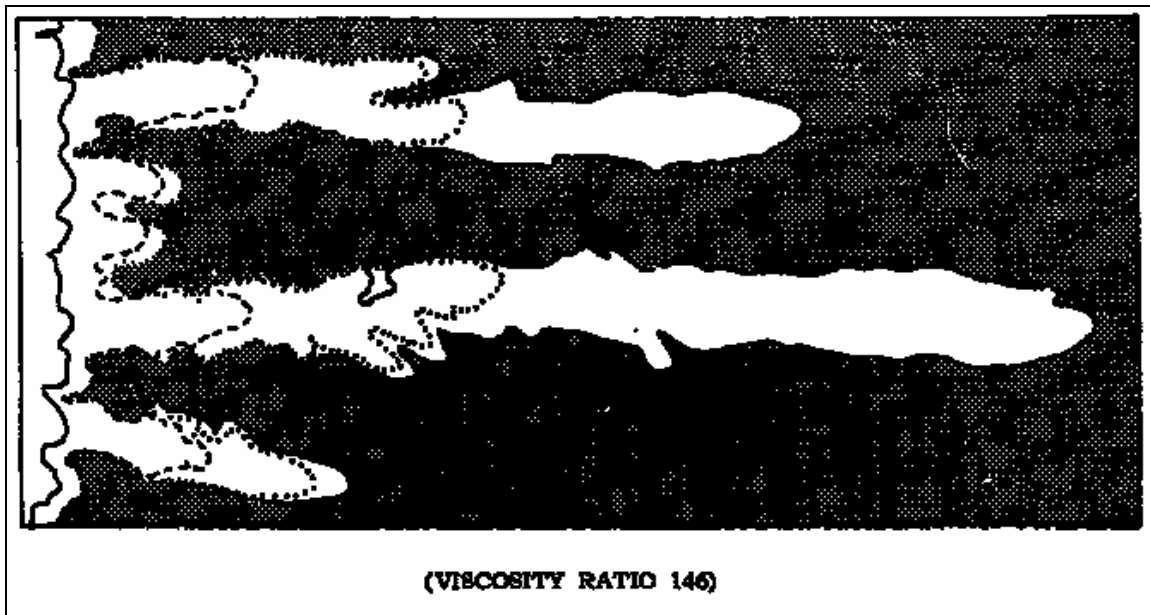
Figure 3.15: Instability of waterfront

(from Perkins and Johnston, 1969)

Perkins and Johnston (1969) reported that at unfavourable viscosity ratios and high injection rate, many viscous fingers form. They also noted that many small fingers form at the inlet, but as the displacement progresses some of these fingers may coalesce to form larger fingers. Thus, the number and size of the viscous fingers will not be constant. It must be noted that the coalescence of small fingers to generate larger fingers might be particular to each system studied; the growth of fingers depends on the severity of the unstable flood front and this is controlled by many factors such as the mobility ratio, the injection velocity and the degree of water-wetting of the rock (Peters and Flock, 1981).

There has been considerable work done in the literature to study the characteristics of viscous fingers. Most early work focused on determining the width of the fingers (Chuoke *et al*., 1959; Outmans, 1962; Varnon and Greenkorn, 1969). Later researchers studied the condition under which the displacement becomes unstable, thereby giving rise to the instability number concept.

3.3.1.1 Instability Theory for Predicting Breakthrough Recovery

In heavy oil waterflooding, the displaced oil has much lower mobility than water, thus the displacement front may become unstable. When this happens, viscous fingers are said to have formed. This will cause premature breakthrough of the displacing phase, and reduce the breakthrough oil recovery.

Early works on viscous fingering were focused on miscible displacement under unfavorable viscosity ratio conditions (Benham and Olson, 1963). The theoretical descriptions of viscous fingering were focused on solving the equation of continuity of one or both fluids moving in the same direction in a homogeneous porous medium (Varnon and Greenkorn, 1969). Independent researchers obtained different results due to the fact that they used different boundary conditions at the interface, and in some cases the expression for flow was also expressed differently.

Peters and Flock (1981) extended the theory of Chuoke *et al*. (1959) and identified the parameters controlling the stability of the system as: mobility ratio, displacement velocity, system geometry and dimensions, capillary and gravitational forces, and the rock permeability and wettability. Their work focused on performing stability analysis in order to identify the conditions under which a frontal perturbation will grow to become a viscous finger. The instability number (I_{sr}) for a horizontal 1-D system, as defined by Peters and Flock (1981), is as follows:

$$I_{sr} = \frac{(M-1)\nu\mu_w D^2}{C^*\sigma k_{wor}}$$ Eqn (3.33)

Where k_{wor} = permeability to water at the irreducible oil saturation S_{or}

k_{oiw} = permeability to oil at the connate water saturation S_{wi} and

C^* = wettability constant.

The wettability constant C* has different values for varying rock wettability, which indicates that the effect of imbibition on the growth of viscous fingers is different in oil wet versus water wet porous media. In smaller diameter cores, there is also less potential for fingers to grow. This means that in actual field scale waterfloods the effect of instability may be more pronounced than in a linear core system. I_{sr} is also directly proportional to the fluid mobility; in heavy oil systems the mobility ratio is very large, which leads to very high values of I_{sr} (i.e. very unstable floods).

At the onset of instability, I_{sr} was found to be 13.56 (Peters and Flock, 1981). When $I_{sr} <$ 13.56, the displacement is stable: in at this range of flood conditions, viscous fingers will not grow if a frontal perturbation develops. When $I_{sr} >$ 13.56 the displacement is deemed fully unstable. In the transition zone ($13.56 < I_{sr} < 900$) the flood is becoming increasingly unstable, and breakthrough recovery decreases rapidly as I_{sr} increases. In the "pseudo stable" region of $I_{sr} > 900$ the breakthrough recovery tends to become constant again (Bentsen, 1987). In this range, displacement is actually so unstable that most of the injected fluid will simply pass through a few fingers, and recovery is low and relatively independent of instability number.

Instability theory therefore dictates that before $I_{sr} = 900$, the displacement rate determines the finger properties. At a high injection rate in an unstable system, the finger wavelength will be short, thus numerous fingers can form. At a low rate the finger wavelength will be long, thus only a few fingers can form in the porous medium (Peters and Flock, 1981). Multiple fingers lead to a higher degree of instability, which explains why breakthrough recovery decreases with increasing values of I_{sr}. Therefore in heavy oil systems it becomes important to perform experiments more slowly when conditions are unstable, in order to limit the generation and growth of fingers.

Peters and Flock (1981) stressed the importance of the wettability number in their formulation of I_{sr}. This number gives an indication of the ability of the porous medium to imbibe the displacing water, which can help to stabilize the flood front. They found that

in water-wet media the influence of water imbibition is strong, thus the wettability number would be large (C* = 306.25). For oil-wet media, the wettability number was found to be much smaller (5.45). This is because under drainage, water will only move through the largest channels, so the front cannot be stabilized by additional flow into smaller pores.

Bentsen (1985) also derived a different version of the instability number, based upon force potentials rather than the velocity potentials used by Peters and Flock (1981). His version of instability number is proportional to the one proposed by Peters and Flock, with an additional factor to take into consideration the larger size difference of water and oil fingers.

The instability number developed by Bentsen (1985) is:

$$I_{sr} = \frac{\mu_w v (M - 1 - N_g)}{k_{wor} \sigma_e} \frac{M^{5/3} + 1}{(M+1)\left(M^{1/3} + 1\right)^2} \frac{4h^2 b^2}{h^2 + b^2} \qquad \text{Eqn (3.34)}$$

It should be noted that Bentsen (1985) derived his version of the instability number for a rectangular system, where b and h are dimensions of the rectangular model.

In Eqn (3.34) σ_e is the effective or the pseudo-interfacial tension, as described by:

$$\sigma_e = \frac{A_c \phi (1 - S_{wi} - S_{or})}{2/\bar{r}_m} \qquad \text{Eqn (3.35)}$$

Where A_c is the area under the capillary pressure curve and $\bar{r}_m$ is the average macroscopic mean radius. The effective interfacial tension is therefore an average value derived using the capillary pressure curve for a given rock-fluid system. The parameter N_g in Eqn. (3.34) is the gravity number (Bentsen, 1985), which is given by:

$$N_g = \frac{(\rho_w - \rho_o)g\cos\alpha k_{wor}}{\mu_w v}$$

Eqn (3.36)

N_g is therefore the ratio of the gravitational forces to the viscous forces, which accounts for the dipping of the formation. In a horizontal system, when the dip angle $\alpha = 0$, this results in a value of $N_g = 0$.

Sarma and Bentsen (1987) also developed the theory further to predict the recovery at breakthrough (R_{bt}) for two situations: stable displacement ($I_{sr} < 13.56$) and pseudo-stable ($I_{sr} > 900$) displacement.

For a stable displacement ($I_{sr} < 13.56$):

$$R_{bt} = \frac{1 - S_{wi} - S_{or}}{1 - S_{wi}}\left[\frac{X_o}{L} + \frac{1 - \dfrac{X_o}{L}}{1 + \dfrac{M - 1 - N_g}{M + 1}\dfrac{M^{2/3} - 1}{M^{2/3}}}\right]$$

Eqn (3.37)

Where X_0 is the location where the frontal perturbation or the viscous fingers start to form. This location is not easily identifiable, thus for most practical purposes, X_0 is assumed to be 0. This means that the perturbation occurs right at the inlet of the model.

For a pseudo-stable displacement ($I_{sr} > 900$):

$$R_{bt} = \frac{1 - S_{wi} - S_{or}}{1 - S_{wi}}\left[\frac{X_o}{L} + \frac{1 - \dfrac{X_o}{L}}{1 + \dfrac{3(M - 1 - N_g)}{M + 1}\dfrac{M^{2/3} - 1}{M^{2/3}}}\right]$$

Eqn (3.38)

This equation was obtained under the assumption that under pseudo-stable conditions, the perturbation velocity of a finger is three times that of the critical perturbation velocity

(Sarma and Bentsen, 1987). It is important to note that for both stable and pseudo-stable displacement the breakthrough recovery is not directly related to the injection rate. Therefore, in these two ranges recovery is expected to be only a function of the mobility ratio, and cannot be controlled by reducing the waterflood injection rate.

Despite the fact that Sarma and Bentsen (1987) developed a the theoretical method to predict recovery at breakthrough, there has actually been very little data presented in literature to verify this model, other than the results reported by the authors (Sarma and Bentsen, 1987). Figure 3.16 shows the relationship between breakthrough recovery and instability number as a function of mobility ratio, for a limited data set.
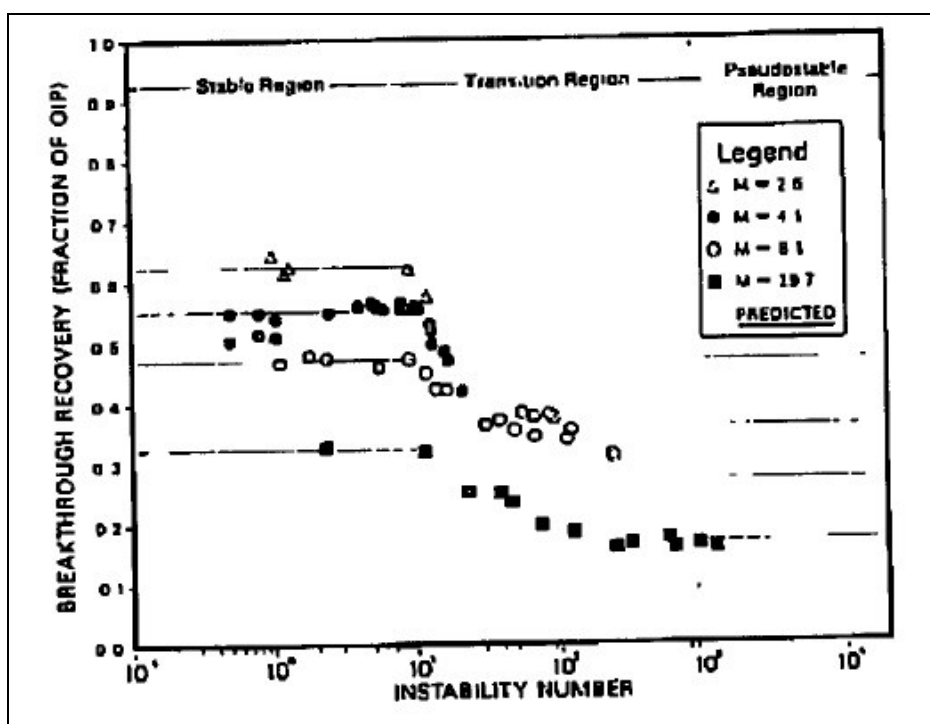
Figure 3.16: Breakthrough recovery as a function of instability number
(from Sarma and Bentsen, 1987)

From Figure 3.15 it can be seen that breakthrough recovery is related to instability number, but that this relationship is different for different mobility ratio waterfloods. This is surprising considering the fact that instability number itself is already a function

of mobility ratio. In general, it can be seen that under stable displacement conditions (I_{sr} < 13.56) the breakthrough recoveries remain fairly consistent for any given mobility ratio. During the transition region (13.56 < I_{sr} < 900) breakthrough recovery decreases as the instability number increases. Unfortunately, this relationship could not be defined in an equation, and it appears to be different for each mobility ratio. Even though Bentsen (1985) and Peters and Flock (1981) reported that in the pseudo-stable region the breakthrough recovery remains constant over a range of instability numbers, there is very little data to support this.

The waterflooding results of Bentsen (1985) and Peters and Flock (1981) are compared against one another in Figure 3.17. Both show similar trends: under stable displacement the breakthrough recovery is better than for unstable displacement, and as the mobility ratio increases the breakthrough recovery decreases. However, it is significant that the results from the different authors are not in agreement. Although Peters and Flock (1981) worked with higher mobility ratio systems their breakthrough recoveries are more optimistic when compared to the values reported by Bentsen (1985).
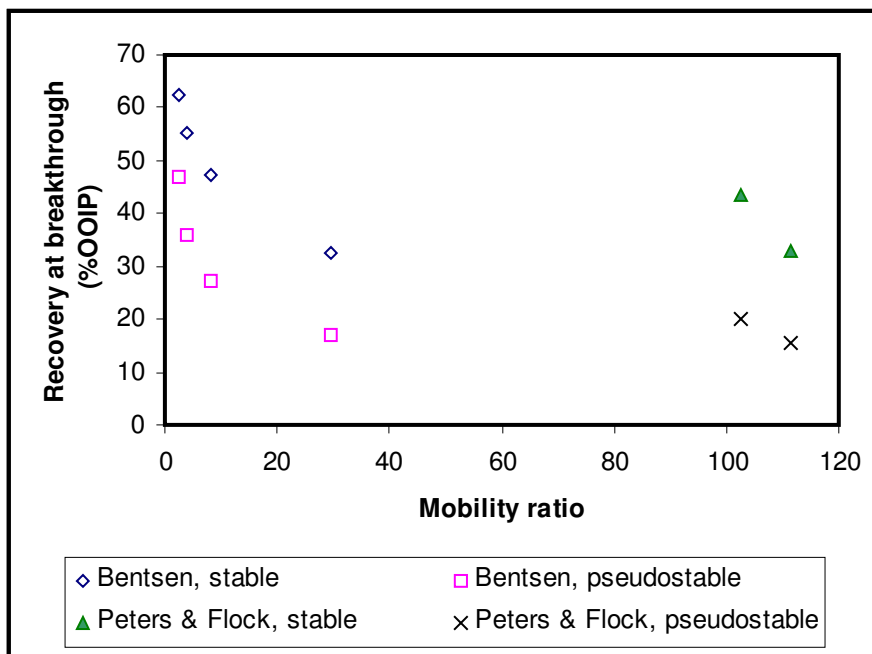
Figure 3.17: Comparison of recovery data under different stability regimes

The recovery data in Figure 3.16 implies that if the correlation by Bentsen (1985) is used to predict breakthrough recoveries under the conditions that Peters and Flock imposed, it would not match the actual breakthrough recoveries measured by Peters and Flock (1981). Thus, although both the proposed equations for breakthrough recovery show the correct trend in recovery as a function of mobility ratio and stability, it appears that they do not properly account for all relevant variables, and as a result the different data sets do not correlate with one another.

The theory of instability is basically a balance of forces. In an immiscible displacement, if the combined forces of gravity and capillarity are greater than the viscous force, then the displacement will be stable. If the reverse is true then the displacement will be unstable, and at least in the transition zone with all else being equal the degree of instability depends on the rate of injection. In heavy oil systems such as the ones in the Canadian oil sands, the difference between oil and water viscosity is so great that I_{sr} will always tend to be very large (i.e. unstable or pseudo-stable). This theory therefore indicates a dominance of viscous forces during waterflooding, and explains the low waterflood recovery expected.

3.3.2 Breakthrough Recovery and Residual Oil after Waterflooding in Heavy Oil

Due to viscous fingering, the recovery of heavy oil at breakthrough is very low. After water has found a continuous path from the inlet to the outlet of a core or a reservoir, it will continue to channel through in this path of least resistance where the water saturation (and relative permeability) is high, and the fluid viscosity is low. The result is that there should be very little additional oil recovered after breakthrough under the influence of viscous forces. This ensures that the process of waterflooding of heavy oil is inefficient compared to its response in conventional oil.

From a laboratory perspective, it is not simple to define the breakthrough point in a heavy oil waterflood. Breakthrough was originally defined as the point when water is first

produced along with oil. For waterflooding of conventional oil in a homogeneous porous medium, water will sweep the entire area of the rock and thus oil will be initially produced as a single phase as brine is injected. Eventually the water-front breaks through at the outlet, and only continuous oil still ahead of the front can flow. As a result, very little additional oil is recovered (Craig, 1971) and the recovery at breakthrough is more or less the same as the ultimate recovery from waterflood. However, waterflooding of heavy oil tends to create many fingers, which induce early water breakthrough and very low breakthrough recoveries. At early times under constant rate injection, water also cannot displace oil at the same rate due to the high pressure gradients required for oil to flow. Thus, water builds up inside the porous medium close to the inlet of the core, creating instabilities of the flood front and leading to viscous fingering.

At first glance the recovery profile of the heavy oil waterflood resembles the production profile of a drainage process, where oil is still produced after breakthrough (Craig, 1971). However, if the porous medium is water wet, the recovery process cannot be drainage. The continuous oil production after breakthrough, added with difficulties in visually distinguishing oil and water due to the viscous nature of the oil, makes it difficult to locate the breakthrough point. If breakthrough is still defined as the point where water is first produced, then the recovery at breakthrough for all heavy oil waterflood is very small, and in some cases is insignificant.

At the conclusion of the waterflood, trapped conventional oil is due to capillary forces. However, this is not the case in a heavy oil waterflood, where a significant amount of continuous oil is bypassed at the time of breakthrough. Thus, within the water channel, the oil may be trapped due to capillarity, but in the bypassed region most of the oil is undisturbed and still capable of flowing. Therefore, the true residual oil saturation is impossible to define for heavy oil applications unless enough water is injected to reach the true S_{or}, and this is usually not done in waterfloods (Maini, 1998).

3.3.3 Field reports of heavy oil waterfloods

There are a limited number of literature sources reporting the results of field data for heavy oil waterflooding. This is due to the fact that many deem this process to be inappropriate for oil viscosity over 200 mPa·s (Farouq Ali, 1976).

Two successful waterfloods were detailed Sutton (1963) and by Oefelein and Walker (1964). Sutton (1963) showed that for an oil viscosity of 48 mPa·s, the ultimate recovery due to waterflooding could be as high as 58% of the pore volume due to favorable permeability distribution. Oefelein and Walker (1964) reported waterflooding results for the Inglewood field in California. The oil in this reservoir has a viscosity of 65 mPa·s. Again, the actual recovery observed from the waterflood was actually much better than anticipated.

Adams (1982) reported waterflooding results for a Lloydminster heavy oil reservoir with oil viscosity ranging from 950 – 6,500 mPa s. He reported that the recovery of these reservoirs was worse than the values predicted by the Buckley-Leverett solution, which assumes a stable water displacing front. There were also difficulties in finding the areal sweep efficiency for cases where the mobility ratio is large. Interestingly, he noted that when the wells were re-flooded after having been shut-in, the water-oil-ratio decreased and was accompanied by a slight increase in oil production rate. Therefore, it appears that during shut-in, fluids redistribution may have led to an improved waterflood response, but Adams (1982) did not discuss this in detail.

Kasraie *et al*. (1993) reported that for a live oil (an oil saturated with solution gas) with a viscosity of 112 mPa s, the ultimate recovery due to primary production and waterflooding could be 26 – 29% of OOIP. Ko *et al*. (1995) used simulation as a means to predict the behavior of a waterflood in a field with live oil viscosity of 350 mPa·s. From simulation, they concluded that waterflooding of this pool could yield an ultimate recovery of 18 - 22% of OOIP. Yang *et al*. (1998) reported that the waterflooding recovery for oil with viscosity greater than 100 mPa·s would be less than 15% of OOIP.

More recently, Singhal and Holowatuk (2007) summarized results for nine current waterfloods in medium to heavy oil reservoirs in Alberta and Saskatchewan. In all the cases presented, it was shown that as water injection rate increased, this in turn led to higher oil rates, but that the produced water cuts would increase significantly as well (Singhal and Holowatuk, 2007). Unfortunately, no information was provided for the rock permeability or oil viscosity, so these observations could not be quantified or compared against what others had observed.

It appears that the results from waterflooding at the field scale are not trivial to interpret. The recoveries reported cannot be simply correlated to the oil viscosity; but rather that many other factors such as water injection rates and rock permeability will also have a significant impact on oil recovery. In the literature published to date, there is a distinct lack of a definitive study that compares the relative significance of changing viscous and capillary forces on the flood response and the oil recovery. Therefore, while there has been research performed for understanding viscous fingering and their effect on breakthrough recovery, there has been very little work done to investigate the recovery of heavy oil after water breakthrough, and the mechanisms by which water can displace viscous heavy oil.

3.4 Wettability Effects in Waterflooding

In a rock/oil/water system, wettability refers to the preference that the rock has to be contacted by either oil or water. If the rock is water wet, water will tend to occupy small pores and exists as thin films covering the rock surface. In an oil wet system, the reverse is true; oil will exists in small pores and water will tend to be in the center of the larger pores, surrounded by a thin oil film. For either wetting preference, the degree of wettability may change, as shown by the contact angle (Section 3.1.2). In the case of neutral wettability, the rock has no preference for either oil or water. Fractional wettability refers to the situation where some of the pores are water wet while some other pores are oil wet. If a rock is mixed wet, this is a special case of fractional wetting, where the small pores are water wet while the large pores are oil wet (Dullien, 1992).

Obviously, since rock wettability directly influences the location of oil or water in a porous medium, this parameter is extremely important for predicting how a waterflood will be expected to behave. While there is no data to quantitatively relate the degree of wetting to the oil recovery, this is still an important parameter to understand. The wettability of the porous medium can be either measured or inferred. There are many different methods available to determine the wettability. Each method has its own range of uses, and the wettability of unconsolidated sand containing heavy oil is non-trivial to obtain.

3.4.1 Measurement of Wettability

There are many different methods available to determine the wettability of a porous medium. These methods can be either quantitative or qualitative. Regardless of the method chosen, it normally performed using either refined oil or extracted oil at ambient conditions. The quantitative methods include: contact angle measurements, Amott and United States Bureau of Mining (USBM) methods. These tests provide a numerical value of the degree of wetting in a given rock/fluid system. There are no standard methods that are accepted as being the most accurate, however when possible quantitative methods are more commonly used.

The contact angle is considered to be the simplest method of determining the degree of wettability for pure fluids and artificial cores (Anderson, 1986b). However, the extension of this method to reservoir cores encounters various difficulties. On a non-porous smooth surface, the determination of contact angle is straightforward. However, in reservoir rocks there are sharp edges, which make the measurement difficult. Another problem is that the wettability measured might be localized due to the heterogeneous nature of the porous medium. Dullien (1992) shows that for a porous medium consisting of pore bodies and pore throats of changing diameter, the contact angle may change from low values up to even 90° (indicating neutral wet conditions) even though the rock remains

water wet. Rosen (1989) also discusses how impurities on the sand and measurement in finely divided solids are difficult to obtain accurately.

Many researchers have postulated that the contact angle measured at ambient conditions might not be representative of *in-situ* wetting preferences, since the light ends that would have left the oil may play a significant role in establishing wettability. Thus, Rao and Girard (1996) proposed a method to measure the contact angle under reservoir conditions. The successful application of this method would solve the problem of the effects of possible light ends evaporation, but there are still other uncertainties in contact angle measurements.

Hysteresis is another common problem associated with the contact angle measurement. This is a condition where the advancing angle does not equal the receding angle, due to the fact that a liquid drop may have many different stable contact angles (Anderson, 1986b). Other common problems with contact angle measurements include contamination of the solid, surface roughness effects, and the inability to measure contact angle accurately on a porous surface (Rosen, 1989). As a result, it becomes difficult to know if the contact angles measured, and their relationship to the degree of wetting preference of a given rock, will be valid at the pore scale.

The Amott method is another quantitative measurement of wettability that combines both spontaneous and forced imbibition (Amott, 1959). There are four main steps involved in the Amott test. The core sample that is saturated with water is first immersed in oil and the volume of water produced by spontaneous imbibition of oil is measured. The sample is then centrifuged in oil (forced drainage of water) until the irreducible water saturation is reached. The same processes are repeated for the same sample that is saturated with oil (immersed in water and then centrifuged in water). The wettability index is the measure of the volumes displaced by spontaneous versus forced processes (Anderson, 1986a). The Amott test works well for samples that are strongly wetted, however it is insensitive in near neutral wet conditions (Anderson, 1986b).

The USBM test is another quantitative measurement of wettability that is also fast to perform (Donaldson, 1969). Its advantage over the Amott test is that it is still quite sensitive near neutral wetting conditions. This method compares the work required for one fluid to displace another. The work required for a wetting fluid to displace a nonwetting fluid is less than the opposite case.

Qualitative methods of measuring wettability involve tests such as determining if spontaneous imbibition of water can occur, and measuring the shape of the capillary pressure and oil/water relative permeability curves. Other methods include microscopic examination of films or apparent contact angles, displacement capillary pressure, nuclear magnetic resonance, and dye adsorption (Anderson, 1986b). The problem with these qualitative methods is that, while they provide an indication of whether a rock is oil or water wet, there is no criterion to determine the degree of water wetness.

3.4.2 Effect of Wettability on Waterflooding Recovery

The wettability of the porous medium will significantly affect the behavior and recovery of the waterflood since it is a major factor that controls the location, flow and distribution of fluids in the porous medium. In a strongly water wet system, breakthrough occurs relatively late and the recovery of oil at breakthrough is high, with very little oil being recovered after breakthrough (Craig, 1971). The water-oil ratio also rises very quickly after breakthrough. In oil wet systems, breakthrough occurs at earlier times with lower oil recovery. However, a significant amount of oil could be recovered after breakthrough with the water-oil ratio increasing gradually. The influence of wettability on oil recovery can be seen in Figure 3.18, which presents the results of a gravity stable immiscible flood using n-decane as the oil in a sandpack of 5 D permeability (Paidin and Rao, 2007).
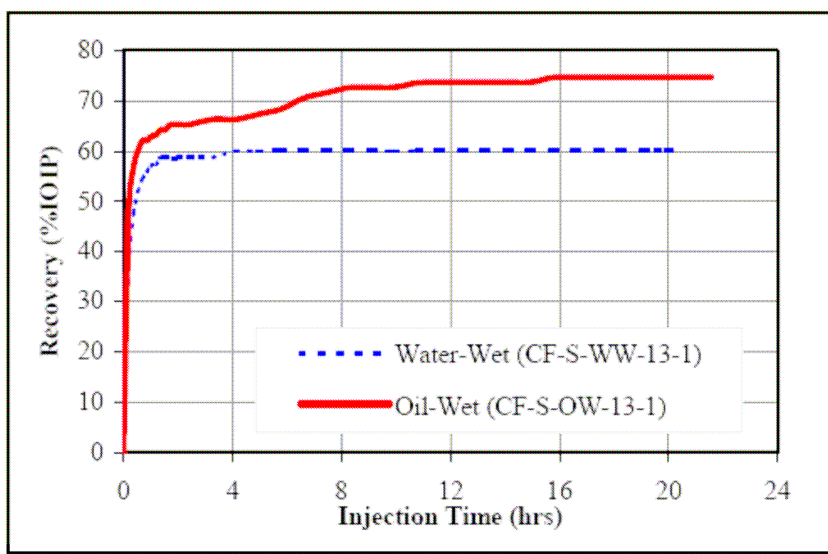
Figure 3.18: Influence of wettability on oil recovery during immiscible displacement (from Paidin and Rao, 2007)

The recovery profile presented in Figure 3.17 can be understood in terms of where oil is physically located in oil wet versus water wet porous media. If oil is a non-wetting fluid, then water injection is an imbibition process, and for low viscosity oils at the point of breakthrough water has swept the entire porous medium. Trapped oil behind the water front exists as discontinuous ganglia, thus after water breakthrough occurs there should be little to no additional oil recovery. In the case of an oil wet medium, water becomes the non-wetting fluid, and at the point of breakthrough the oil will still be continuous and therefore additional oil can still flow out of the core at later times. Therefore, the oil recovery profile becomes more gradual at the point of water breakthrough, as evidenced in Figure 3.18. Craig (1971) noted that in water wet porous media, the majority of the oil would be recovered at lower water cuts, and that oil recovery is slower when the reservoir is oil wet. Due to this fact, waterflooding in a water wet medium is considered to be more economic as the amount of water required to recover the same amount of oil increases with decreasing water wetness.

There are many sources in the literature that provide experimental data to verify this theory. Bobek *et al*. (1958) reported that the oil recoveries from water wet rocks are

significantly better than those from oil wet. Wagner and Leach (1959) also found that by altering wettability from oil wet to water wet conditions, greater oil displacement was seen. Anderson (1987) provided an excellent summary of the effect of wettability on waterflooding recovery. According to Craig (1971), the displacement of a wetting fluid by a non-wetting fluid (i.e. drainage) is less efficient than that of a wetting fluid displacing a non-wetting fluid (i.e. imbibition). Therefore, waterfloods are expected to be more efficient in water wet rocks. Anderson (1986b) also reported that waterflooding in an oil wet reservoir is less efficient. However, there have been some experimental data published that disagree with these findings. Zhou *et al*. (2000) have found that recovery by waterflood increases with increasing aging time; where increasing aging time implies that the sample is more oil wet. Jadhunandan and Morrow (1995) have also found that as the sample changes its wettability from water wet to neutrally water wet, recovery by waterflooding increases. There are also other reports of better waterflood oil recovery from intermediate wettability compare to those that are oil wet or water wet (Moore and Slobod, 1956; Kennedy *et al*., 1955). Thus, there is some discrepancy in interpreting the results of waterfloods in different wettability systems.

With the exception of these few reports, such as that of Figure 3.18, most evidence seems to suggest better waterflood response in water wet systems. The differences in opinion are attributed to the lack of quantitative measurement of wettability using crude oil (Donaldson *et al*., 1969). Another possible explanation for these contradictory findings is that the characteristics of the porous media tested by the different researchers were not all consistent, or that wettability alone is not sufficient to determine the recovery from waterflooding. For example, for water imbibition in a well sorted homogenous rock, the response of a waterflood will be considerably different than for a rock containing a much higher aspect ratio between the pore bodies and throats. While wettability is a very important parameter, it is not trivial to correlate oil recovery directly to the degree of wetting, due to these other factors that will also influence the flood response.

For heavy oil waterfloods, Jennings (1966) reported that no difference was measured in the recovery profile for oil wet and water wet cases. It is possible that for heavy oil the effect of viscous instability and fingering masked the effect of wettability at the conditions that he studied. In a highly viscous oil, when water imbibes into a pore it must first displace the equivalent volume of oil out of that pore. Since oil flows more easily in larger pores (according to Darcy's Law), it is possible that in heavy oil systems water will take the path of lowest viscous resistance (i.e. the drainage pathway) independent of the wetting preference of the core. However, Anderson (1986b) presented data showing that even at high viscosity ratio, waterflooding of oil wet reservoirs is still less efficient. The differences in opinion could not be resolved due to the fact that unless these experiments are repeated, it cannot be determined which report is more trustworthy.

3.4.3 Wettability of Oil Sands

Oil sand reservoirs contain highly viscous heavy oil or bitumen in unconsolidated sand. The unique nature of these reservoirs makes it extremely difficult to obtain true measurements of the rock wettability. However, when considering mechanisms of oil recovery in heavy oil waterflooding, it is important to understand the location of injected water in these reservoirs.

The application of the Amott test for oil sand systems is questionable, due to the fact that heavy oil is highly viscous, so even if the core sample is strongly water wet, the production of oil due to spontaneous imbibition might be very slow. The time generally left for spontaneous imbibition is around 20 hrs (Anderson, 1986b). Thus, for the period of time imposed for spontaneous imbibition, very little oil displacement may have occurred and the core would be mistakenly shown to be neutral or oil wet. It is not clear how long the imbibition process should actually take in a heavy oil system; this will likely be a function of both the oil viscosity and the rock permeability (which will be present in both the capillary forces and will also govern how quickly oil can flow out of the system under only a capillary pressure differential).

Qualitative measurements of wettability (capillary pressure, spontaneous imbibition and relative permeability characterization) are also poorly defined in heavy oil systems. The pore sizes of unconsolidated sand are a function of the overburden pressure, and this will directly affect both the capillary pressure and the viscous flow rates that can be sustained in these cores. The high oil viscosity will lead to extremely slow imbibition rates, even in strongly water wet sands. Therefore, a common assumption made in heavy oil systems is that wettability effects and capillary pressure are negligible in relation to the viscous forces from the high oil viscosity.

It is commonly accepted that the oil sands in Alberta and Saskatchewan are water wet. However, Czarnecki *et al*. (2005) provides a review of the pertinent literature in this area, and turns up a surprising lack of conclusive evidence of this water wetting. It is known that sand as a mineral is hydrophilic, but the evidence for water wetting (i.e. an actual water film surrounding sand grains) is weak. One commonly referenced work is that of Clark (1944). In the hot water process for extracting bitumen (Clark, 1944), hot water that is added to oil sand can separate the bitumen from the sand. However, Czarnecki *et al*. (2005) explain that the electrical double layer forces generated through the addition of water may be responsible for the dislocation of the oil from the sand grains. Therefore, the fact that the hot water flotation process works does not definitely prove that water films are present in sand grains.

Takamura (1982) provided a theoretical analysis of attractive and repulsive molecular forces in oil sands. In his work, he proposed that oil sands are water wet, and that sand grains are covered with a very thin film of water (~ 10 nm thick), and pendular rings of water at grain-to-grain contact points. Based on this theoretical model development, Takamura suggested the following schematic for an oil sand structure.
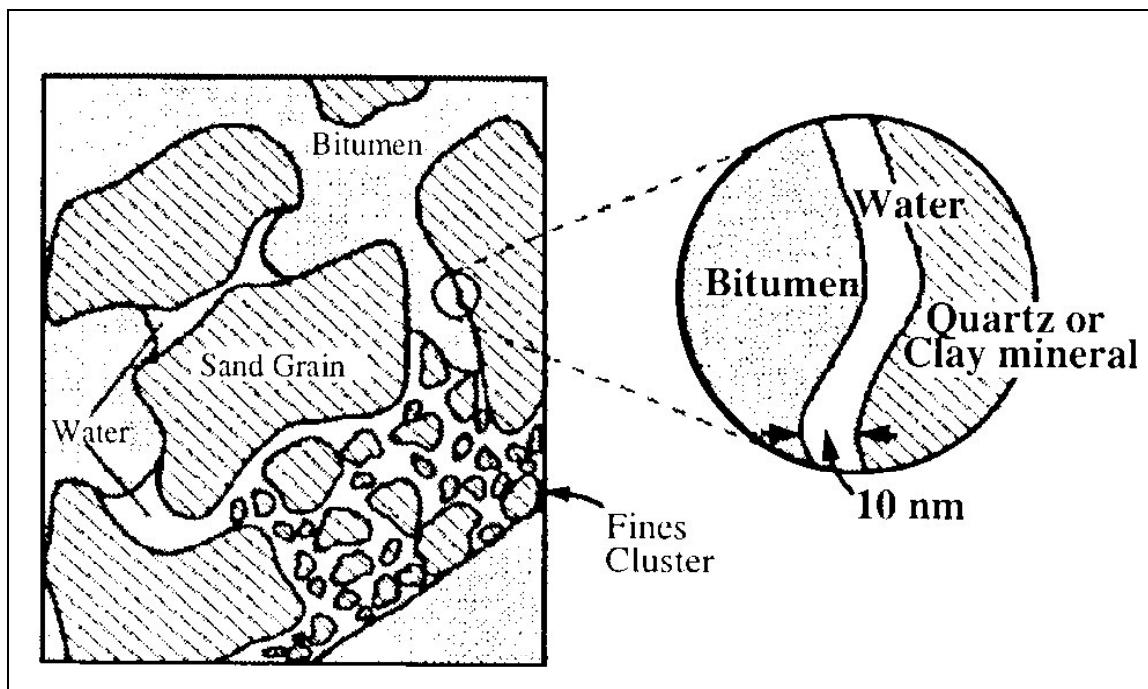
Figure 3.19: Schematic diagram of Athabasca oil sand structure
(from Takamura, 1982)

Figure 3.19 is commonly referenced as evidence of the water wet nature of the oil sands. However, it should be emphasized that this figure is only a schematic, suggested by theoretical calculations in a simplified system. Sobol *et al*. (1985) used NMR measurements in an attempt to provide a direct measurement of water films in oil sands. Two water relaxation times were measured: one signal at approximately 2 ms, and one signal at around 0.4 – 1 ms. Sobol *et al*. (1985) tentatively characterized the longer relaxation time as the contribution from pendular rings, and the faster time to be that of water films. Unfortunately, they were not able to relate these T_2 values to actual effective surface to volume ratios, so their conclusion could not be verified. In addition, it is unlikely that such similar relaxation times will correspond to significantly different water structures, as pendular rings should yield significantly longer relaxation times than thin water films.

Other indirect measurements have also been made to infer the wettability of oil sands. Carrigy (1962) provided an analysis of bitumen and fines content in oil sands, and showed that as the water wet fines fraction increased, the bitumen content decreases accordingly. Alternatively, Hum and Kantzas (2006) used NMR to measure water uptake in asphaltene coated sands, and concluded that in situations where asphaltenes have coated sand (as may happen in heavy oil systems) the sand may initially behave as if it were oil wet and will only gradually return to water wet conditions over extended periods of time in contact with water. This does not necessarily indicate that oil sands are not water wet, but does provide evidence of possible situations where the wettability may be altered to less water wet conditions.

In general, while it is generally accepted that sand is a hydrophilic substance, there is a distinct lack of conclusive information in the literature providing evidence for actual water wetting and water films in oil sands. Even if these water films are present, Takamura (1982) concluded that they would be so thin that they will not provide any hydraulic conductivity in transferring water through film flow. The evidence for water wetting of oil sands is therefore suspect, and more definitive experimental data is still required to prove that this condition actually exists.

3.5 Imbibition

Spontaneous imbibition is a process by which a wetting fluid is drawn into the porous medium by capillary action (Morrow and Mason, 2001). This process occurs when a porous medium that is initially filled with one fluid is immersed or brought in contact with a second fluid that preferentially wets the solid. In a water wet reservoir that contains oil and water films, imbibition refers to the process of water (the wetting phase) invading the porous medium. Therefore, waterflooding of a water wet reservoir is an imbibition process. Imbibition can occur either co-currently or counter-currently. In co-current imbibition, the direction of oil movement is in the same as that of water uptake while counter-current imbibition implies that water and oil moves in opposite directions (i.e. oil is produced at the same face as the injected water). Regardless of the direction,

the behavior of spontaneous imbibition of the wetting phase is consistent with near piston-like displacement (Fischer *et al.*, 2006).

Capillary pressure is the driving mechanism for spontaneous imbibition. Blair (1964) reported that a change in the capillary pressure caused a significant change in the time required to imbibe water and produce an equivalent volume of oil. However, the rate of oil recovery depends on many other factors as well, such as: fluid properties, the degree of rock wettability, initial saturations and boundary conditions (Cuiec *et al.*, 1994). The relative permeability to oil and water is a property of the rock, and should also be considered, although Blair (1964) found that changes in relative permeability curves induced very little change in the time required to imbibe a certain amount of water. Naturally, this observation relies on the assumption of similar oil and water viscosity, meaning that even if relative permeability changes water is still sweeping the entire porous medium and is not fingering through and by-passing continuous oil zones.

Conventionally, many studies on imbibition have focused on the imbibition of water into the rock matrix to displace gas or oil. The theory of these scenarios is discussed below. The nature of imbibition of water to recover heavy oil has not reported in the literature. However, the effect of oil viscosity has been mentioned in several publications. The main application for most imbibition studies is the recovery of gas or oil from fractured reservoirs (Bourbiaux and Kalaydjian, 1990). Since the network of fractures is usually poorly understood and each block produces independently from other matrix blocks, researchers often only study the behavior a single block surrounded by fractures.

3.5.1 Co- and Counter-Current Imbibition

A considerable amount of work in the literature has been devoted to counter-current imbibition due to the fact that the imbibition phenomenon in fractured reservoirs is usually thought to be counter-current. Pooladi-Darvish and Firoozabadi (2000) have observed that water does not instantly fill up the fractures, as was originally expected. Thus the recovery mechanism at early times is actually co-current imbibition until the

matrix block is fully surrounded by water. At this time, water can begin to invade from all faces of the rock, and the imbibition process becomes counter-current.

Co-current imbibition is the condition when the two opposing faces of the sample are open to flow. Water enters from one face, while oil is produced from the other face. Until breakthrough, oil has many pathways to flow out of the rock since the water front is behind the oil. At the point of breakthrough, as discussed previously in Section 3.2, only the oil ahead of the water is still continuous, thus the breakthrough point corresponds roughly to the final recovery that will be achieved by imbibition. Counter-current imbibition is a condition in which water and oil flow through the same face but in opposite directions. In order to directly compare against the co-current situation, the model for counter-current imbibition has all faces being impermeable except for one open face, through which water enters the core and oil flows out. In fractured reservoir applications, all four faces of the core are open to flow. Oil will be displaced by water imbibition into the fractures surrounding the rock matrix, and once in these fractures the oil can easily be produced based on its density difference with water.

Pooladi-Darvish and Firrozabadi (2000) calculated that under co-current imbibition, the boundary conditions applied lead to the generation of an oil pressure gradient over the length of the porous medium. As a result, the recovery rate of co-current imbibition is better than that of counter-current. In counter-current imbibition, oil must flow backwards in the direction of the water, which limits the number of continuous oil channels available and results in a slower rate. The oil may either flow in its own channels, or in the same channels as the invading water, in a two-phase flow regime. One important point to note is that the validity of the standard macroscopic equations of two-phase flow in porous media are not satisfied in counter-current imbibition due to the fact that relative permeabilities are only defined for fluids moving in the same direction (Bourbiaux and Kalaydjian, 1990).

There are two flowing periods in counter-current imbibition (Reis and Cil, 1993). The first period is called the infinite-acting regime, and occurs before the imbibition front reaches the end of the matrix block. The driving force for imbibition during this period is a fixed capillary pressure between the oil and water at the imbibition front. The second period is called the late-acting period, and occurs after the imbibition front reaches the end of the matrix block. The driving force for this period is the declining capillary pressure at the end of the matrix block. This is relatively small, which is why at late times imbibition occurs much more slowly.

3.5.2 Modeling Imbibition Rates in Water-Gas and Oil-Water Systems

Many attempts have been made to model the response of imbibition. One of the earliest attempts was Aronofsky and Masse (1958). From the laboratory data collected, they concluded that oil production rates could be fitted into the following form of an equation:

$$\frac{Q_o}{Q_\infty} = 1 - \exp(-\omega t) \qquad\qquad \text{Eqn (3.39)}$$

Where Q_o = cumulative oil production

Q_∞ = ultimate cumulative oil production

ω = a rate of convergence constant.

The main concern with this model is that ω is found empirically, thus this parameter had to be determined for each sample, which is very time consuming and also defeats the purpose of being able to predict the behavior of imbibition.

Mattax and Kyte (1962) later extended the scaling laws for waterflooding that had been developed earlier by Rapoport (1955), to model oil recovery by capillary imbibition. They identified a scaling group that takes into consideration different rock and fluid properties as follows:

$$t_D = \sqrt{\frac{k}{\phi}} \frac{\sigma}{\mu_w L_a^2} t \qquad\qquad\qquad \text{Eqn (3.40)}$$

Where t_D = dimensionless time

L_a = characteristic dimension of the matrix block.

This scaling group allows the imbibition response of any system of varying rock properties and dimensions to collapse into a single "S-shaped" curve where the recovery could be predicted.

Reis and Cil (1993) combined the scaling law of Mattax and Kyte (1962) with the model proposed by Aronofsky *et al*. (1958) to determine an expression for ω that is calculated based on the rock and fluid properties of a given system:

$$\omega = \frac{\sigma}{\lambda \mu_w L^2} \sqrt{\frac{k}{\phi}} \qquad\qquad\qquad \text{Eqn (3.41)}$$

Where λ = dimensionless empirical constant.

While this model no longer required ω to be obtained empirically, the problem was that it introduced another constant, λ. This constant depends on the petrophysical and fluid properties of the system. Thus, this model also could not be easily employed.

A significant effort was later devoted to modify Mattax and Kyte's expression to describe imbibition in any given system. The goal was to develop a general equation that could be used to describe both co- and counter-current imbibition through the definition of a characteristic length of a system, L_a. Various efforts have been made to define a characteristic length that properly describes the flow at various combinations of flow

paths (Zhang *et al*., 1996; Ma *et al*., 1997). The application of this equation was also studied for a weakly water wet system by Xina and Morrow (2001).

3.5.3 Modeling Imbibition Rates in Heavy-Oil Systems

A research of available literature provides no references for imbibition in heavy oil – water systems. However, there have been several imbibition experiments in the literature that involved higher viscosity oil, even though the range was still lower than that of heavy oil. Thus, these observations were noted to identify the effect of oil viscosity on imbibition.

Many researchers have agreed that the oil viscosity does in fact have some influence on the imbibition rate. Graham (1959) was the first to report that the rate of imbibition is a function of the viscosity of both the oil and water, and stated that the rate of water imbibition is inversely proportional to the viscosity of either fluid. Blair (1964) reported that the time required to imbibe a fixed volume of water into the same rock matrix is approximately proportional to the square root of the oil viscosity, provided that oil viscosity is greater than water viscosity. Therefore, as oil viscosity increases, imbibition rate will also decrease proportionally to the square root of the viscosity.

As shown in Eqn (3.40) the effect of viscosity could be incorporated into μ_m. However, there is no agreement between researchers regarding the mathematical representation of this effect. Ma *et al*. (1997) reported that imbibition time is proportional to the geometric mean of water and oil viscosity, which is:

$$\mu_m = \sqrt{\mu_o \mu_w} \qquad\qquad \text{Eqn (3.42)}$$

However, Fischer *et al*. (2006) have raised the concern that the use of the geometric mean of the oil and water viscosities was based on the experimental studies in a few select systems, and should not be used outside the range of the measurement conditions. Wang (1999) has proposed a different empirical correlation for the mixture viscosity as:

$$\mu_m = \mu_l^{3/4} \mu_g^{1/4} \qquad\qquad\qquad\qquad\qquad \text{Eqn (3.43)}$$

This correlation was found as a solution to the extreme difference in viscosity ratios for air and liquid, in which he noted that the imbibition rate would be dominated by the resistance to flow of the liquid phase. In extrapolating this theory to heavy oil and water, where the overall resistance to flow will reside in the oil viscosity, this correlation could be altered to:

$$\mu_m = \mu_o^{3/4} \mu_w^{1/4} \qquad\qquad\qquad\qquad\qquad \text{Eqn (3.44)}$$

This equation was generated under the assumption that for heavy oil - water systems, the oil viscosity is enormously greater than that of water, which is similar to the variability between water and gas. However, due to the fact that this equation was derived empirically, its range of application might still be limited. So far there has been no independent verification of these empirical models for a wide range of oil viscosity.

3.6 Summary

The distribution and flow of two phases in porous media are governed by Darcy's Law with relative permeabilities, and by capillary pressure. As a result, flow is controlled by fluid saturations and viscosities, and by rock wettability and permeability. Relative permeability and wettability can be measured with relative confidence in conventional oil systems, but in oil sands containing viscous oil in unconsolidated sand these measurements are non-trivial and laboratory data must be interpreted with a higher degree of caution.

In conventional oil reservoirs, waterfloods in water wet porous media are imbibition processes, whereby water invades the porous medium through the smallest pores and then progresses to larger pores upon increase of the water injection pressure. As a result,

water moves through the reservoir in essentially a piston-like fashion, displacing oil ahead of the water front. The result is that very little additional oil can be recovered after breakthrough, and the oil that is trapped behind the water front exists as discontinuous ganglia as defined by capillary forces. Waterflood recoveries and the potential for improved oil recovery can be interpreted in terms of the capillary number, which relates the viscous and capillary forces in a water wet system. There are many formulations of the capillary number available in the literature, but they all show that an increase in the relative magnitude of the viscous forces compared to the capillary forces will result in better oil recovery.

In heavy oil reservoirs, the mechanisms of oil displacement and trapping are considerably different than in conventional oil systems. Water is much more mobile than the oil, and as a result injected water will tend to finger through the reservoir, by-passing significant zones of continuous oil. Instability theory can be used to predict if a waterflood will be unstable, and it is shown that under adverse mobility ratio conditions at reasonable injection rates, waterfloods will always be unstable. Breakthrough recovery can also be predicted based on instability theory, although it appears that this theory is still not complete because different heavy oil systems respond differently to waterfloods, and as a result there are considerable errors in predictions of breakthrough recovery. Overall, however, it has been shown by several researchers that as floods become more unstable the breakthrough recovery will decrease accordingly.

Heavy oil systems respond uniquely to waterflooding, in that water breakthrough occurs very early in the life of a waterflood and significant oil can still be recovered after water breakthrough. In Chapter 2, the recovery mechanism proposed to explain this occurrence is that of water imbibition, which leads to slow recovery of oil at low applied pressure gradients. In order for this to occur, however, this means that oil sands must be water wet and imbibition rates must be significant despite the high oil viscosity. A review of the pertinent literature turns up a surprising lack of quantifiable evidence of the water wet nature of oil sands. Water wetting is generally assumed based on theoretical models and

field observations, and there is a considerable need for conclusive evidence of this wetting condition. Additionally, while imbibition processes are described in pure co-current versus counter-current systems and in rocks containing mobile fluids, there is no information available regarding how imbibition is expected to perform in a heavy oil reservoir. It is generally expected that in higher viscosity oils, imbibition rates should be slow. However, there is no single model available to predict these rates, and there is very little data available for imbibition in higher viscosity oils. The experimental work plan outlined and the data collected in these next chapters will attempt to address some of the gaps in the literature regarding imbibition in heavy oil systems.

CHAPTER 4: PROCEDURE AND EXPERIMENTAL METHODS

In order to study the relative significance of viscous and capillary forces it is necessary to perform experiments at different injection rates and with different oils in sands of varying permeability. Many experiments were conducted, whereby the parameters were all kept constant except for the one parameter being varied (injection rate, oil viscosity or sand permeability). The experimental work plan could be divided into two categories: the actual waterfloods and other tests to determine relevant parameters such as measurements of rock and fluid properties.

During the waterflooding experiments the temperature, pressure and produced fluids were collected. These parameters could give a production profile for each experiment, but they do not illustrate the mechanism of recovery. Thus, Nuclear Magnetic Resonance (NMR) was used to assist in the determination of the saturation and location of oil and water in the porous medium. Computerized Tomography (CT) scanning was also used show the invasion of water as the waterflood progressed. Special core holders had to be designed specifically to allow for NMR or CT measurements. Thus, prior to starting the experiments, the core sleeves had to be designed properly in order to obtain the desired results. Once the core sleeves were available, the sandpacks could be assembled. The properties of the sandpacks were evaluated for each waterflood performed. Along the course of the experiment the properties of live oil and dead oil were evaluated.

Waterflooding was performed on sandpacks saturated with gas-free oil and connate water (primary dead oil waterfloods) and on sandpacks that had previously undergone primary depletion (secondary waterfloods). The sequence of steps carried out is fairly similar for primary versus secondary waterflooding, however for larger sandpacks with primary production extra steps were required to prepare the cores for the state where waterflooding could begin.

In experiments where CT was used to monitor the displacement of oil by water, it is important to first calibrate the CT numbers to density and to choose the right dopant and its concentration. These had to be done prior to any actual core flooding. NMR measurements were additionally obtained, for two applications: to determine the oil and water content of the produced fluids in all of the waterfloods, and to determine the *in-situ* distribution of oil and water inside the porous medium in several select experiments.

Due to the fact that some of these sandpacks have a relatively low pore volume, it became a concern that the results might not be highly accurate. Thus, it was also necessary to perform some repeat measurements in order to assess the repeatability of the data and establish confidence in the results.

4.1 Design of Core Holders

In the most ideal case, the sandpack should be cleaned and reused to investigate the effect of a specific changing parameter without the added complexity of possible variations between cores. Also, the core holder should allow for overburden pressure to be applied, along with the capability for NMR and CT measurements. However, it is impossible to incorporate all these aspects due to fact that in order to satisfy one component (e.g. the ability to clean and re-use cores) the others must be sacrificed. In some cases new core sleeves were built, and in other cases the readily available core sleeves were modified to suit the goals of the experiments, and cores were re-packed in between floods. All of the core holders were constructed to investigate linear displacement, using a distribution plate on the injection end to ensure that water is injected into the entire cross-sectional area of the sand.

4.1.1 Small Aluminum Core Holder for Dead Oil Waterflooding Experiments

The design for this core holder includes an aluminum outer sleeve (aluminum bore) and an inner rubber sleeve with two end pieces to contain the actual sand. Sand was packed into the rubber sleeve, and overburden pressure was applied using nitrogen

between the rubber and the aluminum bore. The design of this core sleeve is shown in Figure 4.1.
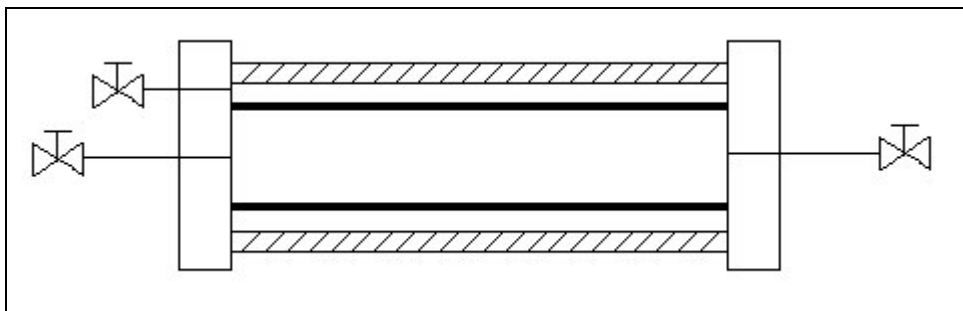
Figure 4.1: Design of aluminum core holder with a rubber sleeve

With testing, it was discovered that the overburden pressure could not be sustained initially, and nitrogen constantly leaked out of the system. The aluminum bore had been used many times before, and the interior of the metal contained many scratches and small pits. The overburden seal is provided by o-rings on the end caps of the core, acting against the internal wall of the tube. Thus the presence of the small pits and scratches on the bore wall made sealing impossible. The scratches were removed by the Machine Shop in the Chemical and Petroleum Engineering department at the University of Calgary, but the pits could not be removed by fill-ups, and the core continued to lose overburden pressure. A new end piece eventually had to be constructed in order to eliminate this problem. The new end piece is longer than the old end caps, and has slots for four o-rings instead of just two, which was designed such that even if there are still some pits in the aluminum bore, other o-rings will provide the seal for the overburden pressure. The addition of more o-rings serves to increase the area of contact between the o-rings and the wall of the borehole, and thus provides a better seal.

The overburden pressure that was applied to these cores was approximately 7,000 kPa (1,000 psi). This coreholder was used in many waterflooding experiments of dead (gas-free) oil systems at various flow rates. Since the bore was made of aluminum, the sandpack could be CT scanned throughout the waterflood. Again, it would have been

ideal to use the same sandpack in all these experiments, but unfortunately the rubber sleeve does not enable a solvent flush for cleaning the core since rubber is broken down by toluene. Therefore, a new sandpack was created for each subsequent waterflood. For each core, porosity and permeability was re-measured and the CT numbers were compared in order to verify that the rock properties were similar and the results of different core floods could be compared against one another. In this manner, an attempt was made to minimize differences between experiments.

In this aluminum core holder, twelve waterfloods were performed. The parameters varied were water injection rate and the oil viscosity. The permeability of the sand was kept relatively constant between experiments since the same sand and the same packing method was employed in these experiments.

4.1.2 Core Holders for Waterflooding Experiments Involving Saturation Using NMR

An additional series of waterfloods were designed to monitor the location of water and oil in the porous medium as the waterflood progressed. This core sleeve was very difficult to design due to many restrictions. Since the experiment was being performed inside an NMR, the material has to be non-metallic. TECAPEEK^{TM} is a high-performance plastic that is capable of withstanding high temperatures and pressures without melting or rupturing. This material was selected for construction of NMR core holders due to its inability to interfere with the magnet or electronic signals generated in NMR experiments. Another concern was the borehole of the NMR, which is only 5.08 cm (2") in one machine, and 4.45 cm (1.75") in the other NMR. The total diameter of the core holder obviously cannot be larger than the diameter of the NMR bore or the core holder cannot be placed into the NMR. This placed a limitation on the maximum size of the core, and the minimum size was dictated by the fact that NMR measures the response of fluid, thus in order to get an accurate measurement the fluid volume in the NMR has to be as large as possible. There was also another issue of the limited length of the region of magnetic homogeneity (the "sweet spot"), in the NMR. In the machines used in these experiments, the sweet spot is only 5 cm long, and only the portion of the core that is

inside the sweet spot was measured. The core could be longer, but it is desirable to measure the section that is most representative of the sandpack. This section should be in the middle of the sandpack since packing inaccuracies may lead to poor packing at the ends of the core. Therefore, considering that larger fluid volumes yield more accurate spectra and that the length of the measured volume is only 5 cm, the walls of the bore holder should be designed to be as thin as possible to hold the pressure while maximizing the pore volume in the sweet spot.

Even though it would have been optimal to apply overburden pressure to the cores so that they could be compared directly against the other waterfloods, the walls of the core holder had to be thick enough to withstand possible large pressure gradients induced during dead oil waterflooding, thus the space remaining for the actual core was reduced. As a result of this size limitation and the need to measure significant signal to get accurate spectra, experiments had to be done without overburden pressure.

Due to the fact that the oil is highly viscous, even if the injection rate is kept low, the pressure induced at early times (before water breakthrough) can still be quite significant. By setting a pressure limit, a minimum thickness of the core sleeve was calculated. The calculations of wall thickness were made using published values of PEEK tensile strength, and are shown in Appendix B. Based on the required thickness and the NMR borehole limit, the inside diameter of the sandpack was established. From previous work (Goodarzi *et al.*, 2007) one PEEK pipe (OD = 3.81 cm, ID = 2.6 cm) had already been constructed. It was decided that this pipe could act as an NMR-transparent core holder. When the pipe was packed with sand, this resulted in a core that was 53.2 cm long. Again, due to the design of this pipe, no overburden pressure could be applied to the core. For this longer core, NMR measurements could be taken at several positions along the core, to determine if water saturation changes with length from the injector to the producer. Three waterfloods at different constant injection rates were carried out in this long core. The sand was a sieved fraction of the sand used in other cores, thus the permeability in this core was the lowest of all the systems tested.

A difficulty that arose out of using the PEEK pipe as a core holder was that the threads connecting the end faces to the pipe walls were on the insides of the pipe. During sand packing, it became difficult to keep sand out of the threads, which would affect the sealing capabilities of the core. In the design of a second NMR-transparent core holder, another design issue was therefore that the threading of the end caps should be from the outside of the core sleeve, where sand could not deposit during the packing process. The final design of the core holder that was constructed is shown in the Figure 4.2.
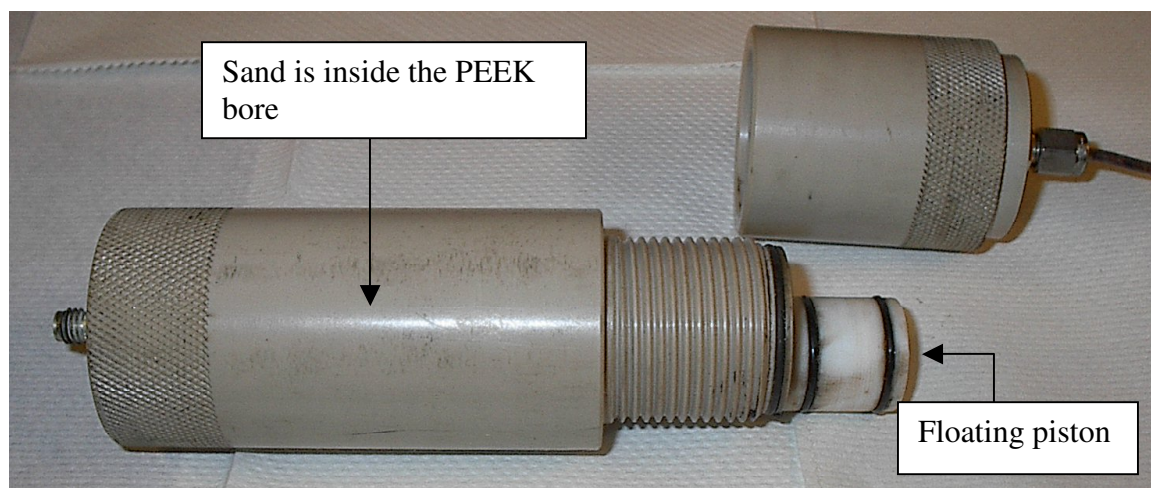
Figure 4.2: Design of PEEK core holder for NMR experiments

A final design element that was added to this new core was that of a floating piston (shown in Figure 4.2), placed at the edge of the sand so that when the lid was screwed on, it would further compact the sand to yield a tighter pack. This was designed to alleviate the problem of non-uniformity along the length of the sandpack. After wet-packing the core with sand and methanol, the core was leak tested to ensure that it could withstand the injection pressures in the system. No leaking was encountered for this core holder. The only negative result of this core holder design was the fact that the packing of the sand could not be compacted to the same degree as in other cores where overburden pressure could be applied. As a result, although the same sand was used as in cores with overburden pressure, the measured permeability to brine was much larger for this core.

Two experiments were performed on this core holder at distinctively different injection rates, using the same oil. The permeability of this core was the highest of all the cores tested due to the lack of overburden pressure.

4.1.3 Sand Pack in an Aluminum Sleeve for Dead Oil Waterflooding Experiments

In order to speed up the data collection, two additional waterfloods were performed using a core holder that was built using a PEEK borehole that has a setup similar to Figure 4.1. At first a rubber sleeve was used to allow for the same overburden pressure to be applied. However, after many attempts the end pieces could not be sealed with the rubber sleeve and nitrogen from the overburden consistently leaked into the core. By packing the sand into a thin-walled aluminum sleeve (thickness = 0.09 cm) and welding the aluminum end caps to the sleeve, this made it impossible for gas from the overburden to leak into the core. Since this new core sleeve material is resistant to toluene, the core could be cleaned between experiments and the effect of changing injection rate could be tested for the same porous medium. Unfortunately, the problem with using the aluminum sleeve was that the same overburden pressure could not be applied as for the cores with a rubber sleeve. Due to the rigid nature of the aluminum sleeve, tapping the sand as it settled did not transmit the same agitation as with rubber, thus it is possible that the packing was not as tight as in the core with the rubber sleeve. Additionally, the aluminum sleeve could not withstand a significant overburden pressure. For the thickness of the aluminum sleeve used (0.09 cm), the maximum pressure that it could withstand without deforming is about 2,500 kPa (400 psi). This was identified by CT scanning of previous cores, which were observed to have deformed under higher overburden pressure. For these experiments, therefore, overburden pressures of 2,070 kPa (300 psi) were applied, and it is not clear how much of this overburden pressure was actually transmitted to the core.

The core was cleaned in between experiments by flushing it first with toluene to remove any residual organic components, which could potentially have altered the rock

wettability if they were not removed. The core was then flooded with de-ionized water followed by acetone. The core was then dried, and its porosity re-measured. Finally, the core was placed under vacuum and saturated with brine, and its permeability to brine was measured. In this manner, the same sandpack could be re-used for other experiments. This condition is more ideal than preparing another sandpack, since two sandpacks can never be identical. It is important to note, however, that the properties of the sandpack were still evaluated before each experiment to prove that during the course of the previous experiment no change had occurred inside the porous medium. This was also necessary in order to ensure that the core had been properly cleaned and dried, and that there were no issues of plugging of the sand grains at the injection or production ports.

Two experiments were performed with this core holder at fixed injection rates with the same oil. Although the same sand is also used in these experiments, due to the lower overburden pressure the properties of the sandpacks are slightly different than the sandpacks prepared in the aluminum core holder.

4.1.4 Large Fiberglass Sandpacks

Three waterfloods were performed on full-diameter (8.89 cm) cores that were approximately 1.2 m in length. Due to the size of the cores, these systems were very difficult to pack and seal. In the first year of this project, multiple configurations for the core end caps were evaluated, but nitrogen from the overburden consistently leaked into the core. After many attempts, the final configuration consisted of sand being packed into a seamless rubber sleeve with special clamps designed by Mr. John Schnitzler of TIPM Laboratory, to provide the seal against the overburden pressure entering the porous medium through the end caps. The end caps were modified to include two o-rings to increase the contact area between the o-rings and the fiberglass borehole and provide more effective sealing. The core holder is similar to the schematic shown in Figure 4.1, except the aluminum bore is now replaced by fiberglass. The overburden is transmitted through the rubber sleeve to the sandpack inside the bore.

The sand was wet packed using acetone and the sleeve was tapped using a rubber mallet while sand was being added in order to dislodge trapped gas pockets and provide a tighter pack. However, the diameter of these sandpacks is much larger than the other sandpacks, thus the sand compaction is not as good as in the small cores packed in rubber sleeves. This is illustrated in the higher sand permeability of these cores, despite the fact that they were made using the same sand and were flooded under the same overburden pressure.

In the three large cores, sand compaction was achieved through two different means. When sand was first added, a rubber mallet was used to gently tap the sand along the length of the sleeve, which was also the procedure followed in preparing all of the smaller cores (in rubber, PEEK and aluminum sleeves). For the large cores, a vibrating agitator was also later attached to outside of the rubber sleeve to further enhance sand compaction. Even with such attention paid to properly packing the core, due to the long length of the sandpack, the cores still tended to sag in the middle when placed into the fiberglass bore. This causes the rubber to lift, thus eliminating the contacts between the o-rings and the rubber and allowing nitrogen from the overburden to enter the core. This problem was rectified by Mr. John Schnitzler through the addition of clamps pinning the rubber to the metal end caps to ensure that the rubber cannot lift up off the end caps. Additionally, water was injected into the space in between the rubber and the fiberglass to provide the overburden pressure. In these large core systems, water was chosen over gas for several reasons. First, due to the low compressibility of water, if there is a leak all the pressure would be lost in a short period of time. When nitrogen gas was used, a small leak would not be noticeable for a long time. Additionally, the manual clamp system design worked better in systems where the overburden fluid is not as effective as gas in entering the core. The overburden pressure applied in these large cores was approximately 7,000 kPa (1,000 psi), which was the same as the small aluminum core holder experiments.

Three large sandpacks were prepared. Two of these cores were saturated with live oil to undergo primary depletion, followed by secondary waterflooding of these cores. The

other sandpack was saturated with dead oil to perform a primary dead oil waterflood at this same length scale.

4.2 Packing, Testing for Leaks and Drying

As mentioned previously, all cores prepared in this thesis were wet packed with methanol. Methanol was chosen because of its ability to evaporate and thus dry quickly. The goal of wet packing is to yield a sandpack with uniform properties along its length – when the core is packed wet instead of dry, sand settling is enhanced and this should yield a more uniform pack. In addition, in order to avoid layering of the sand it was preferable for sand to be added all at once. This procedure was mostly followed, however due to the fact that it was not possible to identify the exact amount of sand to be added, in some cases additional sand had to be added in a second batch. While sand was being added, the sleeve was gently tapped to dislodge any trapped gas bubbles and allow for a more compact porous medium. Sand in rubber sleeve tends to pack tighter than sand in the aluminum sleeve, since rubber is much more effective for transferring the force during tapping. Also, for the larger diameter sandpacks, the sand grains are not packed together as tightly. This is due to the fact that for a smaller rubber sleeve more force could be exerted on the sand by the overburden than in the larger diameter rubber sleeve. After packing was completed, the core was placed into the bore and the core holder was assembled. Overburden pressure was then applied. In small sandpacks, nitrogen was used to provide the overburden pressure, whereas in larger sandpacks water was used instead.

At this point, leak testing was performed in order to ascertain that the core could be used in waterflood experiments. Primarily, it is important to establish that the overburden pressure does not leak into the porous medium or the surrounding. If overburden fluid is entering the core, a situation of two-phase flow occurs at this point and the experiment is no longer valid. Alternatively, if overburden fluid is lost to the surroundings, it is difficult to keep the core at a constant overburden pressure and again results between successive experiments may be difficult to compare directly. Leak testing was performed

by attaching the sandpack to a large pressure calibration tray that contained high accuracy pressure gauge (± 1 kPa). The overburden pressure was then monitored over at least a few hours to determine whether it was constant.

Once it was determined that a sandpack did not leak, it was CT scanned to determine that the density of the pack is fairly uniform with length. If the sandpack was not uniform, it would be removed from the core holder and re-packed. Once it was determined that a sandpack was uniform in density, it was then drained and dried overnight with compressed air at low pressure. Nitrogen was then flowed through the sandpack at low pressure for another day to remove any residual methanol. The sandpack was then CT scanned again to ensure that it is dry.   If the sandpack is not dry, further drying with nitrogen would be required, followed by an additional scan to verify that the core is dry. Failure to begin an experiment with a dry core would lead to underestimation of the pore volume of the sandpack if the sandpack, and possible barriers to flow.

4.3 Evaluation of Properties of Sandpack

The various properties of each sandpack were evaluated at different saturation states. Initially when the sandpack was dry, gas expansion was used to determine the pore volume of the porous medium. After the sandpack was saturated with brine, permeability to brine was determined. The irreducible water saturation was then determined by flooding the brine-saturated sandpack with oil at a fixed injection rate. Oil (and subsequent waterflood) injection was performed using a digital ISCO pump and a piston cylinder either containing oil or brine.

In addition to these parameters, it would have been ideal to determine the wettability and capillary pressure curve for each sand-fluid system. However, as previously discussed in Chapter 3, determination of these properties is not trivial in unconsolidated sand, heavy oil systems.

4.3.1 Pore Volume Determination by Gas Expansion

Pore volume of the core was determined for the dried sandpack using a gas expansion apparatus. This method relies on the Ideal Gas Law, and uses the following relationship:

$$P_1 V_1 = P_2 V_2$$

Eqn. (4.1)

Where P_1 = ambient pressure

V_1 = pore volume

P_2 = elevated pressure

V_2 = the gas volume measured at the elevated pressure.

By measuring the volume of gas injected at a fixed injection pressure, the pore volume can then be calculated. In this equation, both V_1 and V_2 contain the contribution of the dead volume (the volume in lines and valves) of the system. Therefore, these volumes have to be removed in order to properly calculate the pore volume.

In these cases the compressibility factor for gas could be ignored because the pressure employed is always less than 35 kPa (5 psi). A schematic of the apparatus that was used is shown in Figure 4.3.

The experimental procedure for measuring pore volume by gas expansion is as follows: nitrogen was injected into the porous medium until the pressure inside reached close to 35 kPa (5 psi). The sandpack was then isolated by closing all the connecting valves and allowing pressure to reach equilibrium. This is a relatively fast process for cores that are porous and is slower for tighter cores – for unconsolidated sandpacks pressure equilibrium is reached within 10 minutes. Once equilibrium had been reached, the nitrogen existing in the porous medium was allowed to expand. As the gas expanded, it displaced water in a chamber attached to the outlet end of the core. The water was collected and the volume of displaced water is the gas volume at P_2 (35 kPa). The

pressure in the core holder was also noted, along with the daily value of the atmospheric pressure.
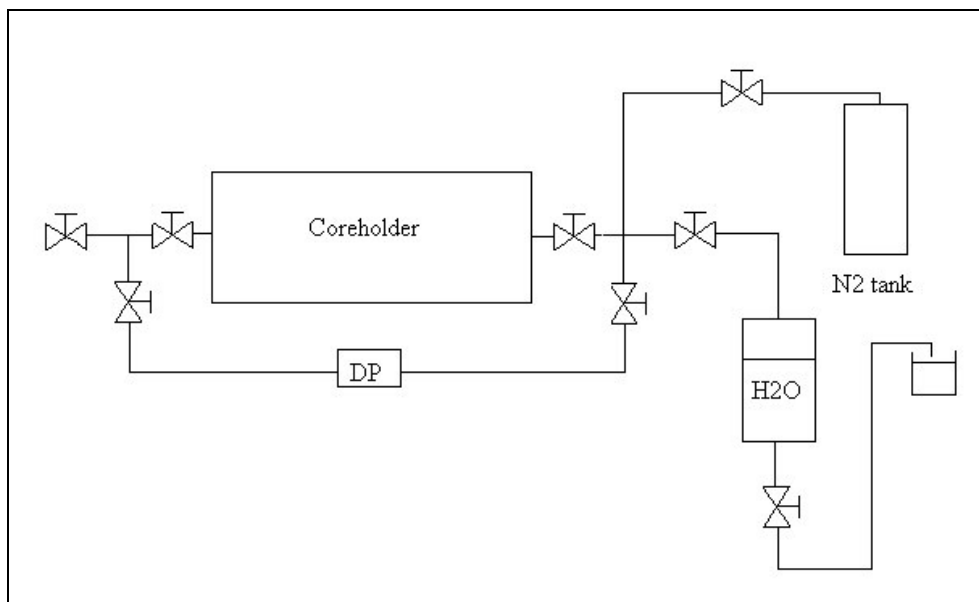
Figure 4.3: Gas expansion apparatus

Using the ideal gas law (Eqn 4.1) the pore volume could then be determined. This same procedure would be repeated three times at approximately the same pressure to ensure that the results were repeatable. As mentioned previously, the volume obtained actually included the pore volume as well as the volume contributed by the inlet and outlet lines.

The dead volume could be approximated by measuring the length and knowing the inside diameter of the lines and fittings, and then calculating their volumes. Once pore volume is known, porosity is calculated as the ratio of the pore volume (with the dead volume subtracted) to the total volume of the core. The calculations of pore volume and porosity are shown in Appendix C.

4.3.2 Brine Permeability

In order to determine the permeability to brine, the sandpack first had to be saturated with brine. This was done by placing the dry sandpack under vacuum for at

least 12 hours, after which point the sandpack was placed in contact with a brine reservoir. Since the core was initially under vacuum, brine was sucked into the core without the formation of any trapped gas pockets. The duration of this saturation stage depends on the size of the sandpack: for small sandpacks an hour was allocated and approximately a day was required for the big sandpacks. After the allotted time for saturation, the outlet of the core was opened and water would instantly be produced. In this manner, it was verified that the cores had indeed been fully saturated with brine.

Darcy's Law was used to estimate the permeability of the sandpack. Brine was injected through the sandpack at four different rates and the corresponding pressure drop across the sandpack was collected. Initially, a pump was used to inject brine at the desired rate, and a digital gauge situated at the inlet was used to record the inlet pressure. The permeability values calculated were poor when comparing the permeability value calculated per trial. The reason is that for small sandpacks with high permeability, the required injection pressure is extremely small, thus even for the lowest range of pressure gauge available (0 – 103 kPa) the equipment was not sensitive enough to detect the true pressure drop. Also, since the pressure drop is so small, any inaccuracies in the calibration of the digital gauge would be magnified. The procedure was then modified for small sandpacks utilizing head pressure of the brine column instead. This brine column is relatively large compared to the pore volume of the sandpacks. At each height of the brine column, the brine was allowed to flow through the small sandpack for 7 – 10 minutes, after which the flow rate of brine was measured by the produced brine collected over a certain period of time (two minutes for the porous sandpacks and three minutes for the tight ones). The height of the brine column before and after flow for each trial was also collected to account for differences in head pressure, although it was noted that they barely change for the small sandpacks due to the small volumes of brine flowing through the sandpack in each trial. In order to minimize any experimental errors, the average heights were used in the calculation of the head pressure. A schematic of the apparatus that was used in these measurements is shown in Figure 4.4.

For the large 1.2 m long, full diameter sandpacks, the pressure drop required is more prominent thus it was possible to use a pump to inject at the desired flow rate. A fixed flow rate of brine set using a digital ISCO pump and brine was injected through the core at this flow rate. The pressure drop was monitored until it reached equilibrium.
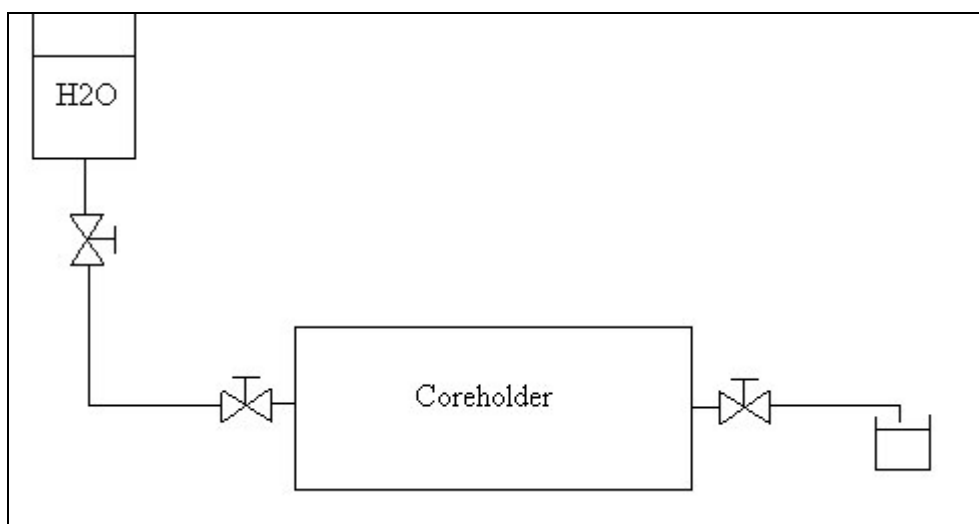
Figure 4.4: Apparatus of brine permeability evaluation using head pressure

Usually, when the pressure drop did not change for approximately half an hour, it was assumed that equilibrium had been reached. The flow rate of brine and the corresponding pressure drop were then recorded. This process was repeated for four different flow rates and permeability was calculated from the plot of (Q/A) vs. ΔP/L. The slope of this plot is equal to (k/μ_w), thus with the known viscosity of water permeability could easily be determined. The calculations for brine permeability of all sandpacks are shown in Appendix C.

4.3.3 Irreducible Water Saturation

In order to correctly quantify the amount of oil recovered through waterflooding, it is important to determine the irreducible water saturation at the beginning of the waterflood. This condition is achieved by flooding the water-saturated sandpack with several volumes of oil at a specific injection rate. The total amount of oil injected is

based on the pore volume of the sandpack. For small sandpacks, approximately five pore volumes of oil were injected. However, for large sandpacks only two pore volumes of oil were injected due to the lack of such large oil volumes. This decision was made based on the observations seen first in small sandpacks, which showed that after around two pore volumes of oil injection essentially all the water had already been displaced due to the good mobility ratio between heavy oil and displaced water.

The produced fluids from the oil flood were then collected and separated to obtain the volume of brine produced. Since the oil is quite viscous and the products contained a large quantity of oil, the separation process is quite extensive. At first the products were all collected in a single beaker and toluene was added to this beaker to reduce the oil viscosity and density, and facilitate water separation. This proved to be a difficult task since a large quantity of toluene was needed to properly dilute the oil. In order to coalesce the water droplets, the mixture of water, oil and toluene must be mixed thoroughly, so after toluene addition the mixture was manually agitated. When the ratio of toluene to heavy oil was too low, this agitation simply served to emulsify the oil and water, and accurate separation was difficult to achieve. Early separation trials severely underestimated the brine volume produced, which yielded an incorrectly high S_{wi}. As a result, the collection and separation process was modified to collect the products in three separate beakers.

The first beaker was used to collect the produced fluids until just after oil production was observed. Separation of this product is relatively easy since there is very little oil. The second beaker then collected an oil and water mixture for another two pore volumes of oil injection. A significantly volume of toluene was added to this mixture and the mixture was left to sit in a separation funnel placed in a fume hood for several days in order to allow enough time for the water to drop out. The last beaker was used the remaining oil produced. Even with toluene addition and long waiting times, little to no brine was recovered from this beaker. Based on this approach, it was concluded that in large cores, fewer pore volumes of oil injection are required to reach S_{wi}.

Once the correct volume of produced water is known, the irreducible water saturation is obtained in the following equation:

$$S_{wi} = \frac{PV - {m_{Tw}}/{\rho_w}}{PV}$$

Eqn (4.2)

Where PV = pore volume of the sandpack

m_{Tw} = the total mass of water collected from separation

ρ_w = density of water.

The calculations of irreducible water saturations are shown in Appendix C.

4.3.4 Measurement of Wettability

Wettability measurements are generally made using contact angles (Anderson, 1986b; Rosen, 1989), measurements of the shape of the capillary pressure curve, and determination of the crossover point in relative permeability curves (Dullien, 1992). Unfortunately, for unconsolidated porous materials containing viscous oil, wettability measurements are non-trivial to make with any degree of certainty. This was previously discussed in Chapter 3.

In unconsolidated, porous sand, contact angles cannot be made accurately. The sand must first be saturated with one phase and then placed in contact with the second phase. Depending on the wettability, some fluid may soak into the porous sand grains, thus any contact angles measured may not be representative of the true wetting condition of the rock. Additionally, when one of the fluids is viscous heavy oil, any water that imbibes into a given rock pore must first displace oil out of the pore, and this will only happen slowly. As a result, wettability tests such as spontaneous imbibition cannot be measured accurately since the imbibition rate is extremely slow. Finally, inferences of wettability based on the shape and crossover point in relative permeability curves cannot be applied

in heavy oil systems, due to the unstable nature of heavy oil waterfloods and the difficulty in measuring the true heavy oil – water relative permeability. Therefore, conventional measurements of wettability cannot be applied in heavy oil/unconsolidated sand systems.

In this work, wettability was only inferred qualitatively by placing water in contact with oil-saturated sand and observing the formation of an oil layer on top of the water. Additionally, measurements were made based on NMR spectra of samples during oil saturation and waterflooding. Details of these methods are presented in Chapter 9. No attempt was made to quantify observations to calculate degrees of wettability of the sand used.

4.3.5 Capillary Pressure Curve

The general methods of determining the capillary pressure curve (e.g. porous plate or centrifugation) could not be used in these experimental systems. It is not possible to apply these methods for unconsolidated porous media. Additionally, in unconsolidated porous media the pore size distribution is a function of the overburden pressure, thus experiments performed at ambient condition are not representative of the conditions during waterflooding. Due to these difficulties, there was unfortunately no attempt made in this study to obtain the capillary pressure information of these systems.

4.4 Evaluation of Dead Oil and Brine Properties

Various properties of gas-free oil were evaluated at ambient temperature (23°C). The properties of interest are the oil density, viscosity, presence and fraction of emulsified water existing in the dead oil supplied by BP and Nexen Inc., and interfacial tension between oil and brine.

The density of both dead oils and brine was measured at room temperature using an Anton Paar DMA 45 digital densitometer with a built in thermostat. Before the density of oil could be measured the densitometer first had to be calibrated with water at the same

temperature. Viscosity of oil was measured by the Wells-Brookfield cone and plate viscometer with a CP51 assembly. This assembly has a cone with a diameter of 12 mm and an angle of 1.5°. The shear rate was increased from 0.8 s^{-1} to a maximum of 100 s^{-1}, and the resulting change in shear stress was digitally output. Viscosity can then be calculated as the ratio between shear stress to shear rate. The viscosity of the injected brine was not measured directly in this work. The viscosity of water is a well-documented property (Heidemann *et al.*, 1987), and even if viscosity increases slightly due to the presence of salt in the brine, water viscosity will still be many orders of magnitude less than that of the oil thus small changes in water viscosity due to salt addition will not have any impact in the viscosity terms of the mobility ratio.

The presence and amount of existing water in oil emulsions was measured by using the NMR. Emulsions are small droplets of water existing in oil, which may be stable due to the high oil viscosity that prevents droplet coalescence. Due to the viscosity difference between oil and water, the signals of these fluids are distinct in NMR spectra even for emulsions that are not visible to the naked eye. A description of the NMR technique will be presented in Section 4.10.

The interfacial tension between water and oil was measured using a Krüss SITE04 Spinning Drop Interfacial Tensiometer. This technique is based on placing a small drop of fluid of lower density into a tube filled with a second fluid of higher density. When the tube is rotated at high velocities, the centrifugal forces present keep the lower density oil in the center of the tube, and the oil droplet stretches. The degree of stretching is a function of the interfacial tension between the oil and water (Vonnegut, 1942; Mannhardt, 1987). For the system used in these tests, interfacial tension is calculated from the following expression (Mannhardt and Kantzas, 2004):

$$\gamma = 3.427 \times 10^{-7} \Delta\rho (fd)^3 n_r^{\ 2} \qquad\qquad \text{Eqn (4.3)}$$

Where γ = interfacial tension between oil and water

Δρ = density difference between oil and water

f = calibration factor

d = drop diameter

n_r = angular velocity.

The interfacial tension measurements performed in this study were made by Ms. Xiaodong Ji of TIPM Laboratory.

A difficulty arose in making interfacial tension measurements due to the similar oil and water densities. In order to measure these values, it was necessary to dilute the oil with varying amounts of n-octane, following the procedure outlined by Schramm *et al*. (2003). After dilution of the oil, the density contrast was sufficient enough to obtain reasonable values of the oil-water interfacial tension.

4.5 Evaluation of Live Oil Properties

Live oil was used in two experiments in the large sandpacks. In order to generate this oil, gas-free oil was mixed with methane at elevated pressures. The properties of this live oil were then evaluated. The properties of interested are the solution gas-oil-ratio (GOR), density and viscosity.

4.5.1 Live Oil Mixing

Live oil was prepared by mixing methane with dead (gas-free) oil at elevated pressure. Initially, oil was poured into the mixing chamber. A methane tank was then connected to the mixer. The gas tank was regulated to provide methane at a pressure of approximately 4,830 kPa (700 psi) to allow a continuous injection of gas into the mixer. The mixer has a magnetic drive pump that could circulate the gas-oil mixture at elevated pressures, thus allowing methane to dissolve into oil. Gas was continuously provided to the mixing chamber for approximately one week, during which time gas was dissolving into the oil and more methane was constantly available. After this period, the gas supply was cut off with the mixer still active to allow for more mixing. If the pressure in the

mixing chamber declined, it was known that the oil was not saturated with methane, and more mixing would be done with the methane supply back on. This procedure was repeated until the oil was mixed with no pressure loss after the gas supply had been turned off. At this point, the gas-oil-ratio of the mixture was measured. The procedure for measuring GOR is described below. The GOR of the oil mixture was monitored over a few days to make sure that it had reached equilibrium. However, in the event that GOR would decrease with time, once again implying that the oil was not yet saturated, more methane would be supplied to the system and the process of evaluating the equilibrium would begin again.

4.5.2 GOR Measurement of Live Oil Mixture

The GOR of the live oil mixture was evaluated by using the apparatus shown in Figure 4.5.
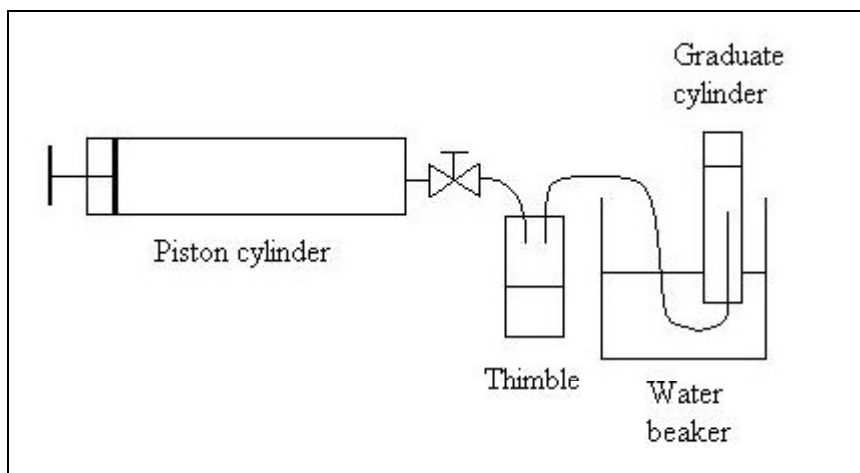
Figure 4.5: Apparatus of a live oil mixing assembly

A live oil sample was extracted from the mixing rig into a small piston cylinder that is essentially a high pressure syringe. The small piston cylinder was then connected to the GOR measurement apparatus. The live oil was displaced into a thimble that is connected to an inverted water column. Once the live oil enters the thimble at ambient pressure, methane will immediately leave the oil solution. This free gas that is produced was

allowed to flow out of the top of the thimble and displaced water in the inverted water column. The volume of gas in the oil was read using the scale on the graduated cylinder in the inverted water column. At least 15 minutes was allowed for the gas to be totally liberated from the oil mixture. The amount of oil was then determined as the mass difference between the empty thimble and the thimble full of oil. From this apparatus the total amount of gas-free oil and the liberated gas could be measured to determine the GOR. For GOR measurement, three consecutive samples were run in order to determine the repeatability of the apparatus. The calculations for GOR are shown in Appendix D.

4.5.3 Density of Live Oil

To measure the density of live oil a simple method was employed. A tube of fixed volume and known weight was used. The fixed volume was determined from the knowledge of the length and the inside diameter of the tube, and could also be calibrated by filling the tube fully with water of known density. The volume of the tube (V_{tube}) is determined first by this simple equation:

$$V_{tube} = \frac{m_{water} - m_{initial}}{\rho_w} \qquad\qquad \text{Eqn (4.4)}$$

Where m_{water} = the mass of the tube filled with water

$m_{initial}$ = the initial mass of the tube at dry condition.

Once the tube volume was accurately determined, the tube was dried and its mass was re-measured to ensure that all the water had been removed. The tube was then positioned vertically, and live oil was injected to the bottom of the tube. The live oil was injected at pressure higher than the bubble point to ensure that the live oil in the tube did not separate into two phases. Naturally, since the tube was initially at ambient pressure, some gas will immediately leave solution with the oil. Therefore, live oil was injected to completely fill the tube, and then some additional live oil was injected to displace any oil out of the tube that could have a low GOR. The total mass of the tube full of live oil was

then obtained. The live oil density is then simply is obtained by mass difference divided by the fixed volume. After each measurement the tube was disconnected, cleaned with toluene to remove all the oil and then dried with acetone and compressed air. The apparatus was then assembled again and the initial weight was obtained. For each batch of live oil, density measurements were performed three times. Calculations are shown in Appendix D.

4.5.4 Viscosity of Live Oil

The viscosity of live oil was measured by injecting live oil through coiled-tubing at various injection rates. Hagen-Poiseuille's Law (Boyle, 1986) was used to determine the viscosity of the live oil. The apparatus is shown in Figure 4.6.
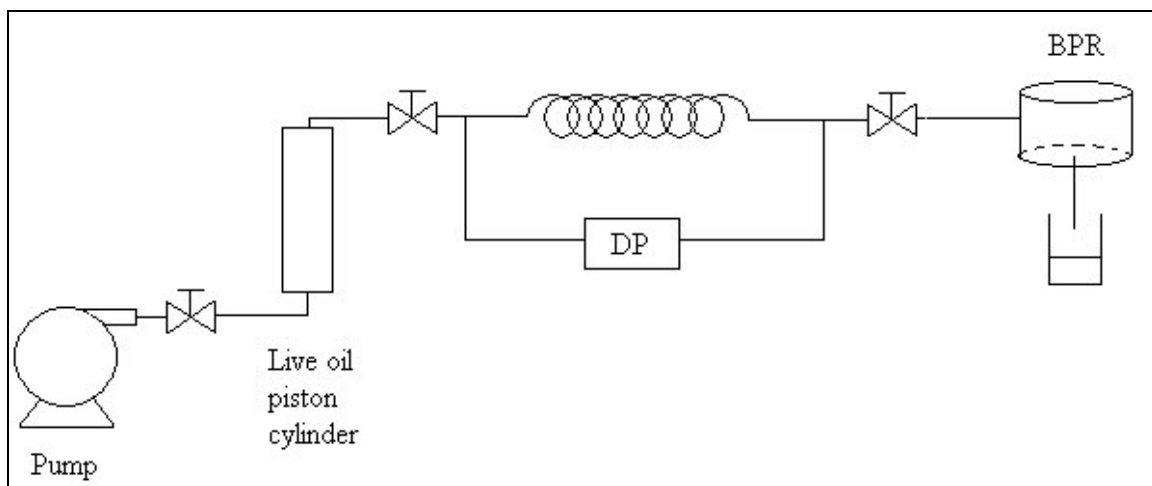
Figure 4.6: Schematic diagram of a high pressure capillary viscometer

A digital ISCO pump was used to inject water onto the bottom of a piston cylinder containing live oil. As water entered the bottom of the cylinder, it displaced an internal piston that transferred live oil at the same fixed injection rate into a long coiled tubing. The differential pressure for each flow rate was measured using a 3,450 kPa (500 psi) Validyne differential pressure transducer. A back pressure regulator (BPR) was attached at the outlet and set at a slightly higher pressure than the mixing pressure of the oil, in order to ensure that the fluid flowing through the coiled tubing was single phase.

In order to measure the oil viscosity, live oil was injected at various fixed flow rates above the bubble point pressure. The oil travels through the coiled-tubing of known length and the pressure drop across the tubing was measured. Hagen-Poiseuille's Law can then be re-arranged to determine oil viscosity:

$$\mu = \frac{\pi D^4 \Delta P}{128 Q L}$$
Eqn (4.5)

Viscosity was calculated from Eqn (4.5) by plotting (Q/A) vs. $\Delta P/L$ for four flow rates, from which the slope is equal to $(R^2/8\mu)$. The calculations of live oil viscosity are shown in Appendix D.

4.6 Primary Depletion

Initially the sandpack was saturated with live oil at irreducible water saturation. The pressure of the sandpack was also set higher than the bubble point pressure by connecting the production end of the core to a BPR. The apparatus primary depletion is shown in Figure 4.7.

The apparatus included two BPR's set in parallel at the core outlet, in order to control the pressure in the core. Two parallel BPR systems were used in case any sand was accidentally produced during primary production, which could plug the BPR and cause a loss of pressure control in the core. The BPR pressure was reduced through two gas cylinders containing high pressure nitrogen, which were connected to a mass flow controller. The mass flow controller was used to withdraw gas from the two cylinders at a fixed rate, which reduced the pressure exerted on the BPR. Since the BPR was connected to the production end of the core, this effectively depleted the pressure at the core outlet at the same fixed rate. The pressure depletion rate was chosen to be 145 kPa/hr (21 psi/hr). The outlet end was also attached to a collection system.
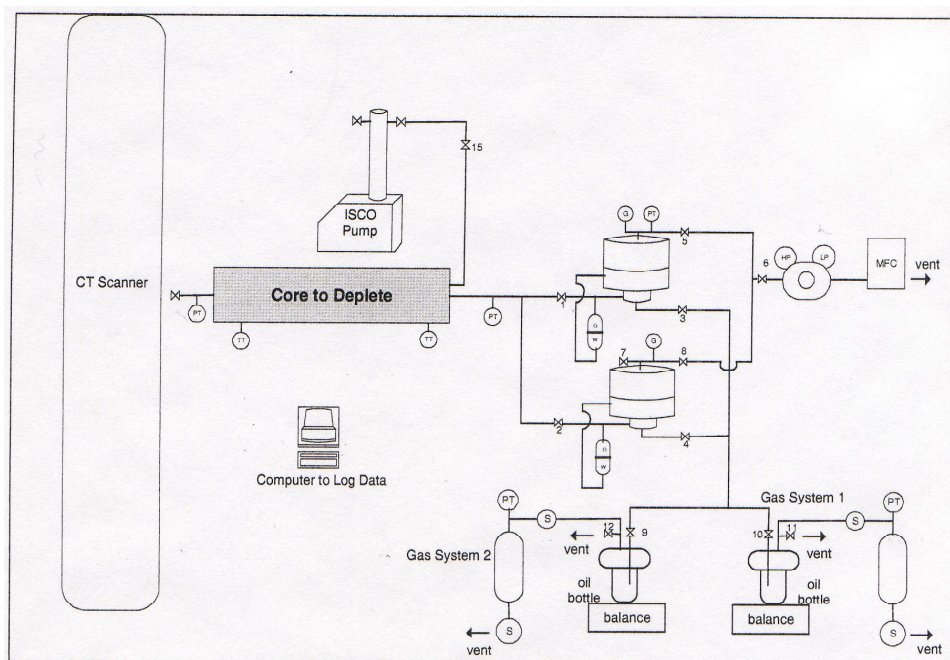
Figure 4.7: Setup for primary depletion
(from Goodarzi, 2006)

As the pressure inside the BPR dropped, the pressure at the outlet correspondingly declined. If the pressure inside the sandpack was larger than the pressure at the outlet, fluids would be produced. The produced fluids, which consist of both oil and gas, were collected in a closed system at ambient pressure. Gas left solution, and the pressure increase in the collection vessel was monitored and used to calculate the volume of gas produced. In order to allow for constant production without a back-pressure building up in the collection vessels, a limit gas pressure was set for this cylinder through an automatic valve, this was designed to open when the pressure in the collection vessel exceeded the set point. When this happened, the free gas was vented and the pressure in the cylinder before and after venting was automatically logged in the data acquisition software. At various times the oil container was disconnected to record its cumulative weight, so discrete values of gas and oil production were measured over time. Each time the produced fluid masses were measured, production was switched into a parallel collection system before the oil container could be detached, so that during the time the

measurement is being taken, production is not disrupted. Details of the procedure for the depletion experiments have previously been described by Goodarzi (2006).

An automatic data acquisition system was used to log various important parameters during depletion. Several pressures were recorded: the inlet pressure, the outlet pressure, the pressure of the BPR, and the pressure of the gas cylinder connected to the production vessel. The time and pressure was also logged at each automatic purge of the gas pressure, which allowed for accurate accounting of the amount of gas produced. The gas saturation remaining in the core was then known by difference from the volume of live oil injected and its GOR, compared to the volume of produced gas.

The calculation of oil and gas production rates is shown in Appendix E.

4.7 Dead Oil Waterflood

The majority of waterfloods performed in this thesis were primary waterfloods, carried out in systems containing dead (gas-free) oil and irreducible water. At the start of these experiments the core had been flushed with several pore volumes of oil in order to displace water to S_{wi}. Prior to starting the waterflood, the inlet line first had to be flushed with brine to remove any oil existing in this line, or additional oil would be entering the core and the recovery calculated would be higher than the true value. After this was done, brine was then injected into the porous medium at the set rate. The apparatus for waterflooding is quite simple, as shown in Figure 4.8.

A digital ISCO pump was used to inject brine at a fixed rate. It is not desirable to fill the pump with salt, since from previous experiences in the laboratory, when brine is stored within the pump for a long period of time the brine would shrink the seals inside the pump and cause it to leak. In these tests, therefore, the pump injected de-ionized (DI) water into a piston cylinder, which contained doped brine on the other side of the piston. The injected DI water then pushed the piston inside the cylinder to transfer the force to the doped brine, thus brine was injected into the sandpack at the same set injection rate.
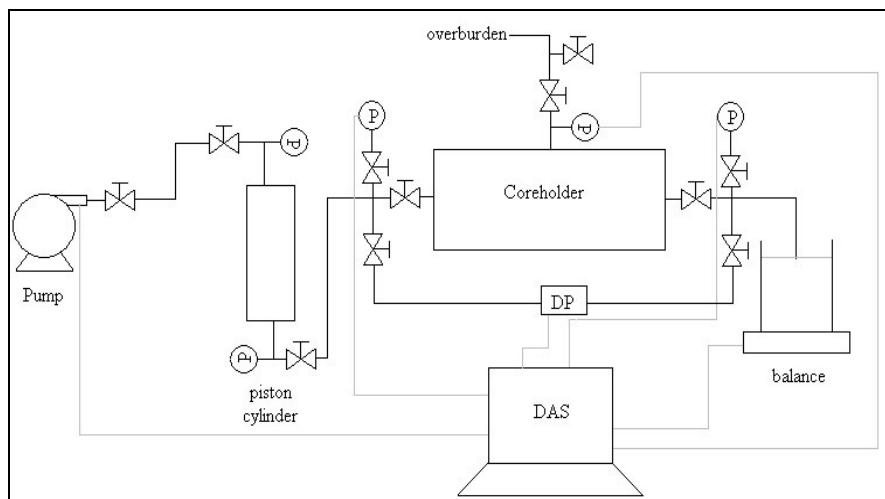
Figure 4.8: Schematic diagram of the experiment set up for dead oil waterflood

During the injection process the pressure at the inlet and outlet were monitored using a Measurement Specialties Inc. (MSP 600 series) gauge pressure transducer, which has an error bar in its measurements of ± 0.25% of its full range. For these waterfloods the transducer used has a range of 172 kPa (25 psi), thus the accuracy of the transducer is ± 0.43 kPa (0.0625 psi). Differential pressure across the core was also measured using a Validyne differential pressure transducer, although it was later discovered that after water breakthrough the pressure gradient in the core was too small to be measured using the differential pressure transducer with the range available in our laboratory. The produced fluids were collected either in beakers (for separation) or Nalgene vials (for NMR measurement). A data acquisition system was used to record the pressures and the cumulative mass of produced fluids.

Oil was not immediately produced as brine was injected. Rather, the pressure at the inlet would build up to a certain pressure before oil was produced. The period of single phase production of oil is very short; afterward water breakthrough occurred and a mixture of oil and water was produced at high water cut. The products were collected and measured through NMR and separation with toluene to obtain the oil and water content. In cases where the pore volumes of the porous medium are small, the fluids are collected in small vials and the content was determined through NMR. For large sandpacks, the fluids are

collected in beakers or 250 cm³ Nalgene bottles, and the amount of oil and water produced was determined by separating the fluids with toluene.

4.8 Secondary Waterflood

At the end of primary production, the dissolved gas in the live oil had been liberated and any gas that was not produced would occupy the space of the produced oil. Further water injection was then performed at ambient pressure.

Prior to the secondary waterflood, various components of the apparatus attached during primary depletion had to be removed. The mass flow controller and its associated parts were disconnected along with the extensive collection system. In secondary waterflooding, once water had traveled through the gas pathways the system was expected to behave similarly to a dead oil two-phase system after water breakthrough. Therefore, there was no more need for the extensive collection system that monitored produced gas and oil fractions. Rather, a simple collection bottle was connected to the outlet of the core. The new collection bottle was a 250 cm³ Nalgene bottle with a fitting drilled into the lid to connect the bottle to the core outlet. The bottle was kept covered in order to prevent evaporation of brine during the production. Samples of the produced oil/water mixture were taken periodically and separated with toluene, at a sampling frequency that depended on the injection rate used.

A total of four secondary waterfloods were performed. Two were done on the large fiberglass sandpacks that were primary depletion. The other two were obtained from Nina Goodarzi from her M.Sc. work.

Overall, the equipment required for a secondary waterflood is similar to those in primary dead oil waterfloods. The only difference is that the collection bottle for secondary waterflood is larger due to the larger pore volume of these sandpacks. The content of the collection bottle were separated to determine the masses of oil and water produced. For the large sandpacks, NMR measurements of the produced fluids were not obtained.

4.9 CT Scanning

Each fluid or solid has a CT number (CTn) value that is directly proportional to effective atomic number and to density. In this manner, CT scanning provides an indication of the density of the sample being measured (Vinegar and Wellington, 1987; Kantzas, 1990). The total density of a sample is the summation of the contribution from the rock and fluid components. Thus, if density contrasts between different fluids such as oil/water or oil/gas can be identified, CT scanning can be used to measure the *in-situ* fluid saturations in a core.

All CT scanning for this project was performed using a third generation General Electric CT/i scanner. In this machine, both the x-ray source and the detectors rotate together around the object. CT scans were taken at a setting of 120 kV and 120 mA. The resolution of the measurement is 0.049 cm x 0.049 cm x 0.03 cm. CT images were cropped and analyzed using software developed internally at TIPM Laboratory.

Prior to scanning of the sandpacks, standard samples were scanned to establish a calibration between density and the CTn. Due to the similar density between water and brine, their CTn values will be very similar, thus for fluids in porous media it is not simple to separate the oil and water contributions. Therefore, one phase also had to be doped in order to establish a CTn contrast between water and oil. The sandpacks were later scanned at various stages of the waterflood.

4.9.1 Calibrations of Standards

Liquids and solids samples of known density were scanned at ambient temperature and pressure to establish a calibration curve. This is required for any CT scanner used, and without this calibration it is not possible to quantify the data from the images obtained. In order to obtain the correct magnitude of CTn values as they would be measured in the cores, each sample was scanned inside the borehole of the core holder, using the same scanning parameters as in measurements during depletions or

waterflooding. For each sample of known density a corresponding average CTn was obtained. Table 4.1 shows the density and measured CTn values of the standard samples.

Table 4.1: Standard samples - CT numbers and densities

Sample	CTn	density (kg/m^3)
Air	-800	0
water	82.2	1000
acetone	-135.6	789.9
methanol	-115.1	791.3
pentane	-261.2	624.8
heptane	-209.9	679.5
decane	-172.3	726.3
toluene	-85.8	862.3
core 118-5	1218.5	2016.7
core 141-6	1335.1	2159.1
core S103	1275.4	2082.6
core 118-6	1211.5	2008.7
Torpedo 70	1192.9	1964.6
core S102	2177.2	2739.3

The density values in Table 4.1 correlated strongly with CTn, as shown in Figure 4.9.
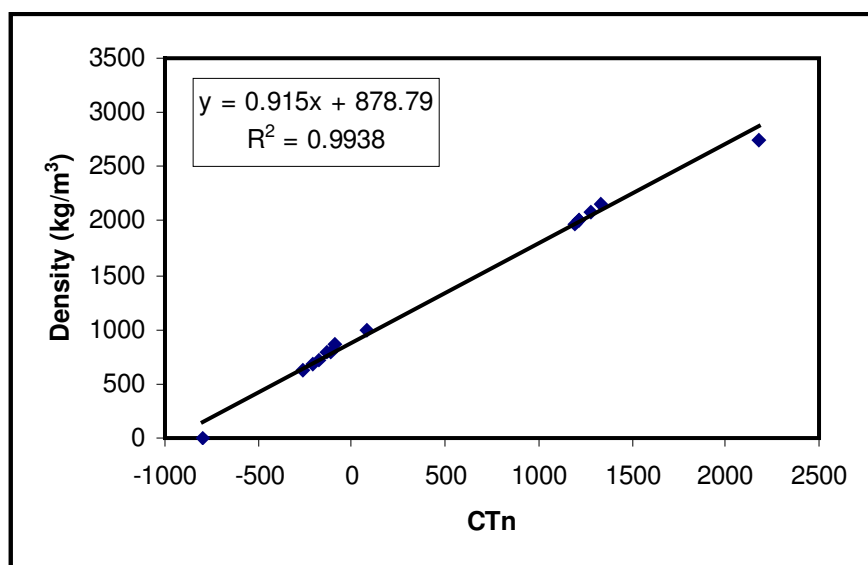
Figure 4.9: Calibration between density and CTn

The relationship yielded by this graph shows that the CTn varies linearly with the density of the samples. Using the correlation shown, CTn from the measured cross-sections of the cores either during primary depletion or waterflooding could now be converted into density units. From density values, the porosity and saturations could also be determined.

4.9.2 Doping of Fluids

CT scanning captures density information, but unfortunately heavy oil and brine have fairly similar values. Thus, in order to distinguish one phase from the other, one fluid has to be doped. Doping is a process by which a chemical is added to increase the atomic number of a fluid. Kantzas (1990) has noted that the addition of a dopant alters the bulk density only slightly, however, the effective atomic number can change quite drastically. Doping allowed the CTn of the fluids to be distinctively different, while not significantly changing the physical properties of the fluids in a way that will influence displacement efficiencies. The amount of dopant added determined the degree of deviation from the actual CTn.

In these heavy oil waterfloods, either oil or brine could be doped. At first it was thought to be more beneficial to dope the oil phase, since this means that doping would only have to be done one time, and also that there would be no salinity variations between connate water and doped injected water. Thus, oil was doped with bromododecane. However, it proved to be extremely difficult to mix bromododecane homogeneously into heavy oil due to the fact that their viscosities and densities are very different. Various concentrations of bromododecane were added to a sample of heavy oil, but it was observed that a significant amount of bromododecane (11%) was required to alter the CTn of the oil by an appreciable amount (170 units). This large fraction of bromododecane considerably altered the properties of the heavy oil: the viscosity of the mixture was considerably lower than the oil viscosity. Another concern was that the bromododecane would separate out of the mixture after an extended period of time in the

piston cylinder. As a result of these concerns, the decision was made to dope the brine phase instead.

In this situation, if there was a difference between connate water and injected water, such as what would be present in secondary waterflooding on the cores prepared by Goodarzi (2006), this would lead to differences between the injected and effective *in-situ* CTn of the water in the core. Since the oil phase was not possible to dope, however, this was an unavoidable experimental uncertainty. Connate water saturation in the cores were relatively low, so it was assumed that this would not cause significant errors in the water saturation predictions.

Brine (consisting of water and 2 wt% NaCl) was doped using potassium iodide (KI). Various concentrations of KI were tested to find the optimized concentration which yields the maximum distinction between oil and brine. It was seen that as the KI concentration increased, the mean CTn of brine increased accordingly. This is shown in Figure 4.10.
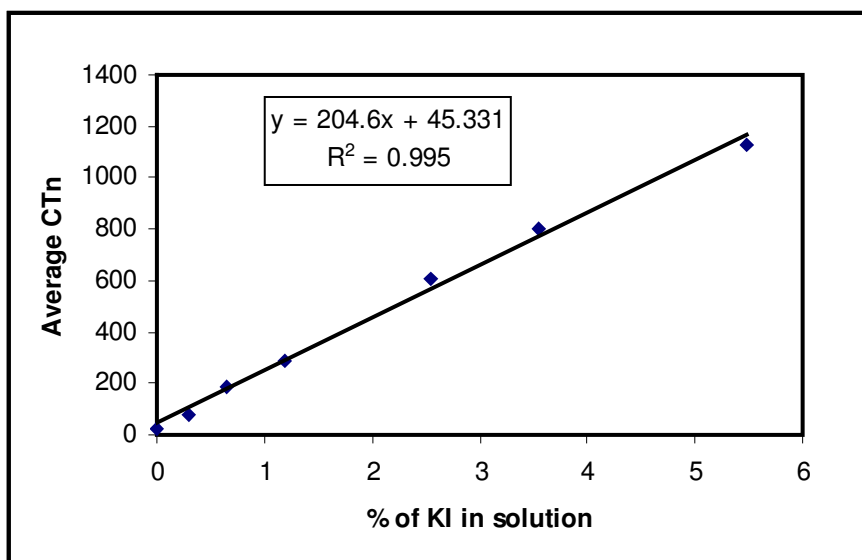
Figure 4.10: Doping of brine with KI

For all the waterfloods a concentration of 5.5% KI was chosen. Even though it is possible to further increase the range of distinction between oil and water through further brine addition, it is known that if salt content in brine is too high, this can have an effect on the oil/water interfacial tension. The doped brine used therefore contains 7.5% salinity in total: 5.5% KI and 2% NaCl.

4.9.3 Scanning of Sandpacks

As mentioned earlier, the sandpacks were all initially scanned when they were fully saturated with methanol to determine the quality of packing. Each sandpack employed in the dead oil waterfloods was also scanned at other conditions: dry, fully saturated with brine, at irreducible water saturation and at the end of the waterflood. Even though it was desirable to scan the at the exactly same locations at each saturation state, it is not possible to leave the sandpack on the scanning bed for the entire course of the experiment, especially in low rate waterfloods that were quite slow. Each time the core is removed and replaced on the scanning bed, it is only possible to re-align the core to within the accuracy of the visual laser alignment tool on the bed. Therefore, small errors in the core positions may lead to additional error in the results, but again this was unavoidable. Also, for some experiments scanning was performed at various times as the waterflood progressed. In these floods, although once again it may not be possible to obtain slices as a function of time at the exact same intervals, a quantitative comparison may still be possible for determining the location of injected water in the core. During primary depletion, the sandpack was also scanned at various time intervals to image the evolution of the free gas phase.

4.10 NMR Measurements

NMR was used in this thesis for two applications: (1) to determine the oil and water masses of the produced fluids, and (2) to obtain additional information about the location of water in pore spaces to aid in the interpretation of the data collected during core flooding. With the exception of the secondary waterfloods performed in the large cores, all the produced fluids were measured using NMR to determine the oil and water

content. The NMR predictions were later verified using manual separation with toluene. An evaluation of the NMR and the separation method was conducted in order to verify the NMR measurements of produced water cut. In several select experiments waterfloods were also carried out in non-metallic PEEK core holders. Spectra of the fluids inside the core were obtained as a function of time during the waterfloods, in order to obtain information regarding the distribution of the fluids existing in the porous medium.

4.10.1 NMR Method of Determining Oil and Brine Fractions in Produced Fluids

Produced fluid samples were collected either in 20 cm³ glass scintillation vials (5 cm in length, 2.5 cm in diameter) or in low density polyethylene Nalgene vials (5 cm in length, 3 cm in diameter). These samples were weighed and NMR measurements were made in a Corespec 1000[TM] low field NMR relaxometer, which operates at a frequency of approximately 1.1 MHz. Measured relaxation data was then converted into spectra using commercial inversion software called "Echofit". This software was developed by Numar, which is now a subsidiary of Halliburton.

Previous works in NMR of oil/water mixtures (Allsopp *et al*., 2001; Wright *et al*., 2004) have already established a method for estimating the oil and water content in the sample. NMR detects the response from hydrogen protons in the fluids, thus the NMR signal contains the contribution of both oil and water. In bulk liquid systems, the NMR relaxation time is proportional to the fluid viscosity. The NMR relaxation rate is given by the expression (Straley *et al*., 1997; Kleinberg and Vinegar, 1996; Coates *et al*., 1999):

$$\frac{1}{T_2} \propto \mu \qquad\qquad \text{Eqn (4.6)}$$

Where μ is the fluid viscosity and $1/T_2$ is the fluid relaxation rate. Eqn (4.6) shows that high viscosity fluids have fast relaxation rates, or low values of T_2. In general, viscous heavy oils have signals at geometric mean relaxation times (T_{2gm}) under 10 ms, while low

viscosity water will relax much slower, on the order of seconds (Allsopp *et al*., 2001; Coates *et al*., 1999).

Example NMR spectra of bulk oil and oil-water mixtures are shown in Figure 4.11.
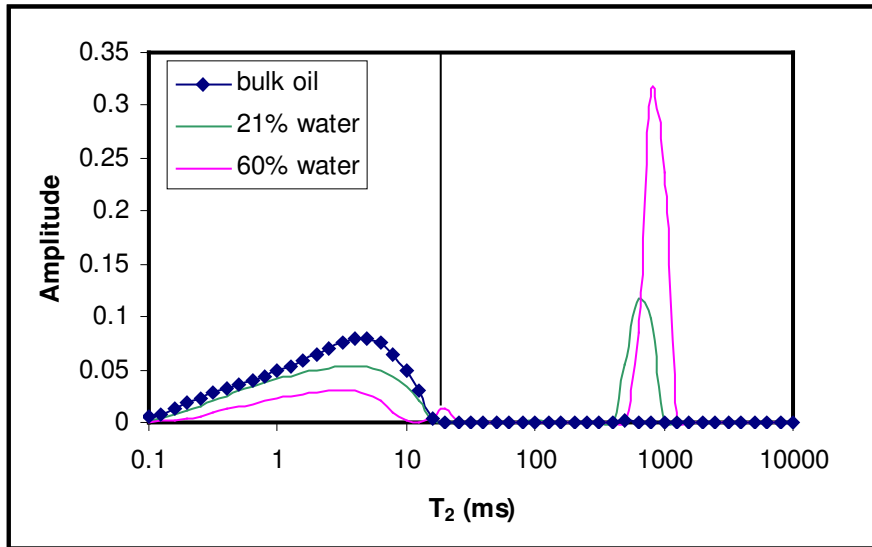
Figure 4.11: NMR spectra of various bulk fluid mixtures

As expected, viscous oil generally relaxes below 100 ms while bulk water relaxes at approximately 1,000 ms. Since the signals are very distinct due to the considerable viscosity contrast between oil and water, a cutoff can be assigned at the end of the oil peak and any signal beyond this point is assigned to be the amplitude from water. The oil and water amplitudes are then linearly related to fluid masses.

Two different oils were used in the waterflood experiments performed in dead oil systems. HO1 has a viscosity of around 4,650 mPa·s at ambient temperature (23°C), and a geometric mean relaxation time of around 2.1 ms. The other heavy oil used in this study, HO2, has a viscosity of 11,500 mPa·s and a T_{2gm} of around 1.1 ms at the same temperature. As expected, HO2 relaxes faster than HO1 due to its higher viscosity.

Figure 4.12 shows the spectrum of HO1 compared to HO2, in order to illustrate this difference.
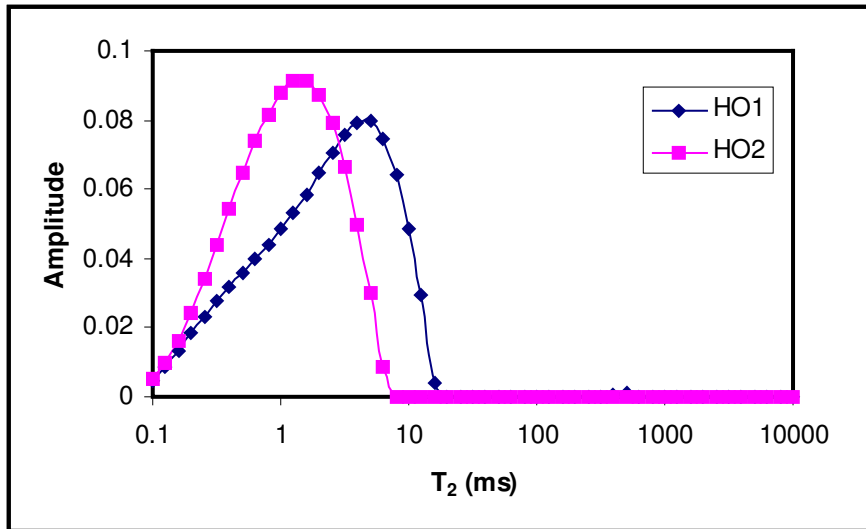
Figure 4.12: NMR spectra of two heavy oil samples with varying viscosity

The bulk HO1 spectrum does not have any signal beyond 20 ms, and the cutoff for HO2 is 10 ms. These were the cutoff values applied to separate oil and water in the produced fluid mixtures.

From Figure 4.11 it is evident that as the percentage of water in a mixture increases, the amplitudes in the second peak of the spectrum also increase accordingly. By summing up all the amplitude after the cutoff, the water amplitude can be known. The water amplitude can then be converted into a physical amount of water from the following relationship (Mirotchnik *et al.*, 2001):

$$m_w = \frac{A_w}{AI_w} \qquad\qquad \text{Eqn (4.7)}$$

The parameter AI_w is the amplitude index of brine, defined as the NMR amplitude per unit mass of brine. This value can be found by obtaining an NMR spectrum and

measuring the water amplitude for a known mass of brine. With the AI_w value known, water amplitudes can be converted into water mass. In general, AI_w will be relatively constant for a given NMR machine.

One limitation of the NMR method for determining produced oil and water content is the sample size, due to the restriction of the NMR borehole diameter and the length of the NMR region of magnetic field homogeneity (the "sweet spot"). As noted previously, the NMR systems in our laboratory only have a sweet spot of approximately 5 cm in length, and a maximum sample diameter of 3.81 cm. Thus, the maximum size of the sample that the NMR can measure is approximately 30 g. The other limitation is the inaccuracies in the direct NMR measurements of oil mass, especially at low oil contents. Oil is a heterogeneous compound and is also more difficult to measure due to its higher viscosity. Thus, oil mass predictions are difficult when very little oil is present to give an NMR signal. In order to account for this second limitation, the water fraction was calculated by determining the water mass from NMR, and measuring the oil content by difference from the total sample mass. Produced fluid cuts were then found by dividing the water and oil masses by density, and water cut was reported on a volume basis.

4.10.2 Evaluation of NMR Method for Monitoring of Produced Fluids

Before the NMR method could be employed in the determination of oil and water content in actual produced fluids, its accuracy had to be established. Samples with known masses of oil and water were created and their NMR spectra were obtained. Amplitudes were converted to mass using Eqn (4.7), and NMR estimates of oil mass were found by difference.

The NMR parameters can be tuned to pick up a specific signal, focusing on either the oil or water response. Previous work with heavy oil systems has shown that NMR can much more accurately measure the signal of brine, thus the NMR parameters were chosen such that the water signal was fully captured. In addition, the samples evaluated generally contain a significant amount of brine, since oil is produced at high water cuts during

heavy oil waterflooding. Different combinations of NMR parameters were evaluated to identify the set that would yield the best accuracy. Both sets of parameters used an echo spacing of 0.3 ms, with 5,000 echoes and 15,000 ms re-polarization time between trains. The only difference is the number of trains run: set 1 was run with 25 trains (a 15 minute measurement) while set 2 was run with 49 trains (a 30 minute measurement). The comparison of NMR water mass to measured water mass is shown in Figure 4.13.
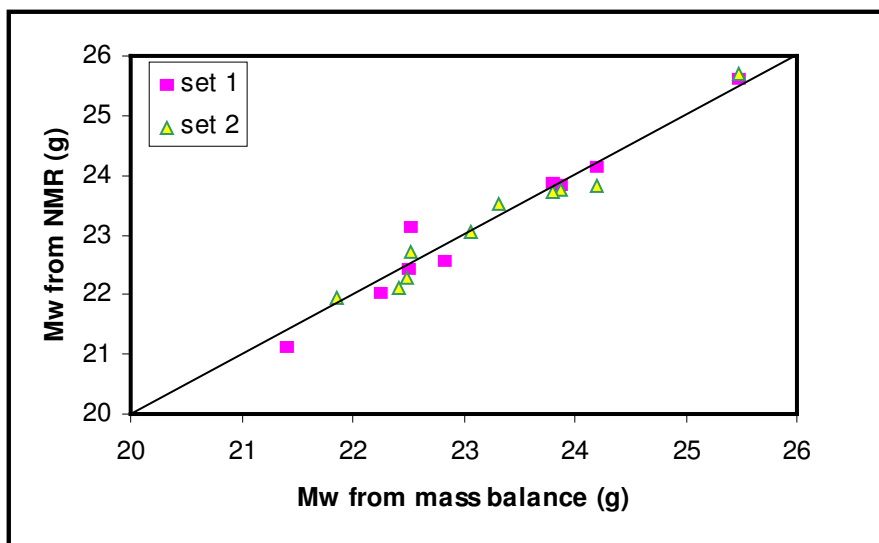
Figure 4.13: Determination of brine masses by NMR

The masses of brine and oil used in this testing data set were chosen to cover a range of water cuts for the actual size of our samples (about 30 g). From Figure 4.13 it can be seen that the prediction for water is quite accurate for both parameter sets. In general, however, the NMR parameters of set 2 (49 trains compared to 25) provided better estimations of the water content. In an NMR measurement the number of trains is the number of times that the NMR decay is measured, and the final decay curve output from the machine is the average of the data from each train. Thus a higher number of trains mean that the NMR decay is obtained over a larger number of re-iterations, which should lead to a cleaner signal and more accurate water content estimates. If using NMR for online water cut estimation, this parameter is important because of the need to acquire water cut information in a fast measurement. For the application of interpreting core

flood data, however, accuracy is more important than speed, thus the longer measurement was used in this work.

From previous experience it has been shown that NMR has difficulty in correctly estimating the oil content in samples containing very little oil (Bryan *et al.*, 2006). In these heavy oil waterflood experiments after water has broken through, the water cut will be quite high and the oil cut will in turn be relatively small. Thus it was important to evaluate the NMR predictions with very small fraction of oil since these samples will have the greatest inaccuracy. The NMR oil content predictions (by difference from the measured sample mass and the NMR water mass estimate) are shown in Figure 4.14.
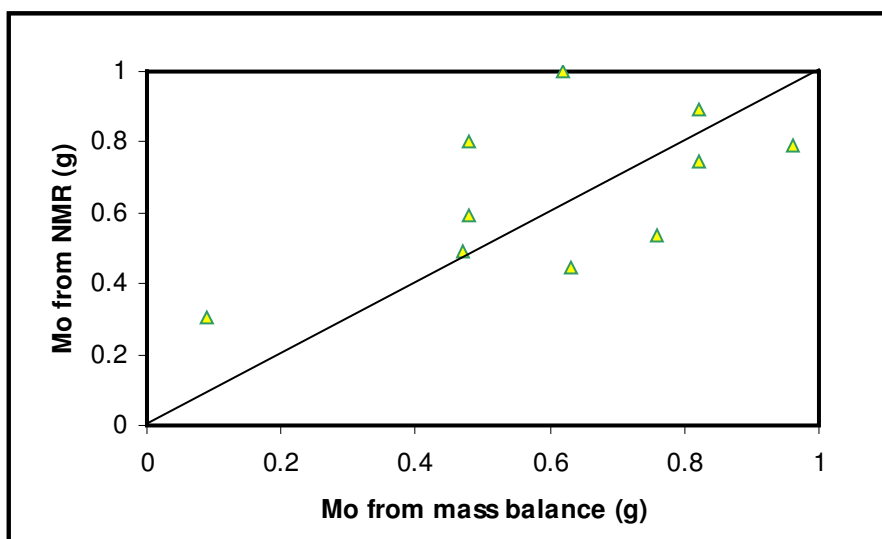
Figure 4.14: Determination of oil mass from NMR

It was calculated that the oil predictions were accurate to within ± 0.18 g. This prediction seems poor, considering the total oil mass in the sample is generally less than 1 g. The reason for this error is that water mass predictions were made assuming a constant value of AI_w. This is theoretically what should happen, since water is a relatively simple component and does not contain many different molecules, in contrast to something like oil. However, NMR measurements are also statistical in nature, since the final decay curve used is the average of many measurements. As a result, in some samples the actual

AI_w may be slightly different from the average value. This will lead to small errors in the water mass predictions, which in turn will lead to more significant errors in the mass predictions of the oil produced.

Water cut predictions were improved by also performing separation studies using toluene to dilute the oil, and measuring the total produced water mass for each experiment. The water masses by separation were then used to tune AI_w values at different points in the waterflood. In this manner, separation using toluene was used to get a measured value of the total water produced. Knowing this number, and the total mass of all the produced fluid, the produced oil could also be determined accurately. Then, with this number, NMR AI_w values are tuned and NMR to give a measurement of the water cut of each produced fluid sample. In this procedure, therefore, produced fluids were interpreted using a combination of NMR (for produced water cut) and separation with toluene (for the total oil recovery).

4.10.3 Evaluation of the Separation Method

If separation is assumed to be the "true" measure of total produced water mass and the water from separation is used to tune the NMR predictions, then it is important to first verify the accuracy of the separation method. To do this, five samples with known water and oil masses were used to evaluate the numbers obtained by separation. These samples were agitated to mix the oil and water and smear oil against the walls of the containers, in order to most closely represent actual produced oil and water. The samples were then separated individually to determine the oil and water components. The sample sizes ranged from 10 g to more than 30 g. These samples were chosen to be small on purpose since for smaller samples errors were expected to be higher. Heavy oil is quite thick and sticky, thus a mixture of oil and water may contain water droplets in oil. Toluene is miscible with heavy oil and will not cause precipitation of asphaltenes, thus it was added to the mixture to dilute the oil and free suspended water droplets that may have been trapped in the viscous oil. After toluene was added, the solution was lightly shaken to allow water droplets to coalesce. The solution was then left to settle for a short

period of time (approximately five minutes) in a separation funnel location in a fume hood. Due to its higher density, water will gravitate toward the bottom of the separator, and a clear distinction can be made between clear water and diluted oil. The water could then be collected and weighed, with oil mass obtained by difference from the total sample mass. The results are shown in Figure 4.15.
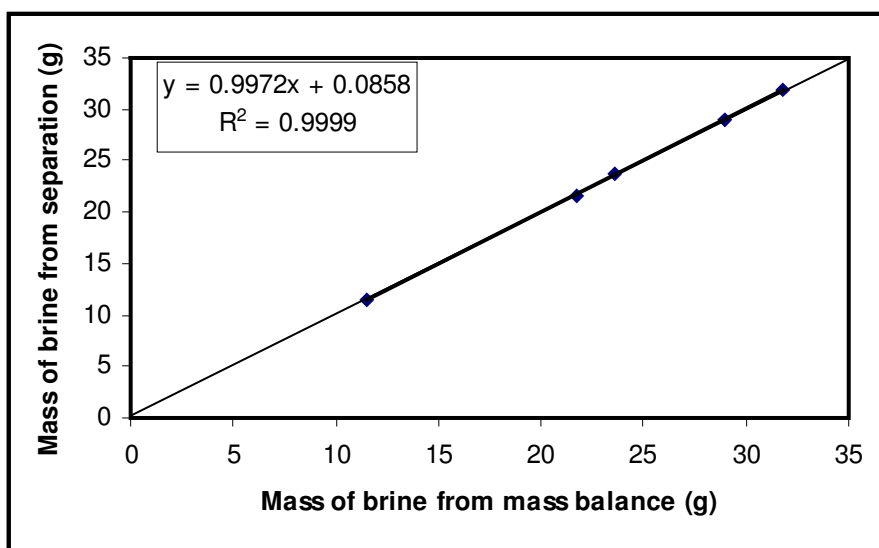
Figure 4.15: Evaluation of separation method

This figure shows that the separation method yields highly accurate results. The average error is 0.06 g with the largest error of 0.15 g, which is 0.56 % of the total mass. Thus it could be established that the separation method is highly accurate for determining the mass of oil and water in a mixture. From the error bar it could be seen that the error induced by this method is smaller than the NMR methods. Therefore, the methodology of using the data from separation to tune the NMR AI_w values appears to be valid.

4.10.4 NMR Measurements of Imbibition in Static Systems

A set of NMR spectra was obtained for oil/water/sand systems in static vials. This experiment was developed to investigate the nature of imbibition in closed systems, and will be discussed in Chapter 9. In order to prepare these samples, Lane Mountain 70 sand was manually mixed with a heavy oil (HO2 from Figure 4.12). The oil and sand

were thoroughly mixed for approximately 10 minutes, and the resulting oil sand (containing no connate water) was divided and packed into four different vials. For each vial a certain amount of water was added. In order to maintain consistency with the core floods performed, water should ideally have been added first before mixing the sand with oil. However, this was not possible for several reasons. First of all, it is not possible to add a known amount of brine corresponding to the S_{wi} values from core flooding, since the porosity of the loose sand is not known. Second, the brine might not occupy the small pores like it would in a reservoir, but might instead spread on the bottom of the vial due to gravitational forces. Most importantly, while mixing sand with oil, any brine added earlier could evaporate and the timing at which imbibition starts to occur could not be identified. Thus, for these static systems the brine was added on top of the oil sand only after dry sand had been thoroughly mixed with oil. This procedure also allowed the amount of brine added to be varied, in order to investigate the effect of the brine volume fraction on the system response.

NMR measurements were taken at various times to monitor the movement of water in the porous medium. The weight of the sample was also measured at the same times that NMR measurements were performed. This was done to monitor evaporation of these samples over time. If there was any evaporation, it was assumed to originate from any bulk brine not yet soaked into the sand.

4.10.5 NMR Measurement of In-Situ Water Distribution

In several select experiments, the goal was to acquire NMR data in order to monitor the *in-situ* distribution and location of injected water. In order to obtain spectra of cores at various stages of waterflooding, the floods had to be performed in core holders that would not interfere with the NMR signal. Two NMR core holders were therefore constructed out of TECAPEEK^{TM} PVX, which is a high performance plastic capable of withstanding high pressure. The design of these core holders was previously discussed in Section 4.1.2. The sand packs were made by wet-packing the core holders with LM 70 sand and methanol. After packing and leak-testing, the cores were dried under air and

nitrogen. In each core, porosity was then measured using gas expansion. The core was then placed under vacuum for at least 12 hours, followed by saturation with brine and measurements of brine permeability using constant head pressure. Finally, the cores were flooded with heavy oil at constant rates until irreducible water saturation was reached. Waterfloods were then performed at fixed rates using a digital ISCO pump. The procedure for these cores is the same as what was carried out in other dead oil waterfloods. The only difference is that in these core holders, NMR spectra were obtained throughout the waterflood to monitor the location of injected water over time.

In one core (L = 9 cm, D = 2.54 cm), the effect of injection rate was studied by performing waterfloods at two fixed rates: 8.89 cm³/hr and 0.45 cm³/hr. Inlet pressures were monitored using two parallel Measurement Specialties Inc. (MSP 600 series) pressure transducers (0 – 7,000 kPa and 0 – 175 kPa), and spectra were measured using an Ecotek FTB low field NMR relaxometer. This machine operates at a frequency of around 1.78 MHz. The core is slightly longer than the region of magnetic field homogeneity, thus measurements at different saturation states can only be compared by relating the amplitudes to the signal of the core fully saturated with water. NMR measurements were made using an echo spacing of 0.16 ms, 5,000 echoes, a recovery time of 10,000 ms and 25 trains. Since these measurements were taken during flowing conditions, it was necessary to test the stability of spectra using different parameters. The parameters finally chosen were optimized to give repeatable spectra.

In the other TECKPEEK^{TM} core (L = 53.2 cm, D = 2.6 cm), spectra were acquired during the waterflood at different lengths in order to investigate the distribution of water as a function of length as well as time. These measurements were obtained using an Ecotek FT low field NMR relaxometer, which operates at a frequency of around 1.95 MHz. In this machine, the optimal parameter choice was found to be an echo spacing of 0.16 ms, 5,000 echoes, a recovery time of 5,000 ms and 16 trains. These parameters allowed for repeatable NMR measurements, which were significantly faster than the velocity of the flood front. In this manner, measurements at different length scales were assumed to

have been taken at approximately the same time. Spectra were measured at fixed locations expressed as fractions (0.09, 0.35, 0.65 and 0.78) of the core length.

4.11 Accuracy of the Waterflooding Results

Sections 4.10.2 and 4.10.3 addressed the methodology for measuring the oil and water content in the produced samples. When performing core flood experiments, with the goal of comparing results from different experiments with one another, there are also other factors that must be considered as well, when ensuring that the results obtained are representative of physical differences in the systems. The following section addresses issues of repeatability and reliability of data in laboratory core floods.

4.11.1 End Effect Issues

Due to the fact that several pore volumes of fluids had to be injected for each experiment and generally a small injection rate was applied, the pore volume of the sandpack was limited to prevent the experiment from becoming too time consuming.

It should be noted that before any flood could be carried out a significant amount of preparation time was required, including packing and sealing the core, drying, measurement of pore volume, saturation with brine and measurement of permeability to brine. Then the core was flooded to irreducible water saturation, and only at this point the waterflood would begin. At the fastest injection rates studied, at least five pore volumes of brine were injected during the waterflood. The fastest experiment therefore would require at least a month (including the time to prepare the core for the waterflood), whereas the slowest injection rate could take easily a few months to conduct. Therefore, it was necessary to keep the pore volume small so that sufficient core floods could be performed such that different flood parameters could be investigated. However, if the pore volume was too small this may in turn pose other problems regarding the quality of the collected data. In general, it is important that the pore volume of the sand pack be much larger than the dead volume of the core holder and lines, due to concerns with oil sticking or smearing in the lines. When the pore volume is small, any error in the

estimation of oil recovery will be magnified since produced oil volumes would be divided by a smaller value of original oil in place (OOIP). OOIP must therefore be large enough that these effects are negligible compared to the production trends observed.

An additional concern that has been noted in many sources in the literature is that of end effects in waterflooding experiments (Rapoport and Leas, 1953). End effects consist of either outlet or inlet end effects. These end effects are caused by the fact that no matter how much care is taken in packing a core, there will exist a small gap between the edge of the core and the end plate of the core holder. During an oil flood, this gap will be fully filled with oil. In practical terms, this gap or oil film can be thought of as a very large pore.

Outlet end effects occur in water wet rocks, where the injection of water into the core is an imbibition process. During imbibition, water enters first through the smallest pores and only at lower capillary pressures are larger pores invaded. At the outlet of the core, therefore, water will tend to remain in the porous medium instead of entering the gap between the core and the end plate. This will lead to an apparent delay in the breakthrough of the water, and incorrectly high values of oil recovery at breakthrough. It is expected that in oil wet rocks, where waterflooding is a drainage process, this will not be as significant since water will easily enter the gap at the edge of the core.

Inlet end effects occur when water contacts the sand pack, at the start of the experiment. Even before water injection begins, some water may move into the smallest pores at the entrance to the porous medium due to capillary imbibition. This would increase the water saturation even before the experiment begins which would in turn reduce the relative permeability to oil at the entrance to the core and prevent the generation of a stable water displacement front. If a stable front does not form, this is analogous to the development of viscous fingers in heavy oil systems, and will tend to be a more pronounced effect in short cores. In heavy oil cores, viscous fingering will occur even

with inlet end effects, but the nature of the viscous fingers are expected to be related to the mobility ratio and injection conditions, and not an artifact of the system.

Using data for conventional oil waterflooding, Rapoport and Leas (1953) suggested a criterion to design a laboratory waterflood such that end effects are negligible. This criterion is:

$$Lv\mu_w \geq 1 \qquad\qquad\qquad\qquad\qquad Eqn \ (4.8)$$

The scaling criterion shown in Eqn (4.8) has units of cm²/min·cP. It was shown experimentally (Rapoport and Leas, 1953) that when this criterion is met in conventional oil, the results obtained will be indicative of porous media properties and will not be an artifact of the experiment. Unfortunately, it is not possible to apply this criterion to a heavy oil waterflood. In order to get $Lv\mu_w > 1$, either the injection rate or the length of the sand pack has to be large. In heavy oil waterfloods a high injection rate would lead to severe viscous fingering, which would in turn mask other properties of the waterflood response. Likewise, a long sandpack would make it impossible to investigate multiple aspects of heavy oil waterfloods due to the extended time requirements for each flood in a long system. These experimental difficulties were previously discussed in more detail in Chapter 3.

Most investigations on displacement of heavy oil tend to neglect issues of end effects. The reason is that under adverse mobility ratio displacement of heavy oil, viscous fingers will always be present whether care is taken to eliminate inlet end effects or not. Likewise, due to the high oil viscosity, if water is to displace heavy oil it is expected that water will follow the paths of least resistance at early times, which will be the largest pore channels in the sand pack. Therefore, regardless of the wettability of the porous medium, water will theoretically displace oil through a pore pathway that is representative of a drainage process, so the delay in breakthrough recovery will not be significant. Additionally, due to viscous fingering and bypassing of large sections of the

core, water breakthrough occurs very early in the life of a heavy oil waterflood (Adams, 1982; Smith, 1992). While it is important to consider the efficiency of the waterflood at the point of breakthrough, a significant fraction of oil is also recovered after breakthrough, which is no longer affected by end effects. For these reasons, heavy oil waterfloods generally do not need to satisfy the criterion for eliminating end effects, and it is possible to conduct waterflooding experiments in shorter cores. Of course, the first criterion regarding the necessity of a pore volume much larger than the system dead volume still holds.

In the experimental work plan developed in this thesis, care was taken to ensure that the pore volumes of the different sand packs were large enough that the results were repeatable. However, no attempt was made to address the issues of end effects, in deference to the reasoning provided by other researchers. In Chapter 7, evidence is provided for repeat measurements performed in different sand packs, at the same injection rates and oil viscosity. The results are repeatable, indicating that end effects (which may be different in different cores) are truly not a concern in these heavy oil systems.

4.11.2 Repeatability of Waterflooding Experiments

Assuming that the pore volume in the core is much larger than the system dead volume and that end effects are negligible, it is expected that the trends obtained will be representative of physical parameters such as injection rate, oil viscosity or rock permeability. To prove that this was true, displacement experiments were repeated and the results were compared. Figure 4.16 shows the oil recovery profile for two waterfloods, both performed at 10 cm³/hr. The properties of these two experiments will be summarized in Chapter 5: these are the results of Experiment # 4 and # 9 listed in Table 5.2. The properties of these experiments reported in Table 5.3. Both of these sandpacks were saturated with the same fluids (the same heavy oil and irreducible saturation of doped brine). In Experiment # 4, water was injected at 10 cm³/hr for approximately 5 PVs. In Experiment 9, water was also injected at 10 cm³/hr but only for

about 2 PVs, after which the injection rate was reduced to 1 cm³/hr. Therefore, the results can be compared at early times (< 2 PVs) when the water injection rates are the same.
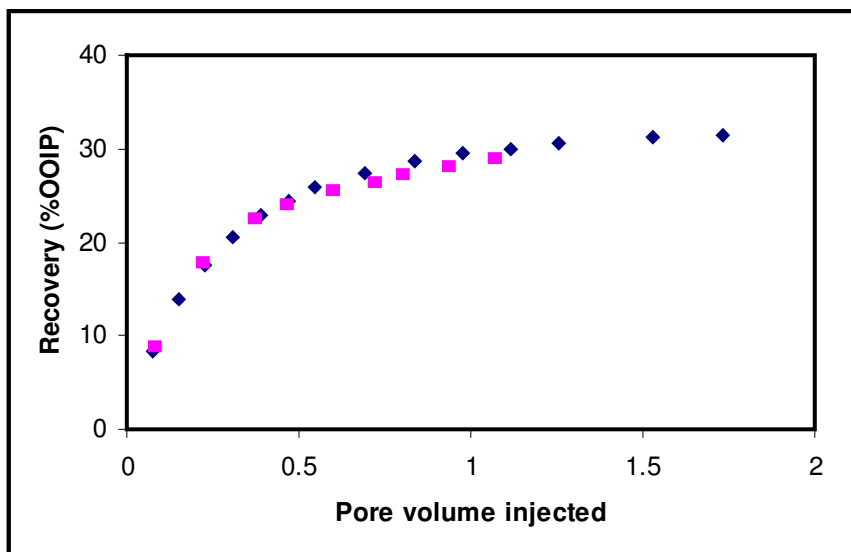
Figure 4.16: Repeatability of a waterflood at the same injection rate

Considering that these experiments were performed on different sand packs that had similar characteristics, the variation in the oil recovery profile is very small: within 1% of OOIP. There is possibly some minor variation between the two experimental runs, however the overall agreement in the results is very satisfactory. Thus, it was concluded that the results obtained from different waterfloods are actually representative of planned changes in the flood parameters, since repeat measurements on similar systems yielded essentially the same trend for recovery.

At this point, confidence was generated both in the measurement of produced oil and water and also in the reliability of the core flooding data. The trends observed from experiments are therefore indicative of physical properties of the systems studied.

CHAPTER 5: SUMMARY OF WATERFLOOD EXPERIMENTS

The previous chapter provided details for the procedures in all the experiments performed. For this thesis, many tests were completed with different oils, different sands and various sizes of sandpacks. The full extent of the experimental program consisted of dead oil waterfloods, primary depletion, secondary waterfloods, imbibition studies and other complimentary investigations. Before the results of these experiments can be discussed, the properties of these experiments need to be summarized. This chapter provides a description of the experiments performed, and includes details of the porous medium, as well as the fluids used in each experiment. The goals of the experimental work plan are also presented.

5.1 Oil Properties

In this thesis, two heavy oil samples were used in the waterflood experiments. The oil samples came from fields Saskatchewan and Alberta. The two oils are referred to as HO1 (supplied by BP) and HO2 (supplied by Nexen). HO1 has a density of 0.97 g/cm^3 and a viscosity of 4,650 mPa·s at 23°C. HO2 has a density of 0.9815 kg/cm^3 with a viscosity of 11,500 mPa·s at the same temperature. By performing waterflooding studies for both of these oils in cores of similar permeability, this allows for a comparison to be made for the efficiency of these waterfloods in oils of varying viscosity.

As discussed in Chapter 4, interfacial tension measurements between oil and brine were difficult to make using the spinning drop apparatus, due to the similar density of these two fluids. The interfacial tension measurement was therefore made by diluting the oil with varying amounts of octane, following the procedure outlined by Schramm *et al.* (2003). Figure 5.1 is a plot of the interfacial tension behavior of HO2 and brine at varying concentrations of n-octane. It can be seen that for n-octane concentrations under 50%, the interfacial tension is roughly constant at approximate 14 mN/m. This is in the same range of values as many conventional oil – water systems (Green and Whillhite, 1998). The interfacial tension between brine and HO1 was not measured, but since this is

still an oil – water system it is expected that the interfacial tension for this system will also be of the same order of magnitude.
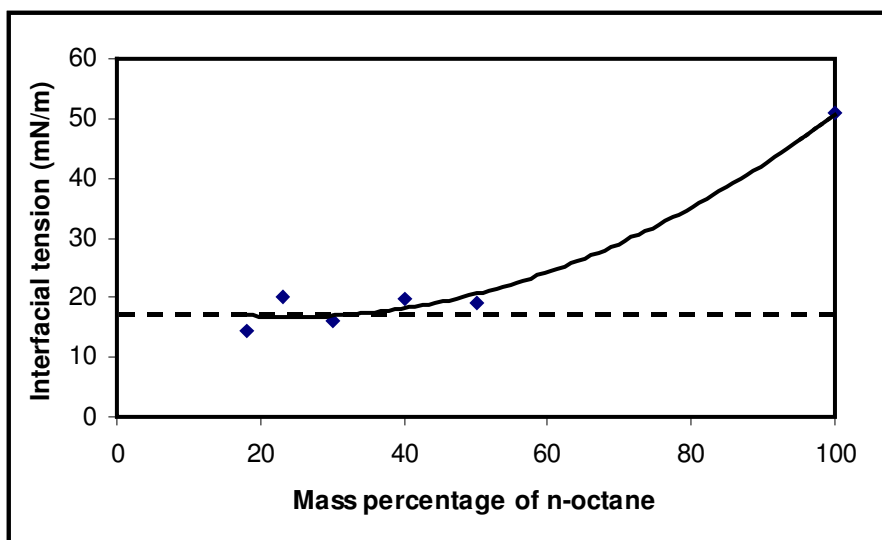
Figure 5.1: Interfacial tension between brine and HO1/n-octane mixtures

All measurements of interfacial tension were made at 23°C. The actual value of interfacial tension was not used directly in this study, except for calculations of capillary number in Chapter 11. The measurement of interfacial tension has been made only to demonstrate that the systems studied are immiscible fluids. Therefore, capillary forces should be present in these systems, and the magnitude of these forces is governed by properties such as the rock wettability and the pore size distribution of the sand grains.

5.2 Dead Oil Waterfloods

Various waterflood experiments were performed with dead oil. Initially, several waterflooding experiments were performed to fine-tune the procedure in order to yield the most accurate results. This was necessary because dead oil waterfloods in unconsolidated cores are inherently unstable, and it was necessary to ensure that the results were actually representative of rock or fluid properties and were not experimental artifacts caused by things like end effects. Additionally, the procedures for proper core preparation and measurement of produced fluids were still being developed, so these

early experiments also served as trouble shooting tests. Once the experimental procedures had been defined, many waterflooding experiments were performed. These consisted of floods at multiple rates in cores with varying water injection rates, rock permeability and oil viscosity. The sandpacks have different properties, as well as different production scheme for different experiments.

5.2.1 Development of Proper Procedure for Waterflooding

Lane Mountain 70 sand was packed into a rubber sleeve with an inside diameter of 3.81 cm and a length of 22.8 cm. The core was then placed inside the aluminum bore, and overburden pressure was applied against the sleeve, as discussed in Chapter 4. The particle size distribution of this sand is shown in Figure 5.2. The majority (approximately 80%) of the sand grains are in the range of 150 – 250 μm. This particle size distribution also shows that the range of pore size is fairly narrow, with only a small fraction of tight pores.
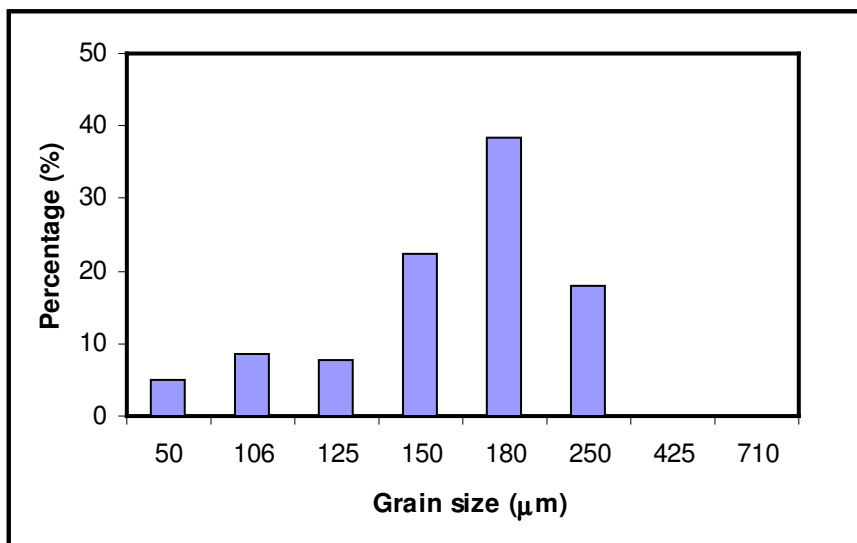
Figure 5.2: Particle size distribution of Lane Mountain 70 sand

Once the sandpack was saturated with oil and irreducible water, it was waterflooded at a fixed rate and the products were collected and separated to measure the oil and water content. This method of determining oil and water content limited the number of data

points that could be collected, since a sufficient volume of fluids was required before separation could be performed with a high degree of accuracy. However, it was necessary to obtain a fairly detailed recovery profile, particularly at early time before and immediately after water breakthrough. Thus, the process of determining oil and water masses was later modified to combine the usage of both NMR (at early times) and separation (at late times). As discussed previously, NMR samples were also fine-tuned by separation with toluene.

The goal of the dead oil waterfloods was to investigate the relative influence of viscous and capillary forces on heavy oil recovery by waterflooding. In order to do this, experiments were designed which varied the viscous forces by changing the water injection rate and oil viscosity. The effect of changing the rock permeability was also studied, as this term relates to both viscous and capillary forces. In any experiment, it was necessary to keep all variables constant save the one parameter that was being investigated, thus care was taken to eliminate as many uncertainties as possible. It would have been most convenient to use the same sandpack in all experiments to allow for a more direct comparison. However, due to the fact that a rubber sleeve was used to contain the porous medium, it is not possible to clean the sandpack with solvents after each experiment.

It is common practice to use the same sandpack for multiple waterfloods by simply flooding the sandpack with dead oil after each experiment to get back to the initial irreducible water saturation. This has the advantage of by-passing the cleaning stage, which allows for shorter times between core floods. This method was initially tested: at the end of a waterflood dead oil was re-injected to attempt to return the same saturation condition before waterflooding.

The first three experiments were performed on the same sandpack, using Lane Mountain 70 sand. In between waterfloods, the core was simply flooded with oil and the resulting water saturation was measured. The properties of this sandpack are shown in Table 5.1.

Table 5.1: Properties of sandpack used in the first three dead oil waterfloods

Diameter	3.81 cm
Length	22.8 cm
Porosity	0.361
Permeability to brine	1.31 D
S_{wi}	12.86 %

The fluids used in these experiments consisted of HO1 and doped brine. As mentioned previously, HO1 has a density of 0.97 kg/cm^3 and a viscosity of 6,500 mPa·s, whereas doped brine has a density of 1.0487 kg/cm^3 with a viscosity of approximately 1 mPa·s. Waterfloods were performed at a fixed injection rate of 5, 10 and 1 cm³/hr, which gives frontal velocities of 0.10, 0.21 and 0.02 m/day, respectively.

In an attempt to achieve the original S_{wi} many pore volumes of oil were injected in between waterfloods. The new S_{wi} was obtained by separation, based on the amount of brine collected during the oil flood. In each waterflood the amount of oil recovered was known, so the water in the core prior to the new oil flood was the original S_{wi} plus the volume of oil recovered from the previous waterflood. During re-saturation with oil it was hoped that the oil would displace a similar volume of water to retain the original irreducible water saturation. However, despite the low mobility ratio between injected oil and water and the large pore volumes of oil injected, the initial S_{wi} condition could not be reached. Table 5.2 shows the calculated S_{wi} based on the mass balance of the brine produced.

Table 5.2: S_{wi} variations for repeat measurements without cleaning core using solvents

Experiment #	S_{wi} (%)
1	12.86
2	22.38
3	29.32

From Table 5.2 it is clear that consecutive experiments had significantly higher irreducible water saturation when oil was re-injected without first cleaning the core. At

first the accuracy of the separation method was questioned. However, it was previously shown in Chapter 4 that the separation procedure followed provides very accurate quantification of water in produced fluids. In order to further eliminate this possible experimental error, a more rigorous separation technique was performed after the final oil flood (Experiment # 3). The produced fluid was poured into several separation flasks, allowing a much higher volume fraction of toluene to be added to dilute the mixture and ensure that water was not trapped within the oil phase. A longer time period was also allowed for water to separate. All these efforts, however, still yielded irreducible water saturation that was higher than the previous experiment. This implies that the S_{wi} obtained earlier for Experiment # 2 was also truly higher than the true irreducible water saturation.

The results of Table 5.2 were also confirmed by the presence of progressively higher CT numbers obtained at the end of the each oil flood, as shown in Figure 5.3.
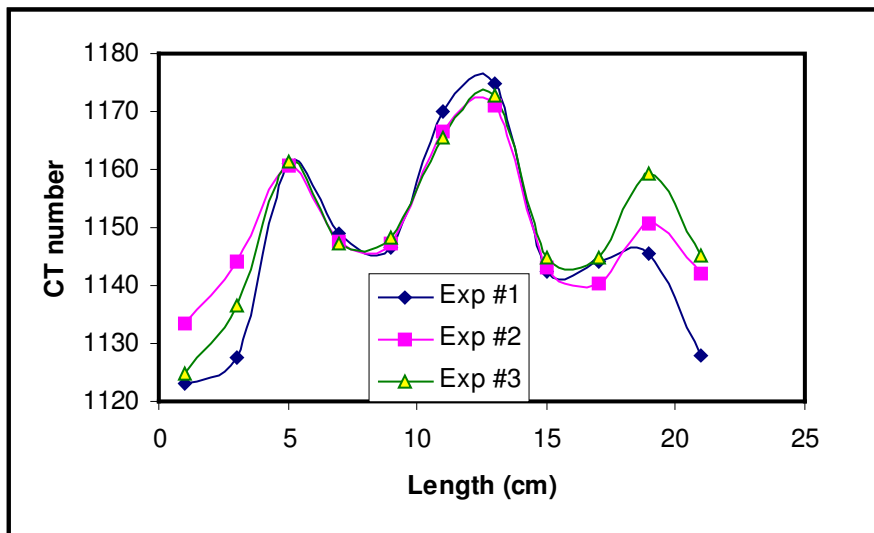
Figure 5.3: CTn variations at varying S_{wi} conditions

When the fluids are inside a porous medium, the overall CTn measured contains the contribution from sand (which is essentially constant between experiments) and the fluids in the pores. Water was doped with 5.5% of KI to give a CT number of about 1,130,

while the CT number of bulk oil is approximately –30. Therefore, larger CT numbers of the core after oil flooding are indicative of higher water saturations. In most slices along the length of the core, the CT numbers in Experiments # 2 and # 3 are higher than the original core. The greatest change in the CT number occurs at the inlet and outlet.

Due to the fact that the original irreducible water saturation could not be achieved by simply flooding with oil at the conclusion of a waterflood, it is possible that the results of Experiments # 2 and # 3 could not be directly compared to those of Experiment # 1.

Table 5.3 shows the measured recovery information for different injection rates in Experiments # 1 – # 3. Despite the fact that lower injection rates should lead to reduced viscous fingering, there was no strong correlation apparent between injection rate and oil recovery. In fact, it appears that for higher S_{wi} at the start of the waterflood, the oil recovery was reduced even for more efficient waterflood conditions.

Table 5.3: Properties of experiments performed on sandpacks with L = 22.8 cm

Experiment #	S_{wi}	OOIP (cm^3)	Injection rate (cm^3/hr)	Volume of oil prod (cm^3)	Recovery (%OOIP)
1	12.86	81.78	5	28.18	34.46
2	22.38	72.85	10	20.74	28.47
3	29.32	66.33	1	20.35	30.68

It is not known what the reason is for the different values of S_{wi} in Experiments # 2 and # 3. Assuming that the sand is water wet, then the first oil flood constitutes a primary drainage process. Subsequent oil floods are then representative of secondary and tertiary drainage. Although there is hysteresis between drainage and imbibition curves, it is generally expected that similar values of S_{wi} can be reached in subsequent drainage floods (Dullien, 1992). The increasing water saturation indicates by-passing of water, which is unexpected for the excellent mobility ratios obtained during the oil floods.

The difference in the recovery profile for different values of S_{wi} is possibly related to the physical location of this connate water. In an oil flood, the oil will very effectively

displace the continuous water channels in the core, and the irreducible water saturation in these zones should be close to the original values. If injected water was also partially traveling through hydraulically connected water films, it may access other portions of the core that do not get displaced in subsequent oil floods. Without additional data, however, this is simply speculation. Since it cannot be known for certain why S_{wi} changed in subsequent core floods, these data were excluded from the subsequent dead oil waterflood analyses.

These first three waterflooding experiments necessitated some very useful modifications to the experimental procedure. The determination of produced oil and water volumes was modified to include NMR measurements at early times to provide a better description of the production profile. Additionally, the inability to return the cores to the same value of S_{wi} between waterfloods prompted a decision to prepare a new sandpack for each experiment. It was accepted that this approach may lead to differences in pore structure between experiments, but the same packing procedure was followed for each flood. Rock porosity and permeability were also re-measured for each core, and CT measurements were taken to ensure that subsequent cores were all similar, so that results from different sandpacks could be compared with reasonable certainty.

After three waterfloods had been performed in the aluminum core holder at this length, another sandpack was prepared to repeat one of the previous experiments. However, at this point the core holder was no longer able to retain the overburden pressure. It was found that nitrogen from the overburden was not leaking into the porous medium. This was an important finding, since it meant that the packing and core sealing procedure was still working. However, the core porosity and permeability are a function of the overburden pressure, so the core holder was taken apart to find the source of the leak. Various scratches and pits were observed inside the borehole. The seal for the overburden pressure was provided by the o-rings on the end plates of the sandpack, acting against the surface of the borehole. With an inner borehole surface that is not smooth, gas can escape at these rough points, promoting a slow leak in the overburden

pressure. In order to seal the core, the o-rings had to be placed in a different location in the borehole, and the design of the new end piece was discussed previously in Chapter 4. The use of this new end piece required the sandpack to be shorter in subsequent experiments. Afterward, the overburden pressure did not leak and the remaining experiments were performed at the new length using the same rubber sleeve.

By performing these initial trouble-shooting core floods, issues in the proper preparation of the core and measurement of the connate water were identified. With these experimental errors corrected, this allowed for confidence in future core flooding results.

5.2.2 Dead Oil Waterfloods on Small Sandpacks in Aluminum Core Holder

Various waterflooding experiments were performed in the aluminum core holder. All of these experiments used Lane Mountain 70 sand and a consistent overburden pressure of approximately 7,000 kPa (1,000 psi). A summary of all the experiments performed with these sandpacks is listed in Table 5.4.

In all of these sandpacks, similar values of rock porosity and permeability were measured. In Experiments # 4 - # 7 the same oil was used (HO1) and the water injection rate was varied. These experiments were performed to establish the effect of injection rate on recovery for an oil of constant viscosity.

In the end of Experiment # 7, the same sandpack was re-used by re-flooding with the same oil to establish a new irreducible water saturation. The same water injection rate (as in Experiment # 8) was then applied. It was known from the trouble-shooting tests that subsequent oil floods did not produce the same value of S_{wi}, thus Experiment # 8 was designed to investigate the effect of irreducible water saturation on the overall recovery of the waterflood, at the same injection rate.

Table 5.4: Summary of experiments performed on sandpacks with L ~ 17 cm

Experiment #	Oil used	Brine used	Q_{inj} (cm³/hr)	Description of waterflood
4	HO1	Doped	10	
5	HO1	Doped	15	
6	HO1	Doped	5	
7	HO1	Doped	1	
8	HO1	Doped	1	This exp used the sandpack of Exp 7 and re-flooded with oil to obtain new S_{wi}
9	HO1	Doped	10 & 1	Inject for 2 PVs at 10, then reduced to 1
10	HO2	Doped	20 & 1	Inject approx 5 PVs, then reduced to 1
11	HO2	Doped	10 & 1	Inject approx 5 PVs, then reduced to 1
12	HO2	Doped	1	
13	HO2	Doped	10 & 1	Inject for 2 PVs at 10, then reduced to 1
14	HO1	2% NaCl	10 & 1	Inject for 2 PVs at 10, then reduced to 1
15	HO2	Doped	1 & 10	Inject for 6 PVs at 1, then increased to 10

Experiment # 9 was designed both to measure the repeatability of the waterflood data and also to investigate the effect of reducing injection rate at late times in a waterflood. While the sandpack was still saturated with HO1, it was waterflooded at 10 cm³/hr for two pore volumes and then waterflooded at 1 cm³/hr for at another three pore volumes. At the lower injection rate, the magnitude of the viscous forces is reduced and the response of the flood efficiency was recorded.

Experiments # 10 – 12 also investigated the effect of injection rate on recovery, however these sandpacks were saturated with HO2. HO2 has a density of 0.9815 kg/cm³ with a viscosity of 11,500 mPa·s, so the viscosity ratio was increased by a factor of 2.5. The effect of higher oil viscosity was studied by comparing the results of these experiments against those obtained earlier for HO1 at similar injection rates. It must be noted that for the cases where the injection rate is 10 and 20 cm³/hr, after five pore volumes of brine were injected, the injection rate was also reduced to 1 cm³/hr. Again, this was done to observe the effect of reducing viscous forces late in the life of a waterflood.

Experiment # 13 was performed with the same purposes as Experiment # 9 (i.e. high rate water injection was only performed for the first two pore volumes). By repeating Experiment # 6 with the higher viscosity heavy oil, these two experiments could be directly compared to identify the effect of oil viscosity.

In Experiment # 14, different brine was used in the waterflood to investigate the effect of brine salinity on recovery. This experiment was performed since the doped brine used in previous experiments is fairly saline, and some researchers have reported improved oil recovery for low salinity systems (Zhang *et al*., 2007). Finally, Experiment # 15 was conducted to examine if a different flood response would be observed if constant pressure injection was applied instead of constant rate. However, the small pressure applied did not induce any oil production. Thus, the experiment was modified to inject at 1 cm^3/hr for about 6.8 PVs, afterwhich the injection rate was increased to 10 cm^3/hr for another 41 PVs, and after that the injection rate was reduced to 1 cm^3/hr.

The properties of these sandpacks are shown in Table 5.5.

Table 5.5: Properties of experiments performed on sandpacks with L ~ 17 cm

Experiment #	Length (cm)	PV (cm^3)	Porosity (fraction)	Permeability (D)	S_{wi} (%)	OOIP (cm^3)
4	16.50	69.99	0.372	1.86	12.25	61.42
5	17.40	71.71	0.361	1.79	12.77	62.55
6	16.70	69.40	0.364	2.80	11.65	61.31
7	16.60	68.00	0.359	2.43	11.62	60.10
8	16.60	68.00	0.359	2.43	15.68	57.34
9	16.65	68.91	0.363	2.87	10.72	61.52
10	17.20	71.75	0.366	2.76	10.33	64.34
11	16.95	68.70	0.356	2.79	10.61	61.41
12	17.55	71.01	0.355	2.79	10.34	63.67
13	17.40	71.04	0.358	2.44	10.28	63.74
14	17.25	70.64	0.359	2.20	10.83	62.99
15	16.95	69.16	0.358	2.58	11.17	61.44

The length of the sandpack was obtained from CT scanning, which could distinctively show the location of the inlet and outlet of the core. Permeability to brine was obtained when the sandpack was saturated with brine. The irreducible water saturation was obtained after five pore volumes of oil were injected at a fixed rate of 5 cm³/hr.

The first two sandpacks have permeability values that appear to be quite different than the remaining sandpacks, despite the fact that all cores were constructed using the same sand and with the same packing procedure. The difference in measured permeability is due to the fact that in these first experiments, brine was injected at a constant rate using a digital ISCO pump and the corresponding pressure drop was monitored using a digital gauge. As mentioned earlier, the digital gauge could not accurately display the true pressure drop in these high permeability systems, and the permeability calculated is not correct. Subsequent measurements were performed using constant head pressure injection, and the permeability was consistently larger. In reality, the sand permeability for the first two sandpacks is most likely in the same range of permeability measured in the subsequent cores, which all measured brine permeability using a constant head pressure approach.

The irreducible water saturation of the first two cases is also slightly higher than the remaining sandpacks (with the exception of Experiment # 8). This was due to underestimation of brine produced, since for these first two tests the separation method was still being fine-tuned. Results were later improved by adding significantly more toluene to the produced mixture to allow for the water droplets trapped in the oil phase to coalesce, thus the high S_{wi} values in the first two cores is likely incorrect, and S_{wi} should be similar to what was measured in subsequent systems.

As mentioned previously, Experiment # 8 was the results of re-flooding the core from Experiment # 7 with oil at the end of the waterflooding. For this reason, this experiment has a much higher S_{wi} than the other experiments.

Overall, the physical rock properties and S_{wi} values indicate that there is very little variation in the cores between experiments. CT scanning was done for most of these sandpacks dry, fully saturated with brine, at irreducible water saturation and at the end of waterflood. However, in Experiments # 10 and # 12 scans were also obtained at various stages of the waterflood. This was done to image the water advancement in the porous medium under conditions of high and low viscous forces.

These experiments were performed in order to investigate the significance of various parameters on heavy oil recovery. A detailed discussion on the results will be addressed in Chapters 7, 10 and 11.

5.2.3 Dead Oil Waterfloods on High Permeability Sandpacks

Lane Mountain 70 sand was also packed into an aluminum sleeve, on which a low overburden pressure of 2,000 kPa (300 psi) was applied between the sleeve and the PEEK bore. Even though the same sand was used, the difference in overburden pressure led to a significant difference in the properties of the sand, as shown in Table 5.6.

Table 5.6: Properties of Lane Mountain 70 core at low overburden pressure

Experiment #	16	17
Length (cm)	21.1	21.1
Diameter (cm)	3.63	3.63
Pore volume (cm^3)	97.64	101.53
Porosity (fraction)	0.447	0.464
Permeability (D)	9.05	9.73
S_{wi} (fraction)	0.115	0.132
OOIP (cm^3)	86.41	88.13
Injection rate (m/day)	0.412	0.023

At the lower overburden pressure, there was less force compacting the porous medium. The pore size distribution of this unconsolidated sand system is therefore expected to be larger than the case in the aluminum core holder, which used a rubber sleeve and higher overburden pressure. The result is a much higher porosity and permeability, as shown in Table 5.6. The irreducible water saturation is also slightly larger. At the end of the

waterflood, the core was cleaned by low rate injection of many pore volumes of toluene. When the produced toluene was clear, this was followed by high rate toluene injection and then injection of de-ionized water. Finally, acetone was used to displace water from the core and the core was dried using compressed air. It is interesting to note that even though the same sandpack was used in the second core flood, the rock properties measured still varied to some extent. This is an indication that the sand was not packed as well in the aluminum sleeve, due to the fact that tapping a rubber sleeve leads to a more compact pack than tapping an aluminum sleeve.

Other than exploring the obvious effect of rates, the significance of permeability of these sandpacks was also examined. Permeability should be an important factor in both viscous dominated and capillary dominated processes, and this will be discussed further in Chapter 7.

5.2.4 Dead Oil Waterfloods on Low Permeability Sandpacks

The core holder and the sand used in this suite of experiments is different than in the other systems. In these cores, the sand is still from Lane Mountain 70, but it was sieved to collect only the portion that is less than 75 μm. As a result, the sand is much finer and has a narrow grain size distribution. The sand was packed into a PEEK core holder, and there was no overburden pressure applied. Despite this fact, the fine sieved sand has a much lower permeability than in the other cores. Table 5.7 summarizes the properties of the experiments performed with these sandpacks.

Table 5.7: Properties of experiments performed on intermediate sandpacks

Experiment #	18	19	20
Length (cm)	53.2	53.2	53.2
Diameter (cm)	2.60	2.60	2.60
Pore volume (cm^3)	116.42	116.38	116.42
Porosity (fraction)	0.412	0.412	0.412
Permeability (D)	0.79	0.77	0.78
S_{wi} (fraction)	0.069	0.050	0.053
OOIP (cm^3)	108.45	110.61	110.25
Injection rate (m/day)	0.512	0.09	0.045

Similar to the experiments in the high permeability core, at the end of a waterflood the sandpack was cleaned with toluene, de-ionized water and acetone. The core was then dried and its porosity re-measured before placing the core under vacuum and re-saturating with brine.

In the first experiment of this set, a high rate waterflood was performed for five PVs. In the second experiment on this same sandpack water was injected at 0.09 m/day (2 cm^3/hr) for approximately five PVs after which the injection rate was reduced to half of its original value for another one PV. Finally, in the last experiment the flood was run at 0.045 m/day (1 cm^3/hr) for all five PVs. Again, the effect of injection rate and permeability is investigated through this suite of experiments and will be discussed in Chapter 7.

5.2.5 Dead Oil Waterflood on Large Sandpack

Several primary depletions studies and secondary waterfloods were performed on large sandpacks (D = 8.89 cm, L > 100 cm). A primary (dead oil) waterflood was also performed in another core that had similar dimensions, in order to directly compare primary and secondary waterflooding profiles. Lane Mountain 70 sand was again used in this experiment. This experiment was also designed to be similar to the dead oil floods in the small cores. Other than the dimensions of the sandpack, the overburden of this sandpack is also smaller: 5,600 kPa (800 psi). The reason for this lower overburden pressure is that in the other two large sandpacks after primary depletion the overburden pressure had decreased to around 5,600 kPa, so the overburden was reduced in this system as well to keep the rock properties consistent in the larger cores.

The properties of the sandpack (labeled "C") are shown in Table 5.8. The waterflood rates for this core were determined so as to have a comparison against the secondary waterflood rates in the other large sandpacks (discussed in Section 5.3). As a result, the core was waterflooded at 0.0106 m/day (2.75 cm³/hr) for approximately 1.7 PVs, after

which the injection rate was reduced to 0.00213 m/day (0.55 cm³/hr). At various times the sandpack was also CT scanned at fixed positions along its length.

Table 5.8: Properties of the large sandpack C

Length (cm)	114.8
Diameter (cm)	8.89
Pore volume (cm^3)	2477.22
Porosity (fraction)	0.348
Permeability (D)	3.86
S_{wi} (fraction)	0.081
OOIP (cm^3)	2277

This experiment was performed in order to study the relationship of viscous and capillary forces in a larger scale. The goal was to determine whether the results obtained for the small cores could be duplicated in a larger system, and also to have a direct comparison of primary versus secondary waterflood response for the same scale of core.

5.3 Secondary Waterfloods

Four sandpacks underwent secondary waterflooding after primary depletion. Two of these cores were packed using glass beads instead of LM 70 sand. One of these cores (labeled "E") was considerably smaller than the others. This core (D = 3.8 cm. L = 42.6 cm) is similar in dimensions to the small cores that had undergone primary (dead oil) waterflooding. The other core (labeled "D") has similar dimensions to the large dead oil waterflood system and the other two cores that underwent primary production followed by waterflooding in this study, however its permeability is higher. The rock properties and primary recovery for both of these systems are shown in Table 5.9. Primary depletion of these two sandpacks had previously been completed by Goodarzi (2006) and Goodarzi and Kantzas (2006). This work began with the cores at this state, and secondary waterfloods at fixed injection rates were performed. The glass beads in the cores were a sieved fraction of 80 – 100 mesh, which corresponds to sizes in the range of 150 – 180 μm.

Table 5.9: Properties of glass beads porous media

Sandpack	D	E
Length (cm)	118	42.6
Diameter (cm)	8.89	3.80
Pore volume (cm^3)	2178	165
Porosity (fraction)	0.318	0.377
Permeability (D)	3.5	6.67
S_{wi} (fraction)	0.0839	0.1099
OOIP (cm^3)	1995.27	146.87
Primary recovery (%OOIP)	30	38

For core E, it could be seen from Table 5.9 that primary depletion recovered 38% of OOIP. At the end of primary production, therefore, a large amount of oil had already been recovered and the reservoir energy has been depleted. The fluids existing in the porous medium at this point consist of oil and gas, and both could possibly be displaced by injected water in a secondary waterflood. For this sandpack an injection rate of 1 cm^3/hr (velocity 0.021 m/day) was employed. Unlike in primary waterflooding experiments at this same injection rate, very little oil was produced. Thus, the injected rate was then reduced to 0.1 cm^3/hr (0.0021 m/day), and at this lower rate oil was steadily produced with high water cuts. The produced oil and water mixtures were collected and a combination of NMR and separation was used to determine the volume of oil produced.

Similar observations were made when waterflooding sandpack D. Initially, this sandpack was flooded at a rate of 2.75 cm^3/hr (0.0106 m/day). Again, very little oil was produced at this condition, so the injection rate was reduced to 0.1 cm^3/hr (3.866 x 10^{-4} m/day).

Two other large cores (similar dimensions to core D) were also packed using LM 70 sand, and were saturated with live oil (HO2) and connate water. These cores had lower permeability than the glass bead systems. Primary production was performed, followed by constant low rate secondary waterfloods. The properties of these sandpacks (labeled as "A" and "B") are listed in Table 5.10.

Table 5.10: Properties of large secondary waterflood sandpacks

Sandpack	A	B
Length (cm)	115	118
Diameter (cm)	8.89	8.89
Pore volume (cm^3)	2592.38	2680.27
Porosity (fraction)	0.363	0.366
Permeability (D)	3.0	3.8
S_{wi} (fraction)	0.089	0.086
OOIP (cm^3)	2360.51	2451.04
Primary recovery (%OOIP)	20.4	27.0

The details of the primary production profiles for systems A and B are provided in Chapter 6, and secondary waterflooding is discussed in Chapter 8.

5.4 Waterflooding and NMR Monitoring

Two dead oil waterfloods were performed in a small PEEK core holder that is non-magnetic. The same sand LM 70 was used in these experiments and the properties of these sandpacks are shown in Table 5.11.

Table 5.11: Properties of waterfloods in small NMR core holder

Experiment #	21	22
Length (cm)	9.30	9.27
Diameter (cm)	2.54	2.54
Pore volume (cm^3)	21.68	21.45
Porosity (fraction)	0.460	0.457
Permeability (D)	14.5	15
S_{wi} (fraction)	0.089	0.090
OOIP (cm^3)	19.75	19.52
Injection rate (m/day)	0.0213	0.421

Due to the design of this core holder (previously discussed in Chapter 4), it was not possible to apply any overburden pressure to the sand, thus the permeability of both cores is quite high. These experiments were conducted in order to investigate the distribution of injected water under fast and slow injection cases. The goal of this study was to formulate an understanding at the pore scale regarding the nature of water invasion in viscous and capillary dominated process.

Further NMR measurements were also obtained on the low rate waterflood in the low permeability sandpack (Experiment # 20 in Table 5.7). In this longer sandpack, the goal was to use NMR to monitor the progress of the waterflood and the in-situ water saturation along the length of the sandpack. The two short core floods performed in Table 5.11 could only establish how brine displaces oil under high and low viscous forces, but they could not show this effect along the length. Thus, this experiment was performed in order to determine if this effect changes with length.

In summary, 22 waterfloods were performed in dead oil systems of varying scale. In some of these waterfloods, along with monitoring of pressure and produced fluid fractions, NMR or CT measurements were also obtained in order to obtain more information about the nature of the waterflood. The parameters investigated were the oil viscosity, the water injection rate, and the sand permeability. Four secondary waterfloods were also performed, which studied, which also investigated the effect of changing water injection rate in systems of varying permeability. The goal of all of these waterfloods was to investigate the relative significance of viscous and capillary forces during low rate waterflooding in heavy oil systems.

CHAPTER 6: PRIMARY DEPLETION RESULTS

The main goal of the primary depletion experiments was to establish the primary production stage so that secondary waterfloods could be performed. A secondary objective was to interpret the data collected from the primary production experiments in order to characterize of the nature of the cores at the end of primary production. This is important for understanding if primary production will affect the waterflood response compared to dead oil systems. The two sandpacks were packed and depleted in the same manner in the hope of establishing the same condition at the end of primary production. Despite these efforts, the properties of the sandpacks and the resulting depletion were not exactly the same, as can be seen from the table below.

Table 6.1: Properties of sandpacks and its fluids

Sandpack	A	B
Length (cm)	115	118
Diameter (cm)	8.89	8.89
Pore volume (cm^3)	2,592.38	2,680.27
Porosity (fracion)	0.363	0.366
Permeability (D)	3.0	3.8
S_{wi} (fraction)	0.089	0.086
OOIP (cm^3)	2,360.51	2,451.04
Density of dead oil (g/cm^3)	0.9815	0.9815
Density of live oil (g/cm^3)	0.973	0.963
Viscosity of dead oil (mPa·s)	11,500	11,500 (?)
Viscosity of live oil (mPa·s)	4,245	3,759
GOR	12.4	11.6
Density of brine (g/cm^3)	1.0487	1.0487
Rate of depletion (kPa/min and psi/min)	2.41 (0.35)	2.41 (0.35)
Recovery (% OOIP)	20.4	27.0

Although the two sandpacks were depleted at the same rate, the recoveries obtained were not the same. Before beginning secondary waterflooding, this difference first had to be reconciled. Specifically, the variation in primary recovery had to be explained physically, in order to determine if this would affect the subsequent waterflood response. Table 6.1 shows that the permeability of sandpack B is higher than that of sandpack A.

This difference is most likely due to the fact that even with agitation and wet packing, it is not trivial to replicate a full diameter, unconsolidated core. Another difference in the two depletion experiments is that the live oil used in sandpack B is less viscous than the oil used in sandpack A. There are several possible explanations for this difference. First, it is not always possible to create the same live oil (similar viscosity and density) due to the inability to reproduce the exact same mixing conditions. This is because the regulator controlling the input of methane has a certain accuracy that does not easily allow the same mixing pressure for different batch of oil. Additionally, although the same dead oil was used in both core floods, it is possible that the oil viscosity was lower in the second flood due to heterogeneities in the oil between different batches. The oil that was provided by Nexen came in several buckets and samples were initially taken from each bucket to ensure that the oil was all the same, but sub-sampling of viscosity was not performed at later times or as a function of depth in the buckets. Therefore, it is possible that the oil itself may have been more viscous in sandpack A.

In the literature, the effects of varying both the rock and fluid properties on primary depletion have been discussed in considerable detail. Various researchers have investigated the influence of permeability on the production of foamy oil. They essentially have observed that for higher permeability sand, the production is higher as well. Dumore (1970) showed that for a higher permeability sandpack, the liberated gas remained dispersed for a longer period. Wall and Khurana (1971) proposed that the free gas saturation is controlled by capillary forces, and is therefore a function of permeability. Ostos and Maini (2005) related the influence of permeability to gas trapping versus flow in a capillary number-type analysis. Goodarzi and Kantzas (2006) also showed that in higher permeability porous media the pore sizes are relatively larger, thus the capillary trapping forces are lower, although in longer systems this was not uniform with length. The permeability effect can be understood by comparing the rate of production to the rate of gas liberation from the oil. The flow of fluid in larger pores is easier, thus the newly nucleated gas has less time to grow within the pores before it would be swept up by the moving oil. This resulted in small gas bubbles remaining

dispersed within the flowing oil for a longer period of time. While gas bubbles are not connected, the mixture is a highly compressible foamy oil flowing in the rock pores. This allows the pressure gradient across the core to remain high, and the end result is higher production rates and recovery for the higher permeability porous medium.

The effect of live oil viscosity on primary recovery is more obvious. From Darcy's Law it is obvious that if the pressure drop is the same in both cases, the sandpack saturated with a lower viscosity oil would yield a better production rate. Thus one would expect the case of lower viscosity would have better primary recovery. Naturally, once gas begins to leave solution the liquid viscosity will begin to increase for any live oil viscosity (Huerta *et al*., 1996; Bora *et al*., 2003; Shen and Batycky, 1999). In general, however, if live oil viscosity is lower, the viscosity of the liquid at any elevated pressure will be proportionally lower as well.

From the fundamental theory and data presented in the literature it is apparent that the combination of higher permeability and less viscous fluid would result in better primary recovery. Thus the recoveries obtained from both sandpacks are not too surprising. The results of the two sandpacks are further analyzed below, to determine the state of the cores at the point when secondary waterflooding can commence.

6.1 Pressure Response during Depletion

The various pressures collected from the two sandpacks are compared in Figures 6.1 and 6.2. Pressure was measured using digital transducers (range 0 – 7,000 kPa) at the inlet and outlet of the core. In the primary production experiments, the pressure in the system was depleted linearly by steadily reducing the pressure on a back-pressure regulator (BPR) located at the backend of the system. Pressure declined at a set rate of 2.41 kPa/min (0.36 psi/min), which was set using a mass flow controller connected to the gas side of the BPR.
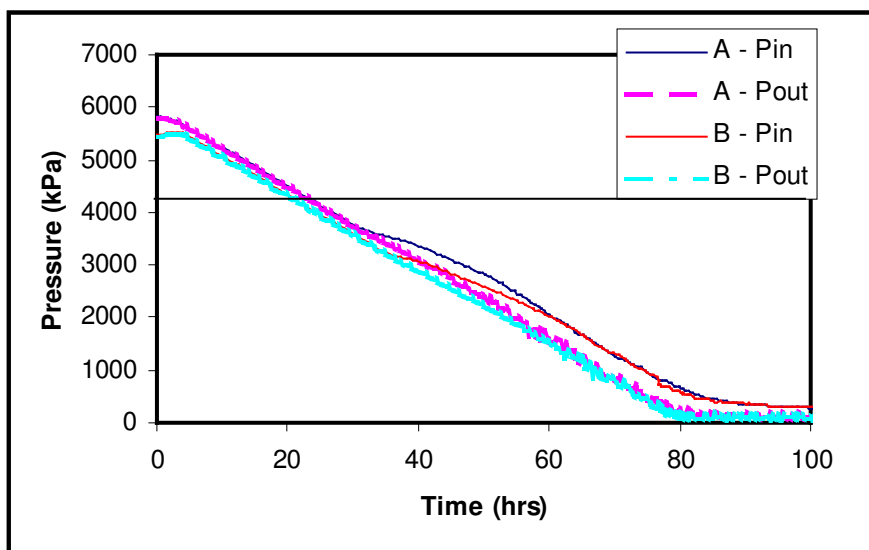
Figure 6.1: Primary depletion of systems A and B – inlet and outlet pressure change with time

As the BPR pressure dropped, the pressure at the outlet decreased accordingly, since fluid from the outlet of the core flowed directly into the BPR. At early times, the slope of the pressure change with time (dP/dt) at the inlet to the core also dropped steadily with time, indicating that the core pressure was declining according to the rate set by the mass flow controller. During this period, the declining pressure at the core outlet very quickly transmitted through the core, and the inlet pressure dropped accordingly as well. This shows that at these early times and elevated core pressures, there was only a single phase, relatively low compressibility fluid present in the core (Craft *et al*., 1991). The core was initially saturated with live oil, which does have a greater compressibility than dead (gas-free) heavy oil or water, however the fact that pressure was transmitting so quickly through the core indicates that the fluid was a single-phase liquid, and that no free gas was present. Thus, as expected, the core was initially above the bubble point pressure.

The fast pressure response in the inlet pressures also indicates that for this size of core (approximately 115 cm in length), pressure was able transmit very quickly along the entire length of the core. In a longer core system or a reservoir, even at pressures above the bubble point, the length of the system is much greater and a pressure gradient will

therefore exist even in the time before gas leaves solution in the oil (Goodarzi and Kantzas, 2006). In these sandpacks, with the presence of the declining pressure at the core outlet felt all along the length of the core, gas will leave solution everywhere in the core once pressure has declined below the supersaturation threshold. Since gas evolution will occur all along the core and not just near to the outlet, the recovery from these cores will be higher than what is expected in the field. In longer systems, most of the gas evolution and oil production occurs close to the production wells (Goodarzi and Kantzas, 2006). Therefore, sand production may be required in order to induce significant recovery from heavy oil primary production. In shorter core systems, the fact that pressure can quickly transmit along the entire core length means that enhanced recoveries can be expected even with no sand production in the experiment.

After close to 30 hours of pressure depletion, the inlet pressure decline began to deviate from the outlet pressure values, as shown in Figure 6.1. Figure 6.2 plots just the inlet pressures for systems A and B, in the first 100 hours of the depletion.
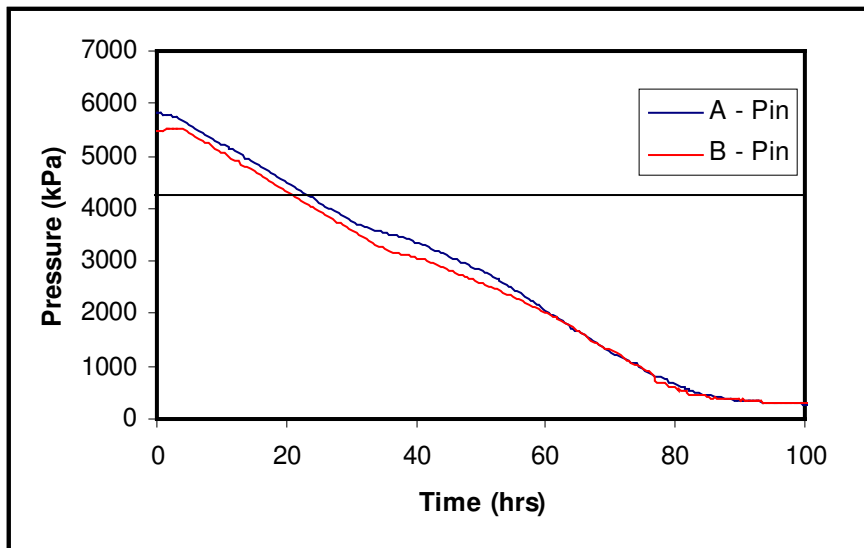
Figure 6.2: Inlet pressures for systems A and B for the first 100 hours of depletion

Up to approximately 30 hours of depletion, the inlet pressures for systems A and B declined linearly, as discussed previously. At approximately 30 hours, however, the

slopes of the dP/dt relationship reduced for both systems. This is an indication that something had changed in the system, whereby the inlet pressure was now dropping more slowly than it was before. Since there was no sand production, rock properties should remain constant, and the decrease in the inlet pressure decline rate implies that a more compressible fluid was now present in the rock pores. At this point, a second phase (gas) had evolved. The change in slope occurred at approximately 3,640 kPa (528 psi) for system A and 3,175 kPa (461 psi) for system B. Since the measured bubble point pressure for this oil was found to be 4,200 kPa (610 psi), this indicates supersaturation pressures of 560 and 1,025 kPa (80 and 150 psi) for systems A and B respectively. Below the supersaturation pressure, a highly compressible gas phase existed in the system. The change in the dP/dt slope indicates that this gas exists, but it cannot provide any insight into whether the gas is a continuous phase, or if gas bubbles are discontinuous in the oil.

Figure 6.3 shows the differential pressure (inlet – outlet pressure) measured across the cores as a function of time. At early times, when pressure is dropping at equal rates at both the inlet and outlet, the differential pressure across the core is low, once again indicating a low compressibility liquid present. Once the free gas phase forms and the pressure decline rate changes at the inlet, this shows up as a large pressure drop evolving across the core in Figure 6.3.

The increase in differential pressure occurred after around 30.5 hrs of depletion in system A, and after 35 hrs in system B. This is a verification of the higher supersaturation for system B, since both depletions began at similar pressures and the outlet pressures were decreased at the same rate. In system A, the differential pressure drop across the core increased to 680 kPa (99 psi), and then leveled off at around 470 kPa (68 psi) until around 82 hrs of depletion, at which point the differential pressure decreased again. In system B, the maximum differential pressure is similar to A but the elevated pressure drop region has a higher value of approximately 500 kPa (73 psi). For the length of these

core systems, this corresponds to elevated pressure gradients of 392 kPa/m (17 psi/ft) and 417 kPa/m (18 psi/ft) for systems A and B respectively.
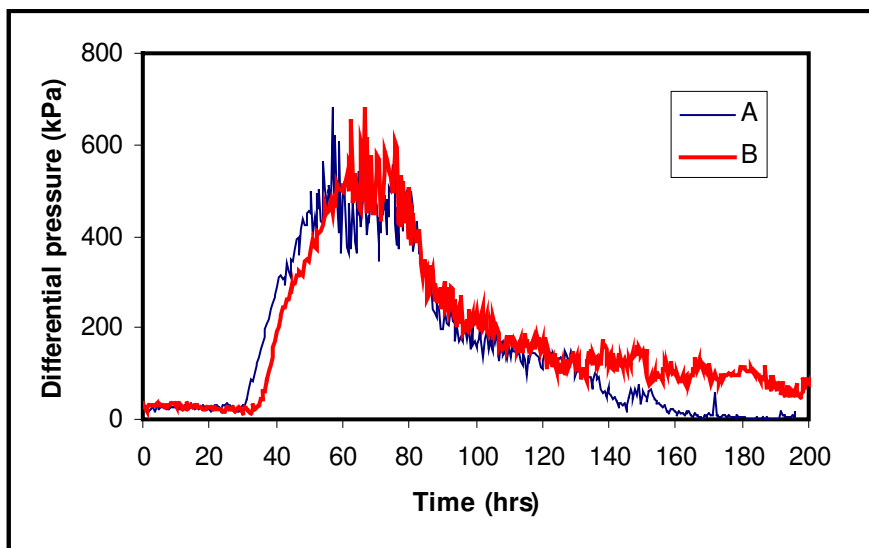
Figure 6.3: Differential pressure vs. time for systems A and B

Several comments can be made regarding the differential pressure profiles shown in Figure 6.3. First, the reason for the high pressure gradients should be explained. As gas leaves solution, the liquid phase is becoming more viscous (Goodarzi *et al*., 2006). This will slow the rate of pressure propagation through the core, and could be partly responsible for the elevated pressure differential in Figure 6.3. However, if this were the primary cause of the pressure drop, then the production rates should also decrease as oil becomes more viscous, and this was not seen in foamy oil experiments. Therefore, the main reason for the increased pressure differentials is the formation of a highly compressible free gas phase that expands and keeps the pressure in the core elevated.

A second observation is that the differential pressure profiles provide an indication of the nature of the free gas phase. While pressure gradients are high, this indicates that some of the gas has left solution, but this gas cannot flow out easily. Once the gas becomes continuous, the free highly mobile gas will then quickly flow out of the core, and the pressure differential will decrease. This point is taken to be the critical gas saturation in

conventional oil solution gas drive (Craft *et al*., 1991). In these cores, the critical gas saturation is reached at approximately 80 hrs of depletion for both cores. Finally, the fact that system B has a higher pressure gradient than system A indicates that, with all else being equal, the oil production rates and recovery are expected to be better for this core.

6.2 Production Response during Depletion

The calculation of the oil and gas production rates for both systems A and B are shown in Appendix E. The oil production and the corresponding pressure drop for system A are shown in Figure 6.4. It is not surprising that the oil rates and the increase in the pressure gradient mirror one another, in accordance with Darcy's Law. It should be noted, however, that in the time where the oil rate is increasing, the pressure has already exceeded the supersaturation so some gas has now left solution with the oil. Although the fluid viscosity is increasing, oil rates still increase. This shows that the high pressure gradient formed in the core is responsible for the enhanced recovery of foamy oil flow, even with increasing fluid viscosity. During this time, oil is produced due to enhanced viscous forces in the system. System B also has similar behaviour: the high oil rates correspond to the times during which the pressure gradient in the core is high. As gas connects and flows out of the core as a free gas phase, the pressure gradient decreases and oil production rates decrease accordingly.
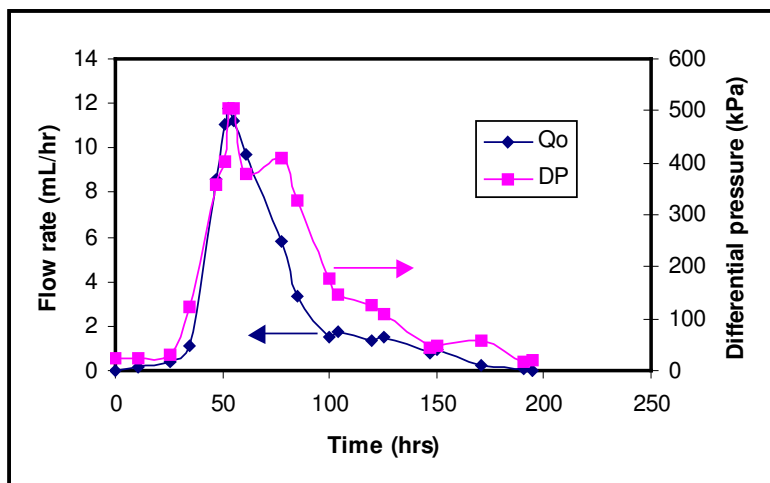
Figure 6.4: Oil production rate and pressure drop for system A

The oil production rates obtained during primary recovery of both systems are compared in Figure 6.5. This figure shows that the oil rates increase at similar times, but that the oil production rate in system B is higher than in system A. From Table 6.1, it could be seen that the total oil recovery is also higher for this system.
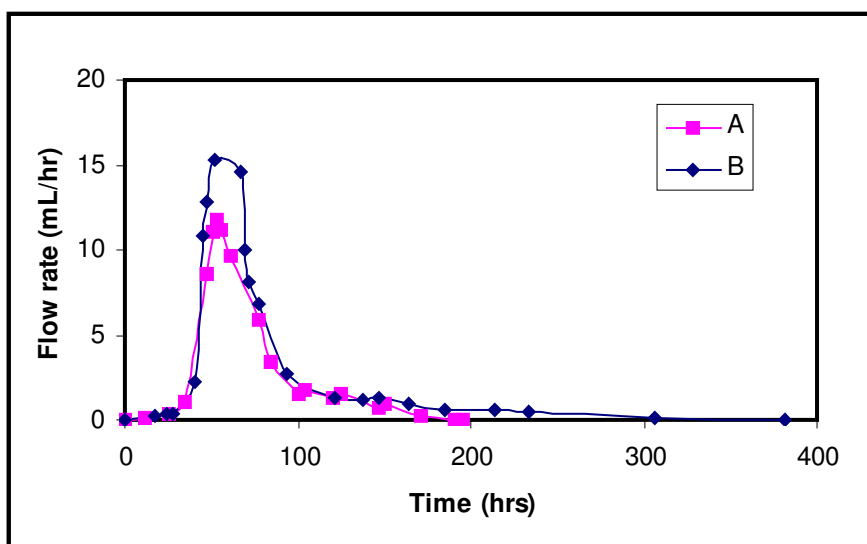
Figure 6.5: Oil production rates for systems A and B

Figure 6.3 previously showed that the differential pressure in system B was higher than in system A. This should lead to enhanced rates in this core, which was observed in Figure 6.5. Additionally, it was previously shown that system B also had a higher supersaturation than system A. Higher supersaturation means that the pressure drops by a larger extent before free gas bubbles are formed in the system, so supersaturation is the driving force for gas phase formation. Firoozabadi *et al*. (1992) showed that smaller supersaturation values (i.e. a lower gas phase formation driving force) led to lower values of critical gas saturation. At the point of the critical gas saturation gas can flow as a continuous phase, so this indicates the end of the enhanced "foamy oil" flow rates. A system with a higher supersaturation will therefore perform better than a system with a lower supersaturation, and this is another reason for the higher rates in system B, in Figure 6.5.

Figure 6.6 shows the oil flow rate divided by the pressure difference in the core, for both systems A and B.
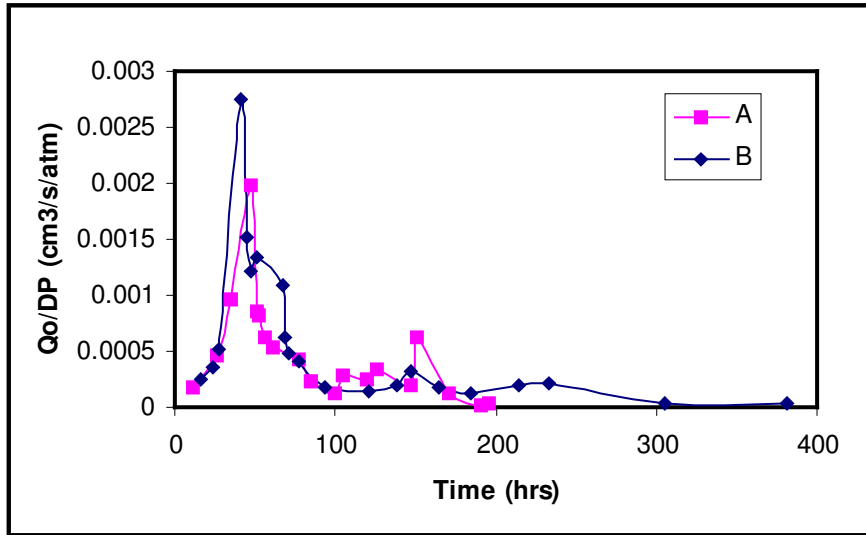
Figure 6.6: Relative fluid mobility values for systems A and B

From Darcy's Law of single phase flow in cores of similar length, the ratio of flow rate to pressure drop (in cores with the same cross-sectional area) gives an indication of the fluid mobility (k/μ). As expected from the rates plotted previously, the oil in system B is more mobile than in system A. This is expected, given the higher rates and recovery in this system.

It was discussed previously that a higher degree of supersaturation and a higher developed pressure gradient will lead to enhanced rates in the core, which corresponds to a higher mobility fluid. At the same depletion rate, the factors that can be responsible for the higher oil mobility in system B are the sand permeability and the oil viscosity at any pressure. Table 6.1 shows that system B has both a higher sand permeability (leading to slower gas coalescence) and also a lower live oil viscosity, but the overall effect of viscosity is unclear since the oil viscosity changes with pressure in the system were not measured directly. In order to identify the contribution of the fluid viscosity, Figure 6.7

plots the ratio of oil flow rate to pressure drop once again for both systems, but now the ratio also includes the sand permeability. In this manner, the effect of oil viscosity can be inferred.
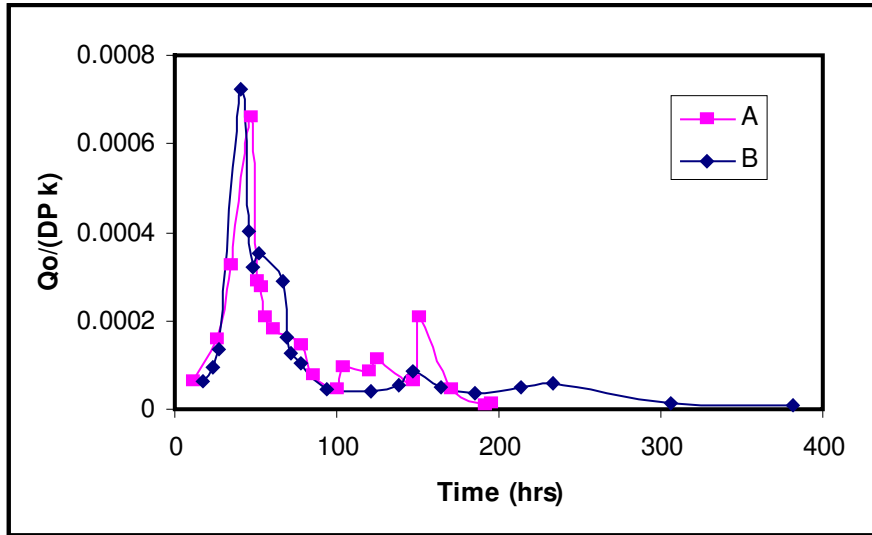
Figure 6.7: Effect of oil viscosity on fluid mobility for sandpacks A and B

The profiles in Figure 6.7 are now much more similar between cores A and B. Therefore, by incorporating the absolute permeability into the y-axis of Figure 6.7, it can be seen that the improved oil mobility in system B was much more strongly a function of the higher permeability of this core than of the lower fluid viscosity. It should be noted that although both cores peak at similar values of maximum Q_o/ (DP k), the values for system A drop more quickly than those in system B. The term plotted in Figure 6.7 is inversely proportional to the fluid viscosity, therefore part of the enhanced oil mobility in system B is due to the oil viscosity remaining low for a longer time in this core. Once gas leaves solution with oil, the oil viscosity will increase. However, when the growth of gas bubbles is slow compared to the pressure depletion rate, even gas bubbles that have left solution may be small enough that they still act to swell the oil and reduce its apparent viscosity (Goodarzi *et al.*, 2007). Additionally, when the free gas becomes continuous, this is an indication of the end of the enhanced primary production response. For these two cores it appears that the influence of the pore space on the development of the

continuous free gas phase is more important than the difference in the fluid viscosity between the two cores.

Figure 6.8 shows the differential pressure profile for system A, along with the cumulative produced gas-oil-ratio (GOR). This figure shows the effect of the produced gas on the pressure of the system. At early times, when the differential pressure is low, the produced GOR is constant. After approximately 30 hrs the differential pressure in the system begins to increase, indicating that a compressible gas phase has formed in the system. However, the produced GOR does not actually increase until after 50 hrs of depletion. At the point where the GOR starts to increase, pressure in the core begins to drop. After 85 hrs of depletion the GOR has reached its final value; at this point there is little differential pressure remaining in the core. By comparing Figures 6.4 and 6.8 it is also apparent that as the GOR increases, or as a higher proportion of gas is produced from the core, oil rate also begins to decrease along with the system pressure. The point where the produced GOR begins to increase indicates the presence of free gas flowing as a continuous phase in the core. When this occurs, the relative permeability to oil decreases and the oil rate declines accordingly.
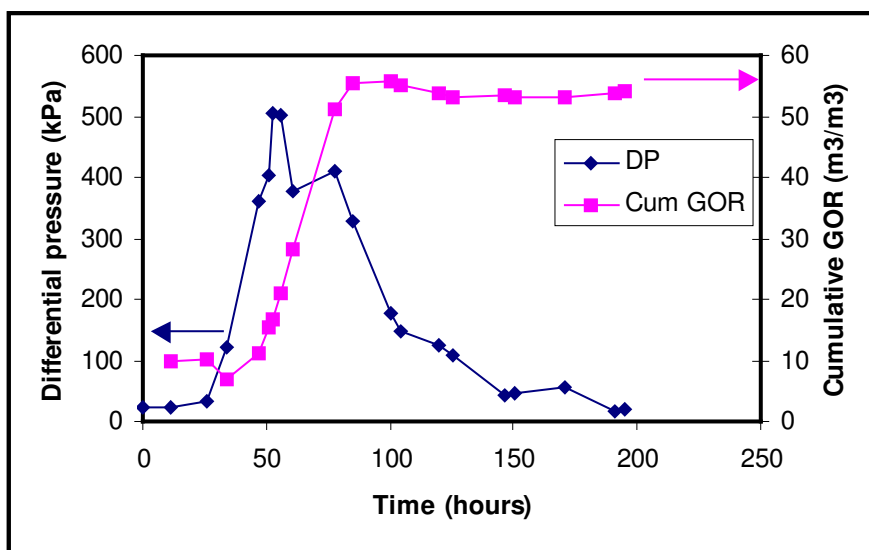
Figure 6.8: System A – differential pressure profile and cumulative produced GOR

Figure 6.9 shows the same correlation between the differential pressure across the core and the produced GOR for system B. In this case, although the differential pressure in the system begins to build up after 35 hrs, the produced GOR does not increase until after approximately 51 hrs of depletion, at which point the differential pressure in the system begins to drop as well. By 95 hrs the produced GOR has reached its final value.
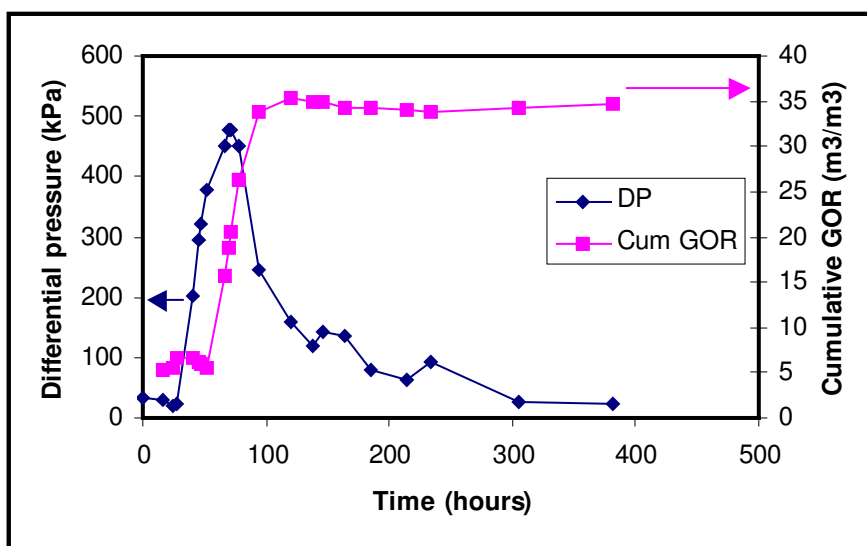
Figure 6.9: System B – differential pressure profile and cumulative produced GOR

In cores A and B, once the produced GOR begins to increase, the differential pressure across the core correspondingly begins to drop and this means that the critical gas saturation has been reached. The critical gas saturation occurs at similar times in both sandpacks A and B, and the final GOR value is also reached at similar times. In system B, however, the decline in the differential pressure occurs much more slowly than in system A. In Figure 6.9, it can be seen that even after the produced GOR reaches its final value there is still a significant differential pressure in the system. Additionally, the core requires almost 400 hrs for the pressure to be fully depleted, compared to only 200 hrs for system A. This indicates that in system B, although the GOR response is similar in both cores, the gas is somehow less mobile than in system A and this translates to improved oil rates and recovery.

Figure 6.10 plots the cumulative oil and gas production along with the average pressure in the core for system A. This plot also shows the influence of gas production on the oil production and the system pressure.
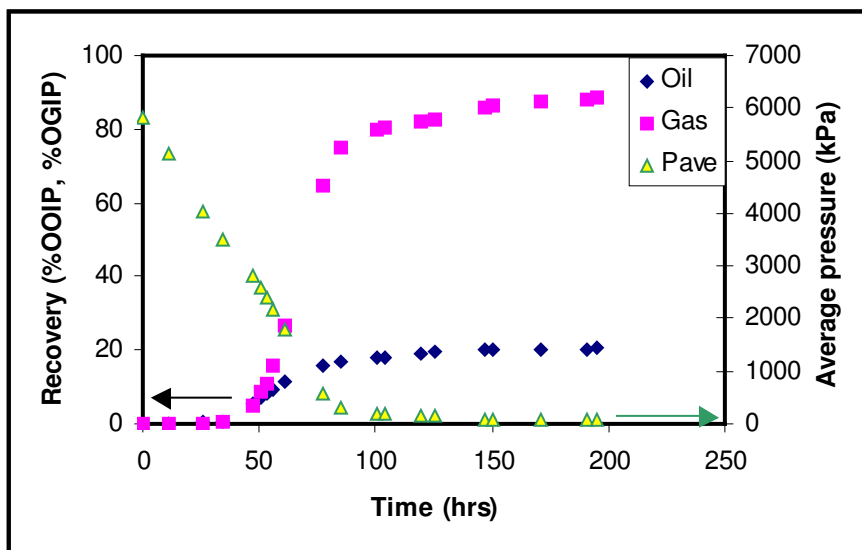
Figure 6.10: System A – oil and gas recovery and average core pressure with time

The final oil recovery factor after 200 hrs of pressure depletion in system A is 20% of OOIP, and the gas recovery factor is 89% of the original gas in place (OGIP). At the end of the depletion there is still some gas trapped in the system, even though the pressure in the core has been fully depleted. This indicates that, although all the gas has likely left solution with the oil, some of the free gas is not connected to the core outlet. The oil and gas production and average core pressure for system B is shown in Figure 6.11. In this core, the final oil recovery factor after approximately 400 hrs of depletion is 27% of OOIP, and the gas recovery factor is 80% of OGIP. The fact that the gas volumes remaining are larger than the evacuated volumes from the oil production means that even in the final state of the cores, when the pressures are low, the gas is still relatively compressed.
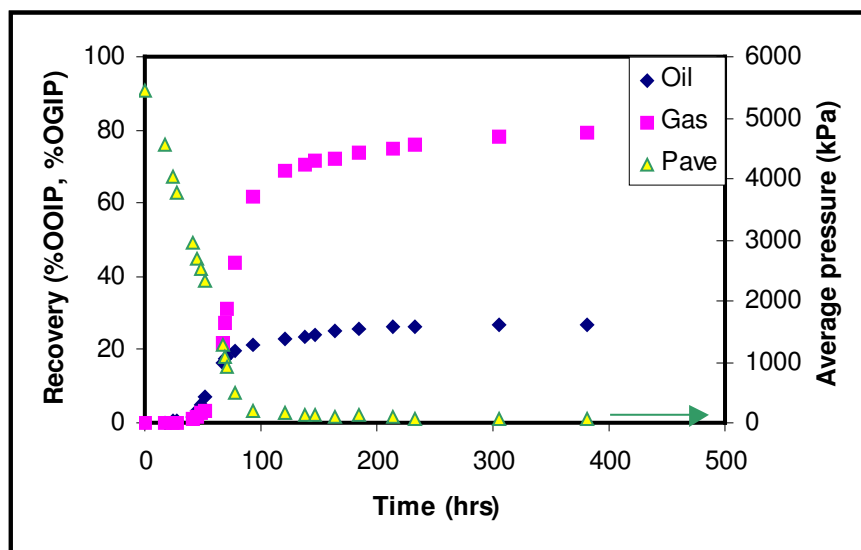
Figure 6.11: System B – oil and gas recovery and average core pressure with time

For both cores, at early times while the pressure in the system is high, this is single-phase flow. During this time, the oil and gas production are both low. Once the system pressure drops further and the differential pressure in the system increases, both the oil and gas production increase as well. In these cores, therefore, it has been demonstrated that the presence of foamy oil (discontinuous gas) is required in order to recover oil.

6.3 Comparison of Systems A and B against Other Depletion Study

Other primary depletion studies were previously performed and have been summarized by Goodarzi (2006) and Goodarzi and Kantzas (2006). These cores utilize the same heavy oil as in systems A and B, but the live oil was mixed at different pressures and depleted in sand packs of varying dimensions. These are defined as systems D and E. In Chapter 8, secondary waterfloods will also be performed in these two other sand packs, thus there is value to first comparing the primary production response in all four systems. Table 6.2 compares the rock and fluid properties of these four sand packs. Along with the live oil viscosity and the sand permeability, the maximum pressure gradient was also determined for all four systems. In order to compare the primary production responses, the maximum value of velocity, as

represented by Darcy's law, is also shown in Table 6.2. This value is calculated using the maximum pressure gradient and the value of the initial live oil viscosity. Obviously, at the point where the maximum pressure gradient occurs the oil is no longer merely live oil, since some gas has left solution and the dispersed gas bubbles are responsible for the high pressure gradients developed. Thus, a simple Darcy's law calculation like the one shown in Table 6.2 is not representative of any actual flow rate, but this term can be thought of as a representation of flow due to viscous forces.

Table 6.2: Properties and recovery of primary depletion in various systems

System ID	Length (m)	Live oil viscosity (mPa·s)	Permeability (D)	Max ΔP/L (kPa/m)	Max $(k/\mu)(\Delta P/L)$	Oil recovery (% OOIP)
A	1.15	4,245	3.0	437	0.309	20
B	1.18	3,759	3.8	404	0.409	27
D	1.20	6,949	3.5	2096	1.056	38
E	0.43	4,780	6.7	1233	1.269	38

As can be seen, the depletions performed in systems D and E had much higher maximum pressure gradients than systems A and B. However, the live oil viscosity was also higher for these cores. Overall, it appears that the oil recovered through primary production can be correlated to the maximum of the right-hand side of Darcy's Law (i.e. the maximum Darcy velocity, or the representation of the viscous forces). This is shown in Figure 6.12.

The results of Table 6.2 and Figure 6.12 show that in primary production, the oil recovery is directly proportional to the magnitude of the viscous forces, as shown in the simplified Darcy's law calculation. In other words, in systems where free gas bubbles nucleate but cannot coalesce into a continuous gas phase, this disconnected highly compressible phase allows for the development of a high pressure gradient in the core, and this in turn leads to improved oil flow rates and recovery.
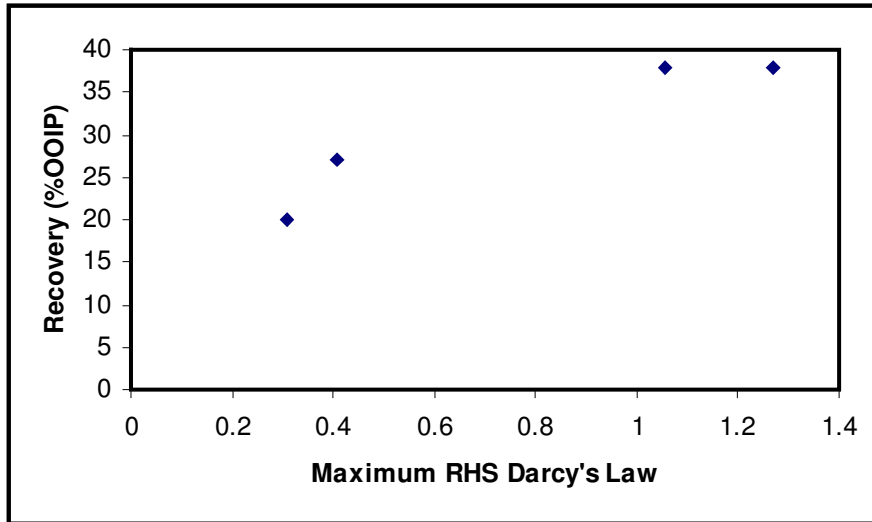
Figure 6.12: Oil recovered by primary production plotted as a function of viscous forces

In primary production, therefore, oil recovery is due to viscous forces and recovery is optimal in high permeability cores or systems with developed pressure gradients.

6.4 Gas Saturation in the Cores

Calculations of gas saturation were made using CT scanning, by applying the equations presented in the literature (Vinegar and Wellington, 1987; Kantzas, 1990). In this calculation, the pore space is filled with oil, gas and irreducible water. By comparing the CT numbers at various saturation stages – dry, water saturated, live oil with S_{wi}, and during primary depletion – measurements of the free gas saturation in the core can be made. It should be emphasized that in this approach, the connate water was assumed to be irreducible and immobile, thus as oil was produced from the core at pressures below the bubble point, the void space left in the pores was assumed to be filled with free solution gas. Figure 6.13 plots the gas saturation with length at various times in the depletion of core A.
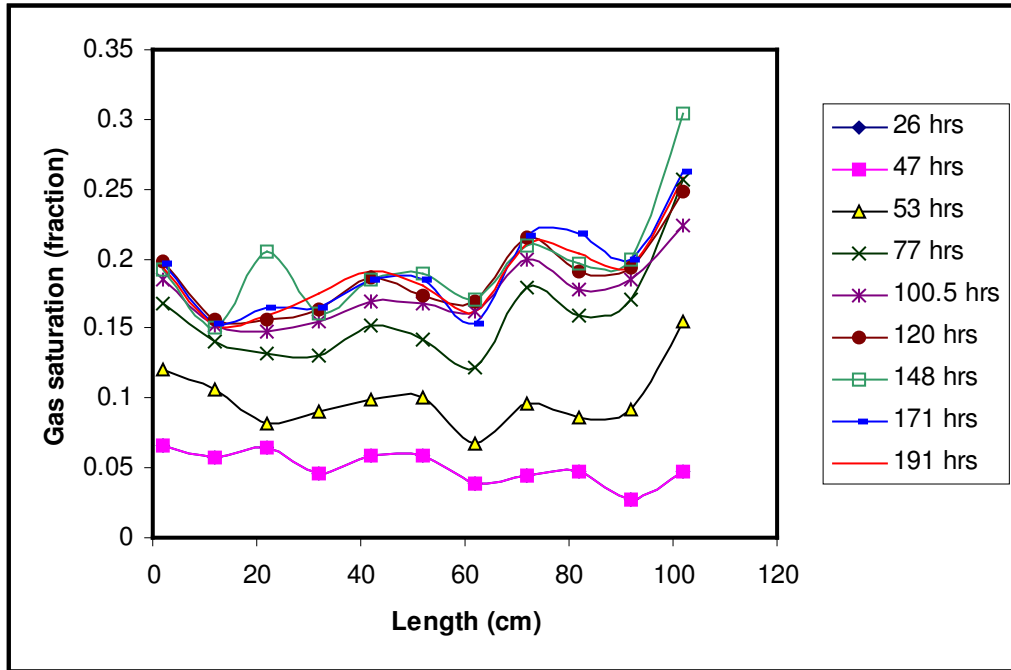
Figure 6.13: CT calculations of free gas saturation vs. length for system A

It is interesting to note that at early times, when pressure in the core is still high, the free gas fraction forms along the length of the whole sandpack. This implies that gas leaves solution all over the core, which was also previously measured in bulk liquid studies (Goodarzi *et al*., 2007). During this period, the differential pressure gradient in the core is high and oil production rates are enhanced. Despite this high pressure gradient, more oil is recovered from the latter half of the core (after 60 cm), thus at the end of the primary depletion the free gas saturation is higher (i.e. the oil saturation is lower) closer to the production end. Goodarzi and Kantzas (2006) also observed this effect in 1.2 m cores compared to a shorter core (system E in Table 6.2), where gas saturations were more uniform with length at the end of primary production.

Figure 6.14 shows the CT calculations of gas saturation with length in core B. In this core, the oil recovery factor was higher than in core A, and this is evident in the higher gas saturations compared to Figure 6.13. The high gas saturations near to the inlet (length = 0) at early times are an experimental artifact; overall the gas saturations in both

systems A and B matched the values obtained by mass balance of the produced oil. It can be concluded for both systems that significant free gas is present throughout the core, but that gas saturation is not uniform with length.
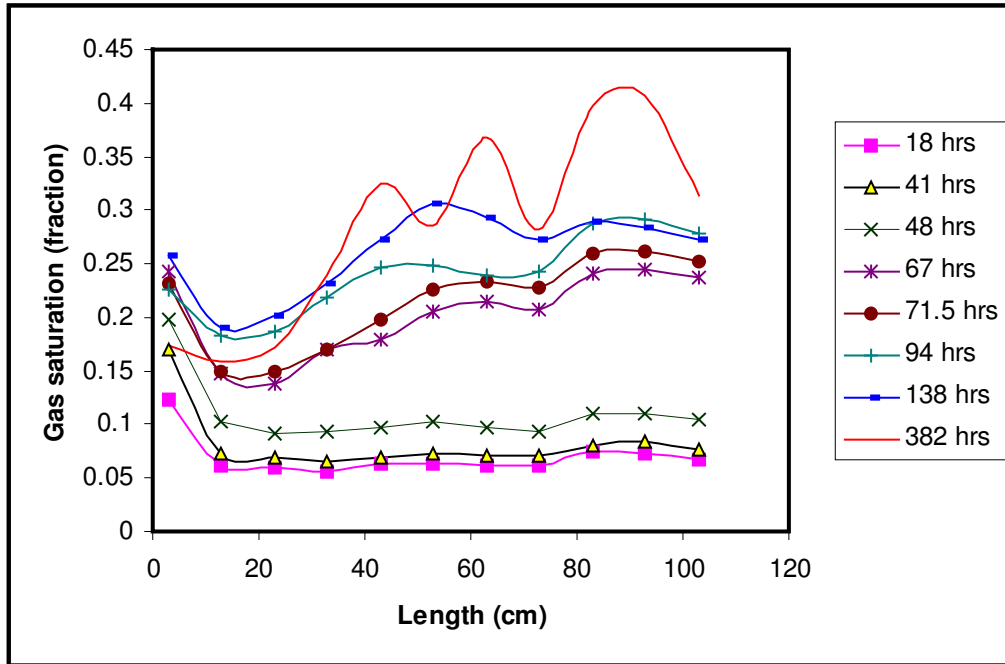
Figure 6.14: CT calculations of gas saturation vs. length for system B

An additional piece of information that can be extracted from the analysis of the CT data is the physical location of this free gas in the core. As mentioned previously, gas initially leaves solution at nucleation points throughout the whole core. Gas bubbles grow due to local pressure gradients and variances in capillary pressure in different sized pores. Eventually, gas becomes continuous and this corresponds to the point where the produced GOR increases, accompanied by a decrease in the oil rates. At the end of primary production, if the oil can drain through gravitational forces (i.e. differences between oil and gas density) the gas will collect near to the top of the core as a gas cap. In heavy oil systems, oil does not flow easily in order to drain, thus it is not clear if this will happen. CT images from different saturation states were compared in order to obtain an

understanding of where in the core the free gas is located. Images of gas saturation versus length are shown for system A in Figure 6.15.
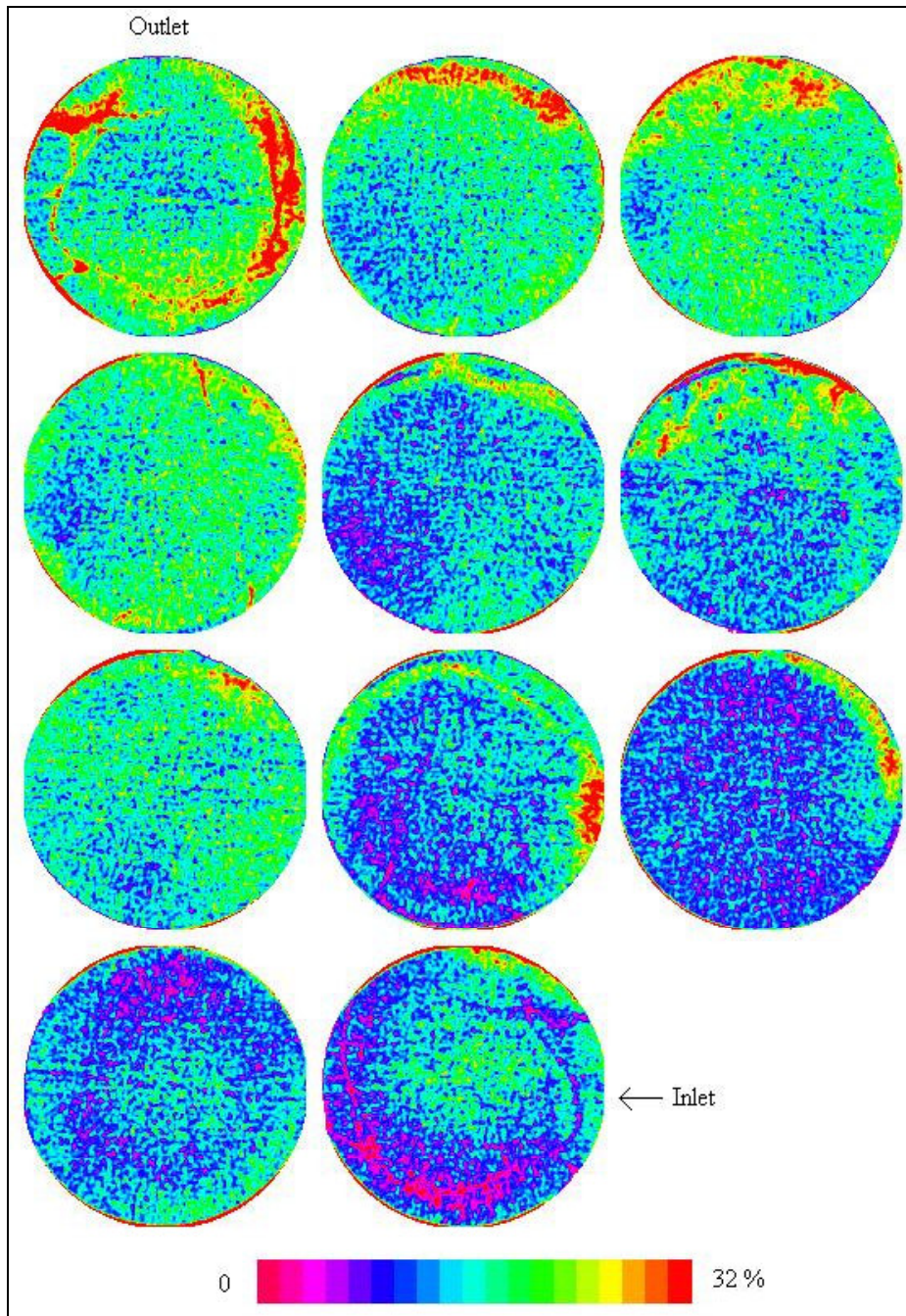
Figure 6.15: Cross-sectional CT images of gas saturation vs. length in system A

In order to construct this figure, cross-sectional images were taken at the same values of length for the condition of the core containing oil with irreducible water, and compared to

the images at the end of primary depletion. Since the location of the images is the same, by subtracting the final images from the initial state, the effect of the sand is removed. The difference in the CT numbers can then be related to the gas saturation: regions with higher differences can be converted into lower density ranges, which correspond to higher gas saturation.

Both Figure 6.14 and 6.15 shows that, as expected, the regions of higher gas saturation are located close to the outlet end of the core, where the gas saturation is high all over the core. Close to the inlet, the gas saturation is lower in each entire cross section. However, even at the outlet end, the regions of highest gas saturation do not always occur at the top of the sandpack. In certain cross-sections, the gas is located near to the sides of the core instead of at the top. In all cases, the regions of highest gas saturation occur close to the core edge, where the sand meets the rubber sleeve. Although the core was compressed using a high overburden pressure, in general there can still be larger spaces at the edge of the pore material. This corresponds to larger pores, where capillary forces will be lower and the non-wetting gas phase can more easily grow and travel. Figure 6.15 shows that in this 1D heavy oil system, the viscous oil at the end of primary production cannot easily drain by gravity, thus the gas channels formed tend to be tortuous and possibly disconnected, instead of forming a gas cap in the upper region of the core.

6.5 State of the Core at the End of Primary Production

As was shown in the production and CT data for these two cores, at the end of primary production a significant fraction of oil had been already recovered, and the cores both contained free gas saturation. Since there was no sand production (i.e. wormhole formation) in these tests, these are the only two conditions that are different from the state of the core without any primary production. The pressure is low at this stage, and gas has left solution with the oil, thus there are sections of low viscosity free gas present in the core. The low pressure in the system is an indication that the gas will have left solution in the oil, so the oil viscosity will be the dead oil value, which is the same as in primary (dead oil) waterflooding.

The regions of high gas saturation exist throughout the entire length of the core, with the outlet end having higher gas saturation compared to the inlet. These regions of low viscosity gas will act as channels of low resistance for injected water during a waterflood. However, it cannot be determined from the CT images or calculated gas saturation values whether the gas channels are connected or discontinuous. This will be investigated in Chapter 8, by monitoring pressure and oil production before water breaks through to the production end of the core.

The lower oil saturation in these systems is the other factor that is significantly different from dead oil waterfloods. The analysis of the CT data shows that gas saturation is higher near to the production end of the core, and in even longer systems without sand production most of the oil recovery and high gas saturation occurs close to the production end (Goodarzi and Kantzas, 2006). In actual oil reservoirs far from the production wells there may not be significant zones of high gas saturation due to lower pressure drop per length, and thus if wells are not hydraulically connected the reservoir may behave more similarly to a dead oil waterflooding scenario. The cores depleted in this chapter therefore represent a "worst case scenario" for post-cold production waterflooding: in these systems there is a high possibility that injected water can easily flow to the production end of the core. Finally, in the reservoir injected water will tend to enter high permeability, low oil saturation wormholes. In these cores, although the porous media properties were not altered, the gas zones that are now present throughout the core may still provide lower resistance pathways for injected water to travel. Therefore, although the primary depletion experiments were performed without allowing for sand production, the reservoir response to secondary waterflooding can still be tested and be expected to be reasonably representative of actual field conditions.

CHAPTER 7: DEAD OIL WATERFLOOD RESULTS

As previously hypothesized, the competing mechanisms in porous media are viscous forces and capillary forces from water imbibition in water wet rocks. The experimental results shown and discussed in this chapter were designed to investigate the relative effect of viscous forces and capillary forces. The evidence and quantification of the contribution of imbibition is introduced here. Further discussion of these results is also presented in Chapters 9 - 11.

The results of all waterflood experiments in dead (gas-free) heavy oil systems are presented here. In the waterflood experiments, water was injected at fixed rates into cores containing heavy oil and connate water. At early times, before water breakthrough, a high pressure gradient developed in the system since viscous heavy oil cannot flow out of the core as quickly as water can be injected in. After water breakthrough, however, the water can now flow along low resistance pathways, and pressure in the system declined quickly. In order to understand the influence of viscous and capillary forces the recovery profile both before and after water breakthrough is extremely important. After breakthrough, oil is recovered with very small pressure drops, and at very high water cuts.

This chapter investigates the relative significance of viscous and capillary forces by altering parameters such as the oil viscosity, the water injection rate and the sand permeability. Trends in recovery are related to the various forces present in these systems, in order to infer oil recovery mechanisms before and after water breakthrough. More detailed analyses of this data for identifying fluid locations in-situ and predictions of oil recovery are performed later, in Chapters 10 and 11.

7.1 Breakthrough Recovery

The analysis of waterflooding of conventional oil often focuses on breakthrough recovery. Conveniently, the results of waterflooding of conventional oil often show very

distinct breakthrough points, after which very little additional oil is produced in cases where the porous medium is water-wet (Mungan, 1966). However, for heavy oil waterflooding it is not trivial to identify the breakthrough point. Figure 7.1 shows the recovery and pressure response of a heavy oil waterflood.
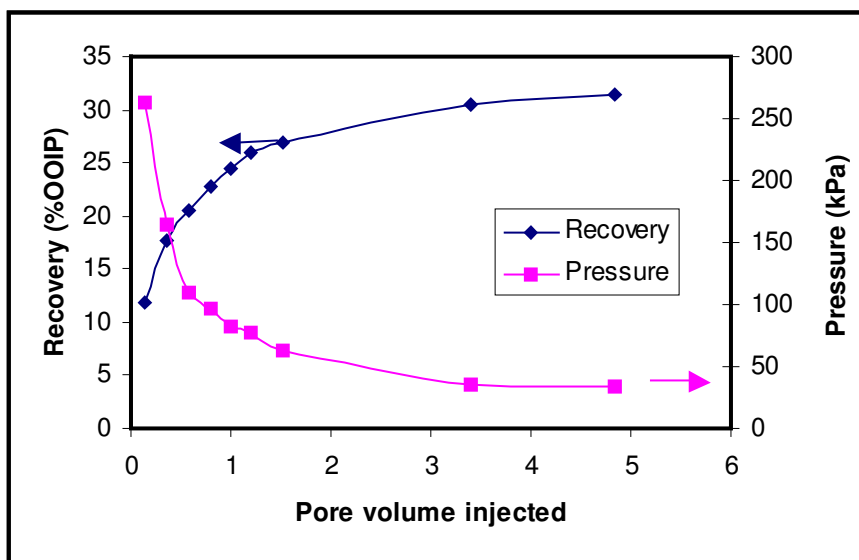
Figure 7.1: Recovery and pressure profile of a heavy oil waterflood

Figure 7.1 shows that in the case of displacement of heavy oil under adverse mobility ratio conditions, oil production continues for several pore volumes of injection, and the breakthrough recovery is not easily identifiable as a sharp change in the recovery profile.

When considering breakthrough recovery, it is important to understand the difference between conventional and heavy oil waterflooding in linear systems. In a 1-D waterflooding of conventional oil assumes that the flood front progresses as a relatively stable front, due to a similarity in mobility between water and oil. Thus, the movement of water is controlled by the rock permeability and the oil-water interfaces, and at the point of water breakthrough water has swept the entire core. After the water front reaches the outlet very little additional oil will be produced, since the oil that was not pushed ahead of the water front is mainly trapped as discontinuous ganglia (Dullien,

1992). For this reason, the breakthrough recovery is a very significant parameter in conventional oil. Additionally, after water breakthrough occurs, issues of water separation and handling become important as well, so in field scale operations the economics of the waterflood change at the point of breakthrough.

In conventional oil waterflooding, the breakthrough point is defined as the instance when water is first produced. This definition, however, cannot be applied in heavy oil waterfloods since the injected water forms viscous fingers and channels to the outlet, bypassing large sections of the core. If the same definition were used in a heavy oil waterflood, the breakthrough recovery would be insignificant. Thus a new definition is required to describe the breakthrough recovery in heavy oil systems.

In heavy oil waterfloods, it was observed that as water was injected at a constant rate, oil was not immediately produced at this same rate. At early times the pressure in the system is low, but in order for viscous heavy oil to flow at the same rate as the injected water, a large pressure drop would be required. Therefore, the oil production rate is initially much lower than the injected water rate, and since water is being forced into the porous medium pressure would begin to build up in the sand pack. Pressure never builds up to the level needed for oil to flow at the fixed injection rate, since water is not simply collecting at the inlet to the core. Rather, water is fingering through the porous medium, taking the most permeable pathways (the paths of least resistance) to the outlet, and pressure will only increase up to the point where water breaks though. After that point, pressure can quickly transmit through these low viscosity pathways (Craft *et al*., 1991), so pressure in the core will decline abruptly.

As a result of the viscous fingering and inability of oil to be produced at the fixed water injection rates, water would break through relatively early on in the life of the flood and oil then continued to be produced at high water cuts. It is important to stress that even though the produced fluids contained a significant fraction of brine, oil was still consistently produced; this characteristic is very much different from waterflooding of

conventional oil in a water wet porous medium. The early production of water could be attributed to viscous instability of the flood front. After viscous fingers found pathways to reach the outlet, further injected water could then channel through the porous medium, which is the reason for the high water cuts in the produced fluids. The water production can therefore be explained by viscous fingering theory, however the mechanism responsible for the oil production after breakthrough is not as clear.

Figure 7.2 plots the oil recovery profile at different water injection rates at early times for HO1. Again, from these curves the breakthrough point cannot easily be determined, but the data at very early times in the flood (i.e. during the first 0.5 PV injected) can be compared with the data at later times in order to identify the nature of the waterflood response before and after breakthrough.
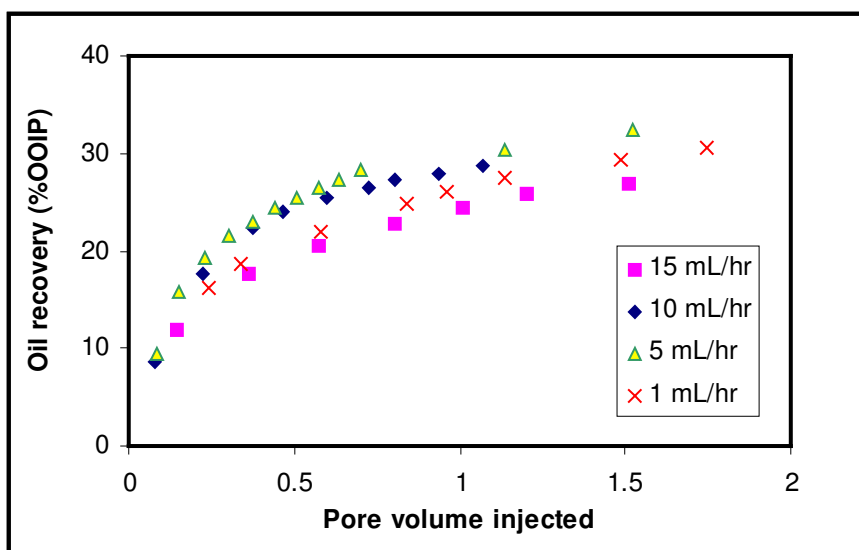
Figure 7.2: Recovery profiles at early stage of the waterflood

Instability theory predicts that at early times (up to water breakthrough), the recovery at the lower injection rates should give better recovery (Bentsen, 1985). This is because, all else being equal, higher injection rates lead to more pronounced viscous fingering under adverse mobility ratio flow, and this will in turn lead to reduced breakthrough efficiency. At first glance, the recoveries at different rates appear to be random. The repeated

measurements from Chapter 4 showed that the experimental results are reliable and repeatable, thus the scatter in Figure 7.2 cannot be attributed to be simply an experimental artifact. The profiles show that at early times the injection rates of 5 and 10 cm^3/hr yield the best recoveries while the highest and lowest injection rates (15 and 1 cm^3/hr) yield poorer recovery. Based on the recovery profiles in Figure 7.2, the breakthrough point could not be easily established in order to test instability theory, thus a new definition of water breakthrough had to be assigned.

As mentioned previously, once water channels are present along the entire length of the core, injected water will flow mainly along these channels and pressure in the system will decline. The recovery at breakthrough was therefore determined by applying a line of constant slope through the data at early times. Water breakthrough was determined to be the point at which the recovery profile begins to deviate from this straight line. This is shown in Figure 7.3. When this happens, the corresponding pressure drop in the system is now much lower than its maximum value.

The reason that this methodology was applied to estimate the point of water breakthrough is that initially, for any injected water to enter the core it must first displace an equivalent volume of viscous heavy oil. At constant rate water injection, therefore, the slope of the oil recovery will initially be linear with time. After breakthrough, however, most of the injected water will simply flow along the water pathways, thus the linearity of the oil recovery curve will be lost. It should be emphasized that these numbers are only approximations, and will be affected by the frequency of acquisition of production data.

169
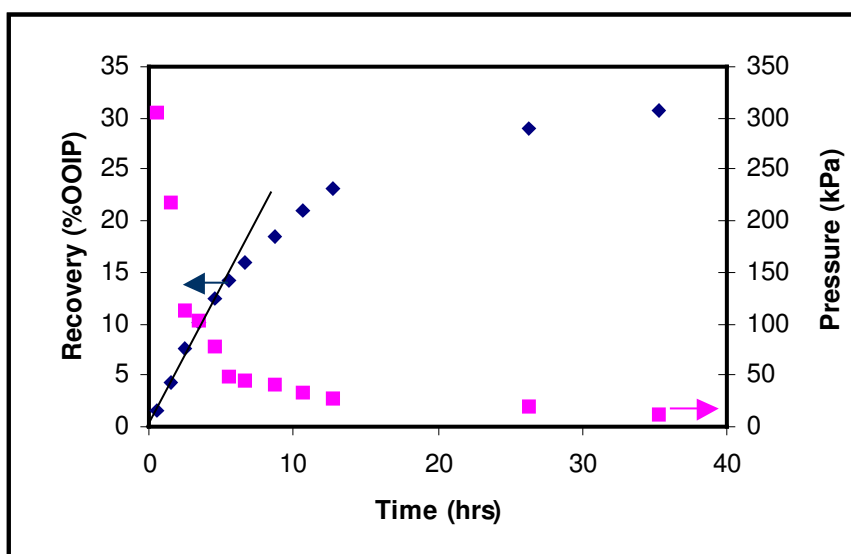
Figure 7.3: Determination of breakthrough recovery

Using this definition of water breakthrough, Figure 7.4 plots the breakthrough recovery values for HO1 and HO2 at various water injection rates. Trend lines have been plotted through the data simply to illustrate the apparent correlation between injection rate and breakthrough recovery for both heavy oils.
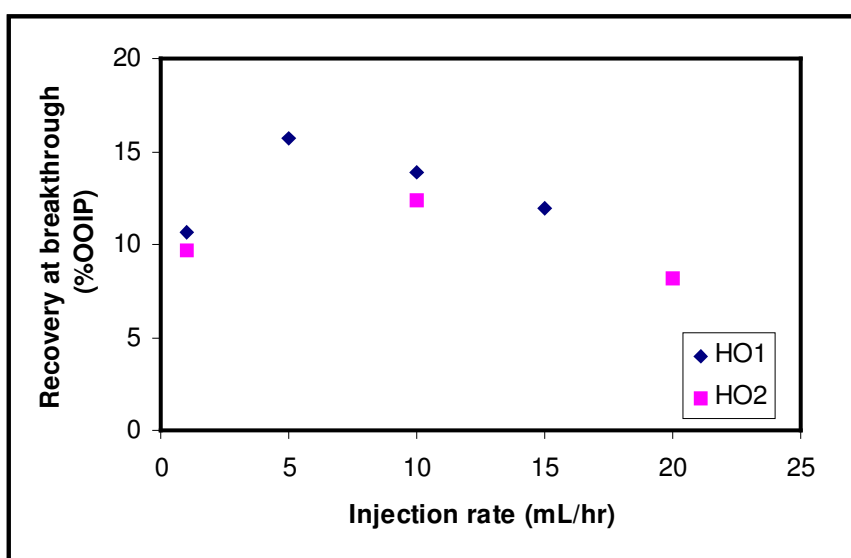
Figure 7.4: Breakthrough recovery as a function of injection rate

From this figure, it appears that the oil recovery at the point of water breakthrough is a non-linear function of the water injection rate. At higher rates, breakthrough recovery decreases with increasing injection rate, as predicted by instability theory. At very low injection rates, however, the breakthrough oil recovery appears to decrease once again. A possible reason for this will be discussed shortly. Recoveries are slightly higher for the lower viscosity oil (HO1) but overall similar results are obtained for both heavy oils.

The breakthrough recoveries, shown in Figure 7.4 for both oils under varying water injection rates, are also summarized in Table 7.1. This data allows for a comparison of the effect of both changing water injection rates and oil viscosity. Table 7.1 also includes the Instability Number, I_{sr} (Eqn 3.33), calculated for these systems.

Table 7.1: R_{bt} and I_{sr} for heavy oil waterfloods

Oil	Q_{inj} (cm^3/hr)	R_{bt} (%OOIP)	I_{sr}
HO1	10	13.82	900
	15	11.94	1200
	5	15.72	500
	1	10.66	100
HO2	20	8.19	6000
	10	12.39	3000
	1	9.63	300

The instability number calculated was based on the definition given by Peters and Flock (1981), and *C** was assumed to be 306.25 (for water wet media). This value was determined by Peters and Flock using 80 –120 mesh unconsolidated Ottawa sand, and was also assumed to be appropriate for Lane Mountain 70 sand.

These data show that the recovery at any injection rate is higher for HO1 (viscosity 4,650 mPa·s) compared to HO2 (viscosity 11,500 mPa·s). The mobility ratio is poor for both floods, but it is expected that recovery should have been higher for the lower viscosity oil. However, when the recoveries at the same flow rates of 10 and 1 cm^3/hr are compared for the different oils, the recovery is only slightly worse for HO2. HO2 is more than two times more viscous than HO1, so all else being equal the mobility ratio

between water and oil should be twice as high in this system. However, the oil recovery after five pore volumes of fluid have been injected is only slightly lower. Other researchers have also shown that relative permeability appears to be higher for lower viscosity oils (Wang *et al.*, 2006), which again would indicate that the difference in oil recovery at the point of water breakthrough should be more significant. This indicates that viscous forces and mobility ratio considerations alone cannot fully explain the nature of recovery in heavy oil waterflooding.

It is also evident from both Figure 7.4 and Table 7.1 that the breakthrough recoveries are not monotonic with changing water injection rates. The breakthrough recovery appears to improve as the water injection rate is decreased from $20 - 10 \text{ cm}^3/\text{hr}$, however once much lower injection rates ($1 \text{ cm}^3/\text{hr}$) are applied the breakthrough recovery actually decreases. Instability number analysis is often used to explain the poor recovery in viscous oil systems. This analysis indicates that for higher oil viscosities or faster water injection rates, the effect of viscous fingering will be greater. This higher instability will lead to lower breakthrough recoveries. Sarma and Bentsen (1987) have provided experimental evidence of this in systems containing oil with viscosity of approximately 30 mPa·s. This appears to be correct as injection rate is decreased from $20 \text{ cm}^3/\text{hr}$ down to 10 or even $5 \text{ cm}^3/\text{hr}$, however the opposite trend is observed at very low rates. At these low injection rates, the relative magnitude between viscous and capillary forces will be very different than at higher rates, thus it is possible that imbibition of water occurring ahead of the front may lead to early breakthrough of water and reduced breakthrough efficiency. This was previously proposed by Smith (1992), although no actual data was provided to support this hypothesis.

In other experiments used to provide evidence for the effects of viscous fingering and instability (Peters and Flock, 1981), the oil used had a viscosity of 100 mPa·s. In this research, experiments were performed with much higher oil viscosities. So instability theory, while it does explain some of the results shown in Figure 7.4 and Table 7.1, may not be applicable for very viscous oils.

Despite the lack of monotonic trends or a significant differentiation in breakthrough recovery, Figure 7.4 still shows that there appears to be an effect of parameters such as oil viscosity and water injection rate on the breakthrough recovery. Additionally, as observed in the oil recovery profile, even after water breakthrough occurs a significant portion of oil can still be recovered. Therefore, interpreting the core flood data just until breakthrough does not provide a complete picture of the response of heavy oil to waterflooding. In the following sections, the focus will be heavy oil recovery both before and after breakthrough, and how manipulation of parameters can affect the waterflood response.

7.2 Effect of Injection Rate on Waterflooding Results

Due to the high viscosity of heavy oil, flow of the oil through porous media is extremely slow and should require high pressure gradients, as depicted by Darcy's Law. For this reason, it is generally accepted as fact that viscous forces dominate the flow behavior of heavy oil, and EOR processes focus on oil viscosity reduction as the main mechanism for producing heavy oil (Green and Wilhite, 1998). The implicit assumption made is that capillary forces are negligible when compared to viscous forces. This is the basis for much of the analysis of heavy oil waterflooding performed in the past, specifically with regards to determination of relative permeability curves in heavy oil systems.

Assuming the dominance of viscous forces is correct, this means that by increasing the viscous forces (i.e. the water injection pressure or rate) in a heavy oil waterflood, recovery should also increase accordingly. Therefore, the purpose of the first suite of experiments was to investigate the effect of changing the injection rate on heavy oil waterflooding recovery. This was done by varying the injection rates for sand packs of similar physical properties (porosity, permeability and pore size distribution), containing the same heavy oil and irreducible water. Care was taken during the preparation of the sand packs to ensure that rock properties were similar, and oil floods were carried out at the same fixed rates in order to keep similar values of S_{wi} between experiments.

Measurements of S_{wi} were also verified through separation. In this part of the experimental plan, four different injection rates were used to waterflood sandpacks that were saturated with HO1 and three different injection rates were studied in sandpacks that were saturated with HO2.

7.2.1 Varying Injection Rate on Sandpacks Saturated With HO1

Four sandpacks with similar rock properties were initially saturated with brine and then flooded to S_{wi} with HO1. Each sandpack was then waterflooded at a fixed rate using a digital ISCO pump. These experiments were outlined previously in section 5.1.1 and their properties are shown in Table 5.3. The results from these experiments are shown in Figure 7.5.
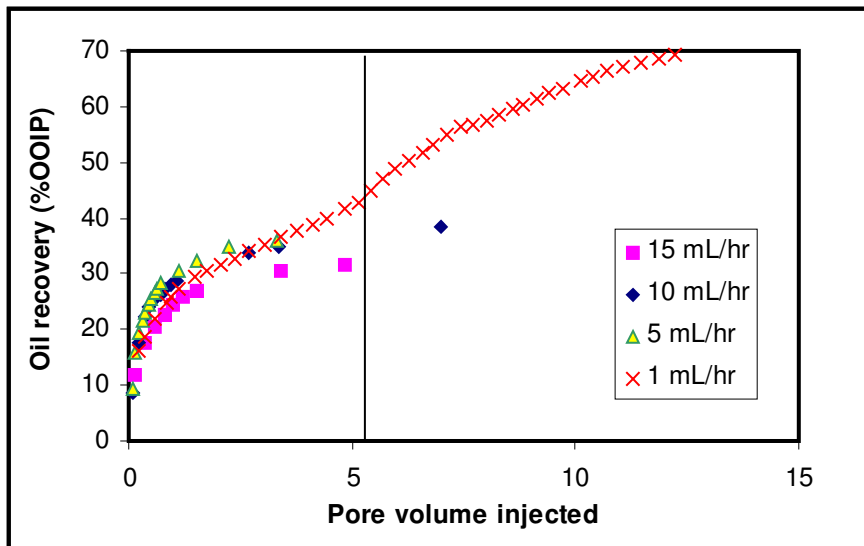
Figure 7.5: Recovery profiles at various injection rate for HO1

In these experiments, brine was injected for approximately 5 pore volumes (PVs) for three flow rates, and for a longer period for the 1 cm^3/hr injection rate. In this low rate flood, after 5 PVs of brine were injected, it was observed that the oil was still steadily being produced even after brine had already broken through for a period of time and the recovery was significantly better than at the other injection rates (as evidenced by the larger slope of the oil recovery profile in Figure 7.5). At this point the waterflood was

stopped to review the steps taken during the course of the experiment, to ensure that the result observed was an actual phenomenon and not an experimental error. The point where the core was shut in is the vertical line just after 5 PVs in Figure 7.5. After it had been satisfied that no error was made in the experiment, brine injection phase was resumed at the same rate. Immediately, the oil cut in the product stream increased, as can be seen by the change in slope of the recovery curve. The mechanism responsible for this improved recovery will be discussed later. After approximately one additional PV of injection, the recovery slope was similar to its value before shutting in the core, and at the slow injection rate significantly more oil was recovered than at higher rates.

In general, the effect of injection rate on recovery at early time (< 1 PV) is difficult to formulate into a trend, however the results after 5 PVs of injection clearly indicate that lower injection rates lead to better recovery. As mentioned earlier, water breaks through quite early in the life of the flood, and after breakthrough oil was consistently produced at high water cuts. The water cut profiles of the produced fluids are shown in Figure 7.6.
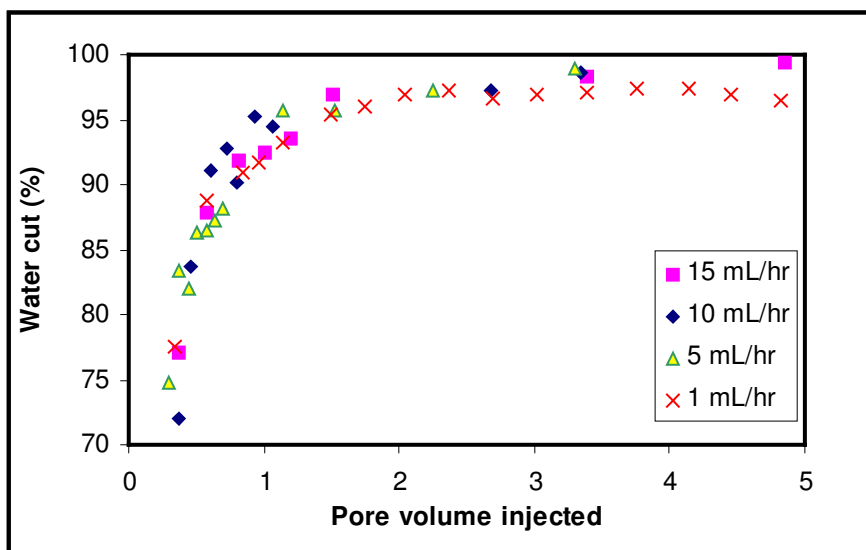
Figure 7.6: Water cut vs. pore volume injected

Observation of Figure 7.6 shows that when injecting at higher rates, the water cut tends to be higher than for lower injection rates. The range of water cuts shown in Figure 7.6 was

shortened to 70 - 100 % to illuminate the results after breakthrough, when oil is produced at high water cut. After several pore volumes of injection, the water cut of the lowest injection rate was almost sustained at a constant value of around 96%; it increased only very slightly over the last 3 PVs injected. For this same case, immediately after shut-in the water cut decreased, thus improving the slope of the oil recovery line. This implies that during the shut-in period, fluids somehow redistributed to a more favorable condition, allowing more oil to be produced. In general, Figure 7.6 shows that for the case of lowest injection rate at late times, the water cut of the produced fluids is lower than those of the higher injection rates. Again, this is an indication that at late times heavy oil displacement by water is more efficient for the lower injection rate.

So far the recovery and water cut profiles qualitatively show that as the injection rate increases (thereby increasing the viscous force) generally the overall recovery decreases after a relatively long period of injection. This is counter-intuitive if the assumption of the dominance of viscous forces is true; with higher viscous forces oil should flow more readily and thus recovery should be higher. However, it should be stressed that simply stating that viscous forces dominate production does not take into account the complexities of instability and viscous fingering, so the production response is actually more complex.

Another observation that can be made from Figures 7.5 and 7.6 is that there does not appear to be a significant difference in the waterflood response at early times. More distinct differences between high and low injection rates are prominent at the later stages of the flood. To investigate these issues in more concrete terms, the results of these waterfloods were further analyzed in Figure 7.7. Figure 7.7 plots the normalized oil production rate against pore volumes injected, for three water injection rates. The normalized oil production rate is the ratio of oil production rate to the injection rate set by the pump.
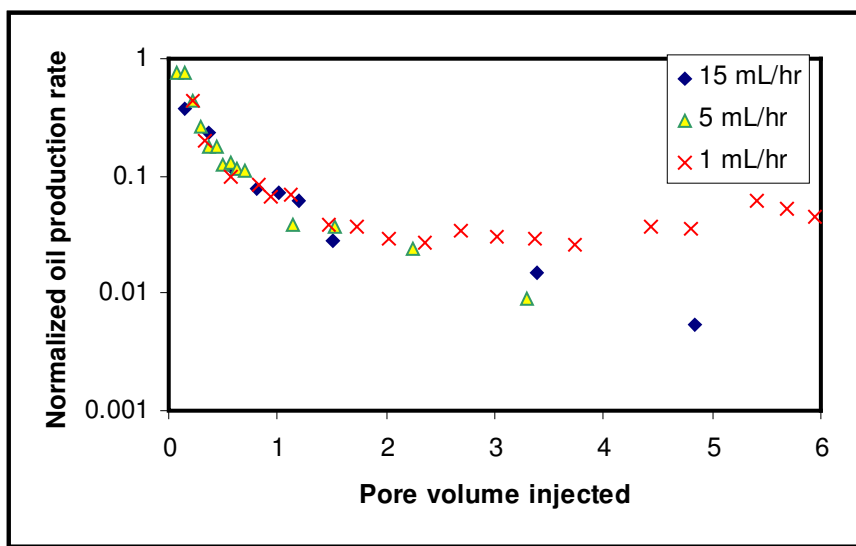
Figure 7.7: Normalized oil production rate vs. pore volume injected for HO1

From this figure it can be seen that at early times (< 1 PV injected) the normalized oil production rates are similar for all the injection rates, meaning that the oil production rates are proportional to the injection rates. This implies that, at this time, the production is dependent on the magnitude of the viscous force. The oil rates are initially highest for the fastest injection rate, but when the production rates are normalized to the injection it can be seen that oil rate is actually declining in the same manner for all three rates shown in Figure 7.7. At early times, therefore, the assumption of viscous forces dominating oil displacement appears to be correct.

However, after 1 pore volume of water has been injected the pattern for each injection rate begins to deviate, with the smallest injection rate being able to maintain its normalized production rate while the normalized rates for the higher rate waterfloods decrease. Larger injection rates appear to correspond to steeper declines in the normalized oil production rate. At later times, therefore, the normalized oil production rates are no longer proportional to injection rates, and the dominance of viscous forces is no longer true. In fact, viscous forces appear to have a negative effect on the normalized oil production rate; Figure 7.7 shows that at higher injection rates the waterflood is consistently less efficient than at lower rates. At an injection rate of 1 cm^3/hr the oil

production rate is approximately 3 % of the injection rate, while at elevated injection rates the normalized oil production rate is almost an entire order of magnitude smaller. At higher injection rates, therefore, a greater fraction of the injected water is simply flowing through water pathways, so injected water is being cycled with less of the water actually being able to displace oil. This result shows that at later times, oil recovery cannot mainly be due to viscous forces.

In order to understand the factor that caused an improvement in recovery at low injection rate, the pressure profile of these core floods were plotted in Figure 7.8.
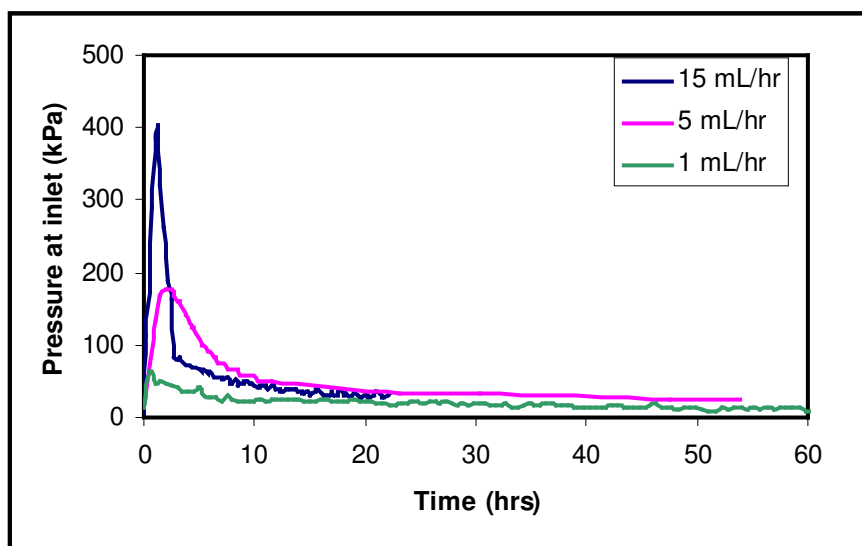
Figure 7.8: Inlet pressure profiles for waterfloods in HO1 cores

The pressure profiles show that the relative size of the maximum pressure corresponds to the injection rate: 15 cm³/hr has a maximum pressure differential of 400 kPa before breakthrough, compared to 175 kPa for 5 cm³/hr and 65 kPa for 1 cm³/hr. As the flood progressed past water breakthrough, the pressure continued to decrease. The pressure at late times could not be used to compare the stabilized pressure drop at each injection rate due to the inaccuracy of the transducers. When injecting at a low rate, and especially at late times with very small pressure drops, the transducer is not very sensitive to the small changes in pressure. In addition, when calibrating the transducers, the dead weight tester

could only apply pressures in excess of 69 kPa (10 psi). Therefore, at low pressures there was no way to validate the accuracy of the tranducers. At earlier times in the waterflood, however, when pressures were still in the range of what could be measured accurately, pressures can be related to oil rates in order to examine the effect of viscous forces on production.

According to theory of multi-phase flow in the porous media, the flow of phase P (oil or water) through a porous medium obeys the relationship for Darcy's law in multiphase systems, as described in Eqn (3.7).

If production were controlled by viscous forces alone, then capillary effects could be ignored and the pressure drop across the core could be assumed to be the same for both the oil and water. Thus the oil production rate could be written as:

$$\frac{Q_o}{A} = \frac{-kk_{ro}}{\mu_o}\frac{\Delta P}{L} \qquad\qquad \text{Eqn (7.1)}$$

With ΔP being the measured pressure drop across the length of the sandpack.

Assuming that this relationship holds, Figure 7.9 plots the oil production rate against the measured pressure drop for the three different rate waterfloods. In this figure, results of waterflooding at 10 cm³/hr were not included because of the fact that the pressure data for this experiment were not collected due to a faulty transducer.
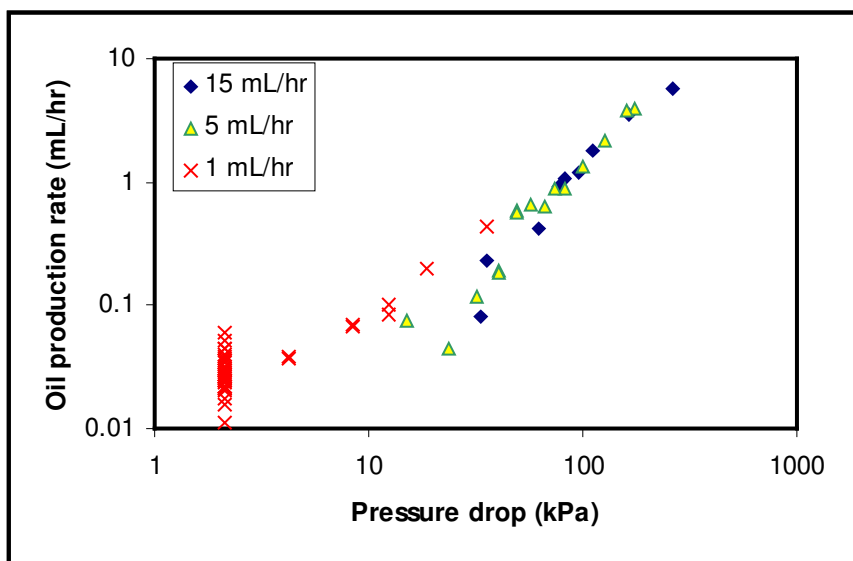
Figure 7.9: Oil production rate vs. pressure drop for HO1

At 15 cm³/hr and 5 cm³/hr injection rates, the oil production rate initially drops linearly with the pressure drop across the core. As pressure becomes low, however, the last data point for the 5 cm³/hr injection rate begins to deviate from this line. For the low injection rate (1 cm³/hr) the oil production rate versus pressure drop trend is markedly different. In fact, the oil rate versus pressure relationship shows higher oil production rates at any given pressure drop, indicating that somehow the oil mobility is higher at the lower injection rate. It is possible that at low pressure drops the slope of the 5 cm³/hr injection rate is approaching the slope of the 1 cm³/hr line, but this cannot be known with certainty due to lack of data at extremely low pressures.

Another observation that can be made from the data for 1 cm³/hr injection rate is the response at 2 – 3 kPa (0.4 psi). The oil production varies by almost one order of magnitude, while the pressure remains constant. This illustrates the measurement limit for the pressure transducers used in this study: at low injection pressure, more accurate transducers would be required. Even with the inaccuracies in the pressure data, Figure 7.9 shows clearly that at lower injection rates the oil rate versus pressure relationship is improved, and that oil production can be sustained under very low pressure gradients. At

very low pressures the relationship between flow rate and pressure gradient changes, implying the existence of another recovery mechanism being also responsible for oil production.

There are several factors that could be responsible for the improved oil production behavior at 1 cm³/hr injection. First, at higher injection rates, while the pressure drop in the core is higher, the impact of viscous fingering will be more pronounced as well. In Table 7.1, the I_{sr} values for HO1 and injection rates of 15, 5 and 1 cm³/hr are approximately 1,200, 500 and 100 respectively. According to instability theory, the lowest values of I_{sr} should correspond to the most stable floods, and correspondingly the highest breakthrough recovery. It should be re-emphasized, however, while the 5 cm³/hr injection did have a better breakthrough recovery than the 15 cm³/hr waterflood, the recovery at 1 cm³/hr injection was lower again. Therefore, instability theory does not fully explain the results of heavy oil waterflooding. Additionally, even if instability theory were to work accurately for all flow rates and oil viscosities, this analysis only concerns the manner in which the growth of viscous fingers will affect the oil recovery at water breakthrough. After breakthrough, when water channels are present along the entire length of the sand pack, it is less clear regarding the effect of the viscous fingers on the flood efficiency. Therefore, viscous fingering alone cannot explain the waterflood response at the injection rate of 1 cm³/hr.

From Eqn (7.1) the slope of lines in Figure 7.9 would correspond to kk_{ro}/μ_o, for constant cross-sectional area and length in the different floods. The data for 1 cm³/hr injection shows a different trend than for the higher injection rates, indicating that at this low injection rate the relative permeability behaviour of the oil flood is noticeably improved. Theoretically, relative permeability should not be a function of rate. However in heavy oil systems a rate effect has been observed by some researchers (Sarma *et al*., 1994; Maini *et al*., 1990; Wang *et al*., 2006). This is likely because the true relative permeability is not measured in heavy oil waterfloods, due to the unknown influence of viscous fingering and bypassing of oil. The data in Figure 7.9 appear to indicate that for

practical purposes, the apparent value of k_{ro} is a function of rate, and at low rates k_{ro} is improved. Even with this conclusion, it should still be emphasized that at low injection rates the flow of oil becomes much less sensitive to the pressure drop in the core, which again indicates that at low pressures, oil production is not only due to viscous forces.

7.2.2 Varying Injection Rate on Sandpacks Saturated with HO2

Three similar sandpacks were prepared and they were saturated with HO2 (viscosity of 11,500 mPa·s at 23°C) and connate water. Each sandpack then underwent a waterflood at a specific injection rate of 20, 10 and 1 cm³/hr. Their recovery profiles are shown in Figure 7.10.
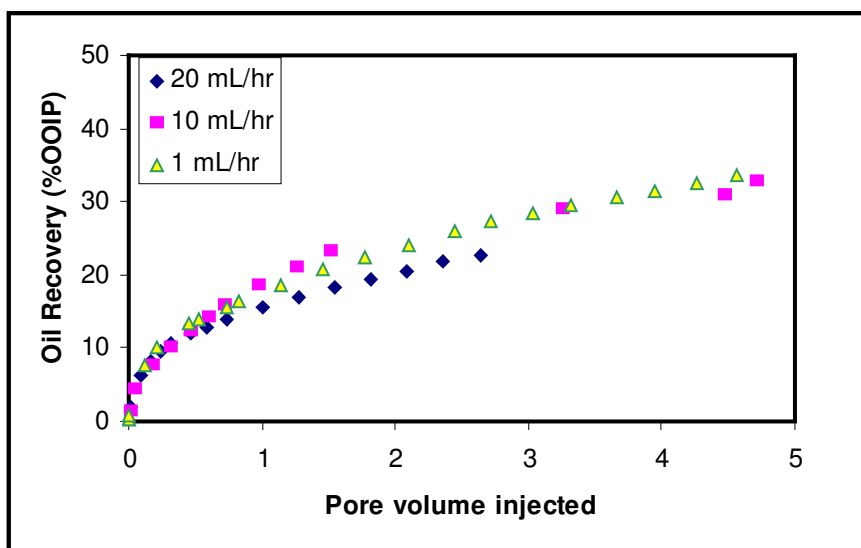
Figure 7.10: Recovery profiles at various injection rate for HO2

This figure shows that the recovery at early times (less than 1 PV) is quite similar for different flow rates. However, as the waterflood progressed the recovery of the slower injection rate is better. This characteristic is similar to the observation made before from Figure 7.5 for varying injection rates in displacing the less viscous HO1. It should be noted that although the recovery after 5 PVs is similar for both 1 cm³/hr and 10 cm³/hr injection rates, the slope of the oil recovery curve at later times is higher for the slower

injection rate. With even longer injection times, therefore, the slower injection rate will eventually outperform the higher rate waterflood.

Figure 7.11 normalizes the oil production rates to the water injection rates, as was also done previously for HO1. The rate of production of oil is low for the first few data points, due to the high oil viscosity. During this time, the oil flow rates are lower than the set values from the pump. The normalized oil rates then go through a local maximum as pressure builds up, before declining again.
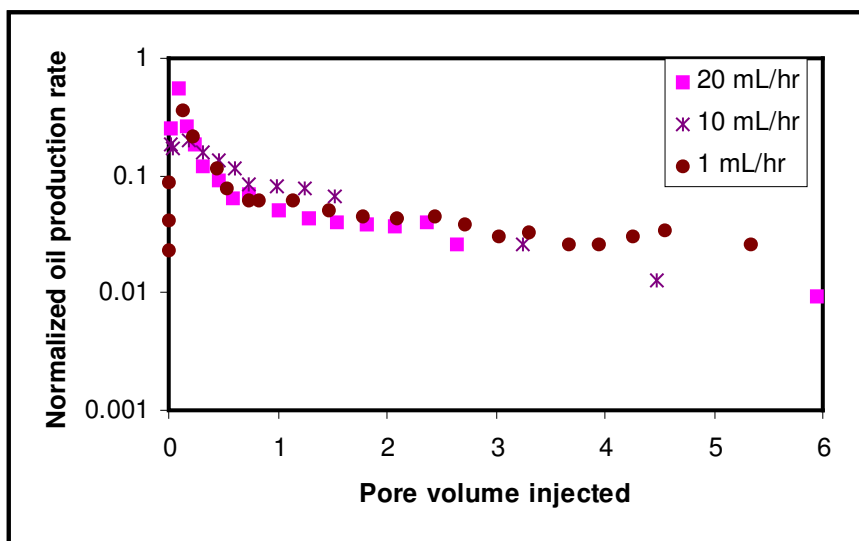
Figure 7.11: Normalized oil production rate vs. pore volume injected for HO2

As with HO1, at early times (< 1 PV injected) there is very little difference in the behavior of the normalized oil rates for the varying injection rates. This again indicates the dominance of viscous forces at early times: here oil production rate is directly proportional to the injection rate. At later times, after 3 PVs injected, the normalized rates once again begin to deviate. At higher water injection rates, the normalized oil rates drop while at 1 cm³/hr the normalized rates decline much more slowly. Again, this indicates that once continuous water channels are present throughout the core, the oil rates are no longer proportional to the water injection since the majority of water will simply travel through the low resistance water pathways. The higher normalized oil

production rates for the 1 cm³/hr waterflood also indicate that with longer injection times, the lowest rate waterflood will be the most efficient.

Figure 7.12 plots the oil production rate against the measured pressure drop across the core. In this more viscous oil, the oil rates were initially lower before pressure built up in the core and water broke through. Thus there appears to be more scatter at the first two pressure points for all three flow rates (i.e. at the highest pressures). Excluding these points, it is once again apparent that for the oil production versus pressure response at the lowest injection rate (1 cm³/hr) deviates from the higher rate waterfloods. This is shown by the deviation of the data from the trend line for 1 cm³/hr injection at pressures under 10 kPa. This again serves as an indication that at this low injection rate, the oil rate is less dependent on the pressure drop (i.e. the viscous forces) in the core.
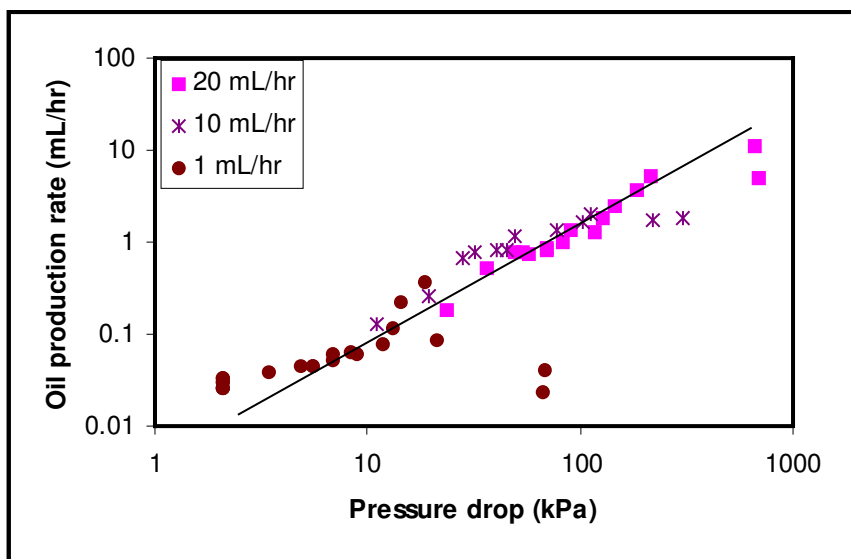
Figure 7.12: Oil production rate vs. pressure drop for HO2

An interesting distinction between the results for HO1 and HO2 is that the spread in the normalized oil production rates seem less distinct for this more viscous oil. Likewise, although the data at 1 cm³/hr in Figure 7.12 still deviates from the higher injection rates, the trend does not become noticeably different until below 10 kPa, as opposed to around

30 kPa in Figure 7.15. This could be the effect of performing the waterflood on more viscous oil; the effects of changing oil viscosity will be examined in more detail later.

7.2.3 Varying Injection Rate with HO2 in High and Low Permeability Cores

Additional experiments were performed on cores of high permeability (around 9 D) and low permeability (around 0.8 D). The properties of these sandpacks are shown in Table 5.7. The cores were saturated with HO2 heavy oil and irreducible water. Waterfloods were performed at two fixed rates into the high permeability core: 18 cm³/hr and 1 cm³/hr. Figure 7.13 shows the oil recovery profile at both injection rates. Similar to previous experiments, the oil recovery is substantially improved at lower injection rates.
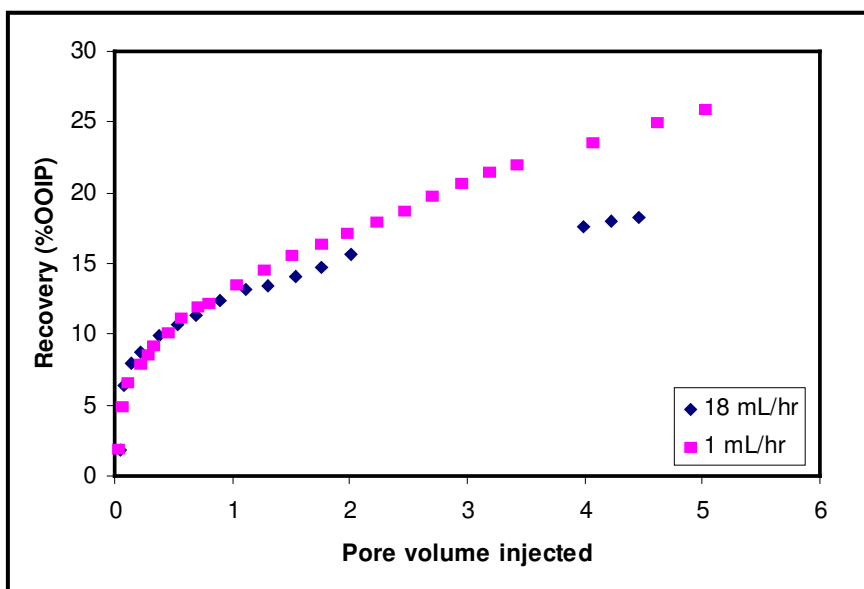
Figure 7.13: Recovery profiles for HO2 in high permeability sandpack

The oil rates are normalized to the injection rate in Figure 7.14. As before, the rates are initially very similar, but at later times the normalized rates at the high injection rate are lower than at the low waterflood rate. Again, this indicates that once water breakthrough occurs and pressure is low in the core, the oil production rates are no longer proportional to injection rates, and low rate water injection is more efficient than high rate injection.
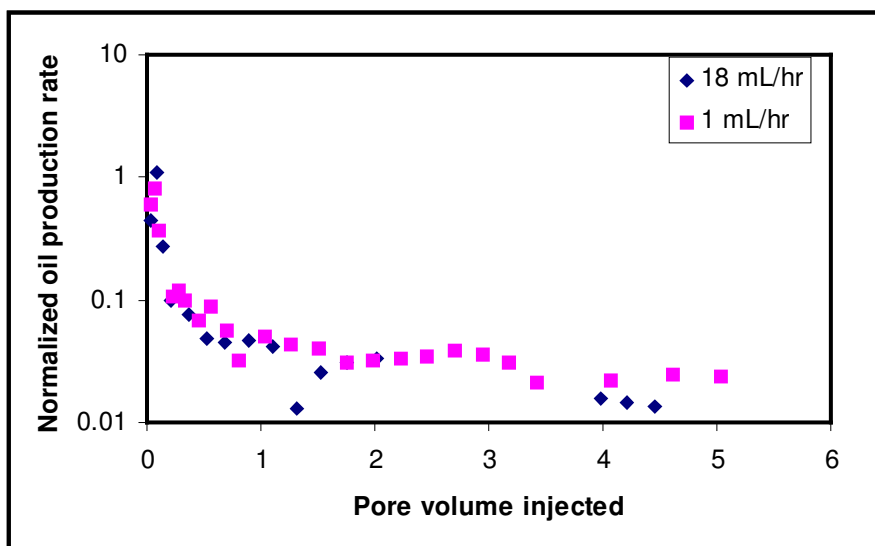
Figure 7.14: Normalized oil production rate vs. PV injected (k ~ 9 D)

In the low permeability core, three waterfloods were performed at constant injection rates of 11.33 cm³/hr, 2 cm³/hr and 1 cm³/hr. Figure 7.15 plots the recovery profiles for all three waterfloods. As before, slower injection leads to higher overall oil recovery. However, the results at early times in this lower permeability core are different from those in higher permeability systems. In this core, it seems that low injection rates yield higher oil recovery even before water breakthrough occurs. In higher permeability systems, the oil recovery at 1 cm³/hr injection was initially lower than at higher injection rates, but became higher over time. As discussed in Chapters 4 and 5, the core holder used in these three waterfloods contained sieved sand and no overburden pressure. Therefore, it is possible that the abnormal results at early times for 1 cm³/hr injection are due to some positive re-arrangement of the sand grains or plugging of the lines, leading to increased injection pressure for that flow rate. Overall, however, the recovery profile for this low permeability sand is still similar to the trends observed in other systems.
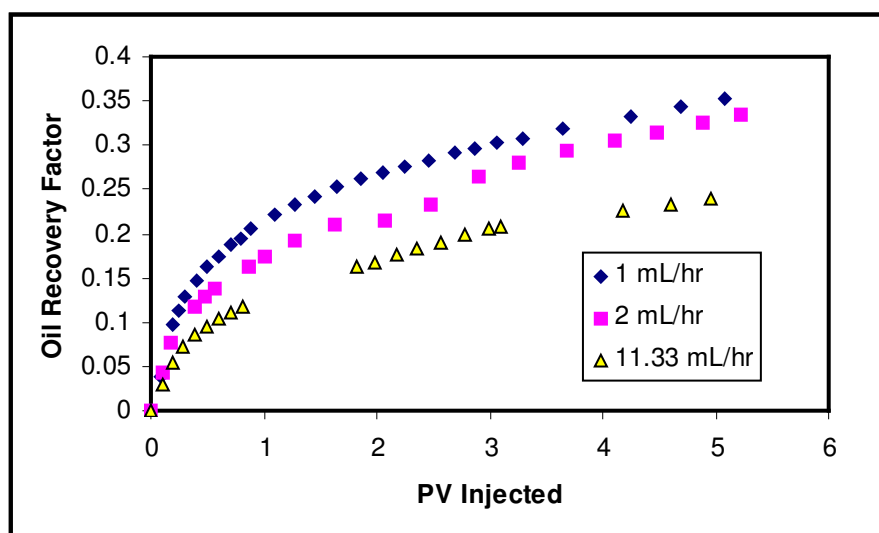
Figure 7.15: Oil recovery factor vs. PV injected (k ~ 0.8 D)

Figure 7.16 plots the oil production rates, again normalized to the injection rates. In this lower permeability core, the normalized oil rates do not collapse at early times the way they do in higher permeability sandpacks. Rather, the normalized rates at 11.33 cm³/hr are consistently the lowest, and the highest initial oil rates are for the lowest injection rate of 1 cm³/hr.
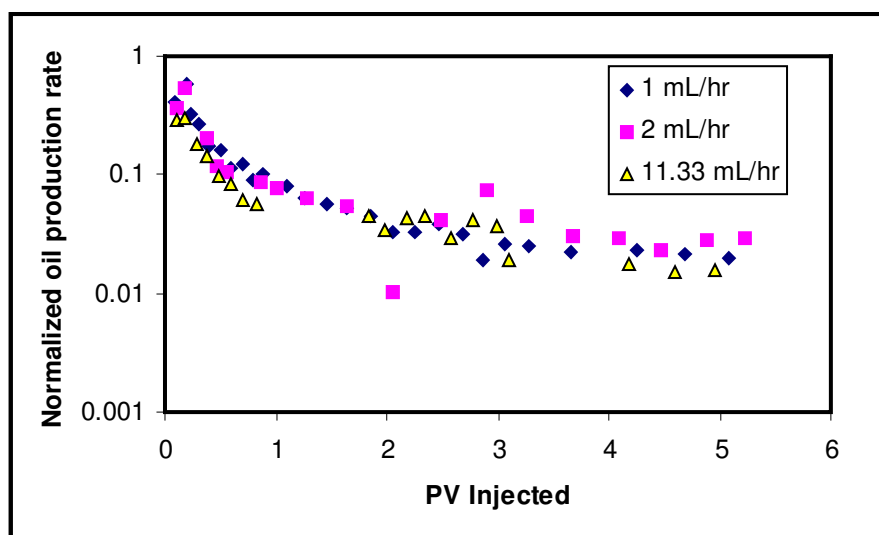
Figure 7.16: Normalized oil production rate at various rates (k ~ 0.8 D)

Figure 7.16 shows that for this lower permeability core, oil rates are not proportional to injection rates even at early times. At late times, the normalized oil rates are still the lowest at the fastest injection rate. The normalized rates for 2 and 1 cm³/hr are similar to one another.

Based upon the results from Figures 7.5 to 7.16, the effect of injection rate appears to change for different parts of a waterflood. At early times, prior to breakthrough, oil production rate is proportional to the injection rate, indicating that viscous forces dominate oil recovery in this region. This is true of cores with higher than 2 D permeability. However, in all cases the breakthrough recovery decreases as the injection rate increases (with the exception of the results at very low injection rates). This corresponds to the fact that instability theory predicts a higher degree of viscous fingering under faster injection. At later times, normalized oil rates are lower for higher injection rates, indicating that viscous forces are no longer dominant after breakthrough. In fact, at elevated injection rates more water channels through previously flooded pathways and proportionally less water is used to displace and recovery oil, thus higher injection rates are less efficient.

Overall, it appears that oil recovery tends to be higher for lower injection rates. This could be partially a reflection of reduced viscous fingering at lower injection rates, however assigning the improved oil recovery at low rates solely to a viscous fingering effect is not correct. With the exception of the values at the lowest injection rates, recovery before breakthrough seems to be improved as injection rate is reduced. This can be explained through reduced viscous fingering at low rates. However, viscous fingering theory does not explain the mechanism for oil recovery after breakthrough. At later times, when the relationship between oil production rate and the pressure drop in the core loses linearity, this is an indication that other mechanisms besides viscous flow are responsible for oil recovery.

7.3 Effect of Changing Injection Rate during Waterflooding

It was observed that with the exception of the low permeability core floods, at water breakthrough the recovery is slightly lower at the lowest injection rates tested. At late times, however, recovery was clearly more efficient at lower injection rates. Even if both injection rates yield the same recovery eventually, from an economic point of view an initial faster injection rate is preferable in order to accelerate oil production. The injection rate should not be too fast, as evidenced by the fact that as the waterflood rate was reduced from 20 cm³/hr to 10 cm³/hr (frontal velocities of 0.42 m/day and 0.21 m/day respectively), both the breakthrough and final recovery improved for HO2. However, it appears that flooding faster than 1 cm³/hr (i.e. a frontal of 0.021 m/day) can accelerate oil production at early times. Therefore, in some of waterfloods after several pore volumes of brine had been injected at a fixed high rate, the injection rate was reduced. The results of lowering injection rate in HO2 are shown in Figure 7.17.
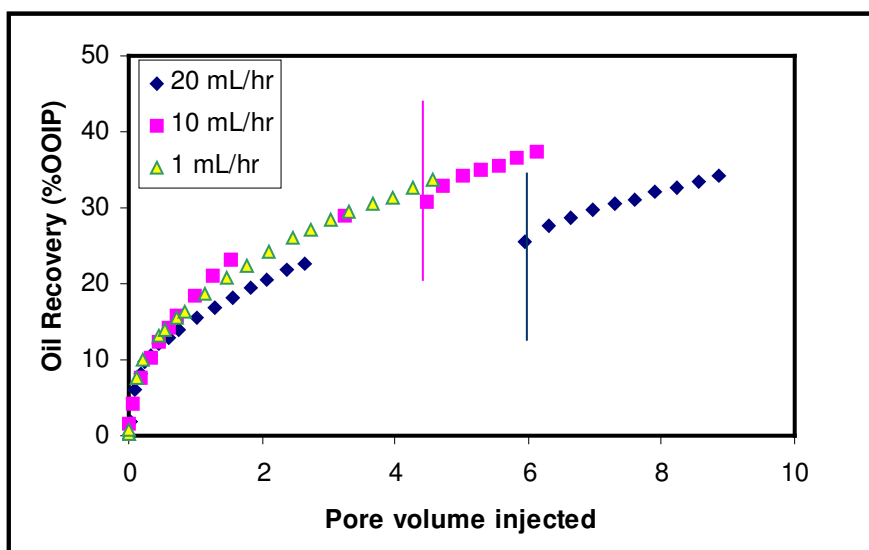
Figure 7.17: Effect of reducing injection rate on oil recovery

At early times, under 1 PV injected, the recovery profiles for all three injection rates appear to be similar. After this time, the 20 cm³/hr waterflood is the least efficient. It should be emphasized, however, that Figure 7.17 plots oil recovery as a function of PV

injected. If the data were instead plotted as a function of real time, it would be seen that similar volumes of oil could be produced much faster at higher injection rates.

The vertical bars in Figure 7.17 denote the instances when the injection rate was reduced from 20 and 10 cm³/hr respectively to 1 cm³/hr. It can be seen that a reduction in the injection rate leads to a corresponding increase in the slope of the recovery curve, indicating that more oil is being produced per pore volume of water injected. Reducing the injection rate will create a more stable front with reduced viscous fingering, however as mentioned previously water breakthrough occurs long before the flow rate is reduced, thus this cannot be the sole mechanism responsible for the improvement in the oil recovery.

The improvements in produced water cut when rates are decreased are shown in Figure 7.18. It is evident in this figure that as the injection rate is reduced, the water cut immediately decreases as well, indicating that the flood has become more efficient.
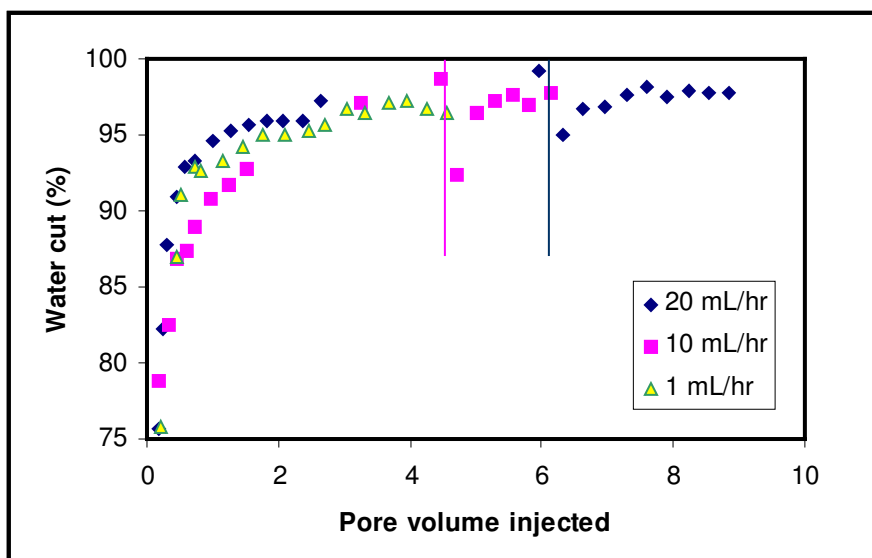
Figure 7.18: Effect of reducing injection rate on water cut

As more brine continued to be injected at the lower rate, the water cut eventually increased again, but more slowly than before. This implies that water still continues to channel through the sandpack, however at the lower injection rate somehow more water is being used to displace heavy oil.

The recoveries of two varying viscosity oils (HO1 and HO2) with the same injection rates are shown in Figure 7.19. In both experiments the injection rate was initially set to be 10 cm³/hr. After 1.8 pore volumes injected in the sandpack saturated with HO1 the injection rate was reduced to 1 cm³/hr and injection rate was also reduced in the sandpack saturated with HO2 after 2 pore volumes of injection.
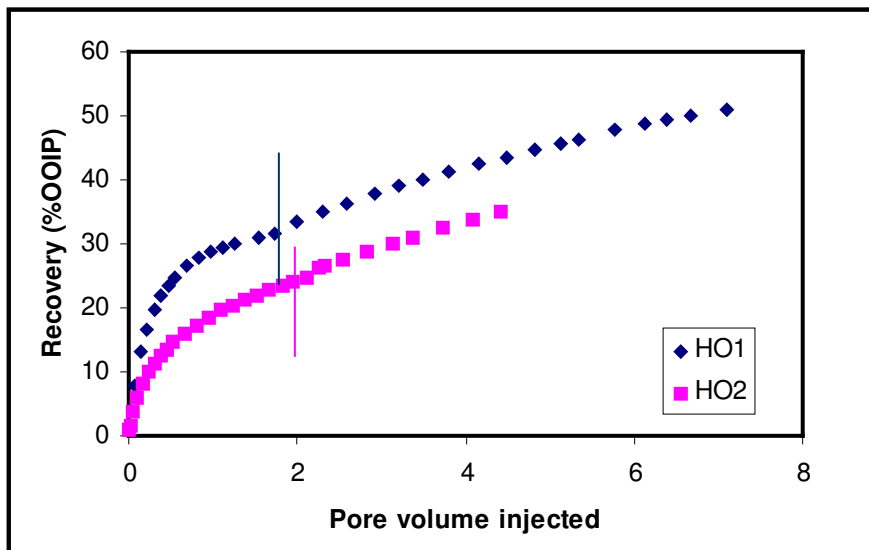
Figure 7.19: Recovery profiles of different oils at the same injection rates

For both heavy oils, the slope of the recovery curve is improved by reducing the injection rate from 10 to 1 cm³/hr. The improved oil recovery can also be seen by the reduction in the water cut at the instant of reduction in the injection rate in Figure 7.20. Again, after the injection rate is reduced, the water cut increases more gradually than at higher injection rates.
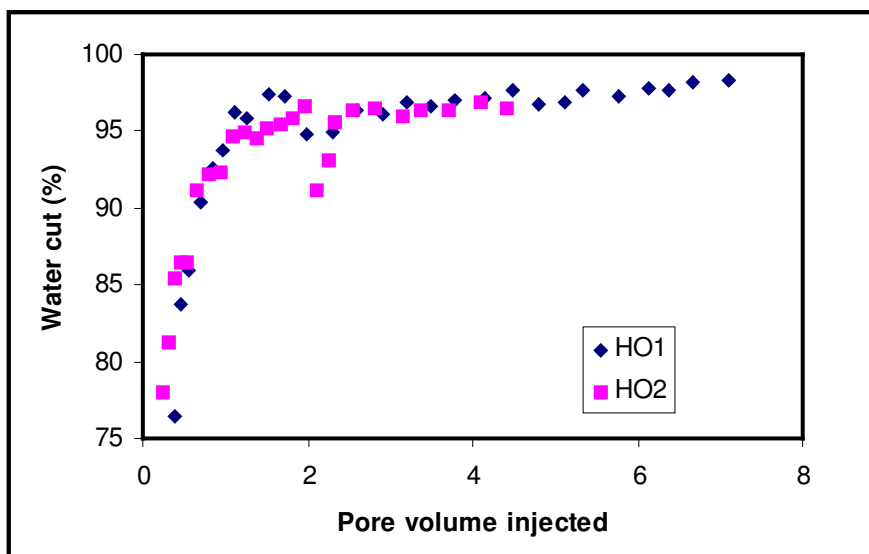
Figure 7.20: Water cut profiles of different oils

A more direct effect of reducing the injection rate is shown in Figure 7.21, where the results of reducing the injection rate is compared against the case where brine was continued to be injected at its original high rate.
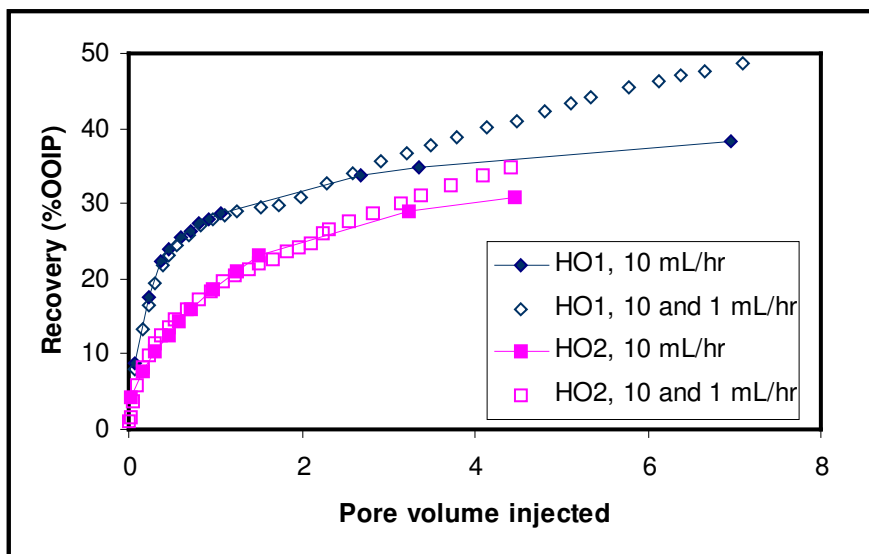
Figure 7.21: Effect of reducing injection rate for both oils

If brine is steadily injected at high rates, the oil recovery eventually levels off. This was seen previously in plots of high water cut and low normalized oil production rates. When the injection rate is later reduced, the oil recovery profile improves and this translates to significant improvements in the oil recovery.   After approximately 5 PVs of brine injected, reducing the oil injection rate led to an increase in 5.5 % and 4 % oil recovery for HO1 and HO2, respectively.

An alternative injection scheme is to inject water slowly at first, followed by high rate injection. This is not expected to be efficient, given the results in Figure 7.21. However, varying injection slow to fast changes the magnitude of the viscous forces late in the life of a waterflood, which can aid in to further understanding of the impact of these forces in heavy oil waterflooding.   Therefore, after waterflooding at 1 cm³/hr for approximately five pore volumes in the high permeability core (9 D permeability), water was injected at a high rate of 18 cm³/hr. The oil production rates are shown in Figure 7.22.
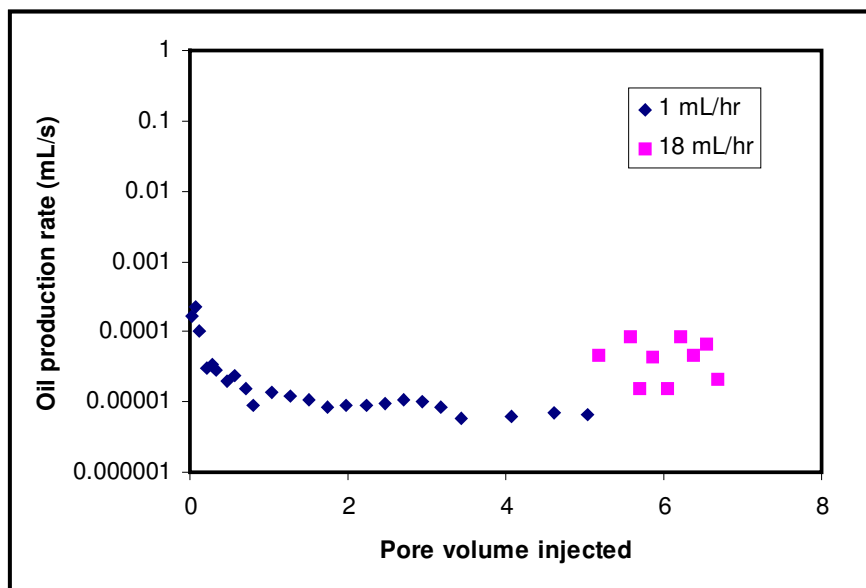
Figure 7.22: Effect of increasing injection rate on oil production rate

Once the water injection rate is increased, the oil production rate also increases. However, the oil rates are scattered: at times the oil is produced at an elevated rate, but at

other times the measured oil rate appears to be much lower again, and in fact is only marginally higher than the production rates at the 1 cm³/hr waterflood. When the oil production rates are normalized to the waterflood rate, it can be seen that increasing the injection rate late in the life of a flood significantly decreases the efficiency of the displacement. This is also shown in the recovery profile plotting in Figure 7.23.
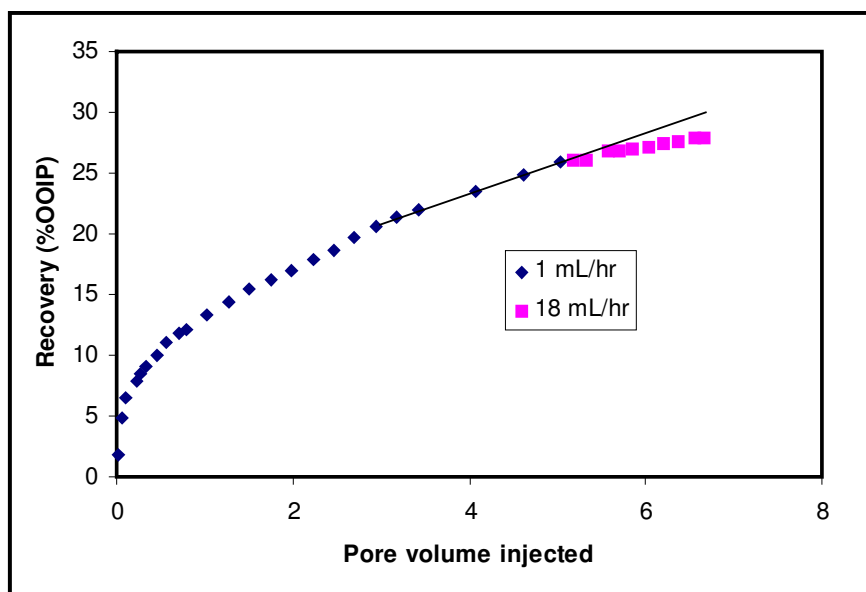
Figure 7.23: Change in slope due to increasing injection rate

In Figure 7.23, a trend line has been drawn through the last few data points acquired at the low injection rate. This line serves to indicate the general recovery profile expected at the low rate. In contrast, the actual recovery is plotted as the pink squares. It can be seen that at when the injection rate is increased late in the life of a waterflood, increasing the viscous forces are not beneficial to oil recovery efficiency. Increasing the waterflood rate does lead to higher oil production rates, so oil is recovered faster, but the efficiency of the flood (denoted by the slope of the recovery profile) suffers.

These results from the tests were injection rate was varied allow for a very important conclusion to be drawn: *viscous forces can be used initially to recover oil quickly, before water breakthrough occurs. At later times, however, viscous forces are actually*

detrimental to the efficiency of a waterflood since water injected at high rates will tend to cycle through the water channels formed during viscous fingering, so a considerable fraction of the injected water is simply by-passing the remaining oil. Reducing the injection rate can therefore lead to more stable floods and improved oil recovery. These results are especially significant for heavy oil fields that are currently undergoing waterflooding. It appears that even in a mature field that has already seen breakthrough, reducing the water injection rate can still lead to improved oil recovery.

7.4 Effect of Oil Viscosity on Waterflooding Results

By comparing the response of heavy oil waterfloods at different rates, the influence of viscous forces on recovery could be interpreted. These are the viscous forces that can be controlled by operators of a heavy oil field. However, parameters such as the oil viscosity or rock permeability are uncontrollable parameters that will also have significant bearing on the magnitude of viscous forces present during flow. In the suite of waterfloods performed, tests were carried out with oils of varying viscosity and also in sands of different permeability. Therefore, results from different core floods can also be interpreted in order to achieve a better understanding of the effect of these parameters.

The effect of oil viscosity was investigated by waterflooding at the same injection rate on sandpacks of similar permeability, but saturated with different oils. Prior to the waterflood, the sandpacks were saturated with HO1 (4,650 mPa·s) and HO2 (11,500 mPa·s), and irreducible water. The recovery profiles for the fixed injection rates into oils with different viscosity are compared in Figure 7.24.

The results shown in this figure came from Experiments #4 and #7 for HO1, and #11 and #12 for HO2. This figure shows that, aside from the fact that lower injection rates are more efficient than higher injection rates, the recovery of the less viscous oil is consistently better than the more viscous oil at any rate of injection. This conclusion, while not surprising, still merits some further discussion.
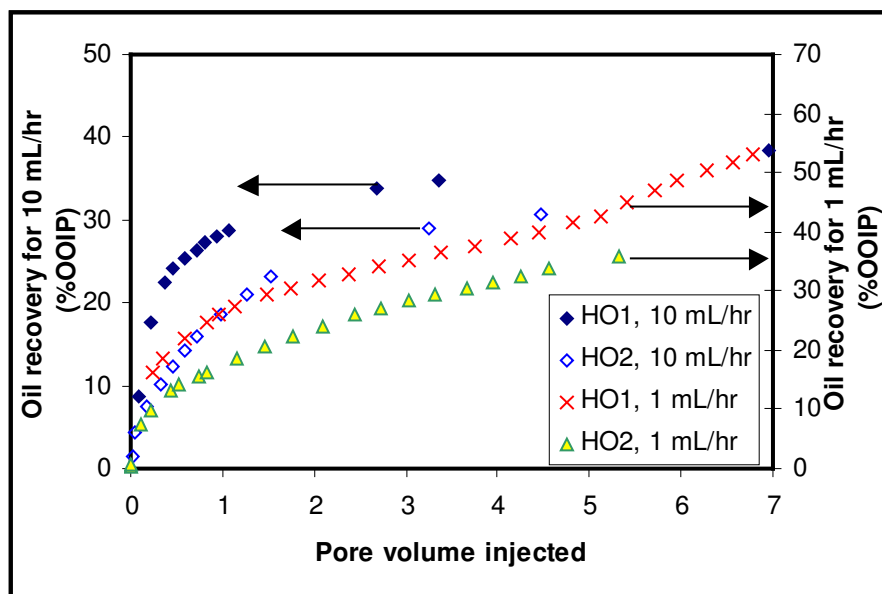
Figure 7.24: Effect of oil viscosity on waterflooding recovery

From instability theory one can expect the recovery at breakthrough to be lower for the more viscous oil. The instability equation (Eqn 3.33) shows that for higher oil viscosity, the instability number increases. This means that the displacement is more unstable, thus the recovery at breakthrough will be less efficient. As mentioned previously it is difficult to establish the true breakthrough point in these experiments, however it can be seen that at early times (less than one pore volume injected) the oil recovery of the less viscous oil is higher. Regardless of the definition of breakthrough, therefore, it can be concluded that the breakthrough recovery decreases as the oil viscosity increases. This means that there will be a limit to heavy oil waterfloods; when the oil viscosity becomes so high that the oil simply is no longer mobile, the waterflood will break through with essentially no oil recovered.

Simply considering the total oil recovery does not differentiate between recovery mechanisms before and after breakthrough. At late times, it appears that the efficiency of the waterflood is much less sensitive to the oil viscosity. Table 7.2 shows the recovery efficiency (i.e. the oil recovered per pore volume of water injected) for the late times in the waterfloods.

Table 7.2: Recovery efficiency of waterfloods at late times for oils of varying viscosity

Experiment #	Oil Viscosity (mPa·s)	Waterflood rate (cm³/hr)	Waterflood Efficiency (% RF/PV injected)
4	4,650	10	1.61
11	11,500	10	1.41
4	4,650	1	3.76
12	11,500	1	3.61

At late times in a waterflood, the recovery efficiency for the lower viscosity oil is still better than that of the higher viscosity oil, but the difference between the two is much less significant than the flood performance before breakthrough. This shows that the waterflood response after breakthrough cannot simply be understood only on the basis of viscous fingering and instability theory. Despite the fact that the viscosity ratio is essentially doubled between HO1 and HO2, the flood only reduces slightly in efficiency at late times. The conclusion that can be drawn from Table 7.2 is that at late times oil is not being produced by water physically pushing the oil through viscous forces.

The water cuts of the produced fluids from these waterfloods are shown in Figure 7.25. The early time data is circled to emphasize the difference in water cut between the two oils.

The water cut profiles show that at early time for the more viscous oil the products have higher water cut, implying that the waterflood is less effective. At late times, however, the water cut profiles appears to be similar. Thus, this figure re-affirms the observations made earlier. Waterfloods are more efficient in lower viscosity heavy oils, but even with significant increases in viscosity the oil recovery efficiency at late times is only marginally lower.
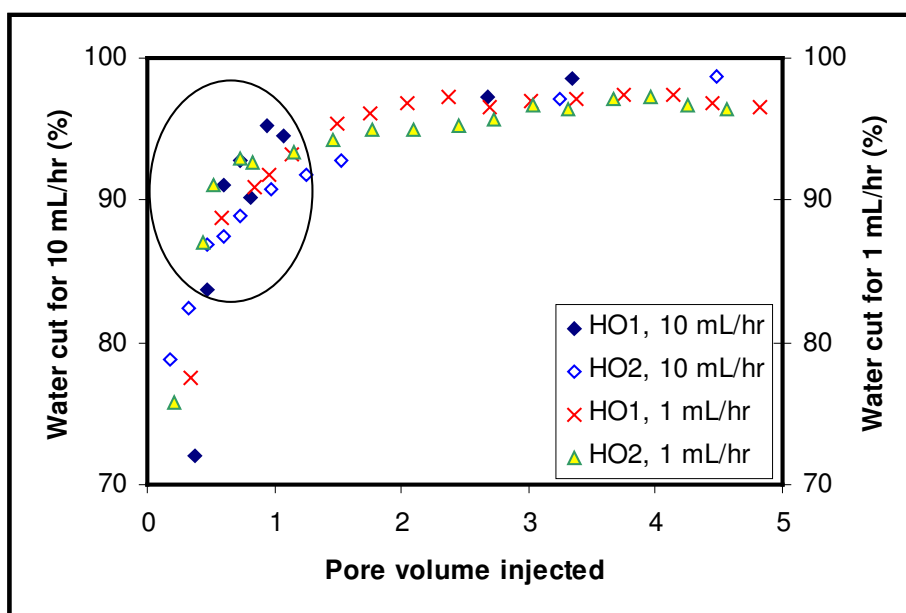
Figure 7.25: Effect of oil viscosity on water cut profiles

The overall recoveries of oil after 5 PVs of brine injected are shown in Figure 7.26. Unlike the breakthrough recovery (shown previously Figure 7.4) the total recovery after 5 PVs of injection are now more linear with injection rate.
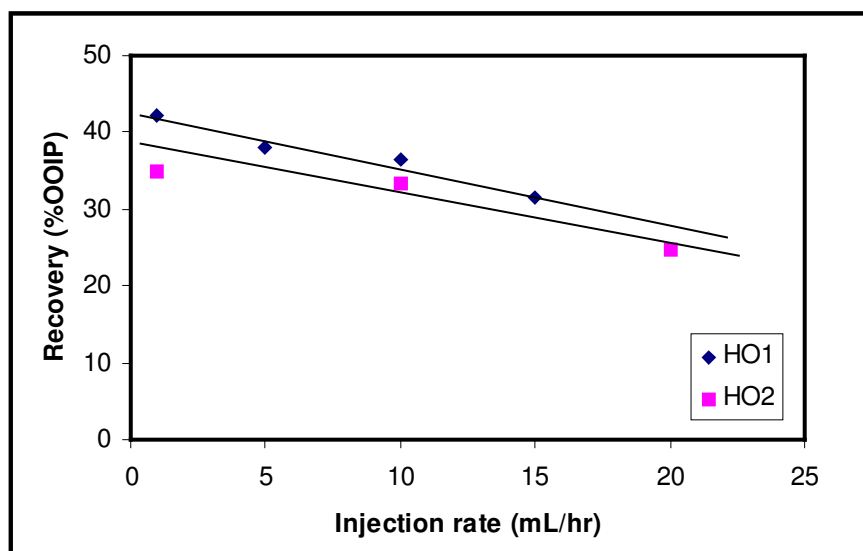
Figure 7.26: Effect of oil viscosity and injection rate on overall recovery

This figure shows that as the injection rate decreased, the recovery increased. Also, at any injection rate, the recovery of the less viscous oil is higher. For a more viscous oil, in order to inject at the same rate the pressure induced must be higher. Thus, at the same injection rate, the viscous force applied is higher as well. Once again, viscous forces and instability of the flood front are important at early times, before water breakthrough occurs. At later times, the effect of the oil viscosity is much less important. When recovery is plotted just up to five pore volumes, this contains the contribution of both early and late time data.

From Figure 7.26 it is also apparent that straight lines of different slopes could be used to show the relationship between recovery and the injection rate. For both heavy oils, recovery decreases with increasing injection rate. Again, recoveries are slightly higher for the lower viscosity oil, however even when oil viscosity is doubled the results are surprisingly similar. It appears that while higher oil viscosity does have a negative impact on waterflood recovery, the effect of the oil viscosity is not as significant as would be expected through an analysis of mobility ratio calculations.

7.5 Effect of Sand Permeability on Waterflooding Results

Experiments were carried out with HO2 in sand packs of varying permeability at the same injection rate (1 cm³/hr). The permeabilities of the cores tested were 0.8 D, 2.8 D and 9 D. The oil recovery profiles for these three systems are compared in Figure 7.27.

Figure 7.27 shows the actual frontal velocity values for the floods, calculated by dividing the injection rate by the cross-sectional area of the cores. Due to the smaller diameter of the 0.8 D core, at the same injection rate the velocity is approximately twice that of the other two cores. Despite this higher injection velocity, the oil recovery is initially highest in this core. The recovery in the 2.8 D sandpack does not become higher until after 4.5 pore volumes of water have been injected, and the recovery is consistently lower in the 9 D core. In general, lower permeability rocks seem to lead to higher oil recovery.
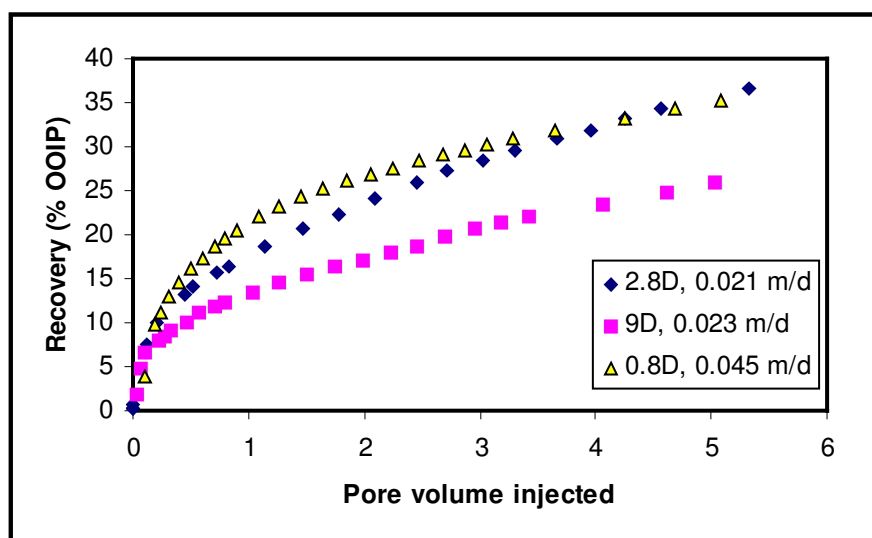
Figure 7.27: Oil recovery at low injection rates for systems of varying permeability

Figure 7.28 plots the oil rates normalized to the injection rates for both the 2.8 D and 9 D cores, at two injection rates. As seen previously, there is little difference between the normalized oil production rates in either core system at early times. After 1 pore volume of water has been injected, however, the normalized oil rates for high rate injection into the large permeability core are noticeably lower than for the other data.
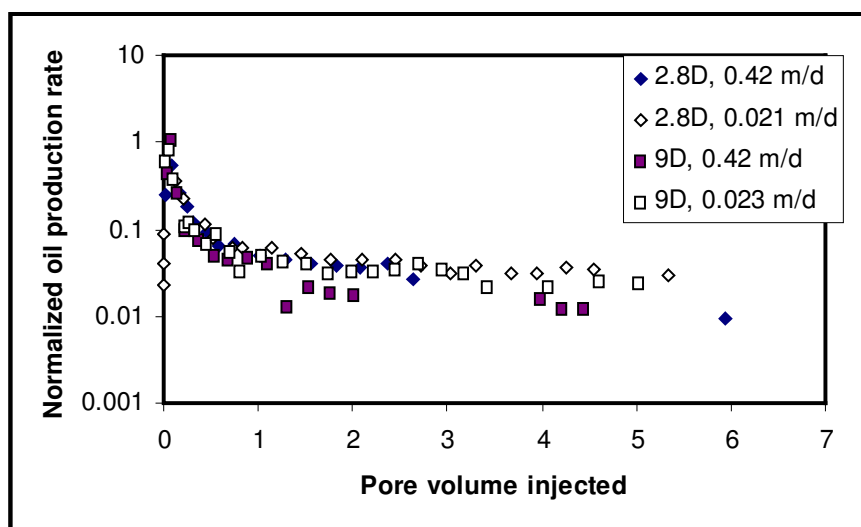
Figure 7.28: Normalized oil production rate for systems with varying permeabilities

Due to the log-scale used to plot Figure 7.28, the difference between high and low rate waterflooding in the different permeability systems is not clear. Therefore, Figure 7.29 plots the same rates on a linear scale, focusing only on the low oil rate portion of the waterfloods. In this more narrow range of normalized production rates, it is clear that the waterfloods are more efficient in the lower permeability core. Comparing the 9 D to 2.8 D cases again shows the higher normalized oil rate in the lower permeability sand.
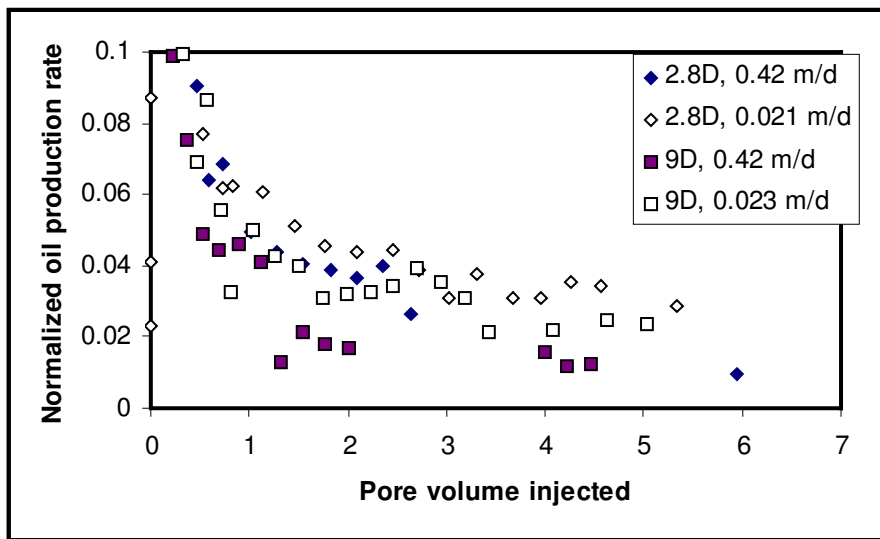
Figure 7.29: Effect of permeability on oil production at similar injection rates

Figure 7.30 plots normalized oil rates for just the lowest injection rate (1 cm³/hr) in all three systems. Again, the plot focuses on the low oil rate portion of the floods. When comparing the results from the three different permeability sandpacks, at early times it is evident that the highest normalized oil rates (i.e. the most efficient waterfloods) are seen in the lowest permeability system. In the later stages of the flood (3 – 5 pore volumes injected) the highest rates are seen in the 2.8 D core. The reason for this is unknown – it can only be speculated that this may be the result of the faster injection velocity in the 0.8 D system. Unfortunately, due to time constraints it was not possible to perform an additional waterflood in the 0.8 D core at the same frontal velocity as in the other systems.
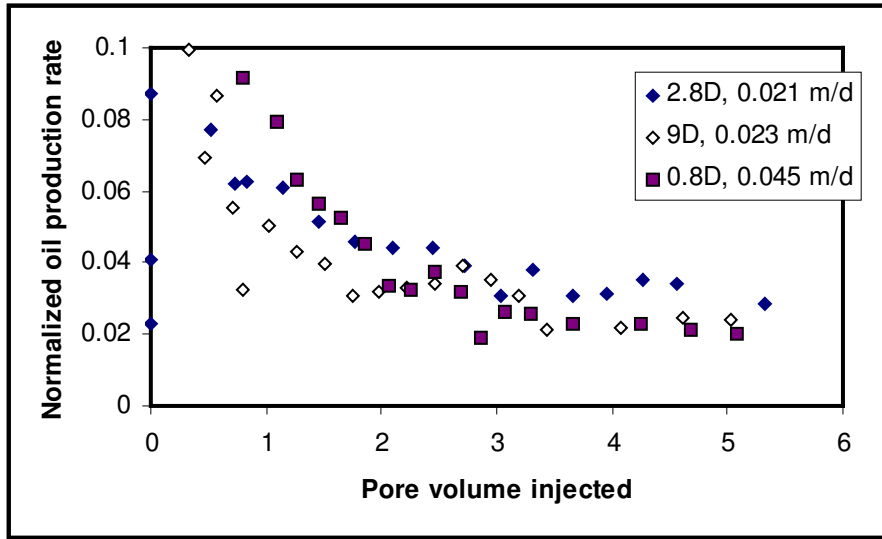
Figure 7.30: Normalized oil production at low injection rates for systems of varying k

Figure 7.31 plots the pressure drop for the low injection rate into the three cores. As expected, the pressure drop increases with reduced sand permeability, since flow of a viscous fluid requires high pressure gradients to flow in these systems. The pressure response is significantly different for the varying permeability cores. The pressure difference between the 0.8 and 2.8 D cores is at least 900 kPa (130 psi), while the difference between the 2.8 D and 9 D cores is close to 100 kPa (14 psi). Despite these significant differences in pressure, the difference in the normalized oil rates is very small. Even at late times in the flood, where the pressure difference between the 2.8 D and 9 D cores is less than 10 kPa (1.5 psi), the difference in the normalized rates is still similar to earlier portions of the flood when the pressure was much higher in the 2.8 D core. Likewise, although at later times the pressure gradient is still significantly higher in the 0.8 D core compared to the 9 D core, the normalized oil rates are similar.
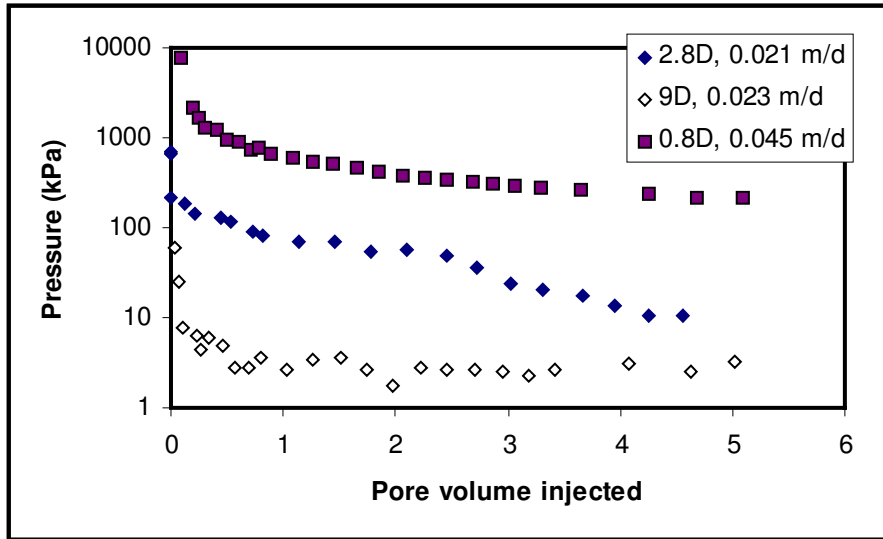
Figure 7.31: Pressure profile at low injection rates for systems of varying permeability

The fact that pressures are significantly different in the three cores while normalized oil rates are only marginally higher in the lower permeability system shows once again that after the initial high pressure region at early times, oil production rates are not proportional to viscous forces. Much higher pressure gradients can be sustained in lower permeability systems, but this does not translate in turn to significantly higher oil rates. The results of Figures 7.29 and 7.30 show that normalized rates are higher in lower permeability rocks, but this cannot be simply attributed to the higher pressure in the cores.

Figure 7.32 plots the oil recovery after 5 pore volumes of injection into the cores of varying permeability, at different water injection rates.   The trend between the improvement in recovery with reduced permeability and reduced injection rate is evident in this figure.   It should be noted, however, that while there is a distinct difference between the 9 D core and the other cores, the results of the 2.8 D and 0.8 D core are similar. This suggests that as permeability is reduced down to the order of 1 – 3 D, the influence of permeability is smaller than it is in much higher permeability systems.
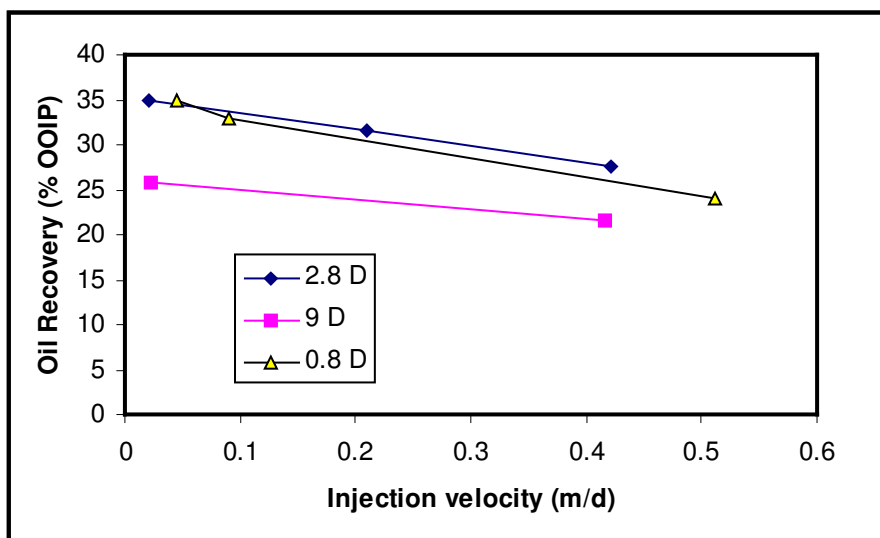
Figure 7.32: Recovery as a function of injection rate for systems of varying permeability

The analysis of normalized oil production rates at early versus late times in the waterflood demonstrates once again that viscous forces are mostly important only at early times in a flood. In reservoirs after primary production, gas is present in the pore spaces and water breakthrough may occur with very little pressure build up. As a result, there is no influence of high pressure gradients at early time, which can aid in oil displacement and recovery. Therefore, in order to properly understand the effect of sand permeability on the oil recovery it is useful to consider the total flood response in relation to the amount of oil recovered at early times (i.e. up to water breakthrough). Table 7.3 shows the breakthrough recovery and the recovery after five pore volumes of water injection into the different systems.

It appears that at early times and high injection rates, when flow is due to viscous forces, breakthrough oil recovery values are slightly higher in higher permeability sands, where oil can flow more easily. This was also observed in the analysis of oil recovery versus viscous forces during primary production (Chapter 6). When injection rates are reduced down to very low frontal velocity values, there does not appear to be any more correlation between the sand permeability and the breakthrough oil recovery.

Table 7.3: Recovery for dead oil waterfloods in different permeability systems

System Permeability (D)	Water injection velocity (m/d)	Breakthrough recovery (%OOIP)	Recovery at 5 PV injected (% OOIP)
2.8	0.42	8.17	27.60
2.8	0.21	12.39	31.59
2.8	0.021	9.63	34.97
9	0.42	8.70	21.60
9	0.023	6.50	25.80
0.78	0.512	7.12	23.90
0.78	0.09	7.60	32.90
0.78	0.045	9.75	35.00

The lack of an apparent trend between permeability and breakthrough recovery at different rates could be partially due to inaccuracies in determining the breakthrough recovery, or could also be due to the competing influences of higher pressure gradients and higher instability obtained for increased injection rates and/or low permeability systems. In general, however, it can be seen that the overall recovery is the highest in the 0.78 D core, despite the fact that frontal velocities are consistently higher in this system. The recovery is also consistently lowest in the 9 D core.

Figure 7.33 plots the oil recovery that is obtained after breakthrough for the different rates and rock permeabilities. The data for this figure is obtained by subtracting the breakthrough recovery from the final oil recovery (after 5 pore volumes of water injection).

The oil recovery after breakthrough is the oil that is produced when the pressure gradient is already low across the core, and the majority of injected water is cycling through low resistance waterflooded channels. When comparing Figure 7.33 to the total oil recovery values in Figure 7.32, it is evident that more oil is recovered for lower permeability systems. The other conclusion that can be reached is that at any permeability lower injection rates lead to higher recovery after water breakthrough.
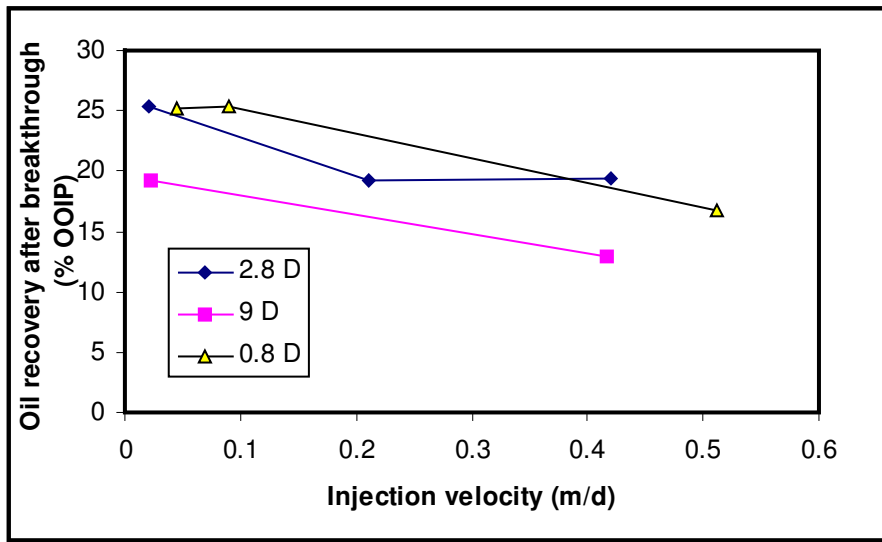
Figure 7.33: Oil recovery after breakthrough for systems of varying k

The trends observed so far all demonstrate that viscous forces are not the main mechanism responsible for oil production at late times in a waterflood. Unlike in primary production of heavy oil, where the presence of high permeability wormholes is often cited as one of the explanations for the oil production rates and recovery (Tremblay *et al.*, 1996, 1999), in the case of waterflooding the opposite trend is observed. It appears that high rock permeability, while providing a greater "ease of flow" for the viscous oil to move through the rock pores, is in fact detrimental to the overall efficiency of a heavy oil waterflood.

7.6 Dead Oil Waterflooding Discussion

The experiments discussed in this chapter were designed to investigate the influence of viscous forces on heavy oil recovery by waterflooding. These viscous forces were manipulated by changing the water injection rate, the oil viscosity, and the rock permeability. In all experiments, parameters such as overall oil recovery, normalized oil production rates, and the relationship between oil recovery and the pressure response in the system were analyzed.

When water injection rates were altered for varying viscosity oils in different rock systems, it was consistently observed that at lower rates, overall oil recovery was higher and oil was produced at reduced water cuts. When oil production rates were normalized to the injection rates, it was observed that at early times the normalized rates were similar for all water injection rates. This indicated that, during these times, viscous forces were dominating flow since oil rates were proportional to the water injection rates. At later times, however, improved normalized rates were consistently measured for lower water injection rates. Additionally, for low waterflood rates after two pore volumes of water injection, the oil production rates were essentially independent of the pressure gradient in the system. Oil could be produced even with very low pressure drop across the cores.

A new definition of breakthrough was employed in order to determine the breakthrough recovery for these heavy oil waterfloods. With the exception of the lowest injection rate, the overall trend observed was that as the instability number increases (due to injection rate or oil viscosity), the breakthrough recovery decreases. Further discussion on instability will be given in Chapter 11. Nevertheless, the results so far indicate that the concept of instability could be used to explain the mechanism up until breakthrough only. At very low injection rates the breakthrough recovery decreased again, although final oil recovery values were highest in these systems.

Elevated injection rates initially led to larger slopes in the oil recovery profiles, indicating that viscous forces (i.e. the generation of a large pressure gradient) can be utilized at early times to improve the oil recovery. Once pressure had dropped in the system, however, injecting at elevated rates led to a decrease in the oil recovery efficiency when compared to the response at lower injection rates. Additionally, reducing the water injection rate at later times led to an increase in the slope of the oil recovery profile, indicating that these lower rates are more efficient at later times.

As expected, when waterfloods were performed on systems of varying oil viscosity, higher recoveries were measured for the lower viscosity oil. A result that was not

expected, however, was that when oil viscosity was more than doubled, the recovery after 5 pore volumes of water injection was only marginally lower. Doubling the oil viscosity was expected to lead to a much more adverse mobility ratio, both in terms of the viscosity ratio and the relative permeability ratio between water and oil. Despite the fact that the flood was now at least twice as unstable, the difference in recovery was much smaller. Therefore, instability and viscous fingering cannot be the mechanism responsible for changes in oil recovery with varying rates and viscosity.

When the results of waterfloods were compared in systems of varying rock permeability, optimal oil recovery was consistently observed at any rate for the lowest permeability rock. This is in direct contrast to primary production of heavy oil, which is controlled by viscous forces and shows a higher recovery in systems with high permeability. The effect of changing the rock permeability can also not be simply explained by the generation of a higher pressure gradient in a lower permeability rock. Even after water breakthrough, when the pressure drop is low across the core, the oil recovery was still consistently highest in the lowest permeability rock.

In primary production of heavy oil (Chapter 6) it was shown that oil recovery is proportional to the magnitude of the viscous forces in the core. All of the evidence compiled for dead oil waterflooding proves that viscous forces are most emphatically not dominant in high viscosity, heavy oil systems. As such, viscous forces cannot be used to explain any of the production behavior observed in these systems after the point of water breakthrough. Observations have been made for reservoirs containing a high permeability streak, or "thief zone", whereby water quickly breaks through in the highest permeability channel and then gradually fluids are displaced in lower permeability sections of the reservoir. This leads to similar behaviour as what was observed in heavy oil systems at low rates: water initially breaks through early in the life of a flood, followed by a much slower change in the water-oil-ratio as other portions of the reservoir are invaded. However, these situations have only been reported for cases with low mobility ratios and high vertical permeabilities (Yortsos *et al*., 1999; Yang and Ershaghi,

2005). In the low rate heavy oil waterfloods studied in this chapter, a similar behaviour is observed, but in linear systems under highly adverse mobility ratios. Therefore, it can be concluded that even in these cores, there is some force that causes water to be displaced out of the water channels, and to access previously unswept portions of the core.

In the absence of any gravitational or inertial forces, the only other force present in these cores is that of capillarity. For water wet rocks, it appears that water imbibition is occurring. As water moves into rocks through imbibition, oil is displaced and oil recovery is improved. Since waterfloods were only carried out to 5 pore volumes of water injection, performing floods at reduced rates allowed more time for imbibition to occur, which lead to overall improvements in the oil recovery profiles in the systems. The effect of capillary forces will therefore be more prominent at lower injection rates, which was observed in these cores. Capillary forces are also higher in lower permeability rocks, which could explain the improved recovery observed in lower permeability cores even at higher frontal velocities. Finally, while imbibition rates are still affected by the oil viscosity, the Laplace equation for capillary pressure is independent of the oil viscosity, which explains how capillary pressure and water imbibition can be a recovery mechanism even for higher viscosity heavy oils.

If capillary forces and imbibition are in fact the mechanism responsible for oil recovery after water breakthrough, then these forces should also be evident in systems where the initial pressure gradients cannot be generated. In the next chapter, therefore, waterfloods are carried out for systems after primary production. In these cores, the effect of viscous flow will be very minor, so if similar trends are observed then this will be strong evidence for water imbibition being responsible for oil production in heavy oil waterfloods.

CHAPTER 8: SECONDARY WATERFLOODING RESULTS

In Chapters 3 and 7, investigations into waterflooding of heavy oil were reported. However, most experimental results are derived from gas-free oil systems. In the field, waterflooding is often commenced after primary production in heavy oil systems, and at this state pressure has been at least partially depleted. As a result, a free gas phase exists in some regions of the porous medium. Thus, in order to properly understand heavy oil waterflooding it is necessary to identify the differences between waterflooding in primary and secondary recovery situations. Additionally, it is beneficial to examine if the results obtained from gas-free systems can be extrapolated to secondary waterfloods.

From the series of waterfloods previously performed in gas-free oil, some important conclusions were reached. It was observed that viscous forces dominate initially at the beginning of the flood. During this time, constant rate water injection leads to the buildup of pressure across the core, and relatively high initial rates of oil recovery. However, these effects diminish as more brine is injected, particularly in cases where the injection rate is slow. At late times oil production rates are no longer proportional to injection rates or pressure, which indicates the presence of another recovery mechanism aiding the process. It was postulated that this is the influence of capillary forces, or water imbibition into water-wet rock. In order to identify if such behaviour can be expected in actual field waterfloods, it is important to establish that the results of secondary waterflooding show similar traits.

Various secondary waterfloods have been performed to investigate the response of oil production rates and recovery to similar factors as in Chapter 7. The purposes of these sets of experiments are fairly similar to the gas-free waterfloods. The effects of viscous forces are investigated by varying the water injection rate; in the secondary waterfloods viscosity is constant (HO2). The effects of changing injection rate in systems of varying permeability in primary and secondary waterfloods are compared. The waterfloods were performed on the cores that had primary production as discussed in Chapter 6.

8.1 Fluid Distribution Prior to Waterflood

It was established previously that the fluid distributions in the porous medium prior to primary versus secondary waterflood are distinctively different. This subsequently influences the behavior of the waterfloods.

8.1.1 Fluid Saturations Prior to Dead (Gas Free) Oil Waterflood

Prior to dead oil waterflooding, only oil and irreducible water exist in the porous medium. The distribution of these fluids is controlled by the wettability preference of the sand. All dead oil waterflood experiments were packed and flooded using the same procedures (i.e. saturating first with water and then flooding with oil at the same rate), and employed the same sand, so the sand wettability should be consistent between experiments. Assuming that the sand is water-wet, oil will likely exist in large pores while water will occupy small pores, and may also cover the surface of the sand grains. The assumption of water wetness of the sand is appropriate according to Peters and Flock (1981), who stated that the sand would be preferentially wetted by the fluid that contacts it first, which in these experiments would be brine. Jamaluddin and Butler (1988) also stated that when cores were saturated with water prior to oil flooding, the sand will tend to be water wet. The wettability assumption will be tested in Chapter 9 against experimental evidence; at this point the sand is simply assumed to be water wet.

Another important aspect of the saturation in a dead oil system is that prior to the waterflood, the oil exists as a continuous phase from inlet to outlet. This is a direct result of the procedure, where the oil displaced brine in a piston-like fashion to reach irreducible water saturation. Due to the absence of a third (gas) phase and primary production of oil, the saturation of oil in the porous medium is also quite high compared to the situation of secondary waterflooding.

As water is injected to displace dead heavy oil, it is unclear which pores are swept first. In a straight imbibition process, water would enter through the smallest pores (the

imbibition pathway) and displace oil out through continuous channels of the largest pores. As shown in Chapter 7, before water breakthrough occurs oil production rates are directly proportional to the water injection rates, which is an indication that viscous forces are dominant during this time. In this scenario, any water entering a given pore must first displace viscous heavy oil out of that pore. Therefore, the high pressure gradient developed will simply push water and oil through the largest (low resistance) pores in preference to smaller pores. This is also indicated in viscous fingering theory. Some oil is produced during this initial stage with no water production, but after a short period water has fingered through to the outlet. Afterwards, any water injected will continue to travel through this path so fluids will be produced at high water cuts, but during the course of injection additional oil may also be produced. This waterflood response can be contrasted to the different state of the reservoir after primary production.

8.1.2 Fluid Saturations Prior to Secondary Waterflood

Prior to secondary waterflooding, oil, water and free gas all exist inside the porous medium. The location of water is expected to be in small pores, assuming that the porous medium is water wet. The experiments that were waterflooded after primary depletion consist of two different types of porous media: sand and unconsolidated glass beads. Glass beads are made of quartz material, thus they should be equally or more water wet than sand.

Dissolved solution gas is liberated from the live oil during primary depletion. At the end of this stage, therefore, a free gas phase has developed and some may exist as disconnected gas bubbles. The mechanisms of primary production of heavy oil through solution gas drive were discussed previously in Chapter 6. During primary depletion some of the oil is mobilized and produced. Goodarzi and Kantzas (2006) showed that although gas nucleation occurs throughout the porous medium, the oil production tends to come mostly from regions close to the outlet, particularly in longer systems. This is confirmed in Figure 8.1, which plots the oil saturations remaining in systems A and B after primary production.
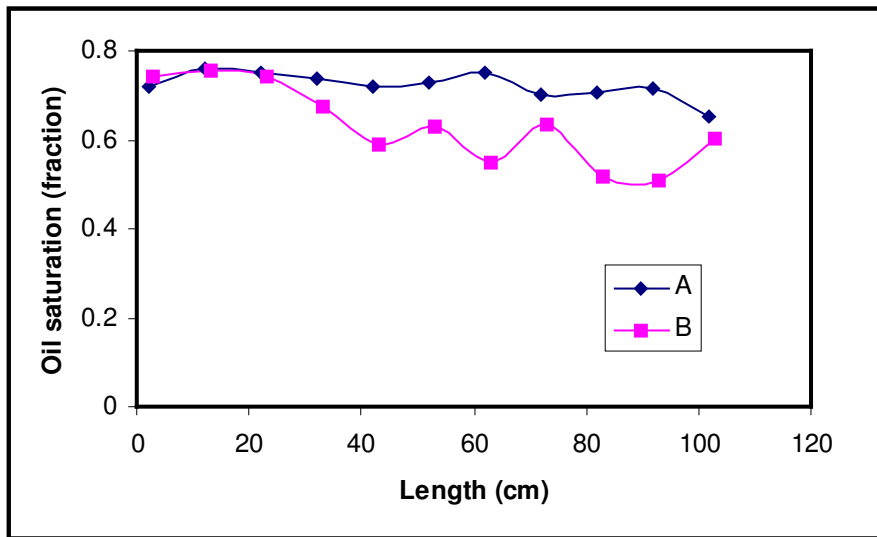
Figure 8.1: Oil saturations remaining in porous media after primary depletion

Figure 8.1 shows fluid distributions obtained from CT scanning at set lengths at the conclusion of primary depletion. At this state, there is still a significant portion of the oil left behind, and the high remaining oil saturation indicates that the oil is likely still continuous. At the end of primary depletion, all the gas originally dissolved in the live oil has evolved due to the low pressures in the core, and most of it has been produced. Thus the oil existing in the porous medium at this stage is essentially gas-free with higher viscosity (Bennion *et al.*, 2003; Goodarzi *et al.*, 2007). The gas may or may not be continuous at this stage. However, it is certain from CT images shown in Chapter 6 that there is a significant free gas existing throughout the length of the cores. The saturation and distribution of irreducible water should not change during primary production, thus at the end of primary production water still exists in small pores while oil and gas (non-wetting fluids) are located in larger pores. Sources in the literature have shown that gas is preferentially liberated in the largest pores of the porous medium, where capillary trapping is the lowest (Stewart *et al.*, 1954; Wall and Khurana, 1971; Bora and Maini, 1997).

When water was injected at a fixed rate after primary depletion, the pressure built up slightly and then later declined again, as can be seen from Figure 8.2.
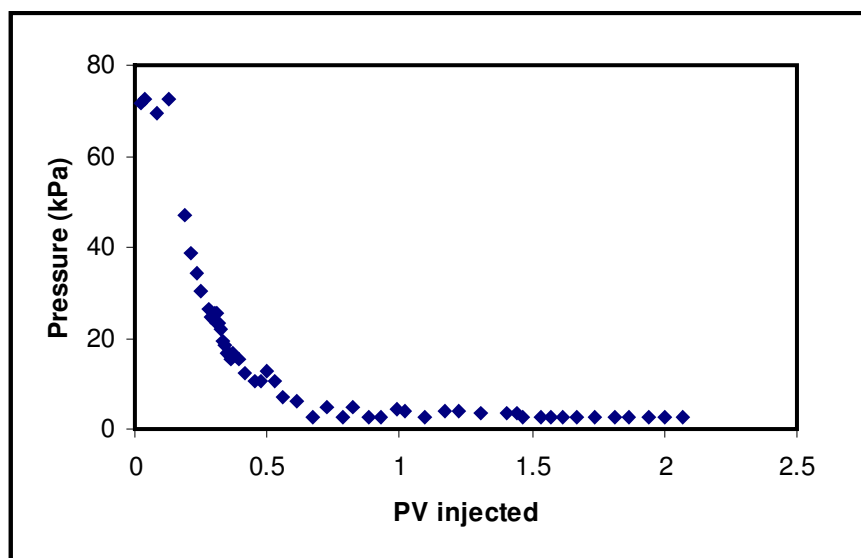
Figure 8.2: Pressure buildup at early times for secondary waterflooding into System A

This figure shows that at an injection rate of 0.0106 m/d, during secondary waterflooding the pressure built up to approximately 70 kPa. Pressure then declined as water breakthrough occurred. Primary waterflooding was also performed in Experiment C, at the same rate in a large core of similar dimensions and rock properties. In this core, the pressure built up to 220 kPa before water breakthrough. This shows that during a secondary waterflood, as brine is injected it automatically seeks the paths of least resistance to flow, thus water will tend to displace gas in the porous medium first. This is due to the fact that the gas flows much more easily than the oil and some of the gas may even be connected, meaning that these regions represent the sections of the core with the highest mobility.

The fact that gas was produced preferentially to oil is shown in two observations. First, the injection pressure was only approximately 1/3 of the pressure required for water injection in a similar permeability sand and similar viscosity oil, but in the absence of a

low resistance gas phase. Second, at the point of water breakthrough in the core, only traces of oil had been produced prior to the production of water. Similar to dead oil waterfloods, water will seek to form continuous channels along the length of the core. In dead oil waterfloods, the pressure at the inlet will increase prior to breakthrough, accompanied by oil production since any water that enters the core must first displace an equal volume of oil. In secondary waterflooding, there was also some pressure build up observed initially, but not to the magnitude seen in dead oil waterfloods.

Since water injection led to a slight increase in the pressure gradient across the core, this indicates that not all the gas is connected, so the injected water also had to displace some oil films that were separating the ganglia of gas. Once water is produced at the outlet it behaves very similarly to the case of dead oil waterflood: injected water flows mainly through the water-continuous channels formed, thus additional oil production is accompanied by very high water cuts.

A comparison of the profiles between the injected and produced fluid volumes shows that after an initial delay period, both the cumulative injected and produced fluid volumes increase correspondingly with time. The difference between them is the volume of gas in the core that was displaced and is now occupied by water. Table 8.1 shows the injected and produced volumes for systems A and B. Also shown are the oil volumes produced during primary production.

Table 8.1: Gas saturations in cores during secondary waterflooding

	System A	System B
Pore volume (cm^3)	2,592.39	2,680.27
OOIP (cm^3)	2,360.51	2,457.04
Oil produced during primary depletion (cm^3)	481.10	661.34
Difference between injected and produced fluids (cm^3)	254.67	272.33
Volume of gas displaced (cm^3)	254.67	272.33
Gas saturation remaining (fraction)	0.087	0.145

At the end of primary production, the pore space containing oil that was produced is now occupied by gas, so this is the free gas saturation in the core. During the initial stage of water injection, water entered the core at a lower injection pressure than for a primary dead oil waterflood, and did not lead to any significant oil production before water breakthrough. Therefore, it was inferred that the water is instead being displaced into the gas-saturated low resistance flow pathways. If all the gas was displaced, the difference between the injected and produced volumes should be essentially the volume of oil produced during primary production, since water would have displaced all the gas and filled this volume of the core. However, in both cores A and B, the difference is less than that of the initial gas volume in the core. This indicates that during secondary waterflooding, there is still a fraction of gas that remains trapped in the core. This is actually not a surprising observation, since gas displacement by water is an immiscible process so it is expected that there should still be some residual gas saturation, trapped by capillary mechanisms (snap-off and by-passing). It is significant that during the initial stage of water displacing gas, a similar gas volume is produced in both sand packs, which have similar rock properties. This means that the water displaced gas at similar efficiencies in both cores. The presence of this trapped gas phase means that compared to primary dead oil waterflooding, there are less drainage pathways for the oil to be produced. Secondary waterfloods are therefore expected to be less efficient than primary waterfloods.

8.2 Secondary Waterflooding Results

As mentioned previously, secondary waterfloods were performed on four different sandpacks that had two different lengths. It should also be noted that the material used to construct the porous media was not all the same, as mentioned previously. The two cores depleted in Chapter 6 were packed using Lane Mountain 70 sand, while the cores prepared and depleted by Goodarzi (2006) contained glass beads.

8.2.1 Summary of Waterfloods on 0.43 m System (Core E)

Goodarzi (2006) prepared this sandpack and performed primary depletion as part of her M.Sc. Thesis. During primary depletion 38% of OOIP was produced, leaving a large free gas phase present in the core after primary production. CT analysis showed that the free gas saturation ranged from 20 – 40% of the pore space along the length of the core (Goodarzi and Kantzas, 2006). The core was used in this project to investigate the nature of waterflooding as a secondary recovery mechanism after such a significant fraction of oil had already been recovered. Another important aspect studied was the effect of porous medium (different permeability and grain size distribution) on the waterflood response. The properties of this sandpack are shown in Table 8.2.

Table 8.2: Properties of 0.43 m sandpack (Core E)

Length (cm)	42.6
Diameter (cm)	3.81
PV (cm³)	165
ϕ (%)	37.7
Permeability (D)	6.67
S_{wi} (%)	10.99

The irreducible water saturation in this core consisted of 2% NaCl brine. However, in the waterflood an attempt was made to track the changes in oil and water saturation as the waterflood progressed using CT scanning. Due to the fact that the density of heavy oil and water are fairly similar, the 2% NaCl brine injected during the waterflood was doped with an additional 5.5% KI. Details of this process have previously been discussed in Chapter 4. The injected water was therefore quite different than the irreducible water in the porous medium. As brine was injected, it would displace not just gas, but would also miscibly displace connate water that was connected to the injection pathways. In this manner, the original (2% NaCl) brine was displaced, and the water existing in the porous medium should be mainly doped brine. The properties of the fluids used in this sandpack are detailed in Table 8.3.

Table 8.3: Properties of fluids used in 0.43 m sandpack

Dead oil density (g/cm^3)	0.982
Dead oil viscosity (mPa·s)	11,500
Density of 2% NaCl brine (g/cm^3)	1.007
Density of doped brine (g/cm^3)	1.0487

The sandpack was waterflooded at a relatively low rate of 1 cm³/hr (frontal velocity of 0.021 m/day). This injection rate was chosen based on the positive response seen in similar cores during dead oil (gas-free) waterfloods. Initially when water was injected into core E, only gas was produced. Unfortunately, the actual amount of gas produced was not measured. Initially when brine was injected, only minute traces of oil were produced at the point of water breakthrough. During this stage, therefore, the injected brine was displacing the free gas and irreducible water in the porous medium, similar to the larger cores discussed in Section 8.1. If the gas liberated from primary depletion is indeed isolated then some oil could be produced while brine coalesced the gas bubbles. Although this was not observed, it was seen in Figure 8.2 that there was some pressure buildup initially in these cores prior to water breakthrough. Therefore, this indicates that even if gas channels were not fully connected, injected water must have ruptured oil films and pushed through these low resistance pathways without actually displacing any viscous gas-free heavy oil out of the core.

From dead oil waterfloods in the short sandpacks (Chapter 7), stable oil recovery profiles were obtained when water was injected at 1 cm³/hr. Thus this injection rate was initially chosen for this experiment to allow for a comparison between dead oil and secondary waterfloods, even the porous media are not the same. However, the results obtained were quite different from the dead oil waterfloods. At first there was a small quantity of oil produced, but then oil production ceased and pure water was produced. Water injection continued at this rate for about 8 days (1.2 PVs). For a total of 194 cm³ of brine injected (1.2 PVs), 1.6 cm³ of oil (1% OOIP) were recovered. The result of the secondary waterflood was surprising, considering that oil recovery was always efficient at a flow rate of 1 cm³/hr in primary waterfloods.

Due to the fact that very little oil was produced at this injection rate, the rate was reduced by an order of magnitude to 0.1 cm³/hr (velocity of 0.0021 m/day). Lower injection rates reduce the viscous forces, so for the same porous medium this allows more time for imbibition to occur (i.e. at reduced viscous forces, less water is pushed through the water channels). After the injection rate was reduced, oil production was steadily measured, with high water cuts. The oil production did not appear to be continuous: visual observations of the produced fluid showed that the production occurred as droplets of pure water followed by droplets of oil, rather than a steady mixture of oil and water. The results of the slow waterflood are shown in Figure 8.3.
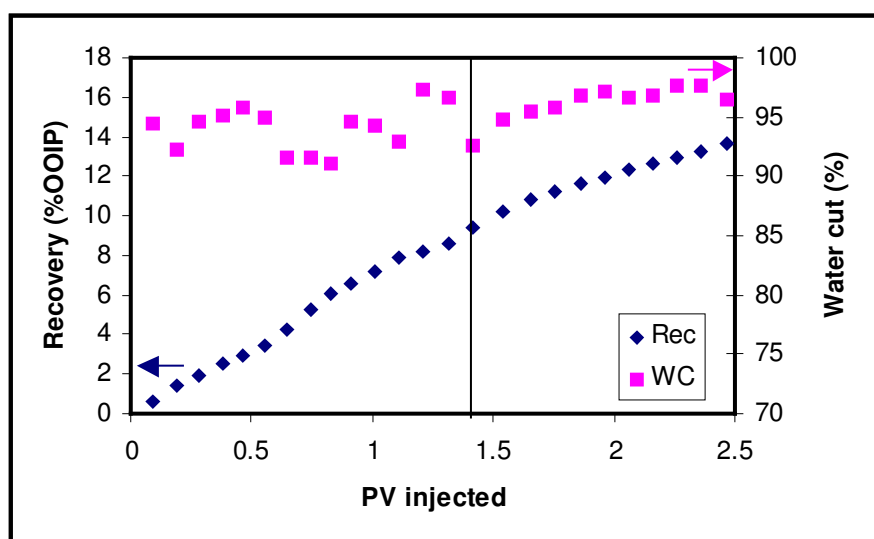
Figure 8.3: Core E oil recovery and water cut for injection at 0.1 cm³/hr

This figure shows a significant amount of scattering initially in the water cut data. This is due to the fact that oil production was not continuous, so for the sample sizes (20 cm³ glass vials), any inaccuracy was magnified. The line in the graph corresponds to a time when the sandpack was shut in for a period of 68 days, after which point the sandpack was flooded again at 0.1 cm³/hr. When the sandpack was shut in and then re-flooded, the water cut of the produced fluids dropped immediately. This was consistent with the observations seen in dead oil waterfloods. The reduction in the water cut, and

correspondingly the improvement in oil recovery, depends on the amount of time the core was shut in. The only mechanism that exists during the shut-in period is capillary pressure, which can lead to fluids re-distribution. This will be discussed further in Chapter 9. It is likely, that during the shut in period, capillary forces redistributed the fluids by imbibing some water from the swept channels into the bypassed regions of the core, thus displacing some oil into pathways that could be produced once injection begins again. Figure 8.4 shows the change in oil rates before and after shutting in the core.
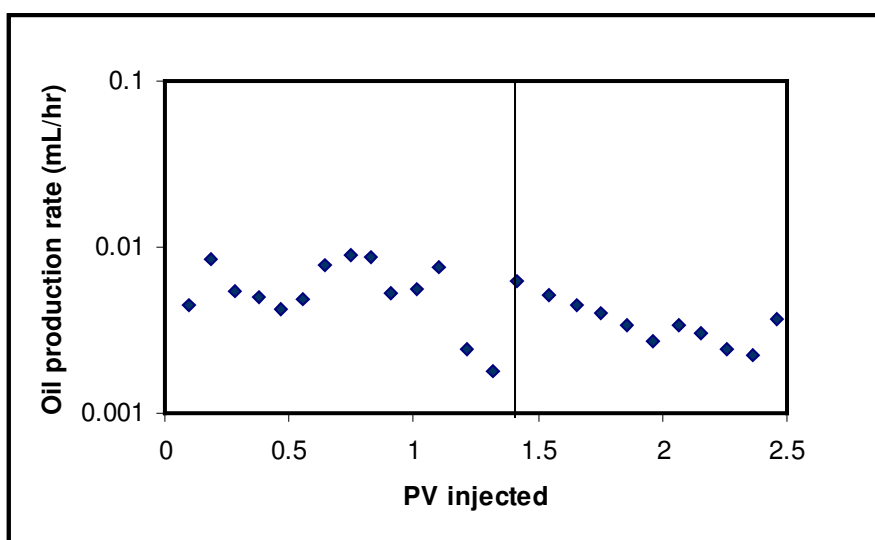
Figure 8.4: Oil production rate improvement after shutting in the core

This figure shows that the oil production rate was relatively steady at first, but then started to decline while produced water cuts became extremely high. At this time, the system was shut in to allow for imbibition to occur. After the waterflood was resumed the oil production rate immediately increased, and as the waterflood progressed the rate decreased again. However, the decline in the oil production rates is less dramatic than before. Although the oil production rate eventually declined to pre-shut in values, the improvement in the waterflood response due to shutting in the core is seen in the difference in the trend of the decreasing oil production rate.

The efficiency of the waterflood is calculated by dividing the oil recovery factor (% OOIP) by the pore volumes of brine injected. This is essentially a numerical calculation the derivative of the oil recovery profile (Figure 8.3), plotted as a function of time. Recovery efficiency is calculated using the following equation:

$$RE_i = \frac{(R_{i+1} - R_{i-1})}{(PV_{i+1} - PV_{i-1})} \qquad\qquad \text{Eqn (8.1)}$$

Where RE_i = the recovery efficiency at the (i[th]) data point

      R_{i-1} = the cumulative recovery at the (i-1) data point

      R_{i+1} = the cumulative recovery at the (i+1) data point

      PV_{i-1} = the pore volume injected at the (i-1) data point

      PV_{i+1} = the pore volume injected at the (i+1) data point.

For each point of production data collected, therefore, the recovery efficiency is the slope found using the data points before and after the current time. This approach was used in an attempt to smooth out the data by averaging over longer time intervals. As water cut increases, a greater volume of brine injection is required in order to recover the same volume of oil, and this will be reflected in a lower waterflood efficiency. Figure 8.5 shows the waterflood efficiency for the 0.1 cm³/hr injection rate, before and after shutting in the core.

In the first 0.5 – 0.75 PV injected at 0.1 cm³/hr, the flood efficiency varied between 5 – 10% of oil recovered per PV injected. The efficiency then dropped sharply down to 3%, at which point the core was shut in. After fluids were allowed to re-distribute, the efficiency increased again to 8%, and did not reduce back to pre-shut in values until another pore volume of water had been injected.
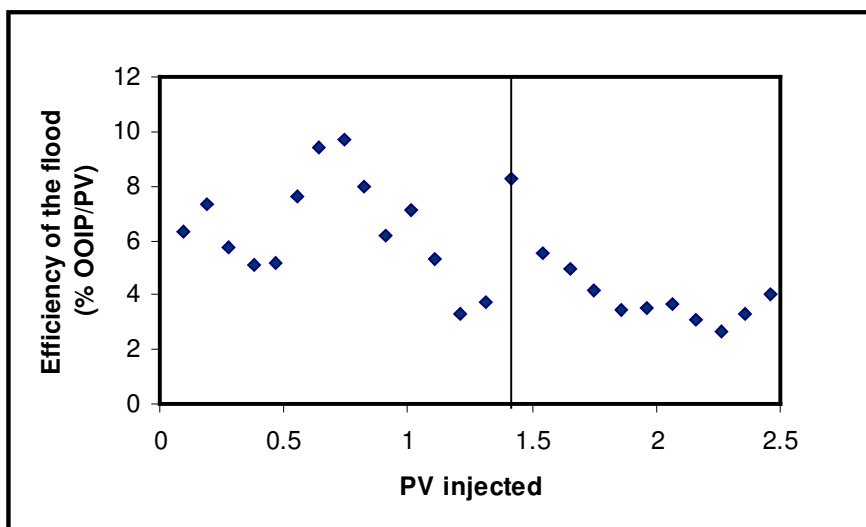
Figure 8.5: Low rate waterflood efficiency before and after core shut in

The pressure profile of this waterflood is shown in Figure 8.6.
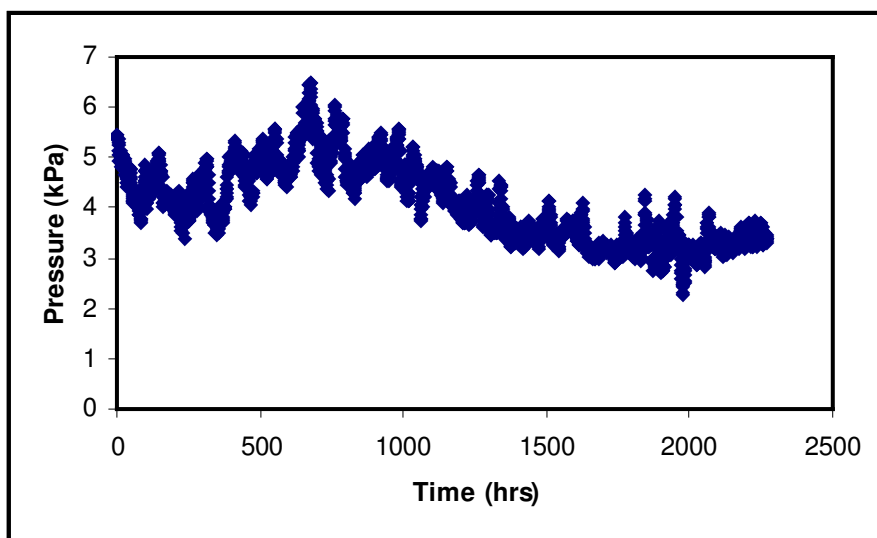
Figure 8.6: Injection pressure profile for 0.1 cm³/hr secondary waterflood

At this low injection rate, the pressure is relatively low, fluctuating around 4 kPa (0.6 psi). This is close to the limit of what can be measured accurately with a 0 – 172 kPa (0 – 25 psi) pressure transducer. Figure 8.6 therefore indicates that in a secondary waterflood,

water is channeling though the porous medium, and the pressure drop required for the injected water to travel through to the outlet for this 6.7 D core is very low.

The low pressure drop observed is a strong indication that viscous forces are not responsible for oil recovery in secondary waterflooding. At such low injection pressures, the oil flow rate predicted from Darcy's Law will be extremely low, and cannot explain the waterflood efficiency values in Figure 8.5. For this core, it appears that oil production is mainly the result of imbibition. The lower water injection rate required is most likely due to the presence of some free gas still in the core, although other factors such as the lower oil saturation and a different pore size distribution may also contribute.

In order to understand the behavior of this waterflood, a comparison of the recovery from this core to a primary waterflood on a core with similar permeability (9 D) is shown in Figure 8.7. As was noted previously, the dead oil waterflood was performed at a rate of 1 cm³/hr, so the viscous forces are an order of magnitude higher in this system.
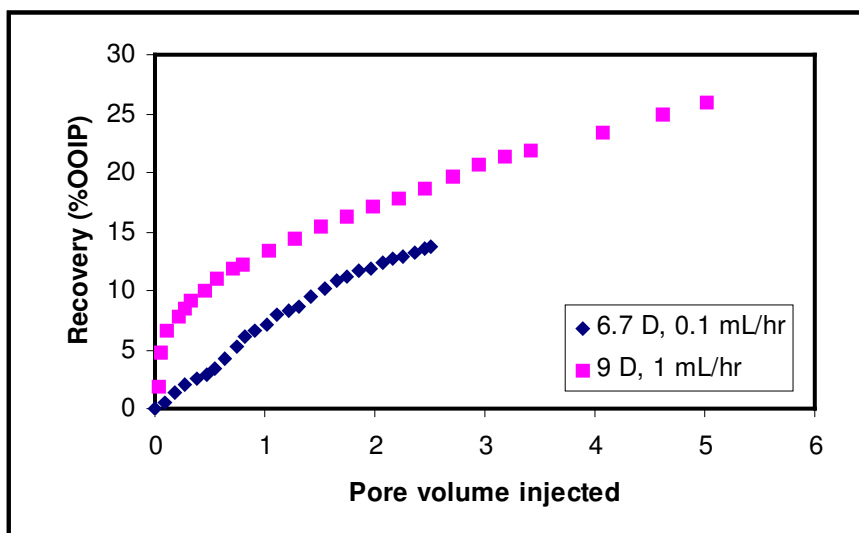
Figure 8.7: Comparison of recovery profiles of sandpacks with similar permeability

Excluding the early time dead oil waterflood data when the oil recovery slope is high, the slope of the oil recovery profile appears similar in both cases. However, in the primary

dead oil waterflood, this recovery is obtained at an injection rate that is ten times that of the secondary waterflood, and in a more permeable sand, which was shown in Chapter 7 to be less efficient for oil recovery. Therefore, the waterflood is more efficient in the primary system. It is unlikely that heterogeneity in the packing alone is responsible for this difference, since both cores were prepared using similar packing procedures and both cores are in aluminum sleeves. There are several differences between the two systems that can contribute to this unexpected response. The differences are outlined in Table 8.4.

Table 8.4: Differences between dead oil and secondary waterflood

	0.43 m	Aluminum
Porous medium used	Glass beads	Lane Mountain 70 sand
Length (cm)	43	21
Permeability (D)	6.67	9
Waterflood recovery as	Secondary	Primary
Initial water saturation (fraction)	0.11	0.13
Recovery from primary depletion (% OOIP)	38	NA
Total recovery after 2 PVs wf (% OOIP)	50	17

Overall, the combination of primary production and waterflooding led to a higher recovery in the secondary waterflood sand pack. However, waterflooding alone appears to be more effective in the primary waterflood core: after 2 PVs of water injection, 17% of the oil had been recovered in the primary waterflood, compared to 12% in the secondary waterflood, at a much lower injection rate. Although the gas saturation change was not monitored in this core, the experience from systems A and B (Table 8.1) shows that a fraction of the free gas at the end of primary depletion will be displaced by water at very early times, with essentially no accompanying oil production. Therefore, at the start of the waterflood in Figure 8.7, the water saturation is considerably higher in the secondary waterflood sand pack. In addition, there is almost certainly still some gas in this sand pack, so the flow pathways for oil and water are distinctly different in this system, compared to the primary waterflood.

After primary production, the pressure inside the core is essentially atmospheric, thus the live oil originally existed in the 0.43 m system has become gas-free. This means that regardless of the nature of the waterflood, primary or secondary, water is still trying to displace the same viscosity oil. However, the condition of the oil is may be different in the two systems. An obvious distinction between the systems in Table 8.4 is the presence of much higher water saturation at the point where the waterflood effectively begins (i.e. after water breaks through) in the secondary waterflood. In a dead oil waterflood, fingers of water move through the channels of least resistance in the core, by-passing significant zones of continuous oil. If recovery after water breakthrough is partially due to water imbibition, in order for oil to be displaced the oil must still be continuous to the core outlet (Dullien, 1992). This is the case after primary waterflooding of dead oil. For waterflooding after primary production, however, gas bubbles have left solution with the oil all over the core. Therefore, it is possible that there are fewer continuous oil pathways in secondary waterflooding. Since not all the gas was displaced by water, there will still be discontinuous gas bubbles in the core, which may have blocked some of the larger flow pathways. Unfortunately, the resolution from CT images was not high enough to determine whether this is the case, so this cannot be concluded with certainty.

It is possible that the lower recovery in core E is reflective of a wettability alteration to less water wet conditions. However, there is no evidence to suggest that the generation of a non-wetting gas phase would have any impact on the rock wettability.

The other major difference between the dead oil (primary) and secondary oil flood is the porous medium. From the PSD information, the range of grains for Lane Mountain 70 ranges from 50 to 250 μm (Figure 5.2), whereas the sizes for glass beads range from 150 to 180 μm. This shows that glass beads have a narrow range of sizes, which may affect imbibition rate and the magnitude of imbibition in this system. From experiments performed in Chapter 7 in gas-free systems, it was shown that heavy oil recovery by waterflooding is less efficient in higher permeability systems, and this was explained

through increased capillary forces in lower permeability cores. The results comparing core E to the dead oil waterfloods indicate that simply relating permeability to capillary pressure may not be correct. Although the dead oil system in Table 8.3 has a higher permeability, the effectiveness of imbibition may also be controlled by the pore size distribution. In the core with LM 70 sand, the wider range of grain sizes also provides a wider pore size distribution. Water can enter through the smaller pores while oil can flow out through larger pores, even if this is not reflected in the overall rock permeability.

8.2.2 Summary of Waterfloods on 1.2 m core D

A second, larger sandpack that had undergone primary production by Goodarzi (2006) was also waterflooded at low rates. The porous medium of this sandpack is made of the same glass beads used in the shorter sandpack (Experiment E). The properties of this sandpack are shown in Table 5.9. Due to the fact that this core was packed in a rubber sleeve with a higher overburden pressure applied, the permeability of the sand was lower: 3.9 D, compared to 6.7 D in core E.

At the start of this experiment, doped brine was injected at 2.75 cm³/hr, which corresponds to a Darcy velocity for this larger core of 0.011 m/day. This injection rate is approximately half the value of the lowest injection velocity tested in the small dead oil cores. The slow injection rate was based on the fact that in core E, the oil recovery at the same injection velocity as the dead oil waterfloods was poor. This injection rate was sustained for 69 days, in which 0.75 PVs of brine were injected to recover about 1.1% OOIP. At this stage the water cut of the produced fluids was 99.7%. Once again, in this glass bead porous medium after primary production, it seemed that injection rates had to be significantly lower than in dead oil waterfloods for LM 70 sands.

In response to the poor waterflood recovery, an attempt was made to improve production by lowering the injection rate to 0.55 cm³/hr. This corresponds to a frontal velocity of 0.0021 m/day and is similar to the optimized rate in core E. Another 1.5 PVs of brine

were injected at this rate to bring the total recovery to brine to 2.1% OOIP. At this point the water cut is 99.0%. These results can also be seen in Figure 8.8.
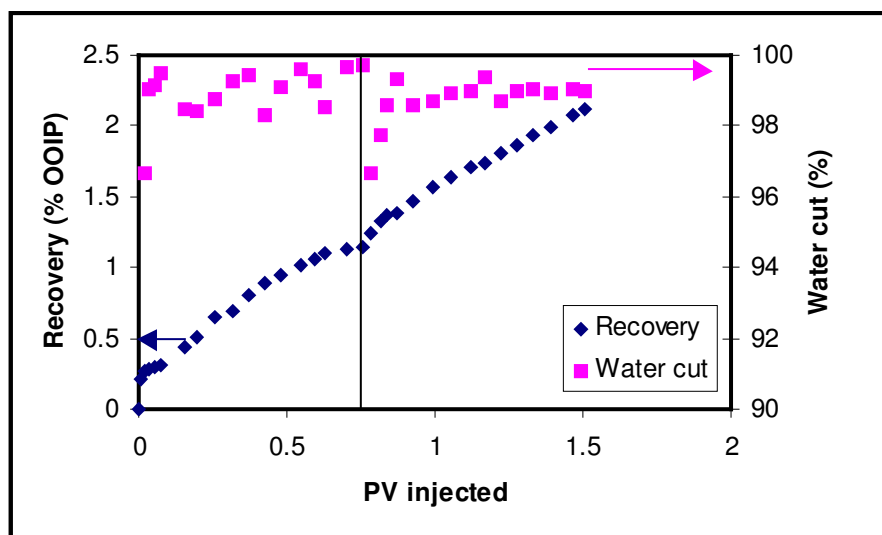
Figure 8.8: Oil recovery and water cut for secondary waterflooding in core D

The vertical line in Figure 8.9 separates the response for the two injection rates studied. At the time that the injection rate was reduced, the system responded by showing a sharp decrease in water cut, corresponding to improving recovery. This also induced a change of slope in the recovery plot, with the lower injection rate having a steeper slope. As with core E, the waterflood recovery efficiency was calculated as the numerical slope of the recovery profile. Recovery efficiency for both injection rates is shown in Figure 8.9.

In general, it could be seen that the recovery factor is marginally better for the lower injection rate. At the injection rate of 2.75 cm³/hr, the efficiency quickly declined to values under 0.5%. With a reduction in velocity (and therefore viscous forces) of 5 times, the efficiency increased to over 3% initially, and then declined to stay constant at just over 1%. At the lower injection rate, the efficiency also seemed to have reached a plateau, meaning that the waterflood was operating at a steady state condition as more brine was injected.
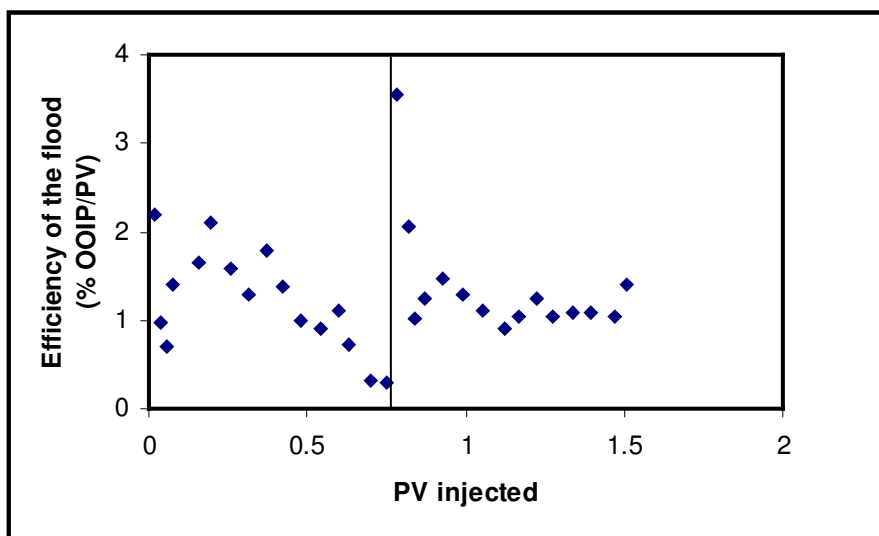
Figure 8.9: Efficiency of waterflooding in core D at two injection rates

From an analysis of the oil volumes produced alone, it is not immediately apparent that the slower injection rate is in fact more efficient in this system. During the first 0.75 PV injected at a higher rate, approximately 1% of OOIP was recovered. Later, after reducing the injection rate by a factor of 5 and injecting twice the volume of water, only 2% OOIP was recovered. It seems that the recovery efficiency is actually identical for the two flow rates. However, Figure 8.9 shows that when this is in fact not true. Oil was recovered initially at the higher injection rate, but by 0.75 PV of injection the recovery efficiency had dropped to very low value, and further water injection would likely not have recovered any more oil. By reducing the flow rate, the recovery efficiency levels out at a slightly higher value. Correspondingly, the oil production rates are shown in Figure 8.10.

This figure shows that as the injection rate was reduced, the oil production initially increased but then decreased and steadied out at an actual oil production rate that is only slightly lower than before. This observation is similar to what was seen in dead oil experiments: the slight reduction in oil production rate does not correspond to the same magnitude of reduction in the viscous force shown in the brine injection rate. This means that viscous forces alone are not responsible for the recovery of oil, and shows the significance of capillary forces on oil production.
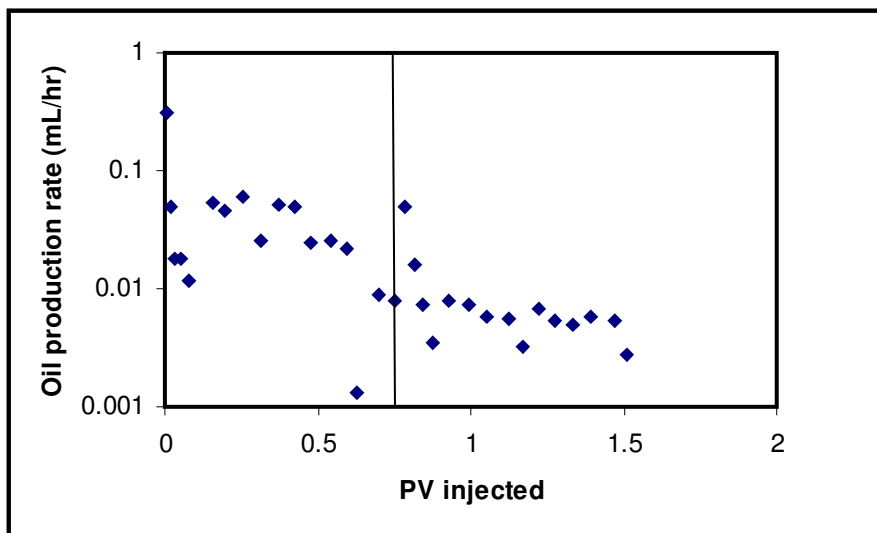
Figure 8.10: Oil production rate in core D during waterfloods at different rates

The effect of viscous force is investigated further in Figure 8.11. In this figure, the oil production rate has been normalized to the injection rates, as was previously shown in Chapter 7. This was done to show the effect of viscous forces on recovery.
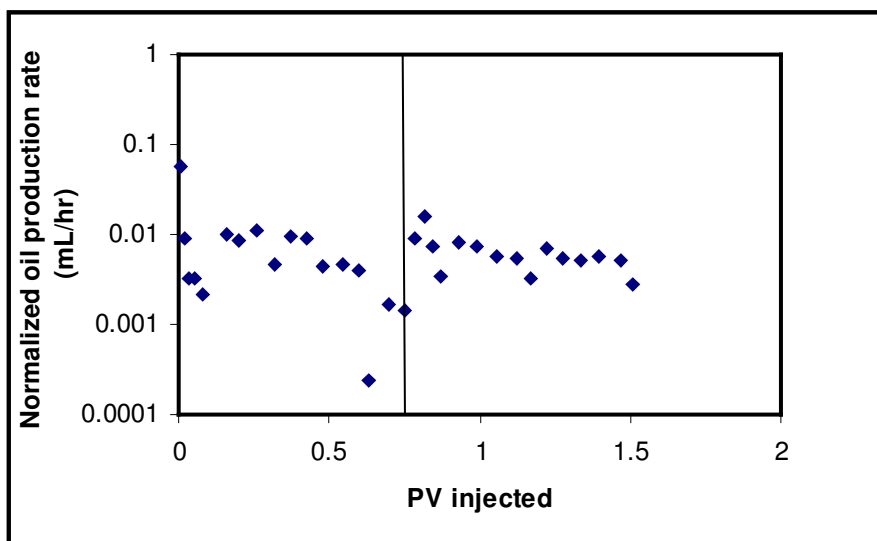
Figure 8.11: Normalized oil production rates for core D

This figure shows that the normalized oil production rates initially hovered at around 0.009 but then as more brine is injected the normalized rates began to decrease. When the injection rate was reduced, the oil production rate was once again sustained at approximately 0.01. By reducing the water injection rates by a factor of five and still measuring similar oil rates, this indicates that the fractional flow of oil is higher than before. This demonstrates that reducing the water injection rate allowed the flood to perform more efficiently. Again, the fact that the normalized oil rate appeared to plateau after the injection rate was reduced indicates that the flood is performing at steady state during this time.

The pressure profile of the waterflood is shown in Figure 8.12. When the injection rate was reduced by a factor of 5.5, the pressure was expected to decrease by a similar value. As can be seen from Figure 8.12, this was not the case.
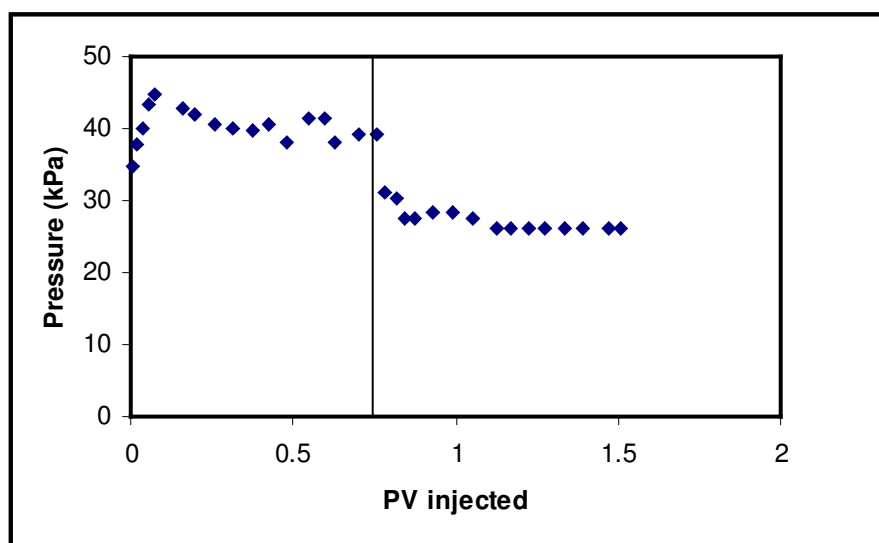
Figure 8.12: Injection pressure for core D at two waterflood rates

It is not certain whether this is a phenomenon of the porous medium or is simply a reflection of the inability of these transducers to measure such low pressure. The difficulty for this system was that initially high pressures were present during primary depletion, thus a large range pressure transducer of $0 - 17,240$ kPa ($0 - 2,500$ psi) was

connected to the inlet of the core. The error bars for these measurements are 0.25% of the range, which corresponds to 43 kPa (6.25 psi). Therefore, the pressures of the secondary waterflood at either rate are at the limits of what can be measured using this range of pressure transducer.

The secondary waterfloods performed on this system yielded similar trends as seen in the short core E. Within the same system, a reduction in injection rate resulted in an improved recovery. It should be noted, however, that if the efficiency values of cores E and D are compared against one another, it appears that core E recovers oil much more effectively. This is despite the fact that both cores were packed with the same glass bead size distribution, and that the permeability was lower in core D, which corresponded to a more efficient waterflood in dead oil systems. It is not clear what was the reason for the poor waterflood performance in core D, but there are several factors that could possibly be responsible. Core D is a much larger system than core E or any of the dead oil waterfloods performed in Chapter 7. However, as will be shown in the next two sections, the recovery efficiency of other large core floods packed with LM 70 sand is similar or better than the efficiency of core E, so it is unlikely that this is simply a scaling issue. The other factor that could affect recovery is the effect of overburden pressure. As the fluids were withdrawn from the porous medium during depletion the overburden fluid expanded and pressure decreased. Thus, at the end of depletion, the overburden pressure is considerably lower than the original overburden pressure exerted. A reduction in overburden pressure would result in an increase in permeability of the system. However, the new permeability value could not be measured since multiple fluids were already present in the core. Therefore, this would in turn affect the behavior of oil recovery during secondary waterflooding.

One other possible reason is that this core had several internal pressure transducers mounted along lines inside the core. The sections of the core corresponding to the lines and transducers are not actually part of the porous medium, so core D is a much more heterogeneous sandpack than any of the other cores. It is possible that this heterogeneity

in the porous medium was somehow acting as barriers to flow, and were either preventing water from entering un-swept regions of the core or are preventing oil from being produced. The nature of how this could be possible is not clear. In the case of secondary waterflooding, water channels form throughout the core, so this is already similar to a heterogeneous sandpack, where water does not displace oil as a single front. In conclusion, the reason for the low recovery efficiency of core D could not be satisfactorily explained.

8.2.3 Summary of Waterfloods on System A

The porous medium for this core consists of Lane Mountain 70 sand. The properties of the sandpack and porous medium are shown in Table 6.1. After primary depletion, the sandpack was waterflooded with brine at 2.75 cm³/hr (velocity of 0.011 m/day). As brine was injected, initially there was no oil or water produced. During this time, brine was replacing some of the free gas that was liberated during primary depletion. After a period of time, small amount of oil and brine were produced, although the pressure in the sandpack was still high. At approximately 0.2 PVs of brine injected, pressure decreased drastically and a water/oil mixture was produced at high water cut. This volume is similar to the free gas saturation in the core (0.19 PVs), although a mass balance of the produced versus injected fluids indicated that there was still some trapped gas remaining in the core. After water breakthrough, the injection rate was reduced to 0.55 cm³/hr (0.0021 m/day), in accordance to the rates required in core D. The point where water injection was reduced is shown by the vertical line in Figure 8.13. The volume of brine that was injected initially to displace gas was not taken into consideration in this figure. At the instance where oil and water were produced, the x-axis was initiated as "0".
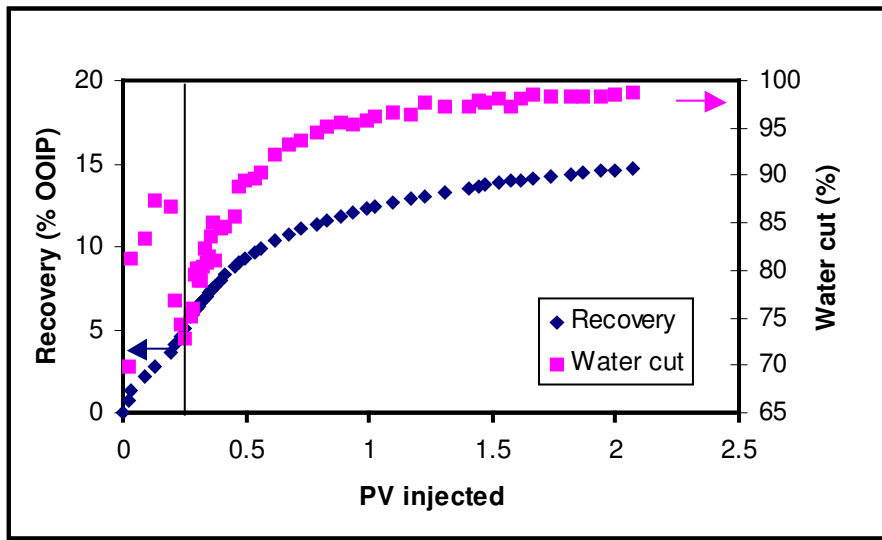
Figure 8.13: Recovery and water cut for secondary waterflood in core A

Figure 8.13 therefore plots the recovery only after water has found a continuous path to the producing end. From the figure it could be seen that due to the large volume of free gas present from primary depletion, the water fingered to the production end with a high water cut immediately after water breakthrough. Therefore, similar to cores D and E, there was no initial period of high injection pressure where the oil recovery is linear with time. This is the major difference between these systems and primary dead oil waterflooding.

The water cut continued to increase as more brine was injected. When the injection rate was reduced, the water cut immediately decreased as well. Similar to the observations made in system D, a decrease in injection rate was followed by a sharp decrease in the water cut and a change of slope on the recovery curve. In this system, however, the response to the waterflood rate reduction is much more distinct than in core D. The oil production rate of this system is shown in Figure 8.14.
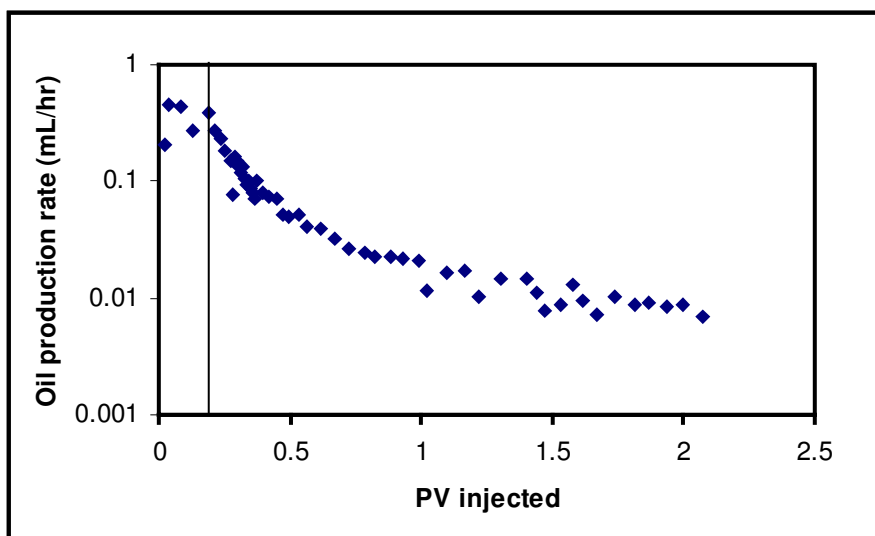
Figure 8.14: Oil production rates for waterflooding in core A

This figure shows the same behavior as what was seen in previous cores: as more brine was injected, the oil production rate decreased. Again, the oil production rate seemed to plateau over time. It is important to note that at the initial injection rate, the oil production was on the order of 0.2 – 0.3 cm³/hr. After the water injection rate was reduced by a factor of five, the oil production rate dropped accordingly. Since absolute oil rates are plotted in Figure 8.15, this may be misleading in that it appears that higher injection rates are more beneficial to oil production. When the oil rates are normalized, it can be seen once more that the lower injection rate was a more efficient waterflood. Normalized oil production rates are shown in Figure 8.15.

In previous measurements of normalized oil rates (Figure 8.11) it was shown that at the higher injection rate the normalized oil rates quickly declined but after the waterflood rate was reduced, the normalized oil rates dropped more slowly to the values that they were at under faster water injection. This trend is not evident in Figure 8.15 since the higher injection rate was only performed for a short time, but it is expected that this system should behave similarly to other cores.
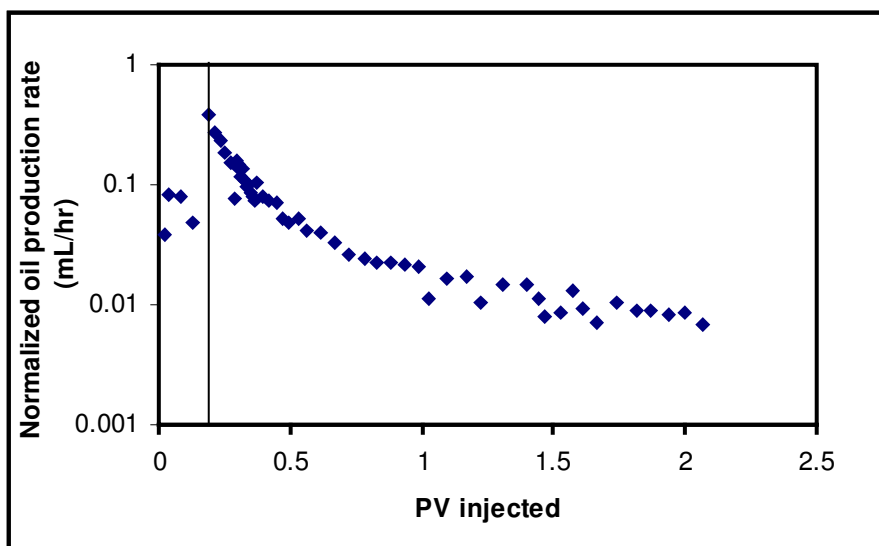
Figure 8.15: Normalized oil production rates for waterflooding in core A

After 1.5 PVs of water had been injected into core A, the normalized oil production rates were still only declining slowly. This indicates that the flood was performing in a relatively stable fashion at that point, and was approaching steady state. The pressure profile also stabled out at later times, as previously shown in Figure 8.2.

The pressure measurements for system A are more descriptive than that of system D (Figure 8.13). From the prior experiment, where it was observed that pressure gradients were extremely low in secondary waterflooding, it was deemed necessary to add more sensitive transducers to the inlet of the sandpack. In this system, two pressure transducers were connected in series. The first had a large pressure range of $0 – 6,900$ kPa ($0 – 1,000$ psi), and was used during the primary depletion step. The accuracy of this transducer is $\pm$ 17 kPa (2.5 psi). During secondary waterflooding, when water was channeling through the sandpack, the pressure drop was fairly small so pressure was recorded using a transducer with a range of $0 – 172$ kPa ($0 – 25$ psi), and an accuracy of $\pm$ 0.43 kPa. However, at pressures around 2 kPa (0.3 psi) even the low range pressure transducer values were no longer accurate. Thus, at late times the true pressure of the system could not be measured.

8.2.4 Summary of Waterflood on System B

This core used the same sand as in system A and in all the dead oil waterfloods. The properties of this sandpack and its fluids are shown in Table 6.1. In this sandpack, over the course of the waterflood various injection rates were applied. In region A of Figure 8.16, brine was injected at 2.75 cm³/hr (velocity of 0.011 m/day). After approximately 2.5 PVs of brine injection, the injection rate was reduced to 0.55 cm³/hr (0.0021 m/day), denoted as region B. In region C, the injection rate was reduced further to 0.1 cm³/hr (0.00039 m/day). In this flood, the efficiency at three orders of magnitude of waterflood rates is compared.
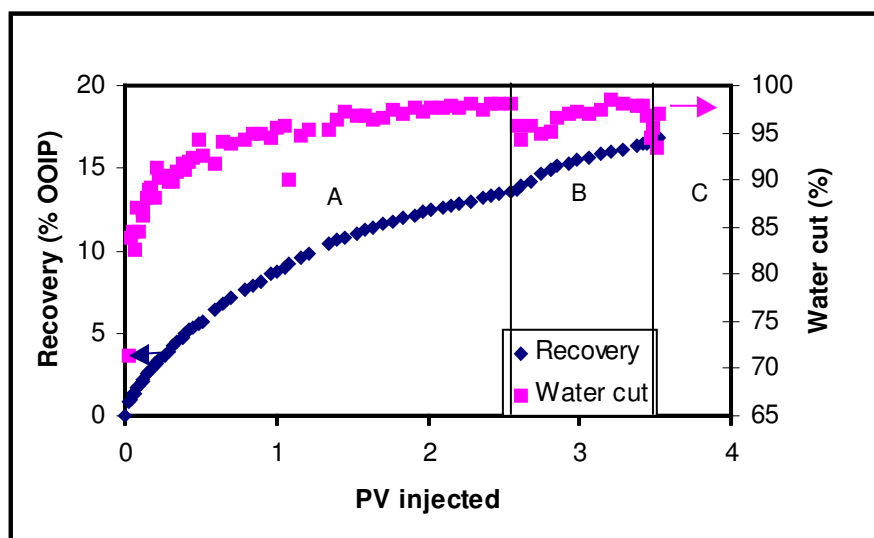
Figure 8.16: Recovery and water cut for secondary waterflood in core B

The responses observed in Figure 8.16 are similar to those seen in system A and D, in that recovery is more efficient for lower injection rates. This is more evident from Figure 8.17, which shows the recovery efficiency at different injection rates. Efficiency, as discussed previously, is a measure of the numerical slope of the oil recovery curve.
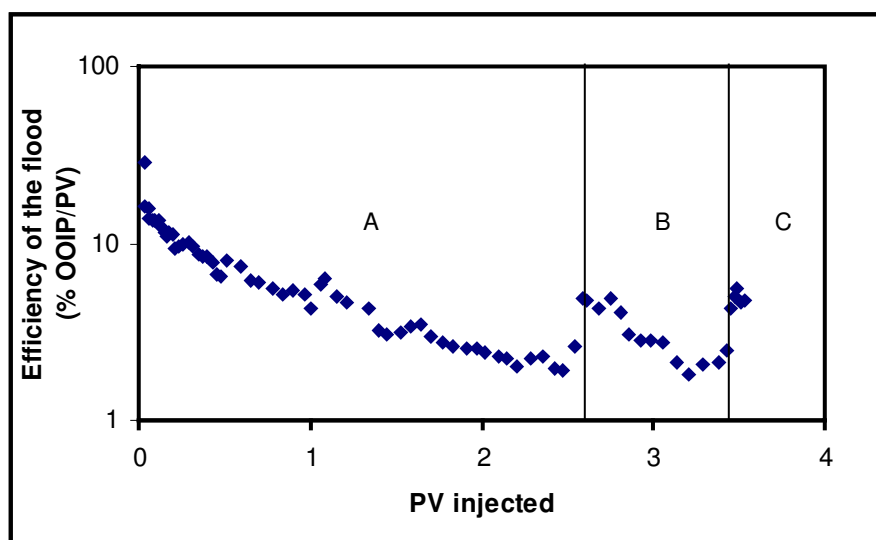
Figure 8.17: Waterflood efficiency at different rates in core B

As was also seen previously, a reduction in injection rate leads to higher efficiency in terms of the fraction of oil recovered for each pore volume of brine injected. This also corresponds to the lower produced water cuts in Figure 8.16. The oil production rate for each corresponding injection rate is shown in Figure 8.18.
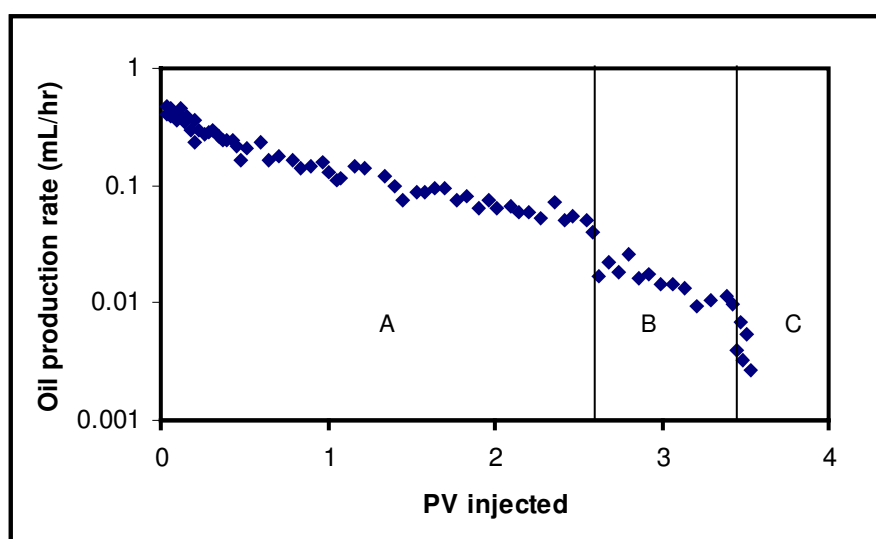
Figure 8.18: Oil production rates at different waterflood rates in core B

Again, it appears that as the waterflood rate was decreased, the oil rate decreased accordingly. However, by plotting the normalized oil rates instead of actual rates, insight is gained once more into the more efficient response at lower injection rates.

Figure 8.19 shows these normalized oil production rates as a function of the pore volumes of brine injected. Shut-in periods are shown by the red dashed lines in Figure 8.19. Comparing Figures 8.18 and 8.19 shows that, while oil rates are higher at faster water injection, normalized oil rates (i.e. fractional flow) is better at lower injection rates.
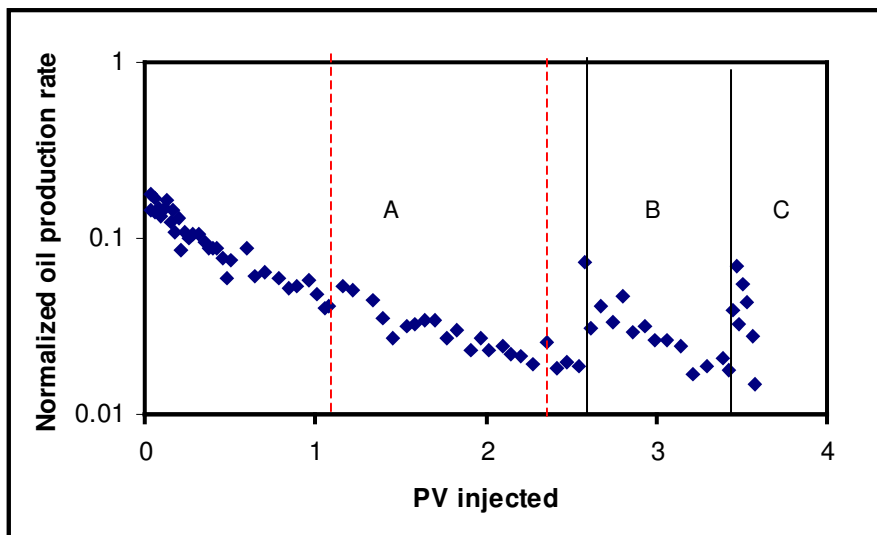
Figure 8.19: Normalized oil production rates for waterflooding of core B

For system B, pressures were once again monitored with a high range transducer during primary depletion, and a low range transducer for the secondary waterflood. The pressure profile for system B was similar to that of system A and D, in that pressure eventually declined to very low rates, and oil was recovered at pressures that were so low that they were at the limits of what could be measured even with the 0 – 172 kPa (0 – 25 psi) transducer.

In system B the sandpack was shut in during two periods to allow for fluids redistribution to occur after 1.06 PVs and 2.68 PVs of brine have been injected. After shut in, the

waterflood was re-initiated and, as had been seen previously in other systems, this corresponded to an improved oil production. It is important to determine the actual amount of oil recovered due to imbibition and fluids re-distribution during shutting in of the core. Figure 8.20 plots the actual water cut values along with expected water cuts, which are the water cuts that would be obtained by following the same trend as if the core had not been shut in. After both shut in periods, the water cuts eventually returned to their pre-shut in values. The enhancement due to fluids redistribution by water imbibition is the additional volume of oil that was recovered during the time before the water cuts returned to the same values as in the "expected water cut" trend line.
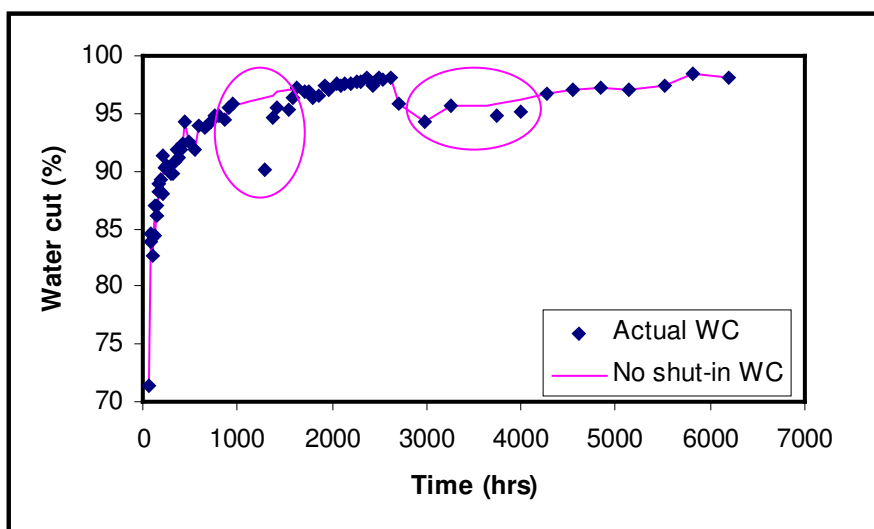
Figure 8.20: Effect of shutting in the core on water cut of system B

From Figure 8.20, values of the "expected water cut" line were interpolated based on the trend of the water cuts prior to shutting in the core. Using these interpolated values of water cut, the oil volumes that would have been produced if the core were not shut in can be calculated. In this manner, the true oil recovery profile can be compared against what the profile would have been if there was no improvement in the water cut. The improvement in recovery from the first shut in period is shown in Figure 8.21.
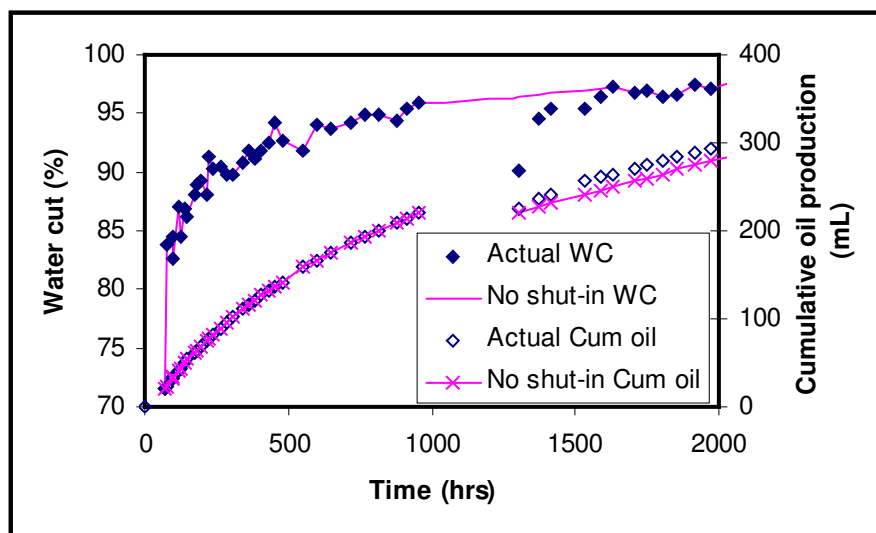
Figure 8.21: Improvement in oil recovery due to 1st shut in period of core B

From the first shut-in period of approximately 13 days, an extra 15.3 cm³ of oil was recovered (0.6 % OOIP). The improvement in recovery due to the second shut-in period was calculated using the same method. The second shut-in period was slightly longer (15 days), but this yielded an improvement of only an additional 5.1 cm³ of oil (0.2 % OOIP). It was seen that the incremental recovery due to shut in appears less significant in subsequent shut in cycles.

The difference in the two shut-in responses can be understood using the principles of water imbibition. During the first shut in cycle, water redistributed into the smallest pores, and displaced an equal volume of oil into larger pores that could be produced upon re-injection of water. In the second cycle, there were less small pores available for water to move into, so for similar capillary pressures there were fewer pore spaces that could be accessed by the water. If the core were shut in for infinitely long times, it is possible that water would completely re-distribute in a single shut in period, and subsequent shutting in of the core would no longer yield any improvement, unless in between shut-in cycles water was somehow allowed to access new sections of the core, as in flow through continuous films. This possibility will be discussed further in Chapter 9.

8.3 Effect of Injection Rate in Secondary Waterflood

In primary dead oil waterfloods, the relative influence of viscous forces on oil recovery was investigated by varying the water injection rates, oil viscosity and sand permeability. In the secondary waterflood systems, it was not possible to investigate this same range of different parameters, since the cores were larger and each waterflood was preceded by a primary production step. However, since injection rates were varied in all the sandpacks, the effect of changing the injection rate can still be analyzed.

In all the secondary waterflooded cores, it was observed that decreasing the injection rate lead to an improvement in the normalized oil rates and the waterflood efficiency. This was also discussed previously in Chapter 7: as viscous forces are reduced this allows more time for water imbibition, which corresponds to better waterflood responses. In the case of secondary waterflooding, however, the response of a core to a waterflood at any given rate will also be a function of other parameters, such as the volume and distribution of water at the start of the flood (i.e. the point of water breakthrough).

Cores A and B have relatively similar values of permeability: 3 D and 3.8 D respectively. From the primary dead oil waterfloods in Chapter 7, differences in the flood response were observed when comparing 2.8 D and 9 D systems, while the difference between 2.8 D and 0.8 D was less pronounced. In these systems, therefore, the influence of permeability on the waterflood results is expected to be small. The water saturation at the start of the secondary waterflood may also have an impact if it is considerably different between the cores. The connate water saturation for cores A and B were 0.089 and 0.086, respectively. System A recovered 20.4% OOIP through primary production, while system B recovered 27% OOIP. This additional volume was filled with free gas at the end of primary production, and some of this gas volume was initially replaced by water without any oil production occurring. Similar gas volumes were displaced during initial water injection, so at the point of water breakthrough in secondary waterflooding the water saturations for systems A and B (from Tables 5.10 and 8.1) were both around 0.188. Thus, there is no effect of varying water saturation in these cores.

Figure 8.22 shows the water cut response for the two secondary waterflood systems, and Figure 8.23 is the production profiles for these two cores. These figures show that the results from systems A and B cannot be easily compared against one another, despite the fact that oil viscosity, water saturation and sand permeability were similar in both cores. System B had a higher primary recovery, and the gas saturation in this core is also higher at the point of water breakthrough. Despite these apparently conditions, system B appears to respond better to secondary waterflooding. At steady state for each injection rate, the water cuts are lower and the recovery profile is better even though the water injection rate is higher in this core.
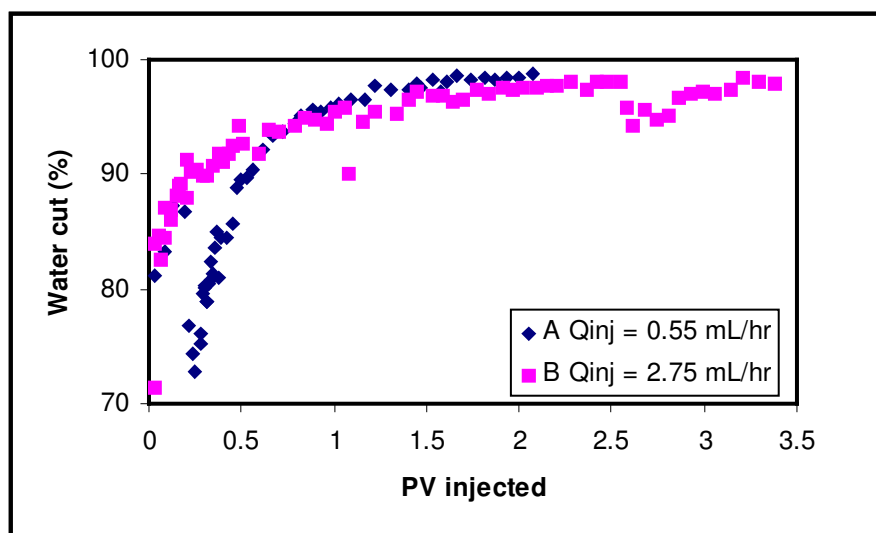
Figure 8.22: Water cut comparison for systems A and B

At early times (i.e. up to around 0.25 PVs) both systems maintained the same injection rate of 2.75 cm³/hr. During this period, the water cut response of the two cases is fairly similar. The injection rate was then reduced to 0.55 cm³/hr in system A, water cut in this system then dropped sharply by approximately 15%. As injection continued, the water cut then steadily increased again. After approximately 1 PV of brine had been injected, the water cut in system A (0.55 cm³/hr) actually became higher than that of system B (2.75 cm³/hr). From previous experiments with dead oil, it was consistently observed

that higher injection rates corresponded to larger water cuts, so the response seen in Figure 8.23 is different from the dead oil system. Individually, the sandpacks behaved consistently with the observations seen in dead oil waterfloods. However, when they were compared against one another, the trend for the water cuts is counter-intuitive. Just after 2.5 PVs of injection, the flow rates in system B were also reduced to 0.55 cm³/hr, and a corresponding decrease in the produced water cut was observed.
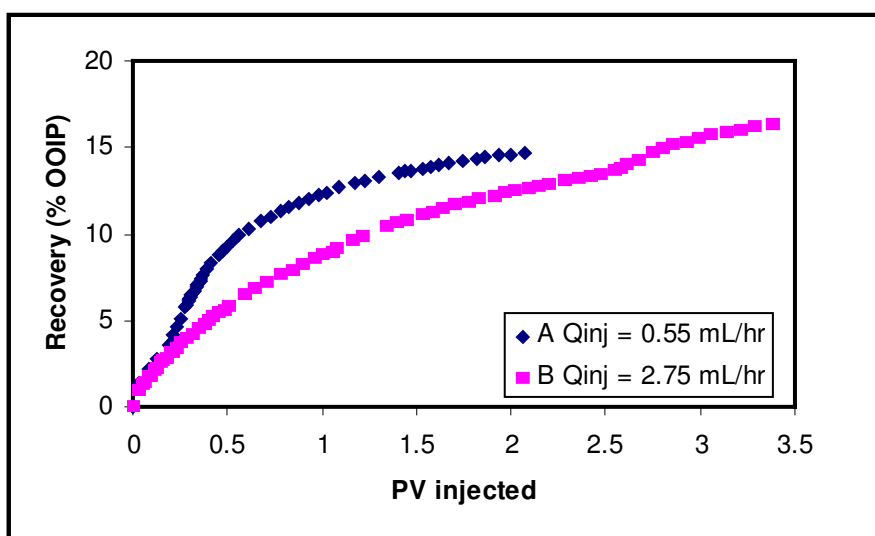
Figure 8.23: Oil recovery profile for cores A and B

Figure 8.23 compares the results of the recovery profile for the cores at different injection rates. At early times, when the injection rates are the same for both cores, the recovery profile was also identical for both systems. However, once the injection rate in system A was reduced, the slope of the recovery profile with the PVs injected became higher than that of system B. After approximately 1 PV, however, the slope of the low rate injection into system A is actually less than the slope of system B, despite the fact that system B was being flooded at a higher rate. After 2.5 PVs when the injection rate was decreased to 0.55 cm³/hr in system B, which is the same as the injection rate in system A, there was a corresponding improvement in the slope of the recovery profile in system B.

After the initial improvement in the oil recovery profile in system A at 0.55 cm³/hr, this system performs with a poorer efficiency, as is evident by the lower slope in the recovery profile compared to the higher rate injection in system B. The difference between the systems that causes the better response in system B is not known. This is the first instance where the lower injection rate did not yield a greater recovery profile.

Even though the flood in system A later became less efficient, its improved response at early time when the injection rate was first reduced leads to a significant increase in oil recovery. It took over 1 PV of extra fluid injection in system B to match the recovery in system A. This is significant in that much less water injection was required to reach the same additional oil recovery of 15% OOIP. It should be noted, however, that Figure 8.23 is plotted as a function of PVs injected. When the recovery information is plotted on a time-scale basis, as shown in Figure 8.24, the results are distinctly different.

Initially, when system B was at a higher rate of 2.75 cm³/hr compared to A, the recovery was higher but the slope appeared to be lower, indicating the eventually the recovery in system A would be higher. However, after system B was shut-in for a period of time, followed by further injection at the same rate, the slope of oil recovery profile improved, implying that after shut-in the waterflood became more efficient. It is due to this fluid re-distribution that the waterflood at 2.75 cm³/hr into system B was so successful. When the recovery profile appeared to plateau, the injection rate was reduced. This is the circled region in Figure 8.24. At this point both systems were being waterflooded at the same rate, and the slope of both recovery profiles was the same.
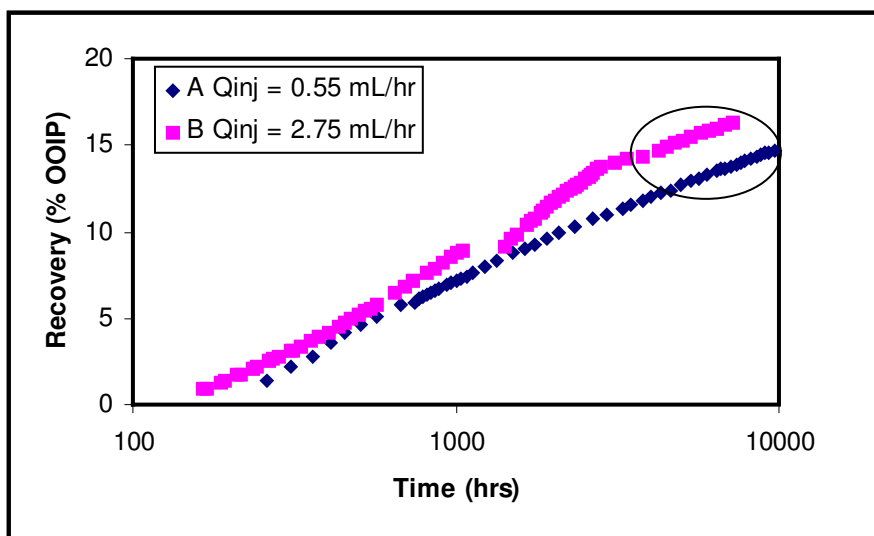
Figure 8.24: Recovery as a function of time of systems A and B

Although both systems did not behave in a consistent manner at early times, eventually when both were waterflooded at the same slow rate, the recovery efficiency is essentially the same.

The efficiency of the two floods is compared in Figure 8.25. Efficiency was calculated using Eqn (8.1), as discussed previously.
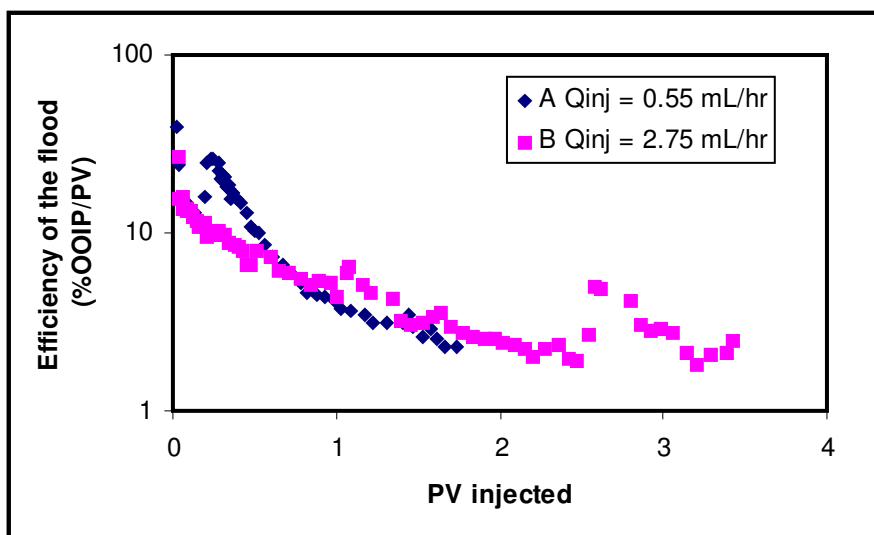
Figure 8.25: Waterflood efficiency for different rates in systems A and B

As expected, at early times in the waterflood the efficiency is high, but it quickly drops in both cores. By reducing the waterflood rate in system A, the efficiency is improved by a factor of two. Eventually, however, the efficiency falls below that of system B. After 2.5 PVs, when the waterflood rate is decreased in system B, the efficiency increases by over a factor of two as well, before once again falling. The system was shut-in after 1 PV of brine was injected, and the efficiency correspondingly increased slightly after injection was resumed. Figure 8.26 plots the normalized oil and water rates for both systems. As expected from the recovery profiles and efficiency calculations, the normalized rates in system A are initially improved considerably by dropping the water injection rate from 2.75 cm³/hr down to 0.55 cm³/hr. Eventually, however, the normalized oil production rates are lower than that of system B, and this is reflected in the improved recovery response in that core.
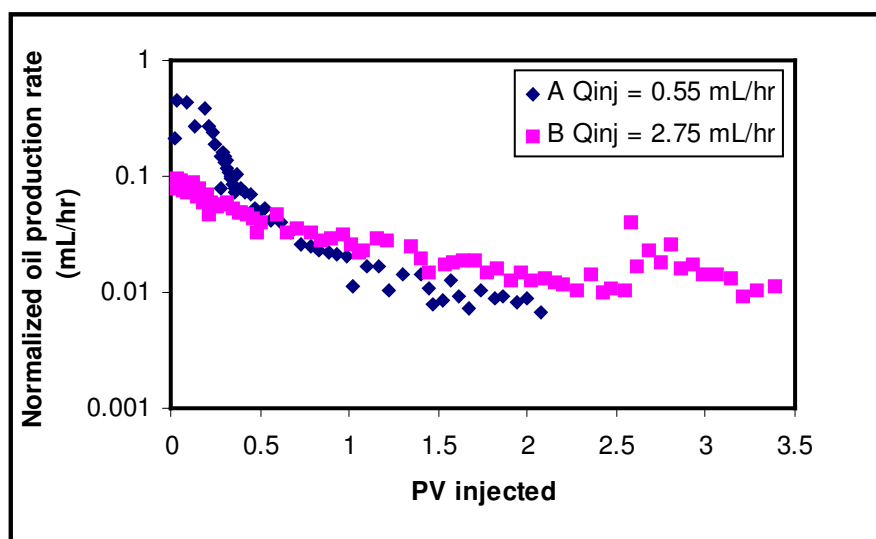
Figure 8.26: Normalized oil production rates for systems A and B

It should be emphasized that in both cores the waterflood was performed at low rates compared to normal field rates, which range from 0.18 m/d to 2.9 m/d (Rojas and Farouq Ali, 1988). At higher rate injection into cores D and E, oil recovery was extremely poor. Therefore, low rate water injection appears to be vital for secondary waterflooding in

heavy oils. It should also be noted that for both systems, the normalized oil production rates are similar to those of the dead oil systems in Chapter 7.

8.4 Comparing Primary and Secondary Waterflood

The value of performing both primary and secondary heavy oil waterfloods is that these experiments can ideally be compared against one another, in order to determine how representative dead oil waterfloods are for studying actual reservoir applications after cold production. In order to make this comparison, a third full diameter core was packed, and its properties are summarized in Table 5.8. This core, labeled "core C", has a permeability of 3.86 D and is similar to systems A and B. Core C was saturated with dead HO2 and connate water. Waterflooding was initially performed at a fixed rate of 2.75 cm³/hr (velocity of 0.0106 m/day), in order to compare the results against systems A and B. During this time, pressure initially built up in the core until water broke through, after which the injection pressure quickly declined, as also observed in the dead oil waterfloods in Chapter 7. After 1.6 PVs of brine had been injected, the injection rate was reduced to 0.55 cm³/hr (0.0021 m/day). Oil production rates were normalized to the injection rates, and are plotted in Figure 8.27.
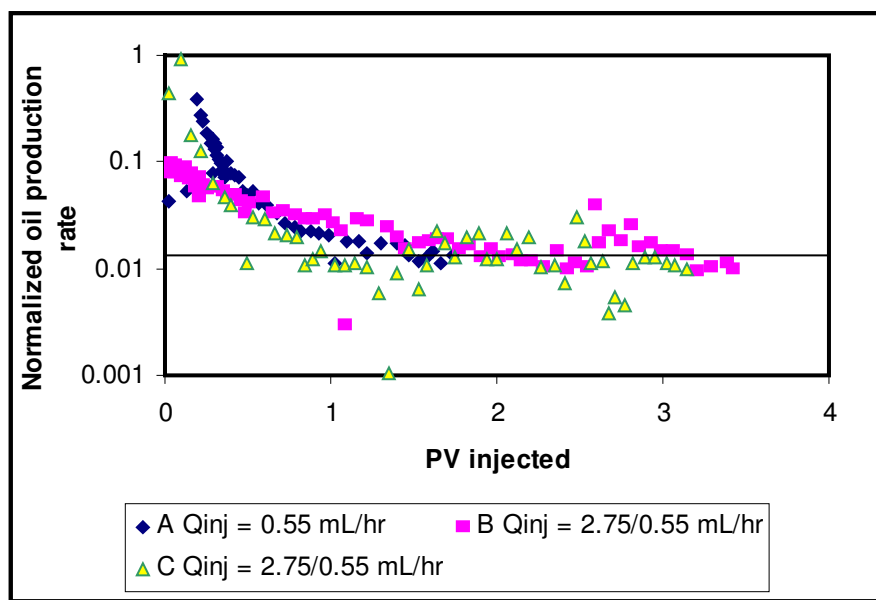
Figure 8.27: Normalized oil production rates for all large cores

At early times, before water breakthrough occurred and pressure in the core decreased, the normalized oil rates in system C were correspondingly very high. In order to match these normalized rates, system A was flooded at 20% of the same frontal velocity. After breakthrough, the majority of injected water would bypass the oil through the continuous water channels, and the normalized oil production rates dropped accordingly. After the waterflood rate was reduced at 1.6 PVs, the normalized oil rates increased again. Finally, at 2.5 PVs of injection the core was shut in for a period of eight days, after which injection began again at the same rate. The effect of the shut in period is shown by the increase in the normalized oil rates at this point. However, the rates quickly return back to their pre-shut in values.

In all three systems, it was observed that the final normalized oil production rate levels out at just over 0.01. This is an indication that at 0.55 cm³/hr injection rate the systems are operating at steady state for both primary and secondary waterfloods. The flood efficiencies were also calculated using Eqn (8.1), and efficiency is plotted against PVs injected in Figure 8.28.
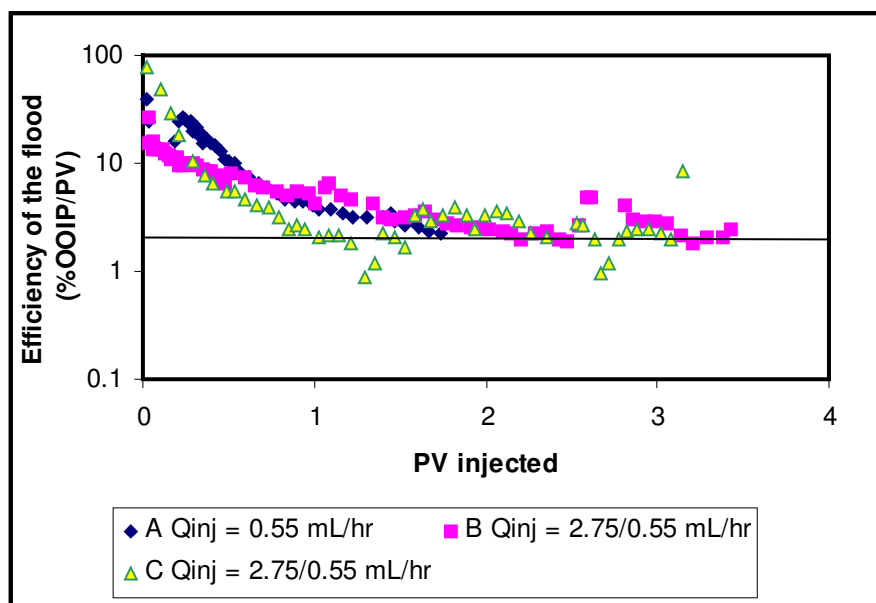
Figure 8.28: Primary vs. secondary waterflood efficiency in large cores

In systems B and C, waterfloods were initially performed at a higher injection rate, until the flood efficiency values dropped to close to 1% OOIP/PV injected. The flood rates were then decreased by a factor of five, leading to improvements in the flood efficiencies. Eventually, however, the values once again decreased down to an efficiency of around 2% OOIP/PV injected, at which point the floods appeared to be performing at steady state.

Figure 8.29 compares the results from Figure 8.27 to the normalized oil production rate from a small (3.81 cm diameter) core in Chapter 7. This small core has a permeability of 2.8 D (Table 5.5), and waterfloods were performed at higher rates than in any of the large core systems (Experiment # 12). The early time data (high pressure gradients) have been excluded from the dead oil core floods, in order to compare these systems. Initially, the highest normalized oil production rates are in system A, after reducing the waterflood rate to 0.55 cm³/hr. Eventually, however, the rates are highest in the small core system.
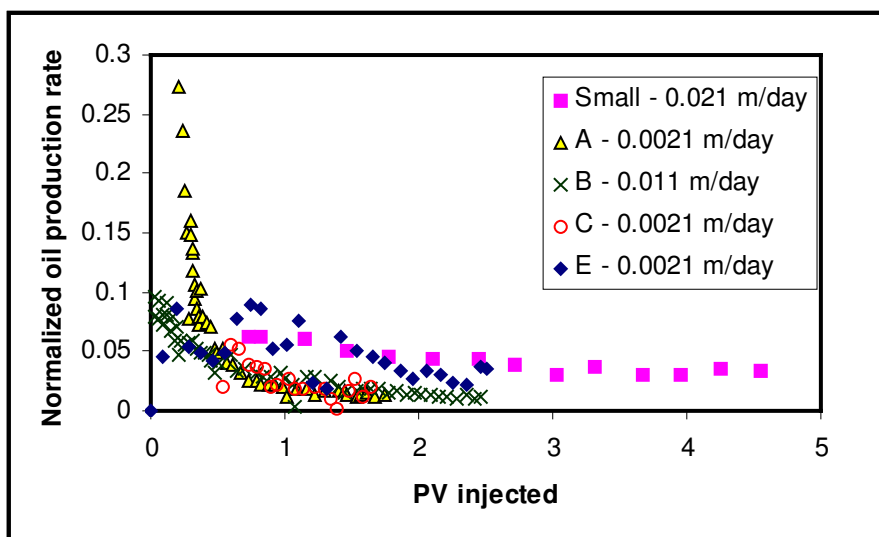
Figure 8.29: Normalized oil production rates in large and small cores

The fact that the normalized oil production rates are higher in the small core system, even though it was being flooded at the highest injection rate, indicates that waterfloods are

somehow more stable in small linear systems. This is not the effect of primary versus secondary recovery, since in Figures 8.27 and 8.28 the rates and efficiencies were similar in both types of waterfloods for similar scale of sandpacks. However, the difference between the small core and the larger systems cannot be simply attributed either to the scale of the system. Figure 8.29 includes the normalized oil production rates for core E, which is also a small core. Although the normalized oil rates for this core are also higher than in the large systems, the injection rate is an entire order of magnitude lower than in the primary dead oil waterflood in the small core.

Instability theory predicts that in larger diameter systems more fingers can form, leading to a higher degree of instability (Peters and Flock, 1981). However, this again deals only with recovery at breakthrough, which has no meaning in secondary waterflooding systems. The case of secondary waterflooding is not that of a water-front displacing the oil, but rather water in channels that may move into bypassed oil zones through capillary imbibition. At this time, it is not clear why the rates are higher in the small core dead oil system. It is possible that the dimensions of the sandpack could influence the behavior of imbibition, and this will be discussed in Chapter 10.

8.5 Discussion

The main finding from the experiments performed in cores after waterflooding is that, qualitatively, the systems respond similarly to primary dead oil waterfloods. In all the cores tested, both large and small, it was observed that a reduction in the water injection rate led to enhancements in the normalized oil production rates and in the calculated efficiency of the waterfloods. Eventually, the rates and efficiency values would decline once again and then level out, indicating that the cores were producing at a pseudo steady-state condition.

An additional observation made was that when the cores were shut in for extended periods of time, the normalized oil rates and water cuts were improved upon re-injection of water at the same rates. The effect of reducing water injection and the response of the

cores to being shut in are both indications of the significance of capillary forces in heavy oil waterfloods. These forces were deemed important in dead oil systems after the first 1 – 2 PVs of fluid injection, once pressures were low and water had broken through to the production end of the cores. During early times in primary dead oil waterflooding, constant rate injection led to the development of high pressure gradients in the core, and oil recovery was correspondingly high during these times. In secondary waterflood systems, water channels through the gas-saturated zones and breaks through with traces of oil production and very little pressure build up, so the influence of high pressure gradients is not present. In these cores, all the recovery is similar to the response of dead oil systems at late times, where capillary forces and water imbibition are used to produce oil.

A main difference between primary and secondary dead oil systems is the rate of the waterfloods. It seems that in secondary waterflooding systems, in order to get steady production of oil at high water cuts, the injection rates have to be reduced by a factor of 2 – 10, compared to the rates in dead oil systems. In secondary waterflood systems, there are many more channels for injected water to travel through, and possible interference of trapped gas ganglia, thus flow rates need to be reduced further in order to allow water imbibition to be significant.

The comparison between absolute and normalized oil production rates (Figures 8.14 and 8.15) is important for understanding how secondary waterfloods are expected to operate. At higher injection rates, the oil production rate is accordingly higher as well, since the total production of oil and water will be equivalent to the fixed water injection rate. At low injection rates, although oil production rates are correspondingly lower as well, they do not decrease by the same factor as the water injection. The waterfloods are also more efficient (i.e. the normalized oil production rates are higher) at low injection rates. More efficient waterfloods will eventually lead to higher oil recovery factors, as also shown in the dead oil systems. The time requirement to recover the oil will be longer, however,

since the time for each pore volume of fluid injection is proportional to the water injection rate.

Normalized rates for HO2 in small linear systems from Chapter 7 were on the order of 0.02 – 0.03. Similar normalized oil rates could be achieved in the small core E containing glassbeads at higher permeability for secondary waterflooding, but the injection rates had to be reduced by a factor of 10. In the larger cores, containing the same oil and sands of slightly higher permeability, normalized rates for systems A, B and C were around 0.01 – 0.02, also at lower water injection rates. There is no significant difference between dead and live oil responses to waterflooding in the large cores. While the normalized oil rates are lower than the values for the small core dead oil systems, these rates are still within the same order of magnitude. Considering the many uncertainties in comparing the different systems against one another, it is not possible to determine why the small core dead oil waterfloods are slightly more efficient than secondary waterflood systems. However, the results of these experiments show that, with proper control, it is possible to recover viscous heavy oil by waterflooding even in systems where significant oil was already recovered by primary production.

CHAPTER 9: EVIDENCE OF IMBIBITION

In the discussion of primary and secondary heavy oil waterflooding, imbibition was mentioned as an important mechanism of oil recovery after water has broken through. In order for imbibition to occur the sand has to be preferentially water wet. However, due to the unconsolidated nature of the sand studied, it is not possible to measure wettability directly, thus wettability could only be inferred from various experiments.   In this analysis, further evidence for water wetting and imbibition was extracted from micro-CT analysis of fluid distributions of oil and water in sand, and fluid redistribution during shut-in. Imbibition was also studied in closed systems, during which oil was expulsed and formed a layer on top of the sand mixture. These analyses have proven that imbibition indeed occurred during static conditions. Finally, it was necessary to prove that imbibition does occur under flowing conditions as well.   This was done by evaluating the results of fast and slow injection in sand packs assembled and run within an NMR.

9.1 Fluid Distribution by Micro-CT Scanning

Rock wettability is an extremely important parameter to consider, when attempting to properly understand reservoir recovery mechanisms. The wettability of the rock governs which fluid will preferentially contact the rock surfaces, which in turn is used to identify the location where the injected water invaded, and the nature of trapped water or oil. Specifically, a waterflood in a water-wet system is an imbibition process, while a waterflood in an oil-wet system is drainage. Due to the high oil viscosity capillary forces are generally thought to be negligible in heavy oil systems, which would lead to the common and perhaps incorrect conclusion that the rock wettability does not matter in terms of the waterflood recovery. In this chapter, that conclusion is shown to be untrue, and the fact that the rock is water-wet becomes extremely important to the oil recovery mechanism.

Since clean quartz is hydrophilic in nature, it is commonly assumed that this also means that sand will be water wet. However, this is not necessarily true (Czarnecki *et al.*, 2005), thus it is important to actually identify the wettability of the system. Contact angle measurements are the most straight-forward way to determine rock wettability in smooth rock systems. Unfortunately, in oil sands these measurements are not simple to perform. Even if they could be obtained, factors such as rock curvature and surface irregularities make it difficult to obtain actual quantifiable values. In this work, the approach used to infer water-wetting of sand grains was through micro-CT imaging of an oil sand sample. This sand was initially saturated with water and then flooded with oil to achieve irreducible water saturation.

The micro-CT scanner used in this study is a Skyscan 1072 x-ray microtomograph. Scans were acquired at a setting of 100 kV and 98 μA, with a power setting of 10 W. The resolution of the images is 2.73 μm/pixel, meaning that any physical features smaller than approximately 3 μm will not be visible in the scanner. However, this resolution is considerably finer than ordinary CT scanners, which have a resolution of approximately 500 μm. 3D imaging of the measured scans was performed using Skyscan's "Ant" 3D creator software.

Figure 9.1 shows an example of a cross-sectional slice of an oil sand sample. This was actually the sand that was recovered from one of the dead oil systems in Chapter 7. The sand had been initially saturated with water and the oil flood was performed at a constant rate until S_{wi} was reached. A low rate waterflood was then performed, and at the end of the waterflood a sample of the core was imaged in the micro-CT scanner. In this image, the colour has been set such that sand is yellow, oil is a darker brown and water is blue. The image in Figure 9.1 represents a single cross-sectional view of the oil sand.
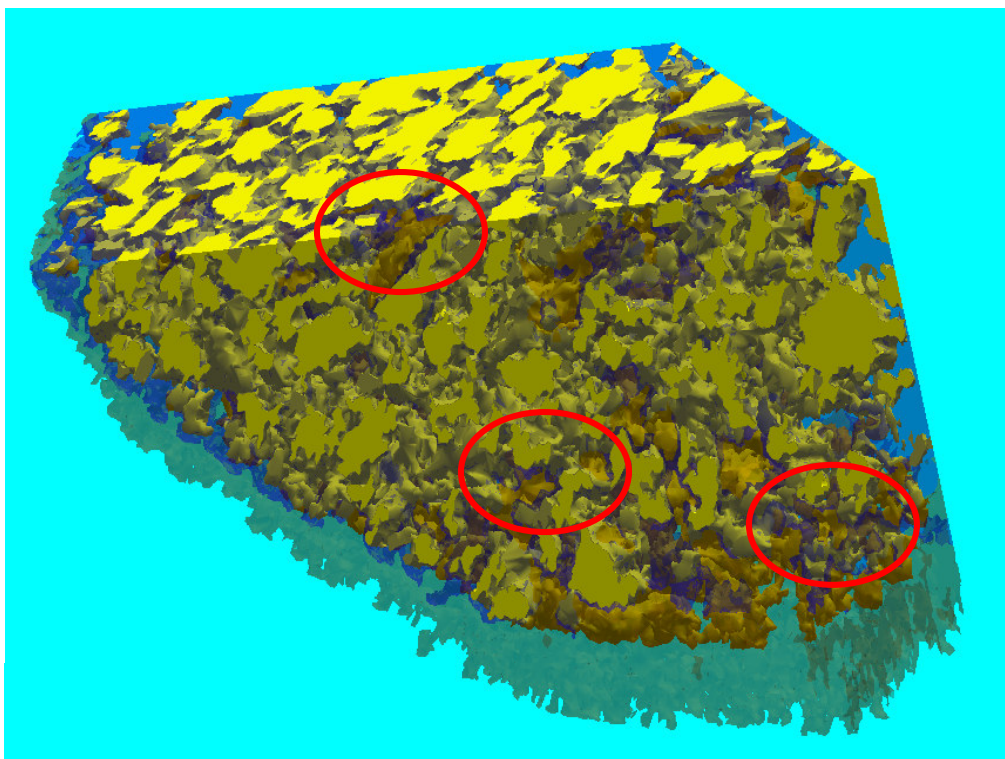
Figure 9.1: Micro-CT image of a cross-sectional slice of an oil sand containing sand, heavy oil and water

The three red-circled regions in Figure 9.1 serve to illustrate the water-wet nature of this sand. In these regions it appears that the sand is coated with a layer of water, while oil exists in the center of the pores. Since the pixel resolution in this image is 6.8 μm, it is evident that if the water films can be measured in the CT scanner, they are relatively thick. In addition, where oil-water interfaces meet sand grains, water appears to have a low contact angle. Additional images of different cross-sections of this same oil sand sample are presented in Appendix F. All of these images show the same properties regarding the location of oil and water.

At the present time, it is still not clear how much of the image properties are due to the actual physics of the sample being measured, and how much is due to the numerical smoothing algorithms applied to generate these 3D images. Micro-CT analysis has therefore only been used qualitatively in this work as further evidence to show that the

water-wet assumption for this sand is generally valid. Quantitative evidence of water wetting, and more importantly, water imbibition in heavy oil waterfloods, will be presented in the following sections.

9.2 Evidence of Imbibition in Closed Systems

Due to the difficulty in obtaining reliable contact angle measurements in unconsolidated sand systems, the presence of spontaneous imbibition of water can also be used to infer if a rock is water wet. Unfortunately, this approach also has its share of uncertainties. Imbibition experiments, which can readily be performed in consolidated cores containing gas or conventional oil, are not trivial to perform in unconsolidated oil sands, where water must imbibe and displace highly viscous heavy oil. Takamura and Isaacs (1989) therefore recommend a simple procedure for inferring if sand is water wet and if water imbibition will happen: a core saturated with oil is placed in an aqueous medium at elevated temperatures, and if a layer of oil forms on top of the water, then imbibition is known to have occurred.

In this work, evidence of imbibition was observed in multiple closed systems. In one experiment oil-coated sand was placed in contact with water in closed vials to observe the formation of an oil layer on top of the sand mixture. This is similar to the recommended method; however experiments were performed at ambient temperature in order to avoid changes in interfacial tension with temperature (Takamura and Isaacs, 1989). NMR spectra were also obtained in order to identify the movement of water in the system. In a second set of tests, waterflooded cores were shut in to allow for fluid redistribution and afterward flow was resumed with an improvement on the oil production rate. In these tests, imbibition is inferred from the production response of the cores before and after shut-in.

9.2.1 Imbibition in Vials

In the first suite of experiments, LM 70 sand was mixed with HO2 heavy oil (viscosity 11,500 mPa·s) and placed into 20 cm³ glass vials. Different amounts of water

were then placed on top of the oil sand mixture, and slowly soaked into the sand. As this happened, heavy oil was displaced out of the sand and formed a layer on top of the water. Aside from visual observations of water displacing oil out of the porous media, NMR spectra of the vials over time were also obtained. The purpose of these measurements was to determine the initial fluids distribution and to establish how the fluids were entering the porous medium. Since NMR is capable of detecting the protons of the fluids existing in the porous medium, it was used to identify both the presence of oil and water and where they exist.

The distribution of fluids is controlled by the wettability of the sand. In general, if the sand is water wet, injected water will preferentially enter the small pores while oil occupies the center of the large pores, and the reverse is true if the sand is preferentially oil wet. Thus, changes in the water and oil location with time should establish the wettability of the sand. It should be emphasized that in this Chapter, wettability is defined as the tendency of the sand to be coated with water in preference to oil. Thus, although the sand was initially not in contact with water, if the sand is water wet then once water comes into contact with sand it will displace oil away from the sand grains thus preferentially follow the imbibition pathways in the pores.

In a closed system the only possible mechanisms responsible for fluids redistribution are gravity and capillarity. The significance of these forces is expressed in the Bond number, which is the ratio of gravitational to capillary forces (Hirasaki and Zhang, 2004). The Bond number (N_B) is defined as:

$$N_B = \frac{\Delta\rho g R^2}{\sigma}$$
Eqn (9.1)

Where $\Delta\rho$ = the density difference between oil and brine

$\quad$ g = the gravity constant

$\quad$ R = the representative radius of the sand.

The densities of oil and brine are 0.9815 and 1.0487 g/cm^3 respectively. The value of interfacial tension between heavy oil and brine was measured to be 14 mN/m. The value of R for this sand must be determined from the properties of the sand. In order to find this value, it was assumed that the porous medium can be approximated by a bundle of capillaries of radius R.

The flow in a capillary tube is described by Hagen-Poiseuille's equation:

$$\nu_{HP} = \frac{R^2 \Delta P}{8 \mu L}$$

Eqn (9.2)

From Darcy's Law:

$$\nu = \frac{k \Delta P}{\mu L}$$

Eqn (9.3)

Eqns (9.2) and (9.3) cannot be directly compared because the Darcy velocity is the velocity of the water front and not the actual velocity of fluid in the pores. Therefore, the Dupuit-Forcheimer assumption (McCauliffe, 1973) was used to convert Darcy velocity to actual (interstitial) velocity:

$$\nu_{pore} = \frac{\nu}{\phi} = \frac{k \Delta P}{\phi \mu L}$$

Eqn (9.4)

Since $\nu_{HP} = \nu_{pore}$, equating eqn (9.2) and eqn (9.4) yields:

$$R = \sqrt{\frac{8k}{\phi}}$$

Eqn (9.5)

Herrick (2004) stated that since rock pores are actually not straight tubes, tortuosity should also be taken into account through multiplying by a factor of 1.5, thus:

$$R = \sqrt{\frac{1.5 \times 8k}{\phi}}$$
<div align="right">Eqn (9.6)</div>

For this particular sand the permeability and porosity have been measured many times. However, these values were usually obtained when the sand is under overburden confining pressure. The worse case scenario is for the experiments in the NMR where the sand was packed into a coreholder with no overburden pressure or stress applied. For these cases the permeability is approximately 15 D and the porosity is about 0.46. In these vials the sand is also loosely packed, thus the properties (permeability and porosity) could be expected to be similar to the values without overburden. With these parameters, the representative radius is then found to be 2.0×10^{-5} m. The Bond number for this experiment was found to be 1.9×10^{-5}, which is much smaller than one where gravity forces are significant. This indicates that the gravitational forces are negligible with respect to the magnitude of the capillary forces. It must be noted that this value is for the worse possible case; in other experiments where overburden was applied the permeability and porosity values would be even smaller, thus the representative radius would be significantly reduced as well. Therefore for systems with smaller pores the Bond number could be expected to be lower and the effectiveness of capillary forces should be proportionally higher.

Prior to conducting the experiment, it is important to establish the characteristic of the oil and water signals, as bulk phases and as they exist in the porous medium. Thus NMR spectra were obtained for various systems and are shown in Figure 9.2. Bulk water relaxes slowly as a narrow peak (~ 2,000 ms) while bulk oil relaxes quickly in a broader peak (< 10 ms) due to its high viscosity (Klinberg and Vinegar, 1996; Straley *et al.*, 1997). The sand was also saturated with brine and its spectrum was obtained. In this state, surface relaxation dominates and the T_2 distribution is analogous to the pore size distribution (Straley *et al.*, 1997; Coates *et al.*, 1999).
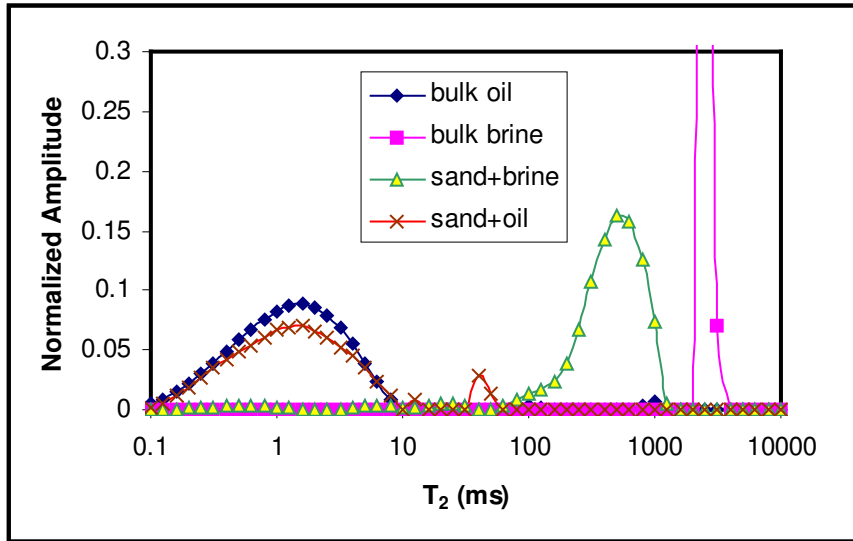
Figure 9.2: NMR spectra of bulk phases and porous medium saturated with fluids

The spectrum of sand and brine shows that a significant fraction of the sand contains large pores. The spectrum for the brine in the porous medium shows only a small signal at $T_2 < 10$ ms; these signals originate from brine occupying very small pores. For normal NMR values of sand surface relaxivity, the signal < 10 ms corresponds to pores with radii less than 1 μm. Calculations showing how T_2 values can be related to pores sizes are presented in Appendix G. Upon comparing the bulk oil and oil in sand, it can be seen that the oil relaxes at relatively the same rate due to its high viscosity, thus for the oil the NMR bulk relaxation term completely dominates over the surface relaxation.

It is also important to note that the oil signal ends before 10 ms, which becomes an important criterion for separating oil and water signals. However, when both oil and water exist in the same porous medium, the signal occurring before 10 ms does not fully originate from oil alone. A portion of it also comes from brine located in either very small pores and/or thin films. Thus, the spectra of the fluids existing in the porous medium illustrate the difficulties in distinguishing the oil and water signal at early time when small pores (fast relaxing water, under 10 ms) are present in the porous medium. This will cause complications in quantifying the amount of oil and water in the porous

medium. However, for this particular experiment it is not a matter of concern since the water signal originally in this range of T_2 values is negligible.

From prior knowledge of the porosity and initial water saturation of this sand, an appropriate amount of oil was mixed with sand. Brine was not initially mixed with the oil and sand for several reasons. First of all, the mixing process requires some time, during which brine would evaporate. Also, it was desired to capture the imbibition process at the moment brine was added and this would not be possible if brine had been added first then mixed with oil. Thus, it was decided that oil and sand would be mixed first and brine would only be added later.

Oil and sand were thoroughly mixed for approximately 15 minutes to ensure that the sample is homogeneous. The oil/sand mixture was then divided into four relatively equal portions and packed into four vials. Then sand was compacted manually, because in these vials the solids could not be confined by overburden pressure. As soon as brine was introduced to the vials, an NMR measurement was taken and these initial measurements are shown in Figure 9.3.
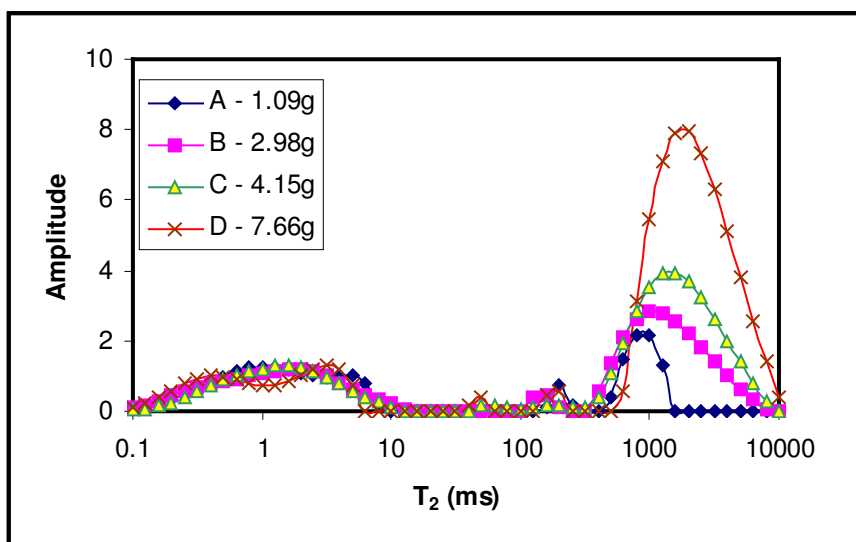
Figure 9.3: NMR spectra of static vials with water added on top of the sand

Each vial, labeled A to D, was given a different amount of brine and the masses listed in Figure 9.3 are the amounts of brine added. NMR measurements were then periodically obtained. The newly added brine initially exists as a bulk phase on top of the oil and sand mixture, and manifests itself in Figure 9.3 as a peak at high T_2 values (on the order of 1,000 - 2,000 ms); the samples with larger amount of brine have larger peaks. This slow relaxing peak is bulk brine that does not have any surface relaxation effects. According to imbibition theory, if the sand is water wet, it is expected to move first into the small pores. However, from this figure it could not be determined whether the brine had invaded the small pores or not. Fortunately, the NMR spectra of two vials (A and C) had also been obtained prior to brine addition. The spectra of these two vials with and without brine are shown in Figure 9.4, which shows that brine addition also increased the amplitude in first peak, thus indicating that brine did immediately occupy some small pores after brine addition. The amplitude increment in the first peak for A and C is 2.684 and 3.577 respectively, which corresponds to 0.17 g and 0.22 g of brine that immediately migrates into small pores. The discrepancy between these samples is not significant considering the fact that sample C is larger in size, and so should have a larger number of small pores.
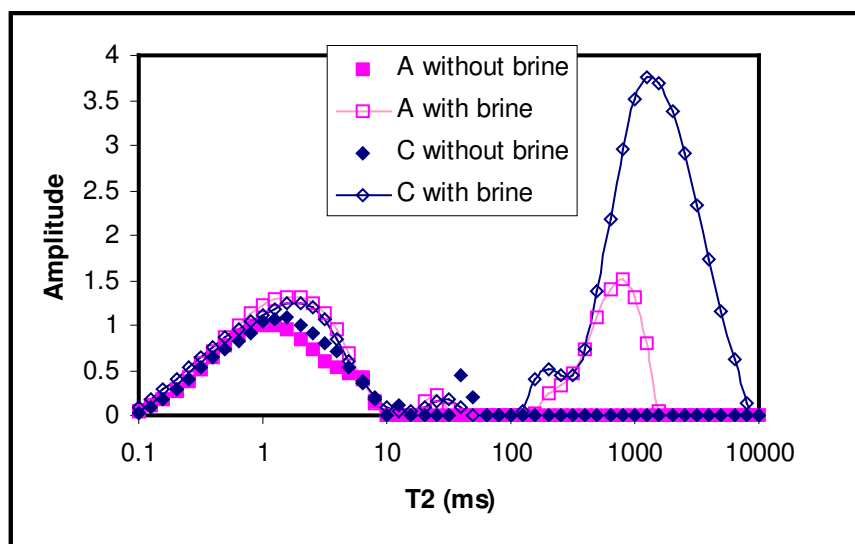
Figure 9.4: NMR spectra of vials A and C prior to and after brine addition

From these spectra, the water signal at time = 0 was de-convoluted by subtracting the amplitudes of the sample without brine from the signal with brine. The resulting distribution of brine is shown in Figure 9.5.
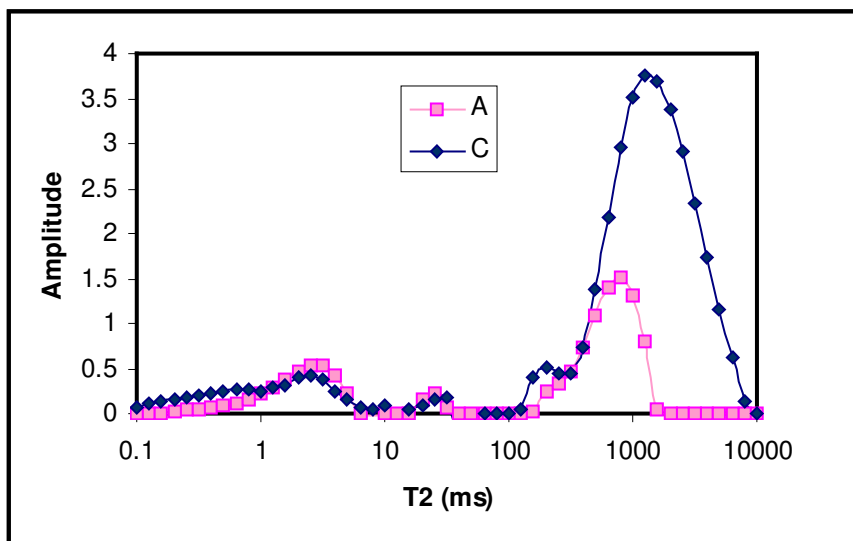
Figure 9.5: Distribution of water signal in vials immediately after brine addition

For both samples, despite the fact that the amount of brine added was different, it seems the brine invaded the porous medium in the same pattern. This figure shows a significant amount of brine relaxing at low T_2 values soon after brine was placed into contact with the oil-coated sand. This signal must come from brine that is present in small pores (radius < 1 µm) or brine that has formed thin films between the sand and oil. The spectrum of sand saturated with brine (in Figure 9.2) does not show a significant fraction of brine relaxing so quickly in the small pores, thus the water signal in Figure 9.5 demonstrates that the brine is present in the form of films that now coat the sand grains.

In relation to the total water signal, it is apparent that the water volume in films can be quite significant. In Figure 9.2, the signal occurring at $T_2 < 10$ ms comes from brine in small pores only. There was no brine relaxing as films since the core was fully saturated with water (only one fluid existing in the porous medium). However, in the case of water moving into oil sand, the oil-coated sand might have inadvertently created smaller

pores spaces between the sand grains. Water might not be able to immediately remove the oil layer coating the sand grain, thus it might exist in these newly formed crevices instead. Alternatively, water could have spread between the oil and the sand, which would be an indication that the sand is strongly water wet. The NMR spectra do not identify which of these situations had occurred, but the fluid distributions measured in the spectra show that the porous medium is preferentially water wet.

Further evidence of imbibition can be seen from the NMR spectra as they track the movement of brine with time. Figure 9.6 shows the shift in the NMR spectra of vial C (4.15 g of brine added) with time. Over time, the signal of the bulk brine shifts to smaller T_2 (under 1,000 ms), indicating that the bulk brine is finding ways to invade into the porous medium.
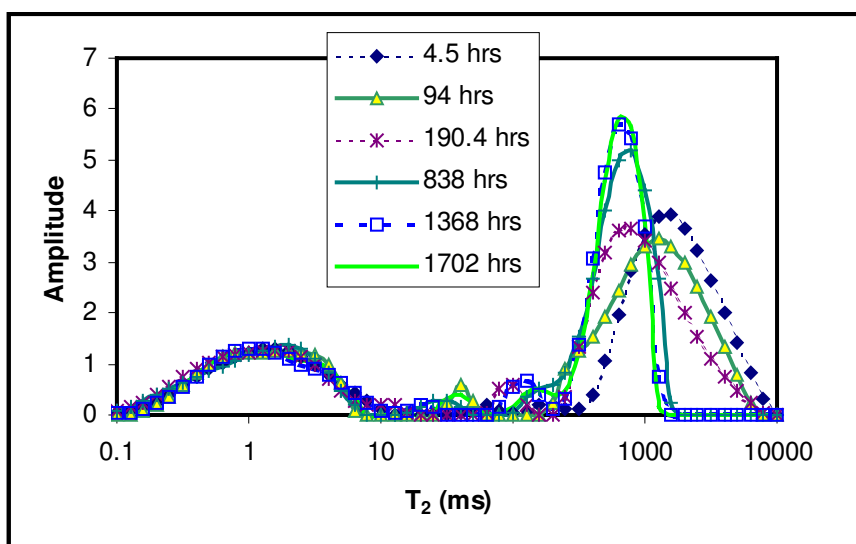
Figure 9.6: NMR spectra of water re-distributing in vial C with time

It must be noted that the issue of brine evaporation was also taken into consideration the interpretation of these results. At any instance when an NMR measurement was taken, the weight of the sample was also obtained. Out of the four vials evaluated only one vial (A) suffered from evaporation, whereas the three other remaining samples had only slight evaporation (approximately 0.5 g of brine lost over the course of three months). Initially

a concern was that evaporation could lead to loss of bulk water and this alteration in the NMR spectra could be wrongly attributed to the effect of imbibition. If this were to happen, only the bulk brine would be subjected to evaporation. If evaporation did occur one would expect the water signal at high T_2 (> 2,000 ms) to slowly diminish in amplitude, while not changing its value of T_2. However, the spectra in Figure 6 are consistently shifting to smaller T_2, thus it could be concluded that the shifts in the spectra are not due to evaporation, but are in fact a reflection of brine slowly invading into smaller pores.

Previous experience with soils coated with organic acids (Manalo *et al*., 2003) or sands contaminated with heavy oil (Hum and Kantzas, 2006) have shown that the trend of water gradually moving into smaller pores is indicative of a porous medium that is initially oil wet and is gradually reverting back to water wet conditions. In this situation, it appears that the sand was always hydrophilic, as evidenced by the water movement into films at early times in Figure 9.5. The gradual movement of water into smaller pores is more likely indicative of the fact that in this system, imbibing water must displace heavy oil out of the pores, and this occurs slowly due to the high oil viscosity. However, even if the wettability reversal hypothesis proposed is accepted (Manalo *et al*., 2003; Hum and Kantzas, 2006), this still indicates that eventually the sand behaves as a water wet porous medium and imbibition of water is occurring.

This shift in the spectra can be described by plotting the geometric mean of the signal after the first peak (at T_2 > 10 ms), as shown in Figure 9.7. In a closed system, if water moves into the smaller pores, then oil that was originally located in these spaces must be transferred either into larger pores or be expelled out of the porous medium. This redistribution of fluids is a direct indication that imbibition is occurring in this water wet sand.
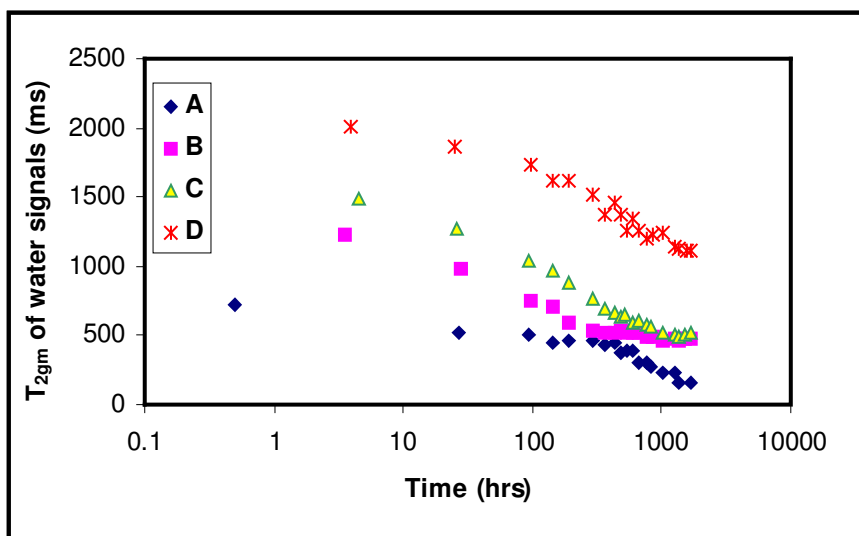
Figure 9.7: Shift in the water signals with time for static vials

The evidence of brine invading smaller pores could be further illustrated by plotting the amplitudes of the second and third peak (10 – 200 ms) as a function of time. These are the surface water peaks (the signal in pores that are filled with water), as shown previously in Figure 9.2. If the pore water signal is increasing, this indicates that more water is relaxing in rock pores. The pore water amplitude signal is plotted in Figure 9.8.
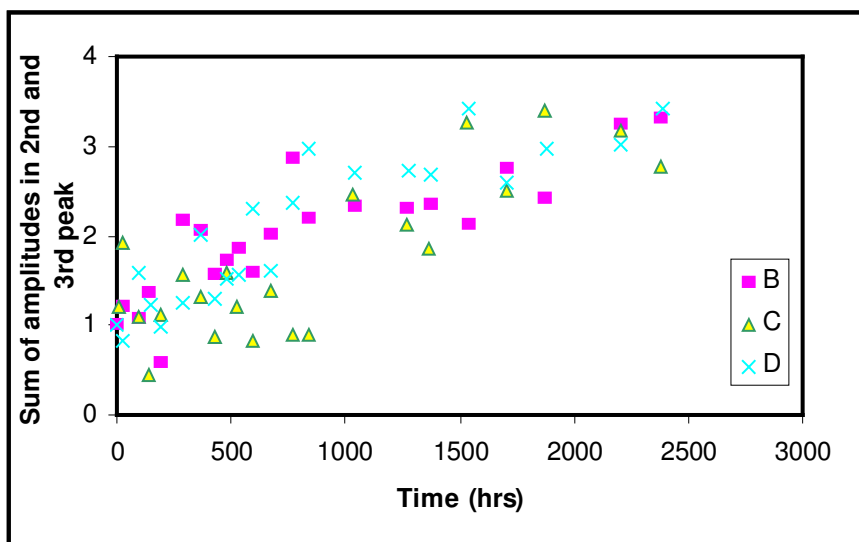
Figure 9.8: Growth of water signal in pores as a function of time

This figure shows the response of only three samples because the data from sample A was excluded due to severe evaporation. As mentioned earlier, the signal beyond 10 ms must come from water and water is tighter pores relaxes faster than water existing in larger pores. Thus, the second and third peak (10 – 200 ms) represented water existing in smaller pores in the porous medium, as opposed to a bulk water phase. Although the total amplitudes in the second and third peak are small, they do show an obvious trend. As time progressed, the amplitude of these peaks increased, proving once again the water existing in larger pores was gradually relocating into smaller pores. The increments in all three cases are fairly consistent despite the scatter, which is a reflection of the small water volumes in this range of T_2.

At the end of the experiment, in the vials where there was excess water added (i.e. the amount of brine originally added is greater than the pore space) a layer of oil sits above the oil and sand mixture, as shown in Figure 9.9. Due to its lighter density (0.9815 g/cm^3) oil will sit on top of water (1.0415 g/cm^3). From the shift in the spectra and the low Bond number (1.9 x 10^{-5}) it can be concluded that gravitational forces were not responsible for the rearrangement of the oil and water distribution, thus the fluid re-distribution must be due to water imbibition.
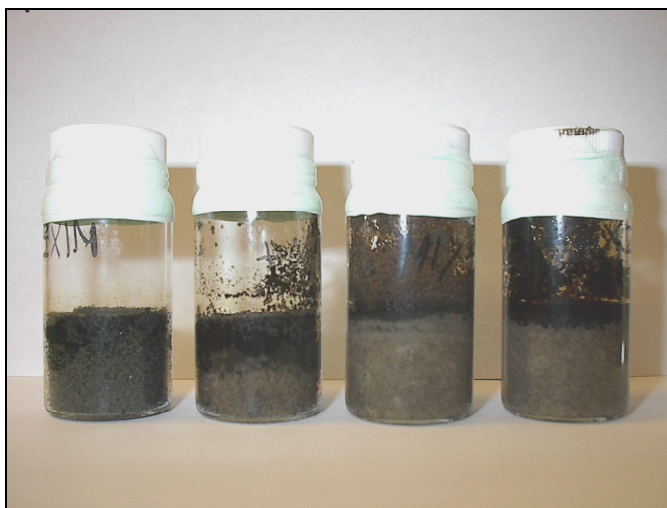
Figure 9.9: Fluids redistribution in vials

From the visual observation of the vials, it was seen that the oil that was originally mixed with sand was removed by water and formed a layer of bulk oil above water. It must be noted that this is possible because the oil density is less than that of water. If the reverse is true, where oil density is higher than that of water, the formation of the oil layer would not occur. In those samples, where oil accumulated on top of the sand mixture, the sand also appeared to be cleaner, or less dark. Through NMR monitoring, it was seen that the added brine immediately occupied the small pores with the excess brine existing as a free phase. As time progressed brine accessed other pores and thus expelled the oil out of the porous medium. Incidentally, this picture shows that bulk water no longer exists on top of the sand. Once bulk oil has been released and spreads over the air/water interface, brine evaporation reduces, which explains why evaporation was low in samples B to D.

One point that should be addressed is the issue of how water initially moves into the porous medium, since there was initially no water present in the sand. Water could either enter the sand through the density contrast between oil and water (i.e. gravity) or water movement may initially have been caused by a spontaneous water emulsification mechanism suggested by Vittoratos *et al*. (2006). In either case, once water has invaded the porous medium, the analysis of the Bond number shows that gravitational forces are insignificant. The NMR spectra also show that some water is initially present in films, while other water gradually moves into smaller pores with time. Thus, once the water is in the porous medium the mechanism of fluid re-distribution is no longer the spontaneous formation of W/O (water in oil) emulsions, as has been proposed in the literature (Vittoratos *et al*., 2006). All of this is evidence that the sand is water wet and imbibition is responsible for fluid redistribution.

9.2.2 Imbibition in Sandpacks during Shut-In

Fluid redistribution was also observed in the core floods when they were shut in for extended periods of time. In these experiments after a period of shut-in, flow was re-initiated, and the produced oil cut was consistently higher than its previous value, before

shutting in the system. This production response was previously discussed in Chapter 8, and the result for one experiment is plotted in Figure 9.10.
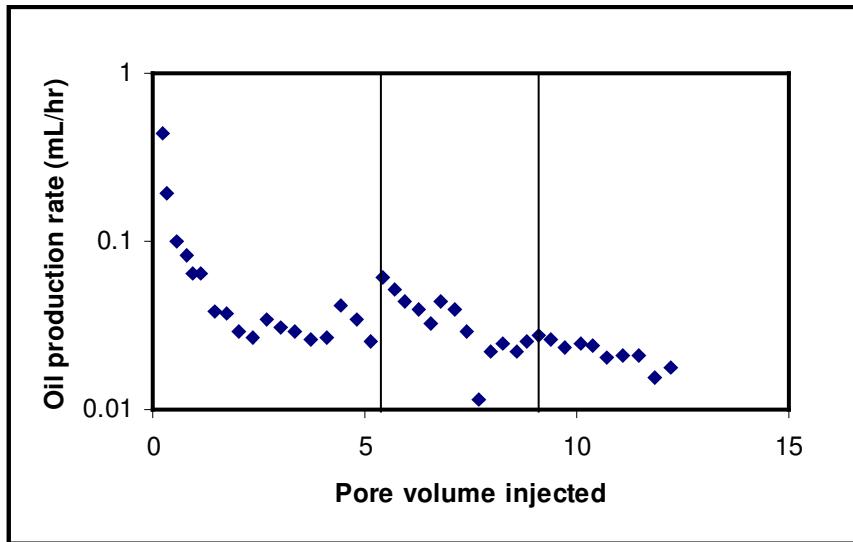
Figure 9.10: Improvement in oil production rates after shut-in (Experiment # 7)

Due to the fact that the core flood has been subjected to brine injection immediately before shut-in, there is still a pressure drop across the sandpack during the shut-in period. Therefore, two forces are acting during this time: viscous forces and capillary forces. The residual effect of viscous forces during shut-in must also be considered. Although the viscous pressure drop was very low, during the shut-in period the sandpack would seek to achieve its equilibrium by balancing the pressure inside the porous medium. Thus, mobile brine along with some oil could find its way toward the outlet. The amount of oil mobilized due to the residual viscous forces is controlled by the relative permeability to oil, and it should be similar to the previous oil cut of the total fluids. At the moment of brine re-injection, the residual viscous forces would cause the oil and water to be produced at water cuts that are similar to their pre-shut in values. However, the actual production after shut-in shows an improvement in oil cut, which cannot be explained through residual viscous forces. Thus, the improvement in the oil production must be due to imbibition during the shut-in period. When there is no flow, water will

move into smaller pores through imbibition, displacing oil into the large, highest permeability pores. Upon the re-generation of flow, the displaced oil can be produced.

The improvement in oil recovery was also seen to be a function of time, as shown in Figure 9.11.
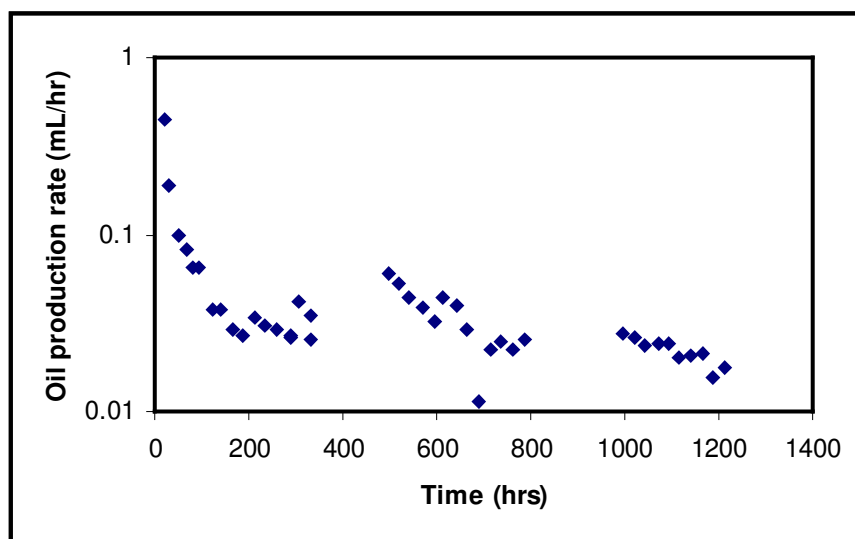
Figure 9.11: Oil production rate vs. time – effect of shutting in core (Experiment # 7)

As oil saturation decreases in successive shut-in cycles, the improvement in the oil flow rate after shut-in becomes less dramatic. This could be due to lower oil relative permeability since oil saturation is lower, or it could also be the effect of fewer channels for the oil and water to invade at each subsequent time. Even though the improvement is not consistent in terms of oil production rate, it is clear that each time the system is shut-in for fluid re-distribution, the oil rate improves and gradually reduces back to the pre-shut in values.

The evidence from both NMR measurements in static vials and from shutting in core floods demonstrates that capillary forces can be potentially used to aid recovery in water wet porous media.

9.3 NMR Spectra of Heavy Oil Waterfloods

The tests performed in the previous section have demonstrated that in the absence of viscous forces (flow), fluid re-distribution due to capillary imbibition in water wet sand can lead to additional oil recovery. The question that must be answered is whether these capillary forces are also present and significant during flowing conditions.

9.3.1 Properties of Sandpacks

Two heavy oil waterfloods were performed, at fixed injection rates. Table 9.1 shows the properties of the two sand packs. Both cores were initially saturated with brine and then were flooded at a constant rate with a heavy oil of viscosity 11,500 mPa·s (HO2) until irreducible water saturation (S_{wi}) was reached. Brine was then injected at a fixed rate for several pore volumes, and NMR spectra of the sandpack were obtained during the flood, in order to measure fluid saturation and the location of water as a function of time.

Table 9.1: NMR Heavy Oil Waterflood Properties

Experiment	Experiment # 21	Experiment # 22
Length (cm)	9.30	9.27
Diameter (cm)	2.54	2.54
Pore volume (cm^3)	21.68	21.45
Porosity (fraction)	0.460	0.457
Permeability (D)	14.5	15
S_{wi} (fraction)	0.089	0.090
OOIP (cm^3)	19.75	19.52
Injection rate (cm^3/hr)	0.45	8.89
Injection velocity (m/day)	0.0213	0.421

Figure 9.12 shows repeat measurements for the Experiment # 21, fully saturated with brine. In this state, the water relaxation times are governed by surface relaxation, thus the NMR relaxation is proportional to the pore size distribution.
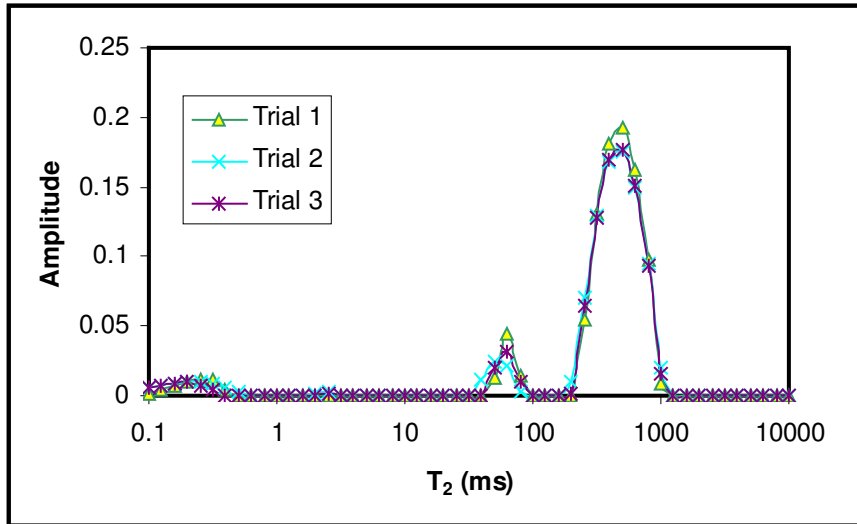
Figure 9.12: Repeatability of NMR spectra at fully saturated with brine condition

The spectra shown in Figure 9.12 are similar to the water-saturated spectrum in Figure 9.2, and were also essentially identical to the spectrum of Experiment # 22 as well. Since the pore size distribution is similar for both cores, this indicates that capillary forces (proportional to pore size) will also be similar in both core floods. A similar pore size distribution also is indicative of similar rock permeability. Viscous forces, represented by the injection velocity, were varied. The goal of this suite of experiments was to identify what is the relative magnitude of the contribution of viscous versus capillary forces to oil production in heavy oil waterflooding.

9.3.2 Determination of Oil and Water Signals in NMR Spectra

A major difference between these NMR core floods and the previous static vials is that the cores were initially saturated with water and then flooded to S_{wi}. The configuration for the flood is therefore different than the vials, but is consistent with all the other waterfloods. In a core flood, until water is continuous across the core, imbibed water must displace viscous heavy oil ahead of the water front, all the way to the production end. Imbibition therefore should occur more slowly at early times.

Figure 9.13 shows an example spectrum of the Experiment # 21, at irreducible water saturation. The core contains a large, fast relaxing peak that relaxes fully by around 10 ms. This is similar to the T_2 location of the bulk heavy oil, and it has been shown that for high viscosity heavy oils, the bulk relaxation time is so fast that this dominates the fluid relaxation. The relaxation rate for heavy oil is therefore largely independent of the surface relaxation effects in the porous medium, and this large fast peak in the oil sand spectrum contains the full contribution of the oil amplitude.
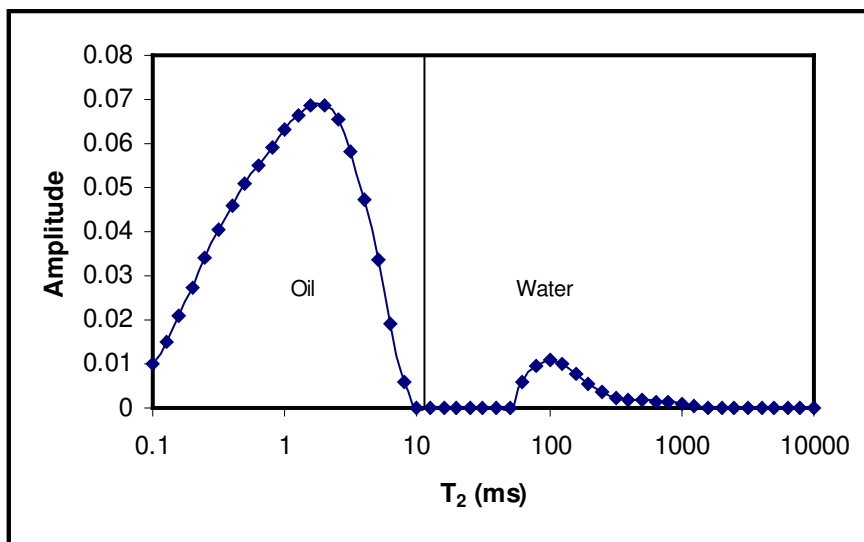
Figure 9.13: Characteristic of oil and water in porous medium

From the brine saturated spectra in Figure 9.12 it can be seen that the T_2 values for water, controlled by surface relaxation, are represented by a peak at approximately 100 ms and another peak between 300 – 500 ms. In the core containing oil and S_{wi}, the peak at long relaxation times has disappeared. This is an indication that water no longer exists in pores large enough to give a relaxation time of 300 – 500 ms, or that the oil is now in the large pores. This is the nature of fluid distribution during drainage, and provides further evidence of the water wetting nature of this sand. The remaining pores that were by-passed and still contain water are the smaller pores, with relaxation times in the range of 100 ms.

In a water wet rock, there may be thin water films surrounding the sand grains. This water may lead to very fast relaxation times, therefore a portion of the water signal may also be relaxing very quickly and overlapping with the oil signal under 10 ms, as was seen previously in the NMR vial experiments. It is not possible to determine *a priori* how much of the signal in the first peak is due to water, however it was known by mass balance of the produced fluids that the irreducible water saturation is low in these cores. Therefore, the large first amplitude peak in the NMR spectra is mainly the contribution of the oil. Since there is no mechanism that can cause the oil to relax more slowly than the signal from bulk oil, it is also certain that any signal after the first peak is the contribution only from water. As a first-pass approach in this study, therefore, the amplitude in the first peak was taken to be the signal from oil and any signal after this peak was taken to be that of water.

Figure 9.14 shows the spectra at various times in a heavy oil waterflood. As expected, the amplitude in the first peak decreases with time, which is indicative of reducing oil saturation in the core. Likewise, the amplitudes in the water portion of the spectra increase, which shows increasing water saturation in the core.
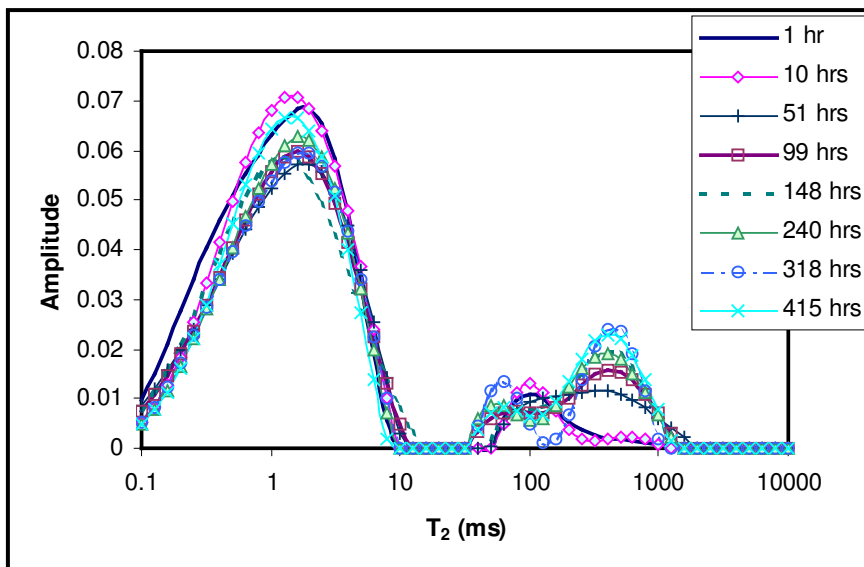
Figure 9.14: NMR spectra of fluids in a core as the waterflood progressed

In order to quantify the trends observed in the NMR spectra as a function of time, several parameters need to be considered. Obviously, the oil and water amplitudes can potentially be related to fluid saturations in the core. Saturation was also obtained by analysis of the produced oil/water mixtures, thus the NMR estimates of saturation could be compared against the production values in order to validate the division of the oil and water amplitudes shown in Figure 9.13. In the signal that is known to be the contribution solely from water, the T_{2gm} of the water can provide additional information about the location of the injected water in the porous medium.

9.3.3 Interpretation of Water Relaxation Times

It was previously observed that for the sand used in this study, large pores have a T_2 peak occurring in the range of several hundred ms, and a smaller peak at around 100 ms. The mean relaxation time for the sand fully saturated with water is around 260 ms. Upon waterflooding, an analysis of the water mean relaxation time (T_{2gm}) can provide an indication of whether the injected water is flowing through the large or the small pores. In order to separate the oil and water response, water mean relaxation time was defined as the geometric mean of the water signal beyond 10 ms.

Figure 9.15 shows the water T_{2gm} values as a function of time for both injection rates. At the fast injection rate, the water T_{2gm} values begin to increase after only an hour of injection, and after five hours the water is relaxing at its final value, which is similar to the fully saturated T_{2gm}. At the slower injection rate, the water T_{2gm} values do not begin to increase until after ten hours of injection, and only reach the fully saturated T_{2gm} value after around 24 hours. In both floods, once the water relaxation times in the core begin to change, the increase to the final T_{2gm} value occurs within approximately 10 hours.
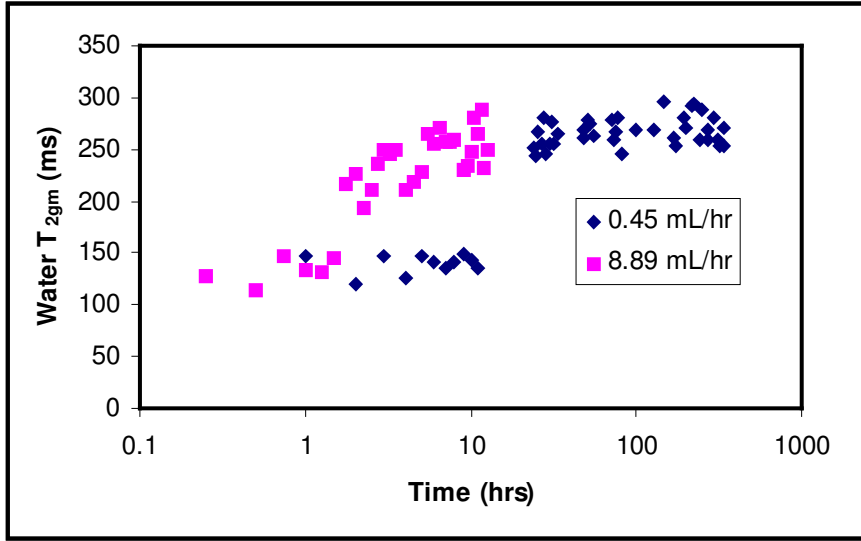
Figure 9.15: Water T$_{2gm}$ after 10 ms for fast and slow injection rates

In order to compare the results from different injection rates, dimensionless time was used instead of time in hours. Dimensionless time (t$_D$) is defined as:

$$t_D = \frac{q_{inj}t}{PV}$$
Eqn (9.7)

Where q$_{inj}$ = fluid injection rate

t = time.

Although t$_D$ appears to be the same as the measurement of pore volumes of brine injected from previous chapters, it should be emphasized that these terms are defined differently in this work. Pore volumes of fluid injected are calculated based on the produced fluid volumes, while t$_D$ comes from the set injection rate from the pump. Dimensionless time is equal to the pore volumes of fluid injected if the injected water could enter the core without obstruction at the rate set by the pump. In reality, this is not the case at early times, when viscous heavy oil cannot flow at the same fixed rate as the water and pressure is building up in the system. After these early times, however, then dimensionless time is the same as the pore volumes of fluid injected, and can be

understood in the same way. Due to the small core sizes used for these experiments, time was represented by Eqn (9.7) for the analysis of this data. Figure 9.16 shows the water T_{2gm} values as a function of dimensionless time in the waterflood.
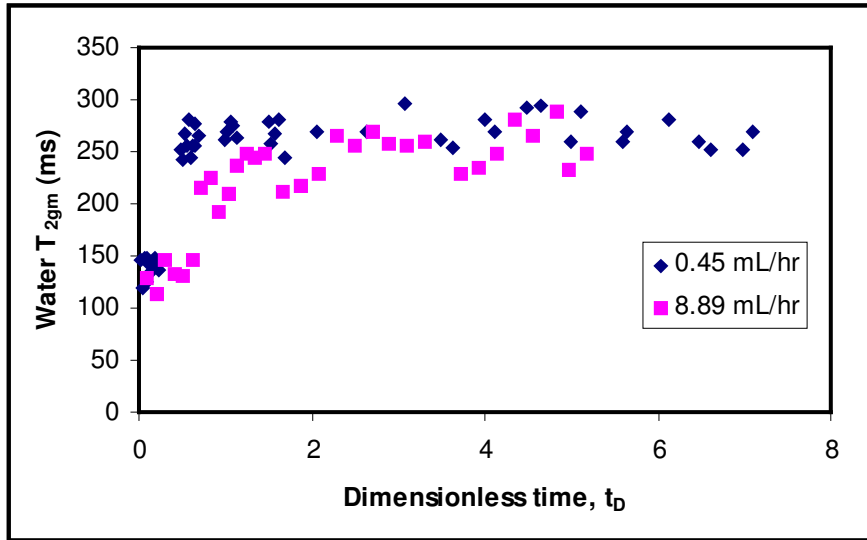
Figure 9.16: Water T_{2gm} after 10 ms as a function of dimensionless time

When water T_{2gm} is plotted as a function of dimensionless time instead of actual time, it is apparent that the measured water T_{2gm} values actually increase faster at the slower injection rate, instead of at the faster injection rate as was observed in Figure 9.15. After around 0.6 pore volumes injected at the low rate, the water T_{2gm} is already at its final value. At a high injection rate, however, almost two pore volumes of injection are required in order for the water T_{2gm} to approach its final value. By looking at the water mean relaxation times alone, therefore, it may appear as if at the lower injection rate water displaces oil and moves into larger pores (as evident by the sudden step change in T_{2gm} values), while at higher injection rates water is somehow entering through the smaller pores (thereby increasing the water T_{2gm} slowly). This is counter-intuitive; it was expected that at higher injection rates, viscous forces would be more dominant and thus water would move through the largest pores in the rock matrix. These results demonstrate that simply looking at water relaxation times without regard to the physical

situation being addressed can lead to errors in interpretation. The water relaxation times must be further analyzed based on the production data gathered from the water flood.

Figure 9.17 shows the measured oil recovery as a function of pore volumes injected. At early times (below two pore volumes injected), although the measured water T_{2gm} values are higher at the lower injection rate the recovery is actually similar or even slightly higher at the faster injection rate. This was also observed in the other 0.8 D core floods that were discussed previously (Chapter 7).
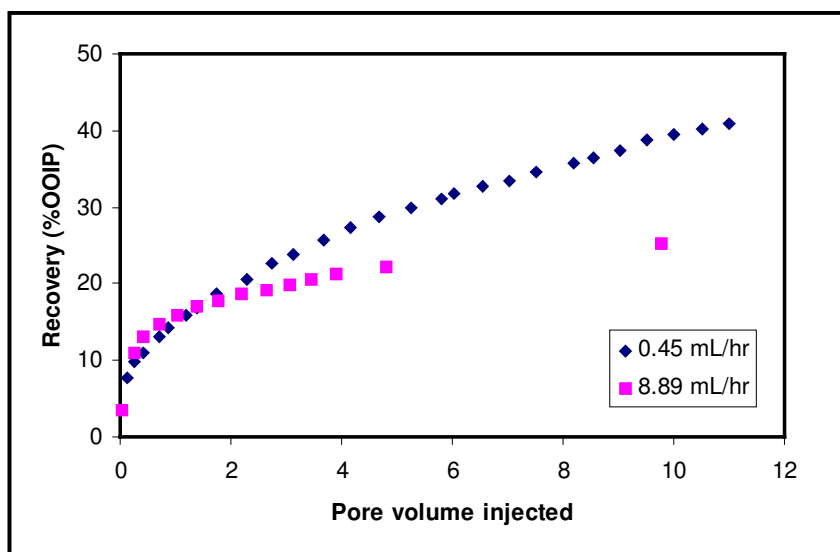
Figure 9.17: Recovery profiles for fast and slow injection

The implications from Figure 9.16 and 9.17 initially appeared to be contradictory. A higher water T_{2gm} value would seem to indicate that more water has displaced oil completely out of rock pores, but this was not shown in the production data. In addition, instability theory would also dictate that at a slower injection rate the displacement front is more stable, thus recovery up to breakthrough should be better at the lower injection rate, but again this was not observed in Figure 9.17. These production profiles have been fairly consistent with the other results presented in Chapter 7, where breakthrough recovery at extremely low injection rate is actually lower than at faster rates. One possibility for this unexpected, but repeatable, behaviour is that at low injection rates

brine is imbibed ahead of the front, causing the front to be less sharp and thus decreasing recovery at breakthrough. Peters and Flock (1981) mentioned the possibility of imbibition as a stabilizing force in an unstable waterflood. In the results shown in Figure 9.17 and in Chapter 7, it appears that this is true only for a certain range of flow rates, and when injection rates are too low, capillary forces may lead to a reduced breakthrough recovery. Overall, however, the recovery will be higher under lower injection.

If brine imbibition does in fact lead to early breakthrough under very low injection rates, then one would expect the brine to be imbibed into the small pores, which would manifest as a more gradual increase in water T_{2gm} in Figure 9.16. Another possibility is that the definition of water T_{2gm} as coming from the signal above 10 ms does not encompass the whole water signal. Specifically, any water signal in very confined spaces may be masked by the oil signal in the first peak.

The first assumption tested is that all the water signal exists only after 10 ms. If this is true, the water T_{2gm} values are a reflection of whether injected water is in large or small pores. The T_{2gm} values at the lower injection rate should therefore mean that the injected water is flowing mainly through the large pores, so recovery should accordingly be higher at early times, but this was not observed in Figure 9.17. In order to reconcile the water T_{2gm} values to the recovery, the water amplitude (i.e. the amount of water in the core) must also be considered. The water amplitude fraction at both injection rates is plotted in Figure 9.18. Water amplitude fraction is defined as the water amplitude (after the first peak) divided by the total amplitude in each spectrum.

The water amplitude should be proportional to the amount of water present in the core. At early times (below 1 PV injected) the water amplitude fraction actually increases faster at the slower injection rate, but in Figure 9.17 the measured oil recovery was higher in the higher rate waterflood. Eventually the water amplitude fraction in the fast injection rate begins to increase and by the time one pore volume of fluid has been injected, the amplitude fraction is actually higher in the core with the faster injection rate.
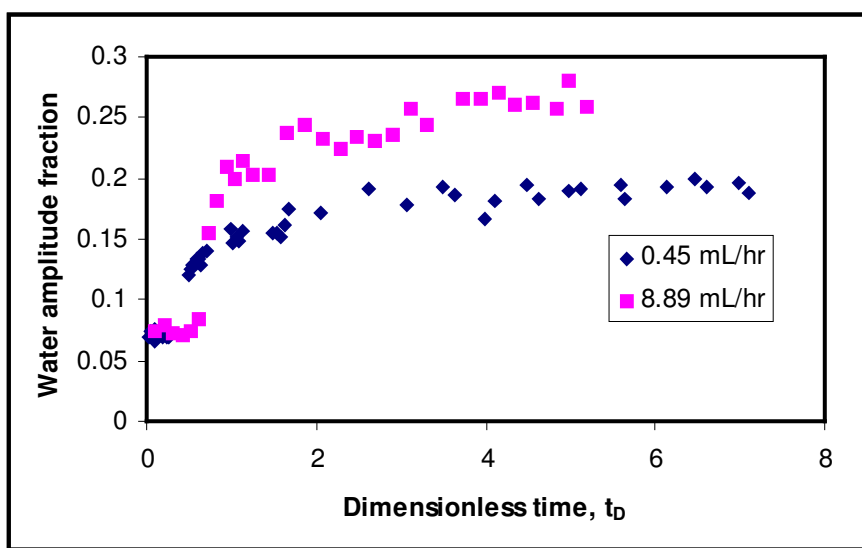
Figure 9.18: Water amplitude fraction after 10 ms for fast and slow injection

From the recovery profile (Figure 9.17) at early dimensionless time of less than 1 PV, the recovery is similar or even slightly higher for the fast injection rate. The NMR water amplitude fraction appears to show the opposite trend. In order to properly understand this apparent discrepancy and how this affects the water T_{2gm}, it is necessary to understand how the NMR measurements are taken. Figure 9.19 shows a schematic of the NMR core holder. The NMR signal only comes from the region of constant magnetic strength, indicated in Figure 9.19. The signal from injected water does not become visible until the water enters this region that is detectible in the NMR.
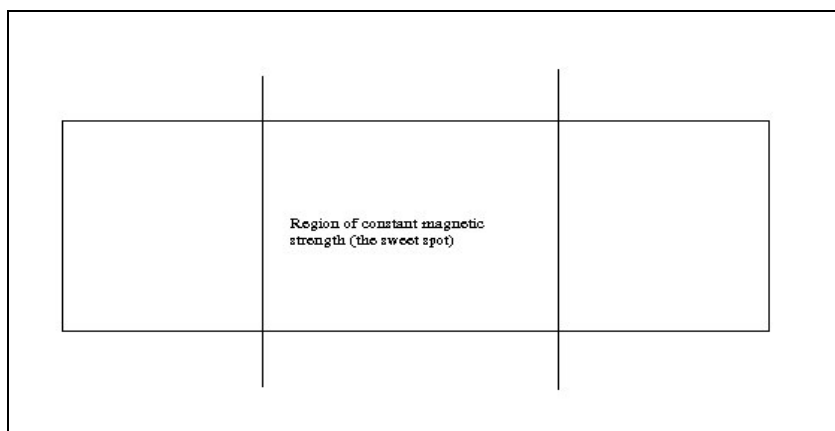
Figure 9.19: Schematic diagram of long core passing through the magnet sweet spot

At early time the flood fronts may take one of two possible forms. Figure 9.20 shows schematically how water signal could potentially enter the NMR sweet spot faster at the lower injection rate, due to increased movement of water (imbibition). This can be verified by also considering the measured pressure drop across the core.
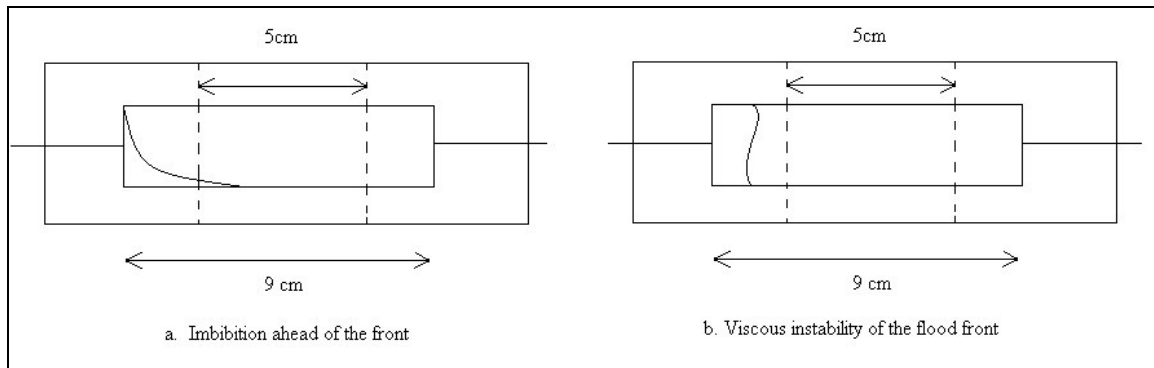
Figure 9.20: Schematic diagrams of water profile for fast and slow injection

Figure 9.21 shows the pressure profile for the waterfloods at low and high injection rates. At the high injection rate, viscous heavy oil cannot flow out as quickly as water is injected into the system. Therefore pressure built up as injected water collected near the entrance to the core. Eventually the pressure in the system became high enough for oil to be produced, and water fingered through the core and broke through to the production end. After water breakthrough, injected water can now flow through continuous channels so pressure quickly declines in the system. For the slow injection rate the pressure peaked after 0.4 PVs of brine injected, whereas the pressure of the faster injection rate peaked after 0.6 PVs of brine injected.
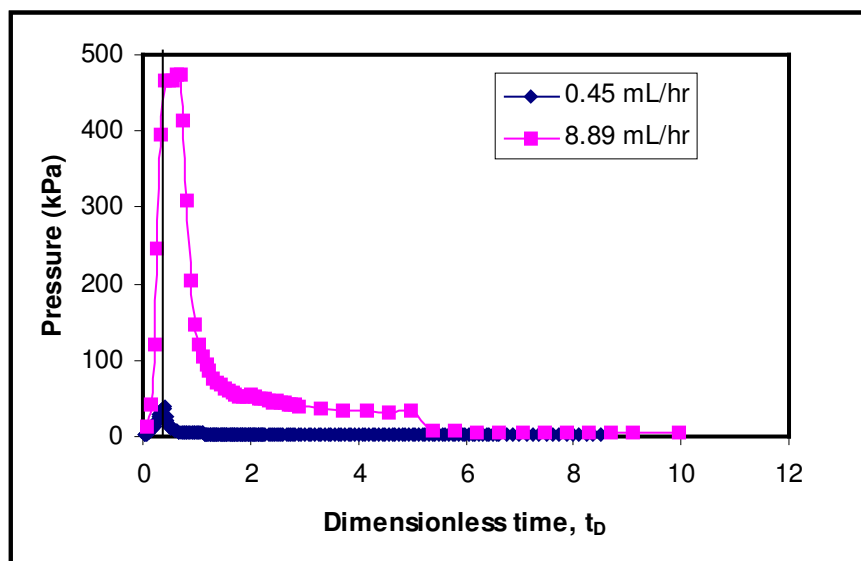
Figure 9.21: Pressure profiles for fast and slow waterfloods

By comparing the pressure profiles to the production behavior and the NMR spectra properties, the response of the varying rate waterfloods can now be properly understood. At a high injection rate, water initially collects near to the entrance of the core while pressure increases. During this time, displaced oil from the core entrance is flowing through continuous channels oil pathways, thus in the NMR spectra the water fraction does not appear to increase and the water relaxation times are constant. However, due to the higher pressure drop across the core, more oil is flowing so the recovery will initially be slightly faster, even if it is less efficient. This again demonstrates the dominance of viscous forces at early times, before water breaks through. At lower injection rates, pressure does not need to build up as much in the core, therefore water can progress further into the core at early times, leading to increasing water amplitudes in the core.

Once water enters into the region of constant magnetic field strength, the water T_{2gm} values quickly increase to the same range of relaxation times as for the water-saturated core. This means that the injected water is now located in large pores and relaxes more slowly than the original connate water. After this point, the water portions of the NMR spectra all indicate that the injected water is in the larger pores, so the water relaxation

times do not provide any more information about the recovery mechanisms at the later portions of the flood, after water breakthrough. Additional understanding comes from a more detailed interpretation of the water amplitudes.

9.3.4 Interpretation of Water Amplitude and Fluid Saturation

By comparing the measured production response (Figure 9.17) to the NMR water amplitude fraction (Figure 9.18), an important observation can be made: the NMR water amplitude fraction does not follow the same trend as the production response. In Figure 9.17 the total recovery of the lower injection rate is significantly better than the recovery of the faster injection rate. However, Figure 9.18 shows that the water signal after 10 ms, which is a reflection of the water saturation in the system, is actually higher for the higher injection rate. The water amplitudes therefore illustrate the opposite relationship as the actual production data. The early time NMR response was explained based on the pressure build up in the core, but it cannot explain the significantly higher water amplitudes at the fast injection rate during later times in the flood. In order to quantify the NMR water amplitude, water saturation was calculated from the NMR spectra. Water saturation was defined to be:

$$S_w = \frac{A_w}{A_{w\_fs}} \qquad\qquad \text{Eqn (9.8)}$$

Where A_w = the NMR water amplitude at any time

A_{w_fs} = the NMR water amplitude of the core fully saturated with water.

This equation is applicable if it could be assumed that the NMR captured the same porous medium at all the times when NMR measurement was obtained. This is a valid assumption since the sandpack was mounted inside the NMR during the waterflood. Eqn (9.8) was defined based on the fact that the water amplitude index (i.e. amplitude per unit mass or volume) is a constant. At the fully saturated condition, the entire measurable porosity was full of brine, thus the amplitude at this condition corresponds to the pore

volume filled with water. At any point during the waterflood, the water amplitude divided by this initial amplitude gives a measure of the water saturation. Due to differences in calibration of the NMR, A_{w_fs} was measured separately for the two floods.

When Eqn (9.8) was used to calculate the water saturation in the core under the assumption that water signals are beyond 10 ms, it was discovered that the NMR estimates of water saturation were consistently lower than the values obtained from mass balance of the produced fluids. For Experiment # 21, the NMR estimate of S_{wi} was approximately 0.067, while the measured S_{wi} was 0.09. Likewise, in Experiment # 22 the NMR predicted a S_{wi} value of 0.063, while the mass balance showed S_{wi} to be 0.083. This showed that in both cores around 2% of the actual water is relaxing in thin films or small pores, such that the water T_2 values are hidden by the oil. Unfortunately, from a T_2 NMR measurement alone cannot conclude where exactly this water amplitude is located.

Figure 9.22 compares the NMR water saturation to the saturation values obtained by separation of the produced fluids in Experiment # 22 (the high rate waterflood). In this figure, NMR water is taken only as the signal after 10 ms.
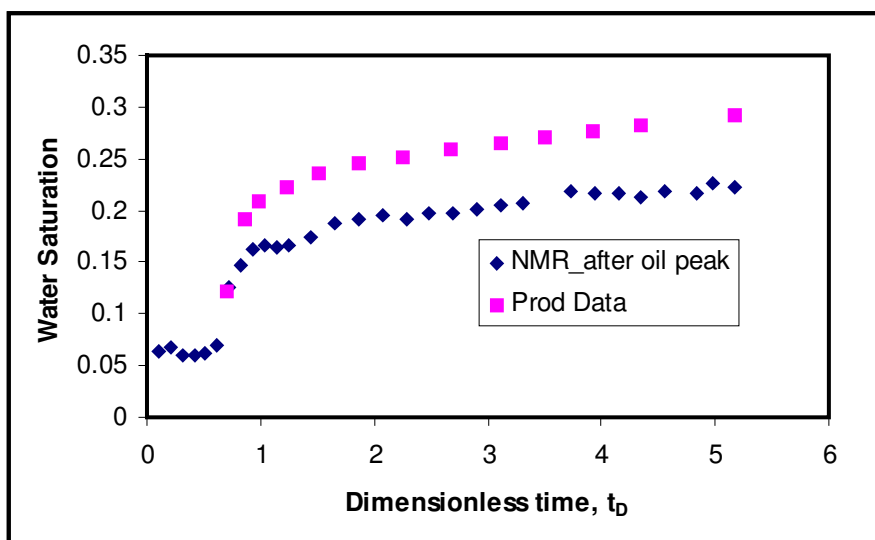
Figure 9.22: NMR water saturation only for signal after 10 ms for fast injection

The shape of the water saturation profile for NMR and production data are very similar, however the NMR values are consistently low. Likewise, NMR oil saturation predictions $(1 - S_w)$ would follow the same trend as the production data but the numbers would be consistently high. This is an indication that additional water amplitude is hidden within the first peak. Eqn (9.9) was therefore used to calculate the water amplitude in the first peak:

$$A_{w\_f} = (S_w)A_{w\_fs} - A_{w\_p}$$
<div align="right">Eqn (9.9)</div>

Where A_{w_f} = the water amplitude within the first peak

A_{w_p} = the water amplitude in the pores (after the first peak).

Using the production data and Eqn (9.9), the water amplitude in the first peak was calculated and is plotted in Figure 9.23. This fast-relaxing water is termed "water in films" and its physical meaning will be discussed shortly.
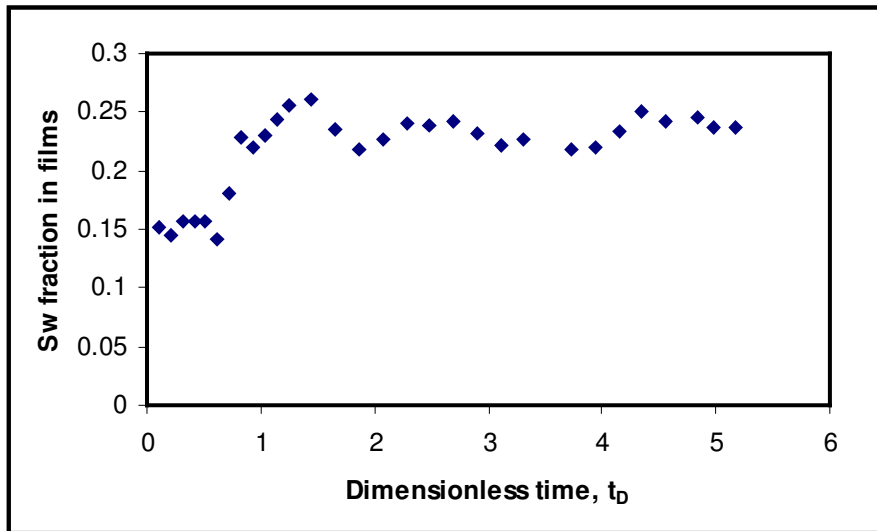
Figure 9.23: NMR water saturation fraction of films for fast injection

Once the water in films have been determined, the total water amplitude is the summation of the film (in the first peak) and pore (after the first peak) amplitude values. NMR water

saturation can then be calculated using Eqn (9.8). Figure 9.24 plots the tuned NMR water saturation values against the measured water saturation for Experiment # 22.
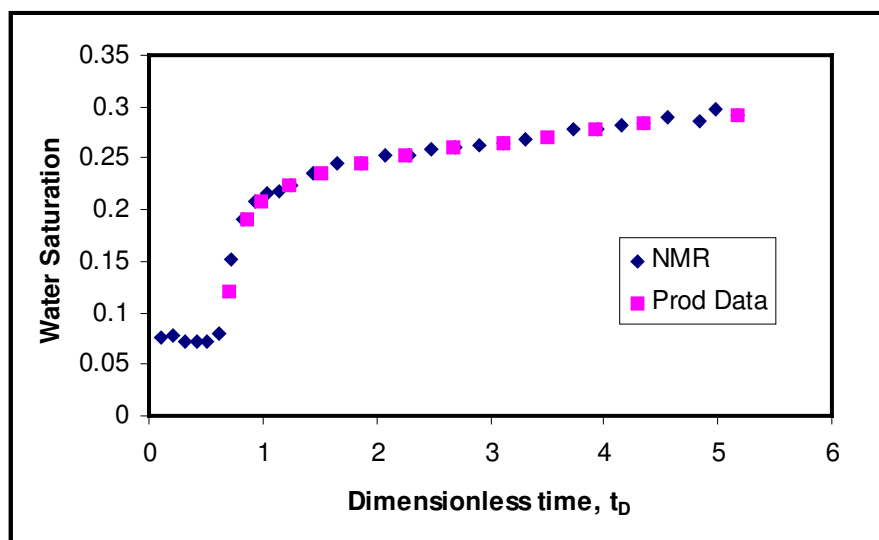
Figure 9.24: Corrected NMR water saturation for fast injection

The identification of the water signal in the first peak was based on the measured water saturation, so it is to be expected that the NMR water predictions match perfectly with the measured values. It should be noted that this methodology is no longer predictive, but unlike in past NMR oil sand studies (Bryan *et al.*, 2006), where the goal was to infer the connate water saturation in a reservoir or a mine, this methodology now has a different focus. The goal in this case is to tune the NMR predictions to match the measured values, and in doing so to calculate the fraction of water that is relaxing in thin films.

Figure 9.25 plots the NMR water saturation prediction without considering water films against the measured values for Experiment # 21, which was the low rate waterflood. As before, the NMR values consistently underestimate the actual water saturation in the core.
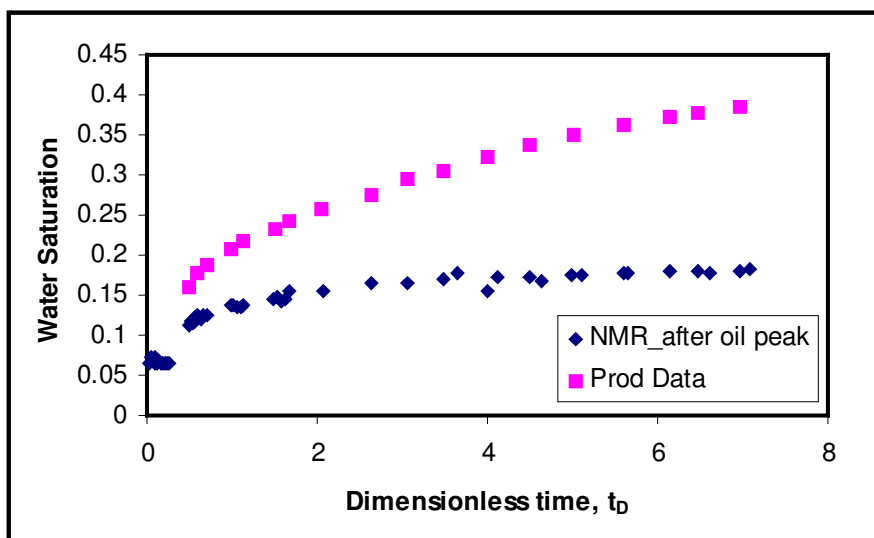
Figure 9.25: NMR water saturation for signal after 10 ms for slow injection

In the low rate waterflood, the NMR water estimate appears to level out at approximately 0.15, while the actual water saturation calculated from the production data increases steadily with time to 0.38 after seven pore volumes of water had been injected. The NMR is greatly under-estimating the water saturation in the system, which means that it is under-estimating the waterflood recovery. In the low rate waterflood, therefore, the NMR estimates of water saturation with the assumption of water only being after 10 ms in the core are not correct. Figure 9.26 plots the change in the fraction of both the amplitude of the first peak and the amplitude after the first peak with time.

It was stated previously that the first peak contains the entire contribution of the oil signal. In Figure 9.26, it appears after approximately 150 hours the amplitudes in the first peak have leveled off. From the production data oil was continuously being produced, thus one would expect the amplitudes in the first peak to decrease with time as well, but this was not observed. This must therefore be the effect of water films thickening and relaxing in the first peak. Oil amplitude is decreasing due to oil production but water amplitude is increasing at similar T_2 values due to film thickening during imbibition, so overall the signal in the first peak appears to have leveled off.
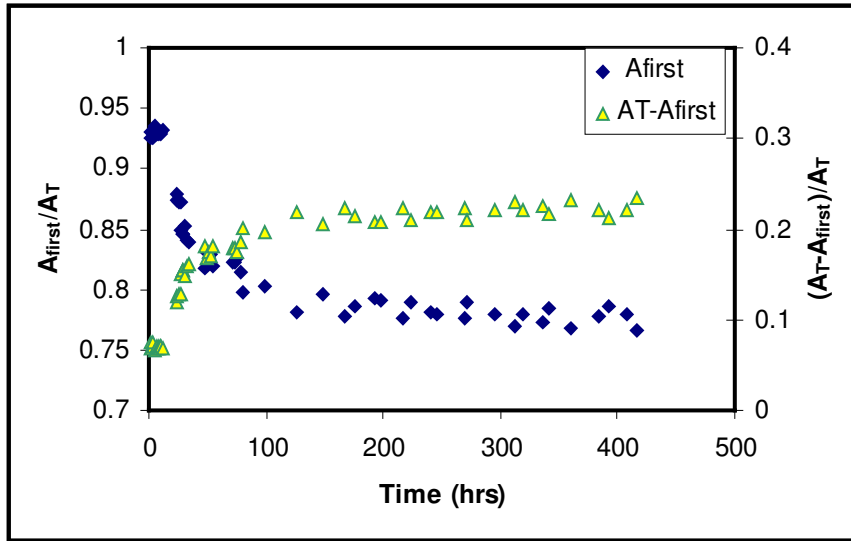
Figure 9.26: Change in amplitude fractions of different peaks for slow injection

If the water amplitude in the films is added to the water amplitude in the pores, the NMR saturation predictions in the low rate waterflood now once again match the measured values. While this methodology of tuning the water amplitudes to the measured values makes it virtually impossible to predict the water saturation upfront using NMR, it does however, indicate a very fundamental difference in the location of the injected water in a low rate waterflood.

From the NMR spectra of the core fully saturated with water (Figure 9.12), it is evident that the pore sizes are large enough that there is very little signal below 10 ms, which is where the first peak relaxes in the waterflood spectra. At S_{wi}, about 2% of the water saturation relaxes this quickly. This cannot be water in small pores, since there are no such small pores. Therefore, this is an indication of water relaxing in regions of higher surface-to-volume ratio than what is given by the pore sizes themselves. The presence of thin films could not be observed directly, but there are various sources in the literature detailing their existence.

Takamura (1982) provided a theoretical analysis of the location of water in oil sands. Assuming that the oil sands were initially saturated with water, and oil displaced water

through a drainage process, it is expected that irreducible water saturation in a packing of relatively uniform spheres will be in the range of 6 – 8%, and is slightly higher for systems containing irregularly shaped particles (Takamura, 1982). In these systems, containing a distribution of grain sizes, S_{wi} ranges from 7.5 – 9%, which is similar to the values predicted. This water will generally tend to be found in pendular rings surrounding the grain-to-grain contact points. Takamura (1982) provided a theoretical calculation of disjoining pressure to indicate that there may also be stable water films present surrounding the sand grains. These films will be thin, and calculations of disjoining pressure for particles in the range of sizes of sand grains show that they will be on the order of 10 – 15 nm. Takamura (1982) stated that these films are so thin that they do not contribute to the hydraulic conductivity of water and they are responsible for only approximately 0.05% of the water volume. The majority of connate water is found in the pendular rings at the grain-to-grain contacts, and water surrounding fine particles. Figure 3.19 presents a schematic of the nature of connate water in oil sands, showing both water locations.

Other researchers (Clark, 1944; Sobol *et al.*, 1985, Czarnecki *et al.*, 2005) have attempted to provide both physical and theoretical evidence for the presence of thin water films, however there is still some uncertainty about their existence in oil sands. This work provides definitive evidence not only for their existence, but also for their importance to oil recovery.

In the core at S_{wi}, there is still a small fraction of water signal present at similar T_2 values as the water-saturated core. This indicates that some of the large pores are surrounded by smaller pores, and will therefore not be easily accessed during drainage by oil. As a result, water is present in both small and larger pores due to non-uniformity in the sand grains. In a packing of spheres of uniform size, it is expected that there will be little by-passing of water in large pores, and all the water will exist in the form of pendular rings (Morrow, 1971) and possibly thin water films over the sand. The NMR spectra at S_{wi} indicate that these cores are not made of uniform sized spheres.

Additionally, it has been shown that there is some water amplitude relaxing much more quickly, below 10 ms. Calculations are presented in Appendix G for relating the signal of fast-relaxing water in the first peak of the core flooding spectra to the possible thickness of water films. First, based on the water-saturated NMR spectra, the surface relaxivity can be found. Surface relaxivity is defined in Eqn (9.10) (Straley *et al.*, 1997, Coates *et al.*, 1999).

$$\frac{1}{T_2} = \left(\frac{1}{T_{2B}} + \frac{1}{T_{2S}}\right) = \left(\frac{1}{T_{2B}} + \rho_s \frac{S}{V}\right)$$ Eqn (9.10)

Where T_{2B} = the bulk relaxation

T_{2s} = the surface relaxation T_2 value

ρ_s = surface relaxivity

S/V = the surface to volume ratio of the pore.

Using the measured permeability of the system and relating permeability to an average pore radius using the Depuit-Forcheimer expression (Scheidegger, 1974), the value of the surface relaxivity for this system was found to be approximately 36 μm/s. Details of this calculation are shown in Appendix G. Since the pore space containing the fluids is more complex than that of cylindrical pores, the value of ρ_s found is actually an effective value. It is a function of the true surface relaxivity and the surface roughness of the sand grains. Other researchers (Chen *et al.*, 2007) have reported similar values of apparent ρ_s. With this value known, the water relaxation times in the first peak can be converted into values of film thickness.

The first peak of the core spectra, containing oil and fast-relaxing bound water, exists below 10 ms. Since there is no way to de-convolute the oil and water signals at this point, it is not possible to accurately determine the T_{2gm} of the water in this peak. In Appendix G, calculations are provided to convert different NMR T_{2gm} values into surface

to volume ratios and equivalent pore sizes. A summary of these calculations is presented in Table 9.2.

Table 9.2: NMR estimates of film thickness based on varying T_{2gm} values

NMR T_{2gm} (ms)	Calculated film thickness (µm)
230	19
10	0.73
5	0.36
1	0.073
0.1	0.0073

For the NMR T_{2gm} value of the fully saturated sandpack, the average pore size is 19 µm. Other possible values of water relaxation time under 10 ms result in calculations of pore sizes, or film thickness, that are considerably smaller than the average pore size. NMR T_{2gm} values on the order of 0.1 – 0.2 ms would be representative of a film thickness of approximately 15 nm, which is in the range of water film thickness predicted by Takamura (1982). Higher T_2 values (still under 10 ms) would be indicative of pendular rings. Unfortunately, since it is not known what the actual water T_{2gm} is, these are only approximate values. It is certain, however, that these values of thickness are well below that of the pore sizes, thus the NMR is measuring the response of water in either pendular rings or films, or even possibly both. Since most of the water volume is expected to exist in the form of pendular rings, it is likely that the T_{2gm} values come mainly from amplitude greater than 1 ms.   In this analysis, however, all the fast-relaxing water amplitude is termed "water in films" for simplicity. This term encompasses both pendular rings and thin water films. Water in very small pores could also contribute to NMR T_{2gm} values in this range, however in Figure 9.12 it was previously observed that there are very few of these small pores present in the absence of overburden pressure.

Figure 9.27 plots the water saturation change in these fast-relaxing pores as a function of dimensionless injection time. Again, saturation values are calculated from comparing the NMR spectra to the produced fluids.
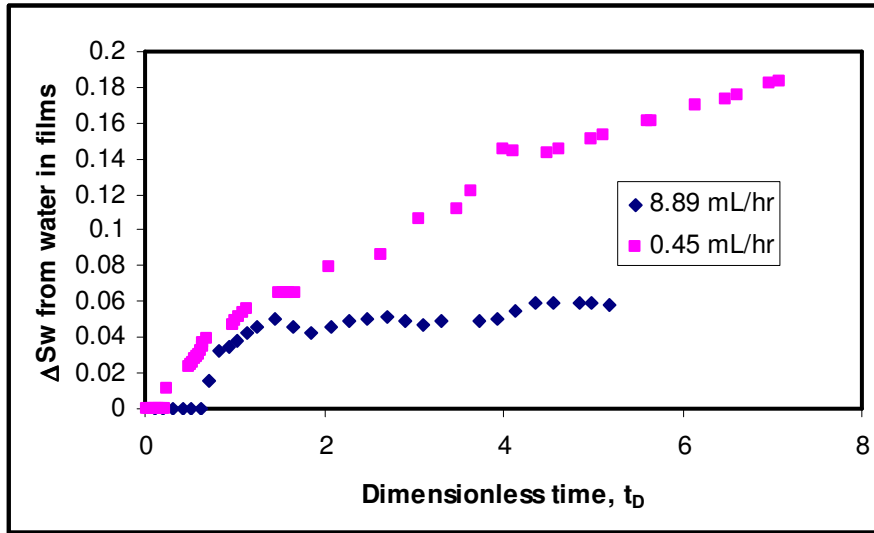
Figure 9.27: Increase in water saturation in films for fast and slow injection

While there is a significant difference between the changes in water saturation with time at fast versus slow injection rates, it is important that in both core floods, the water saturation is increasing at these fast relaxation times. This is the effect of the thickening of pendular rings and possibly water films. These rings are still considerably smaller than the pores, since for a 15 D core the expected average pore size is around 19 μm. Thus, if water saturation is changing in these small pores, this indicates that thickening of the pendular rings has led to oil production. Since the water still continues to relax below 10 ms, this indicates that the rings are still much smaller than the average pore sizes, so oil is not being trapped due to snap-off.

The other significant observation from the increasing water saturation at fast relaxation times is that pendular rings are in fact hydraulically connected, in contrast to what was predicted in the literature (Morrow, 1971; Takamura, 1982). Water must be somehow transmitting from the waterflooded zones to these pendular rings in channels that are still saturated with oil and connate water. This is evidence that, although they cannot be measured directly, there must be thin water films present coating the sand grains, which allows for this hydraulic conductivity.

9.3.5 Effect of Injection Rate on Oil Production in Pores vs. Films

Figure 9.28 compares the water amplitude fraction that is due to films for both injection rates. Again, the term "films" relates to both the thin films covering the surfaces of grains and also the pendular ring structures that contain the majority of the water.
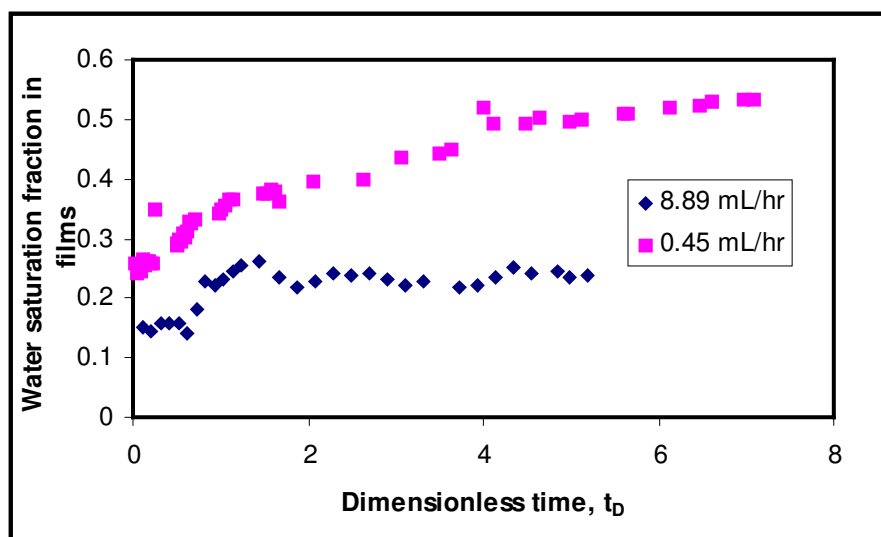
Figure 9.28: Water saturation fraction in films for fast and slow injection

At the fast injection rate, the water fraction in thin films is relatively constant, at around 24% of the total water fraction. The fact that the water film fraction increased at the start of injection demonstrates that even in high viscosity oil reservoirs, imbibition of water will occur so long as the sand is water wet. After this initial increase, however, the water film fraction stays constant and the trend of water amplitude growth in pores matches that of the measured production data. Alternatively, at the slow injection rate, the water amplitude fraction from thickening water films continues to increase, indicating that while water saturation in the pores is constant, the thickening of water films is responsible for the oil recovery at this stage. This allows the conclusion to be made that at low rates, water film thickening is the dominant recovery mechanism responsible for the higher oil recovery.

At early times in a waterflood oil recovery is strongly affected by viscous forces, as shown by the large increase in recovery in the first two pore volumes of dimensionless time in Figure 9.17. After water has broken through, the oil phase is still mainly continuous as a result of severe by-passing due to the adverse mobility ratio. Therefore, while there is still a pressure drop existing in the system, some oil can still flow due to viscous forces (i.e. the relative permeability to oil is still high at high oil saturations). As the system pressure decreases, the effect of the viscous forces should diminish and oil production will decrease. The other mechanism responsible for oil recovery is that of capillary forces, where water imbibition occurs through water films thickening and relaxing very quickly. As these films thicken, they displace oil. The recovery due to capillary forces and film thickening can be significant, as shown in Figure 9.28, even at later times in the flood when the pressure gradient in the system is low.

Figure 9.29 plots the change in oil saturation due to water moving into pores.
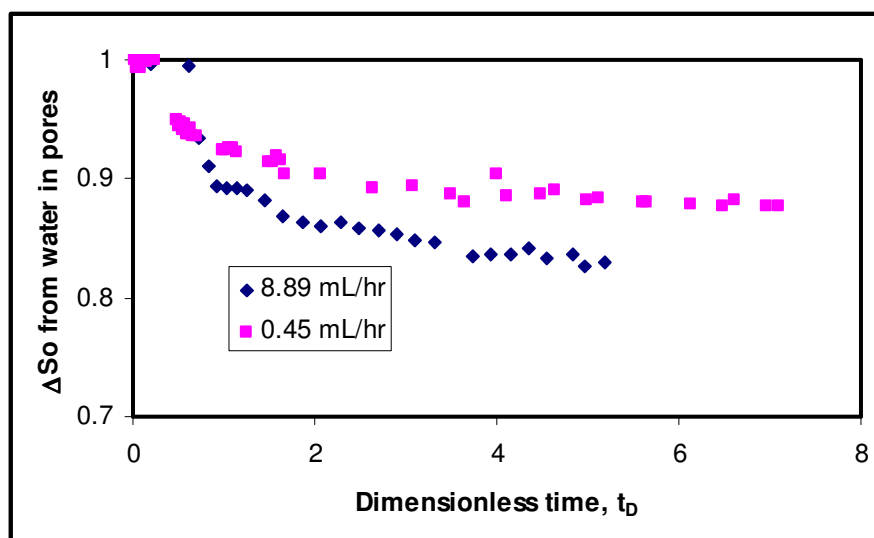
Figure 9.29: Recovery due to water displacing oil out of pores for fast and slow injection

The calculation for water saturation was shown previously (Eqn 9.8), and oil saturation is thus $(1 - S_w)$. The water saturation growth in pores comes from T_2 values after the first peak. Such values occur at similar relaxation times to that of the water-saturated core.

When oil saturation decreases in this range of T_2 values, this indicates that water is completely filling a pore, pushing oil out in a piston-like fashion. At a higher water injection rate, viscous forces are higher so more oil can be fully displaced out of pores, thus oil saturation is lower.

Figure 9.30 plots the change in oil saturation due to the thickening of water films. In this recovery mechanism, the water is still confined in pendular ring/thin film structures, which leads to water relaxation times that overlap with the viscous oil signal. These films swell or thicken, thus displacing a fraction of the oil out of the pores, but do not become continuous and block the oil.

The result from Figure 9.30 demonstrates that in this system, the change in oil and water saturation is due in a large part to water film thickening as opposed to frontal displacement of oil completely out of pores. In other words, water can travel beyond the actual water channels and displace oil in other portions of the porous medium through film thickening, instead of through a simple linear displacement mechanism. In higher viscosity oils, where linear displacement may be even more difficult, the effect of water film thickening may be even more important.
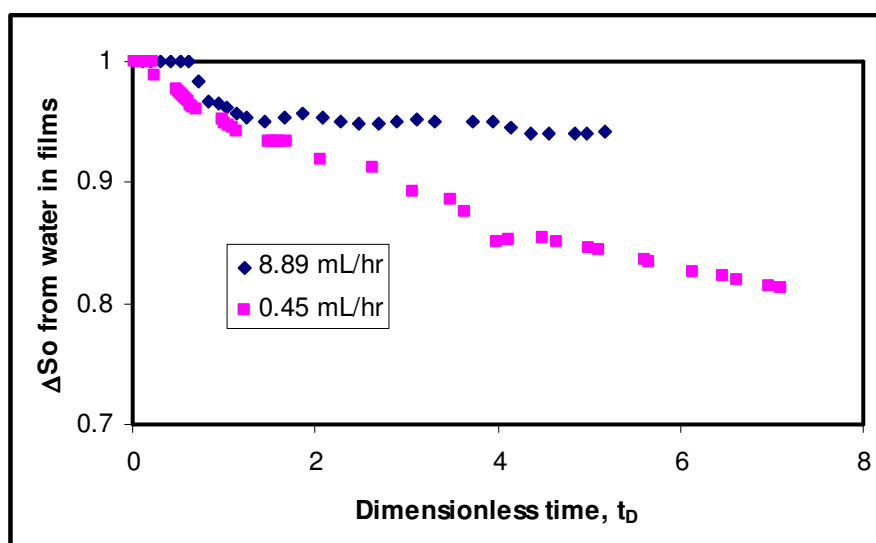
Figure 9.30: Oil recovery due to water film thickening for fast and slow injection

The result of Figure 9.30 could also be a possible explanation why in heavy oil systems, re-flooding with oil at the conclusion of a waterflood still led to a higher value of S_{wi} in the system. If some water had traveled into the porous medium through film thickening, this water will not be displaced in a secondary oil flood.

The results of Figures 9.29 and 9.30 can be better interpreted by separating the effects of early versus late times in the waterfloods. At early times (under 2 pore volumes injected), the efficiency of the oil recovery is affected strongly by viscous forces. As a result, the oil saturation decreases more sharply at the high injection rate. At these early times, the thickening of water films is similar in both systems. The response of the systems after water breakthrough is shown by considering the oil recovery efficiency after two pore volumes of water have been injected. Recovery efficiency is defined as:

$$RF\_Eff = \frac{dS_o}{dt_D}$$ Eqn (9.11)

Where RF_Eff = the efficiency of the waterflood

dS_o/dt_D = the slope of the oil saturation vs. dimensionless time plots.

The values of RF_Eff are shown in Table 9.3. It should be noted that since oil saturation is decreasing, the values are actually negative; RF_Eff in Table 9.3 is therefore the absolute value of the slopes.

Table 9.3: Recovery efficiency in high permeability core after water breakthrough

Injection velocity (m/d)	RF_Eff from water in pores	RF_Eff from water in films
0.021	0.0044	0.0206
0.42	0.011	0.0041

Table 9.3 shows that despite the fact that the injection velocity is 20 times faster at the high injection rate (i.e. viscous forces applied are 20 times greater), the efficiency of

water displacing oil out of complete pores is only approximately 2.5 times higher. This demonstrates the ineffectiveness of viscous forces after water breakthrough. In contrast, the efficiency of the oil recovery due to thickening of water films is approximately 5 times greater at the low injection rate. Overall, therefore, recovery will be higher at the lower injection rate. This proves the importance of capillary forces to heavy oil recovery by waterflooding. At late times in a flood, capillary forces are much more efficient that viscous forces.

9.4 NMR Waterfloods in Systems of Varying Permeability

Injecting water at low rates allows for capillary forces to improve the flood efficiency. However the time requirement for the project is now much longer. In this high permeability sandpacks used in Experiment # 21 and # 22, the pore sizes are relatively large so capillary forces will generally tend to be low. In order to examine the relative importance of capillary forces in lower permeability sand, the results of the previous core floods were compared against those obtained in a lower permeability core.

The core used in this experiment is an unconsolidated sand pack, which contains sand grains that are a sieved fraction (< 100 μm) of the sand used in the previous cores. The core has a diameter of 2.6 cm, a length of 53 cm, and a porosity of 0.41. The permeability of the sand is approximately 0.78 D. A low rate waterflood was carried out at an injection rate of 1 cm³/hr. For the smaller cross-sectional area of this core, this was equivalent to an injection velocity of 0.042 m/d, which is twice the velocity of the low rate waterflood in the 15 D core.

Figure 9.31 plots the oil recovery as a function of dimensionless time, which is analogous to the pore volumes of fluid injected as was previously discussed. As was also observed previously in Chapter 7, when waterfloods are performed in high versus low permeability cores the recovery will be better in the lower permeability system. When comparing the response from the two rates in the 15 D core, the lower injection rate performs better. In the 0.78D core, the oil recovery is the highest and the slope of the recovery profile is

similar to the low rate injection into the 15 D core, despite the fact that the injection velocity in this core is roughly twice the value of the injection velocity into the 15 D core. This improved recovery for the lower permeability sand is expected if imbibition is the mechanism responsible for oil recovery after water breakthrough occurs.
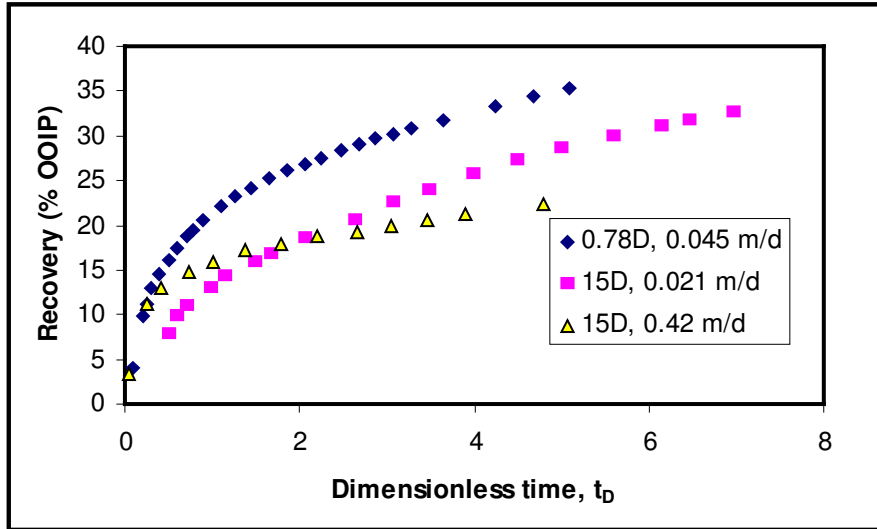
Figure 9.31: Recovery profile for waterfloods in systems of varying permeability

Since NMR spectra were obtained for the 0.78 D core as well, the spectra could once again be calibrated using the production data in order to calculate the oil saturation reduction due to water displacing oil in pores versus water film thickening. Figure 9.32 shows the oil recovery prediction due to the thickening of water films.
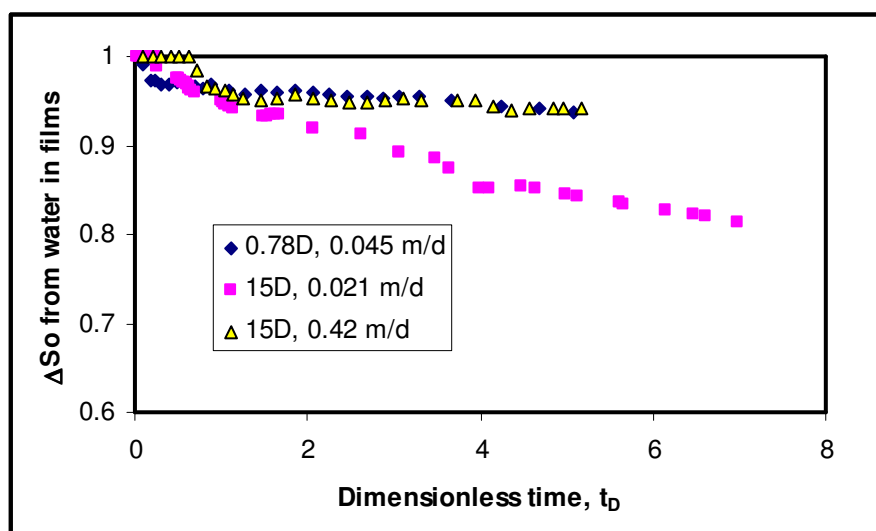
Figure 9.32: Oil recovery due to water film thickening in low and high permeability sand

Surprisingly, the oil recovered due to thickening of water films is small in the low permeability core, and in fact appears to be only slightly better than the response at high flow rates into the 15 D core. In contrast, the recovery due to water displacing oil completely out of pores is much higher in this system, as shown in Figure 9.33. The flow of water into pores is the dominant mechanism responsible for the higher recovery in the lower permeability core.
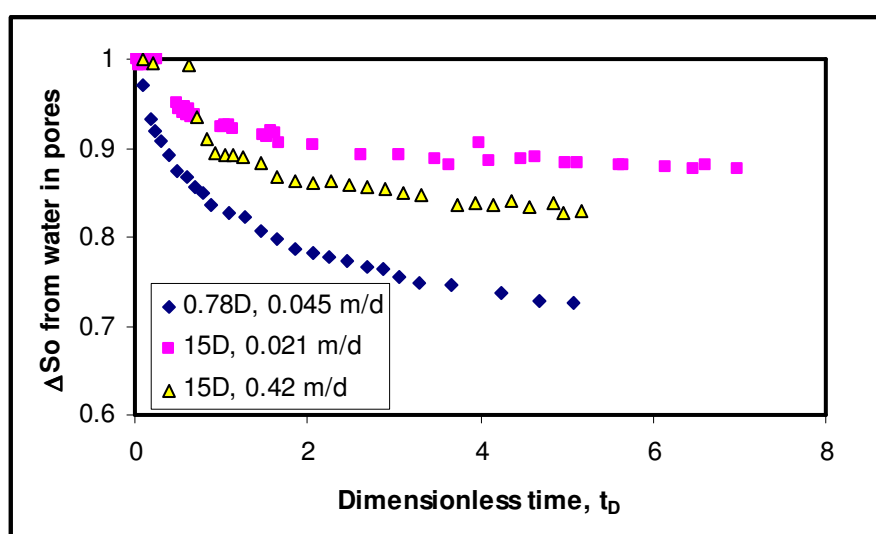
Figure 9.33: Recovery due to water displacing oil out of pores for low and high k sand

After two pore volumes of water injection, the recovery efficiency of the waterfloods in the three cores is shown in Table 9.4. This includes the data previously shown in Table 9.2, along with the recovery efficiency from water film thickening versus flow into pores for the 0.78 D core.

Table 9.4: Recovery efficiency in high permeability core after water breakthrough

Permeability (D)	Injection velocity (m/d)	RF_Eff from water in pores	RF_Eff from water in films	Total RF_Eff
15	0.021	0.0044	0.0206	0.025
15	0.42	0.011	0.0041	0.015
0.78	0.045	0.019	0.007	0.026

The results of efficiency in these three waterfloods can be compared against the relative magnitude of viscous and capillary forces. For the two permeability systems investigated, the Depuit-Forcheimer equation (Scheidegger, 1974) can be used to relative permeability to an average pore size. For the 15 D cores, this average pore size is approximately 19 µm, while the average pore size for the 0.78 D core is only 3.68 µm. Assuming similar wettability for sieved versus un-sieved sand, capillary forces are therefore inversely proportional to the average pore size. Therefore, the capillary forces in the 0.78 D system are approximately 5.1 times larger than for the 15 D cores.

Viscous forces are given by Darcy's law. Assuming that these forces are represented by the pressure gradient that can be developed in the system of identical oil viscosity, viscous forces can be represented in the following expression:

$$P_{visc} \propto \frac{\Delta P}{L} \propto \frac{\nu}{k} \qquad \qquad \text{Eqn (9.12)}$$

Where P_{visc} = viscous forces.

In the calculation of viscous forces, the units for velocity used were m/d, and darcies were used for rock permeability. The units are not important; once viscous forces are calculated for the three systems, the important parameter is the magnitude of these forces in relation to one another. Table 9.4 compare the relative magnitude of viscous and capillary forces to the ratio of the recovery due to water displacing oil out of pores versus through film thickening. These ratios are calculated using the RF_Eff values in Table 9.5.

Table 9.5: Magnitude of viscous and capillary forces and relation to recovery efficiency

	0.78 D core	15 D core low rate	15 D core high rate
P_c	5.1	1	1
P_{visc}	41	1	20
Velocity ratio	2.1	1	20
RF ratio from pores	4.3	1	2.5
RF ratio from films	1.6	5	1
P_c/P_{visc}	0.11	1	0.05

Due to the sizeable difference in permeability between the systems, although the flow rates are only twice the value of the low rate injection into the 15 D core, and only 10% of the high injection rate, the viscous forces in this system are the highest. Correspondingly, the recovery from water displacing oil fully out of pores is the highest in this system: the reduction in oil saturation in pores is 4.3 times the value in the 15 D core at low rates, and 2.5 times the efficiency of the high injection rate. This illustrates an important point regarding viscous forces in a heavy oil waterflood. Namely, although the results in the high permeability system show that capillary forces are a more important recovery mechanism, viscous forces cannot totally be neglected. If the magnitude of the viscous forces is increased, this will in turn lead to higher fraction of oil being fully displaced out of rock pores by water. However, this mechanism is extremely inefficient: by increasing the viscous forces by 20 times, the recovery efficiency from water in pores only improves by a factor of 2.5. Likewise, by increasing the viscous forces by 41 times, the oil displaced fully out of pores only increases by a factor of 4.3. The reason for this inefficiency is that once water has broken through to the production

end of the core, the majority of water cycles through these formed channels of water, and if a pressure gradient in the core cannot be sustained then it is difficult to push oil out of rock pores. The conclusion that can be reached from Figure 9.33 and Table 9.4 is that in lower permeability systems, where higher pressure gradients can be sustained, the displacement of oil by water is more linear. In higher permeability cores, film thickening may lead to oil production from regions that are not necessarily close to the water channels.

It is unexpected that although the relative magnitude of the capillary forces in the 0.78 D core have been increased by a factor of 5.1, the recovery of oil due to thickening of water films is still the highest in the low rate waterflood into the 15 D core. This can be understood by considering the ratio of capillary to viscous forces, shown in Table 9.4. Although the capillary forces are indeed higher in the lower permeability core, the competing viscous forces are also considerably higher as well. Therefore, the optimal recovery from water film thickening occurs for the low rate waterflood in the 15 D system, where the ratio of P_c/P_{visc} is the highest. At this improved ratio, less water is spent cycling through the waterflooded channels, and more time is provided for water to slowly imbibe into the porous medium.

In the lowest permeability core, the viscous forces can be used very effectively at early times to optimize the oil recovery. This is a faster process than imbibition, thus some oil can be recovered relatively quickly at first. Eventually, however, the pressure gradient in the system will decline, and additional application of high viscous forces will become extremely inefficient. At this point, it seems that the best approach to optimize production is to reduce the relative magnitude of the viscous forces in relation to the capillary forces, and allow imbibition to improve the oil recovery. While this will be a slow process, the potential exists for improved efficiency of the waterflood and a higher oil recovery at the economic limit of the flood.

CHAPTER 10: PROPOSED MECHANISM OF IMBIBITION

In the previous chapter it was established that imbibition exists during heavy oil waterflooding, and that water invasion through capillary-aided processes can improve the recovery of heavy oil during waterflooding. Chapter 9 showed evidence of imbibition occurring in both static and flowing conditions at the pore scale. The overall contribution of imbibition on oil recovery was also given, however the NMR investigation in small sandpacks could not describe the contribution of imbibition as a function of length. The information obtained from the previous corefloods in the NMR also do not provide insight into co-current or counter-current flow. This chapter addresses imbibition at a pore scale level. In order to explain the mechanism of imbibition during heavy oil waterflooding, several experiments were set up to illustrate the nature of imbibition along the length of the sandpack. CT data were collected at fast versus slow injection rates, in order to monitor the saturation change with length. NMR spectra were also interpreted, and provided a conceptualization into the pore sizes occupied by water at early and late times in a waterflood. Finally, the conventional definitions of co-current versus counter-current imbibition are explored, in terms of how they relate to the situation of heavy oil cores after water breakthrough.

10.1 Evidence of Imbibition along the Length of a Core

At the point of water breakthrough in a heavy oil waterflood, continuous channels of water are now present throughout the core. In other regions of the core, however, there has been essentially no water invasion and those rock pores are still saturated with oil and connate water. An analogy to this situation is that of flow in fractured reservoirs, where the rock matrix (containing oil and connate water) is surrounded by low resistance pathways of water in fractures. Interpretation of water imbibition from fractures has been presented in the literature (Pooladi-Darvish and Firoozabadi, 2000). In these systems, imbibition is thought to be counter-current, meaning that water enters from the fractures into the matrix and oil is expulsed back into the fracture system. In heavy oil waterfloods, where imbibition is important at low rates, it is necessary to establish the

direction of oil and water movement in the porous medium to see if this is a similar process to flow in fractured reservoirs. Ideally, experiments should be performed where oil and water flow could be visualized at a pore scale. However, it was not possible to achieve this while investigating the effects of global parameters such as injection rate and oil viscosity on recovery. While a micro-model study would provide this additional information, the results from the micro-model would then have to be extended to the core flooding results. An alternative approach that was used in this study was to perform core floods, but to use tomographic imaging tools (CT scanning and NMR) to acquire additional information about the flow behavior of oil and water in the rock pores.

Several experiments were set up to monitor the presence of oil and water along the length of the sandpack. These experiments were designed to shed more light into the nature of imbibition after water has broken through. In order to identify the effect of imbibition, the significance of viscous forces on the in-situ saturation profiles had to be identified and isolated. Detailed CT information was obtained for HO2 (11,500 mPa·s) for cases of fast and slow injection. The production results of these experiments were discussed earlier in Chapter 7. In this chapter, the analysis of the CT images is also included. It was necessary to perform a fast injection case to establish the behavior of a waterflood under the influence of high viscous forces. This was then compared against the improved recovery of a low rate waterflood. Since water was doped to provide a greater distinction between water and oil, CT scanning could be used to track the saturation changes. Thus, the saturation change along the length of the core could be observed. These results were also further validated by NMR data during low rate waterflooding of the same dead oil in a lower permeability sandpack.

10.1.1 CT monitoring of Fast and Slow Waterfloods

For both the high and low rate injection experiments, the sandpack was scanned dry, fully saturated with brine, at irreducible water saturation, and throughout the waterflood. CT images were obtained at the same location along the core at each saturation state, so that the contribution from the rock would be constant in each

subsequent scan. This meant that changes in the CT numbers were reflective of changes in the saturation of oil and water in the core. Scanning was performed more often at early times of the waterflood, where the process was dominated by viscous forces and water fingers were growing in the core. The cross-sectional images of the porous medium were processed and summarized for each slice at different times. The average value of CT number of each slice was also calculated.

Initially the CT numbers obtained on the dry core for both sandpacks are compared in Figure 10.1. This was done in order to establish that the sandpacks are similar for both waterfloods. Since a different sandpack was prepared for each experiment, an initial concern was that the differences between the cores could mask the true effect being studied, which in this case was the effect of injection rate on saturation profiles. Thus, it had to be ensured that the response measured was due to imbibition only, and not due to heterogeneity between sandpacks. For example, if one sandpack were tighter than the other, it could encourage more imbibition due to higher capillary forces. From Figure 10.1 it can be seen that the difference between the sandpacks are not significant. Even though the CT numbers are not uniform along the sandpack, the two sandpacks have the same trend of CTn variation. The maximum difference between the CTn values of the two cores is only 12 units, which corresponds to a density difference of 11 kg/m³ (using the correlation between CTn and density shown in Figure 4.9).

It could also be seen that the CT number along the sandpack is not uniform. This is due to the method of packing, which resulted in one end being more tightly packed than the other. This is reflected by the lower CTn at the inlet and higher CTn at the outlet. Although there appears to be a considerable difference in the CTn values along the length for each core, when this difference is converted to density units this is much less significant. The largest variation in CTn along the length of either core is only around 60 – 65 units, which corresponds to a density difference of only 58 kg/m³. Considering that sand has a density of 2650 kg/m³, a difference in density of 58 kg/m³, when converted to porosity, will lead to a maximum difference of 2% along the length of any one sandpack.
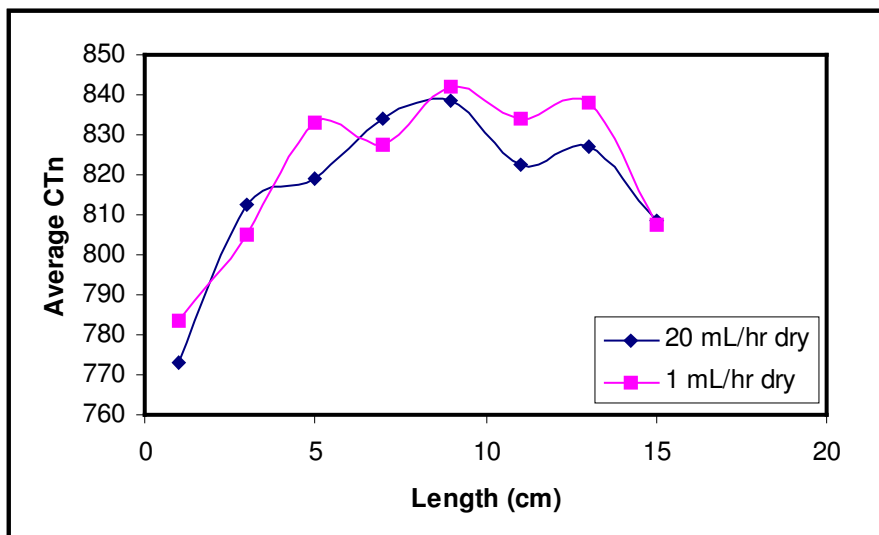
Figure 10.1: CT numbers of dry cores for different injection rate experiments

The goal for the CT scanning of the fast versus slow waterfloods was also not to measure the effect of imbibition along the length for a single waterflood, but rather to study the difference in behavior along the length between the two waterfloods of different rates. CTn is a reflection of density, thus even though the sandpack might not be uniform in length, the figure shows that the sandpacks prepared for fast and slow injection are similar.

The initial oil saturations for the two sandpacks are shown in Figure 10.2. Oil saturation was calculated using the CTn values of the core at several saturation states and the values of the bulk liquids, using the methods outlined by Kantzas (1990). Again, the trends along the length of the sandpacks are fairly similar, so both cores have similar porosity and fluid saturation with length.
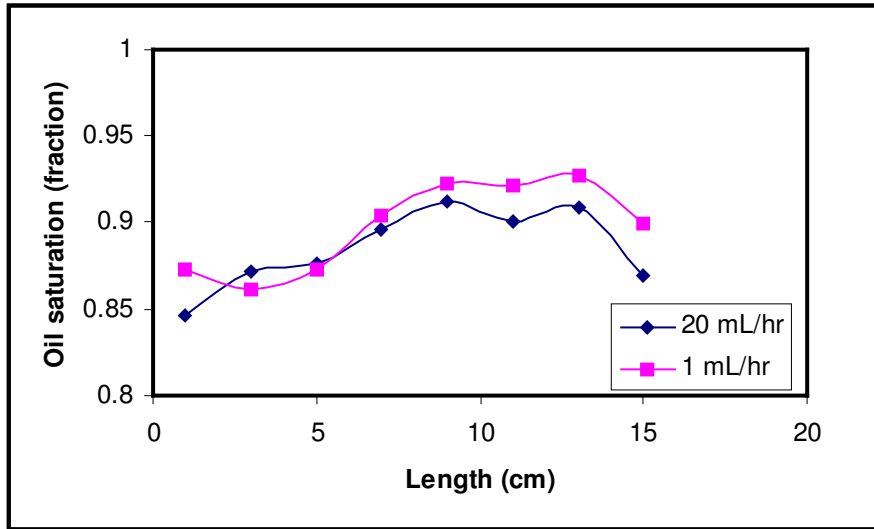
Figure 10.2: Oil saturation in the porous medium for both fast and slow injection cases prior to waterflood

There have been reports in the literature showing that the imbibition rate is a function of irreducible water saturation in the core (Li and Horne, 2002a; 2002b). Thus, Figure 10.2 was generated to show that not only is the initial oil saturation similar between the two systems, but that the distribution of irreducible water $(1 - S_{oi})$ is similar with length as well. The above exercises indicate that the sandpacks have relatively consistent pore structure, so any differences observed in their results during the waterfloods are due to rate variations rather than heterogeneity between different systems.

The CT numbers along the length of the sandpack, as the waterflood progressed for the fast injection rate, are shown in Figure 10.3. This figure shows that as the waterflood progressed, the average CT number in the core increased. In the porous medium the volume of oil displaced is equal to the volume of water replacing the oil. Since the doped brine has a significantly higher CT number than that of oil, the overall increase in CTn corresponds to higher water saturation in the core, which is a measure of the oil production.
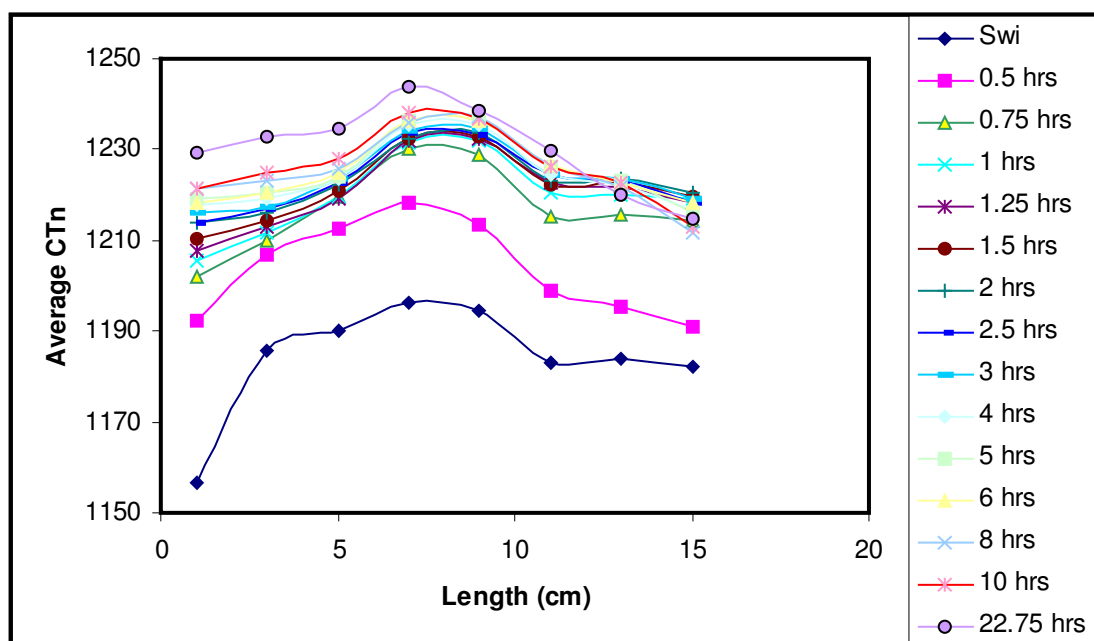
Figure 10.3: CTn changes in fast injection case

At the end of the waterflood, the oil saturation in the core could be calculated, again using the equations presented in the literature (Vinegar and Wellington, 1987; Kantzas, 1990). In Figure 10.4, the final oil saturation as a function of length in the core has been subtracted from the initial oil saturations for the fast injection rate in Figure 10.2. This is a representation of the change in oil saturation in the core due to high water injection rate.
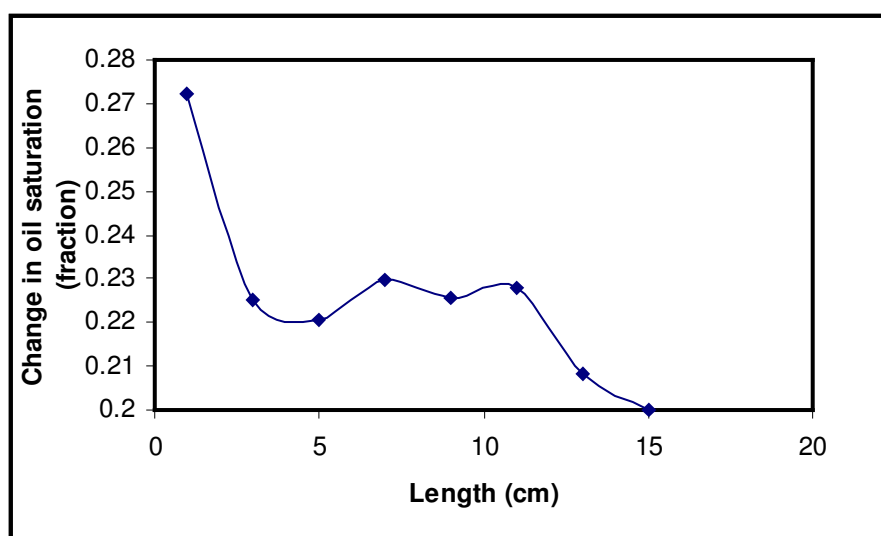
Figure 10.4: Change in oil saturation after waterflooding at a fast injection rate

Figure 10.4 shows that at early times the injected water swept a larger portion of the core close to the inlet, compared to the region of the core that is swept at the outlet. As shown previously in Chapter 7, high water injection rate is accompanied by a large buildup in the pressure of the core prior to water breakthrough. Due to the high pressure gradient developed in the core during this time, high oil rates can be achieved according to Darcy's Law. It seems that when this high pressure gradient is established, this leads to good oil recovery near to the entrance of the core, where water invades at early times. Additional water then fingers through the oil and breaks through to the production end. After this point, the waterflood is not efficient since at high injection rates, water simply travels through the low resistance water pathways, and not enough time is given for imbibition to occur. Therefore, the region close to the inlet of the core is swept to a greater extent than other sections of the core.

The oil recovered after breakthrough is the result of a portion of the injected water that was not flowing through the water channels, but rather was entering into the bypassed regions of the core and displacing heavy oil to the production end. Oil therefore could be recovered from two possible locations: in a two-phase region of intermediate oil and water saturation close to the water channel where both oil and water are mobile, or from core regions saturated with oil and S_{wi}. In Chapter 9, NMR spectra were used to show that some oil was recovered by water displacing oil fully out of pores, while other oil production was due to thickening water films, which expand and displace oil without first connecting and occupying the entire volume of a pore. In order to shed more light upon the difference between fast and slow injection rates, CT images were obtained as a function of both time and length for two displacement velocities: 20 cm³/hr and 1 cm³/hr. The water invasion profile for the high rate waterflood is shown in Figure 10.5.

In this figure, different cross-sectional slices along the length of the core are shown in each row. Different rows correspond to measurements taken at various times, from the condition of S_{wi} to the end of the waterflood. Images were always obtained at the same

location, so the effect of the sand density could be removed. The saturations in Figure 10.5 were obtained by comparing the change in density to the saturation change from the production data.

The CT images show that at the end of the waterflood, there is a higher water saturation region close to the inlet, and a smaller zone of high water saturation close to the outlet. This figure matches the overall water saturation trend in Figure 10.4, for which an average value was calculated for each cross-section. In general, for the fast injection case where viscous forces were used to recover oil faster but much less efficiently, generally oil recovery was better near to the inlet of the core. As time progressed in the waterflood, all cross sections show the same behaviour: there is a region of high water saturation (the red colour in Figure 10.5), surrounded by a small two-phase flow region of intermediate saturation (yellow), and outside of this region the core is mostly green, indicating low water saturation. Therefore, the high rate waterflood response is characterized by a channel of water surrounded mainly by un-swept oil. Most of the injected water is therefore passing through these water channels, and not contacting oil in the surrounding regions of the core. As a result, the oil saturation is not uniform with length, and overall the recovery is low.

It should be noted that the higher swept region close to the core did not correspond to improved final recovery in the core. As mentioned in Chapter 7, even the link between injection rate and breakthrough recovery is unclear due to the presence of viscous fingers that grow faster at higher injection rates. By comparing the results of this waterflood against the response to a waterflood at much lower rates, it can be seen that more oil is recovered in all portions of the core under lower injection rates.
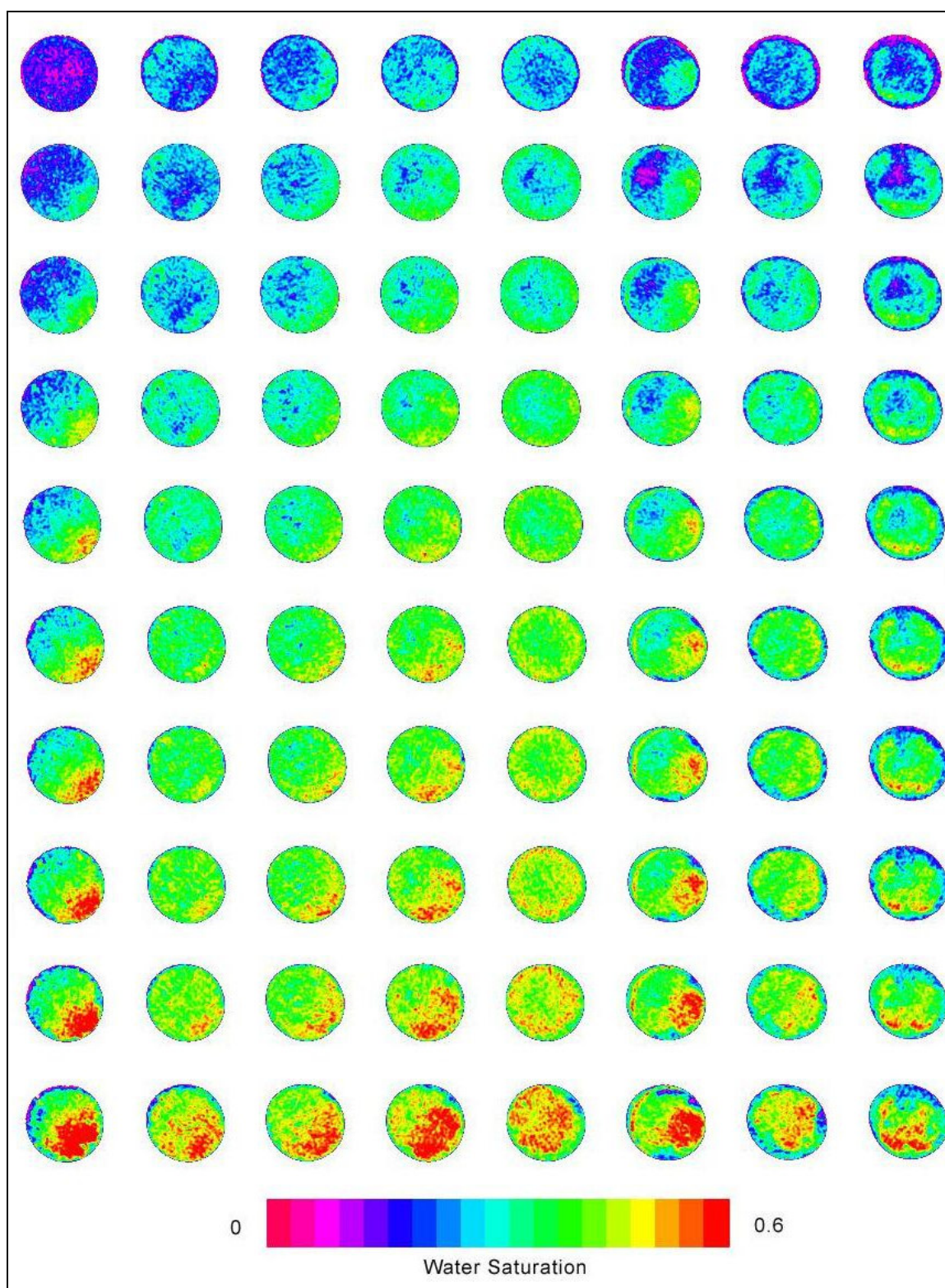
Figure 10.5: Water saturation profile in high rate dead oil waterflood

In order to understand the flood response under lower viscous forces, CT images were also taken at the same lengths for the slow injection rate waterflood (1 cm³/hr). The changes in CTn with time for this waterflood are shown in Figure 10.6.
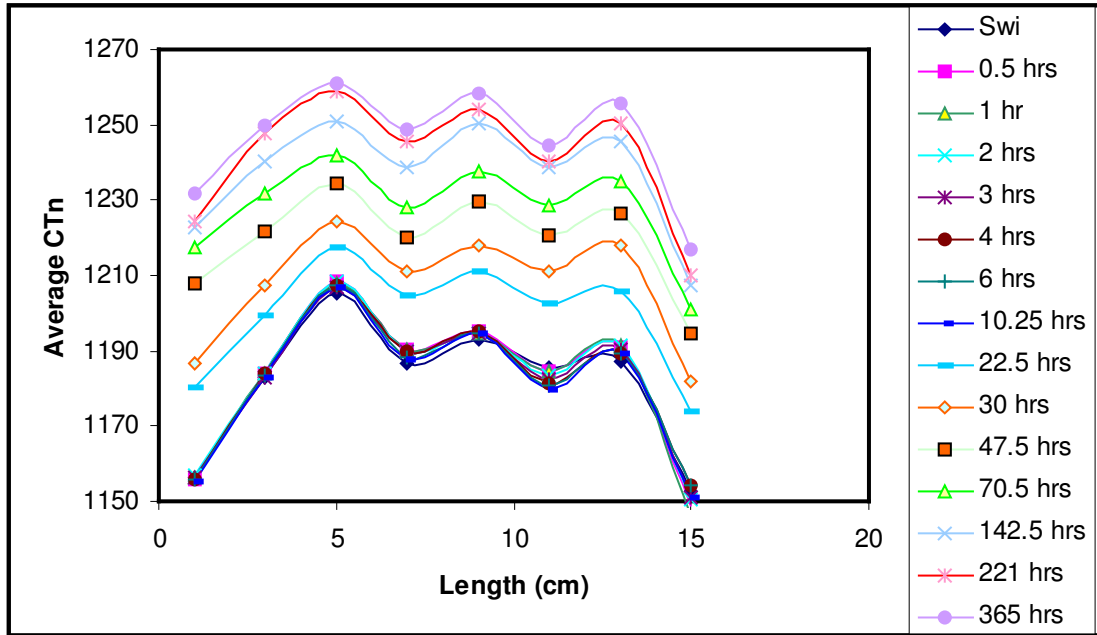
Figure 10.6: CTn changes in the core with time for low rate waterflooding

Once again, there is some variation in the CTn values with length in the core, but these differences are consistently present at all times. This figure shows a very different response, in that CTn increases steadily along the core length at all times, compared to Figure 10.3 where the differences appeared to be more significant near the core inlet. The CTn values were once again converted into water saturation, using the equations proved by Kantzas (1990). Figure 10.7 plots the change in water saturation with length between the core at S_{wi} and after 365 hrs of constant low rate injection, comparing the numbers against the saturation changes from Figure 10.4.
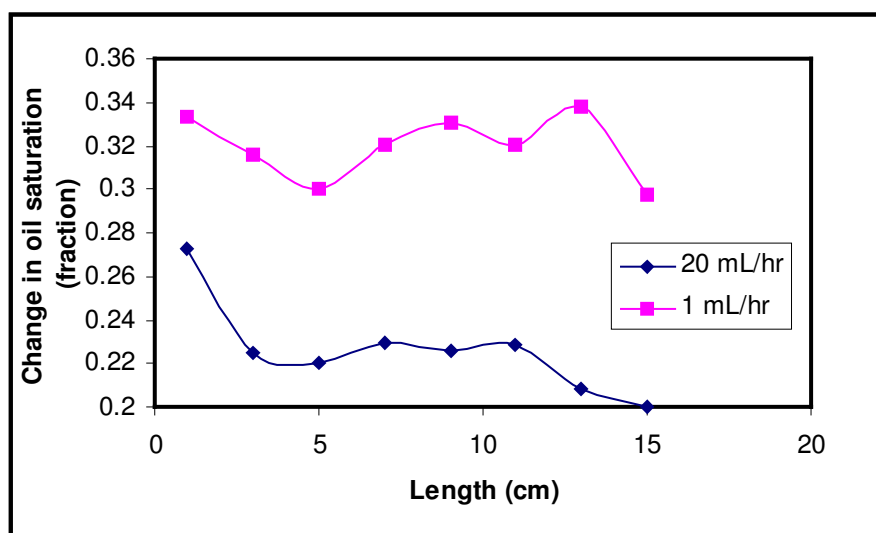
Figure 10.7: Changes in water saturation with length for high vs. low rate injection

A key difference in the low rate waterflood response was that the water swept the oil uniformly along the length of the sandpack. The injection rate for this case was $1/20^{th}$ of the fast injection case, thus the viscous forces were also reduced by a factor of 20. As can be seen the response to the varying injection rate is very distinctive. The difference in the two flood behaviors can be further understood by comparing these results to the NMR T_{2gm} values at fast and slow injection rates from Chapter 9. At the high injection rate, although water was injected more rapidly, there was a delay in the time for the water signal to increase in the pores of the sweet spot. At lower injection rates, with a smaller pressure gradient formed before breakthrough, less oil was displaced by viscous forces and a channel of water passed more quickly through the pores in the magnet sweet spot. Figure 10.7 also shows this same trend: with a higher injection rate the region in the first half of the core is swept more than the region close to the production end. At low rates, however, water simply moves through the core up to breakthrough, and then further recovery is obtained by imbibition into the by-passed oil zones.

The saturation profiles in Figure 10.7 also indicate that the pressure response in the core was most likely non-linear along the length at early times, at high injection rates. This is a property of viscous dead oil systems, where the oil cannot transmit pressure as quickly

as water, as shown in the expression for single-phase pressure diffusivity (Craft *et al.*, 1991). When water quickly enters the core, pressure in the water zone builds up quickly, while pressure ahead of the front increases more slowly. This leads to the higher water saturation close to the inlet of the core. At lower injection rates, the rate of pressure buildup is slower, allowing more time for pressure to be transmitted through the oil, so the pressure profile may be more linear in the core. Unfortunately, no attempt was made in this study to monitor pressure with length, so the relationship between the saturation profile and pressure could not be verified experimentally.

The effect of varying the injection rate serves to show a change in the relative significance of viscous forces, thereby increasing the effect of capillary forces. These two experiments have shown that when viscous forces dominated, aside from more oil being produced close to the inlet of the core, the majority of injected water after breakthrough simply channels through the water pathways, and the total recovery is poor. At low injection rates, alternatively, more time is provided for imbibition to occur. This leads to a more uniform increase in water saturation along the core length, and overall higher oil recovery.

Chapter 7 showed that even at low injection rates viscous forces still dominated production at the beginning of the waterflood, thus it was expected that at the early life of the flood more oil should be recovered from the inlet. However, this was not seen in Figure 10.6. Additionally, after water has broken through, water was consistently removing oil uniformly along the length. Thus, the pattern of sweep was fairly consistent throughout the flood, regardless of the stages of the waterflood. Figure 10.8 shows the CT images of the low rate waterflood as a function of time.
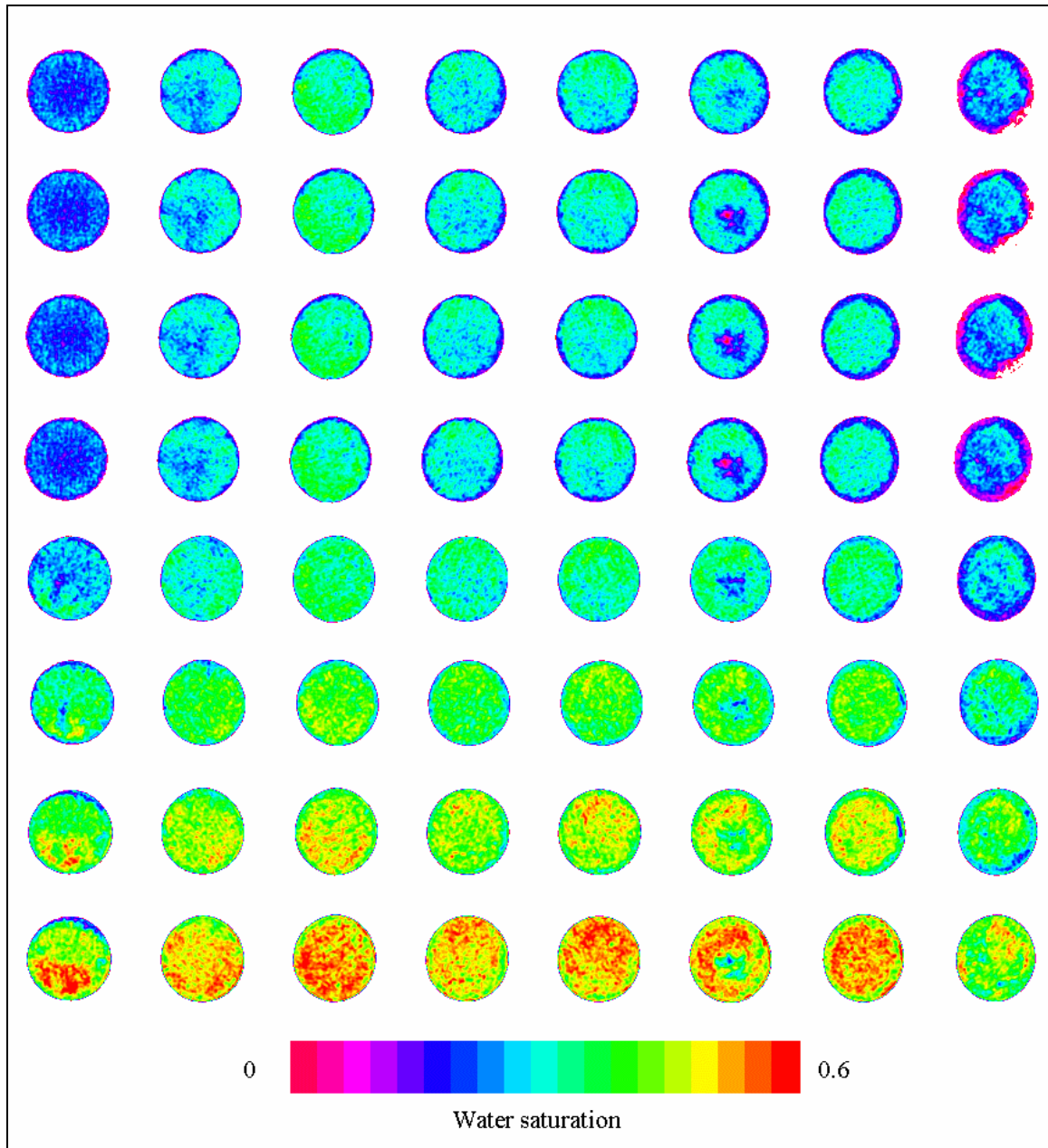
Figure 10.8: Water saturation profile in low rate dead oil waterflood

Again, the images in each row of Figure 10.8 correspond to cross-sections taken along the length of the core, from the inlet to the outlet. The different rows are scans taken at various times in the waterflood, from S_{wi} to the end of the flood. The major difference between the fast and slow waterfloods shown in Figures 10.5 and 10.8 is the generation of high water saturation regions in the core. Figure 10.5, which is for the high rate

waterflood, shows a region of high water saturation developing at a concentrated point in each core. Surrounding this is are zones of intermediate water saturation, and these are surrounded by the remaining core at higher oil saturation. In Figure 10.8, however, although the overall water saturation is higher, the region of intermediate water saturation (i.e. the yellow coloured sections) is consistent along the entire core, and this region grows with time everywhere along the core. Therefore, the location of the water in the sand appears to be quite different between the low and high rate injection cases. As opposed to fast injection, where channels of higher water saturation are surrounded by regions of high oil saturation, slow injection leads to a more even distribution of water everywhere in the core. This is due to a greater influence of capillary forces at low injection rates. This is also possibly an indication of higher oil recovery by film flow at the low injection rate, since water appeared to be recovering oil across the entire cross section of the core and not just close to the water channels. Water saturation and the in-situ location of water was also investigated using low field NMR, in order to provide further evidence of imbibition occurring at all lengths in the core.

10.1.2 NMR Monitoring of Slow Waterflood

In Chapter 9, an experiment was detailed whereby a low rate waterflood (1 cm³/hr, or 0.045 m/day) was performed in an unconsolidated sandpack with a permeability of around 0.78 D. The core holder used was made of PEEK, which does not interfere with magnetic fields and therefore allowed for NMR measurements to be made of the fluid inside the core. This core had a length of 53 cm, and NMR spectra were obtained at four fixed intervals along the core: length fractions of 0.09, 0.36, 0.65 and 0.78. The average water saturation in pores and films was calculated and the results were presented in Chapter 9. In this section, the spectra of the in-situ oil and water are interpreted for the different length fractions measured, in order to obtain additional information about the movement of water in the core from the injection end to the production end of the core.

Figure 10.9 shows the spectra at each of the four locations measured, while the core was fully saturated with water. In this state, the relaxation of water is dominated by surface relaxation, so the spectrum is analogous to a pore size distribution (Straley *et al.*, 1997; Coates *et al.*, 1999).
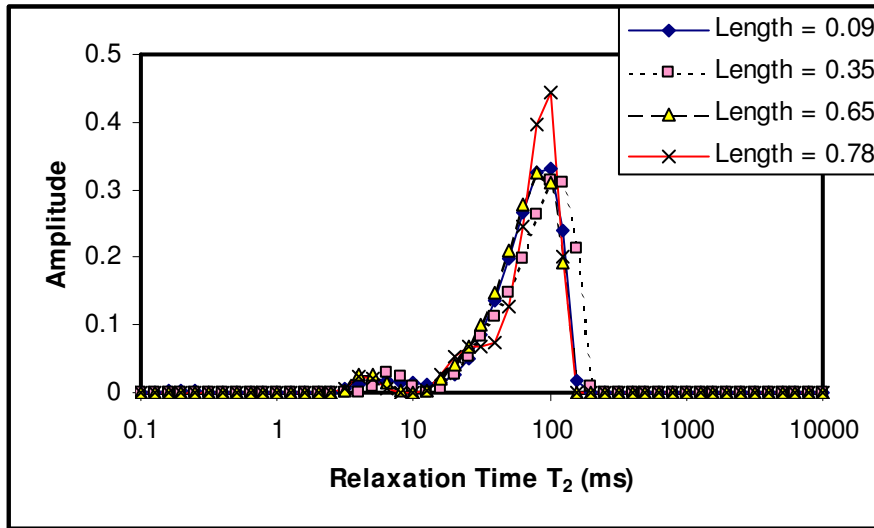
Figure 10.9: NMR spectra of the 0.78 D core fully saturated with water

Figure 10.9 shows that the water signal relaxes at essentially the same T_2 values for all four locations measured. This means that the pore sizes and the rock permeability are homogeneous with length along the core, thus any differences in the waterflood response with length would be due to the balance of viscous and capillary forces in the flood and would not be a property of the sandpack. The core was then flooded with HO2 (viscosity 11,500 mPa·s) to S_{wi}, followed by a low rate waterflood.

Water saturations were calculated from by comparing the NMR water amplitude in pores (after the first peak of the spectra) to the production data. The saturation predictions with length as the waterflood progressed are shown in Figure 10.10.
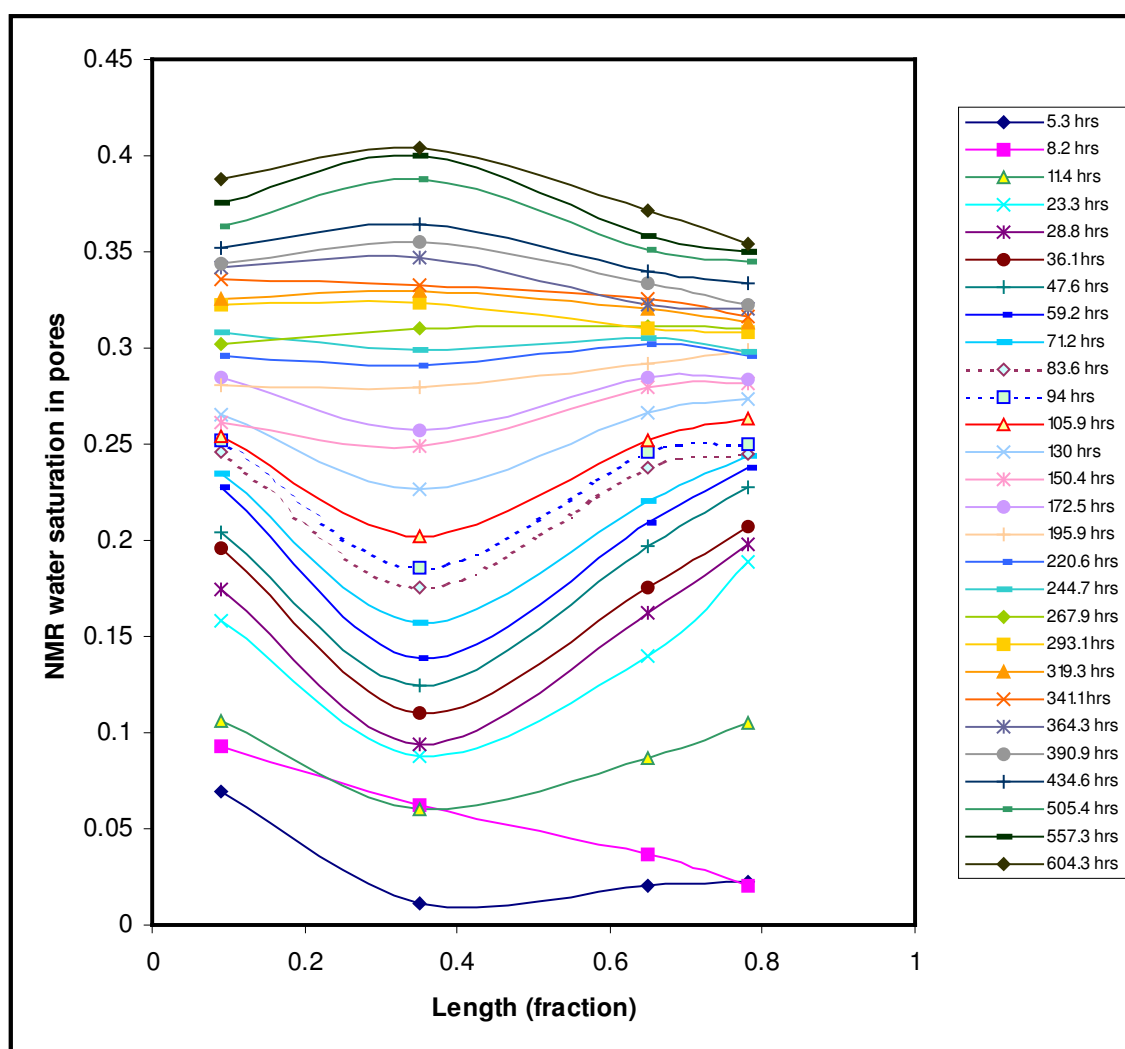
Figure 10.10: NMR water saturation in pores along the length of the core

At early times in the waterflood, before water broke through to the production end of the core, the pressure built up considerably, despite the low injection rate used. Using the definition of breakthrough defined in Chapter 7, breakthrough occurred after approximately 11.4 hrs. Observing the NMR spectra obtained prior to this time, when viscous forces (the pressure gradient) were dominant in the core, it could be seen that the recovery of oil varied with length, similar to the high rate injection into the higher permeability sandpack. In fact, as also observed in Figure 10.4, the water saturation was higher near the inlet of the core. After water breakthrough, the water saturation close to the outlet begins to increase. It is not clear why at early times the water saturation at a

length fraction of 0.36 is consistently lower than other sections in the core. However, over time the water saturation became uniform with length, and eventually water saturation rose uniformly everywhere in the core.

The NMR predictions of water saturation with length at late times in the flood match well with the trend shown using CT for the slow injection case. Under low rate waterflooding after water breakthrough, water is injected slowly enough that capillary imbibition of water can occur into the by-passed oil zones in the core. The NMR experiment therefore shows that with the dominance of viscous forces, oil is recovered close to the inlet, so the pressure distribution is once again likely not to be linear with length. Eventually, however, capillary forces allow oil to be recovered along the entire length of the core, and this leads to overall recovery of oil, as shown by the increasing water saturation all along the length of the core with the passing of time.

Figure 10.11 shows the geometric mean relaxation time of water in the core as a function of time. Water spectra were actually acquired at four lengths along the core, and the values for each of the four lengths have been averaged to give one total value of water T_{2gm} at any given time. This approach is valid since the NMR spectra show that after early times, water is displacing oil all along the length of the core, thus the water T_{2gm} can be represented as a mean of the four measurements. The dashed line at approximately 50 ms represents the T_{2gm} of the pores when the core was fully saturated with water. Since the relaxation times of water in porous media are controlled by surface relaxation, the water T_{2gm} is a measure of the average pore size occupied by water in the core.

Initially, when the core contains oil at irreducible water, water was displaced out of the large pores by the non-wetting oil phase. Therefore, the remaining water signal is found in films within the first peak, and a few by-passed larger pores. Once waterflooding began, water moved through the path of lowest resistance, displacing a fraction of oil out of large pores where the viscous pressure gradient required for the oil to flow was lowest. The water T_{2gm} values therefore quickly increased during this time. Additionally, a

portion of the water was traveling through connecting films to increase the thickness of water films. At later times, when imbibition is the main mechanism causing displacement of oil, the water T_{2gm} values change less sharply, and eventually even level out just above 40 ms.
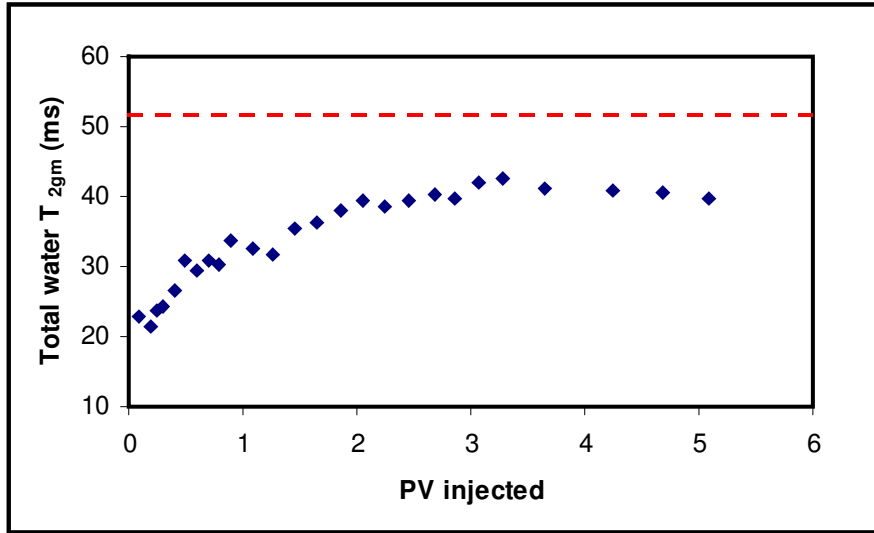
Figure 10.11: Average water T_{2gm} with time for the 0.78 D core

The final water T_{2gm} values contain the contribution of both water in pores (at 50 ms) and water in films (with T_{2gm} values under 10 ms). The fact that the total water T_{2gm} is still less than the T_{2gm} of the water saturated pores therefore shows the influence of enhanced surface relaxation of water in films. The T_{2gm} values in Figure 10.11 include the contribution of the geometric mean relaxation of water both within the first peak and at later T_2 values. For the water amplitude within the first peak, the actual water T_{2gm} is not known, therefore the film T_{2gm} was taken to be the mean relaxation time of the first peak. The T_{2gm} of water after the first peak could be calculated directly. The total water T_{2gm} is the logarithmically weighted average of the water T_{2gm} after the first peak and the water T_{2gm} within the first peak, where both T_{2gm} values are weighted by the amplitude fraction in the pores and films, respectively.

If the water film contribution were not considered, the water T_{2gm} is simply the mean relaxation time for the entire signal after the first peak. This is the mean relaxation time for water in pores alone. This value, denoted as "no films", is compared against the complete water T_{2gm} in Figure 10.12.
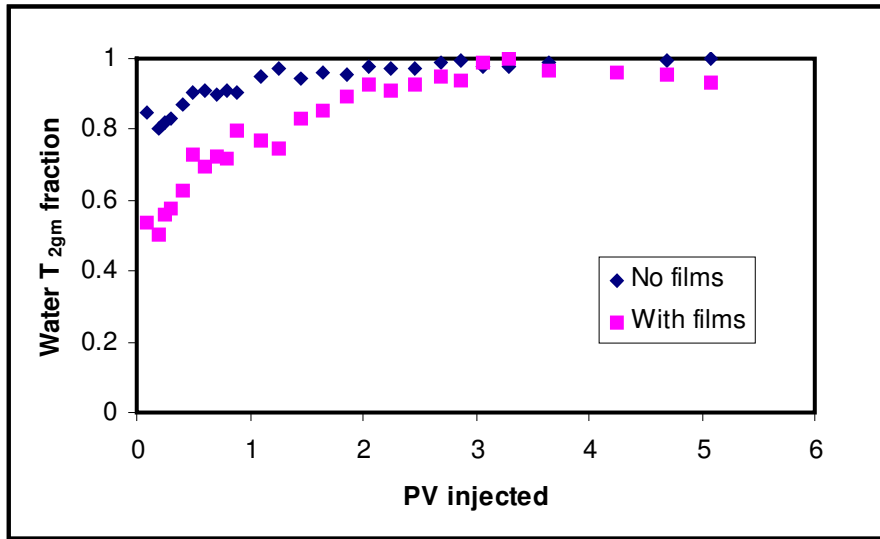
Figure 10.12: Change in total water T_{2gm} and water T_{2gm} in pores during a waterflood

The T_{2gm} fractions plotted in Figure 10.12 are the water values, with and without the effect of water in films, normalized to the maximum T_{2gm} for each case. It can be seen that if the water in films is neglected, the water T_{2gm} quickly increases, and by 1 PV injected the values are already essentially at their final relaxation time. This shows that in a heavy oil waterflood, water very quickly moves through the low resistance (i.e. the most permeable) pathways, so after injection of just over 1 PV the water signal in the pores is a constant. Despite the fact that the core is water wet, the high oil viscosity forces the water to enter the larges pores first, which is the drainage pathway. After breakthrough water channels are already present, whereby water is fully occupying some of the pores. During later injection, a significant portion of water will continue to flow through these channels and the water relaxation times are essentially constant. By including the water in films, the water T_{2gm} values do not approach their final value until after 2 PVs of water have been injected. This shows that if all the water is considered

and not just the water that fully displaced oil out of pores, the water is actually moving through small surface-to-volume pathways as well as through pores. This is the contribution of water film thickening, which has been shown to be responsible for additional oil production.

The results from the NMR measurements of the low rate waterflood therefore reveal several important findings. First, as also shown in the CT measurements of low rate waterflooding, imbibition recovers oil all along the length of the core. Second, during the waterflood a portion of the water initially travels through low resistance pathways, and completely displaces oil out of these pores. In this manner, the waterflood is behaving almost like a drainage process. However, as a result of imbibition, a portion of the water is also displacing oil through movement in films, and overall the water T_{2gm} values are faster than those of the fully saturated core. Finally, the total water T_{2gm} is consistently lower than the water-saturated core, meaning that the core is still water wet and the viscous heavy oil did not adsorb and alter the wettability of the sand.

10.2 Definition of Imbibition in Heavy Oil Waterflood

It was previously established that imbibition is strongly evident in slow water injection situations. A remaining question, however, is whether imbibition occurs in a co-current or a counter-current fashion. Before this could be explored, it is necessary to first examine the conventional notation for the different imbibition mechanisms.

All conventional imbibition experiments detailed in the literature involve a static condition where a wetting fluid (water) is introduced to the surrounding environment of the porous medium that is saturated with another non-wetting fluid (oil). Water will imbibe due to the wetting preference of the solid and the higher capillary forces in small pores in the rock. In this process, only oil will be produced. The production of oil is monitored as time elapses, and the process is continued until no more oil is produced. This is the mechanism of spontaneous imbibition, and co-current versus counter-current

imbibition refers to the difference in the direction of the oil production relative to the direction of brine movement.

The main difference between counter-current and co-current imbibition is that in counter-current imbibition oil is produced at the same face as the water contact, while in co-current imbibition oil is produced from a different face. Even when oil is produced counter-current to the water, at the pore scale level the fluids are not necessary flowing in the same pore space. Counter-current imbibition does not mean that water will imbibe into the pores as films while oil is expulsed through the middle of the pores. In fact, during counter-current imbibition water may enter through small pores while oil is produced out of continuous larger pores, but the production is collected at the water injection face instead of the other end of the core. Therefore, co-current and counter-current imbibition are macroscopic phenomena; the pore scale mechanism of water imbibition is the same for both processes. The only difference is in the boundary conditions applied that allow for oil to be produced at either face of the core.

As previously discussed in Chapter 3, the study of conventional imbibition was designed to investigate the nature of how these processes will occur in highly fractured reservoirs, where the network of fractures is interconnected. The assumption was that the injected water would immediately occupy the high permeability fractures, and from this location water would then imbibe into the porous medium and displace equal volumes of oil back into these fractures counter-currently. Once oil is in the fracture system, the large sizes of rock fractures means that capillary pressure is essentially negligible and oil may be produced either as a continuous or discontinuous phase through viscous or gravity flow mechanisms. There is no capillary trapping of discontinuous oil droplets in fractures.

In gas-free heavy oil systems, water breakthrough occurs early due to viscous fingering, which leads to a significant portion of by-passed oil still remaining in the porous medium. As noted earlier, the nature of formation of fingers depends on factors such as injection rate, the dimensions of the porous medium and the viscosity ratio between oil

and water. Of these parameters, the injection rate is the only parameter that is controllable in the design of a waterflood. Generally, higher injection rates will result in highly unstable flood fronts, which lead to the formation of multiple small-width viscous fingers. Regardless of the injection rate, after water had broken through, these viscous fingers form paths of low resistance that allow for further injected water to channel through to the outlet.

When comparing the conditions between conventional imbibition and the slow injection rate in heavy oil waterflooding, there are various similarities and differences. In the conventional case water is provided by the fractures and moves into the rock matrix, whereas in a heavy oil waterflood water is supplied by the water channels and may also move into the previously un-swept regions of the core. In this manner, the water channels act like fractures, from which further injected water may enter into the sand perpendicular to the channels. However, the difference between these two scenarios is that water in fractures has unlimited mobility, thus any oil that is expulsed into the fractures due to counter-current imbibition can then be produced without any additional capillary trapping of discontinuous droplets. However, in heavy oil waterflooding the channels themselves are not occupied solely with water; some residual oil still exists in the channels. Additionally, the water channels still consist of pores in unconsolidated sand, as opposed to open fractures. Therefore, if oil is expulsed counter-currently into the channels it would be more difficult to produce this oil than in a fractured rock system. This key difference between flow in fractures and flow in water channels in a sandpack allow for several mechanisms to be proposed regarding how imbibition occurs in heavy oil reservoirs.

10.3 Proposed Mechanism of Imbibition

The pressure data collected during the low rate waterfloods showed that for low injection rates of water, the water carried very little pressure in order to flow through the water channels that had developed. However, while the pressure of the water phase is low, the pressure of the bypassed non-wetting oil will be higher due to the presence of

capillary pressure between the water and oil. Within the water channels, where some oil still exists, the pressure of both oil and water might be small since in these channels the water saturation is high. In the bypassed oil region, however, the water saturation is likely to be small and close to the irreducible saturation, due to the inability of water to sweep this zone. At close to irreducible water saturation, the capillary pressure should be very high (see capillary curve in Figure 3.7). Thus one could expect the pressure of oil and water to be quite similar within the water zones, while the pressure of oil and water could be considerably different in bypassed regions of the core.

It must be noted that the pressure of the water phase is not uniform throughout the channel, since there is a pressure drop induced along the length to facilitate water flow through viscous forces. The pressure gradient is very low at late times in a waterflood, but it should be noted that a gradient always exists. Within the bypassed oil, a simplifying assumption is that the capillary pressure could be consistent, but even with this assumption the oil pressure will vary with length. Since $P_c = P_o - P_w$, the pressure of the oil phase (bypassed oil) is not consistent along the length, and will be higher where the water pressure is correspondingly smaller. Additionally, since viscous fingers follow tortuous pathways through the core, the pressure of the oil phase in different regions of the core is difficult to determine. For conventional imbibition, the boundary conditions are strictly defined, thus a distinctive solution could be obtained. However, in heavy oil waterfloods the boundary condition could not be established due to the complicated nature of the viscous fingers. Overall, this means that the pressure distributions developed in a heavy oil core do not resemble either of the pressure profiles of conventional co-current and counter-current imbibition.

Despite the fact that a simple analytical expression cannot be developed, it can still be concluded that water will experience a pressure imbalance between the water in the viscous finger or water channels and the water in the bypassed regions of the core. The unbalance in pressure will advocate water to be imbibed into the oil region, and the possible directions for water imbibition are shown in Figure 10.13. This figure is a

simple schematic; in reality the viscous fingers are much more complex, as shown in the previous CT images (Figures 10.5 and 10.8).
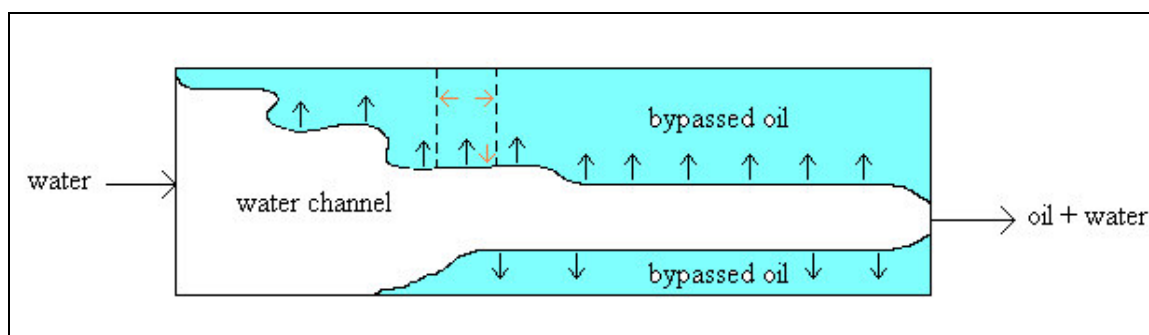
Figure 10.13: Schematic of possible mechanism of imbibition after breakthrough

It is quite simple to predict the direction of brine imbibition (i.e. perpendicular to the water channels), but the behavior of oil is much more complicated to postulate. In conventional imbibition, if both water and oil enter and exit at the same face of the core, this is defined as counter-current imbibition. Likewise, if water enters at one location and oil exits elsewhere then co-current imbibition is said to have occurred. In the situation shown in Figure 10.13, as the water imbibes into the oil region, the oil must be displaced out of the pores into which water is entering. Considering a small slice of the sandpack shown by the dashed lines, the possible directions of oil flow are illustrated by the orange arrows in Figure 10.13. Due to the fact that there is still a pressure drop imposed along the length of the sandpack, with the highest pressure at the inlet, it is not possible for the oil to travel back toward the inlet. This leaves two possibilities: the oil could be expulsed back into the water channels, or oil could instead move further along the length of the sandpack in the direction of the pressure gradient in the core.

If the oil is expelled back into the water stream then the mechanism can be considered to be counter-current imbibition, since water and oil would be traveling in opposite directions at the edge of the water channel. In order for oil to be produced counter-currently, the oil expulsed must form a continuous path within the water channel, since failure to do so would form blockages to flow. If the oil existed in the water channel as

isolated droplets, it would require a significant pressure drop to mobilize and produce this oil. This is called the Jamin effect and is caused by the fact that the radius of curvature of a droplet entering a pore throat is smaller than that of the droplet in a pore body (McAuliffe, 1973), thus the pressure required to force the droplet through the pore throat must exceed this capillary pressure differential. The result of this differential pressure is that oil is trapped in conventional oil waterflooding, and these discontinuous oil ganglia are the targets for enhanced oil recovery. In heavy oil applications, the same forces would also trap oil droplets that approached the size of the pore throats.

For this sand and fluid systems, calculations of the Jamin pressure drop are shown in Appendix H. For an oil droplet the size of a single pore, a pressure of 21,600 kPa/m (950 psi/ft) is required to mobilize the droplet. This pressure is prohibitively high, and if the differential in capillary pressure could not be overcome, this leads to blockages of water pathways that will result in pressure building up at the inlet. During the waterfloods, however, no pressure buildup was observed although oil was continuously produced. From this it is possible to infer that the oil produced must be continuous within the channels or the oil droplets must be sufficiently small enough to be entrained within the water fingers (which is unlikely in an immiscible fluid system). Therefore, if counter-current imbibition is occurring, this will be evidenced by regions of two phase saturation, where water has entered the bypassed regions from the high water saturation channels, and oil has been expulsed backward into these two-phase zones where both oil and water can flow.

The CT images in Figures 10.5 and 10.8 both show that during waterfloods small channels of high water saturation develop along the core. Surrounding these channels are regions of intermediate oil and water saturation, and surrounding these regions is the remaining portion of the core, which contains oil and S_{wi}. These images follow the saturation profiles that would be observed if counter-current imbibition were occurring. If water were to enter the rock pores perpendicular to the water channel and push oil co-currently out of these pores, the CT images would show a region of high water saturation

that grows with time, surrounded by regions of high oil saturation. In contrast, the process of counter-current imbibition would allow for two-phase flow of oil and water, so long as the oil is traveling in its own channels so that there is no trapping of discontinuous oil droplets. This is what was observed in Figures 10.5 and 10.8, therefore it can be inferred that imbibition is at least partially a counter-current process.

If both water and oil exist as continuous phases within the two-phase flow pathways, this means that the pressure drop exerted over the length of the sandpack is also the pressure drop provided for both oil and water to flow through viscous forces in these channels. Thus, from Darcy's law of multiphase flow, the equations for the oil and water phase can be shown as:

$$\frac{Q_o}{A} = \frac{k_{ro}k}{\mu_o}\frac{\Delta P_o}{L}$$
Eqn. (10.1)

$$\frac{Q_w}{A} = \frac{k_{rw}k}{\mu_w}\frac{\Delta P_w}{L}$$
Eqn. (10.2)

In this case, the pressure gradient in each phase is the viscous pressure drop applied through the water at the injection face, thus flow of oil and water occurs through viscous forces and $\Delta P_o = \Delta P_w$. With oil viscosity being 11,500 times that of water, the oil production should be at most 1/11,500 compared to water production rate. This already makes the assumption of equal relative permeability, even though the water saturation is higher in the water channels so it is expected that relative permeability should be lower for the oil. However, as shown by the higher oil cuts in the produced fluid streams (1 – 3% of the total fluid), oil is produced at a higher rate than what is predicted through relative permeability equations.

Viscous coupling has often been cited as a method in which the oil flow rate could be greater than that of water. Viscous coupling is a lubrication effect, which requires oil and water to flow in the same pore. In the case of low S_w and a water film present between

oil and the pore walls, water may be flowing only in the form of thick films (Dullien, 1992). In this state, water is hydraulically connected to oil that is flowing in the center of the pores, and the consequence is that the oil may experience an apparent slip. Dullien (1992) showed that in the case of capillary tubes containing water films and viscous oil, water only flows as films.

In the case of hydraulic slip, the effective oil viscosity is now less than what would be predicted by Hagen-Poiseuille flow. Relative permeability equations would no longer be valid since now oil and water are flowing in the same channels. However, if these equations are used anyway with the actual oil viscosity instead of its lower effective value, then the reduced oil viscosity effect is instead transferred to the relative permeability term. In the case of viscous oil, k_{ro} may be as high as a factor of close to 10 (Dullien, 1992), which would lead to higher oil cuts in the produced fluids. Even with this being the case, however, this would only increase the ratio of the flow of oil to water by a factor of 10/11,500. This is still not enough to explain the higher oil cuts seen in the waterfloods. Thus, viscous coupling might not be possible to produce oil at an oil cut of a few percent, as seen in the experiments.

An alternative imbibition mechanism is that as water enters a rock pore, it displaces heavy oil out of that pore and into a neighboring oil-continuous pore. An equivalent oil volume is then transferred into the next pore, and this is repeated along the entire length of the core. This would be true whether the oil volume is transferred into the oil channels in the two-phase region, or remains in the portions of the core that contain oil and S_{wi}. In either case, the driving force for the oil volume displacement was that of capillary pressure, as opposed to viscous flow of oil. This would be the same for the situation of water films thickening, and thus squeezing equivalent volumes of oil out of the pores. This mechanism can be called co-current imbibition for lack of a better term to describe the oil flow that is not counter-current.

The imbibition is not strictly co-current since the water and oil do not move in the same direction. Rather, water enters the core perpendicular to the water channel and oil is displaced lengthwise along the core to the outlet. In this situation, oil is not moving in opposite direction to water, which is the difference between this and counter-current imbibition. Unlike in conventional co-current imbibition, due to the boundary condition of flow at the outlet (thus, $P_o = 0$ at the outlet), the pressure of the oil is higher at the inlet (due to capillary pressure). This induces an additional pressure drop, which adds to the viscous pressure drop and ultimately increases the oil production rate, as was also shown by Pooladi-Darvish and Firoozabadi (2000).

Figure 10.14 shows the situation of water displacing heavy oil in a single capillary tube. In this situation, water is the wetting phase, and water is injected at a constant pressure, P_{w1} into a capillary tube of radius r.
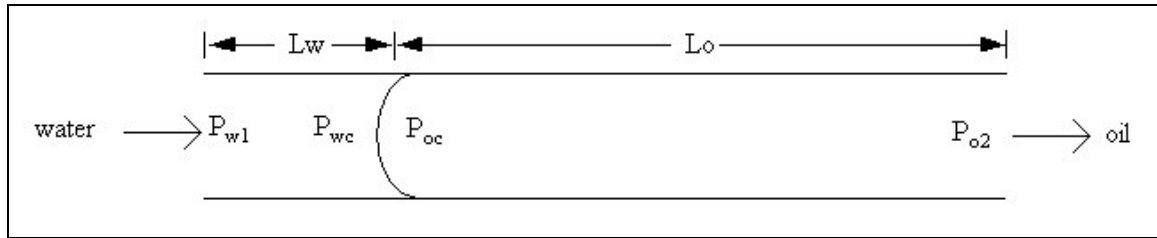
Figure 10.14: Schematic of water displacing oil in a single capillary tube

The pressure drop in this capillary tube is the sum of the viscous pressure drops in the water and oil phases and the capillary pressure difference across the oil-water interface. These can be shown in the following equations:

$$\Delta P_{total} = P_{w1} - P_{o2} = (P_{o1} - P_{wc}) - (P_{oc} - P_{wc}) + (P_{oc} - P_{o2}) \qquad \text{Eqn (10.3)}$$

$$\Delta P_{total} = \frac{8Q\mu_w L_w}{\pi r^4} - \frac{2\sigma \cos\theta}{r} + \frac{8Q\mu_o L_o}{\pi r^4} \qquad \text{Eqn (10.4)}$$

The inclusion of capillary pressure means that the total pressure required to flow oil and water at a fixed rate is less than the simple sum of the viscous pressure drop in each fluid. In co-current imbibition, therefore, the pressure requirement for oil to flow at a given rate is reduced. Of course, in a single capillary tube or pore channel containing viscous heavy oil, the pressure required for oil to flow will still be extremely high, and the effect of capillary forces will be small. However, across the core there are many pore channels present and flow in each pore will be enhanced by this same way. Naturally, this proposed mechanism is a simplification of actual conditions, since it does not consider differences in capillary pressure between pore bodies and pore throats. However, Eqn (10.3) and (10.4) show that co-current imbibition can also be used to explain the fact that oil rates are higher than what is predicted through Darcy's Law and relative permeability.

Ordinarily the pressure information collected in an experiment could be used to assist in the process of identifying the imbibition mechanism as being co-current versus counter-current (Pooladi-Darvish and Firoozabadi, 2000). This is due to the fact that co- and counter-imbibition can have very distinctive pressure profiles. However, the nature of imbibition in heavy oil waterflood is more complicated than in conventional spontaneous imbibition situations. An additional complication in this situation is that there is a pressure drop induced to allow water to be injected, thus the viscous and capillary terms would have to be properly distinguished and this is not trivial. Thus, from the pressure data collected, the only conclusion that could be made is that the systems were not blocked by discontinuous oil droplets in water channels since there was no pressure buildup required to produce the oil after water breakthrough.

From this discussion it could be seen that the actual phenomenon of imbibition in heavy oil waterflood cannot be represented by the conventional definition of imbibition. Also, the mechanisms involved in slow heavy oil waterfloods likely include a combination of both co-current and counter-current imbibition, working together to produce the oil.

10.4 Discussion

This chapter focused on developing a pore level understanding of the mechanisms by which imbibition is occurring in heavy oil waterfloods. By investigating the difference in the CT water saturation profiles with length under fast versus slow injection, the influence of viscous forces on recovery was observed. Under high rate waterflooding, oil cannot flow out as quickly as water is injected. Therefore, water collects near to the inlet and high pressure gradients develop across the core. This leads to higher water saturations at the inlet of the core. Water then breaks through as a result of severe viscous fingering, and under high rate injection experiments are performed quickly, thus there is no time for imbibition to occur. The result is a poor overall recovery from waterflooding. Under low rate injection, more time is provided for imbibition to occur, and the result is water saturation increasing along the entire length of the core, and higher overall recoveries. CT images for high rate injection show a finger of high water saturation, surrounded by a small region of intermediate saturations, and bypassed oil in other regions of the core. In a low rate waterflood, the high saturation finger is reduced, and the intermediate saturation region where two-phase flow is possible is considerably larger in all cross-sections of the core.

The NMR investigation of in-situ water saturation showed that even for low rate waterfloods, there will initially be a higher water saturation near to the inlet of the core. However, as time progresses and imbibition occurs perpendicular to the water fingers, water saturation will eventually become uniform along the entire length of the core. Additionally, it can be seen that a portion of water initially flows through the most permeable sections of the core, essentially following a drainage pathway despite the water wet condition of the sand. Some water saturation also increases in the range of water films, however, and when this effect is considered as part of the water signal, the apparent pore size for which water is present increases much more slowly. Therefore, an analysis that does not consider the water film saturation will be incorrect, and would possibly lead to wrong conclusions regarding the wettability of the sand.

Finally, the core flood data were interpreted in order to identify if imbibition is occurring through co-current versus counter-current processes. In either case, water will imbibe into the bypassed sand perpendicular to the direction of the water fingers. The flow pathways for the oil govern which form of imbibition is actually present. The fact that CT images indicate regions of two-phase flow provide evidence for counter-current imbibition, whereby oil will flow backwards into regions of intermediate oil and water saturation, and will be produced along these continuous oil pathways. However, it can also be shown through an analysis of co-current imbibition in a single pore that the pressure requirement for flow of viscous oil can be reduced in co-current imbibition. Therefore, the produced oil flow rates at such low viscous pressure gradients can also be indicative of co-current imbibition. These systems are different from conventional imbibition systems, thus it is not trivial to develop analytical models for calculating the produced oil flow rates. It is likely that heavy oil is produced through a combination of co-current and counter-current flow.

CHAPTER 11: CONTRIBUTION OF IMBIBITION

In previous chapters, waterflooding results were presented for both dead oil systems and systems after primary production. In both situations, it was demonstrated that normalized oil production rates and oil recovery were superior at low water injection rates. Oil flows in porous media through the combination of both viscous and capillary forces, thus when viscous forces are reduced and enough time is provided for water imbibition to occur, this can improve the overall waterflood response of the system. It was also demonstrated through NMR spectra and the analysis of CT images that imbibition occurs along the entire length of a core, both through water displacing oil out of pores and also through thickening of water films. This chapter investigates how these capillary forces can be quantified, for the purposes of predicting oil production rates and recoveries in a heavy oil waterflood.

11.1 Imbibition Contribution

Handy (1960) performed imbibition experiments with gas – water systems. Based on a theoretical derivation combining the diffusion-convection equation with Darcy's Law for flow in porous media, he found the following expression for the relationship between the volume of water imbibed (N_w) and time:

$$N_w^2 = \left(\frac{2P_c \phi A^2 S_w}{\mu_w} \right) t \qquad\qquad \text{Eqn (11.1)}$$

For an oil-water system, where imbibing water must displace oil of viscosity greater than or equal to that of water, the form of the expression must therefore change and imbibition may occur more slowly than in the gas – water system. However, the significance of Handy's observation is that the imbibition rate is inversely proportional to $\sqrt{t}$. Using a small dataset of cores at multiple temperatures, Handy (1960) showed experimentally that this theoretical relationship between imbibed volume and time actually occurs. It was

shown in the literature (Li and Horne, 2005; Ding *et al.*, 2006) that at early times for water imbibition into a consolidated core gas – water system, this relationship holds true. At later times in these systems, however, the water imbibition volume flattens out and this is an indication that the majority of water has already imbibed into the core. At later times the trend between recovery and the square root of time increases only gradually, and approaches a horizontal line (Ding *et al.*, 2006). Therefore, imbibition rates and water volumes imbibed are greatest at early times, when the driving force for water to enter the pores is high.

Imbibition experiments are often expressed in terms of a capillary dimensionless time, in order to compare the results from different experiments to one another:

$$t_D = \sqrt{\frac{k}{\phi}}\,\frac{\sigma}{\mu_m L_a^2}\,t \qquad\qquad\qquad \text{Eqn (3.40)}$$

The use of this formulation allows the recovery profiles in imbibition experiments to be plotted as "S-shaped" curves that overlay on the dimensionless time scale. In heavy oil waterfloods, although it was demonstrated that capillary forces and imbibition are largely responsible for oil production, it is not possible to plot the recovery profiles using this same expression for dimensionless time. The term "L_a" is the characteristic length of the system, which is defined by the boundary conditions. In a heavy oil waterflood, where imbibition appears to occur either perpendicular to the water channels or further into the core through film thickening, there is no single value for L_a. Additionally, the recovery in heavy oil waterfloods is affected by both viscous and capillary forces, due to the presence of viscous instabilities in the displacement of oil by water at any pressure. This was shown by the fact that for the same viscosity oil and the same porous medium (i.e. where both μ_m and k are fixed), different oil recovery profiles can still be achieved at different injection rates. This is not reflected in the capillary-based value of dimensionless time, so heavy oil waterfloods cannot be collapsed to a single curve using Eqn (3.40).

Despite the inability to plot the recovery profiles from heavy oil waterfloods as a function of capillary-based dimensionless time, it was previously shown that after water breakthrough, imbibition is a strong contributing factor the oil recovery. Thus, the productions of various waterfloods are plotted as a function of $\sqrt{t}$. A linear relationship between the rate of oil produced (or conversely the rate of water entering the core) is indicative of the profile for the time when most of the pores are still available for water to imbibe.
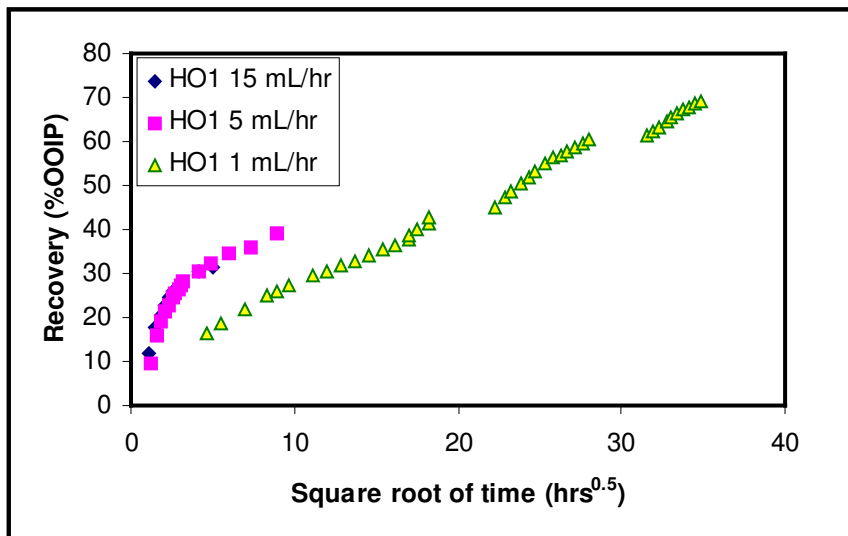
Figure 11.1: Recovery profiles for HO1 at varying injection rates as a function of time

Figure 11.1 shows the oil production at various injection rates. This figure shows that at an injection rate of 1 cm³/hr, the imbibition recovery is evident by the distinctive relationship between oil recovery and square root of time. The breaks in the 1 cm³/hr profile correspond to times when the core was shut in to allow for fluid re-distribution. After each shut in period, the slope increases, indicating that oil was displaced into larger or more mobile regions in the core during the shut-in period. Eventually, however, the slope returns once more to its pre-shut in value.

At higher injection rates, the constant slope was not observed due the influence of viscous forces at early times. At higher injection rates, recovery is initially higher than the $\sqrt{t}$ dependence due to the increased flow from viscous forces when a large pressure gradient is present in the core. Later, it appears as if the profiles could possibly be following the same trend with time as the 1 cm³/hr injection rate. Unfortunately, since these floods were performed on a PV injected basis as opposed to actual units of time, there is a lack of data at later times for higher injection rates, so this cannot be stated with certainty. The same relationship was plotted for HO2 in Figure 11.2.
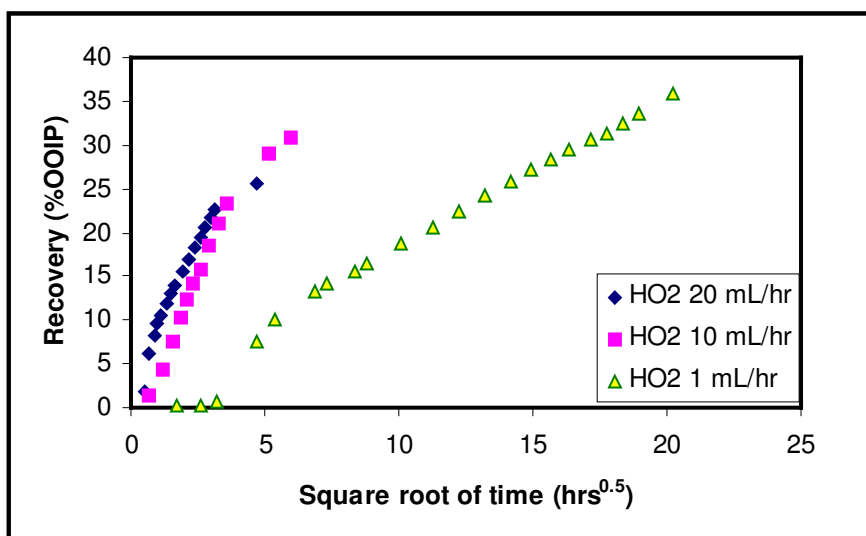
Figure 11.2: Recovery profiles for HO2 at varying injection rates as a function of time

Again, the same trend is observed. The curves of the faster injection rates do not show a linear relationship between recovery and $\sqrt{t}$, but at an injection rate of 1 cm³/hr recovery increases linearly, as was also observed in HO1. For this higher viscosity oil, production appears to be slightly delayed at the low injection rate, due to a higher pressure gradient required to generate flow in this more viscous oil.

There are several major differences between the imbibition response measured in Figures 11.1 and 11.2, compared to gas – water systems. A first major difference is the response

at early times, when the majority of imbibition occurs in a gas – water system. In these cores containing viscous heavy oil, the early time response is instead dominated by high pressure gradients and viscous forces. As a result, the relationship is non-linear at early times or for high rate water injection. This indicates that in these systems, water does not initially enter through imbibition pathways, but instead the paths of lowest resistance for flow are those of the most permeable channels (i.e. the drainage pathway). The CT images in Chapter 10 showed a channel of water breaking through to the production end of the core, followed by increasing water saturation along the entire length of the core, but progressing radially with time. In heavy oil systems, therefore, capillary forces and imbibition become more important later in the life of the waterflood, after water breakthrough and when the pressure gradient in the core has declined.

The second important difference for these systems is the imbibition rate itself, or the time in which the relationship holds between the water volume imbibed and $\sqrt{t}$. In these high viscosity cores, the time in which imbibed water volume and $\sqrt{t}$ are linearly related is much longer than in a simple gas – water system. This is a reflection of the fact that imbibing water must now displace high viscosity oil of limited mobility out of rock pores, as opposed to mobile gas which has infinite mobility. As a result, imbibition is a much slower process in heavy oil systems, which explains why its effects are less noticeable for high rate waterfloods, where several pore volumes of water are injected in relatively short times (on the order or 24 hrs, compared to 400 hrs for a low rate waterflood). Despite these differences, in the low rate waterfloods performed for both HO1 and HO2, both systems show a linear dependence on $\sqrt{t}$, which indicates an imbibition process responsible for recovery in both heavy oils.

Eqn (3.40) also shows that the recovery will be related to the fluid viscosity ratio, which is higher in HO2. Therefore, the viscosity dependence for imbibition in these oils can be determined by plotting the data for the low rate waterfloods together. This is shown in Figure 11.3.
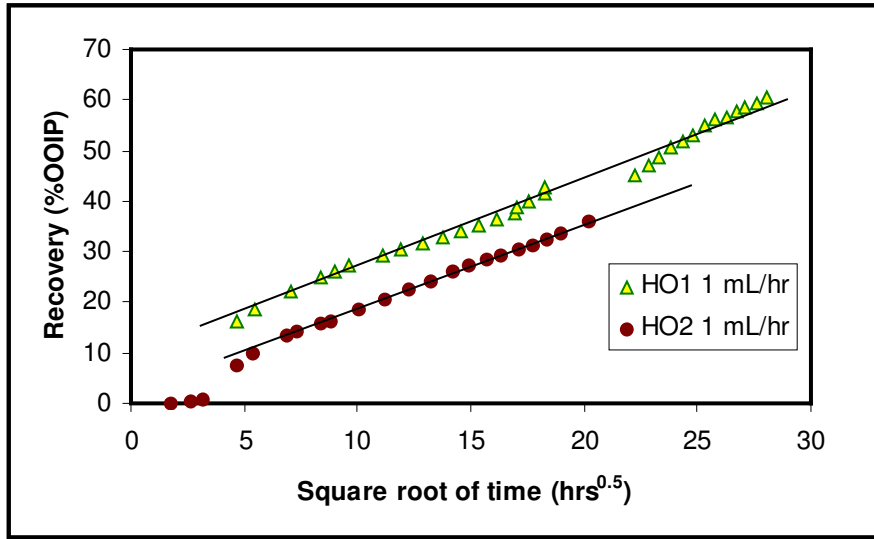
Figure 11.3: Production profile with time for low rate waterflooding in HO1 and HO2

After the initial period where the viscous force effect is very important, the slopes in the recovery profiles are similar for both oils. This is despite the fact that the viscosity ratio is approximate 2.5 times worse for HO2. It appears that for viscous oil systems, the oil viscosity effect is important at early times, but after water breakthrough oil production with time for the same water injection rate is not strongly dependent on oil viscosity. This was also seen previously in Chapter 7, where it was shown that the oil recoveries after 5 PV of water injection were only slightly higher for the lower viscosity HO1. So long as the oil phase is continuous, therefore, it appears that the imbibition rate of water is not a strong function of the oil viscosity. If actual trend lines are plotted through this data, it is shown that the slopes are 1.91 RF/hrs$^{0.5}$ and 1.62 RF/hrs$^{0.5}$ for the 4,650 and 11,500 mPa·s oils, respectively. This is a difference of only 1.18 times, for a 2.5 times increase in the oil viscosity. Therefore, recovery is still better for the lower viscosity oil but is not linearly proportional to the oil viscosity.

11.1.1 Imbibition Contribution under Varying Injection Rates

An additional waterflood was also performed using HO2, whereby the water injection rate was varied from 1 cm³/hr to 10 cm³/hr. The response of this waterflood is compared to the constant rate injection profiles at 1 cm³/hr and 10 cm³/hr in Figure 11.4.
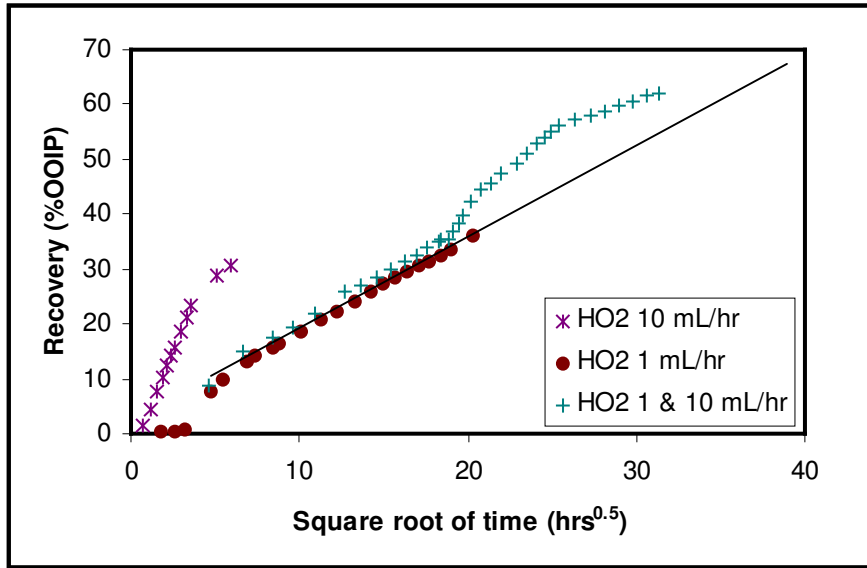
Figure 11.4: Varying injection rate vs. fixed rate recovery profiles for HO2

For the varying rate experiment, when water is injected at 1 cm³/hr at early times, the recovery profile is similar to the constant low rate waterflood. After approximately 400 hrs of injection, the waterflood injection rate was increased by a factor of ten, and Figure 11.4 shows a definitive change in the slope of the recovery profile at this point. The improvement in the oil recovery is therefore attributed to the effect of additional viscous forces applied. When compared to the straight line predicted by the constant 1 cm³/hr injection rate, it appears that additional oil is only recovered at first, and then the recovery efficiency decreases. In fact, the slope at around 25 hrs$^{0.5}$ (625 hrs) appears to be lower than the linear trend predicted by the 1 cm³/hr injection rate. It has been demonstrated (Li and Horne, 2005; Ding *et al.*, 2006) that as the saturations begin to approach S_{or} (i.e. after most of the imbibition has been completed) the relationship between produced volumes and $\sqrt{t}$ loses linearity. Perhaps this is responsible for the decreasing slope in Figure 11.4; unfortunately this was not verified by running the constant 1 cm³/hr for extended periods of time.

If the straight line approximation at 1 cm³/hr is followed assuming that imbibition is mainly responsible for oil recovery at this low injection rate, it will take 27.5 hrs$^{0.5}$ (756

hrs) to reach the recovery of 50% OOIP, which was obtained after only 23 hrs$^{0.5}$ (529 hrs) by increasing the water injection rate. Likewise, even comparing the 1 cm³/hr and 10 cm³/hr constant injection rate data, it took 227 additional hrs at 1 cm³/hr to reach the same oil recovery as what was obtained by injecting fast at first. However, as was shown by plotting normalized oil production rates in Chapters 7 and 8, the waterflood is much less efficient at high rates. Therefore, it appears that the optimal production scheme in terms of balancing recovery and oil production rates is a combination of fast and slow injection. Low rate water injection allows for imbibition, which re-distributes oil and water. Oil is distributed in large pores, either through water film thickening or complete displacement out of other pores. Under increased viscous forces, this oil can then be produced faster than at low rates, although the water cuts will also be higher in this situation. Eventually both the constant low rate injection and the fast/slow combination should yield the same ultimate recovery, which will be the endpoint S_{or}.

While faster injection leads to higher oil rates due to increased viscous forces, it must be stressed that this improvement in oil recovery at ten times the previous injection rate is based on a time scale, thus it does not take into consideration the effect of increasing injection rate on the water cut profile. When evaluating the efficiency of the waterflood based on the recovery of oil per pore volume injected, a different picture is obtained. Figure 11.5 shows the normalized oil production rate for various injection rates in the waterflooding of HO1 at late times, so the data obtained during the initial high pressure gradient is excluded from this analysis.

Although this is known to be a simplification of the actual production response, linear trend lines have been fitted through the different water injection rate data in Figure 11.5. As more water is injected, the normalized oil production rate decreases, and the slopes of these trend lines are related to the efficiency of the waterfloods. At the lowest injection rate (i.e. the most efficient waterflood) the slope is the lowest, meaning that the oil rate is declining slower in this system. Likewise, the oil rate declines the fastest at the highest injection rate.
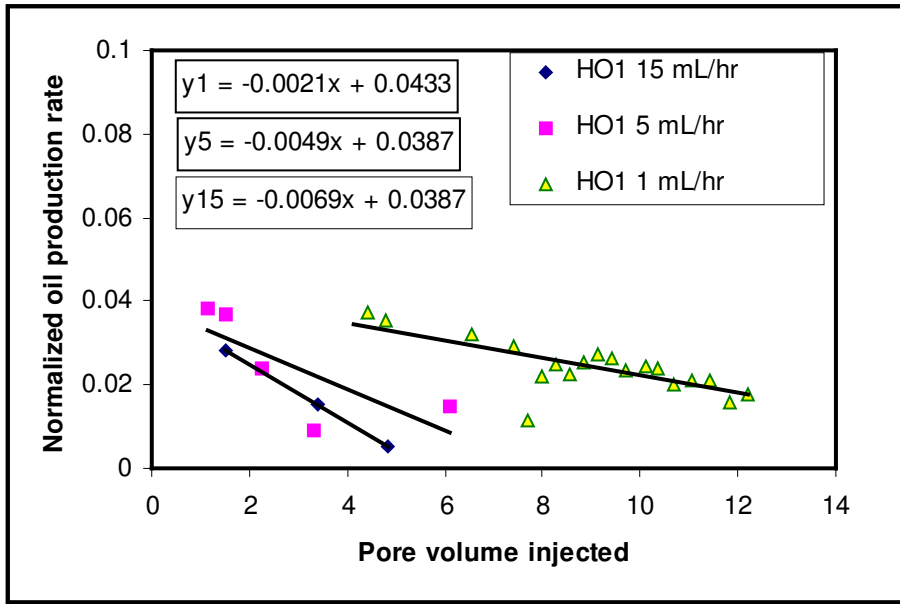
Figure 11.5: Normalized oil production rate for HO1 at varying water injection rates

Oil production rates are the result of both viscous forces (i.e. the force from the varying water injection rate) and capillary forces from water imbibition. Viscous forces are directly proportional to the injection rate, while the production rate from capillary forces are inversely proportional to time. In Figure 11.5, time is shown in terms of PV injected, thus in order to inject the same amount of water into any core, the time requirement is inversely proportional to the injection rate. This can be shown in the following three equations:

$$q_{inj} = 1 \text{ mL/hr} : q_{o\_tot} = q_{o\_visc} + q_{o\_imb} \qquad\qquad \text{Eqn (11.2)}$$

$$q_{inj} = 5 \text{ mL/hr} : q_{o\_tot} = 5(q_{o\_visc}) + q_{o\_imb}/5 \qquad\qquad \text{Eqn (11.3)}$$

$$q_{inj} = 15 \text{ mL/hr} : q_{o\_tot} = 15(q_{o\_visc}) + q_{o\_imb}/15 \qquad\qquad \text{Eqn (11.4)}$$

These simple expressions are valid because the oil viscosity is the same in all three floods, and likewise the porous media properties (porosity and permeability) are also very similar. As a result, the only change between experiments is the water injection rate and

the time of the waterflood. By increasing the viscous component directly with the injection rate, there are several assumptions made for Darcy flow in a two phase system. One assumption is that the pressure gradient is directly proportional to the injection rate, which is a reasonable assumption in dead oil systems. The other assumption is that the oil relative permeability is the same under all three flow rates. For similar ranges of oil saturations, this assumption should also be valid.

Figure 11.5 does not show actual oil rates, however by using the slopes of the lines instead of q_{o_tot} in Eqn (11.2) – (11.4), the loss in oil production due to viscous and capillary forces can be quantified. Eqn (11.2) – (11.4) can therefore be modified in the following fashion:

$$q_{inj} = 1 \text{ mL/hr} : -0.0021 = \frac{dq_{o\_visc}}{dPV\_inj} + \frac{dq_{o\_imb}}{dPV\_inj} \qquad \text{Eqn (11.5)}$$

$$q_{inj} = 5 \text{ mL/hr} : -0.0049 = 5\left(\frac{dq_{o\_visc}}{dPV\_inj}\right) + \frac{1}{5}\left(\frac{dq_{o\_imb}}{dPV\_inj}\right) \qquad \text{Eqn (11.6)}$$

$$q_{inj} = 15 \text{ mL/hr} : -0.0069 = 15\left(\frac{dq_{o\_visc}}{dPV\_inj}\right) + \frac{1}{15}\left(\frac{dq_{o\_imb}}{dPV\_inj}\right) \qquad \text{Eqn (11.7)}$$

By re-arranging Eqn (11.5), (dq_{o_visc}/dPV_inj) can be expressed in terms of the imbibition contribution. This can then be substituted into Eqn (11.6) and (11.7), and the imbibition term can be solved for both 5 and 15 cm³/hr water injection rates. The loss in oil rate due to imbibition is found to be –0.00117 and –0.00166 from Eqn (11.6) and (11.8), respectively. Taking the average of these two, the loss in oil production rate due to imbibition alone can be approximated as –0.00142. The remaining loss in oil production (i.e. the difference between the actual decrease in the normalized oil rates and –0.00142) is the loss in production due to inefficient viscous forces. The effect of the imbibition term can be summarized in Table 11.1.

Table 11.1: Imbibition contribution to loss in oil production at varying injection rates

Inj Rate (cm³/hr)	$\dfrac{dq_{o\_tot}}{dPV\_inj}$	Δ Flood eff from 1 cm³/hr	$\left(\dfrac{dq_{o\_imb}}{dPV\_inj}\right)\Big/ total$
1	-0.0021	1	0.676
5	-0.0049	0.43	0.290
15	-0.0069	0.30	0.206

The second column in Table 11.1 is the total loss in normalized oil production rates, which are the slopes shown in Figure 11.5. The third column in Table 11.1 is found by dividing the total loss in oil production by the value at the lowest injection rate. In this manner, the floods efficiencies have been normalized to the efficiency at 1 cm³/hr injection. Larger slopes indicate that the normalized oil production rate is declining more quickly, or that the flood is less efficient. The imbibition contribution to the decline in production is expressed as a fraction of the total production decline by dividing the imbibition term (-0.00142) by the total slope in column 2.

The results of Table 11.1 clearly show that in systems of similar oil viscosity and rock properties, the loss in the efficiency of the waterflood correlates with the change in the imbibition contribution to the total flow in the system. In other words, increased waterflood efficiency in heavy oil systems is directly proportional to higher contribution of water imbibition, or a lower contribution of viscous forces. Although low rate waterflooding leads to slower recovery of oil on a time scale, as the effect of imbibition becomes more significant, the waterflood efficiency increases by this same degree.

11.1.2 Scaling Results for Systems with Changing Viscous and Capillary Forces

Figure 11.3 plots the oil recovery versus dimensionless time for oils of varying viscosity, illustrates that the effect of oil viscosity on heavy oil waterflooding recovery is not linear. Rather, although there is a viscosity difference of 2.5 between the two oils, the difference in the slopes of the recovery vs. $\sqrt{t}$ is only 1.18. Therefore, imbibition will occur more quickly in lower viscosity oils, but the viscosity effect is not straightforward.

Altering the rock permeability affects both the viscous and capillary forces, and the effect of permeability on overall recovery at low injection rates is considerably more pronounced. Figure 11.6 plots the recovery vs. $\sqrt{t}$ for both HO1 and HO2, in systems of varying permeability. From this figure it is apparent that for a single oil viscosity, recovery is lower in higher permeability cores.
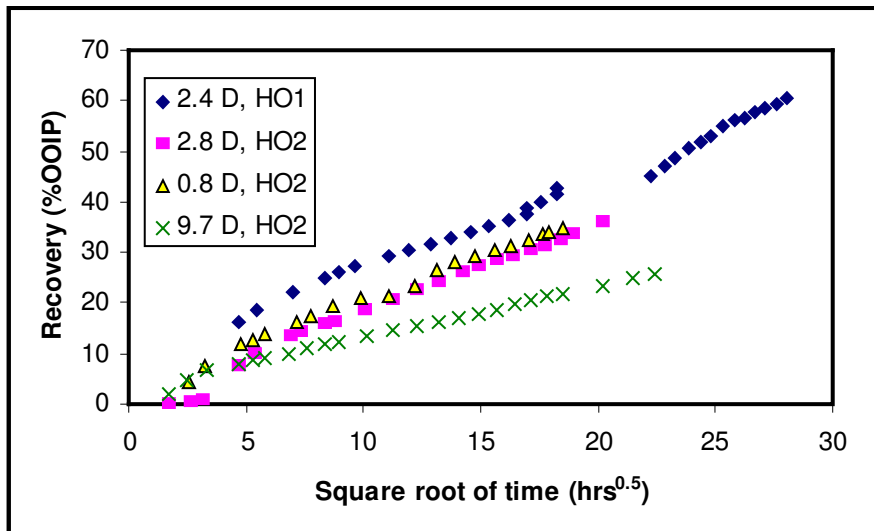
Figure 11.6: Recovery at 1 cm³/hr injection in cores of varying k and μ_o

Again, at late times in the waterfloods, after pressure has already declined in the core, there appears to be a linear relationship between the oil recovery and $\sqrt{t}$, indicating that imbibition has a strong influence on oil recovery at these low injection rates. Three of the cores contained HO2 (11,500 mPa·s), while one core flood was performed on HO1 (viscosity 4,650 mPa·s). The significant differences in the oil recovery with time are strongly related to the differences in the sand permeability. Higher oil viscosity does have an influence as well, but it was shown previously that the slope of the recovery change with time was not significantly different for different oils. The different slopes in Figure 11.6 show that, not surprisingly, different imbibition responses are much more strongly affected by the average pore size (i.e. the permeability) of the sand.

Due to differences in the diameter of the 0.8 D core, there is also a difference in injection velocity in this system. The different parameters for these four waterfloods are summarized in Table 11.2.

Table 11.2: Rock and fluid properties for low rate waterfloods in Figure 11.6

Core Flood	Oil viscosity (mPa·s)	Permeability (D)	Porosity (fraction)	Flood velocity (m/day)
1	4,650	2.43	0.359	0.023
2	11,500	2.79	0.355	0.023
3	11,500	0.78	0.412	0.023
4	11,500	9.73	0.464	0.045

In Eqn (11.1), produced volumes through imbibition are related to $\sqrt{t}$, but are also related to the capillary pressure. In systems of order-of-magnitude similar interfacial tension and similar sand, capillary pressure is inversely proportional to $\sqrt{k}$. Eqn (11.1) also relates the produced volume inversely to the square root of the water viscosity, since this equation was derived for gas – water systems. In the case of oils of varying viscosity, the oil viscosity will have a much more definitive impact on the imbibition rate, as evidenced by the much lower slopes in these systems, compared to the work of Handy (1960).

Washburn (1921) also provided a theoretical calculation of the flow of fluid, due to capillary pressure alone, into a circular capillary. The distance that the fluid would penetrate a horizontal capillary in a given time was developed:

$$L_w = \sqrt{\frac{r\sigma\cos\theta}{2\mu}}\sqrt{t}$$

Eqn (11.8)

Where L_w is the distance penetrated.

For this equation, it could be seen that the penetration distance is related to the square root of the radius of the tube, the inverse of the square root of fluid viscosity and the

square root of time. This expression has much of the same form of Handy's correlation, shown in Eqn (11.1).

Keeping in mind the relationships that had been derived theoretically for capillary driven flow, a new scaled time term, t_s, has been developed in order to compare the results from these different systems against one another:

$$t_s = \sqrt{t} \, \frac{\phi}{\nu \sqrt{k/\phi}} \sqrt{\frac{\mu_{o\_base}}{\mu_o}}$$
Eqn (11.9)

Where μ_{o_base} = the viscosity of the least viscous oil waterflooded

μ_o = the viscosity of any other oil being waterflooded.

Although t_s in Eqn (11.9) is not dimensionless, it appropriately scales time by incorporating the factors that will enhance or reduce imbibition in heavy oil systems. Imbibition is proportional to capillary forces, thus the square root of permeability is in the denominator of the expression. Likewise, at faster injection rates more water cycles through low-resistance water pathways, therefore imbibition will also occur more slowly and velocity is also in the denominator. Finally, the influence of the oil viscosity is incorporated as a square root term, much like Washburn theoretical correlation in Eqn (11.8) and Handy's correlation in Eqn (11.1). Oil viscosity is inversely normalized to the lowest viscosity oil being waterflooded, thus for higher viscosity oils a longer time is required for imbibition. The fact that the viscosity is incorporated as a normalized square root term means that oil viscosity is not ignored, however the viscosity weight is less than a linear dependence, since this was observed in the experimental findings. Therefore, although the scaled time in Eqn (11.9) was developed empirically, the relationship of the different parameters in this expression are based in the theoretical models developed previously (Washburn, 1921; Handy, 1960). When the oil recovery is plotted against the scaled time criterion instead of $\sqrt{t}$, all the recovery profiles collapse to a single curve. This is shown in Figure 11.7.
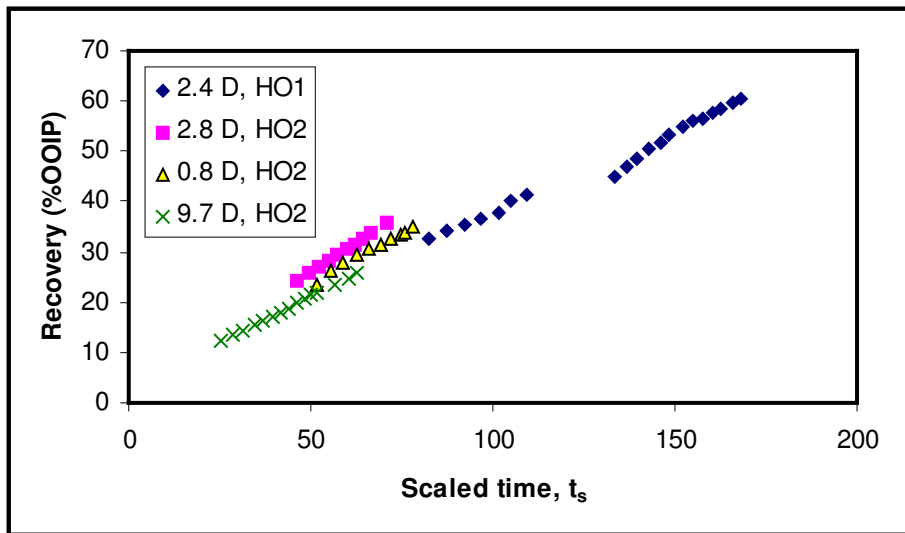
Figure 11.7: Oil recovery at low waterflood rates plotted against scaled time

There is still some scatter in this relationship, however the fact that the curves are now much closer to one another means that the scaled time criterion can potentially be used as a means for calculating the time requirement for a certain oil recovery in a given heavy oil system.

11.2 Effect of Imbibition on Relative Permeability Curves

Due to the problems that are prevalent in adverse mobility waterfloods, there is considerable uncertainty in measurements of heavy oil – water relative permeability (Maini, 1998). Specifically, the effect of viscous fingering and fluids by-passing on the residual oil saturation is not easy to determine. Moreover, relative permeability appears to be a function of the oil viscosity (Wang *et al*., 2006), which is not the case for conventional oil waterfloods. The difficulty in obtaining accurate relative permeability data is also tied in to the fact that imbibition appears to be an important mechanism in these systems. However capillary pressure curves are non-trivial to obtain for heavy oil systems especially in unconsolidated core. Nevertheless, this information is very crucial in reservoir simulation, thus it should be obtained regardless of the difficulties.

Relative permeability information could be extracted from the dead oil waterflooding results via various methods, as described in Chapter 3. In this chapter, the JBN method is used to calculate the relative permeability of the heavy oil waterflood results. It is accepted that this method is a gross simplification of the process and does not properly capture the physics of the oil displacement. However, this method allows for the calculation of apparent relative permeability curves that can be incorporated into reservoir simulators. Additionally, the effect of oil viscosity and injection rates can be addressed through their influence on the apparent relative permeabilities calculated.

11.2.1 Relative Permeability Using JBN Method

The JBN method is an external method of deriving relative permeability data based on unsteady state displacement data. The inherent assumption in this calculation is that although the experiment was conducted under unsteady state conditions, the displacement was still stable. For this assumption to be valid, the criteria of stable flow must be satisfied. The values of the scaling coefficient were calculated for the dead oil waterfloods and shown in the table below. The condition for a stable displacement is that the scaling coefficient ($L\nu\mu_w$) must be greater than or equal to unity, therefore for a given system the core length must be long enough to make any core end effects negligible.

Table 11.3: Scaling coefficient calculations for stability in the JBN method

Experiment #	L (cm)	ν (cm/s)	$L\nu\mu_w$ (cm^2/s·cP)	L required (cm)
4	16.5	2.436E-4	0.00402	4,104
5	17.4	3.655E-4	0.00636	2,736
6	16.7	1.218E-4	0.00203	8,209
7	16.6	2.436E-5	0.000404	41,043
10	17.2	4.873E-4	0.00838	2,052
11	16.95	2.436E-4	0.00413	4,104
12	17.55	2.436E-5	0.000428	41,043

From Table 11.3 it is obvious that none of the heavy oil waterfloods have satisfied the stability criterion. In order to fulfill this condition, either the length of the sandpack studied must be longer or the injection rate must be increased. For all waterflood

performed in Table 11.3, a total five pore volumes of brine was injected. Increasing the length of the cores is not ideal since this would increase the pore volume significantly, thus increasing the amount of time required to inject five pore volumes. In the experimental work plan followed in this thesis, the goal was to perform multiple core floods and investigate the effect of varying the ratio of viscous to capillary forces, thus lengthening each experiment would make it impossible to manipulate the desired number of variables. Likewise, increasing the injection rate is not a feasible solution in heavy oil waterfloods. Instability theory shows that for heavy oil waterfloods, increasing the injection rate will result in severe viscous fingering, which is also far from stabilized flow.

Maini and Okazawa (1987) summarized these concerns by observing that there are various problems associated with using the unsteady state technique in heavy oil systems. These problems include viscous fingering due to unfavorable viscosity ratio, possible invalidation of the incompressible fluid assumption due to high pressure gradients present under constant rate injection before water breakthrough, and the difficulty in determining the true residual oil saturation due to bypassing of continuous oil zones. Thus, it must be noted that the displacement of heavy oil by water almost consistently violates the most fundamental theory of relative permeability.

One other point of concern is that the JBN method ignores capillary effects, by assuming that capillary forces are constant in the system, and thus only viscous forces lead to changes in fluid saturation (Johnson *et al*., 1959). The mathematical formulas employed to determine relative permeability curves obtained via this method are therefore based on the assumption that the capillary differential is constant, or that the pressure gradient in the oil is equal to the pressure gradient in the water. In heavy oil systems, it has been shown that not only is there an effect of capillary pressure, but that this parameter is to a large extent responsible for the oil production at late times in a waterflood.

Despite these concerns, the apparent relative permeability values calculated still allow for observations to be made regarding the efficiency of heavy oil displacement by water, so

the JBN method was used to extrapolate relative permeability based on the production data. This method generates apparent relative permeability relationships for heavy oil and water, whereby the effect of water imbibition is hidden in the relative permeability values calculated. While this methodology is not theoretically accurate, the data is reflective of the oil and water fractional volumes produced in the experiments. Therefore, while they do not properly capture the physics of the displacement, they could still be used in reservoir simulators to predict rates in heavy oil waterfloods.

Four waterfloods were performed in sandpacks saturated with HO1. Unfortunately, in one of the waterfloods (Q_{inj} = 10 cm³/hr), pressure increased too high before water breakthrough and damaged the pressure transducer, thus the pressure was not fully recorded. Additionally, for the case where brine was injected at 1 cm³/hr, the pressure transducer could not accurately measure such small pressure drops (< 5 kPa), thus the pressure recorded could not be trusted in the development of relative permeability data. As a result of these experimental complications, the relative permeability curves were obtained for HO1 at only two injection rates. The oil and water relative permeability curves are plotted in Figure 11.8, and the methodology used to calculate these curves is shown in Appendix I.
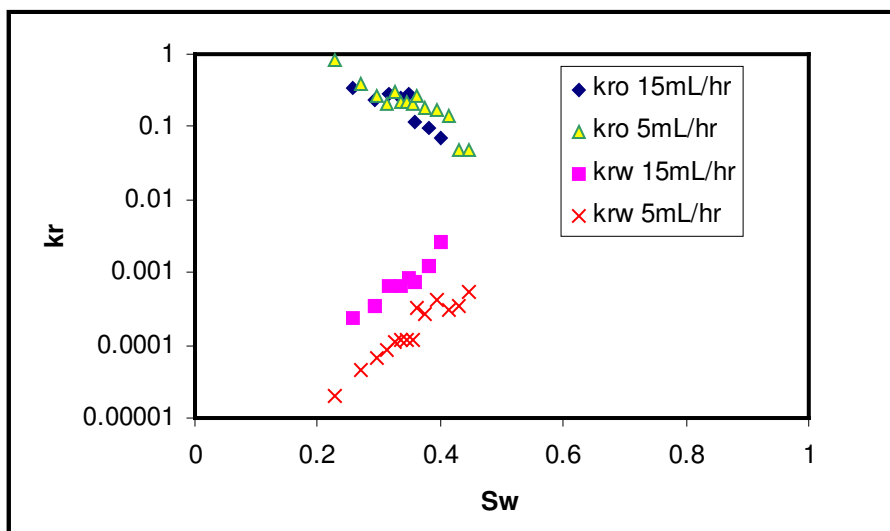
Figure 11.8: Calculated relative permeability for HO1 at varying injection rates

It must be noted that it was not possible to obtain a full relative permeability curve extending from S_{wi} to S_{or} due to the fact that for these adverse mobility conditions, a significant number of pore volumes of brine injection are required before the true S_{or} condition will be reached. For these waterfloods, only a total of five pore volumes were injected, thus the range of water saturations in the model are limited.

The results from Figure 11.8 lead to several significant observations. First, although the fluids were produced at greater than 90% water cuts, the relative permeability to water is several orders of magnitude lower than the relative permeability to oil. This is a reflection of the fact that the viscous pressure gradient measured across the core is not fully responsible for the oil production. At lower water injection rates, the water relative permeability is lower, indicating that the flow of water through continuous pathways is somehow being impeded. This is the result of more water moving into previously unswept regions of the sand, through imbibition.

Due to the small values of k_{rw} for the range of water saturations measured, no cross-over was seen in the oil and water relative permeability curves. As water saturation rises in the core, however, k_{rw} increases by approximately one order of magnitude, while k_{ro} drops accordingly. This is an indication that under high water injection rates, waterfloods become extremely inefficient at later times. This was also shown in Figure 11.5, whereby the normalized oil production rates declined much more rapidly at high waterflood rates, compared to their response at under slower water injection.

The other significant observation from Figure 11.8 is the effect of water injection rate on the oil and water relative permeability. On the logarithmic scale used in Figure 11.8, it appears that for this data set k_{ro} increases marginally for any water saturation when water injection is reduced from 15 to 5 cm³/hr. Therefore, oil relative permeability is improved at lower water injection rates, which is again a result of increased capillary force effects at these conditions. The improvement in k_{ro} is small, however, so if a single oil relative permeability curve were used at both injection rates, the oil production rates could still be

predicted without a severe loss in accuracy. The effect of the water injection rate is much more pronounced in the relative magnitude of the k_{rw} curves. There is a distinct separation in the k_{rw} values at the two injection rates modeled, and k_{rw} is consistently lower at the lower water injection rate. This is again reflective of the physics of the waterflood; in slower waterfloods more time is provided for water to imbibe into the core, thus less water is channeling through the continuous water fingers. Lower k_{rw} also is indicative of higher produced oil cuts, or more efficient waterfloods. It should be noted that at both rates k_{rw} values are low on the logarithmic scale of Figure 11.8, so on a basis of absolute magnitudes of relative permeability, the difference in the water relative permeability values is small. However, if the relative magnitude of the water relative permeability is considered, it can be concluded that these values change much more significantly than for the oil.

As mentioned previously, the pressures recorded during the cases of slowest injection rate (1 cm³/hr) were not accurate since they were at the limits of the accuracy of the 0 – 170 kPa (0 – 25 psi) transducers used. The result is that the relative permeability extracted from this waterflood yielded non-descriptive curves, as shown in Figure 11.9.
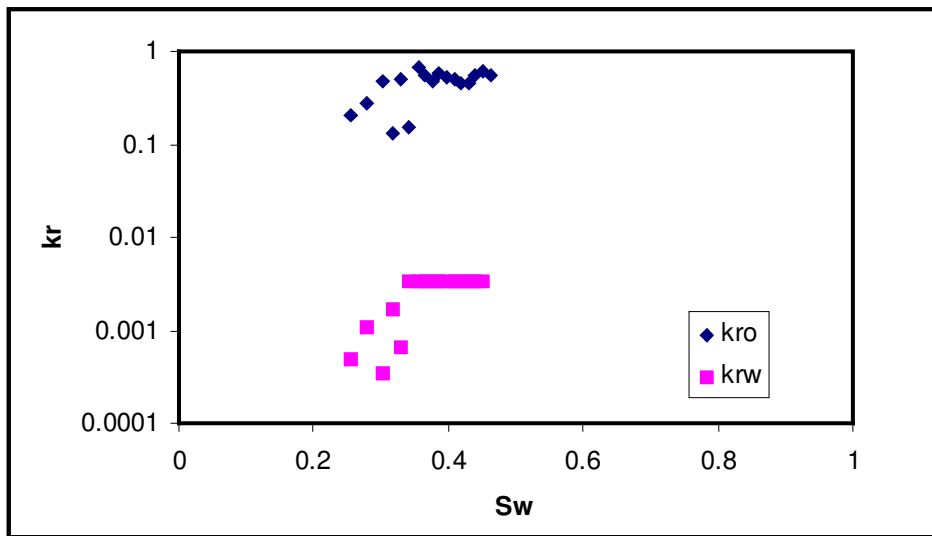
Figure 11.9: Oil and water relative permeability calculated for a 1 cm³/hr waterflood

At this low waterflood rate, the oil relative permeability values do not decrease as much as they do at higher waterflood rates. However, it is obvious from the shape of these curves, especially for the k_{rw} values, that these calculations could not be used for making predictions of very low rate waterflood behavior in heavy oil systems. In order to obtain more accurate data, these floods would have to be repeated with much more sensitive pressure transducers.

The relative permeabilities of two waterfloods performed at fixed rates (20 cm³/hr and 10 cm³/hr) in sandpacks saturated with HO2 were also calculated, and are shown in Figure 11.10. Once again, very low rate water injection was also performed for this oil, but the lack of accurate pressure data made it impossible to use these relative permeability values for predicting the flood performance.
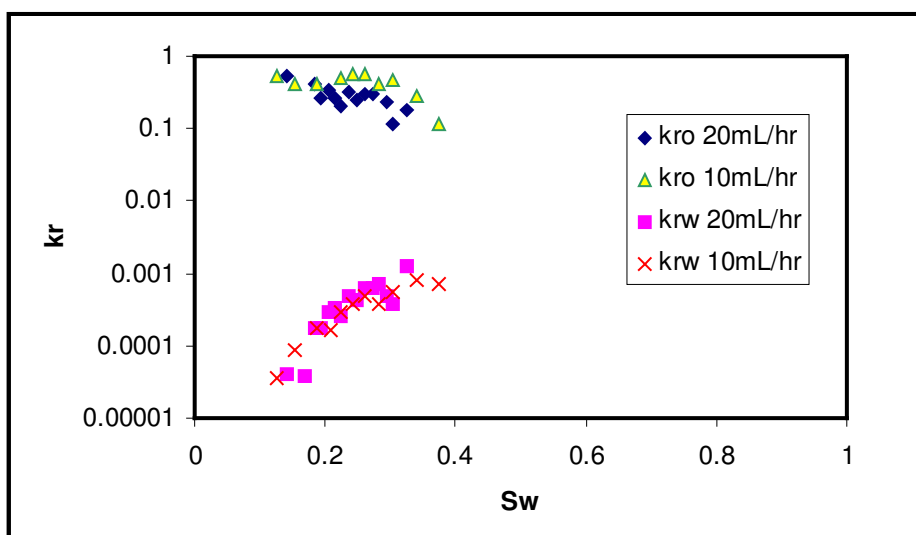
Figure 11.10: Calculated relative permeability for HO2 at varying injection rates

Similar trends were observed for the k_{ro} values in this system: at lower waterflood rates the k_{ro} values were slightly higher than those obtained under faster water injection. What is significant, however, is that for this higher viscosity oil, the k_{rw} values do not appear to be nearly as strong a function of injection rate. This is possibly due to the higher oil viscosity, coupled with the fact that both waterfloods are still relatively fast for heavy oil

systems.   Although it was shown in Section 11.1 that imbibition is not directly proportional to the increase in the oil viscosity, it still does occur more slowly in more viscous oil systems.

Unfortunately, due to the fact the pressure transducer become defective for the case of the waterflood into HO1 at 10 cm³/hr, the pressure data collected was not complete so the effect of oil viscosity cannot be compared directly in these two oils.   However, a qualitative comparison can be made by plotting the k_{ro} and k_{rw} values for HO1 under 15 cm³/hr injection and 10 cm³/hr injection for HO2.   This is shown in Figure 11.11. Although the water injection rate is not the same in both cores, both show a situation where there is a strong contribution of viscous forces, thus the significance of water imbibition is reduced.
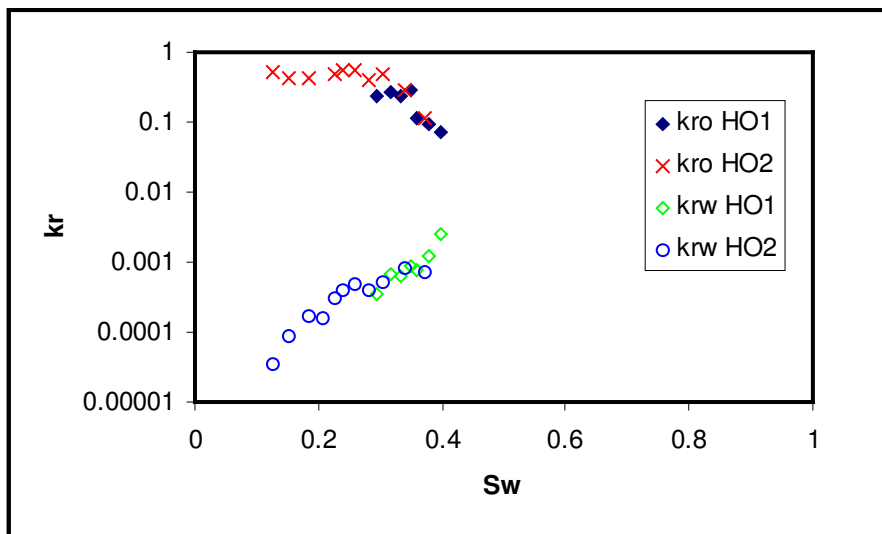
Figure 11.11: Rel perm curves for HO1 and HO2 at high water injection rates

Despite the fact that HO2 is 2.5 times the viscosity of HO1, there is very little difference in the relative permeability curves in these two systems.   It should be emphasized, however, that the velocity of water injection into HO1 is 1.5 times that of the injection into HO2. When the product of velocity and oil viscosity is considered instead of just the viscosity ratio, the difference between the systems becomes less significant.   Therefore,

while Figure 11.11 does not allow for any strong viscosity effect to be determined, this figure shows that viscosity alone does not control the relative permeability behavior of heavy oil waterfloods. Rather, relative permeability is controlled overall by the ratio of viscous and capillary forces, not simply by oil viscosity alone. This will be further investigated in the instability analysis in the next section.

11.2.2 Relationship Between Relative Permeability and Instability

The results of these heavy oil waterfloods have consistently shown that an increase in the injection rate leads to higher water relative permeability, and conversely lower oil relative permeability. For adverse mobility ratio systems, higher injection rates mean that the displacement has become more unstable. The degree of viscous fingering is described by instability theory, thus the instability number was calculated for each experiment and shown in Table 11.4.

Table 11.4: Mobility ratio and instability number for different waterfloods

Experiment	Oil	Q_{inj} (cm³/hr)	M	I_{sr}
5	HO1	15	863	1877
6	HO1	5	863	400
10	HO2	20	2156	4061
11	HO2	10	2156	2009

As expected, as the mobility ratio increases, I_{sr} also increases, which indicate that these floods are less stable. Likewise, for each mobility ratio, the flood becomes more unstable at higher injection rates. Figure 11.12 plots the various relative permeabilities with different instability number.
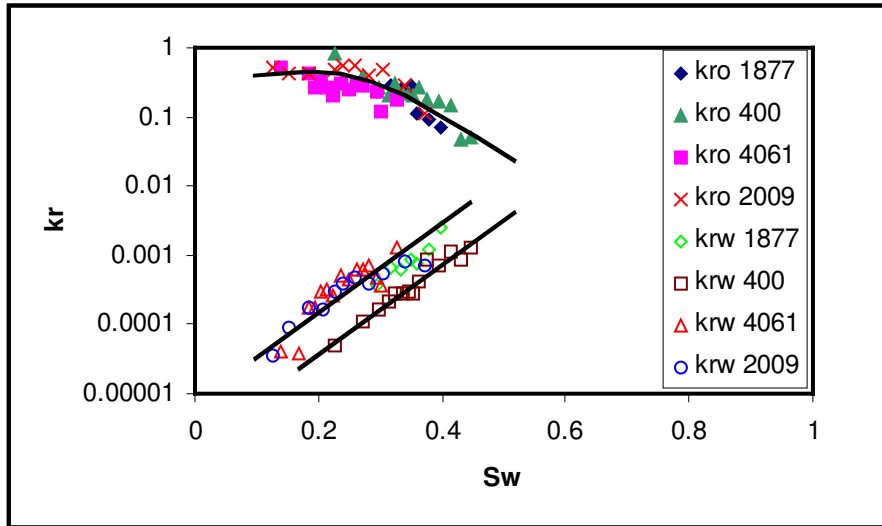
Figure 11.12: Oil and water relative permeability for different instability numbers

Trend lines have been drawn through the data, to show the change in the flood response as I_{sr} increases from 400 to 4,000. Oil relative permeability appears to be relatively insensitive to the instability number. Overall, it appears as if k_{ro} could be fitted by a single non-linear trend line passing through all the data. The water relative permeability response is quite different. It appears that there is no significant change in the slope of k_{rw} as a function of water saturation, but that higher I_{sr} values simply shift the water relative permeability curves over to lower water saturations. This means that under more unstable conditions, the water relative permeability increases at earlier times than for lower I_{sr} system. This is represented by earlier water breakthrough, and reduced oil recovery up to the point of breakthrough. It is also interesting that the shift occurs for I_{sr} of 400, while the data for higher I_{sr} numbers all follow a similar trend. These results are consistent with what Peters and Khataniar (1987) have observed in their experiments, and indicate that perhaps at very high instability numbers the water relative permeability becomes insensitive to the value of the instability number. It should be stressed, however, that all of this data is obtained under relatively high viscous forces. The low rate relative permeability response is significantly different, but unfortunately could not be calculated in this work. In all of these systems, water relative permeability is two to three orders of magnitude lower than that of oil.

Sarma et al. (1990) performed a suite of waterfloods at varying instability numbers, and observed for pseudostable displacement (I_{sr} > 900), k_{ro} was higher and k_{rw} lower than for unstable runs (14 < I_{sr} < 900). These tests were performed at high flow rates, ranging from 108 – 1,908 cm³/hr. At these velocities, the time of each waterflood would be so short that capillary forces have much less significance than in even the highest water injection rate performed in this study. The result of this was higher water relative permeability values: oil and water relative permeability were of the same order of magnitude, indicating that the waterfloods were much less efficient than the ones presented in this study. Sarma et al. (1994) later performed another relative permeability study, where constant rate waterfloods were performed in a very high permeability core (95 D). In the range of flow rates tested, it was concluded that even for unstable displacement, so long as the degree of instability was known it would be possible to predict waterflood behaviour using frontal advance theory and pseudo-relative permeability curves (Sarma et al., 1994). Again, for these waterfloods, the high injection rates coupled with the very high sand permeability negated any benefits of capillary forces, and oil and water relative permeability values were of the same order of magnitude.

Maini et al. (1990) performed constant rate waterfloods into a 400 mPa·s heavy oil in a 3.6 D sand. Water injection rates were varied from 7.5 – 120 cm³/hr. In these experiments, there was a strong correlation between injection rate and relative permeability of water: k_{rw} was reduced at lower injection rates. This was also observed in the results shown in this study. There was no definitive correlation between the injection rate and the k_{ro} values.

Wang et al. (2006) performed low rate waterfloods in heavy oils with viscosity varying from 400 – 13,500 mPa·s. Permeability (7 D) and injection rate (10 cm³/hr) were both in the same range as the experiments shown in this study. A strong correlation was observed between oil viscosity and oil/water relative permeability, which is consistent

with this work. Also, an important finding made was that at these lower injection rates, k_{rw} was approximately two orders of magnitude below the values for oil. This is similar to what was observed in this study, which confirms the improved waterflood efficiency in heavy oil at low rates.

11.3 Predictive Methods

As discussed previously in Chapter 3, there have been methods developed in the literature for estimating the efficiency of conventional oil waterfloods. In heavy oil systems, these methods are not applicable due to issues of viscous fingering and oil by-passing, coupled with the unconventional nature of water imbibition in these systems. Therefore, although the contribution of imbibition has been discussed in terms of oil production rates and fluid relative permeability, the ultimate goal of these experiments is also to predict the oil recovery that can be expected in heavy oil waterflooding. In this section, predictive methods are investigated for providing a means to quickly assess the expected oil recovery.

Predictions of residual oil saturation for conventional oils often involve showing breakthrough recoveries as a function of capillary number (Abrams, 1975). In this section, therefore, the relationship between capillary number and the recovery of heavy oil waterflooding is compared. The effect of oil viscosity is also taken into consideration by modifying the capillary number. Finally, instability theory was also used to characterize heavy oil waterflooding, and a new empirical correlation was developed to predict heavy oil waterflooding recovery based on a wide range of heavy oil waterfloods reported in the literature.

11.3.1 Capillary Number

The analysis of waterflooding results for conventional oils often involves the prediction of breakthrough recoveries as a function of capillary number, in which recovery increases as capillary number increases in water wet cores. Capillary number, N_{ca}, is defined as:

$$N_{ca} = \frac{\nu \mu_w}{\sigma \cos \theta} \qquad\qquad \text{Eqn (11.9)}$$

In conventional oil waterfloods in water wet porous media, oil is trapped in discontinuous ganglia by capillary forces. In this manner, higher capillary numbers are indicative of reduced trapping of oil, and thus higher oil recovery. Capillary number analysis shows that as N_{ca} increases, recovery at breakthrough increases accordingly (Abrams, 1975). In heavy oil waterfloods it is not simple to identify the occurrence of breakthrough. Generally, breakthrough is identified as the point when water was first produced. However, in heavy oil waterfloods, it was shown in Chapter 7 that water is produced very early, at which point the recovery is still very small. Therefore, in Chapter 7 breakthrough recovery values were instead calculated as the point where the slope of the oil recovery versus. PV of water injected began to reduce.

The breakthrough recoveries along with their capillary numbers, as defined by Eqn (11.10) are shown in the Table 11.5. These results show that as injection rate increases, recovery at breakthrough decreases, with the exception of the cases of 1 cm³/hr injection. Table 11.5 also shows that recovery at breakthrough is higher for the less viscous oil. At this range of capillary numbers, the recoveries expected in conventional oil waterfloods are significantly higher than the values in Table 11.5. This illustrates one of the main differences between conventional oil and heavy oil waterfloods: at water breakthrough residual heavy oil is bypassed due to adverse mobility ratio rather than from capillary trapping. Therefore, although for conventional oils there is very little additional recovery after breakthrough, in heavy oil systems water imbibition can lead to significant additional production of oil since most of the oil is still continuous and therefore capable of flow.

Table 11.5: Breakthrough recovery for dead oil systems with varying N_{ca} and I_{sr}

Experiment #	Q_{inj} (cm³/hr)	Oil	R_{bt} (%OOIP)	N_{ca}	I_{sr}
4	10	HO1	13.82	8.122E-8	905
5	15	HO1	11.94	1.218E-7	1877
6	5	HO1	15.72	4.061E-8	400
7	1	HO1	10.66	8.122E-9	118
10	20	HO2	8.17	1.624E-7	4061
11	10	HO2	12.39	8.122E-8	2009
12	1	HO2	9.63	8.122E-9	299
15	1 and 10	HO2	9.42	8.122E-9	299

The relationship between capillary number and breakthrough recovery of these waterflooding experiments is shown in Figure 11.13. As was previously observed in the correlations between breakthrough recovery and injection rate, the relationship between breakthrough recovery and N_{ca} is also non-linear.
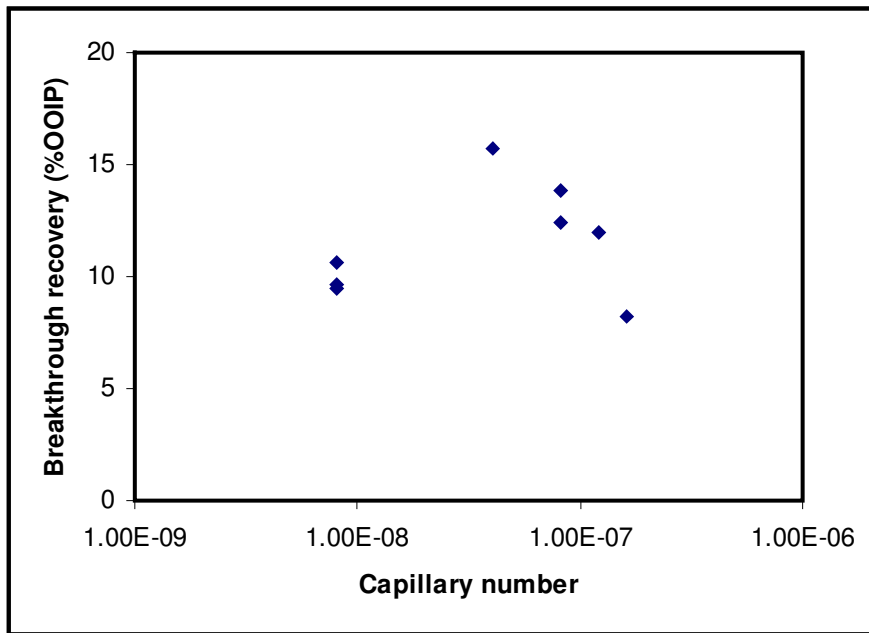
Figure 11.13: Breakthrough recovery for HO1 and HO2 vs. capillary number

In conventional oils, the final oil recovery can be improved by increasing the capillary number. This could be done by increasing the water injection rate, decreasing the oil-water interfacial tension or by increasing the viscosity of the injected water. In a

waterflood with no additional chemical additives, recovery would therefore theoretically improve if waterfloods are performed at high rates. An increase in the water flow rate could potentially create a sufficient pressure drop to mobilize the oil trapped due to capillary pressure, assuming that the oil ganglia are sufficiently large. In heavy oil systems, however, increasing the water injection rate will lead to reduced flood stability and a higher degree of viscous fingering. Figure 11.13 shows that as the capillary number is increases from 10^{-8} to 10^{-7}, the breakthrough recovery does not respond monotonically. Thus, as expected, capillary number cannot be used to predict the recovery in heavy oil waterfloods. The trends that it predicts do not hold in heavy oil systems, and the range of recoveries in heavy oil is much lower than the data shown for conventional oil.

11.3.2 Modification to Capillary Number to Include Viscosity Effect

From Table 11.5, it was seen that capillary number analysis does not apply to heavy oil due to issues regarding severe viscous fingering. Abrams (1975) also observed this limitation in capillary number, and tried to take the influence of the oil viscosity into account by empirically introducing an extra term in the capillary number:

$$N_{ca}^* = \frac{\nu \mu_w}{\sigma \; \cos \theta} \left(\frac{\mu_w}{\mu_o} \right)^{0.4} \qquad\qquad \text{Eqn (11.10)}$$

With this additional viscosity ratio term, Abrams (1975) stated that the capillary number for poorer waterflooding recovery experiments of higher viscosity fluids could be corrected. As the oil viscosity increases, this leads to an apparent decrease in the capillary number, which should therefore correspond to reduced breakthrough recovery, as is observed in adverse mobility conditions. It must be noted that the correction factor in Eqn (11.10) was obtained empirically for the range of viscosity of oils used in Abram's data set, which varied from 0.4 - 37 mPa·s. For the heavy oils used in this study, the oil viscosity is considerably higher. Abram's correlation was applied to the data set used in this study and the results are shown in Figure 11.14.
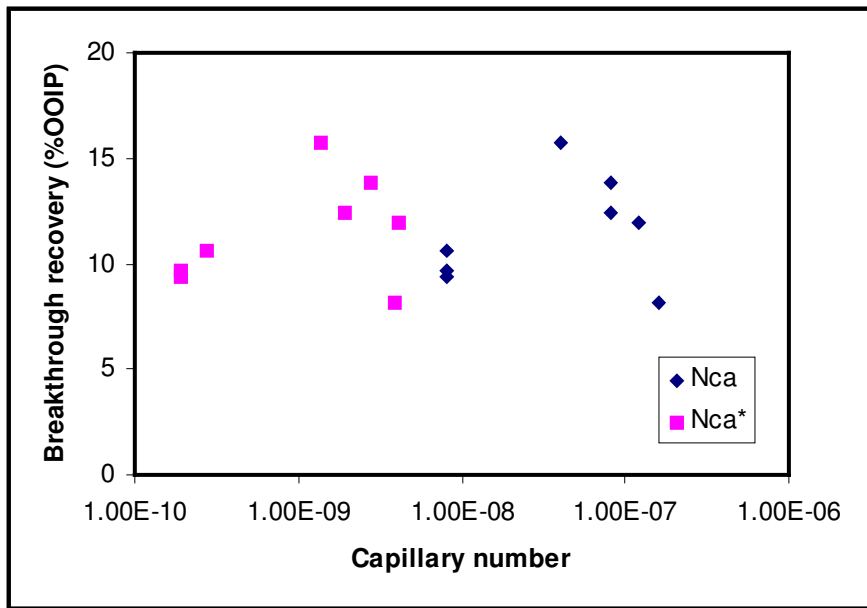
Figure 11.14: Breakthrough recovery for HO1 and HO2 for two definitions of capillary number

By incorporating the viscosity ratio, the relationship between recovery and N_{ca} is skewed toward smaller values, but this still does not improve the correlation between R_{bt} and the capillary number. Even with the additional viscosity effect, the data are separated for HO1 and HO2, and the relationship between R_{bt} and capillary number is still not monotonic. The results from these higher viscosity oils did not show the same trend observed by Abrams (1975), in which it was shown that by incorporating the viscosity ratio, the waterflooding results for the higher viscosity oils all collapsed into a single trend line. One possible reason for the scatter in Figure 11.14 is that the oil viscosities used in these experiments (4,650 and 11,500 mPa.s) are much larger than that studied by Abrams. In these systems, where the ratio of viscous to capillary forces is significantly different than the results expected under maximum oil viscosity values of 37 mPa.s, a simple correction for the viscosity ratio will not be sufficient to properly capture the recovery mechanisms of the waterflood.

11.3.3 Instability Number

The instability number has been widely used to study the nature of waterfloods performed under adverse mobility conditions. Using one expression for the instability number, Bentsen (1985) showed that recovery at breakthrough of certain waterfloods could be determined. However, these correlations were developed to predict recovery under stable ($I_{sr} < 14$) and pseudo-stable ($I_{sr} > 900$) conditions only. The waterflooding experiments performed in this study fall into two categories: the transition region ($14 < I_{sr} < 900$) and the pseudo-stable region. The breakthrough recovery of the pseudo-stable waterfloods can be predicted (Bentsen, 1985) using Eqn (3.38).

$$R_{bt} = \frac{1 - S_{wi} - S_{or}}{1 - S_{wi}} \left[\frac{X_o}{L} + \frac{1 - \dfrac{X_o}{L}}{1 + \dfrac{3(M - 1 - N_g)}{M + 1} \dfrac{M^{2/3} - 1}{M^{2/3}}} \right] \qquad \text{Eqn (3.38)}$$

In order for breakthrough recovery to be calculated using this equation, various assumptions have to be made. There are two unknown variables in the equation: S_{or} and X_o. These are the residual oil saturation and the location in the core where the viscous fingers start to develop, respectively. Due to the nature of heavy oil waterfloods the residual oil saturation cannot be easily determined. In Experiment #15, where extensive waterflooding was carried out at a low injection rate, the recovery under low injection rate waterflooding after 120 PVs injected is approximately 72%, thus in this work S_{or} was assumed to be 25%. In terms of the determination of X_o, there is no way to locate this point, thus it was assumed to have a value of zero. In fact, Sarma and Bentsen (1987) also used this assumption in their work, indicating that for unstable displacement viscous fingers begin to grow immediately at the entrance to the sandpack. The actual and predicted breakthrough recoveries are calculated using Eqn (3.38), and are reported in Table 11.6.

It was observed that Eqn (3.38) does not show any sensitivity to the injection rate. This is due to the fact that instability theory dictates that recovery in the pseudo-stable

condition is the same, regardless of the rate. This is reflected in the calculated values being fairly constant for at different rates for both oils: calculated values of R_{bt} range from 16.18 – 16.75% OOIP, while actual breakthrough recoveries range from 8.17 – 13.82% OOIP.

Table 11.6: Actual and calculated breakthrough recovery based on instability

Experiment #	S_{wi}	R_{bt} (%OOIP)	M	I_{sr}	R_{bt} from Bentsen (%OOIP)
1	12.47	13.82	465	905	16.69
2	12.77	11.94	427	1234	16.68
3	11.65	15.72	543	529	
4	11.62	10.66	606	118	
7	10.33	8.17	1500	5976	16.75
8	10.61	12.39	1500	2988	16.72
9	10.34	9.63	1500	299	
12	11.17	9.42	1500	299	

One other interesting observation is that even though the two oils have fairly different mobility ratios, the breakthrough recoveries predicted are still quite similar. This unexpected results was explained by further studying Eqn (3.38). At very high mobility ratios, this equation reduces to:

$$\left[\frac{1-\dfrac{X_o}{L}}{1+\dfrac{3(M-1-N_g)}{M+1}\dfrac{M^{2/3}-1}{M^{2/3}}} \right] \approx \frac{1}{1+3} \approx 0.25$$

For example, when the mobility ratio is 465, the value of this term is 0.254 while for the case M = 1,500, the value of this term becomes 0.252. Thus, this proves that for high mobility ratio systems the correlation suggested by Bentsen (1985) is no longer sensitive enough to the actual system. The entire term involving the mobility ratio reduces down to approximately 0.25, thus breakthrough recovery is a function of S_{wi} and S_{or}. In heavy oil systems, S_{or} is not a readily available parameter, so although the equation is developed

specifically for adverse mobility ratio situation, it is not very useful for high viscosity heavy oils.

It could also be seen that the breakthrough recoveries calculated using Eqn (3.38) are optimistic compared to the actual breakthrough values. Sarma *et al.* (1994) have also seen conflicting breakthrough recoveries, in which certain sets of data of stable displacement show high breakthrough (Demetre *et al.*, 1982) while other equally stable displacements yielded significantly lower values. They suggested that the wettability constant proposed by Peters and Flock is actually a function of displacement rate, although this could not be validated. Another source of this discrepancy could be the definition of the breakthrough point. It is possible that different researchers defined water breakthrough differently, which would lead to different set of values even for similar fluid systems. In addition, the dimensions of the sandpacks utilized in these waterfloods could also have an influence on the results. Therefore, it was difficult to conclude whether the breakthrough recovery predicted by Bentsen is adequate. The equation is not sensitive to injection velocity or mobility ratio, but it cannot be definitively concluded whether the breakthrough recovery values are in fact too optimistic, or if the differences are simply a reflection of different interpretations.

Currently, there is no correlation to predict breakthrough recovery for heavy oil waterflooding. However, the breakthrough point is not as important as it is in waterflooding of conventional oil, since significant oil production can still continue after breakthrough. Thus, it is desired to develop a correlation between waterflood recovery after breakthrough with various relevant parameters. Although instability theory was only constructed to predict the behavior until breakthrough, the results from Chapter 7 indicate that the total recovery will also be somewhat affected by the same factors that control the stability of the flood front before breakthrough. To further explore this relationship, results from the literature were gathered and plotted along the experimental results obtained in this study. The data are all shown together in Figure 11.15.

Figure 11.15: Recovery after 5 pore volumes of injection vs. instability number

Instability number in Figure 11.15 was calculated using the Peters and Flock (1981) equation of instability:

$$I_{sr} = \frac{(M-1)\nu\mu_w D^2}{C^*\sigma k_{wor}}$$

Eqn (3.33)

It can be seen that as the instability number increases, the total recovery after five pore volumes of water injection decreases. This figure shows that as floods become more unstable, this affects not just the recovery up to water breakthrough, but overall the total flood recovery is also expected to decrease.

The data used to generate Figure 11.15 are summarized in Table 11.7, which lists the literature sources and the rock/fluid properties along with the results of the current floods. The waterfloods performed in this study are labeled as A – F, and other data obtained from literature sources are shown in Roman Numerals. It should be noted that some of these references did not provide the recovery after 5 PVs of brine injection, so the data they provided were either interpolated or extrapolated to obtain the recovery at 5 PVs.

Also, since most of these sources did not report k_{rw} at S_{or} or k_{ro} at S_{wi}, these values had to be approximated in the calculation of mobility ratio. As a result, the mobility ratios are only approximations. Some of the experiments (labeled with *) were performed in 2-D sandpacks.

Table 11.7: Dead oil waterflood data from this study and from literature

Source	D (cm)	L (cm)	ϕ (fraction)	k (D)	μ_o (mPa·s)	v (m/s)	R (%OOIP)
A	8.89	114.8	0.348	3.86	11,500	1.23E-07	24
B	3.63	21.1	0.450	9.7	11,500	2.44E-07	26
C	3.63	21.1	0.450	9.05	11,500	4.39E-06	20
D	2.6	53.2	0.410	0.79	11,500	3.04E-06	27
E	2.54	9.3	0.460	10	11,500	2.35E-07	27
F	2.54	9.27	0.457	10	11,500	4.88E-06	21
I	5.64	46.6	0.348	3.6	10.4	5.92E-05	71.02
	5.64	46.6	0.348	3.6	10.6	6.40E-05	69.71
	5.64	46.6	0.348	3.6	19	1.32E-04	61.13
	5.64	46.6	0.348	3.6	112	1.32E-04	54.52
	5.64	46.6	0.348	3.6	110	1.08E-04	54
	5.64	46.6	0.348	3.6	95	2.12E-04	50.63
II	4.25	14.2	0.356	6.5	430	1.11E-06	51.4
	4.25	14.2	0.358	7.1	1,450	1.96E-06	43.1
III	*20.3x1	50.5	0.390	95.5	717	2.74E-07	26.68
	*20.3x1	50.5	0.390	95.5	717	5.47E-07	21.34
	*20.3x1	50.5	0.390	95.5	717	1.09E-06	19.21
IV	5.64	46.7	0.350	3.6	450	1.11E-07	43.38
	5.64	46.7	0.350	3.6	12	8.89E-07	55.88
V	5	30	0.391	1.3	2,140	4.87E-06	35
VI	5.08	30.48	0.394	3.807	1,649	7.06E-06	35
	5.08	30.48	0.398	1.689	1,600	7.06E-06	48
VII	5	61	0.374	5.11	2,045	9.54E-05	35
VIII	5.04	100	0.338	17.8	408.3	5.56E-06	53.9
	5.04	60	0.387	9.2	18	9.26E-05	60
IX	*4.5x4.5	30	0.236	1.039	51.2	1.16E-05	50.8
X	5.64	43.7	0.344	3	1,190	1.01E-05	44.79
	5.64	43.7	0.344	3	116	9.88E-06	56.27
	5.64	43.7	0.344	3	19.4	1.02E-05	54.59
	5.64	43.7	0.344	3	5.7	1.04E-05	48.99
	5.64	43.7	0.344	3	2.21	1.08E-05	61.59

Table 11.8 provides additional information regarding the source for which data was obtained in each waterflood.

Table 11.8: Reference for waterflood data in Table 11.7

Numeral	Source
I	Sarma *et al*., 1990
II	Liu *et al*., 2006
III	Sarma *et al*., 1994
IV	Maini *et al*., 1990
V	Zhang *et al*., 2006
VI	Farouq Ali *et al*., 1979
VII	Thomas *et al*., 2001
VIII	Symonds *et al*., 2006
IX	Hou *et al*., 2006
X	Maini and Okazawa, 1987

From Figure 11.15 and Table 11.7, it was observed that waterflood recovery appears to be somewhat constant when the instability number is less than 13.56. This was also observed by numerous other researchers (Peters and Flock, 1981, Bentsen, 1985, Sarma & Bentsen, 1987). For higher instability numbers, recovery decreases exponentially with increasing instability number, thus on the semi-logarithmic scale in Figure 11.15 the trend appears linear. However, a significant amount of scatter is present in this relationship. This could be caused by a combination of many factors. As mentioned previously, due to the lack of information some of the data had to be approximated, which has certainly contributed some errors to this figure. It must also be kept in mind that these results were gathered from many different researchers, each using different types of sand, different dimensions and geometry of the sandpacks, as well as different packing techniques. Any of these parameters could have changed the value of $C*$ in Eqn (3.33). Finally, the conditions after breakthrough are not the same as the conditions before breakthrough, therefore total waterflood recovery is only marginally related to the instability number.

Another source of scatter in Figure 11.15 is that there are other aspects of the waterfloods that the instability number did not take into consideration, such as the length or the

permeability of the system. The data from Table 11.7 shows that the range of permeability used to generate Figure 11.15 varies from 0.79 D to 95.5 D. Capillary forces are directly related to permeability, thus the data obtained from high versus low permeability systems will have very different responses from water imbibition. This significant variability would definitely contribute to the scattering seen in Figure 11.15. Therefore, although waterflood recovery can be roughly attributed to the instability number, this will only provide an order of magnitude level of accuracy for recovery.

11.3.4 Empirical Relationship

It has been shown throughout this study that the waterflooding recovery is a function of various parameters, and that capillary forces can aid in recovery. Although recovery can be approximately predicted using the instability number, this is still a fairly cumbersome approach, since it involves estimation of parameters such as end point relative permeability values, which may not be known for a given system. Thus, an attempt was made to develop a new simple empirical correlation for predicting recovery in heavy oil waterfloods, using parameters that are commonly known in these systems.

In any heavy oil waterflood, it has been shown that certain parameters are extremely important for predicting the waterflood response. Oil viscosity has an impact on recovery, since this is directly related to both the viscous forces and also the imbibition rate. Rock permeability is also a critical parameter to the success of a waterflood, as this also contributes to both the viscous and capillary forces in the system. Finally, the injection velocity has been shown to have a considerable impact on the waterflood response. All three parameters are readily available, thus it was decided to relate oil recovery to only these three parameters. The data from this experimental suite was combined with the literature data in Table 11.7, and recovery was once again assumed to be the value after 5 PVs of water injection. The following empirical relationship was found for this data set of waterfloods:

$$R = 105 \frac{v^{0.010}}{k^{0.13}\mu_o^{0.10}}$$
   Eqn (11.11)

Eqn (11.11) shows that oil recovery is inversely proportional to absolute permeability (D) and oil viscosity (mPa·s), and directly proportional to injection velocity (m/s). The effect of permeability and oil viscosity are not unexpected. As permeability decreases (while, of course, still remaining high enough for heavy oil to flow), the effect of imbibition becomes more significant and oil recovery is expected to increase. Likewise, as oil viscosity increases, recovery has been shown to decrease. This is a contribution of both increased instability and also a slower imbibition rate, since water must displace oil in order to imbibe into rock pores.

The effect of velocity is somewhat unexpected, given the results shown throughout this study that clearly indicate recovery should decrease with increasing injection rate. However, upon closer analysis of the response from viscous versus capillary forces, the relationship can be explained. In the first 1 – 2 PVs of water injection, water is injected into the viscous heavy oil at a fixed rate. Before water breakthrough can occur, oil cannot flow out as quickly as water can enter the core, thus a very high pressure gradient develops in the system. During this time, oil production is dominated by viscous forces, which are proportional to fluid velocity. It was only after several pore volumes of water had been injected that the recovery eventually became higher than the values at higher injection rates, which by that point had leveled out. Finally, it should be noted that in Figure 11.4, when the fluid injection rate was increased from 1 – 10 cm³/hr, the oil flow rates did in fact increase. The increase was much smaller than that of the injection rate, and this was reflected in reduced normalized oil flow rates and was indicative of the low efficiency of injecting at high rates. Despite this reduced efficiency, oil flow rates still increased, at least for a time, at higher injection rates. The fact that the velocity term is in the numerator in Eqn (11.11) is due to the complex nature of the velocity relationship to oil recovery. In terms of velocity, imbibition and viscous flow are actually in competition.

The exponent of the velocity term is much smaller than those of permeability and oil viscosity, which reflects the ambiguity in how this parameter affects final recovery. The predicted values are plotted against the actual recoveries in Figure 11.16.
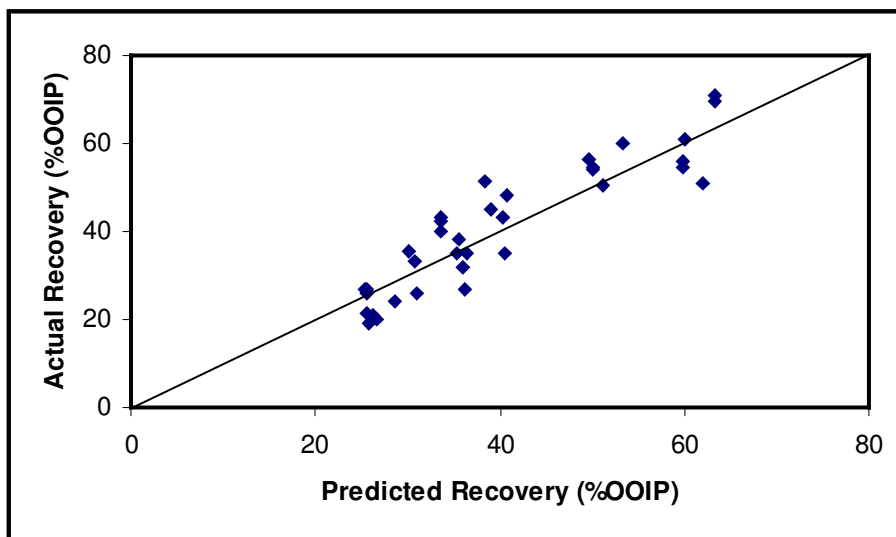
Figure 11.16: Oil recovery predictions made using a simple empirical correlation

The data used in generating this correlation cover a wide range of injection rates (10^{-4} – 10^{-7} m/s), absolute permeability (0.79 – 95.5 D) and oil viscosity (12 – 11,500 mPa·s). This simple empirical correlation therefore appears to be valid for estimating oil recovery in homogeneous water wet systems of widely varying permeability and oil viscosity.

11.4 Discussion

In previous chapters, it was demonstrated that heavy oil recovery by waterflooding is significantly affected by the relative magnitude of viscous and capillary forces present. At lower rates, and with longer times, waterfloods were more efficient and overall oil recovery was higher. Imbibition was demonstrated as a recovery mechanism that is largely responsible for oil production at later times, after water breakthrough has already occurred. Imbibition occurs through a combination of co-current and counter-current processes, and involves film thickening as well as complete displacement of oil out of pores. In this chapter, an attempt was made to quantify some

of these earlier findings. Specifically, the goal of this chapter was to identify the contribution of imbibition to recovery, predict relative permeability for heavy oil and water, and to develop correlations to estimate the recovery that can be expected for heavy oil waterfloods.

It was shown at the start of this chapter that at late times in a waterflood, recovery is proportional to the square root of time, which is indicative of imbibition processes. While the slopes in heavy oil-water systems are obviously much lower than in water – gas cores, the fact that recovery follows the expected imbibition profile shows that imbibition is not only present at this time, but that this mechanism dominates oil recovery. In any heavy oil waterflood, oil production is due to both viscous and capillary forces. Increasing the viscous forces leads to faster oil recovery, however it was shown in this chapter that as the relative size of the capillary term decreases, the flood efficiency decreases proportionally. Therefore, high oil production rates must be balanced by improved flood efficiency in order to maximize recovery.

The optimal waterflood scheme will likely incorporate some mixture of fast and slow injection. High rate injection at early times into dead oil systems develops high pressure gradients, which forces oil flow despite the possibility of increased viscous fingering at these rates. After water breakthrough, when the pressure gradient in the core is low, reducing injection rate will lead to improvement in the waterflood efficiency. Under a lower injection rate, the viscous pressure gradient is low, and this leaves more time for water to imbibe into the core and displace oil. Once the oil has been moved into regions where flow is possible, increasing the injection rate again may lead to faster oil production. Then, once the slope of the oil recovery with time decreases again, water injection rate can be reduced once more. In this manner, capillary forces are used to re-distribute oil while viscous forces allow for faster production.

Oil and water relative permeability measurements cannot be accurately determined in heavy oil systems, due to the many assumptions of relative permeability theory that are

not met in heavy oil waterfloods. However, since this data is required in all reservoir simulators, the JBN method was used to calculate apparent relative permeability relationships that account for the produced oil cuts. It was observed that oil relative permeability is not a strong function of either oil viscosity or water injection rate, but that these parameters have a much more significant impact on the water relative permeability. At reduced rates or for lower viscosity oils (i.e. for lower instability number conditions) apparent water relative permeability is reduced. This is a reflection of more stable waterfloods at these conditions. Unfortunately, due to the lack of accurate pressure data at very low rates, relative permeability curves could not be obtained for the most stable waterfloods. However, it is apparent that in all the heavy oil waterfloods performed in this work, water relative permeability is orders of magnitude less than that of oil.

Oil recovery from waterflooding cannot be predicted by capillary number analysis, even when corrections have been made for the oil/water viscosity ratio. There is a relationship between final oil recovery and I_{sr}, which shows that waterflood recovery decreases as floods become more unstable. Additionally, another empirical correlation was also developed, which relates oil recovery only to three parameters: oil viscosity, sand permeability, and (to a lesser extent) the water injection rate. These parameters are readily defined for any given waterflood. Based on a collection of adverse mobility waterfloods performed in this work and taken from the literature, oil recovery predictions can be made with order of magnitude accuracy in linear, dead oil systems.

Naturally, the inherent assumption in all of this work is that the sand is water wet and rock properties are relatively homogeneous. With water imbibition being the dominant recovery mechanism in heavy oil systems, recovery will obviously be considerably lower in a mixed wet or oil wet reservoir. With these limitations in mind, it appears that it is possible to account for the influence of capillary forces in heavy oil systems, which are shown macroscopically in heavy oil relative permeability information oil recovery predictions.

CHAPTER 12: CONCLUSIONS AND RECOMMENDATIONS

The original hypothesis made in this research was that capillary forces are significant in heavy oil systems, and that after water breakthrough oil recovery is due to displacement from water imbibition. The experimental work plan developed varied the relative significance of viscous and capillary forces, in order to understand the importance of these forces in heavy oil waterflooding. In a waterflood it is not always possible to identify what are the mechanisms that are causing oil to flow, however by varying the viscous forces while keeping the capillary forces relatively constant, the effect of water imbibition could be deduced. Imbibition was later measured directly, through NMR relaxometry and the analysis of CT imaging. Finally, once the presence and importance of imbibition had been proven in these heavy oil cores, an attempt was made to quantify these effects and predict oil recovery.

12.1 Conclusions

The main conclusions reached in this research are the following:

- At late times, viscous forces are not responsible for oil production at low waterflood rates. At low injection rates oil recovery was higher, and fluids were produced at lower water cuts (although still greater than 90%). With slow injection the normalized oil rates are essentially sustained, while at higher injection rates the normalized oil production rate declined much more quickly. The oil rates under low injection rates also appeared to be sustained even for very small pressure drops.

- Viscous forces are significant prior to water breakthrough, and can be used to maximize the initial oil production rates. Later in the life of a waterflood, when the viscous force contribution has been depleted, rates can be reduced to improve the flood efficiency.

- Waterfloods that are currently ongoing at high injection rates will still respond favourably to a rate reduction. It is never too late to allow capillary forces to aid recovery.

- When comparing against dead oil waterfloods, it can be concluded that secondary waterflooding can still lead to significant oil recovery, even without the benefit of oil recovery before water breakthrough. The same mechanisms of oil recovery through imbibition of water at later times are apparent in secondary waterfloods.

- In flowing systems, an analysis of NMR spectra showed that imbibition occurs by a combination of linear displacement and water film thickening. The presence of these thickening water films indicates that sand grains must be completely covered with a thin layer of water, and that the films are hydraulically conductive. Water film thickening was shown to be a significant recovery mechanism at low injection rates into high permeability sand.

- Under low rate waterflooding, imbibition leads to water saturation increasing everywhere in the core, and constant water saturations with length. This indicates a movement of water away from the water channels and into the core. Under these conditions, the presence of water film thickening leads to oil displacement and water saturation increasing in a larger area of the core. Sweep efficiency is therefore improved under low rate injection and with film thickening.

Other conclusions can also be drawn:

- For very unstable floods, Bentsen (1985) discussed the possibility that waterfloods are pseudo-stable, meaning that they are so unstable that recovery will be essentially constant for multiple injection rates, but will still be lower for higher mobility ratio oils. In these core floods, this was not observed. Recovery was only marginally worse for increasing oil viscosity, but recovery improved monotonically with decreasing injection rate, despite the fact that these floods were all performed under the pseudo-stable conditions. It appears that while higher oil viscosity does have a negative impact on waterflood recovery, the effect of the oil viscosity is not as significant as would be expected through an analysis of mobility ratio calculations.

- The effect of sand permeability on oil recovery is not easy to decipher. Lower permeability sand leads to higher capillary forces, but it also alters the viscous forces since higher pressure gradients will develop across the core, and it is more difficult

for oil to flow through the core as well. When the waterflood recovery was interpreted for just the portion of oil recovered after water breakthrough (i.e. excluding the initial production when large pressure gradients could be sustained in the cores), it became apparent that the lowest permeability system gave the highest recovery. Therefore, reservoirs where the significance of capillary forces is higher should respond well to waterflooding.

- During primary depletion of live oil, recovery was better for higher permeability cores, with higher maximum pressure gradients, and for lower live oil viscosity. This means that in primary production, viscous forces control the oil production: higher viscous forces mean better recovery. This is the opposite of what was observed in heavy oil waterflooding, particularly after breakthrough.

- In systems after primary production, as water was injected pressure built up in the core. During this time, very little oil was produced. This indicated that water moved preferentially into the gas channels that were remaining after primary production. The fact that water injection caused pressure to build up meant that not all the gas was connected, and that oil films had to be broken or displaced by the water.

- When comparing the injected versus produced volumes of water in secondary waterflooding, it was determined that similar volumes of water entered the core up until breakthrough, but not all the gas was displaced. This meant that there is still residual gas present during secondary waterflooding, meaning that these displacements are not as efficient as primary waterfloods.

- The major difference between primary and secondary waterflooding is that water injection has to occur at approximately one order of magnitude lower rates. Normalized oil production rates were essentially the same for primary versus secondary waterfloods at the same scale.

- For lower permeability sand, it was observed that although recovery was still optimal overall, linear displacement of oil out of pores was more prominent than film thickening. However, the lower permeability sand also led to higher pressure gradients, which increased the viscous force contribution in this system. In order to

reap the benefits of film thickening, flow rates must be reduced to low levels such that the relative magnitude of the capillary forces is greater.

- Under high rate waterflooding, water prematurely breaks through in a few selected fingers, surrounded by regions of two-phase saturation. This indicates that the majority of injected water is moving through the water channels, and oil recovery after breakthrough occurs in the regions close to the water channels. Other portions of the core remain un-swept.

- When considering the mechanism of imbibition, it was concluded that oil production is likely the result of a combination of co-current and counter-current imbibition. Imbibition cannot be modeled in the same way as conventional analytical expressions.

- It was observed that at later times in waterfloods, oil rates are linear with the square root of time. This is evidence that not only is imbibition present, but that imbibition controls the oil production since the rates follow the relationship described in capillary pressure dominated flow.

- Oil and water relative permeability were calculated from the production data of dead oil waterfloods, and it was seen that the water relative permeability is much more strongly affected by the oil viscosity and injection rate, compared to the oil. Lower water relative permeability (i.e. more stable waterfloods) are measured for lower oil viscosity and lower injection rates.

- In general, water relative permeability is orders of magnitude lower than that of heavy oil. This is the influence of capillary forces and imbibition, where all of these effects are combined into the relative permeability term.

- Heavy oil recovery by waterflooding cannot be predicted by capillary number analysis, even when corrections are made for the difference between oil and water viscosity. There is a correlation between oil recovery and Instability number, showing that oil recovery decreases as waterfloods become more unstable, but this correlation contains significant scatter.

- An empirical equation was developed for predicting oil recovery in dead oil systems from waterflooding as a function of the oil viscosity, the sand permeability and the

water injection rate. Assuming that the sand is water wet, order of magnitude accuracy predictions can be made in linear dead oil systems.

12.2 Recommendations

Although this work provided considerable insight into the influence of capillary forces and water imbibition in heavy oil waterflooding, several recommendations can be made for improving the understanding of these processes:

- One of the biggest problems with interpreting the highest efficiency waterfloods was the lack of accurate pressure data. Low rate waterfloods should be performed using a much lower range pressure transducer (i.e. inches of water) to get better pressure information for relative permeability and mobility calculations for these optimal waterfloods.

- The results to date indicate that oil viscosity is not a strong parameter that affects the production rates and total recovery after water breakthrough. This conclusion should be validated by performing waterfloods for a wider range of oil viscosity values (e.g. 500 mPa·s and 50,000 mPa·s).

- In the CT and NMR analysis of the water saturation at early times or under high injection rates, it was observed that water saturation is not constant along the length of the core. Rather, water saturation is highest near to the inlet, and less oil is recovered close to the outlet of the core. This indicates a non-linear pressure response in the core at early times. It may be instructive to measure pressure versus length to compare the pressure gradient at high versus low injection rates. This would require measurements in a longer core system, where differences in the pressure as a function of length can be measured.

- Primary versus secondary production were compared in the big cores, and it was observed that oil normalized production rates were similar but that water had to be injected at an order of magnitude lower rates in order to get a similar waterflood efficiency. This was attributed to the presence of some remaining gas pockets in the core, but this inference should be validated. This could be done by a CO_2 flood, which would miscibly displace all the remaining methane in the core, followed by a

waterflood. This would allow for a determination if, after recovering the trapped immiscible gas, injection rates could then be increased in secondary waterflood cores, and stable oil production could be obtained faster.

- In waterflooding of lower permeability sandpacks, it was observed that linear displacement of oil completely out of pores appeared to be more significant than water film thickening for recovering oil. In higher permeability cores, water film thickening was an extremely important mechanism. The waterflood in the low permeability sand should therefore be redone at a reduced injection rate, such that the ratio between the viscous and capillary forces decreases, in the manner of Table 9.4. This could allow for more efficient displacement, and would also allow for a validation of film thickening in lower permeability systems.

- Experiments have to be designed to visualize the nature of imbibition. Specifically, when water enters the pore, if oil is produced mainly through so-called co-current or counter-current imbibition. A micro-model or micro-CT study may be valuable to attempt to image mechanisms such as film thickening, and to develop a better understanding of the pore level displacement mechanisms that are occurring during imbibition.

- For waterfloods in NMR transparent core holders, more information could be obtained if the waterflood was followed with a D_2O flood (which gives no water signal) to identify moveable water pathways. This would shed more light on the contribution of linear displacement compared to water film thickening.

- It would also be useful to re-do a waterflood in the NMR, but using silicon oil (which has no NMR signal). This would allow for definitive proof that water is relaxing under 10 ms, and the actual T_{2gm} and water amplitude values could be measured to separate the contribution of water in pendular rings versus thin films covering the sand grains.

- It would be valuable to perform a straight imbibition experiment (similar to an Amott study) in the NMR core holder. This would be similar to the data measured for the static vials in Chapter 9, but the NMR would allow for additional information regarding where water imbibes in the core. This experiment could be performed both

with and without connate water, to identify the difference in water displacement mechanisms in these systems.

- An additional experiment was performed (not included in this thesis) in a 2-D model, where water was injected at infinitely slow rates. In this core, the waterflood recovery is presently over 30% of the oil, with no water breakthrough. This is possibly evidence of oil displacement only through water film thickening. If this experiment could be performed again, either as a 2-D or linear system, and the results could be imaged, it may be possible to identify if water saturation changes just near to injection point (i.e. slow viscous displacement) or if saturation changes everywhere (i.e. film thickening).

- The major conclusion reached in this research was that oil recovery after water breakthrough is the result of imbibition. This can be validated by making a core oil wet (through packing with Teflon beads or washing sand with toluene), and then performing a waterflood. If imbibition is in fact the dominant recovery mechanism, the oil recovered after breakthrough should be negligible, and this should be validated.

- In the low rate waterfloods, it was observed that oil production was linear with the square root of time. It is important to perform high rate waterfloods for these same time scales, and compare the results against those of low rate waterflooding. This will indicate if the slope of the oil production with time is the same (i.e. flow is fully through imbibition), or if viscous forces have an additional influence on the oil production.

- The results from this study have to be compared for a wider data set of secondary waterflooding, in order to determine if a similar empirical correlation can be developed for systems where the initial viscous forces can be neglected. Alternatively, attempts can be made to predict just the recovery of oil after breakthrough in dead oil systems using just the oil viscosity, flow rate and injection rate. However, these numbers cannot be readily obtained from results in the literature, so more experiments would have to be done internally.

CHAPTER 13: REFERENCES

Abrams, A., "The Influence of Fluid Viscosity of Fluid Viscosity, Interfacial Tension, and Flow Velocity on Residual Oil Saturation Left by Waterflood", *SPE Journal*, **15** (5), October 1975, p 437 – 447.

Adams, D.M., "Experiences with Waterflooding Lloydminster Heavy-Oil Reserviors", *Journal of Petroleum Technology*, **34** (8), August 1982, p 1643 – 1650.

AEUB, *Alberta's Energy Reserves 2006 and Supply/Demand Outlook 2007-2016*, EUB Statistical Series ST98-2007, Albertan Energy and Utilities Board, Calgary, AB Canada, June 2007.

Albartamani, N.S., Farouq Ali, S.M. and Lepski, B., "Investigation of Foamy Oil Phenomena in Heavy Oil Reservoirs", presented at the 1999 SPE International Thermal Operations and Heavy Oil Symposium, Bakersfield, California, March 13 – 15, 1999.

Alberta Energy, *North American Oil Reserves*, 2005, internet address www.energy.gov.ab.ca/Oil/pdfs/AB_OilReserves.pdf.

Alikhan, A.A. and Farouq Ali, S.M.,"Current Status of Nonthermal Heavy Oil Recovery", presented at the Rocky Mountain Regional Meeting, Salt Lake, CT, May 23 – 25, 1983.

Allsopp, K., Wright, I., Lastockin, D., Mirotchnik, K. and Kantzas, A., "Determination of Oil and Water Composition of Oil/Water Emulsions Using Low Field NMR Relaxometry", *Journal of Canadian Petroleum Technology,* **40** (7), July 2001, p 58 – 61.

Amott, E., "Observations Relating to the Wettability of Porous Rock", *Trans. AIME,* **216**, 1959, p 156 - 162.

Anderson, W.G., "Wettability Literature Survey – Part 1: Rock/Oil/Brine Interactions and the Effects of Core Handling on Wettability", *Journal of Petroleum Technology*, **38** (10), October 1986, p 1125 – 1144.

Anderson, W.G., "Wettability Literature Survey – Part 2: Wettability Measurement", *Journal of Petroleum Technology*, November 1986, **38** (11), p 1246 – 1262.

Anderson, W.G., "Wettability Literature Survey – Part 6: The Effects of Wettability on Waterflooding", *Journal of Petroleum Technology*, **39** (12), December 1987, p 1605 – 1622.

Aronofsky, J.S. and Masse, L., "A Model for the Mechanism of Oil Recovery from the Porous Matrix Due to Water Invasion in Fractured Reservoirs", *Trans. AIME*, **213**, 1958, p 17 – 19.

Batycky, J.P., McCaffery, F.G., Hodgins, P.K. and Fisher, D.B., "Interpreting Relative Permeability and Wettability From Unsteady-State Displacement Measurements", *SPE Journal*, **21** (3), June 1981, p 296-308.

Benham, A.L. and Olson, R.W., "A Model Study of Viscous Fingering", *SPE Journal*, **3** (2), June 1963, p 138 – 144.

Bennion, D.B., Mastmann, M. and Moustakis, M.L., "A Case Study of Foamy Oil Recovery in the Patos-Marinza Reservoir, Driza Sand, Albania", *Journal of Canadian Petroleum Technology*, **42** (3), March 2003, p 21 – 28.

Bentsen, R.G., "A New Approach to Instability Theory in Porous Media", *SPE Journal*, October 1985, p 765 – 779.

Blair, P.M., "Calculation of Oil Displacement by Countercurrent Water Imbibition", *SPE Journal*, **4** (3), September 1964, p 195 – 202.

Bobek, J.E., Mattax, C.C. and Denekas, M.O., "Reservoir Rock Wettability – Its Significance and Evaluation", *Trans. AIME*, **213**, 1958, p 155 – 160.

Bora, R., Chakma, A. and Maini, B.B., "Experimental Investigation of Foamy Oil Flow Using a High Pressure Etched Glass Micromodel", SPE 84033, SPE Annual Technical Conference and Exbihition, Denver, Colorado, October 5 – 8, 2003.

Bora, R. and Maini, B.B., "Flow Visualization Studies of Solution Gas Drive Process in Heavy Oil Reservoirs Using a Glass Micromodel", SPE 37519, SPE International Thermal Operations and Heavy Oil Symposium, Bakersfield, California, February 10 – 12, 1997.

Bourbiaux, B.J. and Kalaydjian, F.J., "Experimental Study of Cocurrent and Countercurrent Flows in Natural Porous Media", *SPE Res. Eng.*, **5** (3), August 1990, p 361 – 368.

Boyle, W.P., *Applied Fluid Mechanics*, McGraw-Hill Ryerson Ltd., Toronto, ON Canada, 1986.

Bryan, J., Kantzas, A., Badry, R., Emmerson, J. and Hancsicsak, T., "In Situ Viscosity of Heavy Oil: Core and Log Calibrations", *Journal of Canadian Petroleum Technology*, **46** (11), November 2007, p 47 – 55.

Bryan, J., Mai, A., Hum, F. and Kantzas, A., "Oil- and Water-Content Measurements in Bitumen Ore and Froth Samples Using Low Field NMR", SPE 97802, *SPEREE,* **9**(6), December 2006, p 654-663.

Buckley, S.E. and Leverett, M.C., "Mechanism of Fluid Displacement in Sands", *Trans. AIME*, **146**, 1942, p 107-116.

Carrigy, M.A., "Effect of texture on the distribution of oi in the Athabasca oil sands, Alberta, Canada", *J. Sedim. Res*., **62** (2), June 1962, p 312 - 325.

Chatzis, I. and Dullien, F.A.L., "Dynamic Immiscible Displacement Mechanisms in Pore Doublets: Thoery versus Experiment", *J. Coll. Int. Sci*., **91** (1), January 1983, p 199 - 222.

Chatzis, I. and Morrow, N.R., "Correlation of Capillary Number Relationships for Sandstone", *SPE Journal*, **24** (5), October 1984, p 555 – 562.

Chen, J., Gladkikh, M., Chen, S., Jacobi., D. and Kwak, H., "Determination of Grain Size Distribution From NMR Relaxation Time Using Pore Scale Modeling", SCA 2007-49, International Symposium of the Society of Core Analysts, Calgary, Alberta, September 10 –13, 2007.

Chuoke, R.L., van Meurs, P. and van der Poel, C., "The Instability of Slow, Immiscible, Viscous Liquid-Liquid Displacements in Permeable Media", *Trans. AIME*, **216**, p 188 – 194, 1959.

Clark, K.A. "Hot-Water Separation of Alberta Bituminous Sand", *Can. Inst. Min. & Metal. Trans*., **47**, 1944, p 257 - 274.

Coates, G., Xiao, L. and Prammer, M., *NMR Logging Principles and Applications*, Halliburton Energy Services, TX USA, 1999.

Coskuner, G. and Bentsen, R.G., "A Hele-Shaw cell study of a new approach to instability theory in porous media", *Journal of Canadian Petroleum Technology*, January – February 1988, p 87 – 95.

Craft, B.C., Hawkins, M. and Terry, R.E. (revised), *Applied Petroleum Reservoir Engineering*, Second Edition, Prentice Hall PTR, 1991.

Craig, F.F., *The Reservoir Engineering Aspects of Waterflooding*, American Institute of Mining, Metallurgical, and Petroleum Engineers, 1971.

Cuiec, L., Bourbiaux, B. and Kalaydjian, F., "Oil Recovery by Imbibition in Low-Permeability Chalk", *SPE Form. Eval.*, **9** (3), September 1994, p. 200 – 208.

Czarnecki, J., Radoev, B., Schramm, L.L. and Slavchev, R., "On the nature of Athabasca Oil Sands", *Adv. Coll. Int. Sci.*, 114 - 115, 2005, p 53 - 60.

Demetre, G.P., Bentsen, R.G. and Flock, D.L., "A multi-dimensional approach to scaled immiscible fluid displacement", *Journal of Canadian Petroleum Technology*, July – August, 1982, p 49 - 61.

Ding, M., Kantzas, A. and Lastockin, D., "Evaluation of Gas Saturation During Water Imbibition Experiments", *Journal of Canadian Petroleum Technology*, **45** (10), October 2006, p 29 - 35.

Donaldson, E.C., Thomas, R.D. and Lorenz, P.B., "Wettability Determination and Its Effect on Recovery Efficiency", SPE 2338, *SPE Journal*, **9** (1), March 1969, p 13 - 20.

Dullien, F.A.L., *Porous Media Fluid Transport and Pore Structure*, Academic Press, San Diego, CA USA, 1992.

Dumore, J.M., "Development of Gas-Saturation During Solution-Gas Drive in an Oil Layer Below a Gas Cap", SPE 2508, *SPE Journal*, **10** (3), September 1970, p 211 – 218.

Dyes, A.B., "Discussion of Mobility Ratio, Its Influence on Flood Patterns During Water Encroachment", *Trans. AIME*, **195**, 1952, p 22-23.

Engelberts, W.F. and Klinkenberg, L.J., "Laboratory Experiments on the Displacement of Oil by Water from Packs of Granular Materials", Third World Petroleum Congress, The Hague, 1951, p 544.

Farouq Ali, S.M., "Non-Thermal Heavy Oil Recovery Methods", SPE 5893, Rocky Mountain Regional Meeting of the Society of Petroleum Engineers of AIME, Casper, Wyoming, May 11 – 12, 1976.

Farouq Ali, S.M., Figueroa, J.M., Azuaje, E.A. and Farquharson, R.G., "Recovery of Lloydminster and Morichal curdes by caustic, acid and emulsion floods", *Journal of Canadian Petroleum Technology*, January – March 1979, p 53 – 59.

Farouq Ali, S.M. and Thomas, S., "Enhanced Oil Recovery – What We Have Learned", *Journal of Canadian Petroleum Technology*, **39** (2), February 2000, p 7 – 11.

Firoozabadi, A., Ottesen, B. and Mikkelsen, M., "Measurements of Supersaturation and Critical Gas Saturation", SPE Form. Eval., **7** (4), December 1992, p 337 – 344.

Fischer, H., Wo, S. and Morrow, N.R., "Modeling the Effect of Viscosity Ratio on Spontaneous Imbibition", presented at the 2006 SPE Annual Technical Conference and Exhibition, San Antonio, Texas, USA, September 24 – 27, 2006.

Forth, R., Slevinsky, B., Lee, D. and Fedenczuk, L., "Application of Statistical Analysis to Optimize Reservoir Performance", *Journal of Canadian Petroleum Technology*, **36** (9), October 1997, p 36 – 42.

Garb, F.A., "Waterflooding calculations for hand-held computers; part 5 – evaluating areal sweep efficiency", *World Oil*, April 1980, p 136 – 139.

Goodarzi, N.N., *Investigating Heavy Oil Solution Gas Drive Fluid Properties and the Effect of Scale on Depletion Experiments*, M.Sc. Thesis, University of Calgary, Calgary, Alberta, April 2006.

Goodarzi, N., Bryan, J., Mai, A. and Kantzas, A., "Novel Technique for Measuring Heavy Oil Fluid Properties", SPE 97803, *SPE Journal*, **12** (3), September 2007, p 305 – 315.

Goodarzi, N. and Kantzas, A., "The Effect of Scale on the Primary Depletion of Heavy Oil Solution Gas Drive", 57th Annual Technical Meeting of the Petroleum Society of CIM, Calgary, Alberta, June 13 – 15, 2006.

Graham, J.W. and Richardson, J.G., "Theory and Application of Imbibition Phenomena in Recovery of Oil", *Journal of Petroleum Technology*, **11** (2), February 1959, p 65 – 69.

Green, D.W. and Willhite, G.P., *Enhanced Oil Recovery*, SPE Textbook Series, Volume 6, 1998.

Haberman, R., "The Efficiences of Miscible Displacement as a Function of the Mobility Ratio", *Trans. AIME*, **219**, 1960, p 264 - 272.

Handy, L.L., "Determination of Effective Capillary Pressures for Porous Media From Imbibition Data", *Trans. AIME*, **219**, 1960, p 75 – 80.

Heidemann, R.A., Jeje, A.A. and Mohtadi, F., *An Introduction to the Properties of Fluids and Solids*, The University of Calgary Press, 1987.

Herrick, D.C., "Understanding Permeability", 2004 CSPG-CWLS-CHOA Joint Conference, Calgary, AB Canada, May 31 – June 4, 2004.

Hirasaki, G. and Zhang, D.L., "Surface Chemistry of Oil Recovery From Fractured, Oil-Wet, Carbonate Formations", *SPE Journal*, **9** (2), June 2004, p 151 – 162.

Hou, J.R., Dong, M.Z., Yang, J.Z., Liu, Z.C., and Yue, X.A., "Effect of Viscosity of Alkaline/Surfactant/Polymer (ASP) Solution on Enhanced Oil Recovery in Heterogeneous Reservoirs", *Journal of Canadian Petroleum Technology*, **45** (11), November 2006, p 27 – 33.

Huerta, M., Otero, C., Rico, A., de Mirabal, M. and Rojos, G., "Understanding Foamy Oil Mechanisms for Heavy Oil Reservoirs During Primary Production", SPE 36749, SPE Annual Technical Conference, Denver, Colorado, October 6 – 9, 1996.

Hum, F.M. and Kantzas, A., "Using Low-Field NMR to Determine the Wettability of, and Measure Fluid Uptake in, Coated and Uncoated Sands", *Journal of Canadian Petroleum Technology*, **45** (7), July 2006, p 23 - 28.

Jadhunandan, P.P. and Morrow, N.R., "Effect of Wettability on Waterflood Recovery for Crude-Oil/Brine/Rock Systems", *SPE Res. Eng.*, **10** (1), February 1995, p 40 - 46.

Jamaluddin, A.K.M. and Butler, R.M., "Factors Affecting the Formation of Water-in-Oil Emulsions During Thermal Recovery", *AOSTRA J. Research*, **4** (2), 1988, p 109 - 116.

Jayasekera, A.J. and Goodyear, S.G., "The Development of Heavy Oil Fields in the United Kingdom Continental Shelf: Past, Present, and Future", *SPE Res. Eval. & Eng.*, **3** (5), October 2000, p 371 – 379.

Jennings, H.Y. Jr., "Waterflood Behavior of High Viscosity Crudes in Preserved Soft and Unconsolidated Cores", *Journal of Petroleum Technology*, **18** (1), January 1966, p 116 – 120.

Johnson, E.F., Bossler, D.P. and Naumann, V.O., "Calculation of Relative Permeability from Displacement Experiments", *Trans. AIME*, **216**, p 370-372, 1959.

Jones, S.C. and Roszelle, W.O., "Graphical Techniques for Determining Relative Permeability From Displacement Experiments", *Journal of Petroleum Technology*, **30** (5), May 1978, p 807-817.

Kantzas, A., "Investigation of Physical Properties of Porous Rocks and Fluid Flow Phenomena in Porous Media Using Computer Assisted Tomography", *In Situ*, **14**(1), 1990, p 77 – 132.

Kasraie, M., Sammon, P.H. and Jespersen, P.J., "Field Development Options for a Waterflooded Heavy-Oil Reservoir", *Journal of Petroleum Technology*, **45** (9), September 1993, p 888 – 894.

Kennedy, H.T., Burja, E.O. and Boykin, R.S., "An Investigation of the Efects of Wettabiliy on the Recovery of Oil by Water Flooding", *Jour. Phys. Chem*, **59**, 1955, p 867.

Kerig, P.D. and Watson, A.T., "Relative-Permeability Estimation From Displacement Experiments: An Error Analysis", *SPE Res. Eng.*, **1** (2), March 1986, p 175 – 182.

King Hubbert, M., "Darcy's Law and the Field Equations of the Flow of Underground Fluids", *Trans. AIME*, **207**, 1956, p 222 – 239.

Kleinberg, R. and Vinegar, H., "NMR Properties of Reservoir Fluids", *The Log Analyst*, **37** (6), November – December 1996.

Ko, C.M., Domier, D.B. and MacDermott, R.N., "Waterflood Optimization of the Buffalo Coulee Bakken Heavy Oil Pool of Southwestern Saskatchewan", SPE 30285, International Heavy Oil Symposium, Calgary, Alberta, June 19 – 21, 1995.

Kumar, M., Hoang, V., Satik, C. and Rojas, D.H., "High Mobility Ratio Water Flood Performance Prediction: Challenges and New Insights", SPE 97671, SPE International Improved Oil Recovery Conference, Kuala Lumpur, Malaysia, December 5 - 6, 2005.

Kyte, J.R. and Rapoport, L.A., "Linear Waterflood Behavior and End Effects in Water-Wet Porous Media", *Trans. AIME*, **213**, 1958, p 423 – 426.

Larter, S.R., Adams, J., Gates, I.D., Bennett, B. and Huang, H., "The Origin, Prediction and Impact of Oil Viscosity Heterogeneity on the Production Characteristics of Tar Sand and Heavy Oil Reservoirs", 57th Annual Technical Meeting of the Petroleum Society of CIM, Calgary, AB Canada, Jun 13 – 15, 2006.

Leverett, M.C., "Capillary Behavior in Porous Solids", *Trans. AIME*, **142**, 1941, p 152 – 169.

Li, K. and Horne, R.N., "Scaling of Spontaneous Imbition in Gas-Liquid-Rock Systems", SPE 75176, SPE/DOE Improved Oil Recovery Symposium, Tulsa, Oklahoma, April 13 – 17, 2002 (a).

Li, K. and Horne, R.N., "Effect of Initial Water Saturation on Spontaneous Water Imbibition", SPE 76727, SPE Western Regional/AAPG Pacific Section Joint Meeting, Anchorage, Alaska, May 20 – 22, 2002 (b).

Li, K. and Horne, R.N., "Computation of Capillary Pressure and Global Mobility From Spontaneous Water Imbibition Into Oil-Saturated Rock", *SPE Journal*, **10** (4), December 2005, p 458 – 465.

Liu, Q., Dong, M. and Ma, S., "Alkaline/Surfactant Flood Potential in Western Canadian Heavy Oil Reservoirs", SPE 99791, 2006 SPE/DOE Symposium on Improved Oil Recovery, Tulsa, OK USA, Apr 22 – 26, 2006.

Ma, S., Morrow, N.R. and Zhang, X., "Generalized scaling of spontaneous imbibition data for strongly water-wet systems", *Journal of Petroleum Science and Engineering*, **18**, 1997, p 165 - 178.

Macdonald, I.F., El-Sayed, M.S., Mow, K. and Dullien, F.A.L., "Flow through Porous Media – the Ergun Equation Revisited", *Ind. Eng. Chem. Fundam.*, **18** (3), 1979, p 199-208.

Maini, B.B., "Is it Futile to Measure Relative Permeability for Heavy Oil Reservoirs", *Journal of Canadian Petroleum Technology*, **37** (4), April 1998, p 56-62.

Maini, B.B., Coskuner, G. and Jha, K., "A comparison of steady-state and unsteady state relative permeabilities of viscous oil and water in Ottawa sand", *Journal of Canadian Petroleum Technology*, **29** (2), March – April 1990, p 72-77.

Maini, B.B. and Javadpour, F., "Immiscible Displacement Experiment (Waterflooding)", Department of Chemical and Petroleum Engineering, University of Calgary, Canada, September 2000.

Maini, B.B. and Okazawa, T., "Effects of temperature on heavy oil-water relative permeability of sand", *Journal of Canadian Petroleum Technology,* May – June 1987, p 33 – 41.

Manalo, F.P., Kantzas, A. and Langford, C.H., "Soil Wettability as Determined from Using Low-Field Nuclear Magnetic Resonance", *Environmental Science & Technnology*, **37** (12), 2003, p 2701 – 2706.

Mannhardt, K., "The Measurement of Interfacial Tension by the Spinning Drop Method", Petroleum Recovery Institute, Calgary, Alberta, Canada, March 13, 1987.

Mannhardt, K. and Kantzas, A., "Interfacial Tension by the Spinning Drop Method", Laboratory Exercises Enpe 513: Flow in Porous Media, Department of Chemical and Petroleum Engineering, University of Calgary, Calgary, AB Canada, Aug 2004.

Mattax, C.C. and Kyte, J.R., "Imbibition Oil Recovery from Fractured, Water-Drive Reservoir", *SPE Journal*, **2** (2), June 1962, p 177 – 184.

McAuliffe, C.D., "Oil-in-Water Emulsions and Their Flow Properties in Porous Media", *Journal of Petroleum Technology*, **25** (6), June 1973, p 727-733.

Miller, K.A., "Improving the State of the Art of Western Canadian Heavy Oil Waterflood Technology", *Journal of Canadian Petroleum Technology*, **54** (4), April 2006, p 7 – 11.

Mirotchnik, K.D., Allsopp, K., Kantzas, A., Curwen, D. and Badry, R., "Low-Field NMR Method for Bitumen Sands Characterization: A New Approach", SPE 71208, *SPE Res. Eval. & Engg.*, **4** (2), Apr 2001, p 88 – 96.

Moore, T.F. and Slobod, R.L., "The Effect of Viscosity and Capillary On the Displacement of Oil by Water", *Producers Monthly*, August 1956, p 20 – 30.

Morrow, N.R. and Mason, G., "Recovery of oil by spontaneous imbibition", *Current Opinion in Colloid & Interface Science*, **6**, 2001, p 321 – 337.

Mungan, N., "Role of Wettability and Interfacial Tension in Water Flooding", *SPE Journal*, **4** (2), June 1964, p 115 – 123.

Mungan, N., "Certain Wettability Effects In Laboratory Waterfloods", *Journal of Petroleum Technology*, **18** (2), February 1966, p 247 – 252.

Newcombe, J., McGhee, J. and Rzasa, M.J., "Wettability versus Displacement in Water Flooding in Unconsolidated Sand Columns", *Trans. AIME*, **204**, 1955, p 227 – 232.

Oefelein, F.H. and Walker, J.W., "California Flood Yields Profitable Recovery of Heavy Oil from Multilayered Reservoir", *Journal of Petroleum Technology*, **16** (5), May 1964, p. 509 – 514.

Outmans, H.D., "Nonlinear Theory for Frontal Stability and Viscous Fingering in Porous Media", *Trans. AIME*, **2** (2), June 1962, p 165 – 176.

Ostos, A.N. and Maini, B.B., "An Integrated Experimental Study of Foamy Oil Flow During Solution Gas Drive", *Journal of Canadian Petroleum Technology*, **44** (4), April 2005, p 43 – 50.

Paidin, W.R. and Rao, D.N., "Physical Model Experiments to Evaluate the Effect of Wettability and Fractures on the Performance of the Gas Assisted Gravity Drainage (GAGD) Process", SCA 2007-48, International Symposium of the Society of Core Analyst, Calgary, Alberta, September 10 – 13, 2007.

Peters, E.J. and Flock, D.L., "The Onset of Instability During Two-Phase Immiscible Displacement in Porous Media", *SPE Journal*, **21** (2), April 1981, p 249 – 258.

Peters, E.J. and Khataniar, S., "The Effect of Instability on Relative Permeability Curves Obtained by the Dynamic Displacement Method", *SPE Form. Eval.*, **2** (4), December 1987, p 469 – 474.

Perkins, F.M., "An Investigation of the Role of Capillary Forces in Laboratory Water Floods", *Journal of Petroleum Technology*, **9** (11), November 1957, p 49 – 51.

Perkins, T.K. and Johnston, O.C., "A Study of Immiscible Fingering in Linear Models", *SPE Journal*, **9** (1), March 1969, p 39 – 46.

Pooladi-Darvish, M. and Firoozabadi, A., "Cocurrent and Countercurrent Imbibition in a Water-Wet Matrix Block", *SPE Journal,* **5** (1), March 2000, p 3 – 11.

Radler, M., "Oil production, reserves increase slightly in 2006", *Oil & Gas Journal*, **104** (47), Dec 18 2006, p 20-23.

Rao, D.N. and Girard, M.G., "A New Technique for Reservoir Wettability Characterization", *Journal of Canadian Petroleum Technology*, **35** (1), January 1996, p 31-39.

Rapoport, L.A., "Scaling Laws for Use in Design and Operation of Water-Oil Flow Models", *Trans. AIME*, **204**, 1955, p 143 – 150.

Rapoport, L.A. and Leas, W.J., "Properties of Linear Waterfloods", *Trans. AIME*, **198**, 1953, p 139-148.

Reis, J.C. and Cil, M., "A model for oil expulsion by counter-current water imbibition in rocks: one-dimensional geometry", *Journal of Petroleum Science and Engineering*, **10**, 1993, p 97 – 107.

Reisberg, J. and Doscher, T.M., "Interfacial Phenomena in Crude Oil – Water Systems", *Prod. Monthly*, November 1956, p 43 – 50.

Rojas, G.A. and Farouq Ali, S.M., "Dynamics of Subcritical CO_2/Brine Floods for Heavy Oil Recovery", SPE 13598, *SPE Res. Eng.*, **3** (1), February 1988, p 35 – 44.

Rosen, M.J., *Surfactants and Interfacial Phenomena, Second Edition*, John Wiley & Sons, New York, NY USA, 1989.

Sarma, H.K. and Bentsen, R.G., "An experimental verification of a modified instability theory for immiscible displacements in porous media", *Journal of Canadian Petroleum Technology*, **26** (4), July - August 1987, p 88-99.

Sarma, H.K. and Bentsen, R.G., "A new method for estimating relative permeabilities from unstabilized displacement data", *Journal of Canadian Petroleum Technology*, **28** (4), July - August 1989, p 118-128.

Sarma, H.K., Maini, B.B. and Allen, G., "Effects of Viscous Instability on Unsteady-State Permeability", CIM/SPE 90-66, International Technical Meeting, Calgary, Alberta, June 10 – 13, 1990.

Sarma, H.K., Maini, B.B., Purves, R.W. and Jha, K.N., "A Laboratory Investigation of the Pseudo Relative Permeability Characteristics of Unstable Immiscible Displacements", *Journal of Canadian Petroleum Technology*, **33** (1), January 1994, p 42 – 49.

Scott, G.R., Collins, H.N. and Flock, D.L., "Improving Waterflood Recovery of Viscous Crude Oils by Chemical Control", *The Journal of Canadian Petroleum*, October – December, 1965, p 243 – 251.

Scheidegger, A.E., *The Physics of Flow Through Porous Media*, University of Toronto Press, Canada, 1974.

Schramm, L.L., Stasiuk, E.N. and Turner, D., "The influence of interfacial tension in the recovery of bitumen by water-based conditioning and flotation of Athabasca oil sands", *Fuel Proc. Tech.*, **80**, 2003, p 101 – 118.

Selby, R., Alikhan, A.A. and Farouq-Ali, S.M., "Potential of non-thermal methods for heavy oil recovery", *Journal of Canadian Petroleum Technology*, **28** (4), July – August 1989, p 45 - 59.

Shen, C. and Batycky, J.P., "Observation of Mobility Enhancement of Heavy Oils Flowing Through Sand Pack Under Solution Gas Drive", *Journal of Canadian Petroleum Technology*, **38** (4), April 1999, p 46 – 53.

Sigmund, P.M. and McCaffery, F.G., "An Improved Unsteady-State Procedure for Determining the Relative Permeability Characteristics of heterogeneous Porous Media", *SPE Journal*, **19** (1), 1979, p 15-28.

Sigmund, P., Sharma, H., Sheldon, D. and Aziz, K., "Rate Dependence of Unstable Waterfloods", *SPE Res. Eng.*, **3** (2), May 1988, p 401 – 409.

Singhal, A.K. and Holowatuk, C., "Role of Operating Practices on Performance of Waterfloods in Heavy Oil Reservoirs", Petroleum Society's 8th Canadian International Petroleum Conference, Calgary, Alberta, Canada, June 12 – 15, 2007.

Smith, G.E., "Waterflooding Heavy Oils", SPE 24367, SPE Rocky Mountain Regional Meeting, Casper, Wyoming, May 18 – 21, 1992.

Sobol, W.T., Schreiner, L.J., Miljkovic, L., Marcondes-Helene, M.E., Reeves, L.W. and Pintar, M.M., "N.m.r. line shape-relaxation correlation analysis of bitumen and oil sands", *Fuel*, **64**, 1985, p 583 - 590.

Stewart, C.R., Hunt, E.B. Jr. and Berry, V.J. Jr., "The Role of Bubble Formation in Oil Recovery by Solution Gas Drive in Limestones", *Journal of Petroleum Technology*, **5** (12), December, 1954, p 21 – 28.

Straley, C., Rossini, D., Vinegar, H., Tutunjian, P. and Morriss, C., "Core Analysis by Low Field NMR", *The Log Analyst*, **38** (2), March – April 1997.

Sutton, E., "Waterflood Performance in a High Viscosity Oil Reservoir", *Journal of Petroleum Technology*, **15** (12), December 1963, p 1281 – 1284.

Symonds, R.W.P, Farouq Ali, S.M. and Thomas, S., "A laboratory study of caustic flooding for two Alberta crude oils", *Journal of Canadian Petroleum Technology*, **30** (1), January – February 1991, p 44 - 49.

Takamura, K. "Microscopic Structure of Athabasca Oil Sand", *Can. J. Chem. Eng.*, **60**, 1982, p 538 - 545.

Takamura, K. and Isaacs, E.E., "Chapter 5: Interfacial Properties", *AOSTRA Technical Handbook on Oil Sands, Bitumens and Heavy Oils*, AOSTRA Technical Publications Series #6, Hepler, L.G. and Hsi, C., ed., 101 – 128, Alberta Oil Sands Technology and Research Authority, Edmonton, AB Canada, 1989.

Tao, T.M. and Watson, A.T., "Accuracy of JBN Estimates of Relative Permeability: Part 1 – Error Analysis", *SPE Journal*, **24** (2), April 1984, p 209 – 214.

Tao, T.M. and Watson, A.T., "Accuracy of JBN Estimates of Relative Permeability: Part 2 – Algorithms", *SPE Journal*, **24** (2), April 1984, p 215 – 223.

Thomas, S., Farouq Ali, S.M., Scouler, J.R. and Verkoczy, B., "Chemical Methods for Heavy Oil Recovery", *Journal of Canadian Petroleum Technology*, **40** (3), March 2001, p 56 - 61.

Tremblay, B., Sedgwick, G. and Forshner, K., "Simulation of Cold Production in Heavy Oil Reservoir: Wormhole Dynamics", SPE 35387, SPE Symposium on Improved Oil Recovery, Tulsa, Oklahoma, Apr 21 – 24, 1996.

Tremblay, B., Sedgwick, G. and Vu, D., "CT Imaging of Wormhole Growth Under Solution-Gas Drive", *SPE Res. Eval. & Eng.*, **2**(1), February 1999, p 37 – 45.

van Meurs, P. and van der Poel, C., "A Theoretical Description of Water-Drive Processes Involving Viscous Fingering", *Trans. AIME*, **213**, 1958, p 103 - 112.

Varnon, J.E. and Greenkorn, R.A., "Unstable Two-Fluid Flow in a Porous Medium", *SPE Journal*, **9** (3), September 1969, p 293 – 300.

Vinegar, H.J. and Wellington, S.L., "Tomographic imaging of three-phase flow experiments", *Review of Scientific Instruments,* **58** (1), January 1987, p 96 – 107.

Vonnegut, B., "Rotating Bubble Method for the Determination of Surface and Interfacial Tensions", *Review of Scientific Instruments 13*, 1942, p 6 – 9.

Vittoratos, E.S., Brice, B.W., West, C.C., Digert, S.A. and Chambers, B.C., "Optimizing Heavy Oil Waterflooding: Are the Light Oil Paradigms Applicable?", presented at the 1st World Heavy Oil Conference, Beijing, China, Nov 12 – 15, 2006.

Washburn, E.W., "The Dynamics of Capillary Flow", *The Physical Review*, **17** (3), March 1921, p 273 – 283.

Wagner, O.R. and Leach, R.O., "Improving Oil Displacement Efficiency by Wettability Adjustment", *Trans. AIME*, **216**, 1959, p 65 -72.

Wall, C.E. and Khurana, A.K., "Saturation: Permeability Relationships at Low Gas Saturations", *Journal Institute of Petroleum*, **57**, September 1971, p. 261 – 269.

Wang, R., Gas recovery from porous media by spontaneous imbibition of liquid, Master's Thesis, University of Wyoming, December 1999.

Wang, J., Dong, M. and Asghari, K., "Effect of Oil Viscosity on Heavy-Oil/Water Relative Permeability Curves", SPE 99763, 2006 SPE/DOE Symposium on Improved Oil Recovery, Tulsa, Oklahoma, 22-26 April 2006.

Welge, H.J., "A Simplified Method for Computing Oil Recovery by Gas or Water Drive", *Trans. AIME*, **195**, 1952, p 91 – 98.

Wright, I.W., Lastockin, D., Allsopp, K., Evers-Dakers, M. and Kantzas, A., "Low Field NMR Water Cut Metering", technical note, *Journal of Canadian Petroleum Technology*, **43** (5), May 2004, p 17 – 21.

Xie, X. and Morrow, N.R., "Oil Recovery by Spontaneous Imbibition from Weakly Water-Wet Rocks", *Petrophysics*, **42** (4), July – August 2001, p 313 – 322.

Yang, Z. and Ershaghi, I., "A Method for Pattern Recognition for WOR Plots in Waterflood Management", SPE 93870, SPE Western Regional Meeting, Irvine, CA USA, Mar 30 - Apr 1, 2005.

Yang, R., Yang, S., Zou, Z., Zhao, F. and Muhetaer, "Tests of Conversion into Steam Stimulation Following Water Flooding in Karamay Conglomerate Oilfield", SPE 50894, SPE International Conference and Exhibition, Beijing, China, November 2 – 6, 1998.

Yortsos, Y.C., Choi, Y., Yang, Z., and Shah, P.C., "Analysis and Interpretation of Water/Oil Ratio in Waterfloods", *SPE Journal*, **4** (4), Dec 1999, p 413 – 424.

Zhang, X., Morrow, N.R. and Ma, S., "Experimental Verification of a Modified Scaling Group for Spontaneous Imbition", *SPE Res. Eng.*, **11** (4), November 1996, p 280 – 285.

Zhang, Y.P., Sayegh, S.G. and Huang, S., "The Role of Effective Interfacial Tension in Alkaline/Surfactant/Polymer Flooding", CIM 2005-022, 56th Annual Technical Meeting of the Petroleum Society of CIM, Calgary, AB Canada, June 7 – 9, 2005.

Zhang, Y., Xie, X. and Morrow, N.R., "Waterflood Performance by Injection of Brine With Different Salinity for Reservoir Cores", SPE 109849, 2007 SPE Annual Technical Conference and Exhibition, Anaheim, California, November 11 – 14, 2007.

Zhou, X., Morrow, N.R. and Ma., S., "Interrelationship of Wettability, Initial Water Saturation, Aging Time, and Oil Recovery by Spontaneous Imbibition and Waterflooding", *SPE Journal,* **5** (2), June 2000.

APPENDIX A: CALCULATION OF FLOW RATES IN THE PORE DOUBLET MODEL FOR SYSTEMS OF VARYING OIL VISCOSITY

The pore doublet model of Moore and Slobod (1956) was utilized to show fluid movement in two pores of varying size. The physical representation of this model is that of fluid flowing around a sand grain, that is surrounded by other grains.
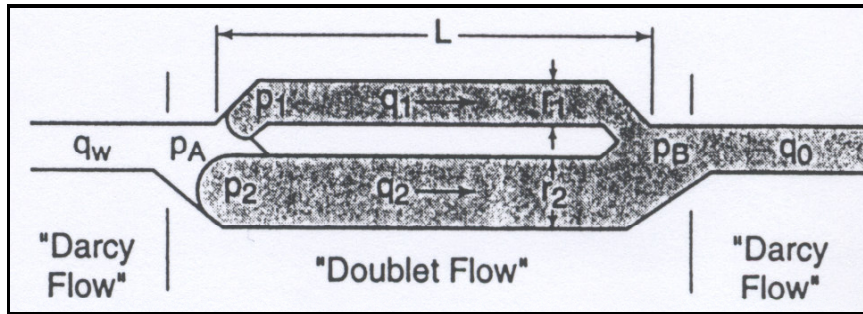
Figure A-1: Displacement of oil in a pore doublet (from Green and Willhite, 1998)

Moore and Slobod (1956) derived equations for flow into both pores (1 and 2) under the assumption that oil and water have similar viscosity. These equations were developed by assuming that fluid was injected at a fixed total injection rate, q, and that flow within each pore is governed by the Hagan-Poiseuille equation for laminar flow.

$$q_1 = \frac{\dfrac{4\mu Lq}{\pi r_2^4} + \left(\dfrac{1}{r_1} - \dfrac{1}{r_2}\right)\sigma\cos\theta}{\dfrac{4\mu L}{\pi}\left(\dfrac{1}{r_1^4} + \dfrac{1}{r_2^4}\right)} \qquad\qquad \text{Eqn (A.1)}$$

$$q_2 = \frac{\dfrac{4\mu Lq}{\pi r_1^4} + \left(\dfrac{1}{r_1} - \dfrac{1}{r_2}\right)\sigma\cos\theta}{\dfrac{4\mu L}{\pi}\left(\dfrac{1}{r_1^4} + \dfrac{1}{r_2^4}\right)} \qquad\qquad \text{Eqn (A.2)}$$

$$v = \frac{v_1}{v_2} = \frac{\dfrac{4Lq\mu}{\pi r_2^2 \sigma \cos\theta} + r_2^2\left(\dfrac{1}{r_1} - \dfrac{1}{r_2}\right)}{\dfrac{4Lq\mu}{\pi r_1^2 \sigma \cos\theta} - r_1^2\left(\dfrac{1}{r_1} - \dfrac{1}{r_2}\right)} \qquad \text{Eqn (A.3)}$$

Eqn (A.3) is a ratio of the fluid velocity in the small pore (1) to the larger pore (2). This equation will be used to calculate the velocity ratio of fluid advancement in both capillaries under various circumstances.

Table A-1 contains the values for the variables to be used in Eqn (A.3).

Table A-1: Relevant parameters for calculations in the pore doublet model

k (D)	3
ϕ (fraction)	0.36
R (average radius, m)	9.93×10^{-6}
r_1 (m)	$= 0.5*R = 4.97 \times 10^{-6}$
r_2 (m)	$= 1.5*R = 1.49 \times 10^{-5}$
L (m)	$= 5*R = 4.97 \times 10^{-5}$
IFT of conventional case (mN/m)	30
IFT of HO1 and HO2 (mN/m)	14
μ of conventional case (mPa·s)	1
μ of HO1 (mPa·s)	4,500
μ of HO2 (mPa·s)	11,500

Using Eqn (A-3) along with the values outlined in Table (A-1) the ratios have been calculated for a wide range of injection rates (frontal velocity) and are plotted in Figure A-2. From this figure, it can be seen that there is a limit at which the rate of advancement in the smaller capillary (1) exceeds that of the larger capillary (2). However, there is also a wide range of frontal advancement rates under which the ratio is negative, implying that fluids is imbibed into the smaller capillary but flows backwards counter-currently through the larger capillary. According to Rojas and Farouq-Ali (1988), the range of flow rates often employed in the reservoir is 0.18 m/d to 2.9 m/d. This means that under

reservoir condition, the ratio of velocities will be negative, which is not physically possible.
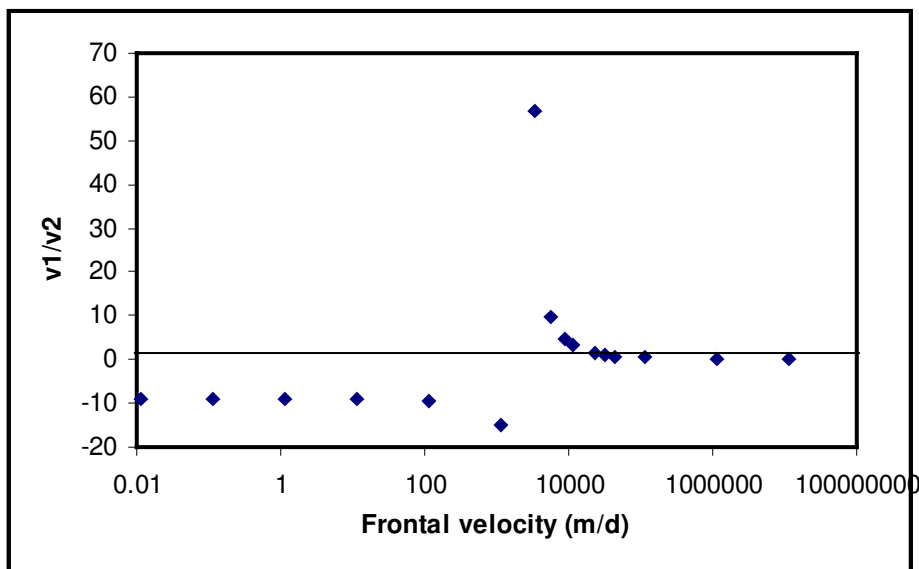
Figure A-2: Ratio of velocity in the pore doublet model for conventional oil

If only the positive values of the ratio are considered, Figure A-2 illustrates a very important concept: in order for the flow in the larger capillary tube to be faster than the flow in the smaller one (i.e. for the ratio to be less than 1), it is necessary to inject at a phenomenally high rate of greater than 32,000 m/d.

Even though the above equations were derived for a system where oil and water have the same viscosity, its application can still be extended to heavy oil cases. This is possible through the use of several assumptions. First, it is assumed that water is at the inlet to the pore doublet, so at the initial state of flow the pore doublet contains oil of higher viscosity. The second assumption made is that, since water is much less viscous than oil, the flow rates given in the Hagan-Poiseuille expression is controlled by the oil viscosity. The last assumption made is that flow instabilities are negligible, so there is no viscous fingering or poor displacement within a single capillary. With these assumptions, the effect of viscosity is investigated and plotted in Figure A-3.
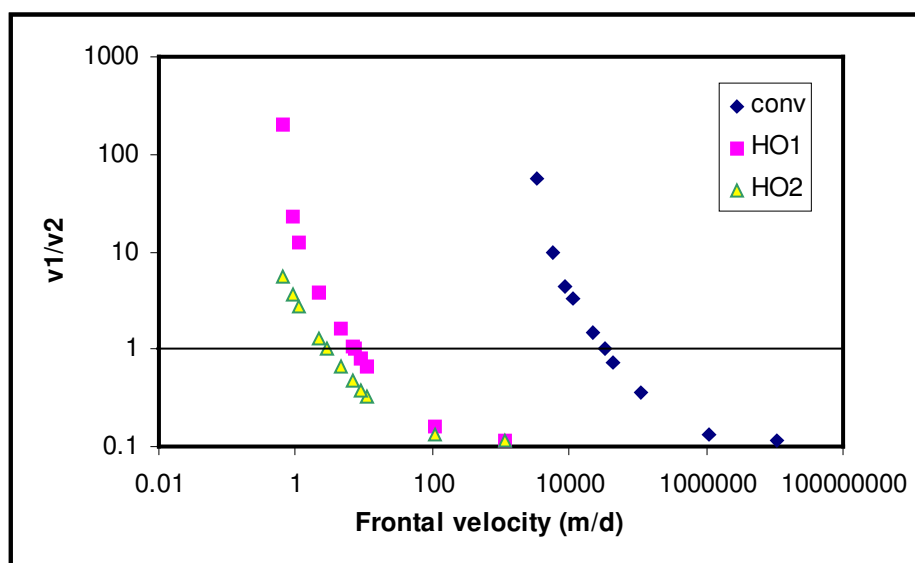
Figure A-3: Effect of changing oil viscosity on the critical velocity required for flow to be faster in the larger capillary

Figure A-3 shows a distinct shift to lower ratios for higher viscosity of oil. This implies that for higher oil viscosity, viscous forces become more important so at lower frontal velocities flow occurs more readily through the larger capillary. Table A-2 shows the required frontal velocity that will yield equal flow through the capillaries. At velocities higher than this critical value, flow is through the larger pore.

Table A-2: Critical velocity for flow occurring faster in the larger capillary

Oil viscosity (mPa·s)	Frontal velocity when v =1 (m/d)
1	32,000
4,500	7
11,500	3

These results indicate that as the oil viscosity increases, viscous forces start to dominate more and flow will preferentially occur in the larger pores even in a water wet core. However, it should be emphasized again that at the range of frontal velocities representative of reservoirs, there exists a negative solution where the pore doublet model is not representative of any physical flow condition.

APPENDIX B: CALCULATION OF WALL THICKNESS AND MAXIMUM ALLOWABLE PRESSURE OF PEEK CORE HOLDERS

Properties of PEEK were provided by Quadrant Engineering Plastic Products. At 23°C the tensile strength of PEEK is 100,000 kPa (15,000 psi).

A core holder is essentially a pipe that has to sustain a certain maximum pressure, which is given by either the overburden pressure in a core that contains overburden, or the injection pressure in a core that has no overburden. In the system studied in the NMR, there was not enough space for a core with a sleeve and overburden pressure, so waterfloods were performed on sandpacks prepared in the absence of overburden. For this application, the maximum allowable pressure is therefore the injection pressure at early times, before water breakthrough occurs.

Pipe strength calculations were performed using the "Engineer Edge" website, which can be found in the following link (http://engineersedge.com/pipe_bust_calc.htm).

For this core, the outer diameter of the core holder (constrained by the diameter of the NMR bore) was 5.08 cm (2 inches). The wall thickness was then varied in order to maximize the size of the core while still giving a high pressure rating for the core. In the calculation of wall thickness (shown on the next page) the safety factor was taken to be five. In this manner, the core can be operated at 20% of the burst pressure. With a wall thickness of 0.635 cm (0.25 inches) the core holder could be operated at a working pressure of 6900 kPa (1000 psi).

Pipe Strength Calculator

Equation: P = (2*S*T)/((O.D.-2*T)*SF)

Where:	P = Fluid Pressure (psi)
	T = Pipe Wall Thickness (in)
	O.D. = Pipe Outside Diameter (in)
	SF = Safety factor (General Calculations 1.5 – 10, Use 1 For Bursting Pressure)
	S = Material Strength (psi)
	Ultimate Tensile strength or Yield strength can be used. Ultimate should be used to determine the bursting pressure. Yield can be used for estimating pressures at which permanent deformation begins.

Engineers Edge Design & Engineering Resources

OD (in)	2	(in)
Wall (in)	.25	(in)
Material Strength	15000	(psi)
Safety Factor (working)	5	See Above
	Calculate!	
Calculated Working Pressure	1000	
Calculated Bursting/Yield Pressure	5000	

APPENDIX C: CALCULATION OF THE PROPERTIES OF THE SANDPACKS

Various properties of the sandpacks were calculated for each experiment. These properties include porosity, permeability and irreducible water saturation (S_{wi}).

Porosity

The porosity of the sandpacks was obtained through gas expansion, in which a small pressure is applied to the porous medium and after the pressure has equalized, the gas is allowed to expand. During gas expansion it displaces water from an attached water reservoir. Due to the fact that the system operates under small pressure, the gas could be assumed to be ideal. Under constant temperature, Boyle's Law can be applied. Boyle's Law states that:

$$P_1V_1 = P_2V_2 \qquad\qquad\qquad \text{Eqn (C-1)}$$

The pore volume of the sandpack can be determined by re-arranging Eqn (C-1) to give:

$$V_1 = \frac{P_2V_2}{P_1} \qquad\qquad\qquad \text{Eqn (C-2)}$$

Where P_2 is the atmospheric pressure, V_2 is the volume of water produced and P_1 is the pressure of the gas. In reality, V_1 is the pore volume plus any dead volume from the associated lines and fittings. Thus, to obtain an accurate pore volume the dead volumes must be calculated and subtracted. The porosity is then equal to the pore volume divided by the bulk volume of the sandpack.

Permeability

The permeability of the sandpack was obtained by flowing brine with a certain head pressure through the sandpack. The data collected is the height of the water column

above the sandpack, and the amount of brine produced in a certain time. Permeability is obtained from Darcy's Law. A sample calculation is shown below:

Trial	Height (cm)	amt of brine (g)	time (s)	ΔP (atm)	ΔP*/L	Q (ml/s)	Q*/A
1	79	20.06	180.66	0.080	0.005	0.106	0.009
2	100	19.66	129.15	0.102	0.006	0.145	0.013
3	118	24.94	131	0.120	0.007	0.182	0.016
4	132	28.36	130.21	0.134	0.008	0.208	0.018

Length of sandpack	16.8 cm
Density of doped brine	1.0487 g/cc
Cross-section area	11.4 cm^2
Flow rate	0.208 cm^3/s
Reynold's number	4.125E-06
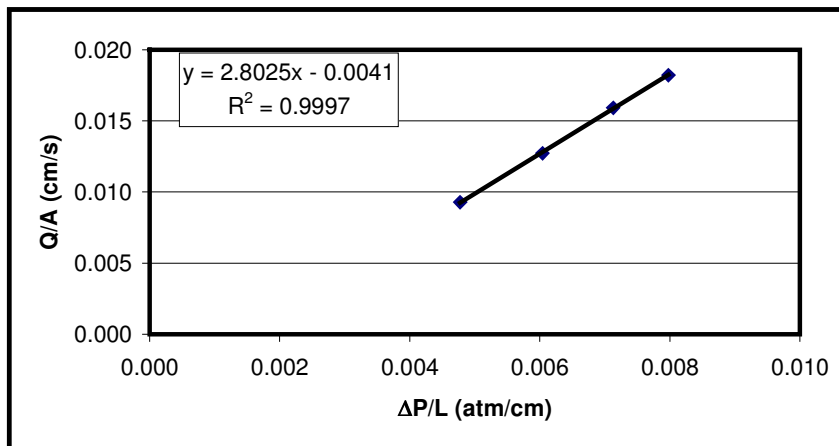
Reynold's number was calculated to make sure that the flow regime is still laminar, in order for Darcy's Law to be applicable. It was calculated using the highest velocity (0.208 cm^3/s) and the average diameter of the pore (9.93 x 10^{-6} m). The small values of the Reynold's number indicate that the flow is in fact laminar, and inertial forces are negligible. The brine permeability is the slope seen in the figure (assuming viscosity of brine is equal to 1).

Irreducible water saturation

During oil saturation, brine is produced and separated. By knowing the total amount of brine produced, the irreducible water saturation could be calculated by using:

$$S_{wi} = \left(\frac{PV - M_{brine}/\rho_{brine}}{PV} \right)$$
Eqn (C-3)

The pore volume (PV) was previously calculated through gas expansion. The mass of brine is obtained through separation with toluene, and brine density can also be measured at the experimental temperature.

APPENDIX D: CALCULATION OF LIVE OIL PROPERTIES

For any batch of live oil generated, the gas oil ratio (GOR), density and viscosity was determined.

Gas oil ratio

During this measurement a sample of live oil is collected in the piston and is transferred to a test tube where the dead oil is collected. Any liberated gas flows out of the top of the test tube and is collected in an inverted graduated cylinder that was full of water. The volume of water displaced is the gas volume.

A sample calculation is shown below.

Table D-1: Calculation of gas oil ratio for a sample of live oil

Trial #	Piston (g)	Test tube (g)	Orig gas (cm³)	Piston +LO (g)	Test tube +DO (g)	Vol of DO (cm³)	Total gas (cm³)	GOR
1	1444.08	12.93	36	1453.41	22.13	9.529	100.471	10.54
2	1444.01	12.94	23	1453.8	22.6	9.998	111.002	11.10
3	1444.07	12.81	30	1453.45	22.32	9.580	107.420	11.21
4	1444.15	12.94	35	1453.32	22.02	9.365	105.635	11.28
5	1444.13	12.75	44	1453.42	22.02	9.488	105.512	11.12
							avg	11.18

The volume of dead oil is obtained by subtracting the weight of the test tube with dead oil from its original weight and dividing by the dead oil density. The total gas volume is the final gas volume, after subtracting the original gas volume plus the volume of the dead oil. The GOR is then the ratio of gas volume to oil volume.

Density

The calculation of live oil density is quite simple. A tube of known volume was filled with live oil and weighed. The change in mass of the tube expressed over the volume of the tube is then the density of the live oil sample. A sample calculation is shown below.

Table D-2: Calculation of live oil density

mass of container (g)	trial 1	trial 2	trial 3	average
filled H_2O (g)	309.59	309.62	309.61	
empty (g)	298.98	299	299.01	
H_2O weight (g)	10.61	10.62	10.6	
volume of container (cm³)	10.63	10.64	10.62	10.63

mass of container (g)	trial 1	trial 2	trial 3	average
filled live oil (g)	309.33	309.34	309.34	
empty (g)	298.89	298.95	298.94	
Live oil weight (g)	10.44	10.39	10.4	
live oil density (g/cm³)	0.98	0.98	0.98	
Density of live oil (kg/m³)	981.75	977.05	977.99	978.93

Viscosity

The live oil viscosity is measured through a capillary tube. Pressure drop was monitored at fixed flow rates, and oil viscosity was calculated using the Hagen-Poiseuille equation.

Q (ml/hr)	ΔP (psi)	Q (cm³/s)	Q/A (cm/s)	ΔP/L (atm/cm)
100	111	0.028	1.151	0.0497
50	56	0.014	0.576	0.0251
75	83	0.021	0.864	0.0372
25	32	0.007	0.288	0.0143

$y = 2.3020E+01x$

$R^2 = 9.9546E-01$
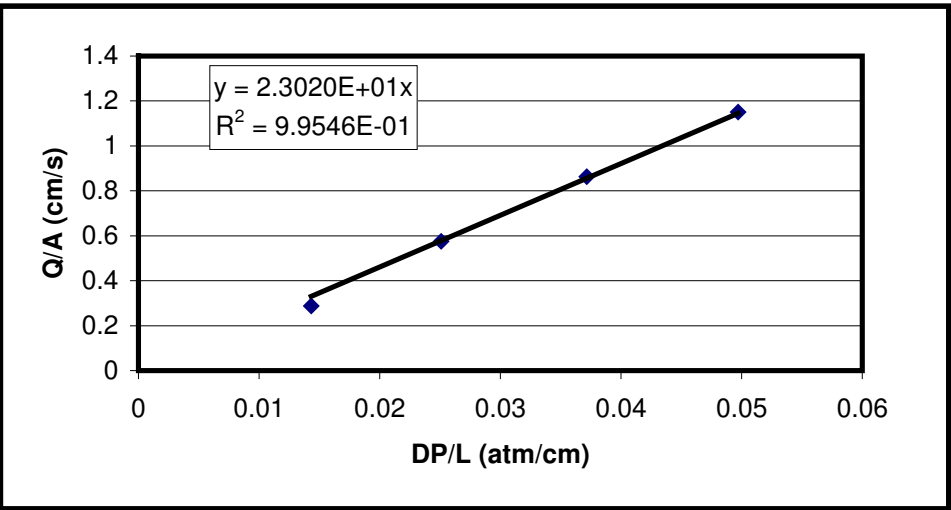
L (cm)	152
k (D)	9.73E+04
slope	2.30E+01
μ (mPas)	4225
Reynold	0.004671652

APPENDIX E: CALCULATION OF GAS AND OIL PRODUCTION RATES DURING PRIMARY DEPLETION

The setup in Figure 4.7 shows that the live oil produced during primary depletion could be collected in one of the two parallel collection systems. Each collection system consists of a container to retain oil, while allowing any liberated gas to be accumulated and in another container. The gas volume is determined from the pressure of the system. This gas container was attached to two automated Solenoid valves, which were controlled using Labview™ software. This allowed a limit pressure to be set, at which point one Solenoid valve would close to isolate the gas collection system and the other Solenoid valve will open to vent the pressurized gas. In these experiments the limit was set at 34 kPa (5 psi). At this pressure, the gas is once again assumed to be ideal. Thus, Boyle's Law could be used to determine the actual volume of gas produced.

The data collection system records the time at which the pressure limit was reached and vented, along with pressure inside the gas container with time. The difference between the pressure limit and the initial pressure was used to calculate the total amount of gas collected during each time period. At various instances the oil container was detached to measure the weight, so produced oil mass was measured as discrete samples. While this was being done, any live oil that was produced was directed to the other collection system as shown in Figure 4.7. Before the oil container is removed, the pressure inside this container is noted and any gas existing in this container was vented. From the known volume of the oil container and the actual volume of oil present in the container, the volume occupied by gas is determined. Thus, the volume of gas liberated during this step could be accounted for.

Table E-1 shows the oil production rate along with the GOR for primary depletion in core B. The determination of oil production rate is very straightforward. At the point where the oil container is measured, an oil production rate could be calculated. The total gas production until this point consisted of all the vented gas.

Table E-1: Primary production data for core B

| Primary depletion of core B										
Date	Time	Time (hrs)	Oil prod (g)	Q_oil (mL/hr)	Cum oil (mL)	R (%OOIP)	Cum gas (mL)	Gas prod (mL)	GOR	Cum GOR
14-Mar-06	16:45	0	0	0	0	0	0			
15-Mar-06	9:34	16.82	4.60	0.28	4.69	0.19	24.59	24.59	5.35	5.35
	16:45	24.00	2.50	0.36	7.24	0.30	38.73	14.14	5.65	5.46
	19:59	27.23	1.10	0.35	8.37	0.34	53.67	14.94	13.58	6.55
16-Mar-06	9:26	40.68	29.70	2.25	38.67	1.58	250.65	196.98	6.63	6.61
	13:49	45.07	46.70	10.87	86.33	3.52	520.73	270.08	5.78	6.16
	16:27	47.70	33.10	12.83	120.10	4.90	704.70	183.97	5.56	5.99
	20:14	51.48	56.60	15.27	177.86	7.26	961.77	257.07	4.54	5.52
17-Mar-06	11:36	66.85	220.80	14.66	403.16	16.45	6190.74	5228.96	23.68	15.67
	13:49	69.07	21.70	9.99	425.31	17.35	7824.79	1634.05	75.30	18.77
	16:09	71.40	18.60	8.13	444.29	18.13	8921.37	1096.59	58.96	20.49
	21:55	77.17	38.60	6.83	483.67	19.73	12434.69	3513.32	91.02	26.23
18-Mar-06	14:30	93.75	44.30	2.73	528.88	21.58	17534.89	5100.20	115.13	33.83
19-Mar-06	17:35	120.83	34.40	1.30	563.98	23.01	19534.57	1999.68	58.13	35.34
20-Mar-06	10:32	137.78	18.70	1.13	583.06	23.79	20001.15	466.59	24.95	35.00
	21:02	146.68	11.70	1.34	595.00	24.28	20365.96	364.81	31.18	34.93
21-Mar-06	14:25	164.07	15.90	0.93	611.22	24.94	20494.76	128.80	8.10	34.21
22-Mar-06	11:05	184.73	12.90	0.64	624.39	25.47	20910.72	415.96	32.25	34.17
23-Mar-06	16:06	213.75	15.40	0.54	640.10	26.12	21306.52	395.80	25.70	33.97
24-Mar-06	10:50	233.48	9.20	0.48	649.49	26.50	21584.09	277.57	30.17	33.91
27-Mar-06	11:11	305.83	10.10	0.14	659.80	26.92	22145.83	561.74	55.62	34.25
30-Mar-06	14:26	381.08	2.50	0.03	662.35	27.02	22546.60	400.78	160.31	34.74

APPENDIX F: MICRO-CT CROSS-SECTIONAL SLICES OF AN OIL SAND

In these micro-CT images, water is a dark blue colour, sand is yellow and oil is dark brown. Micro-CT imaging can only provide a qualitative indication of water wet conditions, since the 3-D representation was developed through computer algorithms and software, and it is not known how much of an impact these numerical processes have on the final results that are visualized. However, in these images, it appears that a water film exists, separating the sand grains and the oil. In the figures below, red circles are used to draw attention to these apparent water films.
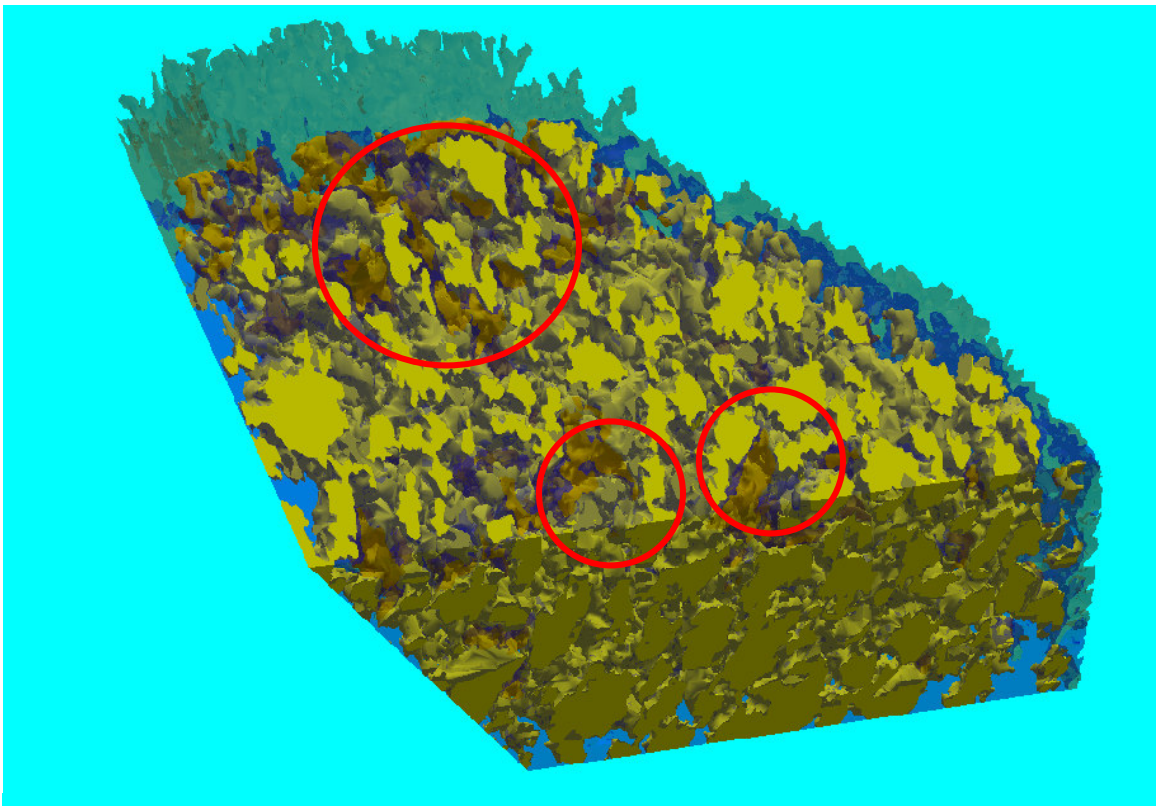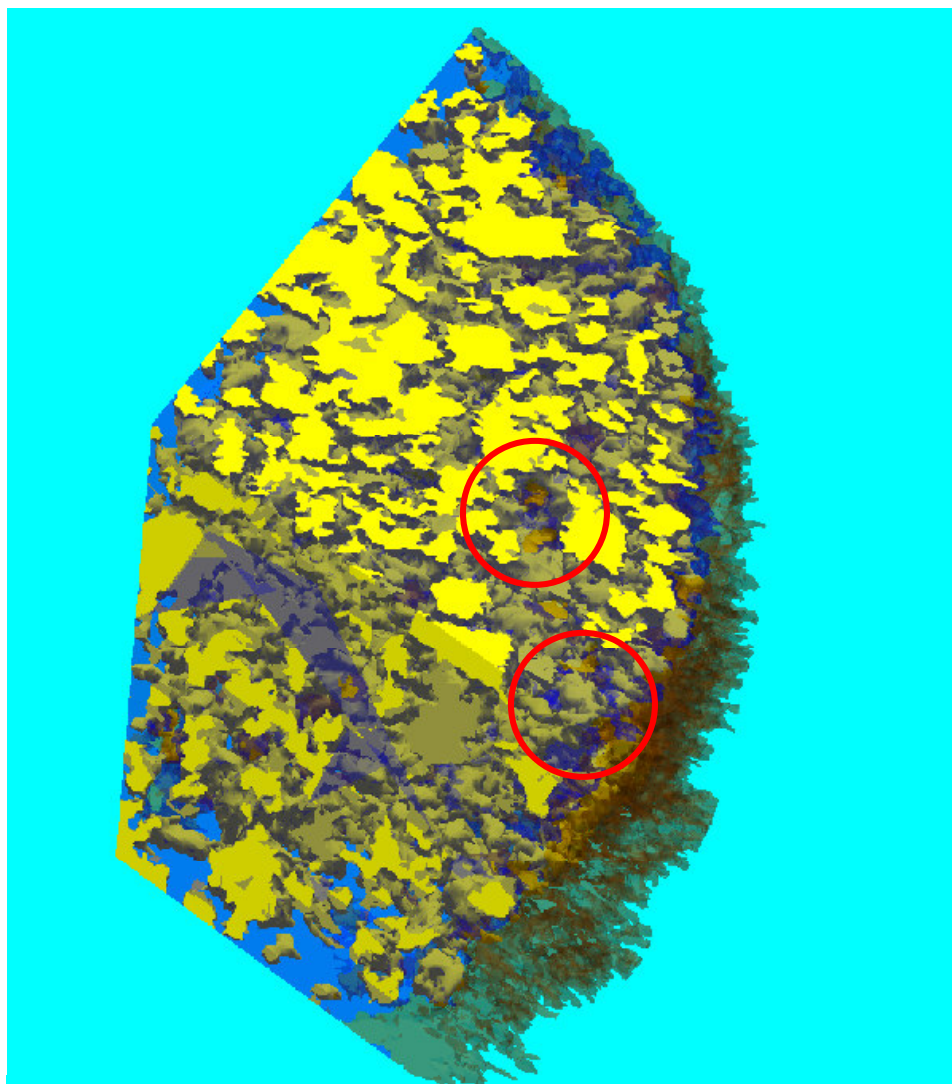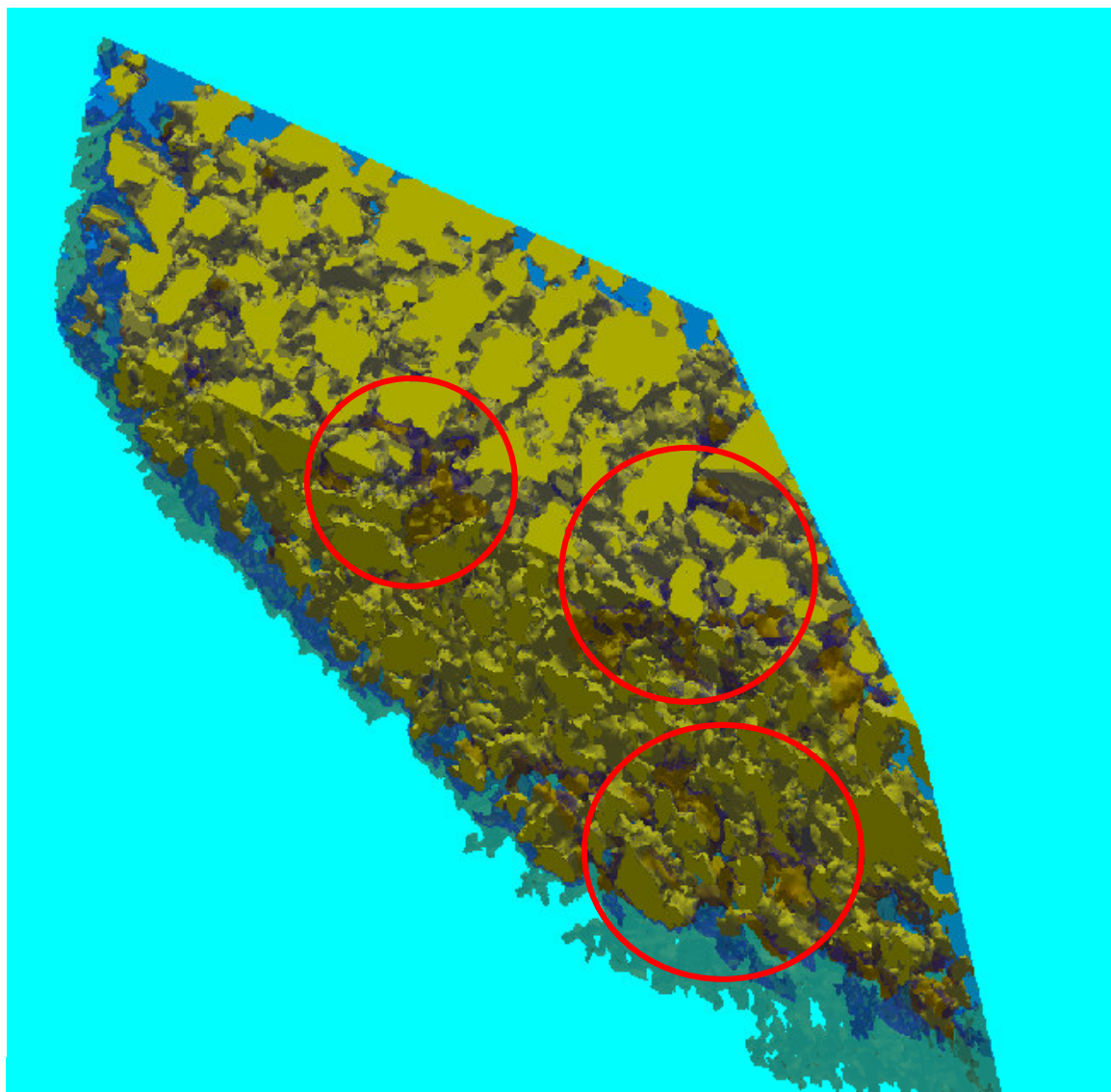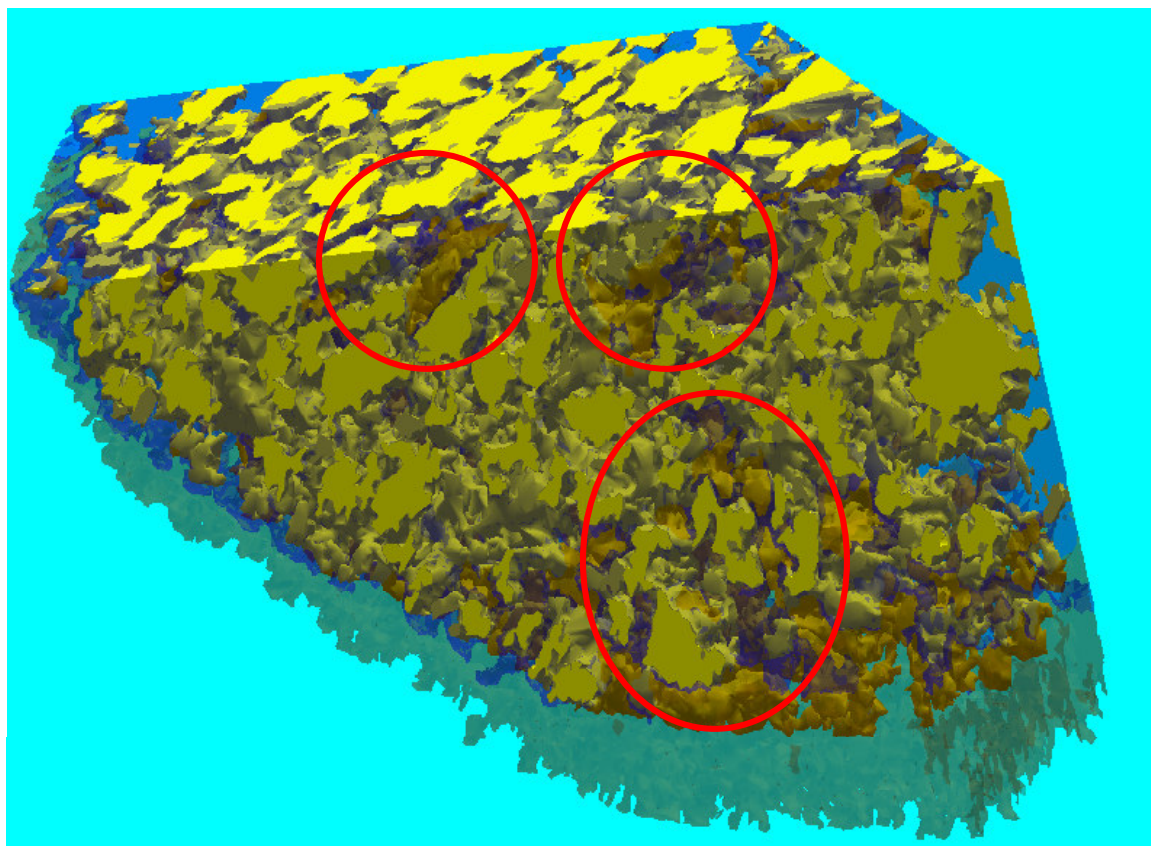
APPENDIX G: CALCULATION OF FILM THICKNESS FROM NMR DATA

The NMR signal of a sample obtained while fully saturated with a fluid is a result of bulk relaxation and surface relaxation, which could be represented by:

$$\frac{1}{T_2} = \left(\frac{1}{T_{2B}} + \frac{1}{T_{2S}}\right) = \left(\frac{1}{T_{2B}} + \rho_s \frac{S}{V}\right) \qquad \text{Eqn (9.10)}$$

In these experiments, the sandpack is saturated with brine with the bulk relaxation of brine 2000 ms. From the NMR data the total relaxation rate is known, as is the bulk relaxation T_2 value of water. Thus, Eqn (9.10) could be rearranged to solve for the surface relaxivity of this sand.

$$\rho_s = \frac{\left(\frac{1}{T_2} - \frac{1}{T_{2B}}\right)}{\left(\frac{S}{V}\right)} \qquad \text{Eqn (G-1)}$$

Assuming that the pore/film can be represented as a cylindrical tube, the surface to volume ratio is 2/r.

The sample calculation below shows the surface relaxivity calculation for a sandpack that is saturated with brine. This same relaxivity is then used to back-calculate the mean pore size in a different sandpack that was saturated with water. The same relaxivity could be used in these cases because of the fact that these sandpacks use the same sand. In the second sandpack, the average pore size is approximately 19 μm, so significantly shorter T_2 values correspond to water this is in a more constricted space (i.e. films).

From NMR spectra obtained while fully saturated with water:

Length frac	Amplitude	T_{2gm}	
0.09	1.786	59.921	
0.35	1.808	71.982	
0.65	1.779	57.196	
0.78	1.765	63.485	
	T_{2gm_avg} (ms)	63.146	0.063 s

k (D)	0.780	7.699E-13 m²	
Porosity	0.41		
Avg radius (m)	4.747E-06	4.7468 µm	
T_{2S} (ms)	6.520E+01	6.520E-02 s	
Relaxivity (µm/s)	36.399		

Film thickness calculation:

Measured T_{2gm} (ms)	230		
$1/T_{2S}$ (ms^{-1})	0.00385	3.84783 s^{-1}	
T_{2S} (s)	0.260		
radius (µm)	18.920		

APPENDIX H: JAMIN PRESSURE DROP

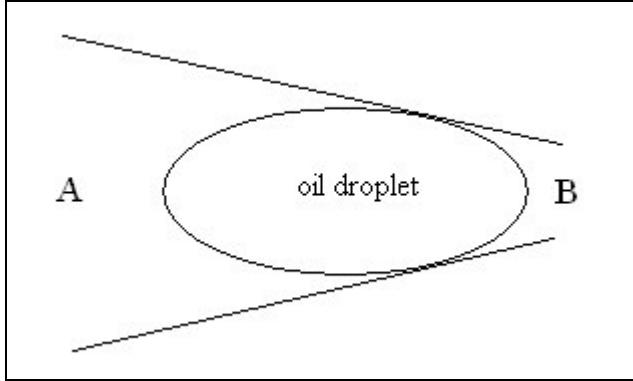This exercise was done to show the amount of pressure required to mobilize trapped oil droplets.

Figure H-1: Oil droplet in a capillary

The pressure drop across this oil droplet is:

$$P_B - P_A = (P_o - P_A) - (P_o - P_B) = \frac{2\sigma\cos\theta}{r_A} - \frac{2\sigma\cos\theta}{r_B} \qquad \text{Eqn (H.1)}$$

In this case σ and θ are assumed to be constant, thus:

$$P_B - P_A = 2\sigma\cos\theta\left(\frac{1}{r_B} - \frac{1}{r_A}\right) \qquad \text{Eqn (H.2)}$$

At equilibrium condition, there is a pressure exists across the droplet (P_B is much higher than P_A). Thus, a significant pressure must be induced across the droplet in order to mobilize it.

For the Lane Mountain 70 sand that was used in essentially all experiments, various properties are noted below in Table H-1.

Table H-1: Porous medium properties

k (D)	3
ϕ (fraction)	0.36
R (average radius, m)	9.93×10^{-6}
r_A (m)	$= 0.5*R = 4.97 \times 10^{-6}$
r_B (m)	$= 1.5*R = 1.49 \times 10^{-5}$
L (m)	1.80×10^{-4}
IFT of HO1 and HO2 (mN/m)	14

The length was assumed to be the size of the grain, which was calculated from the particle size distribution of Lane Mountain 70 sand.

The required pressure drop was calculated to be 20,877 kPa/m.

APPENDIX I: JOHNSON-BOSSLER-NAUMANN (JBN) METHOD FOR CALCULATING RELATIVE PERMEABILITY

Information obtained from dead oil floods was used to extrapolate relative permeability characteristics. The method used to calculate permeability was outlined in detail by Maini and Javadpour (2000), which is based on the JBN method. The JBN method itself employed the frontal advance theory developed by Buckley and Leverett (1942), with further developments by Welge (1952). The principle equations are as follows:

$$W_i = \frac{1}{df_w / dS_w} \qquad \text{Eqn (I-1)}$$

From the waterflood the volume of water injected and the amount of oil recovered is recorded, thus the water saturation could be calculated. From these numbers the oil fraction could be determined.

$$(f_o)_2 = \frac{dS_{avg}}{dW_i} \qquad \text{Eqn (I-2)}$$

I_r is then calculated next by using the following equation:

$$I_r = \frac{\dfrac{u}{\Delta P}}{\left(\dfrac{u}{\Delta P}\right)_{\text{at start of injection}}} = \left(\frac{\Delta P_{\text{at start of injection}}}{\Delta P}\right) \qquad \text{Eqn (I-3)}$$

The relative permeability to oil can be determined from:

$$\frac{f_o}{k_{ro}} = \frac{d\left(\dfrac{1}{W_i I_r}\right)_1}{d\left(\dfrac{1}{W_i}\right)}$$

Eqn (I-4)

The water relative permeability can then be estimated from the following relationship:

$$\frac{f_o}{f_w} = \frac{1-f_w}{f_w} = \frac{k_{rw}\mu_o}{k_{ro}\mu_w}$$

Eqn (I-5)

At any production point, the average water saturation is:

$$\left(S_w\right)_{avg} = \left(S_w\right)_2 + W_i\left(f_o\right)_2$$

Eqn (I-6)

The basic assumptions behind this model are the porous medium is homogeneous, the fluids are incompressible and gravity effects are negligible (Maini and Javadpour, 2000). The JBN method requires two conditions to be met before one can apply this method. First, the flow velocity has to be high enough to achieved stabilized displacement (no capillary effects) so that the capillary pressure gradient can be neglected. Second, the flow velocity is assumed to be constant across the cross section.

Detailed sample calculations for the JBN method are provided in the literature (Maini and Javadpour, 2000).